Issues 1-2 2022 | Volume 18

The Journal on Advanced Studies in Theoretical and Experimental Physics, including Related Themes from Mathematics

PROGRESS IN PHYSICS

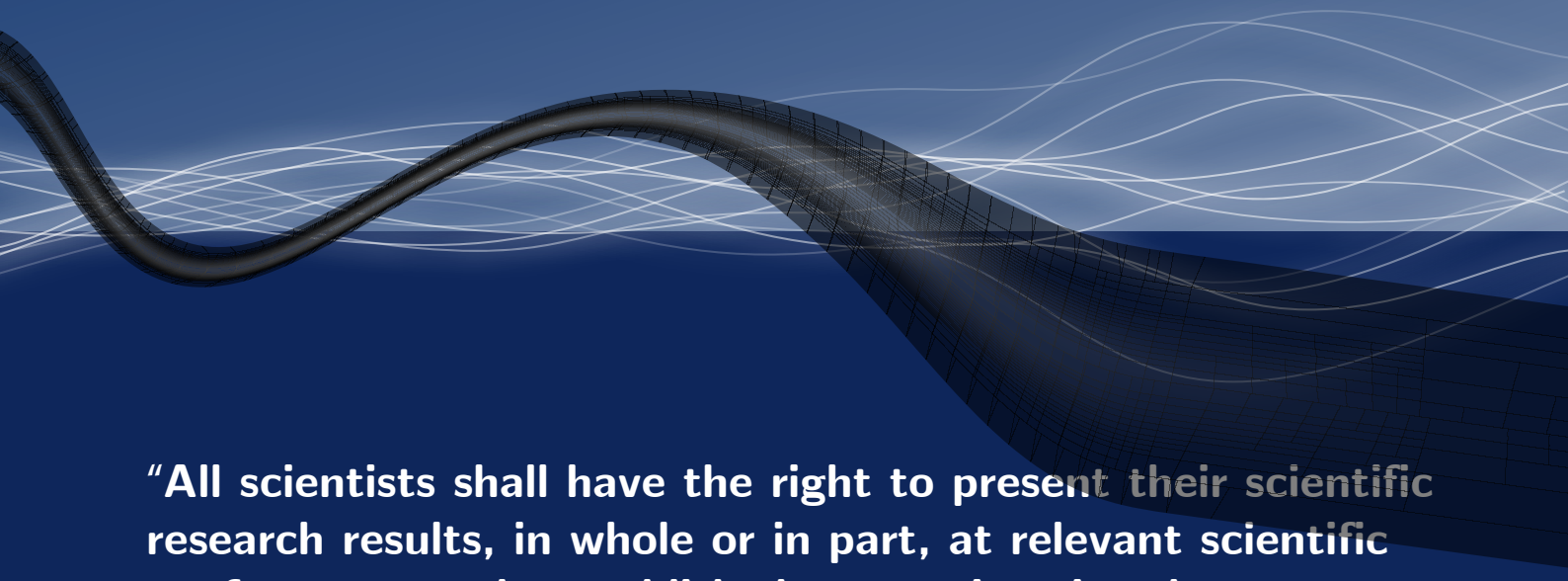

"All scientists shall have the right to present their scientific research results, in whole or in part, at relevant scientific conferences, and to publish the same in printed scientific journals, electronic archives, and any other media." — Declaration of Academic Freedom, Article 8

ISSN 1555-5534

PROGRESS IN PHYSICS

A Scientific Journal on Advanced Studies in Theoretical and Experimental Physics, including Related Themes from Mathematics. This journal is registered with the Library of Congress (DC, USA).

Electronic version of this journal:
http://www.ptep-online.com

Postal Address

Department of Mathematics and Science,
University of New Mexico,
705 Gurley Ave., Gallup, NM 87301, USA

ISSN: 1555-5534 (print)
ISSN: 1555-5615 (online)

Standard Address Number: 297-5092
Printed in the United States of America

April 2022 **Vol. 18, Issue 1**

CONTENTS

Information for Authors

Progress in Physics has been created for rapid publications on advanced studies in theoretical and experimental physics, including related themes from mathematics and astronomy. All submitted papers should be professional, in good English, containing a brief review of a problem and obtained results.

All submissions should be designed in LaTeX format using *Progress in Physics* template. This template can be downloaded from *Progress in Physics* home page http://www.ptep-online.com

Preliminary, authors may submit papers in PDF format. If the paper is accepted, authors can manage LaTeXtyping. Do not send MS Word documents, please: we do not use this software, so unable to read this file format. Incorrectly formatted papers (i.e. not LaTeXwith the template) will not be accepted for publication. Those authors who are unable to prepare their submissions in LaTeXformat can apply to a third-party payable service for LaTeX typing. Our personnel work voluntarily. Authors must assist by conforming to this policy, to make the publication process as easy and fast as possible.

Abstract and the necessary information about author(s) should be included into the papers. To submit a paper, mail the file(s) to the Editor-in-Chief.

All submitted papers should be as brief as possible. Short articles are preferable. Large papers can also be considered. Letters related to the publications in the journal or to the events among the science community can be applied to the section *Letters to Progress in Physics*.

All that has been accepted for the online issue of *Progress in Physics* is printed in the paper version of the journal. To order printed issues, contact the Editors.

Authors retain their rights to use their papers published in *Progress in Physics* as a whole or any part of it in any other publications and in any way they see fit. This copyright agreement shall remain valid even if the authors transfer copyright of their published papers to another party.

Electronic copies of all papers published in *Progress in Physics* are available for free download, copying, and re-distribution, according to the copyright agreement printed on the titlepage of each issue of the journal. This copyright agreement follows the *Budapest Open Initiative* and the *Creative Commons Attribution-Noncommercial-No Derivative Works 2.5 License* declaring that electronic copies of such books and journals should always be accessed for reading, download, and copying for any person, and free of charge.

Consideration and review process does not require any payment from the side of the submitters. Nevertheless the authors of accepted papers are requested to pay the page charges. *Progress in Physics* is a non-profit/academic journal: money collected from the authors cover the cost of printing and distribution of the annual volumes of the journal along the major academic/university libraries of the world. (Look for the current author fee in the online version of *Progress in Physics*.)

The Energy Spectra of Cosmic Ray Protons, the Origin of Gluons, and the Mechanism of Baryon Generation

Osvaldo F. Schilling

Departamento de Física, Universidade Federal de Santa Catarina, Campus, Trindade, 88040-900, Florianópolis, SC. Brazil.
E-mail: osvaldo.neto@ufsc.br

For the past sixty years, the generation of hadrons has been dealt with through a framework of theories devised to describe the so-called Strong interactions. About two years ago, the author put forward an essentially quantum electrodynamical model for the same purpose. The present paper contains the latest development in the interpretation of those results, and we reached a point where a bridge can be extended to existing theories. The main result of our previous work has been the determination of an energetic interval of 2.7 GeV between a "vacuum" parent state and the proton rest-energy. The full interpretation of this finding is that this is the energy advantage (calculated from a Regularization procedure) that stabilizes charge (the baryons) confined in the shape of loops by correlating EM excitations at 3.7 GeV. That is, we have been able to establish that these EM excitations are in fact the Gluons of high-energy physics, and they come straight from relativistic quantum electrodynamics through the Regularization procedure of loop energies. The value 2.7 GeV obtained from Regularization is of the correct magnitude to explain the difference between the strength of Strong and EM interactions (15 versus 1/137). The size of a proton can also be approximately deduced from our arguments.

1 Introduction

The present paper contains the main results of investigations which have directly addressed the long-standing problem of describing the genesis of particles. In particular, the issue of the origin of mass is considered [1, 2]. Many of the ideas and concepts in this work have previously been advanced by Barut [3], Bostick [4], and Jehle [5]. In particular, the starting point in this treatment, is that magnetic moments are fundamental properties of leptons and baryons, and that the presence of magnetic moments in particles can be modelled by the introduction of an intrinsic closed electrical current loop of finite (rather than point-like) size. It might be argued that such hypothesis should be incompatible with QED and that electrons behave experimentally as point-like objects. However, the present treatment may be regarded as describing the earliest stages of a particle condensation process taking place in an extremely dense medium at 10^{13} K. Present day experiments take place under completely different conditions.

The current-loop model refers more properly to the EM fields in this *embryonic* stage, and no specific mass/charge distribution for baryons is explicitly needed or introduced. A blend of fermion/EM fields in loop form act to correlate and confine baryon fields inside the loop. A multiply-connected current path should arise, whose possible topological forms were the object of intense discussions by Bostick and Jehle, but in the absence of more concrete evidence a simple circular loop path is adopted in this treatment. The confinement of magnetic flux within such paths was initially [1] assumed as occurring in numbers of flux quanta determined by the magnetic moments in magneton units, a property easily derived from Barut's semiclassical spinning particle-model, but such assumption is later adjusted to better fit data.

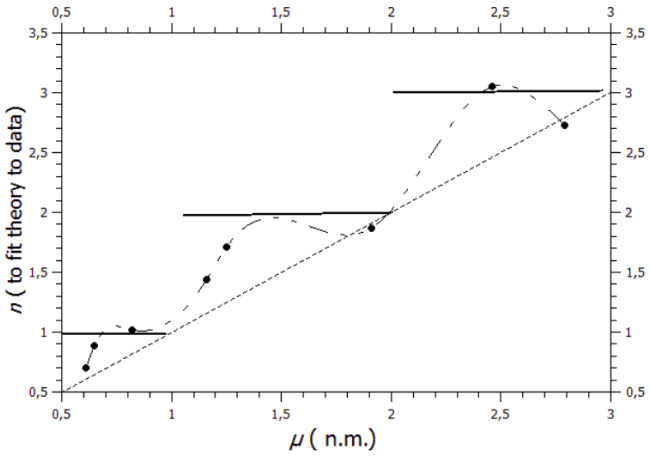

Fig. 1: Plot of n against the magnetic moment for the baryons octet (points) from the definition $n = (2c^2\alpha/e^3)\,\mu\, m$. The diagonal line is the classical prediction of one flux quantum per nuclear magneton (n.m.). Nucleons are on the line. The data display undulations, and a tendency to reach for the steps (traced line as guide) [2].

In paper [1], we have shown that it is possible to describe the masses m of all the baryons of the octet and decuplet in terms of a single formula, involving the magnetic moments μ and corresponding numbers of confined flux quanta n. One might otherwise use this relation to define n from the experimental masses and moments [2]:

$$n = \left(2fc^2\alpha/e^3\right)\mu\, m$$

where $f = 1$ for spin $1/2$ and $\approx 1/\sqrt{3}$ for spin $3/2$, and α is the fine-structure constant (one immediately recovers the often-mentioned inverse relation of mass with the constant α, since n and μ are approximately proportional to each other). The treatment that produces this equation is essentially heuristic, but precise enough for instance to highlight the dependence of mass upon the square-root of the spin angular momentum, as reported in the literature (note that the phenomenological factor f that corrects for spin is related to kinetic energies rather than to magnetic constributions) (cf. Fig. 1 of [1]).

In paper [2], whose main results are reproduced in the following section for the sake of clarity, we took much further the treatment presented in [1]. A key parameter in this analysis is the number of flux quanta n arrested inside a current loop. In particular, we obtain in [2] a very revealing result which has previously been reported mainly through Condensed Matter physics investigations, which is that the energy of currents (here regarded as a particle's rest mass) is a *periodic function* of the confined magnetic flux in multiply-connected structures. Consistently with these results from Condensed Matter systems, the periodic dependence of baryons masses (and confined flux) with the magnetic moments (see Fig. 1) can be regarded as a demonstration that the initial hypotheses of the present investigations are sound. That is, indeed mass is a manifestation of magnetodynamic energies (related to currents) confined in a multiply-connected region. Such hypothesis is therefore consistent with experimental data. With this evidence in hand, the next step clearly was to advance beyond the initial phenomenological-heuristic argumentation and propose a field-theoretical treatment that would describe the observed mass-energy relations for actual particles.

Such kind of treatment has previously been applied for fermion fields flowing around a closed loop containing magnetic flux (see references in [2]). Starting from a Lagrangian suitable to these fields (assumed as built upon a proton "substrate", following Barut), we then obtain an energy spectrum for the possible traveling wave-states around a closed path. To simulate the perturbations coming from the vacuum background which will be added to the proton state, a sum over the states in the energy spectrum of kinetic energies for the EM/fermion quasiparticles is necessary. An Epstein-Riemann Zeta function Regularization procedure previously adopted for the Casimir Effect problem is applied to eliminate divergences when the sum over the energy spectrum states is carried out, and the periodic behavior of the baryon masses with magnetic flux is quantitatively reproduced with no further forms of energies required besides the magnetodynamic terms. A new result of this treatment [2], is the prediction of a parent state at $U_0 = 3.7\,\mathrm{GeV}$, which should be identified with a dense medium (opposite to what we usually qualify as "vacuum"), whose fluctuation instabilities would give origin to baryons. The present work goes beyond [2] in the search for evidence for the existence of this state as well as the source of the correlations. The calculated value of U_0 immediately indicates that protons (of rest mass 0.94 GeV) should become unstable if accelerated to kinetic energies beyond 2.7 GeV if their structure were not strong enough and capable to radiate excess energy. We found out that a very good way to investigate this point is through the analysis of the spectra of protons in cosmic rays, whose energy flux profile peaks at 2.7 GeV kinetic energy (Fig. 3 below) for reasons we will discuss.

In the following sections, we firstly present the field-theoretical model introduced in [2], alongside the comparison with experimental data for mass and magnetic moments for baryons. In the analysis in Section 3, we test the hypothesis of the existence of an energy level for vacuum by examining data collected for protons in cosmic rays and discuss the relation between this energy level and gluons. In Section 4, we show that an estimate for the proton size can be obtained from the theory.

2 Field-theoretical model for generation of baryons

For the developments that led to this field-theoretical treatment, we make reference also to the *Annales* paper [1] (see also references therein and in [2]). Let's consider a fermion field confined by EM energy inside a circular path of length L, enclosing an amount of self induced magnetic flux φ, in a potential A. We need to show that such an EM/fermion packet corresponds to a state detached from a higher state associated with a sea of excitations in equilibrium, and therefore might be used to represent a "quasiparticle". The relativistic Lagrangian for such an object can be modelled through the dressing of a proton of mass m_p (as once proposed by A. Barut) in view of the presence of magnetodynamic terms [2]:

$$L = \overline{\Psi}\left\{ i\alpha_\mu \left(\hbar\partial_\mu - i\,\frac{\mathrm{e}}{\mathrm{c}}\,A_\mu \right) - \alpha_4\, m_p\, c \right\} \Psi \qquad (1)$$

where the α_μ are Dirac matrices. This Lagrangian can readily be transformed into a Hamiltonian form. Assuming a constant potential A around the ring path, the spectrum of possible energies for a confined fermion becomes:

$$\epsilon_k = c\,\left\{ (p_k - eA/c)^2 + m_p^2\, c^2 \right\}^{1/2} \qquad (2)$$

which comes straight from the orthonormalized definition of the Dirac matrices and diagonalization of the Hamiltonian. We now definitely impose a circular closed path. If one takes the Bohr-Sommerfeld quantization conditions, the field momentum p_k (for integer k) is quantized in discrete values $2\pi\hbar\, k/L$. We start from this assumption, but the true boundary conditions to close the wave loop might impose corrections to this rule in the form of a phase factor (a phase factor is introduced in the fit to the data in Fig.3 below). The potential A can be replaced by φ/L. Environmental (vacuum) fluctuation effects on the kinetic energy are accounted for in

a way similar to that applied in the analysis of the Casimir Effect, by summing over all possible integer values of k in (2) [2]. This summation diverges. According to the theory of functions of a complex variable, the removal of such divergences requires that the analytic continuation of the terms be taken, which reveals the diverging parts which are thus considered as contributions from the infinite vacuum reservoir. What remains plays the important role of energetically stabilizing the loops (in a way that resembles the role of phonons in the formation of Cooper pairs). It is necessary to rewrite (2) in terms of Epstein-Riemann Zeta functions [2], including the summation over k from minus to plus infinity integers, and making a Regularization (Reg) transformation. Here $M(\varphi)$ is the flux-dependent dressed mass of a baryon, and $s \to -1$:

$$M\,c^2 \;=\; U_0 + \mathrm{Reg} \sum_k \; c\,\left\{(p_k - e\varphi/Lc)^2 + m_p^2 c^2\right\}^{-s/2} \qquad (3)$$

where we have allowed for the existence of a finite energy U_0 to represent an hypothetical state from which the individual baryons would condense, since they would correspond to lower energy states. Such particles should be characterized as states of energy lower than U_0. It is convenient to define from L a parameter with units of mass $m_0 = 2\pi\hbar/cL$, which will be used to define a scale in the fit to the data. We notice that m_0 is related to the parameter L in the same way field theories regard mass as created from broken symmetries of fields, establishing a range for an otherwise boundless field distribution (e.g. as happens with the London penetration depth at the establishment of a superconductor state, which is related to an electromagnetic field "mass" by a similar expression). For convenience, we define the ratios $m' = m_p/m_0$ and $u_0 = U_0/m_p c^2$. For comparison with the data analysis in our previous work [2], we must introduce also the number of flux quanta n (integer or not) associated to φ, such that $n = \varphi/\varphi_0$. In terms of these parameters one may write (3) in the form:

$$M(n)/m_p = u_0 + (1/m')\,\mathrm{Reg} \sum_k \left\{(k-n)^2 + m'^2\right\}^{-s/2} . \qquad (4)$$

In the analysis of data, the experimental values of M/m_p for baryons will be plotted against n. The sum on the right side of (4) is a particular case of an Epstein Zeta function $Z(s)$, and becomes a Riemann Zeta function, since the summation is over one parameter k only. The summation diverges but it can be analytically continued over the complex plane, since the Epstein Zeta function displays the property of reflection. It has been shown that after the application of reflection, the resulting sum is already regularized, with the divergences eliminated. The reflection formula is [2]:

$$\pi^{-\frac{s}{2}}\,\Gamma\left(\frac{s}{2}\right) Z(s) \;=\; \pi^{\frac{s-1}{2}}\,\Gamma\left(\frac{1-s}{2}\right) Z\,(1-s)\;. \qquad (5)$$

This replaces the diverging $Z(s)$ straight away by the regularized $Z(1-s)$, which is a convergent sum (since $\Gamma\,(-1/2) = -2\,\sqrt{\pi}$ we see that the regularized sums are negative, like in the Casimir Effect solution). The Regularization of (4) is carried out as follows (note that $s \to -1$, and the "reflected" exponent $-(1-s)/2$ replaces $-s/2$ of (4)). $Z(1-s)$ is given as [2]:

$$\begin{gathered}
\sum_k \left\{(k-n)^2 + m'^2\right\}^{-(1-s)/2} = \\
\frac{2}{\Gamma\left(\frac{1-s}{2}\right)} \int_0^\infty t^{\frac{1-s}{2}-1} \left(\sum_k e^{-(k-n)^2 t - m'^2 t}\right) dt = \\
\frac{2\,\sqrt{\pi}}{\Gamma\left(\frac{1-s}{2}\right)} \int_0^\infty t^{-\frac{s}{2}-1} \left(\sum_k e^{-2\pi i k n}\; e^{-\frac{\pi^2 k^2}{t} - m'^2 t}\right) dt = \\
\frac{2\,\sqrt{\pi}}{\Gamma\left(\frac{1-s}{2}\right)} \left(\frac{\Gamma\left(-\frac{s}{2}\right)}{m'^{-s}} + 2\pi^{-s/2} \sum_{k/0} \left(\frac{k}{m'}\right)^{\frac{-s}{2}} K_{\frac{s}{2}}\,(2\pi m' k)\, e^{-2\pi i k n}\right)
\end{gathered} \qquad (6)$$

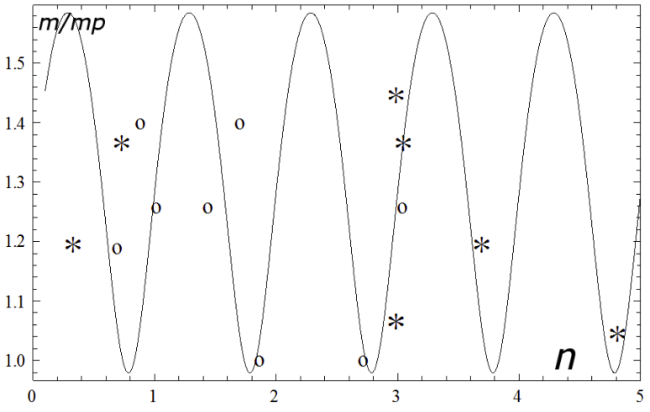

Fig. 2: Comparison of baryons masses calculated from (6) (line) as a function of confined flux n, with data points from Tables I and II of [2] for octet (open circles) and decuplet particles (m_t used [2], stars). Nucleons are on the basis of the figure. The points come from the heuristivc/phenomenological equation $n = (2c^2\alpha/e^3)\,\mu\, m$. The fit produces $U_0 = 3710\,\mathrm{MeV}$ as the vacuum/environment parent level.

The "Reg" summation in (4) then becomes

$$\left(\pi^{\frac{2s-1}{2}}/\Gamma\left(\frac{s}{2}\right)\right)\Gamma\left(\frac{1-s}{2}\right) Z(1-s)\,,$$

and the exponential produces a cosine term.

Since $\Gamma\,(-1/2) = -2\,\sqrt{\pi}$ we see that the regularized sum is negative, corresponding to energies lower than U_0. In the fitting to the data, we will admit that both m' and u_0 are adjustable parameters.

Fig. 2 shows the data for all baryons in Tables I and II of [2], and the plot of mass in (4) regularized by (6), for $u_0 = 3.96$ and $m' = 0.347$ (corresponding to $m_0 = 2.88\ m_p$ and $U_0 = 3710\,\mathrm{MeV}$). The energy $3710\,\mathrm{MeV}$ would represent the environment ("vacuum") energy (state) from which

the baryons would evolve. By comparison with Yukawa's theory of the meson, one may interpret $m_0c^2 = 2710\,\text{MeV}$ as the mass of a particle that provides an internal correlation and keeps the dressed proton stable, a task usually attributed to gluons in particle theory. Such particle is essentially EM energy confined in a loop [4], and the correlated system would follow the behavior of an harmonic oscillator in resonance with the particle motion.

3 Evidence from the energy-flux profile of cosmic rays

This model produced an entirely new result, which is the proposal of a parent vacuum/environment energy state at 3.71 GeV. Flux profiles of cosmic ray (CR) protons display important features [6] that seem related to the existence of a "correlation" energy that keeps the loops dressing of protons, corresponding to the difference between 3.71 GeV and the proton's rest energy of 0.94 GeV.

It is worthwhile to examine some available experimental data, well gathered in [6]. Fig. 3 shows the energy flux profile of protons as detected from interstellar outer space by a space probe. The symmetry of this figure clearly gives an average energy per proton of about 2.7 GeV. Tsallis and collaborators [7] carried out the integration of a related set of data to obtain an averaged energy of about 2.88 GeV, with the comment "Any connection of this value with other cosmological or astrophysical quantities is of course very welcome". Statistical mechanics has several famous similar cases. For instance, in the Maxwell kinetic theory of velocities distribution in a gas, the average energy of a molecule matches the energy provided by the environment under equilibrium conditions, which is measured in terms of the absolute temperature as $3/2\,kT$. According to the theory in [2], in the case of the proton, equilibrium is reached against a vacuum at 3.7 GeV, which is 2.7 GeV higher in energy than the proton's rest energy, corresponding to a local temperature of about 10^{13} K. Therefore, the CR protons, similar to the classical gas case, display an averaged energy consistent with an equilibrium reached against the environment, at the predicted level at 3.7 GeV energy. It must be stressed that such equilibrium does not follow the classical formalism of Maxwell-Gibbs statistics, and requires relativistic effects to be included [7, 8].

4 About the size of the proton

The structure of fully developed protons is known to be formed by (the entanglement of) at least three major quark constituents, each of them with $1/3$ of the proton rest mass (see topological considerations in [4, 5]), with charges of opposite signs. This is a very important detail, since the same external electric fields that accelerate the proton as a whole will stretch this structure with a similar force. Therefore, the proton can be regarded as a stressed/strained ensemble of charged objects strongly connected (entangled) together, and thus its elastic response behavior should be considered. Excited by external forces, a three-dimensional elastic structure will vibrate at its natural frequencies. The proton might be represented by a three-dimensional quantum harmonic oscillator. Following the considerations at the end of Section 2, we shall take 2.7 GeV as the ground state energy of an isolated oscillator [9]. This is the share of the 3.7 GeV that lays beyond the rest-energy. Extremely energetic quasiparticles from the original "vacuum" reservoir at 3.7 GeV would dress the proton fields leading to stabilization of the structure in the form of oscillators, in an energy state lower than the original "vacuum", establishing in this case the rest energy of a proton (in a way probably similar to how low-energy lattice phonons promote electron correlations and make the Cooper pairs stable in the superconductor ground state, which is lower in energy than the Fermi level by a small gap). This stable dressed-proton structure behaves like a vibrating system. The model developed in [2] and Section 2 actually deals with the fields of this correlations calculation. We now treat the elastic response of the particle in equilibrium with those fields.

The natural frequency of three-dimensional oscillations ω is given as: $3/2\,\hbar\omega = 2.7\,\text{GeV}$. One obtains $\omega = 2.7 \times 10^{24}$ rad/s, an extremely high figure, within the gamma-ray range of photons in the EM spectrum. What makes such oscillations regime stable?

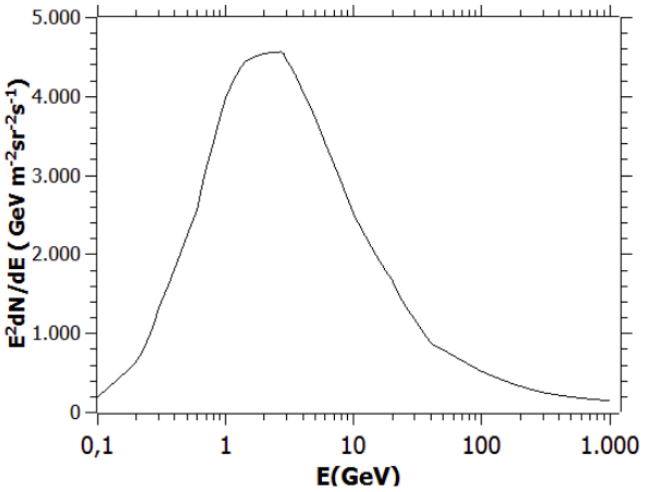

Fig. 3: Interstellar energy-flux profile of protons in CR, which peak at, and have an average energy of 2.7 GeV kinetic energy [3].

The diameter of a proton determined by scattering experiments is $\approx 1.8\,\text{fm}$. This should be taken as the maximum spacing between constituents in a "relaxed" proton structure, but such spacing is deformed by oscillations. Criteria have been developed to evaluate whether the deformation of interatomic spacing in a substance might provoke a change of state. A range of deformation between 5 and 10% of the relaxed "inter-constituent" spacing is usually recognized as within a typical limit for a structure to remain stable. The

maximum possible oscillating displacement is

$$x_m = (2/3\ E/(m\omega^2))^{1/2}\,,$$

where E is 2.7 GeV. We obtain $x_m = 0.16$ fm, which is obtained independently of the knowledge of the proton size. In view of the stability criteria mentioned earlier, this would independently establish a proton size of at least 3 fm at 3.7 GeV conditions. When cooling took place, the structure shrunk to the measured 1.8 fm. One might even conjecture that the observed size of the proton cannot be smaller since smaller particles with same constituents simply break apart as soon as formed due to inelastic strains.

5 Conclusions

It is then possible to summarize all the results in this work: The observed size of the proton, 1.8 fm would be a consequence of its origins in an environment at about 3.7 GeV. According to the model, the particle condenses due to the provision of a 2.7 GeV correlation energy from fields confinement in the form of loops, as calculated by the Regularization procedure. These confined fields play the role of quasiparticles ("vacuum-dynamics" quasiparticles), which provide strongly-binding correlations, which join constituents like in a harmonic oscillator, promoting a stable structure. There is a clear potential association between these energetic quasiparticles and what is called gluons. The magnitude of 2.7 GeV is in a proportion consistent with the ratio of 15 to 1/137, to EM coupling energies, which is the accepted relation between Strong and EM interactions in the range of tenths of a femtometer.

Acknowledgements

The author wishes to thank Dr. Indranu Suhendro for his interest in this Research.

Received on November 29, 2021

References

1. Schilling O. F. A unified phenomenological description for the magnetodynamic origin of mass. *Annales de la Fondation Louis de Broglie*, 2018, v. 43 (1), 1.
2. Schilling O. F. Generation of baryons from EM instabilities of the vacuum. *Progress in Physics*, 2019, v. 15 (3), 185.
3. Barut A. O. Stable particles as building blocks of matter. *Surveys in High Energy Phys.*, 1980, v. 1 (2), 117.
4. Bostick W. H. Mass, charge and current: the essence and morphology. *Physics Essays*, 1991, v. 4 (1), 45.
5. Jehle H. Flux quantization and fractional charges of quarks. *Phys. Rev.*, 1975, v. D11, 2147.
6. Gaisser T. K., Engel R., and Resconi E. Cosmic rays and particle physics. Cambridge University Press, Cambridge, 2016.
7. Tsallis C., Anjos J. C., and Borges E. P. Fluxes of cosmic rays: a delicately balanced stationary state. *Phys. Lett. A*, 2003, v. 310, 372.
8. Kaniadakis G. Statistical mechanics in the context of special relativity. *Phys. Rev.*, 2002, v. E66, 056125.
9. Lapidus I. R. Quantized relativistic motion. *Am. J. Phys.*, 1981, v. 49, 849.

On the Quantification of Relativistic Trajectories

Jean-Pascal Laedermann

Route du Jorat 20, 1052 Le Mont-sur-Lausanne, Switzerland. E-mail: jp.laedermann@laedus.org

Solving the geodesic equation on a relativistic manifold is possible numerically step by step. This process can be transposed into a quantisation. We study here the effect of this quantisation on the Schwarzschild spacetime, more precisely in the Kruskal-Szekeres map.

1 From digitization to quantification

The geodesics are obtained using the Euler-Lagrange variational method, with the Lagrangian $L = g_{\mu\nu}x'^{\mu}x'^{\nu}$ which leads to the well-known equation [1, 8.26]

$$x''^{\alpha} + \Gamma^{\alpha}_{\mu\nu}x'^{\mu}x'^{\nu} = 0\,.$$

The goal is to obtain the extremal solutions for

$$\tau = \int_{\lambda_0}^{\lambda_1} \sqrt{L}\, d\lambda$$

which happens to be the proper time for a test particle subjected to the field g. Except for the mass of the particle, which is in fact an energy, this proper time is an action.

Finding solutions digitally is extremely simple. Given a digitisation step $\delta\lambda$ and an initial state (x, x') of the mobile, the position x is incremented by $x'\delta\lambda$. The geodesic equation gives $x'' = -\Gamma^{\alpha}_{\mu\nu}x'^{\mu}x'^{\nu}$ and the velocity x' is incremented by $x''\delta\lambda$. The process is then iterated.

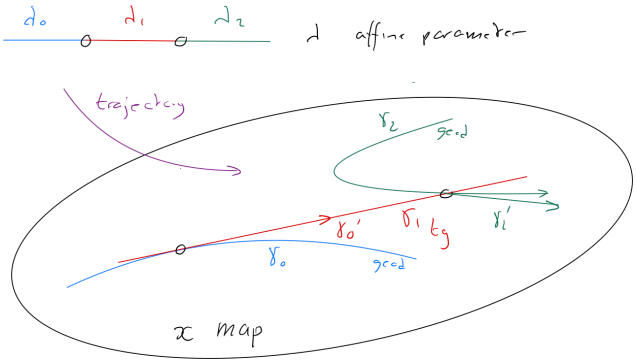

Fig. 1: A test-particle moves from a geodesic $\gamma_0(\lambda_0)$ to a geodesic $\gamma_2(\lambda_2)$ by a trajectory element $\gamma_1(\lambda_1)$ on an interval $\delta\lambda$. This is a straight line in the tangent space. We use the fact that the tangent spaces $T_x\mathbb{R}^n$ are in fact canonically included in $\mathbb{R}^n$.

The choice of the affine step will be made here by keeping the time step constant $\eth\tau$ which gives

$$\delta\lambda = \eth\tau/\sqrt{L}\,.$$

This time step can be physically equated with the quantum of action in the following interpretation.

At each step, the mobile requests a quantum according to the chosen coordinate system x. It uses this quantum to continue its trajectory in its local context, which is the tangent space to the space-time manifold at the current point. Then the new state is considered as such in global space-time. An observer placed on the particle moves during the quantum of time according to a trajectory linearised by the choice of its map.

Some remarkable facts emerge.

First, the coordinate system selected by the observer is essential. The linearisation of the trajectory during $\eth\tau$ depends on the map x and makes the interaction between space-time and the observer contextual. There is an effect of the observation on the trajectory.

Second, it cannot be excluded that the quantisation step involves speeds higher than those of light. This phenomenon can be related to certain quantum effects, such as the possibility for a particle to tunnel through a potential barrier, or to violate the conservation of energy law for a time short enough to be allowed by Heisenberg's uncertainty relations.

Third, in the particular case of the Schwarzschild model with a radius r_S it becomes possible to be in the forbidden zone beyond the naked singularity described below.

2 Reminder on Schwarzschild, Kruskal and Szekeres

Karl Schwarzschild was one of the first to find a solution to the gravitational equations of Einstein's general relativity in 1916. This solution, which describes the field created by a point mass, is expressed by the following metric in polar coordinates, with a speed of light $c = 1$ and a Schwarzschild radius r_S:

$$d\tau^2 = \left(1 - \frac{r_S}{r}\right) dt^2 - \left(1 - \frac{r_S}{r}\right)^{-1} dr^2 - r^2\left(d\theta^2 + \sin^2\theta d\varphi^2\right)\,.$$

Two peculiar radiuses were observed immediately. The first one, $r = r_S$, gives the horizon beyond which a particle cannot escape, giving the name of a black hole to this zone. The second one, $r = 0$, is a singularity of the metric, known as naked, where any particle entering the black hole ends its trajectory in a finite time.

The Kruskal-Szekeres coordinate transformation leads to a formulation in terms of the variables (T, X, θ, ϕ) [2]:

$$d\tau^2 = \frac{4r_s^3}{r}\,\exp\left(-\frac{r}{r_S}\right)\left(dT^2 - dX^2\right) - r^2\left(d\theta^2 + \sin^2\theta\, d\varphi^2\right)\,.$$

The parameter $r = r_S\left(\mathcal{W}_0\left(\frac{1}{e}\left(X^2 - T^2\right)\right) + 1\right)$ is given by the branch 0 of the Lambert function $\mathcal{W}$.

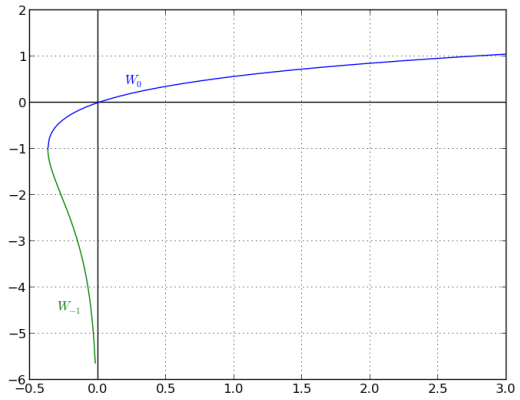

Fig. 2: Real branches of the Lambert function.

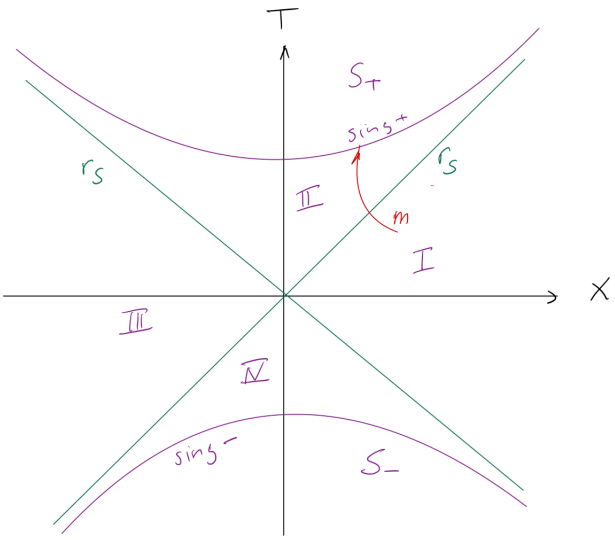

Fig. 3: Kruskal-Szekeres map.

The diagram in Fig. 3 shows the following regions:

I space-time outside the black hole
II black hole
III other component of space-time
IV white hole
S+ inside of the naked singularity
S– other component inside the naked singularity.

This map shows that the Schwarzschild horizon is not a physical singularity, but only an artefact due to the choice of the map.

The diagonal lines represent the Schwarzschild horizon, and the two boundary branches of the **sing+** and **sing–** hyperbola the entrance and exit of the naked singularity.

A particle from region **II** ends its trajectory on **sing+**, without being able to exit. Conversely, a particle in region **IV** cannot do anything else, but exit; hence the name of the white hole. One also finds the expressions *sink* and *source* for these two regions.

S– and **S+** are inaccessible, or forbidden, because they are outside the map domain. These two regions and their boundaries are associated with a single point, the zero of the polar coordinates, and can be considered as collapsed. At least in the hypothesis of a strictly continuous world.

3 Appearance of tachyons

Traditionally, the term *tachyon* has been applied to a hypothetical particle with a speed greater than the speed of light. The exit of the speed of the future light cone is identified by the fact that $L < 0$ and thus an imaginary quantisation step. Here, we propose using a complex proper time:

$$\tau = \tau_r + i\tau_i \in \mathbb{C}\,.$$

This time is measured by two clocks, one real and the other imaginary. The increase in the affine parameter becomes $\delta\lambda = \eth\tau_r/\sqrt{L}$ if $L > 0$ or $\delta\lambda = i\eth\tau_i/\sqrt{-L}$ if $L < 0$. In this way, the trajectory remains real in the map x. For a tachyon, it is the imaginary clock that works, the other one remains fixed, and the opposite is true for a standard particle.

For any coordinate system on space-time, the notions of time and space are found locally by placing an orthonormal basis in the tangent space which diagonalizes the metric. Afterwards, thanks to a possible permutation of the axes and a calibration of the units, we can obtain the diagonal metric of Minkowski Diag$(1,-1,-1,-1)$. The zero coordinate is then time and the others define the space. The base obtained in this manner is generally referred to as a *tetrad*.

The proper speed $\dot{x} = \frac{\delta\lambda}{\eth\tau}x'$ is transformed into a quad-speed $u = \gamma\begin{pmatrix}1\\ \boldsymbol{v}\end{pmatrix}$ where $\boldsymbol{v}$ is the space velocity of the mobile. Let v be its Euclidean norm and $\boldsymbol{n}_G$ be the unit vector $\boldsymbol{v}/v$, the so-called *slip* vector. We easily obtain $\gamma = (1-v^2)^{-1/2}$.

If $v < 1$, it is possible to put the mobile at rest with a Lorentz boost $\Lambda(\boldsymbol{v})$ such as

$$\Lambda(\boldsymbol{v})\,\boldsymbol{u} = \begin{pmatrix}1\\ 0\end{pmatrix}.$$

If $v > 1$, γ becomes purely imaginary. Nevertheless, it is possible to extend this boost by

$$\Lambda(\boldsymbol{v}) = \Lambda\left(\frac{\boldsymbol{n}_G}{v}\right) R\left(\boldsymbol{n}_G, \frac{\pi}{2}\right)$$

where $R(\boldsymbol{n},\theta)$ is the rotation of angle θ and axis $\boldsymbol{n}$. It can be seen that $\Lambda(\boldsymbol{v})\,\boldsymbol{u} = \begin{pmatrix}0\\ i\boldsymbol{n}_G\end{pmatrix}$. The "putting at rest" with this extended boost makes a particle appear in the direction $\boldsymbol{n}_G$ with a proper time marked by its imaginary clock. As $1/v <$

1, this transformation is physically feasible for an external observer, and the tachyon could be visible. One can notice that the factor i in front of $\boldsymbol{n}_G$ is consistent, as it implies a quadrivector of Minkowskian norm one.

4 Transition from black hole to white hole

The appearance of a state in a zone forbidden by the singularity poses a more delicate problem. Indeed, the Christoffel coefficients involve the parameter

$$r = r_s\left(\mathcal{W}_0\left(\frac{1}{e}\left(X^2 - T^2\right)\right) + 1\right).$$

This critical zone is defined by $X^2 - T^2 < -1$ which is outside the domain of $\mathcal{W}_0$.

The solution proposed here is to use the other part of this function on the real line, namely

$$r = r_s\left(\mathcal{W}_{-1}\left(\frac{1}{e}\left(X^2 - T^2\right)^{-1}\right) + 1\right)$$

by reversing the term $X^2 - T^2$ which enters the domain of W_{-1}. The trajectory is then continued by changing the signs of T and X, which moves the mobile from the black hole to the white hole. This idea is supported by the hyperbolic character of the Kruskal map.

5 Cost of quantification

The evolution of the trajectory during the time quantum is no longer geodesic, and therefore requires some work. The force that appears during this displacement is given by

$$f^\alpha = x''^\alpha + \Gamma^\alpha_{\mu\nu} x'^\mu x'^\nu$$

and its work on the affine segment $\delta\lambda$ is given by

$$\delta W = \int_{\lambda_0}^{\lambda_1} g_{\mu\nu} f^\mu x'^\nu d\lambda\,.$$

A quick calculation shows that

$$\delta W = \frac{1}{2}\delta\lambda\, x'^\mu x'^\nu x'^\rho \int_0^1 \frac{\partial g_{\mu\nu}}{\partial x^\rho}\left(x + x'\xi\delta\lambda\right) d\xi$$

$$= \delta\lambda\, x'^\mu x'^\nu x'^\rho \int_0^1 \Gamma_{\rho\mu\nu}\left(x + x'\xi\delta\lambda\right) d\xi\,.$$

This expression makes it possible to estimate the energy needed to quantify the movement.

6 Refutability of the model

Given a time quantum, one can ask which mass M_0 corresponds to a quantum of action equal to Planck's constant. Thus, $M_0 c^2 \delta\tau = \hbar$.

Clearly, the finer the digitisation, the closer the trajectories to the unquantized geodesics, thus deferring the quantum effects mentioned above.

The smaller the quantum, the later the effect, the longer the calculation time. The calculations carried out here allowed us to aim for a time quantum of approximately 10^{-13} s which corresponds to a mass of $10^{-2}\,\mathrm{eV/c^2}$. For example, reaching the mass of the neutrino, which is currently estimated at $1.1\,\mathrm{eV/c^2}$, would require a temporal resolution two orders of magnitude lower, resulting in calculation times that are approximately 100 times longer. As the calculations performed here require several days, it is not impossible to think that an optimisation could be achieved up to the level of actually observable particles.

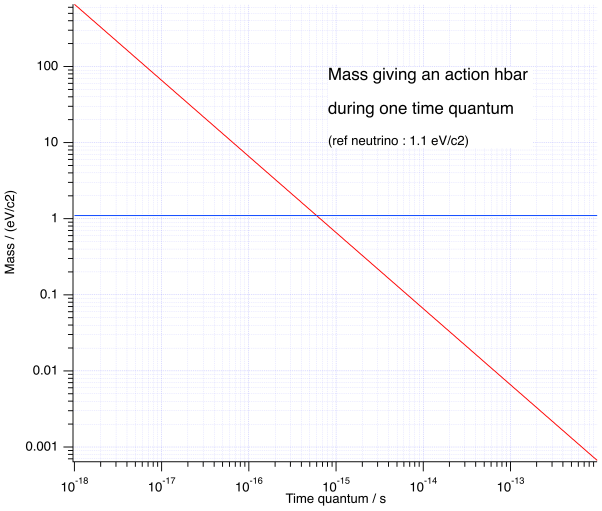

Fig. 4: Mass–time quantum relationship.

7 Two typical trajectories

In general, the trajectories end either with the limiting velocity 1 or at the singularity. Tachyons are short-lived, and return to standard space-time with a final velocity of 1. Two examples are given in Fig. 5 and Fig. 6.

8 Calculation tools

The digital tracking of trajectories requires over several million steps. The standard precision of the current computers (double precision) is 53 bits, which is totally insufficient. The MPFR library [4] implements the calculation with an arbitrary precision, which is only limited by the machine's memory. An interface written by P. Holoborodko [3] then allows the use of the Eigen vector calculation library [6]. The very complete study of F. Johansson [5] on the Lambert function finally makes it possible to carry out the calculation of trajectories, which becomes stable with a precision of 4096 bits (approximately 1200 decimal places).

The exploration of the various trajectories is programmed in C++ and uses a 128-processors machine running in the *Gnu-Linux Ubuntu 20.4* environment.

The trajectories presented here generally require several days of parallel CPU.

9 Analogy with quantum measurement

As we have seen, some of the effects emerging in a time quantum $\eth\tau$ of a relativistic motion are due to the presence of the observer. In summary, the motion naturally follows a geodesic; then during the time of observation, it follows a tangent, and it resumes its natural trajectory, but on another, neighbouring geodesic.

This sequence is similar to the Copenhagen version of quantum measurement, in which two types of evolution coexist in a quantum system. The first, known as unitary (U-type), is governed by the Schrödinger or Dirac equation. The second, which appears when the system is measured, is called wave packet reduction (type R), and consists of projecting the wave function onto an eigenspace associated with the observable to be measured.

Let $\hat{A}$ be the self-adjoint operator translating an observable. To measure A according to Geneva's school [8], the observer asks a series of questions whose answers are *yes* or *no*. A question about A is for example: "Will the value of A appear in a certain interval Δ of the real line?".

Let $\mathrm{Sp}\,\hat{A}$ be the spectrum of the operator $\hat{A}$. This question is represented by the projection operator $J_\Delta = \sum_{a\in\Delta\cap\mathrm{Sp}\hat{A}} J^A_a$ where J^A_a is the projector onto the eigenspace of eigenvalue a. The result of the measurement, i.e. the answer to the question, will be *yes* with probability $p_1 = \langle\psi|J_\Delta|\psi\rangle$ and the system will then be in the state $|1\rangle = J_\Delta\psi \,/\, \|J_\Delta\psi\|$. The answer *no* is treated in the same way, but with the projector $J_{\complement\Delta}$ and gives the final state $|0\rangle$.

One can imagine that the measurement lasts for a time interval $\eth\tau$ and, after the response has been randomly chosen, the wave function evolves "linearly" towards its final state.

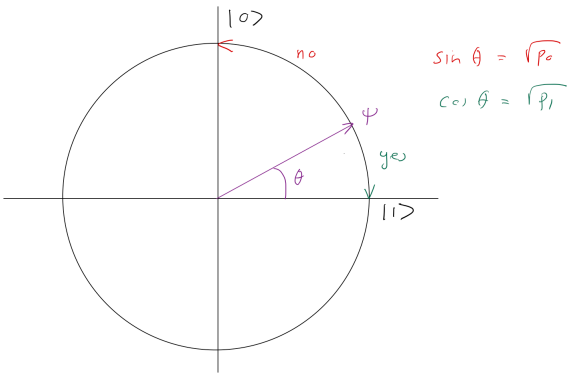

Fig. 7: Evolution of the quantum probability amplitude in R mode.

For example, the path in Fig. 7

$$t \mapsto \psi_t = \cos\left(\theta\left(1-\frac{t}{\eth\tau}\right)\right)|1\rangle + \sin\left(\theta\left(1-\frac{t}{\eth\tau}\right)\right)|0\rangle$$

where $\cos\theta = \sqrt{p_1}$, moves in a uniform and unitary manner from ψ to $|1\rangle$ in case of a *yes* answer.

For the Schrödinger equation, this evolution is governed in the $(|1\rangle, |0\rangle)$ basis by the Hamiltonian operator

$$\hat{H}_1 = \frac{\theta\hbar}{\eth\tau}\,\sigma_2 \quad \theta = \arccos\sqrt{p_1}$$

where σ_2 is the second Pauli matrix. It can be seen that $\langle\hat{H}_1\rangle = 0$, and that we have

$$\psi_t = \exp\frac{\theta t}{i\eth\tau}\sigma_2\psi = \exp\frac{\theta t}{\eth\tau}(|1\rangle\langle 0| - |0\rangle\langle 1|)\psi\,.$$

Initially, the wave function follows a trajectory U given by a Hamiltonian $\hat{H}$. During the measurement, the reduction R is replaced by a trajectory U with a Hamiltonian proportional to σ_2. It then resumes the trajectory U given by $\hat{H}$.

10 From the quantum to the infinitesimal

The infinitesimals of Leibnitz and Newton were only recently given a consistent axiomatic basis. They have been used systematically by mathematicians such as Euler, Lagrange or Wallis with success and without rigorous justification. Physicists use these devices without further ado on a daily basis. The axiomatization of continuity by d'Alembert, Cauchy and Weierstrass almost sounded the death knell of these quantities, as small as one likes, but nonzero.

Nevertheless, they have made a surprising reappearance through topos, equipped with their not necessarily Boolean logic. For smooth infinitesimal analysis, for example, they are defined by the subset of the line $\Delta = \{\varepsilon\,|\,\varepsilon^2 = 0\}$ which is no longer reduced to $\{0\}$. One then speaks of nilpotent real numbers. This has the effect of eliminating all powers greater than or equal to 2 in the Taylor developments on this set. In other words, any function becomes linear on Δ or: Δ is a representation of the tangent space in zero which is included in the real line.

The above analysis performs this integration with the idea that the time quantum could ideally be understood from the nilpotents.

The quantum effects in the vicinity of singularities are reminiscent of John Lane Bell's formula:

Vale *ict*, ave $i\varepsilon$!* [7]

as an extension of the discussion of the introduction of imaginary time by Minkowski [1, Box 2.1 p. 51].

Received on February 1, 2022

References

1. Misner W., Thorne S., Wheeler J.-A. Gravitation. Princeton University Press, 2017.
2. Müller T. Catalogue of Spacetimes, 2.2.5. arXiv: gr-qc/0904.4184v3.

*Goodbye *ict*, welcome $i\varepsilon$!

3. Holoborodko P. MPFR C++. http://www.holoborodko.com/pavel/mpfr/.
4. Gnu MPFR library. https://www.mpfr.org/.
5. Johansson F. Computing the Lambert W function in arbitrary-precision complex interval arithmetic. arXiv: cs.MS/1705.03266.
6. Eigen library. https://gitlab.com/libeigen/eigen.
7. Bell J. L. A Primer of Infinitesimal Analysis, 2nd Edition. Cambridge University Press, 2008, p. 80.
8. Piron C. Quantum Mechanics. Presses polytechniques et universitaires romandes, 1998.

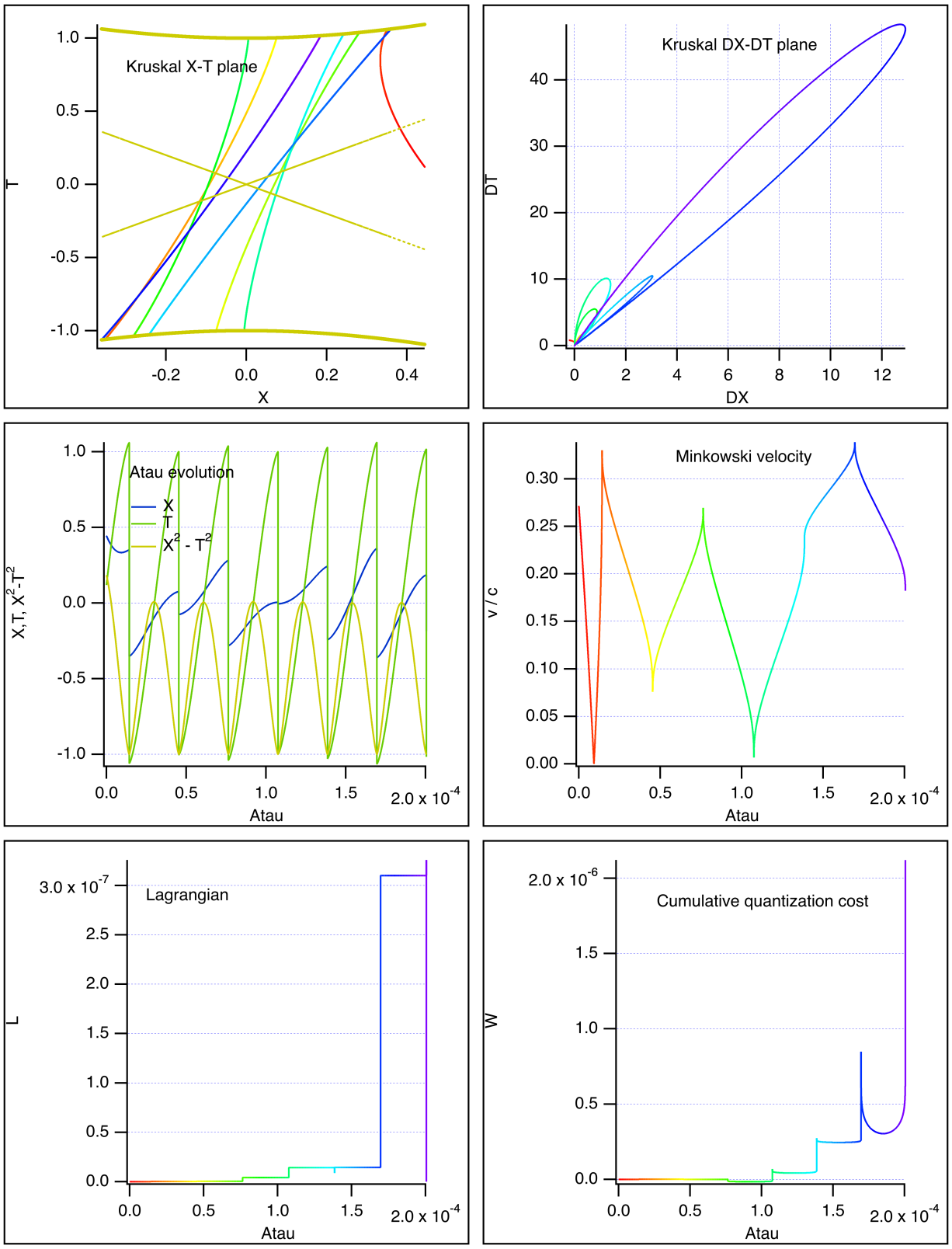

Fig. 5: Trajectory evolving towards the singularity. The variable Atau is simply the addition of the two real and imaginary clocks. The imaginary time is identified by a negative Lagrangian. The start of the trajectory is in red and its end in dark blue. The passages through the singularity are located at the points where $X^2 - T^2 < -1$.

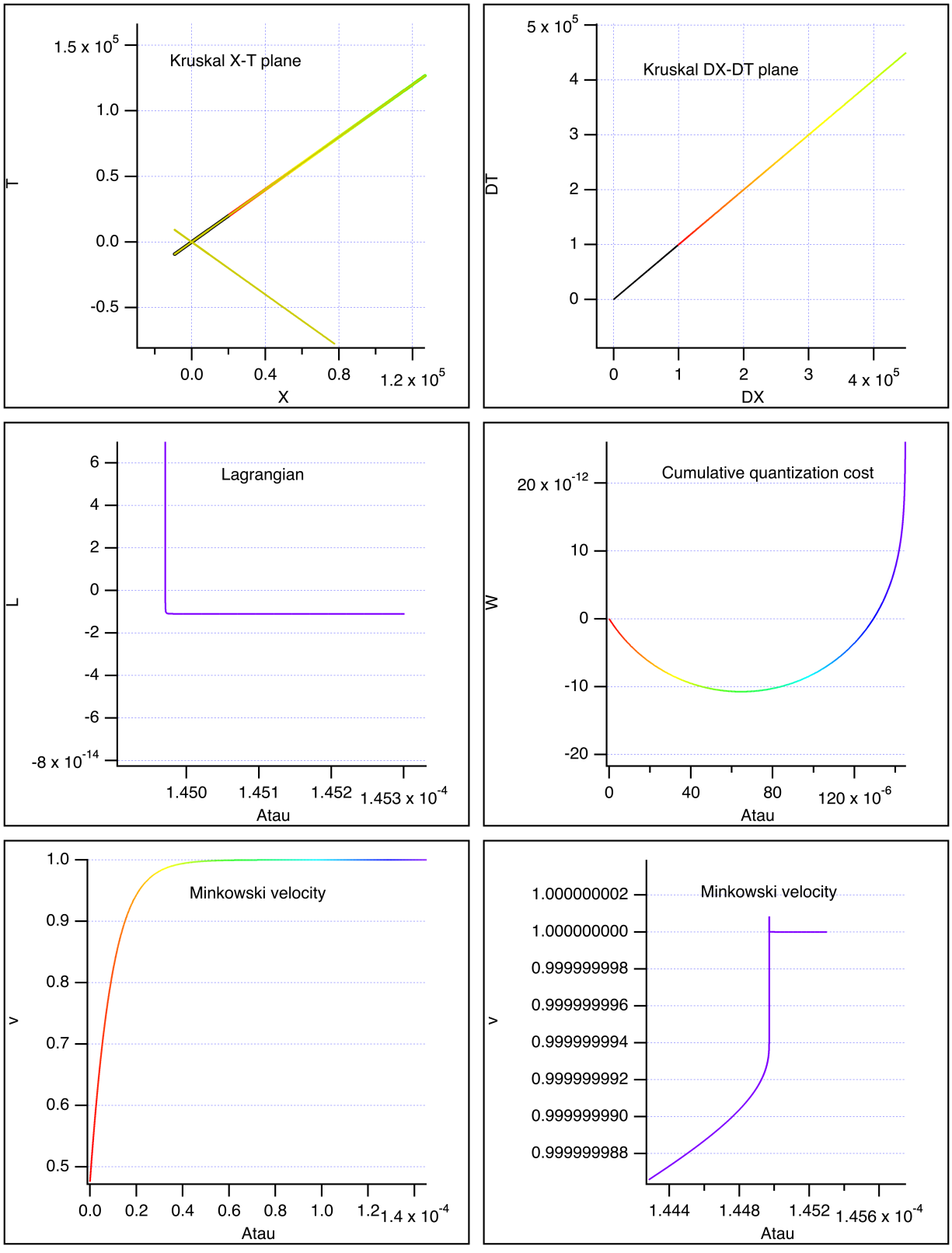

Fig. 6: Trajectory leading to a tachyon, before ending on the singularity. The colouring of the top two graphs is given by the imaginary clock from the black part. The calculation was redone by increasing the precision from 4096 to 8192 bits, with no significant difference.

Combinatorics and Frequency Distributions as the Determining Factors of Electron and Nuclear Spectra

Anatoly V. Belyakov

Tver, Russia. E-mail: belyakov.lih@gmail.com

It has been established that electronic and nuclear spectra can be calculated and formed using combinatorics and frequency distributions (FD) provided that electrons, nucleons and other elementary particles in the composition of an atom are represented as unit structureless elements. The examples given show a good match between the calculated spectra and the experimental ones. The program for calculating spectrograms has been compiled.

1 Introduction

Electronic and nuclear spectra are characterized by a set of emission (absorption) spectral frequency lines arising from the excitation of atoms or by the energy spectrum of split off nucleons in the nuclear decay process. In electronic spectra the spectral lines position for hydrogen and for hydrogen-like atoms is determined by the Balmer-Rydberg formula for the radiation wavelength

$$\lambda_e = \frac{n^2 m^2}{m^2 - n^2} \frac{1}{R_\infty Z^2}, \qquad (1)$$

where n and m are the quantum numbers or orbit numbers, R_∞ is the Rydberg constant, Z is the element atomic number.

For other spectral transitions in multielectron atoms the Rydberg formula gives incorrect results, since the internal electrons screening varies, and for external electrons transitions it is not possible to make a similar correction in the formula to compensate for the nuclear charge weakening, as described above. Therefore, in the general case, to find the position of spectral lines, the Ritz combination principle [1], which has become the basis of modern spectroscopy, is used. Its validity has been confirmed by numerous experimental data. But it is not clear what regularities underlie it, what processes exactly exist, and how the atom internal structure is rearranged in order to cause the waves emission with a frequency corresponding to any spectral line.

Nuclear spectra arise when a nucleus is exposed to hard radiation or high-energy electrons. The nucleons split off in this case have the energy of tens of MeV and form the giant dipole resonance (GDR) [2]. The giant resonance is inherent in all nuclei, it has been studied since 1947 and it manifests itself so brightly and universally that, perhaps, not a single nuclear "event" can compare with it. The giant resonance nature is believed to lie in the nucleus dipole oscillations (displacement of all nucleus protons relative to all its neutrons) under the action of long-wavelength γ-radiation. When irradiated with electrons having an energy of more than 200 MeV, along with dipole vibrations, other types of vibrations can also be excited in the nucleus. These vibrations are of a collective nature and form giant multipole resonances (GMRs) [3]. The photonucleons energy spectra are not described by smooth curves, and when studying the cross sections for the (γ, n) reactions, maxima of the first and subsequent orders are found, forming the GDR structure of three types: rough (gross), intermediate, and fine.

There are several GDR theories, the most detailed being the multiparticle shell model [4]. Its development proceeds through a unified description of various collective motions (rotations, surface oscillations, nucleus dipole oscillations), as well as interactions between them. At present, theories are not yet able to give a good quantitative description of the width and fine structure of the giant resonance and the entire spectrum of nucleons separated during the nuclei decay, since there are large computational difficulties and a lack of reliable information about a number of important parameters of the theory.

2 Initial conditions

In this article, as in previous works, in accordance with the mechanistic interpretation of J. Wheeler's idea, charged particles are considered to be the singular points on the three-dimensional surface of our world (conditionally this is the X-region), connected by vortex tubes (current lines of force) through an additional dimension (conditionally this is the Y-region), which is responsible for the electromagnetic forces and the "hidden" mass of the microparticles [5, 6].

If, as is commonly believed, the microparticles are oscillators, then the atom itself can be considered as a collective oscillator, which consists of the "oscillator-electrons" (X-region) and the "oscillators-protons" (Y-region), and these oscillators are elastically connected to each other by the vortex current tubes. At that, according to [7], the electrons located at the more distant orbits are associated with the protons located at the deeper nucleus levels; thus the layers or envelopes are formed in the nucleus that similarly to the electronic shells.

The multielectron atoms protons number's increasing in proportion to the atomic number Z increases the bonds inflexibility, as if "stretching" the vortex tubes, which reduces the oscillators-electrons wavelength in the X-region in accor-

dance with the formula (1). At the same time, the protons mass's increasing reduces the system as a whole inflexibility, therefore in the same proportion increases the oscillator-protons wavelength in the Y-region.

For multielectronic atoms, the numbers m and n lose their meaning of the electron shell number, and n must be taken equal to Z, since in the limit, when $m \to \infty$ and $n = Z$, in accordance with (1), $\lambda \to 1/R_\infty$, and the atom becomes hydrogen-like one. For the radii smaller than $1/R_\infty$, i.e. when there is "sinking" into the Y-region, quantum numbers formally become inverses of n and m, and the formula (1) for oscillator-protons takes the form

$$\lambda_p = \frac{1}{m^2 - n^2} \frac{Z^2}{R_\infty} . \qquad (2)$$

The dependence of wavelengths on Z^2 is understandable, since, unlike a simple one-dimensional oscillator, where the oscillation period depends on its inflexibility and on its mass to the power of 1/2, the atom (taking into account the additional degree of freedom in Y) is a four-dimensional oscillator and $(Z^{1/2})^4 = Z^2$.

3 Formation of the electronic spectra

The spectra revealed in physical experiments is obvious to be as a joint result of the electronic and proton oscillators oscillations superposition; it is clear that in this case, as a result of interference, both damping and amplification of certain frequencies of the spectrum occur. Therefore, to obtain the spectrum, it is necessary to calculate all possible wavelengths of oscillators-electrons according to (1), as well as all possible wavelengths of oscillators-protons according to (2) for all combinations of n and m, and multiply the results logically.

For this purpose, a calculation program has been drawn up (see Appendix). The essence of the program is as follows: to divide a certain spectrum region into intervals, to calculate the *frequency distributions* (FD) of all functions values according to (1) and (2) in the spectrum selected region, write them into the corresponding arrays and multiply these arrays. The type of the spectra obtained by this program depends on the number of values λ_i falling into the i-th interval (i.e., on the parameter q value in the program) and can have the histogram form of different detail (q-large) or the line spectra form (q-small) [8]. Moreover, the type of histograms can reflect some additional spectrum parameters, since the histogram peaks height is proportional to the probability (intensity) of the corresponding spectral parameter along the Y-ordinate.

Fig. 1 shows the experimental spectrum of the holmium liquid filter (240–650 nm) which is a solution of holmium dissolved in perchloric acid for checking the wavelength accuracy [9], and Fig. 2 shows the calculated histogram for $_{67}$Ho. Here and below, the intervals for substituting variables a and b in the calculation program are indicated.

Fig. 3 shows part of the $_{80}$Hg spectrum as a line spectrum. Above it, the spectral lines experimental values are shown

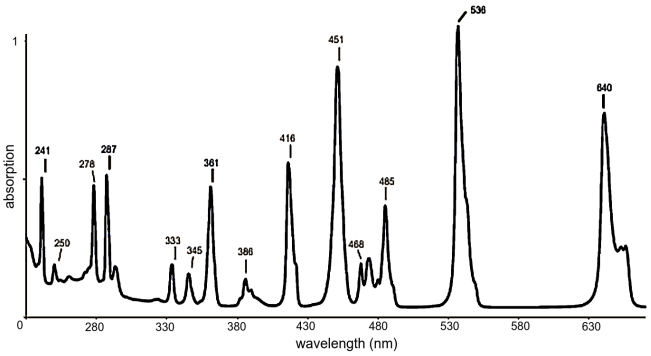

Fig. 1: Typical spectrum of holmium liquid filter (240–650 nm) [9] consists of a solution of holmium dissolved in perchloric acid.

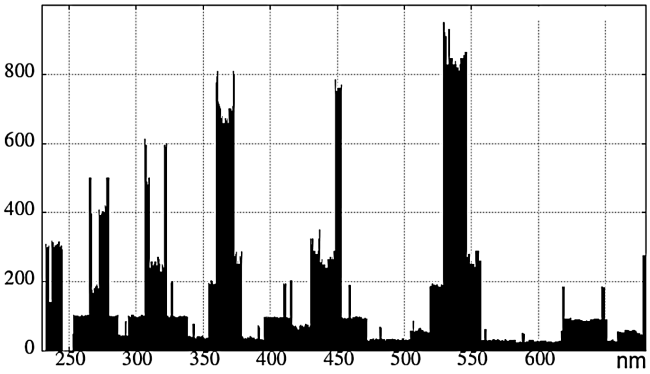

Fig. 2: Calculated spectrum for $_{67}$Ho: $q = 0.026$, $\lambda_t(a,b) = 57$–67, $\lambda_p(a,b) = 1$–67.

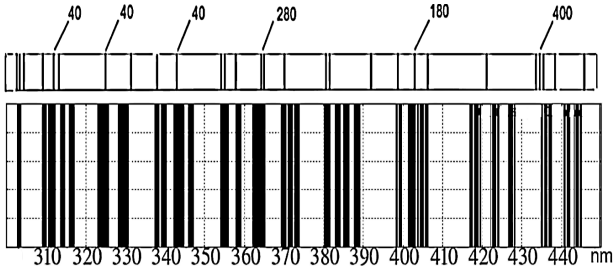

Fig. 3: Calculated spectrum for $_{80}$Hg: $q = 0.0021$, $\lambda_e(a,b) = 50$–80, $\lambda_p(a,b) = 1$–80.

and the brightness values of some of them are given. Note, when changing the interval of substitution of variables the histograms shape changes; in the case of a line spectrum it affects the spectral lines intensity, the presence or absence of some lines, but their position in the spectrum does not change.

Obviously, the constructed spectra are in good agreement with the experimental ones. Of course, one cannot expect the calculated spectra to match exactly with the experimental ones, since the latter are influenced by various factors: the methods of excitation of atoms, the degree of their ionization, the presence of forbidden transitions, the medium which the element is locate in, etc.

Nevertheless, in a number of cases, for some sets of variables, even the external shape of the calculated non-line spectra (the histograms shape) is very similar to the real non-line spectra (see Figs. 1 and 2), which, apparently, corresponds to certain physical conditions. Thus, limiting the function λ_e to variables within 57–67 means that when calculating the spectrum only the electrons in the outer shells of $_{67}$Ho (10 units) are taken into account. Indeed, it is known the inner shells electrons do not take part in the formation of the visible spectrum range for atoms having high numbers Z. For the $_{80}$Hg spectrum 30 electrons are taken into account. This turned out to be sufficient to form the spectrum. With a full set of variables, the short-wavelength spectrum part is enhanced and, in general, the spectrum detail is enhanced.

4 Formation of the nuclear spectra

The region of the giant dipole resonance extends within the energy range of tens of MeV, and its shape and structure are extremely diverse. When the nucleus is exposed to gamma radiation or high-energy electrons, there is both protons and neutrons's splitting off. Thus, the nucleus as an oscillator should contain the maximum number of unit elements (oscillators-nucleons) equal to its mass number A. On the other hand, by analogy with oscillators-electrons, one can imagine that there are oscillators-pions or other mesons, which, as expected, exist in the proton close environment in the form of a virtual meson "coat" [10].

So, to build a nuclear spectrum one should use the same formulas (1) and (2), replacing the element number Z with the mass number A, but at the same time, as it were, "going deeper" along the Y-axis, that is, moving to smaller sizes and higher energies. The transition coefficient, as it turned out, is equal to a^3 — the fine structure constant in the cube $(1/137)^3$. Thus, for the nuclear resonance wavelengths, denoting them λ_π and λ_n, we have

$$\lambda_\pi = \frac{a^3 n^2 m^2}{m^2 - n^2} \frac{1}{A^2 R_\infty}, \tag{3}$$

$$\lambda_n = a^3 \frac{1}{m^2 - n^2} \frac{A^2}{R_\infty}. \tag{4}$$

These formulas, passing to the frequencies and further to the energies in MeV, are written as

$$E_\pi = \frac{m^2 - n^2}{n^2 m^2} \frac{A^2 R_\infty c h}{a^3 k}, \tag{5}$$

$$E_n = \left(m^2 - n^2\right) \frac{R_\infty c h}{a^3 k A^2}, \tag{6}$$

where c is the light speed, h is the Planck's constant, k is the conversion factor 1.602×10^{-13} [J/MeV]. Calculating the constants, we get

$$E_\pi = 35.02\, A^2 \frac{m^2 - n^2}{n^2 m^2}, \tag{7}$$

$$E_n = 35.02 \frac{m^2 - n^2}{A^2}. \tag{8}$$

The general view of the giant resonance for light and heavy nuclei, obtained from the calculation in accordance with (7) and (8), is shown in Fig. 4, which generally agrees with the experimental results. Indeed, in the experiments with irradiation of the nuclei with low mass numbers, even at low resolution, maxima are found in the giant resonance, in contrast to the heavy nuclei, where numerous weak peaks are detected only at high resolution.

The giant resonance has been established to be formed in the heavy nuclei with the participation of nucleons from the two outermost nuclear shells, while the main nucleon core lying under the outer shells is not affected at all by the photo disintegration process. At that, with an increase in the mass number A, the neutron fraction knocked out of the nucleus increases, while the proton fraction decreases, reaching only about 1% in a nucleus with $A \approx 200$ [11].

Therefore, if one takes into account only those nucleons (neutrons) that are not included in clusters and therefore easily splitting off from the nucleus (for Pb^{207}, as indicated in [7], there are 65 units), then when forming a spectrogram for Pb^{207}, one should limit the variables range for E_n within 142–207. In this case, the maximum of the spectrogram shifts to the range of 11–12 MeV and it takes the form close to the Poisson distribution; this is generally match to the experimental data. As in the case of the electronic spectrum, this is, as it were, the formal restriction on the range of variables, coincides with the physical meaning of the phenomenon, otherwise the GDR peak would be shifted towards higher energies.

Fig. 5 shows the experimental cross sections for reactions $Al^{27}(p, \gamma_0)Si^{28}$ according to [12], and Fig. 6 shows the calcu-

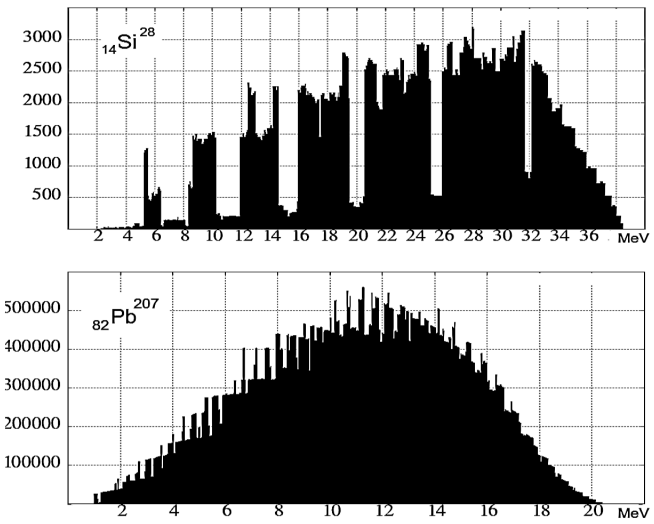

Fig. 4: General view of the GDR for light and heavy nuclei : $q = 0.1$, $A = 28$: $E_\pi, E_n(a, b) = 1$–28, $A = 207$: $E_\pi(a, b) = 1$–207, $E_n(a, b) = 142$–207.

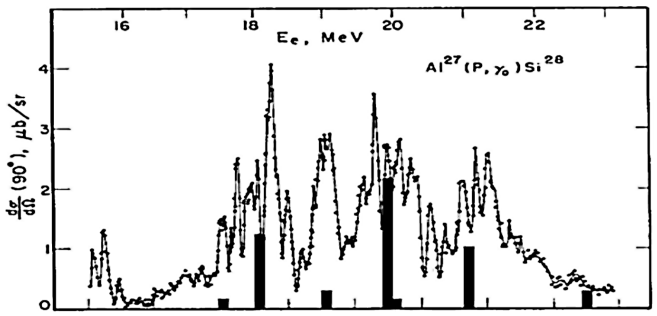

Fig. 5: Reaction cross sections Al^{27} (p, γ_0) Si^{28} [12] and data of theoretical calculations photodisintegration within the multiparticle shell model.

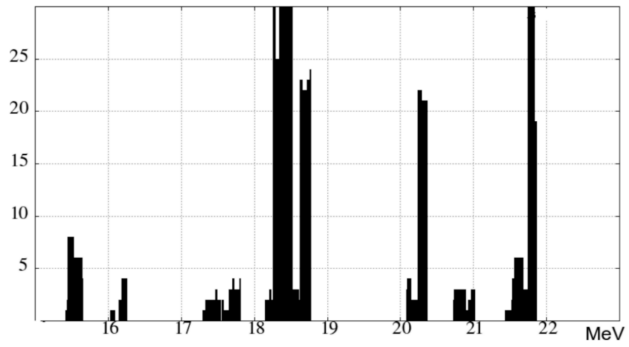

Fig. 6: Calculated spectrum for Al^{27} Si^{28}: $A = 27.5$, $q = 0.007$, $E_\pi, E_n(a, b) = 1$–27.

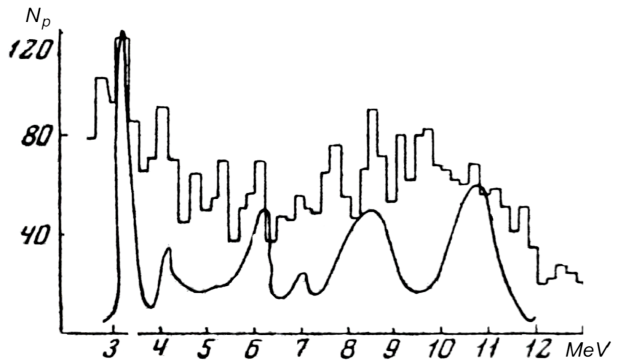

Fig. 7: Spectrum of photoprotons from Ca^{40} upon irradiation with the bremsstrahlung spectrum of γ-quanta with $E_{\gamma max} = 25$ MeV and calculated spectrum in the shell model (smooth curve).

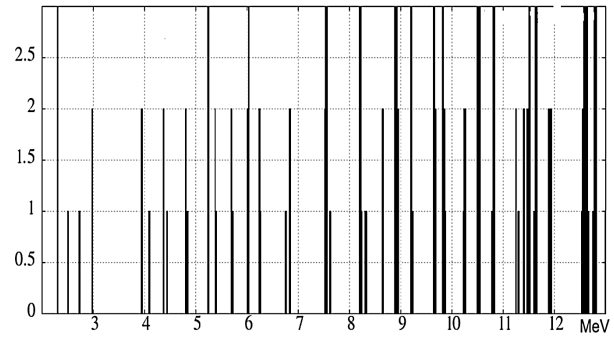

Fig. 8: Calculated spectrum for Ca^{40}: $q = 0.003$, $E_\pi, E_n(a, b) = 1$–40.

lated spectrogram in the histogram form. Obviously, the main peaks of the reaction cross section (p, γ_0) coincide with those in the calculated spectrogram. At the same time, a large number of narrow peaks with a width of 50–100 keV are observed in the reaction cross section against the intermediate structure background (resonances with a width of 0.4–1.0 MeV). The existing theory does not explain the nature of these peaks. But in the calculated spectrograms they are revealed as the parameter q decreases. These coincidences point to the manifestation of combinatorics, to the fact that any maximum is not the result of any particular resonance, but the superposition of many single events.

Fig. 7 shows the experimental spectrum for Ca^{40} [13], and Fig. 8 shows the calculated spectrogram. It also demonstrates good agreement with the experimental data both in terms of the peaks number and the peaks positions for Ca^{40}.

In the process of the studying the atomic nuclei structure by the method of scattering of electrons with energies up to 225 MeV new giant multipole resonances (GMR) were discovered. These resonances go beyond the GDR, which arise during photodisintegration. They have a much more complex structure than that obtained from photonuclear experiments and theoretical predictions. To explain them, quadrupole, octupole, and other types of oscillations was assumed can be excited in the nucleus.

The parameters of the giant resonance in Fe^{56} E_{res}, MeV are given in [3, p. 142] (the plus or minus errors in absolute value are shown in parentheses):

9.5 (0.1)	10.1 (0.1)	10.3 (0.3)	11.3 (0.5)
11.9 (0.9)	13.0 (0.3)	13.0 (0.9)	13.1 (0.1)
14.6 (0.3)	15.0 (0.4)	15.6 (1.2)	16.0 (0.2)
16.1 (0.5)	16.3 (0.1)	16.9 (0.1)	17.3 (0.1)
17.9 (0.2)	18.2 (0.1)	18.3 (0.1)	19.0 (0.5)
19.8 (0.3)	23.9 (0.3)		

On Fig. 9 the calculated spectrogram for Fe^{56} is shown. It can be seen that almost all of the above energy values, within the limits of errors, coincide with the peaks of the first (most) and second orders in the calculated spectrogram.

On Fig. 10 a part of the spectrogram for Fe^{54} in the line spectrum form is shown. Here is a good agreement with experimental data [3, p. 149] too:

Of course, as in the case of electronic spectra, the calculated nuclear spectrograms cannot completely coincide with the real ones, because in addition, there is an incomplete agreement between the data of different experiments. The

9.7 (0.1)	12.4 (0.5)	12.6 (0.4)	13.4 (0.2)	13.8 (0.2)
15.0 (0.9)	15.0 (1.3)	17.5 (0.2)	17.9 (0.2)	19.2 (0.1)
20.2 (0.1)	20.3 (0.1)	23.9 (0.3)	25.4 (0.4)	

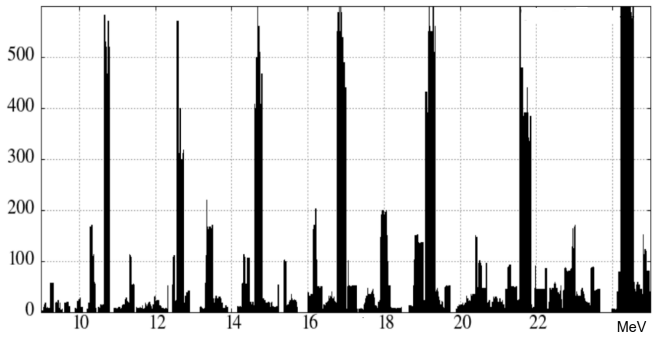

Fig. 9: Calculated spectrum for Fe^{56}: $q = 0.005$, $E_\pi, E_n(a, b) = 1$–56.

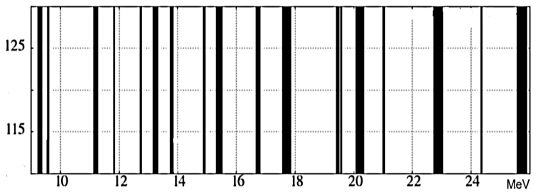

Fig. 10: Calculated spectrum for Fe^{54}: $q = 0.007$, $E_\pi, E_n(a, b) = 1$–54.

instrumental functions of the experiments have very complex shapes, so that the determined cross sections differ in all the main parameters (shape, size, and energy position). It should also be noted that in the above method for calculating spectrograms, the mass number A is the sum of neutrons and protons, and the spectrograms do not differ for nuclei with the same A. The accuracy of the calculated spectra can be improved by introducing additional restrictions or additions to the set of variables.

Nevertheless, the obtained results show this method of analysis can be used as an addition to the instrumental spectrography methods, since it makes it possible to quickly, almost instantly find the statistically most probable form of electronic and nuclear spectra.

5 Conclusions and generalization

The main conclusion from the foregoing is not so much the fact of the emergence of a new analytical method, but that it is possible to obtain results close to reality by considering the complex structure of electronic and nuclear shells as a set of structureless single uniform elements. This contradicts the quantum provisions, according to which elementary particles differ in a set of quantum numbers. On the other hand, each element acquires individuality, since it (and all of them at the same time) moves in the space of variables $n_i - m_i$, and any movement of any element is accompanied by the release of an individual portion of energy E_i, which, being mutually superimposed, eventually form the spectrum. But this again contradicts the quantum principle, this time it contradicts the principle of indistinguishability of identical particles.

Applying a FD to an array of values of the functions E_π and E_n, i.e. to just a set of numbers, gives physically reliable results, but this fact should not be surprising. So in the work of S. E. Shnoll [13], when processing the FD of the experimental data array of the various physical processes, obtained initially in the normal distributions form, these distributions was found are discrete and depend on the algorithms that determine these processes.

The fact that simple formulas for the i-th wavelength or the energy value give results, otherwise obtained through the laborious experiments and complex calculations, leads to the question — do dipole and other resonances affect the nuclear spectra and do they exist in the nucleus at all? Is it really necessary to calculate the nuclear spectra consider nuclei and their components to be the sources of oscillations, or is a set of statistical methods sufficient? This question can only be answered by further wide application of the method described both to the electronic and nuclear spectra and to other physical phenomena in those cases, where it is possible to apply the FD to the functions describing these phenomena.

But now, summing up the above, we can conclude:

— the electronic spectra are reproduced at a deeper level of matter in the nuclear spectra form,

— the type of spectrograms is mainly determined by combinatorics and the frequency distributions of elementary particles, considered as structureless unit elements in the range of their atomic numbers or their mass numbers.

Appendix

A C++ program is written to calculate the wavelength in nanometers. When calculating nuclear spectra, the atomic number Z is replaced by the mass number A, and M is a dimensional coefficient.

```
#include <iomanip>
#include <stdlib.h>
#include <algorithm>
#include <stdio.h>

using namespace std;
struct preobr: binary_function <double, double, double> {
double operator()(double x, double y) const {return x*y;} };

float R, M;
float f1(float x, float y, float z) { return M*(x*x*y*y)
/(y*y – x*x)/z/z/R ;};
float f2(float x, float y, float z) { return M*z*z/(y*y – x*x)/R ;};

FILE *fp = fopen("uuu", "w");

int main() {
```

```
int n=1000000; float*m1 = new float[n]; float*my1 = new float[n];
float*my2 = new float[n]; float*my12 = new float[n];

for (int c=0; c<n; c++) m1[c]=my1[c]=my2[c]=my12[c]= 0;

float z=80, xn=300, xm=500, q=0.002, t=0, c=0; int j=0;
R=1.0974e+7, M=1e+9;
// xn and xm — range limits

for(t=xn; t<xm; t=t+0.001*t) {
j++, m1[j] = t;
// dividing the range into segments
// proportional to its current value

for(int a=1; a<=80; a++) {
for(int b=1; b<=80; b++) {

if(b>a) c = f1(a,b,z);

if(fabs(m1[j] – c) < fabs(q*c)) my1[j]++ ;
// recording the number of values in intervals for f1
}
}
for(int a=1; a<=80; a++) {
for(int b=1; b<=80; b++) {

if(b>a) c = f2(a,b,z);

if(fabs(m1[j] – c) < fabs(q*c)) my2[j]++ ;
// recording the number of values in intervals for f2
}
}
}
transform(my1, my1+j, my2, my12, preobr());

for(int i=0; i<j; i++) {
if(m1[i]!=0)

fprintf(fp, "%20f %20f\n", m1[i], my12[i]);
// writing results to the file "uuu"

std::cout << m1[i] <<" "<< my12[i] << std::endl;
// outputting results to the terminal

}
}
```

Submitted on February 18, 2022

References

1. Ritz W. On a new law of series spectra. *Astroph. Journal*, 1908, October, v. XXVIII, issue 3, 237–243.
2. Bergere R. Features of the Giant E1 Resonance. In: Lecture Notes in Physics, v. 61. Photonuclear Reactions I, Springer-Verlag, Berlin-Heidelberg-New York, 1977.
3. Aizatski N. I., Afanasiev S. N., Buki A.Yu., et al. A Study of Atomic Nuclei Using the Electrons and Photons at Energies Upto 300 MeV. Kharkov, Kharkov Physical Technical Inst. Publ., 2017.
4. Elliot J. P., Flowers B. H. *Proc. Roy. Soc.*, 1957, v. A242, 57.
5. Belyakov A. V. Charge of the electron, and the constants of radiation according to J. Wheeler's geometrodynamic model. *Progress in Physics*, 2010, v. 6, issue 4, 90–94.
6. Belyakov A. V. Macro-analogies and gravitation in the micro-world: further elaboration of J. Wheeler's model of geometrodynamics. *Progress in Physics*, 2012, v. 8, issue 2, 47–57.
7. Belyakov A. V. Nuclear power and the structure of a nucleus according to J. Wheeler's geometrodynamic concept. *Progress in Physics*, 2015, v. 11, issue 1, 89–98.
8. Belyakov A. V. Finding the fine structure of the solutions of complicate logical probabilistic problems. *Progress in Physics*, 2010, v. 6, issue 4, 36–39.
9. https://www.hellma.com/ja/laborbedarf/zertifizierte-referenzmaterialien/messung-der-wellenlaengengenauigkeit/didymium-fluessigfilter
10. Belyakov A. V. The substantive model of the proton according to J. Wheeler's geometrodynamic concept. *Progress in Physics*, 2021, v. 17, issue 1, 15–19.
11. http://nuclphys.sinp.msu.ru/enc/e042.htm
12. Singh P. P., Segel R. E., Meyer-Schützmeister L., Hanna S. S., Allas R. G. *Nucl. Phys.*, 1965, v. 65, 577.
13. Diener E. M., Amann J. F., Paul P. *Phys. Rev.*, 1973, v. C7, 695.
14. Shnoll S. E. Cosmic physical factors in random processes. Svenska fysikarkivet, Stockholm, 2009, 388 pages.

Apparent Unsettled Value of the Recently Measured Muon Magnetic Moment

Ruggero Maria Santilli

The Institute for Basic Research, 35246 U. S. 19N, Suite 215, Palm Harbor, FL 34684, USA.
E-mail: research@i-b-r.org

In this paper, we point out that the anomalous value of the muon magnetic moment recently measured at FERMILAB appears to be unsettled due to the experimentally unresolved behavior of the mean life of muons with speed caused by non-local internal effects as well as the irreversibility of the muon decay.

1 Introduction

In the preceding paper [1], we outlined:

1) Historical and recent verifications of the Einstein-Podolsky-Rosen argument that *"Quantum mechanics is not a complete theory"* (EPR argument) [2];

2) Mathematical, theoretical and experimental foundations of the completion of quantum mechanics into *hadronic mechanics* (hm) for the representation of the extended, thus deformable, and hyperdense hadrons which representation is achieved via the symmetries and physical laws of the completed invariant

$$\hat{x}^{\hat{2}} = \frac{x_1^2}{n_1^2} + \frac{x_2^2}{n_2^2} + \frac{x_3^2}{n_3^2} - t^2 \frac{c^2}{n_4^2}, \tag{1}$$

where $n_k^2 > 0,\ k = 1, 2, 3$ represents the dimension and shape of hadrons normalized to the values $n_k^2 = 1$ for the perfect sphere, and $n_4^2 > 0$ represents the density of hadrons normalized to the value $n_4^2 = 1$ for the vacuum;

3) The representation of *all* characteristics of the muons, including the recently measured difference between the experimental value of the *muon* g-factor, g_μ^{EXP}, and its prediction via quantum electrodynamics, g_μ^{QED},

$$\begin{aligned} & g_\mu^{EXP} - g_\mu^{QED} = \\ & = 2.00233184122 - 2.00233183620 \\ & = 0.00000000502 > 0\,, \end{aligned} \tag{2}$$

which representation is achieved via the hadronic structure model of the muons

$$\mu^\pm = (e^-_\downarrow, e^\pm_\uparrow, e^+_\downarrow)_{hm}\,, \tag{3}$$

with physical constituents produced free in the spontaneous decay with the lowest mode, $\mu^\pm \ \to \ e^- + e^\pm + e^+, \%10^{-12}$, while the presence of an electron-positron pair in the muon structure, which is confirmed by the additional spontaneous decay $\mu^\pm \to e^\pm + 2\gamma, \%10^{-11}$, allows the understanding of the instability of the muons as well as a numeric representation if its mean life. In particular, thanks to the use of hadronic mechanics, [1] has achieved the following numeric values of the n-characteristic quantities of the muons

$$n_1^2 = n_2^2 \approx 0.4926,\ \ n_3^2 \approx 0.0149, \quad n_4^2 \approx 0.0149, \tag{4}$$

with the following EPR completion of the muon g-factor

$$\hat{g}_\mu^{EXP} = \frac{n_4}{n_3} g_\mu^{QED}, \quad \frac{n_4}{n_3} = 1.00000000502. \tag{5}$$

In this paper, we use the preceding results to indicate that, despite the accuracy of measurements [6], the anomalous magnetic moment of the muons appears to remain unsettled due to deviations from the relativistic behavior of mean lives of unstable hadrons with speed that are predicted by internal non-local effects, the time irreversibility of spontaneous decays, and other aspects.

2 Apparent unsettled aspects in the muon magnetic moment

To implement due scientific process on anomalous values (2), we should recall P. A. M. Dirac's [7] and other authoritative doubts on the final character of the numeric values obtained from quantum electrodynamics due to the divergence of Feynman's and other series (see [8] for a recent account on QED divergences).

Additionally, measurements [6] have been done via the assumption that the mean life of muons behaves with speed according to the time dilation law of special relativity

$$t = t_o \sqrt{1 - \frac{v^2}{c^2}}\,. \tag{6}$$

The exact validity of the above law for electrons and other *point-like* particles in vacuum can be considered, nowadays, to be beyond scientific doubt.

However, at this writing there exist unresolved aspects in regard to the experimental behavior of law (6) for the behavior of the mean life with speed (or, equivalently, with energy) of *unstable, thus composite particles.*

In 1965, D. I. Blokhintsev [9] pointed out the expected inapplicability (rather than the violation) of special relativity for the interior of hadrons due to non-local effects in their hyperdense structure and suggested that deviations due to internal effects could be measured in the outside via deviations from time dilation law (6).

In 1983, R. M. Santilli [10, 11] (see also notes [12] from lectures delivered in 1991 by Santilli at the ICTP, Trieste, Italy, and Section 8 of the recent update [4]) showed that the

axioms of special relativity remain valid for time reversible processes of extended particles with invariant (1) when realized via the use of isomathematics with axiom-preserving EPR completion of law (6)

$$t = t_o \sqrt{1 - \frac{v^2/n_3^2}{c^2/n_4^2}}\,. \tag{7}$$

Additionally, Santilli [13, 14] pointed the inapplicability (rather than the violation) of special relativity and relativistic quantum mechanics for time irreversible processes such as the spontaneous decays, due to the known reversibility of said theories. Its origin was identified in the invariance of Lie's theory under anti-Hermiticity, by therefore suggesting the completion of Lie and Lie-isotopic methods into the broader Lie-admissible methods [16, 17] (see [3] for detailed treatments and [4] for a recent update).

These studies triggered a number of generalizations of time dilation law (6), such as those by L. B. Redei [18], D. Y. Kim [19] and others.

In 1989, A. K. Aringazin [20] proved that all preceding generalizations of law (6) are particular cases of the isotopic law (7) because they can be obtained via different expansions of the latter law in terms of different parameters and with different truncation, thus restricting the experiments to the test of law (7).

In 1983, S. H. Aronson *et al* [21] reported the outcome of experiments conducted at FERMILAB showing apparent *deviations* from law (6) for the $K^0 - \bar{K}^0$ system in the energy range from 0 to 100 GeV.

In 1987, N. Grossman *et al* [22] reported counter-experiments also conducted at FERMILAB showing an apparent *confirmation* of law (6), but in the *different energy range* from 100 to 250 GeV.

In 1992, F. Cardone *et al* [23] indicated that counter-measurements [22] from 100 to 350 GeV leave basically unresolved the deviations of law (6) from 0 to 100 GeV [21], and that the isotopic law (7) provides an exact fit for both measurements [21, 22] (Fig. 1).

Finally, in 1998, Yu. Arestov *et al* [24] pointed out apparent flaws in the theoretical elaboration of the experimental data of measurements [22].

3 Concluding remarks

The above results appear to confirm the lack of exact character of time evolution law (6) for the behavior of the mean life of unstable particles with speed. In fact, under the assumption in first approximation that the muon spontaneous decay is time-reversible, isotopic time dilation law (7) with values (5) predicts the *increase* of anomalous value (2)

$$t = t_o \sqrt{1 - 1.00000000502\,\frac{v^2}{c^2}}\,, \tag{8}$$

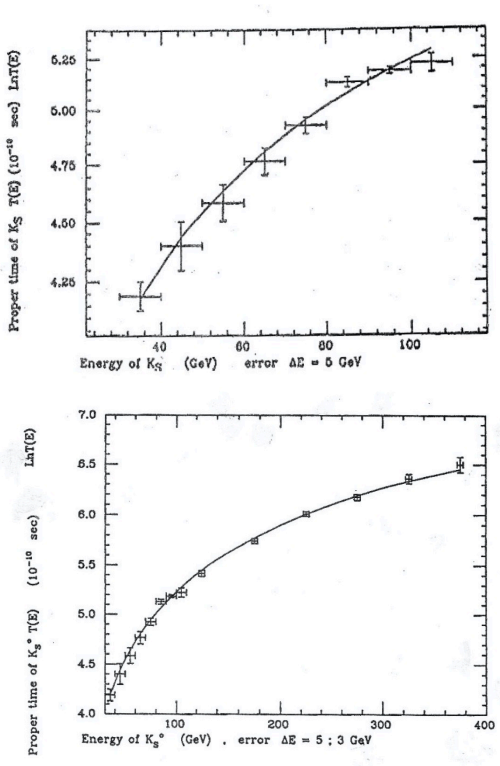

Fig. 1: In this figure, we reproduce the exact fits of isotopic time dilation law (7) obtained by F. Cardone et al [23] of: 1) Deviations [21] from the time dilation law (6) for the behavior of the $K^0 - \bar{K}^0$-system from 0 to 100 GeV (top view); 2) The exact fit of both deviations 0 to 100 GeV [21] and apparent verification in the range from 100 to 350 GeV [22] (bottom view).

with the expectation of bigger deviations for a full time irreversible treatment.

In conclusion, it seems plausible to expect that, in the event deviations [21] from time dilation (6) are confirmed, experimental value (2) of the muon magnetic moment should be correspondently revised.

4 Acknowledgments

The author would like to express sincere thanks for penetrating critical comments received from the participants of the *2020 International Teleconference on the EPR argument.* Additional thanks are due to various colleagues for technical controls and to Mrs. Sherri Stone for linguistic control of the manuscript.

Received on February 16, 2022

References

1. Santilli R. M. Representation of the anomalous magnetic moment of the muons via the Einstein-Podolsky-Rosen completion of quantum into hadronic mechanics. *Progress in Physics*, 2021, v. 17, 210–215.

2. Einstein A., Podolsky B., and Rosen N. Can quantum-mechanical description of physical reality be considered complete? *Phys. Rev.*, 1935, v. 47, 777. www.eprdebates.org/docs/epr-argument.pdf.
3. Santilli R. M. Elements of Hadronic Mechanics. Volumes I, II, III. Ukraine Academy of Sciences, Kiev, 1995 (I), 1995 (II), 2016 (III). www.i-b-r.org/Elements-Hadronic-Mechanics.htm.
4. Santilli R. M. Overview of historical and recent verifications of the Einstein- Podolsky-Rosen argument and their applications to physics, chemistry and biology. APAV - Accademia Piceno Aprutina dei Velati, Pescara, Italy, 2021. www.santilli-foundation.org/epr-overview-2021.pdf.
5. Dunning-Davies J. A Present Day Perspective on Einstein-Podolsky-Rosen and its Consequences. *Journal of Modern Physics*, 2021, v. 12, 887–936.
6. Miller J. P., de Rafael E. and Roberts B. L. Muon (g-2): experiment and theory. *Rep. Prog. Phys.*, 2007, v. 70, 795–881.
7. Dirac P. A. M. The evolution of the physical picture of nature. *Scientific American*, 1963, v. 208, 45–53.
8. Consa C. Something is wrong in the state of QED. arXiv: gem-ph/2110.02078.
9. Blokhintsev D. I. The Philosophy of Quantum Mechanics. JINR (in Russian), 1965. Springer (in English), 1968.
10. Santilli R. M. Lie-isotopic Lifting of Special Relativity for Extended Deformable Particles. *Lettere Nuovo Cimento*, 1983, v. 37, 545–551. www.santilli-foundation.org/docs/Santilli-50.pdf.
11. Santilli R. M. Isotopic Generalizations of Galilei and Einstein Relativities, Vols. I and II. International Academic Press, 1991. www.santilli-foundation.org/docs/Santilli-01.pdf and Santilli-61.pdf.
12. Aringazin A. K., Jannussis A., Lopez F., Nishioka M. and Vel-janosky B. Santilli's Lie-Isotopic Generalization of Galilei and Einstein Relativities. Kostakaris Publishers, Athens, Greece, 1991. www.santilli-foundation.org/docs/Santilli-108.pdf.
13. Santilli R. M. Embedding of Lie-algebras into Lie-admissible algebras. *Nuovo Cimento*, 1967, v. 51, 570. www.santilli-foundation.org/docs/Santilli-54.pdf.
14. Santilli R. M. Lie-admissible invariant representation of irreversibility for matter and antimatter at the classical and operator levels. *Nuovo Cimento B*, 2006, v, 121, 443. www.santilli-foundation.org/docs//Lie-admiss-NCB-I.pdf.
15. Santilli R. M. On a possible Lie-admissible covering of Galilei's relativity in Newtonian mechanics for nonconservative and Galilei form-non-invariant systems. *Hadronic J.*, 1978, v. 1, 223–423. www.santilli-foundation.org/docs/Santilli-58.pdf.
16. Santilli R. M. Lie-Admissible Approach to the Hadronic Structure, Vols. I and II. International Academic Press, 1978 (I) and 1982 (II). www.santilli-foundation.org/docs/Santilli-71.pdf and Santilli-72.pdf.
17. Bhadra Man T., Ed. Proceedings of the third international conference on the Lie-admissible treatment of non-potential interactions, Vols. I and II. Kathmandu University, Nepal, February 2011. www.santilli-foundation.org/docs/2011-nepal-conference-vol-1.pdf and 2011-nepal-conference-vol-2.pdf.
18. Redei L. B. Possible Experimental Test of the Existence of a Universal Length. *Phys. Rev.*, 1966, v. 145, 999–1012.
19. Kim D. Y. The light scalar meson and the anomalous magnetic moment. *Hadronic J.*, 1979, v. 2, 1110–1121.
20. Aringazin A. K. Lie-isotopic Finslerian lifting of the Lorentz group and Blokhintsev-Redei-like behavior of the meson lifetime and of the parameters of the $K^0 - \bar{K}^0$-system. *Hadronic J.*, 1989, v. 12, 71–74.
21. Aronson S. H., Bock G. J., Cheng J. Y., and Fischbach E. Energy dependence of the fundamental parameters of the $K^0 - \bar{K}^0$ system. *Phys. Rev. D*, 1983, v. 28, 495–503.
22. Grossman *et al* Measurement of the lifetime of $K^0 - \bar{K}^0$ mesons in the momentum range 100 to 350 GeV/c. *Phys. Rev. Lett.*, 1987, v. 59, 18–26.
23. Cardone F., Mignani R. and Santilli R. M. On a possible energy-dependence of the K^0 lifetime, I and II. *J. Phys. G: Part. Phys.*, 1992, v. 18, L61–L65 and L141–L144.
24. Arestov Yu., Santilli R. M. and Solovianov V. Experimental evidence on the isominkowskian character of the hadronic structure. *Foundation of Physics Letters*,1998, v. 11, 483–492. www.santilli-foundation.org/docs/Santilli-52.pdf.

Are Tensorial Affinities Possible?

G. G. Nyambuya

National University of Science and Technology, Faculty of Applied Sciences – Department of Applied Physics,
Fundamental Theoretical and Astrophysics Group, P. O. Box 939, Ascot, Bulawayo, Republic of Zimbabwe.
E-mail: physicist.ggn@gmail.com

This short paper is an extraction from our previous work [1], the purpose of which is to make clear that it is very much possible to use Weyl's idea [2] of a conformal metric to achieve tensorial affinities. We are of the strong view that this is very important as it is predominantly assumed that this is not possible. We want to dispel this myth once and for all.

Nature is pleased with simplicity.

Sir Isaac Newton (1642-1727)

1 Introduction

The purpose of this article is to present in a much simpler and succinct form, the ideas presented in our first installation [1] on an attempt to bring the gravitational force and the other forces of Nature (the Electromagnetic, Weak and the Strong Nuclear force) into unity with all the other forces and, as well, unity of all the forces with Quantum Mechanics. For clarity's sake, we have herein removed most of the intricate mathematical and philosophical details found in [1]. We hope this abridged version will make clear to our readers what it is we have done in paper [1].

Further, the purpose and motivation of the present paper has been propelled by one of our favourite Weylian blogger and American physicist – Dr. William O. Straub. He posted on his blog-site* on 28 February 2022 an interesting article entitled: *I'm Still Rooting for the Underdog*. In his article, Dr. Straub expresses his justified frustration on the lack of progress in the search for darkmatter and wonders if it is not time for physicists to abandon this idea/concept and seriously consider much more seriously already existing alternative theories to darkmatter – e.g. Milgrom's *Modified Newtonian Gravity* (MoND) [3–5]. Dr. Straub's frustration is not his alone, it is shared by a plethora of physicists.

To prepare his reader(s) for the conclusion that he seeks, in the introduction of his article, Dr. Straub talks of *perpetual motion machines* and the *luminiferous aether* – i.e. concepts that were once thought to have a direct relation with reality but were eventually found to be worthless/non-physical and were thus abandoned by mainstream science and these ideas are not expected to re-appear anytime soon in mainstream science.

Amongst the many alternative ideas to darkmatter, Dr. Straub considers the subtle flaws in Einstein [6]'s General Theory of Relativity (GTR) and wonders if Weyl's [2] supposed failed unified theory of gravitation and electromagnetism holds any hope as an alternative theory to darkmatter. In the penultimate of his article: of Weyl's [2] theory, Dr. Straub had this to say:

> To me, there is one glaring flaw in Einstein's theory, which is its noninvariance with respect to conformal transformations. Weyl also saw this as a flaw, and he showed us a possible way to fix it.

After reading Dr. Straub's article on the morning of 1 March 2022, I was particularly struck by the first sentence in his statement. I immediately wrote to him saying

> I must say, I hold the same view and like Einstein [7, 8], Schrödinger [9–11], *etc*, I believe this requires that the affinities be tensors. I have worked out a new theory that is just that – I am sure I have sent this to you before.

Rather swiftly, Dr. Straub responded to my email by saying: ... *Turning the connections into true tensors will be a tough job, and I'm inclined to believe it can't be done.* His response challenged me to write a much simpler version of the idea that I used in [1], i.e. the idea of obtaining tensorial affinities. This is what we present below and I hope it is much clearer than it is presented in [1].

2 Riemann geometry

From a viewpoint of geometry, Einstein [6]'s greatest and most beautiful masterpiece, the GTR, has its rock solid foundations anchored in Riemann Geometry† (RG). Fundamental in RG are the affine connections (Christoffel three symbols), namely:

$$\Gamma^{\lambda}_{\mu\nu} = \frac{1}{2} g^{\delta\lambda}\left(g_{\delta\mu,\nu} + g_{\nu\delta,\mu} - g_{\mu\nu,\delta}\right) . \tag{1}$$

Their topological defect, insofar as the GTR is concerned, is that these affine connections are not tensors, as they transform in the following manner:

$$\Gamma^{\lambda'}_{\mu'\nu'} = \frac{\partial x^{\lambda'}}{\partial x^{\lambda}} \frac{\partial x^{\mu}}{\partial x^{\mu'}} \frac{\partial x^{\nu}}{\partial x^{\nu'}} \Gamma^{\lambda}_{\mu\nu} + \frac{\partial x^{\lambda'}}{\partial x^{\lambda}} \frac{\partial^2 x^{\lambda}}{\partial x^{\mu'} \partial x^{\nu'}} . \tag{2}$$

*`http://www.weylmann.com/aftermath.shtml`, visited on 5 Mar. 2022 @ 16h18 GMT+2

†I shall assume that the reader(s) knows very well Riemann geometry together with its symbols as commonly presented in the textbooks. Hence, we will not explain these but assume the reader(s) is/are *in sync* with us.

The first term on the right hand side of (2) has the characteristic transformational properties of a tensor while the second term destroy the *to-be* tensorial character of the affine. If this second term on the right hand side of (2) was not present, the affine would surely be a tensor. These affine connections present a problem when it comes to the geodesic equation of motion, namely:

$$\frac{d^2x^\lambda}{ds^2} - \Gamma^\lambda_{\mu\nu}\frac{dx^\mu}{ds}\frac{dx^\nu}{ds} = 0\,. \tag{3}$$

Because of the nature of the non-tensorial affine connection $\Gamma^\lambda_{\mu\nu}$, this geodesic (3) of motion does not holdfast – in the truest sense – to the depth of the letter and essence of the philosophy deeply espoused and embodied in Einstein's *Principle of Relativity* (PoE) [12], namely that physical laws must require no special set of coordinates where there are to be formulated.

The non-tensorial nature of the affine connections require that the equation of motion must first be formulated in special kind of coordinate systems known as a *geodesic coordinate systems*[*], yet the PoE forbids this. This problem has never been adequately addressed in the GTR. In order to appreciate that this indeed is a real problem, one can for example consider the fact that affinities in the GTR represent forces. A force has no relative sense of existence either by way of a coordinate transformation or a transformation between reference systems – yet, the affine connection speaks to the construction of this seemingly non-physical scenario.

That is to say: if a force exists (i.e. $\Gamma^\lambda_{\mu\nu} \neq 0$) in one coordinate system, it must exist in any arbitrary coordinate system (i.e. $\Gamma^{\lambda'}_{\mu'\nu'} \neq 0$). This surely is not the case if these affinities are to transform as spelt out in (2), because you can have $\Gamma^\lambda_{\mu\nu} = 0$ and $\Gamma^{\lambda'}_{\mu'\nu'} \neq 0$. Against all that is expected from physical and natural reality as we have come to experience it, this literally means a force has a relative sense of existence where it can be made to come into or out of existence by a mere change of the system of coordinates. If anything, coordinates are no more than a convenient way which we use to uniquely label points in space and this should not, in any way imaginable, have any physical effect whatsoever on the resultant physics thereof.

3 Weyl (1918)'s theory

In the first such attempt to bring gravitation and electromagnetism under one mathematical scheme, in which effort one obviously hopes for a unification of these two forces in the resulting theory, Weyl [2] realised that he could forge such a scheme if he were to supplement the metric $\mathrm{g}_{\mu\nu}$ of Riemann geometry with a scalar function ϕ as follows:

$$\bar{\mathrm{g}}_{\mu\nu} = e^{2\phi}\mathrm{g}_{\mu\nu}\,. \tag{4}$$

The resulting affine connections from this modified Riemann metric (4) are:

$$\overline{\Gamma}^\lambda_{\mu\nu} = \Gamma^\lambda_{\mu\nu} + W^\lambda_{\mu\nu}\,, \tag{5}$$

where:

$$W^\lambda_{\mu\nu} = \mathrm{g}^\lambda{}_\mu\partial_\nu\phi + \mathrm{g}^\lambda{}_\nu\partial_\mu\phi - \mathrm{g}_{\mu\nu}\partial^\lambda\phi\,, \tag{6}$$

is the tensorial Weyl connection which results from Weyl's supplemented scalar function ϕ. Insofar as its transformation between coordinates is concerned, this new tensorial affine connection of the modified Riemann geometry (hereafter, *Weyl Geometry* (WG)) is no different from the affine connection of Riemann geometry as it transforms as follows:

$$\overline{\Gamma}^{\lambda'}_{\mu'\nu'} = \frac{\partial x^{\lambda'}}{\partial x^\lambda}\frac{\partial x^\mu}{\partial x^{\mu'}}\frac{\partial x^\nu}{\partial x^{\nu'}}\overline{\Gamma}^\lambda_{\mu\nu} + \frac{\partial x^{\lambda'}}{\partial x^\lambda}\frac{\partial^2 x^\lambda}{\partial x^{\mu'}\partial x^{\nu'}}\,. \tag{7}$$

So, from a viewpoint of topology, WG is the same as RG.

Now, if this Weyl scalar is chosen such that:

$$\phi = \kappa_0\int A_\alpha dx^\alpha, \tag{8}$$

then the tensorial Weyl connection becomes:

$$W^\lambda_{\mu\nu} = \delta^\lambda{}_\mu A_\nu + \delta^\lambda{}_\nu A_\mu - \delta_{\mu\nu}A^\lambda\,, \tag{9}$$

where A_μ, is (here) a (dimensionless) four-vector and the δ's are the usual Kronecker delta functions, and κ_0 is a constant with the dimensions of inverse length and this constant has been introduced for the purposes of dimensional consistency, since we here assume that the four-vector A_μ and the Weyl scalar ϕ are dimensionless physical quantities.

The versatile and agile Weyl [2] was quick to note that this new Christoffel-Weyl affine (5) is invariant under the following rescaling of the metric $\mathrm{g}_{\mu\nu}$ and the four vector A_μ:

$$\left.\begin{array}{rcl} \mathrm{g}_{\mu\nu} & \longmapsto & e^{2\Phi}\mathrm{g}_{\mu\nu} \\ A_\mu & \longmapsto & A_\mu + \kappa_0^{-1}\partial_\mu\Phi \end{array}\right\} \quad \Rightarrow \quad \overline{\Gamma}^\lambda_{\mu\nu} \longmapsto \overline{\Gamma}^\lambda_{\mu\nu}\,, \tag{10}$$

where $\Phi = \Phi(\boldsymbol{r}, t)$ is a well-behaved, arbitrary, smooth, differentiable, integrable and uniform continuous scalar function.

Now, because Maxwell [13]'s electromagnetic theory is invariant under the same gauge transformation which the four-vector A_μ has been subjected to in (10), the great mind of Weyl seized this beautiful golden moment and identified this four-vector A_μ with the electromagnetic four-vector potential. Weyl went on to assume that the resulting theory was a unified field theory of gravitation and Maxwellian electrodynamics. Weyl's hopes were monumentally dashed, first starting with Einstein's lethal critique of the theory. Later, others joined Einstein in their critique and dismissal of Weyl's theory, where they argued that despite its irresistible grandeur and exquisite beauty, Weyl's theory can not possibly describe the measured reality of the order of the present world.

[*] A geodesic coordinate system is one in which the Christoffel three symbols ($\Gamma^\lambda_{\mu\nu}$) vanish at all points on the given set of coordinates – i.e. $\Gamma^\lambda_{\mu\nu} = 0$. An example is the flat rectangular (x, y, z) system of coordinates. However, when one moves from this (x, y, z) rectangular system of coordinates to, say, the spherical (r, θ, φ), the resulting affine ($\Gamma^{\lambda'}_{\mu'\nu'}$) is not zero – i.e. $\Gamma^{\lambda'}_{\mu'\nu'} \neq 0$.

4 Modified Weyl theory

Now, following for example Einstein [7, 8], Eddington [14] and Schrödinger [9–11], we strongly felt that the idea of tensorial affinities is the only way to solve the aforementioned topological issues with RG and at the same time, we felt that the beautiful introduction of the four-vector into the framework of RG in WG needed to be preserved at all cost. To us, this meant modifying WG in such a manner that tensorial affinities are attained. For this, we imagined the metric of WG being modified such that it is now given by:

$$\bar{\mathrm{g}}_{\mu\nu} = e^{2\chi}\mathrm{g}_{\mu\nu}, \tag{11}$$

where, unlike in WG, the function: χ is no longer a scalar, but a pseudo-scalar so designed that the resulting affinities of this new geometry are true tensors.

The new metric given in (11) leads to the following affine connection:

$$\overline{\Gamma}^{\lambda}_{\mu\nu} = \Gamma^{\lambda}_{\mu\nu} + Q^{\lambda}_{\mu\nu}\,, \tag{12}$$

where:

$$Q^{\lambda}_{\mu\nu} = \mathrm{g}^{\lambda}{}_{\mu}\partial_{\nu}\chi + \mathrm{g}^{\lambda}{}_{\nu}\partial_{\mu}\chi - \mathrm{g}_{\mu\nu}\partial^{\lambda}\chi \tag{13}$$

is a new affine connection that transforms as follows:

$$Q^{\lambda'}_{\mu'\nu'} = \frac{\partial x^{\lambda'}}{\partial x^{\lambda}}\frac{\partial x^{\mu}}{\partial x^{\mu'}}\frac{\partial x^{\nu}}{\partial x^{\nu'}}Q^{\lambda}_{\mu\nu} - \frac{\partial x^{\lambda'}}{\partial x^{\lambda}}\frac{\partial^2 x^{\lambda}}{\partial x^{\mu'}\partial x^{\nu'}}\,. \tag{14}$$

Because of the transformational properties of the new Q-affine as spelt out in (14) above, the resultant affine $\overline{\Gamma}^{\lambda}_{\mu\nu}$ in (12) is a tensor. In order for the Q-affine to transform as desired in (14), the χ-function must transform as follows:

$$\chi' = \chi - \frac{\partial x^{\lambda}}{\partial x^{\lambda'}}\,. \tag{15}$$

Further, in order for the χ-function to transform as desired in (15), this function ought to be defined as follows:

$$\chi = \ln\Omega\,, \tag{16}$$

where the Ω-function transforms as follows:

$$\Omega' = \Omega\,\exp\left(-\frac{\partial x^{\lambda}}{\partial x^{\lambda'}}\right). \tag{17}$$

In this way, tensorial affinities are indeed possible.

5 Unified Field Theory

With the nagging topological defect of RG and WG now out of the way, i.e. the problem of non-tensorial affinities, we realised in [1] that Weyl [2]'s idea can be brought back to life. Instead of just supplementing the Riemann metric with the Weyl-scalar, we have to supplement it with both the Weyl-scalar ϕ and the new χ-function as follows:

$$\bar{\mathrm{g}}_{\mu\nu} = e^{2(\phi+\chi)}\mathrm{g}_{\mu\nu}\,. \tag{18}$$

This leads to the affine of the emergent geometry now being defined as follows:

$$\overline{\Gamma}^{\lambda}_{\mu\nu} = \Gamma^{\lambda}_{\mu\nu} + W^{\lambda}_{\mu\nu} + Q^{\lambda}_{\mu\nu}\,. \tag{19}$$

Just like the affine in the previous section defined in (12), this new affine (19) is also a tensor. From this, one can construct a unified field theory of their choice by identifying the Weyl tensor with a field of their choice. Since all our theories are designed in order to model physical and natural reality, the choice one will have to seek is obviously that which can explain physical and natural reality as we experience it and have come to know it. Our work presented in [1] makes a temarious endeavour to that end.

6 General discussion

Without an iota of doubt, we certainly have demonstrated or shown that it is very much possible to attain tensorial affinities by simple redefining Weyl [2]'s scalar so that it is a pseudo-scalar that is, for better or for worse, forced to yield for us the desired tensorial affinities. In closing, we certainly must hasten to say that our foisting of this pseudo-scalar to yield the desired tensorial affinities has been done well within the permissible and legal confines, domains and provinces of physics, mathematics and philosophy.

Received on March 8, 2022

References

1. Nyambuya G. G. Fundamental Geometrodynamic Justification of Gravitomagnetism (I). *Progress in Physics*, 2220, v. 16, 73–91.
2. Weyl H. K. H. Gravitation und Elektrizität. *Sitzungsber. Preuss. Akad. Wiss.*, 1918, v. 26, 465–478.
3. Milgrom M. MOND – A Pedagogical Review. *Acta Phys. Pol. B*, 2001, v. 32, 371–389. arXiv: astro-ph/0112069.
4. Milgrom M. A Modification of the Newtonian Dynamics – Implications for Galaxies. *Ap.J.*, 1983, v. 459, 371–389.
5. Milgrom M. A Modification of the Newtonian Dynamics – Implications for Galaxy Systems. *Ap.J.*, 1983, v. 270, 384–389.
6. Einstein A. Die Feldgleichungun der Gravitation. *Sitzungsberichte der Preussischen Akademie der Wissenschaften zu Berlin*, 1915, 844–847.
7. Einstein A. A Generalisation of the Relativistic Theory of Gravitation. *Ann. Math.*, 1945, v. 46, 578–584.
8. Einstein A. and Straus E. G. *Ann. Math.*, 1946, v. 47, 731. See also: Einstein A. *Rev. Mod. Phys.*, 1948, v. 20, 35; Einstein A. *Can. J. Math.*, 1950. v. 2, 120.
9. Schrödinger E. The Final Affine Field Laws I. *Proceedings of the Royal Irish Academy. A: Math. and Phys. Sc.*, 1945, v. 51, 163–171.
10. Schrödinger E. The Final Affine Field Laws. II. *Proceedings of the Royal Irish Academy. A: Math. and Phys. Sc.*, 1945, v. 51, 205–216.
11. Schrödinger E. The Final Affine Field Laws. III. *Proceedings of the Royal Irish Academy. A: Math. and Phys. Sc.*, 1948, v. 52, 1–9.
12. Einstein A. 1907. Translated in: Schwartz H. M. *Am. J. Phys.*, 1977, v. 45, 10.
13. Maxwell J. C. A Dynamical Theory of the Electromagnetic Field. *Phil. Trans. Royal Soc.*, 1865, v. 155, 459–512.
14. Eddington A. S. The Mathematical Theory of Relativity. Cambridge University Press, Cambridge, 1924.

Conditions for the Riemannian Description of Maxwell's Source-Free Field Equations

G. G. Nyambuya

National University of Science and Technology, Faculty of Applied Sciences – Department of Applied Physics, Fundamental Theoretical and Astrophysics Group, P. O. Box 939, Ascot, Bulawayo, Republic of Zimbabwe.
E-mail: physicist.ggn@gmail.com

In this paper, away from the intricate mathematics and philosophy presented in our earlier work [1], we demonstrate that well within Riemann geometry, Maxwell's electrodynamic source-free field equations [2] are indeed susceptible to a geometric description by the metric tensor, provided: (1) the non-linear term of the Riemann curvature tensor is assumed to vanish identically, and (2) the electromagnetic four-vector field A_μ obeys the gauge condition $A^\alpha \partial_\alpha A_\mu$. We strongly believe that this demonstration is important for physics because if the electromagnetic force can be given a geometric description, this most certainly will lead to the opening of new pathways for incorporating the gravitational force into such a scheme.

Truth is ever to be found in simplicity, and not in the multiplicity and confusion of things.

Sir Isaac Newton (1642-1727)

1 Introduction

As far as prevailing wisdom is concerned, there is only one *Force of Nature* that is described geometrically and this is the force of gravity and its geometric description was handed down to us by Albert Einstein [3] in his intellectual masterpiece – the *General Theory of Relativity* (GTR). By geometric description, we here mean the ability of the force in question to submit to a metric description in a manner redolent or akin to the force of gravity in Einstein [3]'s GTR, where the gravitational force is described by the metric tensor $g_{\mu\nu}$. In turn, the metric tensor $g_{\mu\nu}$ evolves and is governed by the laws governing Riemann Geometry (RG).

Given our opening statement, the question naturally suggests itself: *Can Maxwell's electromagnetic force be given a geometric description?* Our answer to this question is that with the *proviso* that the:

1. Riemann curvature tensor is linearized, i.e. $\Gamma^\lambda_{\delta\sigma}\Gamma^\delta_{\mu\nu} - \Gamma^\lambda_{\delta\nu}\Gamma^\delta_{\mu\sigma} \equiv 0$, and the metric tensor $g_{\mu\nu}$ is decomposed into a product of the components of a four-vector, i.e. $g_{\mu\nu} = A_\mu A_\nu$,
2. Electromagnetic four-vector field A_μ obeys the gauge condition $A^\alpha \partial_\alpha A_\mu$,

then, one can successfully give a geometric description of Maxwell's [2] source-free field equations.

Herein, we have for clarity's sake removed most of the intricate mathematics and philosophy (found in [1]) so that our reader(s) will have a much greater appreciation of our ongoing work. We here only deal with the Riemann tensor and its identities and from that only, we demonstrate that a decomposed metric ($g_{\mu\nu} = A_\mu A_\nu$) can successfully lead one to the source-free Maxwell's equation [2]. This we believe is something that will provoke our reader(s) into thinking further (than meet the eye) by asking about the possibility of doing the same for the source-coupled field equations. Not only will this provoke the reader(s) into thinking about the possibility of a geometrically derived source-coupled Maxwell's equation [2], but of the possibility of a unity between gravitation, electricity and possibly the other two forces of Nature – the *weak* and *strong* nuclear forces.

Lastly, this article is organised as follows: in §2, we present the Riemann tensor and in addition to this, we introduce a gauge condition that linearises this tensor. In §3, we present the metric tensor in its decomposed form and some of the necessary gauge conditions. In §4, we write down the affine connection in terms of the decomposed metric tensor and from this exercise, we show that the Maxwellian electrodynamic tensor can be harnessed. In §5, we delve onto the main task of the day whereby we derive the Maxwellian source-free field equations purely from the Riemann tensor and lastly, in §6, we present a general discussion.

2 Riemann curvature tensor

From the view point of tensors, the Riemann curvature tensor $R^\lambda_{\mu\sigma\nu}$ has two components to it – i.e. the linear and non-linear parts which are themselves tensors. That is to say:

$$R^\lambda_{\mu\sigma\nu} = \overbrace{\Gamma^\lambda_{\mu\nu,\sigma} - \Gamma^\lambda_{\mu\sigma,\nu}}^{\hat{R}^\lambda_{\mu\sigma\nu}} + \overbrace{\Gamma^\lambda_{\delta\sigma}\Gamma^\delta_{\mu\nu} - \Gamma^\lambda_{\delta\nu}\Gamma^\delta_{\mu\sigma}}^{\breve{R}^\lambda_{\mu\sigma\nu}} = \hat{R}^\lambda_{\mu\sigma\nu} + \breve{R}^\lambda_{\mu\sigma\nu}\,, \quad (1)$$

$$\text{linear terms} \qquad \text{non–linear terms}$$

where $\hat{R}^\lambda_{\mu\sigma\nu}$ and $\breve{R}^\lambda_{\mu\sigma\nu}$ are the linear and non-linear components of the Riemann curvature tensor and these are defined as follows:

$$\hat{R}^\lambda_{\mu\sigma\nu} = \Gamma^\lambda_{\mu\nu,\sigma} - \Gamma^\lambda_{\mu\sigma,\nu}\,, \quad (2a)$$

$$\breve{R}^\lambda_{\mu\sigma\nu} = \Gamma^\lambda_{\delta\sigma}\Gamma^\delta_{\mu\nu} - \Gamma^\lambda_{\delta\nu}\Gamma^\delta_{\mu\sigma}\,. \quad (2b)$$

Because $R^{\lambda}_{\mu\sigma\nu}$ and $\hat{R}^{\lambda}_{\mu\sigma\nu}$ are tensors, it directly follows that $\check{R}^{\lambda}_{\mu\sigma\nu}$ is a tensor too. If, as proposed in [1], we are to choose as a natural gauge condition on our desired spacetime the condition $\check{R}^{\lambda}_{\mu\sigma\nu} = 0$, then, in any subsequent system of coordinates and/or reference frame, this condition will hold because $\check{R}^{\lambda}_{\mu\sigma\nu}$ is a tensor. What we now have is a linear Riemann world. Insofar as computations are concerned, such a world is certainly much easier to deal with. Besides this, one is able to obtain exact solutions from the resultant field equations. Whether or not this is the world that we live in, we can only compare our final results with what obtains in Nature.

3 Decomposition of the metric tensor

As is well known, the metric tensor $g_{\mu\nu}$ of RG has a total of sixteen components and as a result of the symmetry in its $\mu\nu$-indices, i.e. $g_{\mu\nu} = g_{\nu\mu}$, it has ten independent components. Starting in [4], we realised that the number of independent terms can be reduced from ten to four by way of casting this metric as a product of a four-vector A_μ, i.e.

$$g_{\mu\nu} = A_\mu A_\nu \,. \tag{3}$$

With the metric now written in this manner, we where able to write down a curved spacetime Dirac equation [4] using the same approach used by Dirac to arrive at the Dirac equation.

This four-vector A_μ is assumed to have unit magnitude throughout all of spacetime, i.e.

$$A^\alpha A_\alpha = 1 \,. \tag{4}$$

In [1], we have called this condition (4), the *Normalization Gauge Condition* (NGC). Differentiating this NGC with respect to: x^μ, we obtain the following corollary condition:

$$A^\alpha \partial_\mu A_\alpha = 0. \tag{5}$$

As will be seen in §5, this corollary condition (5) and the NGC, are necessary for the derivation that we shall carry out.

Apart from the NGC (4) and its corollary (5), we will also need the following condition for our derivation, i.e.

$$A^\alpha \partial_\alpha A_\mu = 0 \,. \tag{6}$$

At present, we have no ready natural justification for this condition, i.e. where it originates from, except that it is a necessary condition for our derivation.

4 Recomposition of the affine connection

The Christoffel three-symbol [5] (affine connection) is given by:

$$\Gamma^{\lambda}_{\mu\nu} = \frac{1}{2}\left(\partial_\nu g^{\lambda}{}_{\mu} + \partial_\mu g^{\lambda}{}_{\nu} - \partial^\lambda g_{\mu\nu}\right) . \tag{7}$$

Under the new decomposition of the metric given in (3), this affine connection can be recomposed or redefined by substituting the decomposed metric tensor. So doing, we obtain:

$$\Gamma^{\lambda}_{\mu\nu} = \frac{1}{2}\left[\partial_\nu\left(A^\lambda A_\mu\right) + \partial_\mu\left(A^\lambda A_\nu\right) - \partial^\lambda\left(A_\mu A_\nu\right)\right] . \tag{8}$$

Differentiating the terms of the metric in (8), we will have:

$$\begin{aligned}\Gamma^{\lambda}_{\mu\nu} = \frac{1}{2}\Big(&\underbrace{A^\lambda\partial_\nu A_\mu}_{\text{Term I}} + \underbrace{A_\mu\partial_\nu A^\lambda}_{\text{Term II}} + \underbrace{A^\lambda\partial_\mu A_\nu}_{\text{Term III}} + \underbrace{A_\nu\partial_\mu A^\lambda}_{\text{Term IV}} - \\ &- \underbrace{A_\nu\partial^\lambda A_\mu}_{\text{Term V}} - \underbrace{A_\mu\partial^\lambda A_\nu}_{\text{Term VII}}\Big) .\end{aligned} \tag{9}$$

Rearranging the differentiated terms of the metric tensor labelled in (9) above as: Term I, II, III, *etc*, we will have:

$$\begin{aligned}\Gamma^{\lambda}_{\mu\nu} = \frac{1}{2}\Big[&\Big(\underbrace{A_\mu\partial_\nu A^\lambda}_{\text{Term II}} - \underbrace{A_\mu\partial^\lambda A_\nu}_{\text{Term VII}}\Big) + \\ &+ \Big(\underbrace{A_\nu\partial_\mu A^\lambda}_{\text{Term IV}} - \underbrace{A_\nu\partial^\lambda A_\mu}_{\text{Term V}}\Big) + \Big(\underbrace{A^\lambda\partial_\nu A_\mu}_{\text{Term I}} + \underbrace{A^\lambda\partial_\mu A_\nu}_{\text{Term III}}\Big)\Big] .\end{aligned} \tag{10}$$

From (10), we can now write the Christoffel as follows:

$$\Gamma^{\lambda}_{\mu\nu} = \frac{1}{2}\left(A_\mu F^{\lambda}{}_{\nu} + A_\nu F^{\lambda}{}_{\mu} + A^\lambda H_{\mu\nu}\right) , \tag{11}$$

where:

$$F_{\mu\nu} = \partial_\mu A_\nu - \partial_\nu A_\mu \,, \tag{12a}$$

$$H_{\mu\nu} = \partial_\mu A_\nu + \partial_\nu A_\mu \,. \tag{12b}$$

The object $F_{\mu\nu}$ in (12a) can easily be identified with Maxwell's electromagnetic field tensor [2] while the object $H_{\mu\nu}$ is a new object which may appear to be unrelated to Maxwell's electromagnetic field tensor [2]. As will be seen in the next section where we are going to derive the electrodynamic source-free field equations, this seemingly unrelated object $H_{\mu\nu}$ is what shall lead us to our desideratum.

Now, on the corollary to the NGC, i.e. (5) and (6), an application of these to (12), leads to the following corollary gauge conditions:

$$A^\alpha F_{\alpha\nu} = A^\alpha F_{\nu\alpha} = 0 \,, \tag{13a}$$

$$A^\alpha H_{\alpha\nu} = A^\alpha H_{\nu\alpha} = 0 \,. \tag{13b}$$

The above completes the necessary package of conditions needed to derive Maxwell's source-free field equations.

We shall now make a further reduction in the symbols by writing the affine connection as follows:

$$\Gamma^{\lambda}_{\mu\nu} = F^{\lambda}_{\mu\nu} + H^{\lambda}_{\mu\nu} \,, \tag{14}$$

where:

$$F^{\lambda}_{\mu\nu} = \frac{1}{2}\left(A_\mu F^{\lambda}{}_{\nu} + A_\nu F^{\lambda}{}_{\mu}\right) , \tag{15a}$$

$$H^{\lambda}_{\mu\nu} = \frac{1}{2}A^\lambda H_{\mu\nu} \,. \tag{15b}$$

With the affine connection written as we have written it in (14), we can now write the linear Riemann tensor as follows:

$$R^{\lambda}_{\mu\sigma\nu} = F^{\lambda}_{\mu\sigma\nu} + H^{\lambda}_{\mu\sigma\nu} \,, \tag{16}$$

where the new curvature tensors $F^{\lambda}_{\mu\sigma\nu}$ and $H^{\lambda}_{\mu\sigma\nu}$ are such that:

$$F^{\lambda}_{\mu\sigma\nu} = \partial_{\sigma}F^{\lambda}_{\mu\nu} - \partial_{\nu}F^{\lambda}_{\mu\sigma}\,, \tag{17a}$$

$$H^{\lambda}_{\mu\sigma\nu} = \partial_{\sigma}H^{\lambda}_{\mu\nu} - \partial_{\nu}H^{\lambda}_{\mu\sigma}\,. \tag{17b}$$

We are now ready to demonstrate that deeply embedded in the Riemann metric under the present metric decomposition (3), are the Maxwell source-free field equations [2].

5 Derivation

We know that the Riemann tensor satisfies the following first Bianchi identity:

$$R^{\lambda}_{\mu\sigma\nu} + R^{\lambda}_{\nu\mu\sigma} + R^{\lambda}_{\sigma\nu\mu} \equiv 0\,. \tag{18}$$

Multiplying this identity (18) throughout by A_{γ}, and then contracting the $\gamma\lambda$-indices of the resulting tensor, i.e. $\gamma = \lambda = \alpha$, (19) will reduce to:

$$A_{\alpha}R^{\alpha}_{\mu\sigma\nu} + A_{\alpha}R^{\alpha}_{\nu\mu\sigma} + A_{\alpha}R^{\alpha}_{\sigma\nu\mu} \equiv 0\,. \tag{19}$$

From the decomposition of $R^{\lambda}_{\mu\sigma\nu}$ into the curvature tensors $F^{\lambda}_{\mu\sigma\nu}$ and $H^{\lambda}_{\mu\sigma\nu}$ given in (16), it follows that we can decompose (19) into two corresponding parts as follows:

$$\begin{aligned}&\left(A_{\alpha}F^{\alpha}_{\mu\sigma\nu} + A_{\alpha}F^{\alpha}_{\nu\mu\sigma} + A_{\alpha}F^{\alpha}_{\sigma\nu\mu}\right) + \\ &+ \left(A_{\alpha}H^{\alpha}_{\mu\sigma\nu} + A_{\alpha}H^{\alpha}_{\nu\mu\sigma} + A_{\alpha}H^{\alpha}_{\sigma\nu\mu}\right) \equiv 0\,.\end{aligned} \tag{20}$$

In our calculation of (19), we shall first compute:

$$A_{\alpha}F^{\alpha}_{\mu\sigma\nu} + A_{\alpha}F^{\alpha}_{\nu\mu\sigma} + A_{\alpha}F^{\alpha}_{\sigma\nu\mu}\,,$$

followed by:

$$A_{\alpha}H^{\alpha}_{\mu\sigma\nu} + A_{\alpha}H^{\alpha}_{\nu\mu\sigma} + A_{\alpha}H^{\alpha}_{\sigma\nu\mu}\,.$$

5.1 Part I

We know that:

$$\begin{aligned}2F^{\lambda}_{\mu\sigma\nu} = &\left(\partial_{\sigma}A_{\mu}F^{\lambda}{}_{\nu} + A_{\mu}\partial_{\sigma}F^{\lambda}{}_{\nu} + \partial_{\sigma}A_{\nu}F^{\lambda}{}_{\mu} + A_{\nu}\partial_{\sigma}F^{\lambda}{}_{\mu}\right) \\ &- \left(\partial_{\nu}A_{\mu}F^{\lambda}{}_{\sigma} + A_{\mu}\partial_{\nu}F^{\lambda}{}_{\sigma} + \partial_{\nu}A_{\sigma}F^{\lambda}{}_{\mu} + A_{\sigma}\partial_{\nu}F^{\lambda}{}_{\mu}\right).\end{aligned} \tag{21}$$

Multiplying $F^{\lambda}_{\mu\sigma\nu}$ by A_{γ}, and then contracting the $\gamma\lambda$-indices of the resulting tensor, i.e. $\gamma = \lambda = \alpha$, and taking into account the gauge condition $A_{\alpha}F^{\alpha}{}_{\mu} = 0$, (21) will reduce to:

$$\begin{aligned}2A_{\alpha}F^{\alpha}_{\mu\sigma\nu} = &\left(A_{\alpha}A_{\mu}\partial_{\sigma}F^{\alpha}{}_{\nu} - A_{\alpha}A_{\mu}\partial_{\nu}F^{\alpha}{}_{\sigma}\right) + \\ &+ \left(A_{\alpha}A_{\nu}\partial_{\sigma}F^{\alpha}{}_{\mu} - A_{\alpha}A_{\sigma}\partial_{\nu}F^{\alpha}{}_{\mu}\right).\end{aligned} \tag{22}$$

Writing $A_{\alpha}A_{\mu} = \mathrm{g}_{\alpha\mu}$, $A_{\alpha}A_{\nu} = \mathrm{g}_{\alpha\nu}$ and $A_{\alpha}A_{\sigma} = \mathrm{g}_{\alpha\sigma}$, we will have:

$$\begin{aligned}2A_{\alpha}F^{\alpha}_{\mu\sigma\nu} = &\left(\mathrm{g}_{\alpha\mu}\partial_{\sigma}F^{\alpha}{}_{\nu} - \mathrm{g}_{\alpha\mu}\partial_{\nu}F^{\alpha}{}_{\sigma}\right) + \\ &+ \left(\mathrm{g}_{\alpha\nu}\partial_{\sigma}F^{\alpha}{}_{\mu} - \mathrm{g}_{\alpha\sigma}\partial_{\nu}F^{\alpha}{}_{\mu}\right),\end{aligned} \tag{23}$$

hence, lowering the indices in (23) where applicable, we will have:

$$2A_{\alpha}F^{\alpha}_{\mu\sigma\nu} = \left(\partial_{\sigma}F_{\mu\nu} - \partial_{\nu}F_{\mu\sigma}\right) + \left(\partial_{\sigma}F_{\nu\mu} - \partial_{\nu}F_{\sigma\mu}\right). \tag{24}$$

Using in (24) the antisymmetry property of the electromagnetic field tensor, namely $F_{\nu\mu} = -F_{\mu\nu}$ and $F_{\sigma\mu} = -F_{\mu\sigma}$, we will have:

$$2A_{\alpha}F^{\alpha}_{\mu\sigma\nu} = 0 \;\;\Rightarrow\;\; A_{\alpha}F^{\alpha}_{\mu\sigma\nu} = 0\,, \tag{25}$$

hence:

$$A_{\alpha}F^{\alpha}_{\mu\sigma\nu} + A_{\alpha}F^{\alpha}_{\nu\mu\sigma} + A_{\alpha}F^{\alpha}_{\sigma\nu\mu} = 0\,. \tag{26}$$

Next, we need to calculate $A_{\alpha}H^{\alpha}_{\mu\sigma\nu} + A_{\alpha}H^{\alpha}_{\nu\mu\sigma} + A_{\alpha}H^{\alpha}_{\sigma\nu\mu}$.

5.2 Part II

We know that:

$$\begin{aligned}2H^{\lambda}_{\mu\sigma\nu} = &\left(A^{\lambda}\partial_{\sigma}H_{\mu\nu} - A^{\lambda}\partial_{\nu}H_{\mu\sigma}\right) + \\ &+ \left(H_{\mu\nu}\partial_{\sigma}A^{\lambda} - H_{\mu\sigma}\partial_{\nu}A^{\lambda}\right).\end{aligned} \tag{27}$$

Multiplying $H^{\lambda}_{\mu\sigma\nu}$ by A_{γ}, and then contracting the $\gamma\lambda$-indices of the resulting tensor, i.e. $\gamma = \lambda = \alpha$, (27) will reduce to:

$$\begin{aligned}2A_{\alpha}H^{\alpha}_{\mu\sigma\nu} = &\left(A_{\alpha}A^{\alpha}\partial_{\sigma}H_{\mu\nu} - A_{\alpha}A^{\alpha}\partial_{\nu}H_{\mu\sigma}\right) + \\ &+ \left(H_{\mu\nu}A_{\alpha}\partial_{\sigma}A^{\alpha} - H_{\mu\sigma}A_{\alpha}\partial_{\nu}A^{\alpha}\right).\end{aligned} \tag{28}$$

From the normalization gauge ($A_{\alpha}A^{\alpha} = 1$), and the corollary of this gauge, namely $A_{\alpha}\partial_{\mu}A^{\alpha} = 0$, (28) reduces to:

$$2A_{\alpha}H^{\alpha}_{\mu\sigma\nu} = \partial_{\sigma}H_{\mu\nu} - \partial_{\nu}H_{\mu\sigma} = \partial_{\sigma}F_{\nu\mu} + \partial_{\nu}F_{\mu\sigma}\,, \tag{29}$$

hence:

$$2A_{\alpha}H^{\alpha}_{\mu\sigma\nu} = \partial_{\sigma}F_{\nu\mu} + \partial_{\nu}F_{\mu\sigma} \neq 0\,, \tag{30a}$$

$$2A_{\alpha}H^{\alpha}_{\nu\mu\sigma} = \partial_{\mu}F_{\sigma\nu} + \partial_{\sigma}F_{\nu\mu} \neq 0\,, \tag{30b}$$

$$2A_{\alpha}H^{\alpha}_{\sigma\nu\mu} = \partial_{\nu}F_{\mu\sigma} + \partial_{\mu}F_{\sigma\nu} \neq 0\,. \tag{30c}$$

From (30), it is clear that:

$$\begin{aligned}&A_{\alpha}H^{\alpha}_{\mu\sigma\nu} + A_{\alpha}H^{\alpha}_{\nu\mu\sigma} + A_{\alpha}H^{\alpha}_{\sigma\nu\mu} = \\ &= \partial_{\mu}F_{\sigma\nu} + \partial_{\nu}F_{\mu\sigma} + \partial_{\sigma}F_{\nu\mu}.\end{aligned} \tag{31}$$

Now, we can put everything together.

5.3 Summary

Putting everything together, i.e. (19), (26) and (31), we will have:

$$\begin{aligned}&A_{\alpha}R^{\alpha}_{\mu\sigma\nu} + A_{\alpha}R^{\alpha}_{\nu\mu\sigma} + A_{\alpha}R^{\alpha}_{\sigma\nu\mu} = \\ &= 0 + \left(\partial_{\mu}F_{\sigma\nu} + \partial_{\nu}F_{\mu\sigma} + \partial_{\sigma}F_{\nu\mu}\right) \equiv 0\,,\end{aligned} \tag{32}$$

hence:

$$\partial_{\mu}F_{\sigma\nu} + \partial_{\nu}F_{\mu\sigma} + \partial_{\sigma}F_{\nu\mu} \equiv 0\,. \tag{33}$$

Of course, (33) is indeed Maxwell's source-free field equations [2].

6 Discussion

Given a linearized Riemann curvature tensor, we have herein demonstrated, in clear and no uncertain terms, the conditions under which Maxwell's electrodynamic source-free field equations [2] are readily susceptible to a geometric description by a metric tensor in much the same way that the force of gravity is described by the metric tensor in Einstein's GTR [3]. This description has come at the following cost:

1. A decomposed metric $g_{\mu\nu} = A_\mu A_\nu$. This reduces the number of independent fields from ten to four. In accordance with *Occam's Razor*, this is a welcome development in any theory, especially if the new theory does not destroy the old but enriches and engenders it.
2. A linearised (i.e. $\Gamma^{\lambda}_{\delta\sigma}\Gamma^{\delta}_{\mu\nu} - \Gamma^{\lambda}_{\delta\nu}\Gamma^{\delta}_{\mu\sigma} \equiv 0$) Riemann curvature tensor. This eliminates the computational complexity that ensues from these non-linear terms.
3. A normalization (i.e. $A^\alpha A_\alpha = 1$) gauge on the four-vector. A corollary to this normalization gauge is that $A^\alpha \partial_\mu A_\alpha = 0$.
4. Introduction of an extra exo-gauge condition to the metric four-vector, i.e. $A^\alpha \partial_\alpha A_\mu = 0$.

Having demonstrated the susceptibility of Maxwell [2]'s source-free field equation to a geometric description, the value of this work is that it indicates that Maxwell's equations [2] may very well be embedded deep inside the labyrinth of Riemann geometry. In addition to this, we strongly believe that this work is important for physics because if the electromagnetic force can be given a geometric description, this most certainly will lead to the opening of new pathways for incorporating the gravitational force into such a scheme.

Received on March 29, 2022

References

1. Nyambuya G. G. Fundamental Geometrodynamic Justification of Gravitomagnetism (I). *Progress in Physics*, 2220, v. 16, 73–91.
2. Maxwell J. C. A Dynamical Theory of the Electromagnetic Field. *Phil. Trans. Royal Soc.*, 1865, v. 155, 459–512.
3. Einstein A. Die Feldgleichungun der Gravitation. *Sitzungsberichte der Preussischen Akademie der Wissenschaften zu Berlin*, 1915, 844–847.
4. Nyambuya G. G. New Curved Spacetime Dirac Equations. *Foundations of Physics*, 2008, v. 37 (7), 665–677.
5. Christoffel E. B. Ueber die Transformation der Homogenen Differentialausdrücke zweiten Grades. *Jour. für die reine und angewandte Mathematik*, 1869, v. B70, 46–70.

Non-Quantum Teleportation in a Rotating Space With a Strong Electromagnetic Field

Dmitri Rabounski and Larissa Borissova

Puschino, Moscow Region, Russia
E-mail: rabounski@yahoo.com, lborissova@yahoo.com

In 1991 we derived the physical conditions opening the gate to a fully degenerate space-time, where from the point of view of a regular observer the observable spatial and time intervals are equal to zero. The one of the conditions, under which the observable interval of time is zero, enables instant displacement (non-quantum teleportation) of physical bodies at any distance. In this article, we derive the teleportation condition for Schwarzschild's mass-point metric, Schwarzschild's metric inside a sphere filled with an incompressible liquid and de Sitter's metric of a space filled with the physical vacuum. We also introduce the modifications of the above three metrics, which contain rotation due to the space-time non-holonomity (non-orthogonality of the time lines to the three-dimensional spatial section) and derive the teleportation condition in each of these spaces. The obtained teleportation condition requires either a near-light-speed rotation or a super-strong gravitational field (depending on the particular space metric), which is very problematic if not impossible in a regular laboratory. On the other hand, the non-orthogonality of the time lines to the three-dimensional section can be implemented not only by a mechanical rotation of the laboratory space, but also using other physical factors. Thus, we are looking for how to do it using a strong electromagnetic field (the latter is not a problem for modern technologies). We introduce a space-time metric, which rotates due to its non-holonomity, and the gravitational field is neglected. Then, substituting the components of the obtained metric into Einstein's field equations with the electromagnetic energy-momentum tensor on the right hand side, we obtain the conditions under which the equations vanish and, therefore, the metric space is Riemannian and contains an electromagnetic field. As a result, we obtain how the electromagnetic field parameters can replace the rotation of space in the teleportation condition. The obtained result shows how to teleport physical bodies from an earth-bound laboratory to any remote point in the Universe using a super-strong electromagnetic field. Creating such devices is a very interesting task for engineers in the near future.

1 The background

In 1991, in the course of our extensive research on the application of the General Theory of Relativity to biophysics, we set ourselves the following primary task. We aimed to deduce such physical conditions, under which the four-dimensional preudo-Riemannian space, which is the basic space-time of the General Theory of Relativity, is fully degenerate from the point of view of a regular observer. In such a fully degenerate region, the four-dimensional space-time interval is equal to zero, as well as the three-dimensional spatial interval and the interval of time, which are observed by a regular observer outside this region (in a regular non-degenerate region of the space-time), are also equal to zero.

In particular, the condition that the interval of physically observable time between two events is equal to zero enables instant displacement (non-quantum teleportation) of a physical body from the observer's laboratory to any remote point in the Universe.

The source and logical basis of this idea was the fact that a partial degeneration of the space-time was already known. In this case the four-dimensional (space-time) interval is equal to zero, and the observable three-dimensional interval and the interval of observable time are not equal to zero, but are equal to each other. Such a partially degenerate region of the space-time is home to light-like trajectories and light-like (massless) particles moving along them, for example, photons (photons belong to the family of massless light-like particles).

In our mathematical search for physical conditions, under which the space-time fully degenerates, we used, as always in our theoretical work, the mathematical apparatus of chronometric invariants, which are physically observable quantities in the General Theory of Relativity. This mathematical apparatus was created in 1944 by our esteemed teacher A. L. Zelmanov (1913–1987), who published it first in 1944 in his PhD thesis [1] and then in two brief journal articles [2, 3]. It just so happened that after Zelmanov's death, we remain the only ones who professionally master this mathematical apparatus and apply it in scientific research. For this reason, before explaining our current study of the non-quantum teleportation condition, we give below a brief introduction to the theory of chronometric invariants.

2 A brief introduction to chronometric invariants

Briefly, *chronometric invariants* are the quantities that are invariant everywhere along a three-dimensional spatial section of the space-time and a line of time, which are linked to a real observer and his laboratory. Mathematically, chronometrically invariant quantities are projections of four-dimensional

(general covariant) quantities onto the three-dimensional spatial section and the line of time of the observer. In the general case, such a real three-dimensional spatial section (local three-dimensional space) can be curved, inhomogeneous, anisotropic, deformed, rotating, be filled with a gravitational field and also have some other properties such as viscosity etc. The lines of real time can have different density of time coordinates depending on the gravitational potential, as well as be non-orthogonal to the three-dimensional spatial section (the latter property is called the space-time non-holonomity, which is manifested as a three-dimensional rotation of the spatial section). As a result, the reference frame of a real observer, consisting of a coordinate grid paved on his real three-dimensional spatial section, as well as a system of real clocks located at each point of the section, has all the geometric and physical properties of his local space. Therefore, chronometrically invariant quantities as projections of four-dimensional (general covariant) quantities onto the real spatial section and real time line in his reference frame take into account the influence of all the geometric and physical factors present in his local space. So, the chronometrically invariant projections of any four-dimensional (general covariant) quantity calculated in the real reference frame of an observer are truly *physically observable quantities* registered by the observer.

The operator of projection onto the time line of an observer is the unit-length four-dimensional vector tangential to the observer's world line at each of its points

$$b^\alpha = \frac{dx^\alpha}{ds}, \qquad b_\alpha b^\alpha = 1,$$

while the operator of projection onto his three-dimensional spatial section is the four-dimensional symmetric tensor

$$h_{\alpha\beta} = -g_{\alpha\beta} + b_\alpha b_\beta.$$

These operators are orthogonal to each other, i.e., their common contraction is always equal to zero

$$h_{\alpha\beta}b^\alpha = 0, \quad h^{\alpha\beta}b_\alpha = 0, \quad h^\alpha_\beta b_\alpha = 0, \quad h^\beta_\alpha b^\alpha = 0.$$

A regular observer rests with respect to his reference body ($b^i = 0$) and, thus, accompanies to his reference space. Thus, the components of the projection operator b^α are

$$b^0 = \frac{1}{\sqrt{g_{00}}}, \quad b^i = 0, \quad b_0 = \sqrt{g_{00}}, \quad b_i = \frac{g_{i0}}{\sqrt{g_{00}}},$$

while the components of $h_{\alpha\beta}$ have the form

$$\begin{aligned}
&h_{00} = 0, && h^{00} = -g^{00} + \frac{1}{g_{00}}, && h^0_0 = 0,\\
&h_{0i} = 0, && h^{0i} = -g^{0i}, && h^i_0 = 0,\\
&h_{i0} = 0, && h^{i0} = -g^{i0}, && h^0_i = \frac{g_{i0}}{g_{00}},\\
&h_{ik} = -g_{ik} + \frac{g_{0i}g_{0k}}{g_{00}}, && h^{ik} = -g^{ik}, && h^i_k = \delta^i_k.
\end{aligned}$$

According to Zelmanov's theorem on the chronometrically invariant (physically observable) projections, the chr.inv.-projections of a four-dimensional vector Q^α are

$$b^\alpha Q_\alpha = \frac{Q_0}{\sqrt{g_{00}}}, \qquad h^i_\alpha Q^\alpha = Q^i,$$

while for a symmetric 2nd rank tensor $Q^{\alpha\beta}$ these are

$$b^\alpha b^\beta Q_{\alpha\beta} = \frac{Q_{00}}{g_{00}}, \quad h^{i\alpha}b^\beta Q_{\alpha\beta} = \frac{Q^i_0}{\sqrt{g_{00}}}, \quad h^i_\alpha h^k_\beta Q^{\alpha\beta} = Q^{ik}.$$

Thus, the chr.inv.-projections of a four-dimensional interval dx^α are the physically observable time interval

$$d\tau = \sqrt{g_{00}}\, dt + \frac{g_{0i}}{c\sqrt{g_{00}}}\, dx^i$$

and the observable three-dimensional interval dx^i which coincides with the spatial coordinate interval. The physically observable velocity is the three-dimensional chr.inv.-vector

$$\mathrm{v}^i = \frac{dx^i}{d\tau}, \qquad \mathrm{v}_i\mathrm{v}^i = h_{ik}\mathrm{v}^i\mathrm{v}^k = \mathrm{v}^2,$$

which, on the trajectories of light, transforms to the three-dimensional chr.inv.-vector of the physically observable velocity of light c^i, the square of which is $c_i c^i = h_{ik}c^i c^k = c^2$.

Calculating the spatial chr.inv.-projections of the fundamental metric tensor $g_{\alpha\beta}$, we see that

$$h^\alpha_i h^\beta_k g_{\alpha\beta} = -h_{ik}, \qquad h^i_\alpha h^k_\beta g^{\alpha\beta} = -h^{ik},$$

i.e., h_{ik} is the physically observable chr.inv.-metric tensor. It has all properties of the fundamental metric tensor $g_{\alpha\beta}$ in the observer's three-dimensional spatial section

$$h^\alpha_i h^k_\alpha = \delta^k_i - b_i b^k = \delta^k_i,$$

where δ^k_i is the unit three-dimensional tensor, which is part of the four-dimensional unit tensor δ^α_β. Therefore, the chr.inv.-metric tensor h_{ik} can lift and lower indices in chronometrically invariant quantities.

The chr.inv.-operators of derivation

$$\frac{{}^*\partial}{\partial t} = \frac{1}{\sqrt{g_{00}}}\frac{\partial}{\partial t}, \qquad \frac{{}^*\partial}{\partial x^i} = \frac{\partial}{\partial x^i} - \frac{g_{0i}}{g_{00}}\frac{\partial}{\partial x^0}$$

are non-commutative

$$\frac{{}^*\partial^2}{\partial x^i \partial t} - \frac{{}^*\partial^2}{\partial t\, \partial x^i} = \frac{1}{c^2}F_i\frac{{}^*\partial}{\partial t}, \quad \frac{{}^*\partial^2}{\partial x^i \partial x^k} - \frac{{}^*\partial^2}{\partial x^k \partial x^i} = \frac{2}{c^2}A_{ik}\frac{{}^*\partial}{\partial t},$$

where

$$F_i = \frac{1}{1 - \frac{\mathrm{w}}{c^2}}\left(\frac{\partial \mathrm{w}}{\partial x^i} - \frac{\partial v_i}{\partial t}\right)$$

is the chr.inv.-vector of the gravitational inertial force,

$$A_{ik} = \frac{1}{2}\left(\frac{\partial v_k}{\partial x^i} - \frac{\partial v_i}{\partial x^k}\right) + \frac{1}{2c^2}\left(F_i v_k - F_k v_i\right)$$

is the antisymmetric chr.inv.-tensor of the three-dimensional angular velocity of rotation of the observer's space, w is the gravitational potential, and v_i is the three-dimensional linear velocity of rotation of the observer's space due to the space-time non-holonomity (non-orthogonality of the time lines to the three-dimensional spatial section)

$$\mathrm{w} = c^2\,(1 - \sqrt{g_{00}})\,, \quad v_i = -c\,\frac{g_{0i}}{\sqrt{g_{00}}}\,, \quad v^i = -c\,g^{0i}\,\sqrt{g_{00}}\,.$$

In particular, v_i gives a detailed formula for the chr.inv.-metric tensor h_{ik}, which is

$$h_{ik} = -\,g_{ik} + \frac{1}{c^2}\,v_i\,v_k\,.$$

It should be noted that the quantities w and v_i do not have chronometric invariance, despite the fact that $v_i = h_{ik}\,v^k$ and $v^2 = v_k v^k = h_{ik}\,v^i v^k$ as for a chr.inv.-quantity.

The reference space can deform, changing its coordinate grids with time that is expressed with the three-dimensional symmetric chr.inv.-tensor of the space deformation

$$D_{ik} = \frac{1}{2}\,\frac{{}^*\partial h_{ik}}{\partial t}\,, \quad D^{ik} = -\frac{1}{2}\,\frac{{}^*\partial h^{ik}}{\partial t}\,, \quad D = h^{ik}D_{ik} = \frac{{}^*\partial \ln\sqrt{h}}{\partial t}\,,$$

where $h = \det \| h_{ik} \|$.

The regular 2nd rank Christoffel symbols $\Gamma^{\alpha}_{\mu\nu}$ and the 1st rank Christoffel symbols $\Gamma_{\mu\nu,\sigma}$ are replaced with the respective chr.inv.-Christoffel symbols

$$\Delta^i_{jk} = h^{im}\Delta_{jk,m} = \frac{1}{2}\,h^{im}\left(\frac{{}^*\partial h_{jm}}{\partial x^k} + \frac{{}^*\partial h_{km}}{\partial x^j} - \frac{{}^*\partial h_{jk}}{\partial x^m}\right),$$

where the chr.inv.-metric tensor h_{ik} is used instead of the fundamental metric tensor $g_{\alpha\beta}$.

The chr.inv.-curvature tensor is derived similarly to the Riemann-Christoffel tensor from the non-commutativity of the 2nd chr.inv.-derivatives of an arbitrary vector

$${}^*\nabla_i {}^*\nabla_k\,Q_l - {}^*\nabla_k {}^*\nabla_i\,Q_l = \frac{2A_{ik}}{c^2}\,\frac{{}^*\partial Q_l}{\partial t} + H^{\cdots j}_{lki\cdot}\,Q_j\,,$$

where the 4th rank chr.inv.-tensor

$$H^{\cdots j}_{lki\cdot} = \frac{{}^*\partial\Delta^j_{il}}{\partial x^k} - \frac{{}^*\partial\Delta^j_{kl}}{\partial x^i} + \Delta^m_{il}\Delta^j_{km} - \Delta^m_{kl}\Delta^j_{im}\,,$$

is the basis for the chr.inv.-curvature tensor C_{lkij},

$$C_{lkij} = \frac{1}{4}\left(H_{lkij} - H_{jkil} + H_{klji} - H_{iljk}\right),$$

$$C_{lk} = C^{\cdots i}_{lki\cdot}\,, \qquad C = h^{lk}C_{lk}\,,$$

which has all properties of the Riemann-Christoffel tensor in the observer's three-dimensional spatial section, and its contraction gives the observable chr.inv.-curvature C. Also

$$H_{lkij} = C_{lkij} + \frac{1}{2}\left(2A_{ki}D_{jl} + A_{ij}D_{kl} + \right.$$
$$\left. + A_{jk}D_{il} + A_{kl}D_{ij} + A_{li}D_{jk}\right),$$

$$H_{lk} = C_{lk} + \frac{1}{2}\left(A_{kj}D^j_l + A_{lj}D^j_k + A_{kl}D\right),$$

$$H = h^{lk}H_{lk} = C\,.$$

Please note that, as was found by Zelmanov, the physically observable chr.inv.-curvature of a space is depended on not only the gravitational inertial force acting in the space, but also the space rotation and deformation, and, therefore, does not vanish in the absence of the gravitational field.

The general covariant Einstein equations

$$R_{\alpha\beta} - \frac{1}{2}\,g_{\alpha\beta}R = -\varkappa\,T_{\alpha\beta} + \lambda g_{\alpha\beta}$$

with taking all possible factors into account have the chr.inv.-projections called the chr.inv.-Einstein equations

$$\left.\begin{aligned}
&\frac{{}^*\partial D}{\partial t} + D_{jl}D^{jl} + A_{jl}A^{lj} + {}^*\nabla_j F^j - \frac{1}{c^2}\,F_j F^j = \\
&\qquad\qquad = -\,\frac{\varkappa}{2}\left(\varrho c^2 + U\right) + \lambda c^2 \\
&{}^*\nabla_j\left(h^{ij}D - D^{ij} - A^{ij}\right) + \frac{2}{c^2}\,F_j A^{ij} = \varkappa J^i \\
&\frac{{}^*\partial D_{ik}}{\partial t} - \left(D_{ij} + A_{ij}\right)\left(D^j_k + A^{\cdot j}_{k\cdot}\right) + D\,D_{ik} + 3A_{ij}A^{\cdot j}_{k\cdot} - \\
&\qquad - \frac{1}{c^2}\,F_i F_k + \frac{1}{2}\left({}^*\nabla_i F_k + {}^*\nabla_k F_i\right) - c^2 C_{ik} = \\
&\qquad\qquad = \frac{\varkappa}{2}\left(\varrho c^2 h_{ik} + 2U_{ik} - U h_{ik}\right) + \lambda c^2 h_{ik}
\end{aligned}\right\},$$

where the chr.inv.-derivative of the A^{ij} by x^j

$${}^*\nabla_j A^{ij} = \frac{{}^*\partial A^{ij}}{\partial x^j} + \Delta^i_{jl}A^{jl} + \Delta^l_{lj}A^{ij}, \quad \Delta^l_{lj} = \frac{{}^*\partial \ln\sqrt{h}}{\partial x^j}$$

is determined, as well as all other chr.inv.-derivatives

$$\begin{aligned}
&{}^*\nabla_i Q_k = \frac{{}^*\partial Q_k}{dx^i} - \Delta^l_{ik}Q_l\,, \\
&{}^*\nabla_i Q^k = \frac{{}^*\partial Q^k}{dx^i} + \Delta^k_{il}Q^l\,, \\
&{}^*\nabla_i Q_{jk} = \frac{{}^*\partial Q_{jk}}{dx^i} - \Delta^l_{ij}Q_{lk} - \Delta^l_{ik}Q_{jl}\,, \\
&{}^*\nabla_i Q^k_j = \frac{{}^*\partial Q^k_j}{dx^i} - \Delta^l_{ij}Q^k_l + \Delta^k_{il}Q^l_j\,, \\
&{}^*\nabla_i Q^{jk} = \frac{{}^*\partial Q^{jk}}{dx^i} + \Delta^j_{il}Q^{lk} + \Delta^k_{il}Q^{jl}\,, \\
&{}^*\nabla_i Q^i = \frac{{}^*\partial Q^i}{\partial x^i} + \Delta^j_{ji}Q^i\,, \qquad\qquad \Delta^j_{ji} = \frac{{}^*\partial \ln\sqrt{h}}{\partial x^i}\,, \\
&{}^*\nabla_i Q^{ji} = \frac{{}^*\partial Q^{ji}}{\partial x^i} + \Delta^j_{il}Q^{il} + \Delta^l_{li}Q^{ji}, \quad \Delta^l_{li} = \frac{{}^*\partial \ln\sqrt{h}}{\partial x^i}\,,
\end{aligned}$$

by analogy with the respective absolute derivative, and

$$\varrho = \frac{T_{00}}{g_{00}}\,, \qquad J^i = \frac{c\,T^i_0}{\sqrt{g_{00}}}\,, \qquad U^{ik} = c^2 T^{ik}$$

are the chr.inv.-projections of the energy-momentum tensor $T_{\alpha\beta}$ of the distributed matter that fills the space, e.g., an electromagnetic field: ϱ is the physically observable density of the field energy, J^i is the physically observable density of the field momentum, and U^{ik} is the physically observable stress-tensor of the field (its trace is $U = h^{mn}U_{mn}$).

The electromagnetic field tensor is the curl of the four-dimensional electromagnetic field potential A^α, i.e.,

$$F_{\mu\nu} = \nabla_\mu A_\nu - \nabla_\nu A_\mu = \frac{\partial A_\nu}{\partial x^\mu} - \frac{\partial A_\mu}{\partial x^\nu},$$

where

$$\nabla_\mu A_\nu = \frac{\partial A_\nu}{\partial x^\mu} - \Gamma^\sigma_{\nu\mu} A_\sigma$$

is the absolute derivative of the A_ν by x^μ. The electromagnetic field tensor has the physically observable projections

$$E^i = \frac{F^{\cdot i}_{0\cdot}}{\sqrt{g_{00}}} = \frac{g^{i\alpha}F_{0\alpha}}{\sqrt{g_{00}}}, \qquad H^{ik} = F^{ik} = g^{i\alpha}g^{k\beta}F_{\alpha\beta},$$

called the chr.inv.-electric strength E^i and chr.inv.-magnetic strength H^{ik} of the field. The respective chr.inv.-pseudovector H^{*i} and chr.inv.-pseudotensor E^{*ik}

$$H_{*i} = \frac{1}{2}\,\varepsilon_{ikm}H^{km}, \quad H^{*i} = \frac{1}{2}\,\varepsilon^{ikm}H_{km},$$

$$E^{*ik} = -\varepsilon^{ikm}E_m, \quad \varepsilon^{ipq}H_{*i} = \frac{1}{2}\,\varepsilon^{ipq}\varepsilon_{imn}H^{mn} = H^{pq}$$

are created in accordance with the transposition of indices in the antisymmetric "discriminant" chr.inv.-tensor

$$\varepsilon^{ikm} = \frac{e^{ikm}}{\sqrt{h}}, \qquad \varepsilon_{ikm} = e_{ikm}\sqrt{h},$$

which was introduced by Zelmanov by analogy with the Levi-Civita antisymmetric unit tensor e^{ikm}. Using ε^{ikm} and ε_{ikm}, we can transform chr.inv.-tensors into chr.inv.-pseudotensors (see §2.3 in our monograph [5]).

Thus, the general covariant energy-momentum tensor of an electromagnetic field

$$T_{\alpha\beta} = \frac{1}{4\pi}\left(-F_{\alpha\sigma}F^{\cdot\sigma}_{\beta\cdot} + \frac{1}{4}\,g_{\alpha\beta}F_{\mu\nu}F^{\mu\nu}\right)$$

has the following chr.inv.-projections

$$\varrho = \frac{T_{00}}{g_{00}} = \frac{1}{8\pi}\left(E_iE^i + H_{*i}H^{*i}\right),$$

$$J^i = \frac{cT^i_0}{\sqrt{g_{00}}} = \frac{c}{4\pi}\,\varepsilon^{ikm}E_kH_{*m},$$

$$U^{ik} = c^2T^{ik} = \varrho c^2h^{ik} - \frac{c^2}{4\pi}\left(E^iE^k + H^{*i}H^{*k}\right).$$

Generally speaking, the mathematical apparatus of chronometric invariants is extensive. We have given above only that part of it that is necessary for understanding this article. For a deeper study of this mathematics, we recommend the respective chapters of our monographs [4, 5], especially — the chapter Tensor Algebra and the Analysis in [5]. You can also study Zelmanov's publications [1–3], of which his 1957 presentation [3] is the most useful and complete.

3 The physical conditions under which the space-time is fully degenerate

To deduce the physical conditions, under which the space-time is fully degenerate, we considered the square of the four-dimensional space-time interval $ds^2 = g_{\alpha\beta}dx^\alpha dx^\beta$ in the form, expressed in terms of chr.inv.-quantities, i.e.

$$ds^2 = c^2d\tau^2 - d\sigma^2,$$

where $d\tau$ is the interval of physically observable time, $d\sigma$ is the physically observable three-dimensional interval

$$d\tau = \left(1 - \frac{\mathrm{w}}{c^2}\right)dt - \frac{1}{c^2}\,v_i\,dx^i, \quad d\sigma^2 = h_{ik}\,dx^i dx^k,$$

while w is the gravitational potential, and v_i is the linear velocity of rotation of the observer's space due to the space-time non-holonomity. Thus, considering the space-time interval the path travelled by a particle, we have

$$ds^2 = c^2d\tau^2\left(1 - \frac{\mathrm{v}^2}{c^2}\right), \qquad \mathrm{v}^i = \frac{dx^i}{d\tau},$$

where v^i is the physically observable chr.inv.-velocity of the particle registered by the observer (see above).

Prior to our study, two types of trajectories and, respectively, two types of particles were known in the General Theory of Relativity. First, these are the so-called non-isotropic trajectories, along which, in terms of chr.inv.-quantities,

$$ds^2 = c^2d\tau^2 - d\sigma^2 \neq 0, \qquad c^2d\tau^2 \neq d\sigma^2 \neq 0.$$

They lie in the so-called non-isotropic region of the space-time, which is home to mass-bearing particles, and "mass-bearing" means that the rest-mass of such a particle is non-zero ($m_0 \neq 0$). The relativistic mass (mass of motion) of such a particle is non-zero too ($m \neq 0$). Such particles make up substances.

Trajectories of the second type are the so-called isotropic trajectories, along which, in terms of chr.inv.-quantities,

$$ds^2 = c^2d\tau^2 - d\sigma^2 = 0, \qquad c^2d\tau^2 = d\sigma^2 \neq 0.$$

They lie in the so-called isotropic region of the space-time, which is home to massless particles, for which "massless" means that the rest-mass of such a particle is equal to zero ($m_0 = 0$), while its relativistic mass (mass of motion) is non-zero ($m \neq 0$). Re-writting $ds^2 = 0$ in the form

$$ds^2 = c^2d\tau^2\left(1 - \frac{\mathrm{v}^2}{c^2}\right) = 0, \qquad c^2d\tau^2 \neq 0,$$

we see that massless particles travel at the velocity of light ($\mathrm{v}^2 = h_{ik}\,\mathrm{v}^i\mathrm{v}^k = c^2$). The latter mean that massless particles are related to the light-like family of particles.

The fact that $ds^2 = c^2d\tau^2 - d\sigma^2 = 0$ and $c^2d\tau^2 = d\sigma^2 \neq 0$ along the isotropic trajectories means that this is a partially degenerate region of the space-time.

Taking the above into account, we logically supposed that the space-time becomes fully degenerate, if

$$ds^2 = c^2d\tau^2 - d\sigma^2 = 0, \quad c^2d\tau^2 = 0, \quad d\sigma^2 = 0.$$

Our expectations found full justification. Below we will explain why.

As it is known from the geometry of metric spaces, a metric space is fully degenerate if the determinant of its metric tensor is equal to zero. In the four-dimensional pseudo-Riemannian space, which is the basic space-time of the General Theory of Relativity, the determinant of the fundamental metric tensor is $g < 0$. This means that the basic space-time of the General Theory of Relativity is non-degenerate.

The condition $d\tau = 0$ means that the physically observable time interval between any two events in this space-time region, when registered by an observer, whose home is the regular (non-degenerate) space-time region, is equal to zero. We re-write $d\tau = 0$ in the form

$$d\tau = \left[1 - \frac{1}{c^2}\left(\mathrm{w} + v_i u^i\right)\right] dt = 0, \qquad u^i = \frac{dx^i}{dt},$$

where u^i is the three-dimensional coordinate velocity of motion with respect to the observer, which is not a physically observable chr.inv.-quantity; the u^i is based on the time coordinate increment dt, which is not equal to zero between the events ($dt \neq 0$).

The condition $d\sigma^2 = 0$ in the extended form is

$$d\sigma^2 = h_{ik}\,dx^i dx^k = 0, \qquad dx^i \neq 0$$

and means that in this space-time region the physically observable three-dimensional distance $d\sigma$ between any two different points ($dx^i \neq 0$) when registered by an observer, whose home is a regular non-degenerate space-time region, is equal to zero. This condition satisfies only if the determinant of the chr.inv.-metric tensor h_{ik} is equal to zero

$$h = \det\| h_{ik}\| = h_{11}h_{22}h_{33} + h_{31}h_{12}h_{23} + h_{21}h_{13}h_{32} - \\ - h_{31}h_{22}h_{13} - h_{21}h_{12}h_{33} - h_{11}h_{23}h_{32} = 0.$$

Zelmanov proved that the determinant of the fundamental metric tensor $g = \det\| g_{\alpha\beta}\|$ is connected with that of the chr.inv.-metric tensor $h = \det\| h_{ik}\|$ by the formula

$$h = -\frac{g}{g_{00}},$$

i.e., once the chr.inv.-metric tensor h_{ik} is degenerate, the fundamental metric tensor $g_{\alpha\beta}$ is degenerate too.

The above is an exact proof to why the entire space of the Universe or a local space region in it, wherein $c^2d\tau^2 = 0$ and $d\sigma^2 = 0$, is fully degenerate. We therefore called such a space-time *zero-space*, while the trajectories that lie in it — *zero-trajectories*.

Using the formulae for $d\tau$ and h_{ik}, we obtained the *physical conditions for full degeneracy*, i.e., the physical conditions in a fully degenerate space-time (zero-space)

$$\mathrm{w} + v_i u^i = c^2, \qquad \left(1 - \frac{\mathrm{w}}{c^2}\right)^2 c^2dt^2 = g_{ik}\,dx^i dx^k.$$

From a geometric point of view, the conditions for full degeneracy mean the following.

Within the infinitesimal vicinity of any point in a Rimeannian space, we can introduce a flat space, which is tangential to the Riemannian space in this point. The latter means that the basis vectors $\vec{e}_{(\alpha)}$ of the tangential flat space are tangential to the curved coordinate lines of the Riemannian space. But, since the coordinate lines in a Riemannian space are curved and non-orthogonal to each other (if the space is non-holonomic), the lengths of the basis vectors $\vec{e}_{(\alpha)}$ in the tangential flat space are different from the unit length. The vector of an infinitesimal displacement in the Riemannian space is expressed through the tangential basis vectors as

$$d\vec{r} = \vec{e}_{(\alpha)}dx^\alpha,$$

and, since the scalar product of the vector $d\vec{r}$ with itself gives $d\vec{r}d\vec{r} = ds^2$ and also it is $ds^2 = g_{\alpha\beta}\,dx^\alpha dx^\beta$, we obtain

$$g_{\alpha\beta} = \vec{e}_{(\alpha)}\vec{e}_{(\beta)} = e_{(\alpha)}e_{(\beta)}\cos(x^\alpha; x^\beta),$$

i.e., $g_{00} = e^2_{(0)}$, $g_{0i} = e_{(0)}e_{(i)}\cos(x^0; x^i)$, $g_{ik} = e_{(i)}e_{(k)}\cos(x^i; x^k)$. Thus, according to the definitions of v_i and h_{ik}, we have

$$v_i = -\,c\,e_{(i)}\cos(x^0; x^i),$$

$$h_{ik} = e_{(i)}e_{(k)}\Big[\cos(x^0; x^i)\cos(x^0; x^k) - \cos(x^i; x^k)\Big].$$

Taking into account that $d\tau = 0$ and $d\sigma^2 = 0$ in the zero-space (the latter, as was shown above, means $h = 0$), we obtain the *geometric conditions for full degeneracy*

$$e_{(0)} = -\,\frac{1}{c}\,e_{(i)}u^i\cos(x^0; x^i),$$

$$\cos(x^0; x^i)\cos(x^0; x^k) = \cos(x^i; x^k).$$

So, once the rotation of the observer's space reaches the light speed, $\cos(x^0; x^i) = 1$ and, thus, $\cos(x^i; x^k) = 1$: the lines of time become "fallen" into the three-dimensional spatial section (time becomes "fallen" into space), wherein all three spatial axes become coinciding with each other.

As for the particles located is the zero-space, their physical sense is derived based on Levi-Civita's rule, according to which, in a Riemannian space of n dimensions the length of

any n-dimensional vector Q^α transferred in parallel to itself remains unchanged ($Q_\alpha Q^\alpha = const$).

As it is known, any mass-bearing particle is characterized by the four-dimensional momentum vector P^α, and any massless (i.e., having the zero rest-mass) particle is characterized by the four-dimensional wave vector K^α,

$$P^\alpha = m_0 \frac{dx^\alpha}{ds}, \qquad K^\alpha = \frac{\omega_0}{c}\frac{dx^\alpha}{ds},$$

each of which is transferred in parallel to itself along the particle's trajectory in the space-time. The chr.inv.-projections of the P^α and K^α onto the time line and the three-dimensional spatial section of a regular observer are equal to

$$\frac{P_0}{\sqrt{g_{00}}} = m, \qquad P^i = \frac{m}{c}\,\mathrm{v}^i,$$

$$\frac{K_0}{\sqrt{g_{00}}} = \frac{\omega}{c}, \qquad K^i = \frac{\omega}{c}\,c^i.$$

To adapt the P^α and K^α to the zero-space condition, we are looking for the condition in their structure. Based on the interval of physically observable time $d\tau$ (page 32), we obtain how the physically observable velocity depends on the condition for full degeneracy $\mathrm{w} + v_i u^i = c^2$, i.e.,

$$\mathrm{v}^i = \frac{u^i}{1 - \frac{1}{c^2}\left(\mathrm{w} + v_k u^k\right)},$$

and then express ds^2 in the form

$$ds^2 = c^2 d\tau^2 \left(1 - \frac{\mathrm{v}^2}{c^2}\right) = c^2 dt^2 \left\{\left[1 - \frac{1}{c^2}\left(\mathrm{w} + v_k u^k\right)\right]^2 - \frac{u^2}{c^2}\right\},$$

which gives

$$P^\alpha = m_0 \frac{dx^\alpha}{ds} = \frac{M}{c}\frac{dx^\alpha}{dt}, \quad K^\alpha = \frac{\omega_0}{c}\frac{dx^\alpha}{ds} = \frac{\omega}{c^2}\frac{dx^\alpha}{dt},$$

where $dt \neq 0$, and

$$M = \frac{m}{1 - \frac{1}{c^2}\left(\mathrm{w} + v_k u^k\right)}, \quad \omega = \frac{\omega}{1 - \frac{1}{c^2}\left(\mathrm{w} + v_k u^k\right)}$$

take the condition for full degeneracy $\mathrm{w} + v_i u^i = c^2$ into account and are not equal to zero in the zero-space.

For zero-space particles, the chr.inv.-projections of their momentum vector P^α and wave vector K^α onto the time line and the three-dimensional space of a regular observer outside the zero-space are equal to

$$\frac{P_0}{\sqrt{g_{00}}} = M\left[1 - \frac{1}{c^2}\left(\mathrm{w} + v_i u^i\right)\right] = 0, \qquad P^i = \frac{1}{c} M u^i \neq 0,$$

$$\frac{K_0}{\sqrt{g_{00}}} = \frac{\omega}{c}\left[1 - \frac{1}{c^2}\left(\mathrm{w} + v_i u^i\right)\right] = 0, \qquad K^i = \frac{1}{c^2}\,\omega u^i \neq 0.$$

The above result means that all zero-space particles have zero rest-masses $m_0 = 0$, zero relativistic masses $m = 0$ and zero relativistic frequencies $\omega = 0$. We therefore called the particles, whose home is the zero-space, *zero-particles*.

This is the third, new type of particles in addition to mass-bearing and massless (light-like) particles, already known in the General Theory of Relativity.

As it is known, for any regular mass-bearing and massless particle (their home is the regular non-degenerate space-time), the relation between its energy and momentum remains unchanged along its trajectory

$$E^2 - c^2 p^2 = const.$$

This follows from Levi-Civita's rule $P_\alpha P^\alpha = const$ and $K_\alpha K^\alpha \neq const$ having the form for mass-bearing particles and massless particles, respectively,

$$E^2 - c^2 p^2 = E_0^2, \qquad E^2 - c^2 p^2 = 0,$$

where $E = mc^2$, $p^2 = m^2 \mathrm{v}^2$, $E_0 = m_0 c^2$. For massless particles this relation, taking into account that $p^2 = m^2 \mathrm{v}^2 = m^2 h_{ik}\,\mathrm{v}^i \mathrm{v}^k$, transforms into the banal formula $h_{ik}\,\mathrm{v}^i \mathrm{v}^k = c^2$ meaning that they travel at the velocity of light.

On the other hand, $P_\alpha P^\alpha \neq const$ and $K_\alpha K^\alpha \neq const$ for zero-particles: anyone can verify this fact by his own calculations based on the above. This fact means that Levi-Civita's rule is violated along the trajectories of zero-particles, and, hence, the observed geometry along their trajectories is not Riemannian.

The said does not necessarily mean that the zero-space geometry is non-Riemannian itself, but only that it looks like that from the point of view of a regular observer.

Of all the types of particles known in modern physics, only virtual particles have $E^2 - c^2 p^2 \neq const$. Feynman diagrams show that virtual particles are carriers of the interaction between elementary particles, i.e., between each two branching points on the diagrams. According to Quantum Electrodynamics, all physical processes in our world are based on the emission and absorption of virtual particles by real mass and massless (light-like) particles.

That is, the interaction between particles in our regular space-time is transmitted through an "exchange buffer" that is the zero-space, while zero-particles transmitting the interaction through this "buffer space" (zero-space) are *virtual particles* known in Quantum Electrodynamics.

The above is the solely interpretation of virtual particles and Feynman diagrams in the framework of the space-time geometry, and is a "bridge" connecting Quantum Electrodynamics with the General Theory of Relativity.

To understand how zero-particles could be registered in an experiment conducted by a regular observer, consider them as waves travelling along their space-time trajectories.

As it is known, any massless particle in the framework of the geometric optics approximation is characterized by the

four-dimensional wave vector determined in the lower-index form K_α through the wave phase ψ called eikonal. In analogy to it, we introduce the four-dimensional momentum vector characteristic of any mass-bearing particle, respectively,

$$K_\alpha = \frac{\partial\psi}{\partial x^\alpha}, \qquad P_\alpha = \frac{\hbar}{c}\frac{\partial\psi}{\partial x^\alpha},$$

where $\hbar$ is Planck's constant. Their physically observable chr.inv.-projections onto the observer's line of time are

$$\frac{K_0}{\sqrt{g_{00}}} = \frac{1}{c}\frac{^*\partial\psi}{\partial t}, \qquad \frac{P_0}{\sqrt{g_{00}}} = \frac{\hbar}{c^2}\frac{^*\partial\psi}{\partial t},$$

and, since these chr.inv.-projections are also equal to ω/c and m (see above), we obtain that, in the framework of the geometric optics approximation,

$$\omega = \frac{^*\partial\psi}{\partial t}, \qquad m = \frac{\hbar}{c^2}\frac{^*\partial\psi}{\partial t}.$$

Therefore, on the transition to the zero-space, i.e., under the condition for full degeneracy $\mathrm{w} + v_i u^i = c^2$, since $\omega = 0$ and $m = 0$ (see above), we obtain

$$\frac{^*\partial\psi}{\partial t} = 0.$$

The eikonal equation $K_\alpha K^\alpha = const$ means that the length of the four-dimensional wave vector transferred in parallel to itself remains unchanged. The chr.inv.-eikonal equation for regular massless (light-like) particles and mass-bearing particles, taking the main property $g_{\alpha\sigma}g^{\beta\sigma} = \delta^\beta_\alpha$ of the fundamental metric tensor $g_{\alpha\beta}$ into account, has the form, respectively,

$$\frac{1}{c^2}\left(\frac{^*\partial\psi}{\partial t}\right)^2 - h^{ik}\frac{^*\partial\psi}{\partial x^i}\frac{^*\partial\psi}{\partial x^k} = 0,$$

$$\frac{1}{c^2}\left(\frac{^*\partial\psi}{\partial t}\right)^2 - h^{ik}\frac{^*\partial\psi}{\partial x^i}\frac{^*\partial\psi}{\partial x^k} = \frac{m_0^2c^2}{\hbar^2},$$

and is a travelling wave equation. On the transition to the zero-space, the above eikonal equations take the same form

$$h^{ik}\frac{^*\partial\psi}{\partial x^i}\frac{^*\partial\psi}{\partial x^k} = 0,$$

which is a standing wave equation.

To understand the result we have obtained, we should take into account the fact that a regular observer does not register zero-space objects themselves, but only what he sees on the transition to or from the zero-space (we assume that Levi-Civita's rule is satisfied on this boundary), and the zero-space itself is the fully degenerate case of the isotropic space (home to massless light-like particles).

Therefore, zero-particles, i.e., all particles, whose home is the zero-space, should appear to a regular observer outside the zero-space as *standing light waves*, while the zero-space should appear as a point containing a system of standing light waves (a *light-like hologram*) inside itself.

4 Non-quantum teleportation

Teleportation is the instant displacement of particles from one point in the three-dimensional space to another.

Initially, scientists considered only quantum teleportation. In fact, quantum teleportation is not a real instant displacement, but a "probabilistic trick" based on the laws of Quantum Mechanics [7]. This is despite the fact that, using quantum teleportation, photons were first "teleported" in 1998 [8], and atoms were "teleported" in 2004 [9, 10].

On the contrary, we considered instant displacement in accordance with the geometric structure of the space-time of the General Theory of Relativity, which is real teleportation without any "probabilistic tricks". This is why we called this regular non-quantum method of particle teleportation *non-quantum teleportation*.

In terms of physically observable chr.inv.-quantities, teleportation is a process of displacement in which the interval of physically observable time between its beginning and end is equal to zero ($d\tau = 0$). If a mass-bearing particle is teleported (mass-bearing particles make up substances), the teleportation condition $d\tau = 0$ is added with the physically observable three-dimensional interval between the point of departure and the point of arrival, which is not equal to zero, i.e. $d\sigma \neq 0$. Therefore, the space-time metric along the trajectories of non-quantum teleportation of mass-bearing particles is

$$ds^2 = c^2d\tau^2 - d\sigma^2 = -d\sigma^2, \quad c^2d\tau^2 = 0, \quad d\sigma^2 \neq 0.$$

Since $d\sigma^2 = h_{ik}dx^idx^k$ and taking into account the condition $\mathrm{w} + v_i u^i = c^2$ under which $d\tau = 0$, the space-time metric takes the form, which we called the *non-quantum teleportation metric*

$$ds^2 = -d\sigma^2 = -\left(1 - \frac{\mathrm{w}}{c^2}\right)^2 c^2dt^2 + g_{ik}dx^idx^k = \\ = -\frac{1}{c^2}v_iu^iv_ku^kdt^2 + g_{ik}dx^idx^k.$$

As you can see, in the non-quantum teleportation metric, the regular signature $(+---)$ of space-time is replaced with the inverted signature $(-+++)$. That is, from the point of view of a regular observer, "time" and "space" are replaced with each other on the teleportation trajectories: "time" of a teleporting particle is "space" of a regular observer, and "space" of the teleporting particle is "time" of the regular observer.

The same is true for the non-quantum teleportation metric, derived for massless (light-like) particles. If a massless (light-like) particle is teleported, the teleportation condition $d\tau = 0$ is added with $c^2d\tau^2 = d\sigma^2$, since the latter is characteristic of the isotropic region of the space-time, which is home to such particles. Therefore, the space-time metric along the trajectories of non-quantum teleportation of massless (light-like) particles is fully degenerate

$$ds^2 = c^2d\tau^2 - d\sigma^2 = 0, \qquad c^2d\tau^2 = d\sigma^2 = 0,$$

which means that the trajectories along which massless particles are teleported lie in the fully degenerate space-time (zero-space). The equation of such trajectories is derived from the non-quantum teleportation metric (see above) equalized to zero, and is the fully degenerate light hypercone equation

$$\left(1 - \frac{\mathrm{w}}{c^2}\right)^2 c^2 dt^2 = g_{ik}\, dx^i dx^k.$$

So, according to the General Theory of Relativity, as soon as we realize the physical condition

$$\mathrm{w} + v_i u^i = c^2$$

in the local space inside a device in our laboratory (under this condition, $d\tau = 0$), a mass-bearing or massless (light-like) particle that is inside this device enters a teleportation trajectory and, thus, can be instantly teleported to any other place in our Universe. For this reason, we call $\mathrm{w} + v_i u^i = c^2$ also the *physical condition for non-quantum teleportation*.

5 Finding the teleportation condition accessible in a real laboratory. Problem statement

The above results, which we obtained in the early 1990s, were presented in our two monographs in 2001 [4, 5], and then in the brief article [6]. The reason for such a long overview of these results in the present article is that without a detailed acquaintance with the above results, it would be impossible to understand everything that follows, including the engineering implementation of non-quantum teleportation at any distance in our Universe.

So, the physical condition $\mathrm{w} + v_i u^i = c^2$ under which the interval of physically observable time is degenerate ($d\tau = 0$) is also the physical condition for non-quantum teleportation. To implement this physical condition, a super-strong gravitational potential and a near-light-speed rotation of the observer's space are required. Obviously, in a real laboratory, this is extremely difficult, if not impossible.

On the other hand, when deriving the teleportation condition $\mathrm{w} + v_i u^i = c^2$ from $d\tau = 0$, we did not indicate the formulas for the individual components of the fundamental metric tensor $g_{\alpha\beta}$ and the chr.inv.-metric tensor h_{ik}. That is, we did not specify the specific local space of the real laboratory in which we are going to teleport particles.

It is obvious that, as soon as we specify the metric of the local space in a real laboratory, the teleportation condition derived from this metric will be different from its general form $\mathrm{w} + v_i u^i = c^2$. Say, we have an electromagnetic field generator installed and running in our laboratory. If so, then the local space in our laboratory has an electromagnetic field. Accordingly, we expect that the characteristics of the electromagnetic field will appear in the teleportation condition derived from $d\tau = 0$. In particular, if the generated electromagnetic field is super-strong (this is not a big problem when using modern technologies), then the numerical values of the electromagnetic field terms in the teleportation condition can be so significant that "replace" the gravitational potential and rotation of the laboratory space. In such a case, the teleportation condition, i.e., the condition under which particles enter teleportation trajectories and, thus, can be instantly teleported to any other place in our Universe, can be implemented in a real laboratory.

Which specific space metric is suitable for a real laboratory? Such a local space is connected either with the Earth, or with another planet, or with another star system, and, at first glance, is described by Schwarzschild's mass-point metric. On the other hand, the mass-point metric does not take into account the rotation of space, which is one of the two "core" factors in the teleportation condition $\mathrm{w} + v_i u^i = c^2$. Another drawback is that the space described by the mass-point metric is filled only with a gravitational field, and does not have an electromagnetic field. The third drawback is that the gravitational field is so weak in a real earth-bound laboratory that this factor can be neglected in the teleportation condition.

We therefore have drafted the following research plan for the next Sections of this article.

At our first step we will derive and analyze the teleportation condition for each of the three most popular space metrics. These are Schwarzschild's mass-point metric, Schwarzschild's metric inside a sphere filled with an incompressible liquid and de Sitter's metric of a space filled with the physical vacuum. Then, based on the above metrics, we will introduce three similar metrics containing a three-dimensional rotation due to the space-time non-holonomity (expressed by $g_{0i} \neq 0$). After that we will derive and analyze the teleportation condition in each of these three types of rotating space.

At our second step, we will introduce the metric of a space that rotates due to the space-time non-holonomity, but free from the gravitational field. This metric will be our "working metric" in this research.

It is not a fact that the introduced metric containing rotation describes a Riemannian space. As it is known, a Riemannian space metric must not only have the Riemann square form $ds^2 = g_{\alpha\beta}\, dx^\alpha dx^\beta$, determined by the Riemann fundamental metric tensor $g_{\alpha\beta}$, and be invariant $ds^2 = inv$ everywhere in the space. It must also satisfy Einstein's field equations — the relation between the Ricci curvature tensor, the fundamental metric tensor multiplied by the curvature scalar, and the energy-momentum tensor of the "space filler", which is satisfied in any Riemannian space. The latter means that as soon as we substitute the components of the fundamental metric tensor $g_{\alpha\beta}$ (taken from the formula of a particular Riemannian space metric) and the components of the energy-momentum tensor of the medium filling the space into the component notation of the field equations, this must turn the field equations into the zero identity. This is why not many space metrics are proven to be Riemannian and, thus, are used in the General Theory of Relativity.

So, most likely, the introduced metric containing rotation will turn out to be non-Riemannian due to the term taking the

three-dimensional space rotation into account.

To correct this situation, at our second step, we will take the $g_{\alpha\beta}$ components from the introduced metric, then substitute them into the chr.inv.-Einstein equations, the right hand side of which is non-zero and contains the energy-momentum tensor of an electromagnetic field. The relations that vanish the resulting chr.inv.-Einstein equations (we call them the *Riemannian conditions*), are the conditions under which the metric is Riemannian and describes a non-holonomic (rotating) space-time filled with an electromagnetic field.

Please note that, as was found by Zelmanov (see page 33), the physically observable chr.inv.-curvature of a space is depended on not only the acting gravitational inertial force, but also the space rotation and deformation, and, therefore, does not vanish in the absence of the gravitational field.

At our third step, we will consider the teleportation condition, derived for the introduced metric containing rotation, and the Riemannian conditions for this metric in the presence of an electromagnetic field (the latter follow from the Einstein equations, see above).

The obtained system of equations will show how strong the electromagnetic field should be and what additional conditions are required to launch particles on teleportation trajectories in a slow rotating laboratory space. Super-strong electromagnetic fields are not a big problem when using modern technologies. For this reason, the obtained electromagnetic field parameters and additional conditions will show how, under the conditions of a real earth-bound laboratory, real physical bodies and photons can be instantly teleported to any other place in our Universe.

6 The teleportation condition in the space of a mass-point body

Schwarzschild's mass-point metric describes a spherically symmetric space filled with the gravitational field created in emptiness by a spherically symmetrical massive island, which is considered as a point-like mass. The metric has the form

$$ds^2 = \left(1 - \frac{r_g}{r}\right)c^2dt^2 - \frac{dr^2}{1 - \frac{r_g}{r}} - r^2\left(d\theta^2 + \sin^2\theta\, d\varphi^2\right),$$

where r is the distance from the centre of the island, while $r_g = 2GM/c^2$ is its gravitational radius.

Here and below, in terms of the spherical coordinates, r is the radial coordinate, θ is the polar angle, φ is the geographical longitude, dr is the elementary segment length along the r-axis, $r\,d\theta$ is the elementary arc length along the θ-axis, and $r\sin\theta\, d\varphi$ is the elementary arc length along the φ-axis.

Therefore, the non-zero components of the fundamental metric tensor $g_{\alpha\beta}$ of the mass-point metric expressed in terms of the spherical coordinates are equal to

$$g_{00} = 1 - \frac{r_g}{r},\quad g_{11} = -\frac{1}{1 - \frac{r_g}{r}},\quad g_{22} = -r^2,\quad g_{33} = -r^2\sin^2\theta.$$

With the above $g_{\alpha\beta}$ components, we obtain that the interval of physically observable time in the space of the mass-point metric has the form

$$d\tau = \sqrt{g_{00}}\, dt + \frac{g_{0i}}{c\sqrt{g_{00}}}\, dx^i = \sqrt{1 - \frac{r_g}{r}}\, dt,$$

and the teleportation condition, which is $d\tau = 0$ with $dt \neq 0$, has the following form

$$1 - \frac{r_g}{r} = 0 \quad \Longrightarrow \quad r = r_g.$$

In addition to the above, because g_{00} is expressed through the gravitational potential w in the form

$$g_{00} = \left(1 - \frac{\mathrm{w}}{c^2}\right)^2,$$

the obtained teleportation condition can be re-written as

$$1 - \frac{\mathrm{w}}{c^2} = 0 \quad \Longrightarrow \quad \mathrm{w} = c^2.$$

The obtained result means that, in the space of the mass-point metric, i.e., in the field of a spherically symmetric non-rotating mass, a particle enters a teleportation trajectory under the condition of gravitational collapse, i.e., on the surface of a gravitational collapsar.

In other words, if you are in the field of a spherically symmetric non-rotating mass, in order to launch a particle on a teleportation trajectory, you need to simulate a mini black hole in your laboratory.

7 The teleportation condition in the space of a rotating mass-point body

Introduce a mass-point metric, where a gravitational field is created in emptiness by a spherically symmetrical massive island, which rotates due to the space-time non-holonomity. We use Schwarzschild's mass-point metric as a basis. Assume that the space rotates along the φ-axis (along the geographical longitudes) with the linear velocity $v_3 = \omega r^2\sin^2\theta$, where $\omega = const$ is the angular velocity of this rotation. Since, according to the definition of v_i,

$$v_3 = \omega r^2\sin^2\theta = -\frac{c\, g_{03}}{\sqrt{g_{00}}},$$

we obtain

$$g_{03} = -\frac{1}{c}\, v_3\sqrt{g_{00}} = -\frac{\omega r^2\sin^2\theta}{c}\sqrt{1 - \frac{r_g}{r}},$$

and, thus, we obtain a Schwarzschild-like mass-point metric containing the above rotation, i.e.,

$$ds^2 = \left(1 - \frac{r_g}{r}\right)c^2dt^2 - 2\,\omega r^2\sin^2\theta\sqrt{1 - \frac{r_g}{r}}\, dt\, d\varphi - \frac{dr^2}{1 - \frac{r_g}{r}} - r^2\left(d\theta^2 + \sin^2\theta\, d\varphi^2\right).$$

Accordingly, the interval of physically observable time in the rotating space of the Schwarzschild-like metric we have introduced is

$$d\tau = \sqrt{g_{00}}\,dt + \frac{g_{0i}}{c\sqrt{g_{00}}}\,dx^i = \left(\sqrt{1-\frac{r_g}{r}} - \frac{\omega r^2\sin^2\theta}{c^2}\,\frac{d\varphi}{dt}\right)dt,$$

and the teleportation condition, i.e., $d\tau = 0$ with $dt \neq 0$, written in the spherical coordinates has the form

$$\sqrt{1-\frac{r_g}{r}} - \frac{\omega r^2\sin^2\theta}{c^2}\,\frac{d\varphi}{dt} = 0,$$

or, that is the same

$$\mathrm{w} + \omega r^2\sin^2\theta\,\frac{d\varphi}{dt} = c^2,$$

where $\sin\theta = 1$ for the observer's laboratory located at the equator, and the last multiplier is the coordinate velocity of the teleporting particle along the φ-direction, which is the geographical longitude (we assume that the particle travels either in the same or in the opposite direction in which the space rotates).

This condition is different from that in the space of the Schwarzschild mass-point metric in only the second term depending on the rotation of space due to the space-time non-holonomity: the faster the rotation of space and the faster the teleporting particle, the farther the teleportation trajectory from the surface of gravitational collapse.

8 The teleportation condition in the space inside a liquid sphere

Consider the metric of the space inside a liquid sphere, which was introduced by Schwarzschild. It describes the space inside a sphere, which is not empty, but filled with an incompressible liquid. The gravitational field inside such a sphere is created by a spherically symmetrical imcompressible liquid that fills it. As it is known, this metric has the form

$$ds^2 = \frac{1}{4}\left(3\sqrt{1-\frac{r_g}{a}} - \sqrt{1-\frac{r^2 r_g}{a^3}}\right)^2 c^2dt^2 - \frac{dr^2}{1-\frac{r^2 r_g}{a^3}} - r^2\left(d\theta^2 + \sin^2\theta\,d\varphi^2\right),$$

where $r_g = 2GM/c^2$ is the gravitational radius calculated for the entire mass M of the liquid (source of the gravitational field) inside the sphere, and $a = const$ is the radius of the sphere. Respectively, the non-zero components of the fundamental metric tensor $g_{\alpha\beta}$ of this metric are

$$g_{00} = \frac{1}{4}\left(3\sqrt{1-\frac{r_g}{a}} - \sqrt{1-\frac{r^2 r_g}{a^3}}\right)^2,$$

$$g_{11} = -\frac{1}{1-\frac{r^2 r_g}{a^3}}, \quad g_{22} = -r^2, \quad g_{33} = -r^2\sin^2\theta.$$

As a result, we obtain that the interval of physically observable time inside such a sphere has the form

$$d\tau = \sqrt{g_{00}}\,dt + \frac{g_{0i}}{c\sqrt{g_{00}}}\,dx^i = \frac{1}{2}\left(3\sqrt{1-\frac{r_g}{a}} - \sqrt{1-\frac{r^2 r_g}{a^3}}\right)dt,$$

and the teleportation condition, i.e., $d\tau = 0$ with $dt \neq 0$, has the following form

$$3\sqrt{1-\frac{r_g}{a}} - \sqrt{1-\frac{r^2 r_g}{a^3}} = 0.$$

The obtained formula is a condition under which a particle enters a teleportation trajectory inside a sphere filled with an incompressible liquid.

It is obvious that the obtained teleportation condition is satisfied if

$$r = r_g = a,$$

which means that a particle enters a teleportation trajectory on only the surface of the liquid sphere (where the particle's radial coordinate is $r = a$), and the liquid sphere is a gravitational collapsar ($a = r_g$).

9 The teleportation condition in the space inside a rotating liquid sphere

Introduce the metric of the space inside a sphere filled with an incompressible liquid, which rotates due to the space-time non-holonomity.

We use the metric of a liquid sphere as a basis. Assume that the liquid sphere has a radius $a = const$, a mass M and rotates along the φ-axis (along the geographical longitudes) with the linear velocity $v_3 = \omega r^2\sin^2\theta$, where $\omega = const$ is the angular velocity of this rotation. With these characteristic parameters, according to the definition of v_i, we obtain

$$v_3 = \omega r^2\sin^2\theta = -\frac{c\,g_{03}}{\sqrt{g_{00}}},$$

$$g_{03} = -\frac{1}{c}\,v_3\sqrt{g_{00}} = -\frac{\omega r^2\sin^2\theta}{2c}\left(3\sqrt{1-\frac{r_g}{a}} - \sqrt{1-\frac{r^2 r_g}{a^3}}\right).$$

Thus, the metric inside such a rotating liquid sphere is

$$ds^2 = \frac{1}{4}\left(3\sqrt{1-\frac{r_g}{a}} - \sqrt{1-\frac{r^2 r_g}{a^3}}\right)^2 c^2dt^2 - \omega r^2\sin^2\theta\left(3\sqrt{1-\frac{r_g}{a}} - \sqrt{1-\frac{r^2 r_g}{a^3}}\right)dt\,d\varphi - \frac{dr^2}{1-\frac{r^2 r_g}{a^3}} - r^2\left(d\theta^2 + \sin^2\theta\,d\varphi^2\right).$$

Therefore, the interval of physically observable time inside such a rotating sphere has the form

$$d\tau = \sqrt{g_{00}}\,dt + \frac{g_{0i}}{c\sqrt{g_{00}}}\,dx^i = \\ = \left\{\frac{1}{2}\left(3\sqrt{1-\frac{r_g}{a}} - \sqrt{1-\frac{r^2 r_g}{a^3}}\right) - \frac{\omega r^2 \sin^2\theta}{c^2}\,\frac{d\varphi}{dt}\right\} dt.$$

where $\sin\theta = 1$ for the observer's laboratory located at the equator, and the last multiplier is the coordinate velocity of the teleporting particle along the φ-direction, which is the geographical longitude (we assume that the particle travels either in the same or in the opposite direction in which the space rotates).

As a result, the teleportation condition ($d\tau = 0$ with $dt \neq 0$) inside such a rotating liquid sphere has the form

$$\frac{1}{2}\left(3\sqrt{1-\frac{r_g}{a}} - \sqrt{1-\frac{r^2 r_g}{a^3}}\right) - \frac{\omega r^2 \sin^2\theta}{c^2}\,\frac{d\varphi}{dt} = 0.$$

This is a condition under which a particle enters a teleportation trajectory inside the space of a rotating sphere filled with an incompressible liquid. It is different from that in the space inside a non-rotating liquid sphere in only the second term depending on the rotation of space due to the space-time non-holonomity. The smaller the gravitational radius r_g of the rotating liquid sphere and the smaller the distance r from the centre of the sphere, the faster the sphere should rotate and a particle should travel in order for this particle to enter a teleportation trajectory.

According to the obtained teleportation condition, two ultimate cases of particle teleportation are conceivable in the space inside a rotating liquid sphere.

1. In the first ultimate case of particle teleportation, the gravitational radius r_g of the liquid sphere is much smaller than the distance r of the teleporting particle from the centre of the sphere, and this distance r is much smaller than the radius a of the sphere

$$r_g \ll r, \qquad r \ll a,$$

which is possible if the liquid sphere has a small mass, the liquid itself is very rarefied, and the teleporting particle is close to the centre of the sphere.

In this case, the obtained teleportation condition takes the simplified form

$$\omega r^2 \sin^2\theta\,\frac{d\varphi}{dt} = c^2,$$

i.e., the liquid sphere should rotate at the velocity of light and the particle should travel at the velocity of light in order for this particle to enter a teleportation trajectory.

2. In the second ultimate case of particle teleportation,

$$r r_g = a^2 \quad \Longrightarrow \quad r = r_g = a,$$

and g_{00} of the metric is equal to zero

$$g_{00} = \frac{1}{4}\left(3\sqrt{1-\frac{r_g}{a}} - \sqrt{1-\frac{r^2 r_g}{a^3}}\right)^2 = 0,$$

which means gravitational collapse. In this case, the teleporting particle is on the surface of the liquid sphere, which is a gravitational collapsar. In this case, the obtained teleportation condition takes the form

$$\omega r^2 \sin^2\theta\,\frac{d\varphi}{dt} = 0 \quad \Longrightarrow \quad \frac{d\varphi}{dt} = 0,$$

which means that the teleporting particle rests with respect to the liquid sphere, since the sphere rotates ($v_3 \neq 0$) according to the initial formulation of the problem.

In other words, in order for a particle to enter a teleportation trajectory on the surface of a liquid sphere, which is a gravitational collapsar, the particle should be at rest with respect to the sphere.

10 The teleportation condition in the space filled with the physical vacuum

De Sitter's metric describes a space filled with the physical vacuum (λ-field) and does not include any island of mass or a distributed matter. The curvature is the same everywhere in such a space, so it is a constant curvature space. The physical vacuum (λ-field) produces a non-Newtonian gravitational force, which is proportional to the distance in the space, i.e., the force of non-Newtonian gravitation (λ-force) grows with distance. If $\lambda < 0$, it is an attraction force. If $\lambda > 0$, it is a repulsion force.

For details about the physical vacuum, its physically observable properties, and also the non-Newtonian gravitational force, see Chapter 5 in our monograph [5].

As it is known, de Sitter's metric has the form

$$ds^2 = \left(1 - \frac{\lambda r^2}{3}\right)c^2 dt^2 - \frac{dr^2}{1-\frac{\lambda r^2}{3}} - r^2\left(d\theta^2 + \sin^2\theta\,d\varphi^2\right),$$

and, hence, the non-zero components of the fundamental metric tensor $g_{\alpha\beta}$ of this metric are

$$g_{00} = 1 - \frac{\lambda r^2}{3}, \quad g_{11} = -\frac{1}{1-\frac{\lambda r^2}{3}}, \quad g_{22} = -r^2, \quad g_{33} = -r^2\sin^2\theta.$$

Using these components, we obtain that the interval of physically observable time in a de Sitter space is

$$d\tau = \sqrt{g_{00}}\,dt + \frac{g_{0i}}{c\sqrt{g_{00}}}\,dx^i = \sqrt{1-\frac{\lambda r^2}{3}}\,dt,$$

and the teleportation condition, i.e., $d\tau = 0$ with $dt \neq 0$, has the following form

$$1 - \frac{\lambda r^2}{3} = 0 \quad \Longrightarrow \quad r = \sqrt{\frac{3}{\lambda}},$$

where, since $\lambda = const$, the r means the maximum distance in the space. As it is known, $\lambda \leqslant 10^{-56}$ cm^{-2} with today's measurement accuracy. So, if our Universe is a de Sitter space, the maximum distance in it is $r \geqslant 10^{28}$ cm.

In addition, the teleportation condition we have obtained above means that the space is in the state of collapse, i.e.,

$$g_{00} = 1 - \frac{\lambda r^2}{3} = 0.$$

The above means that a particle in a de Sitter space, i.e., in a space filled with the physical vacuum in the absence of any other matter, enters a teleportation trajectory at the maximum distance from the observer, which is conceivable in the space. Besides that, since the state of collapse occurs at the same distance from the observer, we conclude that the entire space should be in the state of collapse, i.e., the entire space filled with the physical vacuum should be a collapsar.

11 The teleportation condition in the rotating space filled with the physical vacuum

Introduce the metric of a space filled with the physical vacuum in the absence of other matter, which rotates due to the space-time non-holonomity.

We derive the metric based on de Sitter's metric. Assume that the space rotates along the φ-axis (along the geographical longitudes) with the linear velocity $v_3 = \omega r^2 \sin^2\theta$, where $\omega = const$ is the angular velocity of this rotation. Thus, according to the definition of v_i, we obtain

$$v_3 = \omega r^2 \sin^2\theta = -\frac{c\, g_{03}}{\sqrt{g_{00}}},$$

$$g_{03} = -\frac{1}{c}\, v_3 \sqrt{g_{00}} = -\frac{\omega r^2 \sin^2\theta}{c} \sqrt{1 - \frac{\lambda r^2}{3}}\,.$$

As a result, we obtain the metric of a rotating space filled with the physical vacuum

$$ds^2 = \left(1 - \frac{\lambda r^2}{3}\right) c^2 dt^2 - 2\,\omega r^2 \sin^2\theta \sqrt{1 - \frac{\lambda r^2}{3}}\, dt\, d\varphi - \\ - \frac{dr^2}{1 - \frac{\lambda r^2}{3}} - r^2 \left(d\theta^2 + \sin^2\theta\, d\varphi^2\right),$$

and, hence, the interval of physically observable time in such a space has the form

$$d\tau = \sqrt{g_{00}}\, dt + \frac{g_{0i}}{c\sqrt{g_{00}}}\, dx^i = \\ = \left(\sqrt{1 - \frac{\lambda r^2}{3}} - \frac{\omega r^2 \sin^2\theta}{c^2}\, \frac{d\varphi}{dt}\right) dt,$$

and the teleportation condition ($d\tau = 0$ with $dt \neq 0$) has the following form

$$\sqrt{1 - \frac{\lambda r^2}{3}} - \frac{\omega r^2 \sin^2\theta}{c^2}\, \frac{d\varphi}{dt} = 0,$$

where r is the distance between the teleporting particle and the observer, $\sin\theta = 1$ for the observer's laboratory located at the equator, and the last multiplier is the coordinate velocity of the teleporting particle along the φ-direction, which is the geographical longitude (assuming that the particle travels either in the same or in the opposite direction in which the space rotates).

The above formula we have obtained is the condition under which a particle enters a teleportation trajectory in a rotating de Sitter space, which is a rotating space filled with the physical vacuum in the absence of any other matter.

According to the obtained teleportation condition, two ultimate cases are conceivable for particle teleportation in a rotating de Sitter space.

1. In the first ultimate case of particle teleportation,

$$\lambda r^2 \ll 1,$$

and the obtained teleportation condition takes the following simplified form

$$\omega r^2 \sin^2\theta\, \frac{d\varphi}{dt} = c^2.$$

Since $\lambda \leqslant 10^{-56}$ cm^{-2} (according to modern astronomy), in this ultimate case of particle teleportation in a rotating de Sitter space, the teleporting particle should be at the distance $r \ll 10^{28}$ cm from the observer. In addition, the space should rotate at the velocity of light and the particle should travel at the velocity of light.

2. In the second ultimate case of particle teleportation, the teleporting particle should be very far from the observer

$$r = \sqrt{\frac{3}{\lambda}} \geqslant 10^{28} \text{ cm},$$

i.e., at the edge of the observable Universe or even beyond that observable edge.

In this case, g_{00} of the metric is equal to zero

$$g_{00} = 1 - \frac{\lambda r^2}{3} = 0,$$

which means that the space is in the state of collapse (i.e., the entire space is a huge collapsar), and the obtained teleportation condition takes the form

$$\omega r^2 \sin^2\theta\, \frac{d\varphi}{dt} = 0 \quad \Longrightarrow \quad \frac{d\varphi}{dt} = 0,$$

which, since the space rotates ($v_3 \neq 0$), means that the teleporting particle is at rest.

In other words, in the second ultimate case of particle teleportation in a rotating de Sitter space, the teleporting particle should be resting with respect to the space, be at the maximum distance from the observer, which is conceivable in the space, while the entire space should be in the state of collapse (it should be a huge collapsar).

12 The metric of the space, which rotates, but is free from the gravitational field

Introduce the metric of a space, where the three-dimensional space rotates due to the space-time non-holonomity, but there is no field of gravitation. This space metric most accurately describes the local space of an observer, who is located in an earth-bound laboratory, since the gravitational potential on the Earth's surface is so weak that its factor under the teleportation condition can be neglected. Only the factors of rotation of space and the teleporting particle's speed affect teleportation in this case. An addition, in the space of this metric, the effect of rotation of space due to the space-time non-holonomity is most clearly manifested.

For the above reasons, we will deduce the characteristics of such a simplest rotating space in more detail.

Assuming that the space rotates along the φ-axis (along the geographical longitudes) with the velocity $v_3 = \omega r^2 \sin^2\theta$, where $\omega = const$ is the angular velocity of this rotation, and, according to the definition of v_i,

$$v_3 = \omega r^2 \sin^2\theta = -\frac{c\, g_{03}}{\sqrt{g_{00}}}, \qquad g_{03} = -\frac{\omega r^2 \sin^2\theta}{c},$$

we obtain the metric of such a space. It has the form

$$ds^2 = c^2 dt^2 - 2\omega r^2 \sin^2\theta\, dt\, d\varphi - \\ - dr^2 - r^2\left(d\theta^2 + \sin^2\theta\, d\varphi^2\right),$$

where the rest non-zero components of the fundamental metric tensor $g_{\alpha\beta}$ are

$$g_{00} = 1, \quad g_{11} = -1, \quad g_{22} = -r^2, \quad g_{33} = -r^2 \sin^2\theta.$$

So forth, using the general formula for the chr.inv.-metric tensor, which is

$$h_{ik} = -g_{ik} + \frac{g_{0i}\, g_{0k}}{g_{00}} = -g_{ik} + \frac{1}{c^2}\, v_i\, v_k,$$

we obtain that its non-zero components in the specific space we are considering are equal to

$$h_{11} = 1, \quad h_{22} = r^2, \quad h_{33} = r^2 \sin^2\theta\left(1 + \frac{\omega^2 r^2 \sin^2\theta}{c^2}\right),$$

$$h^{11} = 1, \quad h^{22} = \frac{1}{r^2}, \quad h^{33} = \frac{1}{r^2 \sin^2\theta\left(1 + \frac{\omega^2 r^2 \sin^2\theta}{c^2}\right)},$$

where, since the matrix h_{ik} is diagonal, the upper-index components of h_{ik} are obtained as $h^{ik} = (h_{ik})^{-1}$ just like the invertible matrix components to any diagonal matrix.

To check the correctness of the above construction of the space metric, we calculate $v^2 = v_i v^i = h_{ik} v^i v^k$. Since $v^i = h^{ik} v_k$, we obtain the following

$$v^2 = v_i v^i = \frac{\omega^2 r^2 \sin^2\theta}{1 + \frac{\omega^2 r^2 \sin^2\theta}{c^2}}, \qquad v = \frac{\omega r \sin\theta}{\sqrt{1 + \frac{\omega^2 r^2 \sin^2\theta}{c^2}}},$$

hence, the dimension of v is [cm/sec]. If the space rotates slowly, the above formula transforms to $v = \omega r \sin\theta$ [cm/sec] that is completely "comme il faut".

Based on the above formula for v_3 and using the corresponding h^{ik} components, we obtain that the antisymmetric chr.inv.-tensor of the angular velocity of rotation of space, A_{ik} (see page 32), has the following non-zero components

$$A_{13} = \omega r \sin^2\theta, \qquad A_{31} = -A_{13},$$

$$A_{23} = \omega r^2 \sin\theta\cos\theta, \qquad A_{32} = -A_{23},$$

$$A^{13} = \frac{\omega}{r\left(1 + \frac{\omega^2 r^2 \sin^2\theta}{c^2}\right)}, \qquad A^{31} = -A^{13},$$

$$A^{23} = \frac{\omega \cot\theta}{r^2\left(1 + \frac{\omega^2 r^2 \sin^2\theta}{c^2}\right)}, \qquad A^{32} = -A^{23}.$$

To check the correctness of the above, we calculate the square of the chr.inv.-pseudovector of the angular velocity of rotation of space, $\Omega^2 = \Omega_{*i}\Omega^{*i} = h_{ik}\,\Omega^{*i}\Omega^{*i}$. Since

$$\Omega^{*i} = \frac{1}{2}\,\varepsilon^{ikm} A_{km}, \quad \varepsilon^{ikm} = \frac{e^{ikm}}{\sqrt{h}}, \quad \Omega_{*i} = h_{ik}\,\Omega^{*k}$$

as for any pseudovector (see page 34 in this paper; for more details on pseudovectors and pseudotensors see §2.3 of our monograph [5]), after some algebra we obtain

$$\Omega^2 = \Omega_{*i}\Omega^{*i} = \frac{\omega^2}{1 + \frac{\omega^2 r^2 \sin^2\theta}{c^2}}, \quad \Omega = \frac{\omega}{\sqrt{1 + \frac{\omega^2 r^2 \sin^2\theta}{c^2}}},$$

so, the dimension of Ω is $[\sec^{-1}]$. If the space rotates slowly, the obtained formula transforms to $\Omega = \omega$ $[\sec^{-1}]$ that is completely "comme il faut".

Using the non-zero h_{ik} components, we obtain the determinant of the chr.inv.-metric tensor h_{ik} (see page 35)

$$h = \det\| h_{ik} \| = r^4 \sin^2\theta\left(1 + \frac{\omega^2 r^2 \sin^2\theta}{c^2}\right).$$

So forth, we obtain nonzero chr.inv.-derivatives of $\ln\sqrt{h}$. According to the mathematical apparatus of chronometric invariants, they are equal to the respective chr.inv.-Christoffel symbols, in which two indices have been contracted, i.e., Δ^i_{ik}. Such Christoffel symbols are used in our further calculation of the chr.inv.-divergence of A^{ik}, as well as the chr.inv.-Ricci curvature tensor C_{ik}, which are the left hand side terms of the chr.inv.-Einstein equations. After some algebra, we obtain

$$\Delta^i_{i1} = \frac{{}^*\partial \ln\sqrt{h}}{\partial r} = \frac{2}{r\left(1 + \frac{\omega^2 r^2 \sin^2\theta}{c^2}\right)}\left(1 + \frac{3\,\omega^2 r^2 \sin^2\theta}{2\,c^2}\right),$$

$$\Delta^i_{i2} = \frac{{}^*\partial \ln\sqrt{h}}{\partial \theta} = \frac{\cot\theta}{1 + \frac{\omega^2 r^2 \sin^2\theta}{c^2}}\left(1 + \frac{2\,\omega^2 r^2 \sin^2\theta}{c^2}\right),$$

as well as their chr.inv.-derivatives

$$\frac{{}^{*}\partial\Delta^i_{i1}}{\partial r} = -\frac{2}{r^2\left(1+\frac{\omega^2r^2\sin^2\theta}{c^2}\right)^2} - \frac{3\,\omega^2\sin^2\theta}{c^2\left(1+\frac{\omega^2r^2\sin^2\theta}{c^2}\right)^2} - \frac{3\,\omega^4r^2\sin^4\theta}{c^4\left(1+\frac{\omega^2r^2\sin^2\theta}{c^2}\right)^2},$$

$$\frac{{}^{*}\partial\Delta^i_{i1}}{\partial\theta} = \frac{2\,\omega^2r\sin\theta\cos\theta}{c^2\left(1+\frac{\omega^2r^2\sin^2\theta}{c^2}\right)^2},$$

$$\frac{{}^{*}\partial\Delta^i_{i2}}{\partial r} = \frac{2\,\omega^2r\sin\theta\cos\theta}{c^2\left(1+\frac{\omega^2r^2\sin^2\theta}{c^2}\right)^2} = \frac{{}^{*}\partial\Delta^i_{i1}}{\partial\theta},$$

$$\frac{{}^{*}\partial\Delta^i_{i2}}{\partial\theta} = -\frac{1}{\sin^2\theta\left(1+\frac{\omega^2r^2\sin^2\theta}{c^2}\right)} - \frac{2\,\omega^2r^2\sin^2\theta}{c^2\left(1+\frac{\omega^2r^2\sin^2\theta}{c^2}\right)^2} - \frac{2\,\omega^4r^4\sin^2\theta}{c^4\left(1+\frac{\omega^2r^2\sin^4\theta}{c^2}\right)^2}.$$

The chr.inv.-Ricci curvature tensor C_{lk} is one of the terms contained in the tensorial equation of the chr.inv.-Einstein equations (see page 33). Its formula (page 33) is based on the chr.inv.-Christoffel symbols Δ^i_{jk} and their chr.inv.-derivatives. Therefore, to calculate the chr.inv.-Ricci curvature tensor C_{lk} in the specific space we are considering, we need to calculate the chr.inv.-Christoffel symbols. They are re-combinations of the chr.inv.-derivatives of the chr.inv.-metric tensor h_{ik} (see page 33). Thus, first, we obtain non-zero chr.inv.-derivatives of the chr.inv.-metric tensor h_{ik} for the space we are considering. They have the form

$$\frac{{}^{*}\partial h_{22}}{\partial r} = 2r,$$

$$\frac{{}^{*}\partial h_{33}}{\partial r} = 2r\sin^2\theta\left(1+\frac{2\,\omega^2r^2\sin^2\theta}{c^2}\right),$$

$$\frac{{}^{*}\partial h_{33}}{\partial\theta} = 2r^2\sin\theta\cos\theta\left(1+\frac{2\,\omega^2r^2\sin^2\theta}{c^2}\right).$$

So forth, according to the general formula for the chr.inv.-Christoffel symbols (see page 33), we calculate all them one by one in the specific space we are considering. After some algebra, we obtain formulae for those of them that are different from zero, i.e.,

$$\Delta^1_{22} = -r,$$

$$\Delta^1_{33} = -r\sin^2\theta\left(1+\frac{2\,\omega^2r^2\sin^2\theta}{c^2}\right),$$

$$\Delta^2_{12} = \Delta^2_{21} = \frac{1}{r},$$

$$\Delta^2_{33} = -\sin\theta\cos\theta\left(1+\frac{2\,\omega^2r^2\sin^2\theta}{c^2}\right),$$

$$\Delta^3_{13} = \Delta^3_{13} = \frac{1}{r\left(1+\frac{\omega^2r^2\sin^2\theta}{c^2}\right)}\left(1+\frac{2\,\omega^2r^2\sin^2\theta}{c^2}\right),$$

$$\Delta^3_{23} = \Delta^3_{32} = \frac{\cot\theta}{1+\frac{\omega^2r^2\sin^2\theta}{c^2}}\left(1+\frac{2\,\omega^2r^2\sin^2\theta}{c^2}\right).$$

Then, we look for non-zero components of the contracted 4th rank chr.inv.-tensor $H^{\cdots i}_{lki\cdot}$, which, since the space we are considering is free from deformations ($D_{ik}=0$), is equal to the chr.inv.-Ricci curvature tensor C_{lk} (for the full formulae of the chr.inv.-curvature tensors see page 33)

$$C_{lk} = C^{\cdots i}_{lki\cdot} = H^{\cdots i}_{lki\cdot} = \frac{{}^{*}\partial\Delta^i_{il}}{\partial x^k} - \frac{{}^{*}\partial\Delta^i_{kl}}{\partial x^i} + \Delta^m_{il}\Delta^i_{km} - \Delta^m_{kl}\Delta^i_{im},$$

where, according to the mathematical apparatus of chronometric invariants (see page 33), we have

$$\Delta^i_{ik} = \frac{{}^{*}\partial\ln\sqrt{h}}{\partial x^k}.$$

As a result, we obtain that the chr.inv.-Ricci tensor in the specific space we are considering has the following non-zero components

$$C_{11} = H^{\cdots i}_{11i\cdot} = \frac{{}^{*}\partial\Delta^i_{i1}}{\partial r} + \Delta^2_{21}\Delta^2_{12} + \Delta^3_{31}\Delta^3_{13},$$

$$C_{12} = H^{\cdots i}_{12i\cdot} = \frac{{}^{*}\partial\Delta^i_{i1}}{\partial\theta} + \Delta^3_{31}\Delta^3_{23} - \Delta^2_{21}\Delta^i_{i2},$$

$$C_{21} = H^{\cdots i}_{21i\cdot} = \frac{{}^{*}\partial\Delta^i_{i2}}{\partial r} + \Delta^3_{32}\Delta^3_{13} - \Delta^2_{12}\Delta^i_{i2},$$

$$C_{22} = H^{\cdots i}_{22i\cdot} = \frac{{}^{*}\partial\Delta^i_{i2}}{\partial\theta} - \frac{{}^{*}\partial\Delta^1_{22}}{\partial r} + 2\Delta^2_{12}\Delta^1_{22} + \Delta^3_{32}\Delta^3_{23} - \Delta^1_{22}\Delta^i_{i1},$$

$$C_{33} = H^{\cdots i}_{33i\cdot} = -\frac{{}^{*}\partial\Delta^1_{33}}{\partial r} - \frac{{}^{*}\partial\Delta^2_{33}}{\partial\theta} + 2\Delta^3_{13}\Delta^1_{33} + 2\Delta^3_{23}\Delta^2_{33} - \Delta^1_{33}\Delta^i_{i1} - \Delta^2_{33}\Delta^i_{i2},$$

where

$$\Delta^i_{i1} = \frac{{}^{*}\partial\ln\sqrt{h}}{\partial r}, \qquad \Delta^i_{i2} = \frac{{}^{*}\partial\ln\sqrt{h}}{\partial\theta}.$$

To calculate the components of the chr.inv.-Ricci tensor, we already have the specific formulae for Δ^i_{i1} and Δ^i_{i2} in the metric we are considering (see page 43). In addition, we need formulae for the chr.inv.-derivatives of Δ^1_{33} with respect to r and Δ^2_{33} with respect to θ, which are contained in the chr.inv.-Ricci tensor. We obtain that they are equal to

$$\frac{{}^{*}\partial\Delta^1_{33}}{\partial r} = -\sin^2\theta\left(1+\frac{6\,\omega^2r^2\sin^2\theta}{c^2}\right),$$

$$\frac{{}^{*}\partial\Delta^2_{33}}{\partial\theta} = \sin^2\theta + \frac{2\,\omega^2r^2\sin^4\theta}{c^2} - \cos^2\theta - \frac{6\,\omega^2r^2\sin^2\theta\cos^2\theta}{c^2}.$$

So forth, after some algebra, we obtain formulae for the non-zero components of the chr.inv.-Ricci tensor

$$C_{11} = \frac{3\,\omega^2 \sin^2\theta}{c^2\left(1+\frac{\omega^2 r^2\sin^2\theta}{c^2}\right)} - \frac{\omega^4 r^2 \sin^4\theta}{c^4\left(1+\frac{\omega^2 r^2\sin^2\theta}{c^2}\right)^2},$$

$$C_{12} = \frac{3\,\omega^2 r \sin\theta\cos\theta}{c^2\left(1+\frac{\omega^2 r^2\sin^2\theta}{c^2}\right)} - \frac{\omega^4 r^3 \sin^3\theta\cos\theta}{c^4\left(1+\frac{\omega^2 r^2\sin^2\theta}{c^2}\right)^2},$$

$$C_{21} = \frac{3\,\omega^2 r \sin\theta\cos\theta}{c^2\left(1+\frac{\omega^2 r^2\sin^2\theta}{c^2}\right)} - \frac{\omega^4 r^3 \sin^3\theta\cos\theta}{c^4\left(1+\frac{\omega^2 r^2\sin^2\theta}{c^2}\right)^2},$$

$$C_{22} = \frac{3\,\omega^2 r^2 \cos^2\theta}{c^2\left(1+\frac{\omega^2 r^2\sin^2\theta}{c^2}\right)} - \frac{\omega^4 r^4 \sin^2\theta\cos^2\theta}{c^4\left(1+\frac{\omega^2 r^2\sin^2\theta}{c^2}\right)^2},$$

$$C_{33} = \frac{3\,\omega^2 r^2 \sin^2\theta}{c^2} - \frac{\omega^4 r^4 \sin^4\theta}{c^4\left(1+\frac{\omega^2 r^2\sin^2\theta}{c^2}\right)},$$

where, in particular, we see that $C_{12} = C_{21}$ that means a certain curvature symmetry in the space we are considering.

As a result, the physically observable chr.inv.-scalar curvature $C = h^{lk}C_{lk}$ (see page 33) of the rotating space we are considering is equal to

$$C = \frac{6\,\omega^2}{c^2\left(1+\frac{\omega^2 r^2\sin^2\theta}{c^2}\right)} - \frac{2\,\omega^4 r^2 \sin^2\theta}{c^4\left(1+\frac{\omega^2 r^2\sin^2\theta}{c^2}\right)^2},$$

i.e., the origin of the physically observable chr.inv.-curvature of such a space is only its three-dimensional rotation due to the space-time non-holonomity (non-orthogonality of the time lines to the three-dimensional spatial section).

As you can see, the obtained formula for the scalar curvature and also every component of the obtained chr.inv.-Ricci curvature tensor (used in the chr.inv.-Einstein equations, see below) consists of two terms: the first order term, the goal of which is very significant, and the second order (additional) term, the influence of which is tiny. When Larissa first saw the above formulae, she immediately said: "You just made a fundamental theoretical discovery: if a space rotates due its space-time non-holonomity, its curvature produces the first order effect."

The above characteristics of the space we are considering will be used further to calculate the individual components of the chr.inv.-Einstein equations in this space.

So forth, we obtain that the interval of physically observable time in such a rotating space has the formula

$$d\tau = \sqrt{g_{00}}\,dt + \frac{g_{0i}}{c\,\sqrt{g_{00}}}\,dx^i = \left(1 - \frac{\omega\, r^2\sin^2\theta}{c^2}\,\frac{d\varphi}{dt}\right)dt,$$

where $\sin\theta = 1$ (the polar angle θ is equal to $\frac{\pi}{2}$) for the observer's laboratory located at the equator, and the last multiplier is the coordinate velocity of the teleporting particle along the φ-direction, which is the geographical longitude (assuming that it travels either in the same or in the opposite direction in which the space rotates).

As a result, we obtain that the teleportation condition, i.e., $d\tau = 0$ with $dt \neq 0$, has the form

$$\omega\, r^2\sin^2\theta\,\frac{d\varphi}{dt} = c^2.$$

The obtained formula is the teleportation condition in a rotating space that is free from the field of gravitation and a distributed matter. In this case, as you can see from the above formula, a particle enters a teleportation trajectory in such a space, if it travels at the velocity of light, and the space rotates at the velocity of light.

Next, we will look how this condition changes if the rotating space is not empty, but filled with an electromagnetic field. To do it we will consider Einstein's field equations for a space of the above metric, where the right hand side of the equations is non-zero, but contains the energy-momentum tensor of the electromagnetic field (such Einstein equations characterize a space filled with an electromagnetic field).

As it is known, Einstein's equations are one of the necessary conditions for a space metric to be Riemannian. Therefore, the considered rotating space filled with an electromagnetic field is Riemannian under some particular conditions by which the Einstein equations for this space metric vanish (for this reason we call them *Riemannian conditions*).

We hope, the derived Riemannian conditions will somehow replace the rotation of space (the main factor in the teleportation condition) with the electromagnetic field parameters, thereby giving us the opportunity to "strengthen" the space-time non-holonomity to the level necessary for particle teleportation without the need to mechanically rotate the observer's local space at the light speed.

13 Using Einstein's field equations to find conditions under which the introduced metric is Riemannian

In an empty rotating space of the metric we have introduced above, the gravitational inertial force, the space deformation and the λ-term are equal to zero, while the space curvature and rotation are non-zero

$$F_i = 0, \quad D_{ik} = 0, \quad \lambda = 0, \quad C_{ik} \neq 0, \quad A_{ik} \neq 0.$$

The chr.inv.-Einstein equations (for their full formulae see page 33) very simplify under the above conditions. If the rotating space is filled with a distributed matter, they have the non-zero right hand side and take the form

$$\left.\begin{aligned} & A_{ik}A^{ki} = -\frac{\varkappa}{2}\left(\varrho c^2 + U\right) \\ & {}^{*}\nabla_k A^{ik} = -\varkappa J^i \\ & 2A_{ij}A^{\cdot j}_{k\cdot} - c^2 C_{ik} = \frac{\varkappa}{2}\left(\varrho c^2 h_{ik} + 2U_{ik} - U h_{ik}\right) \end{aligned}\right\},$$

where the right hand side contains the physically observable projections of the energy-momentum tensor of the matter that fills the space: ϱ is the chr.inv.-density of the field energy, J^i is the chr.inv.-density of the field momentum, and U^{ik} is the chr.inv.-stress-tensor of the field.

Calculate $U = h_{mn}U^{mn}$, i.e., the trace of the electromagnetic field chr.inv.-stress-tensor U^{ik} (see page 34). Since the trace of the chr.inv.-metric tensor is $h_{mn}h^{mn} = 3$, we obtain $U = \varrho c^2$. Thus, the chr.inv.-Einstein equations in a rotating space filled with an electromagnetic field have the form

$$\left.\begin{aligned} & A_{ik}A^{ki} = -\varkappa\varrho c^2 \\ & {}^{*}\nabla_k A^{ik} = -\varkappa J^i \\ & 2A_{ij}A^{\cdot j}_{k\cdot} - c^2 C_{ik} = \varkappa U_{ik} \end{aligned}\right\},$$

or, extending the electromagnetic field characteristics,

$$\left.\begin{aligned} & A_{ik}A^{ki} = -\frac{\varkappa c^2}{8\pi}\left(E_i E^i + H_{*i}H^{*i}\right) \\ & {}^{*}\nabla_k A^{ik} = -\frac{\varkappa c}{4\pi}\,\varepsilon^{ikm}E_k H_{*m} \\ & 2A_{ij}A^{\cdot j}_{k\cdot} - c^2 C_{ik} = \\ & \quad = \frac{\varkappa c^2}{8\pi}\left(E_j E^j + H_{*j}H^{*j}\right)h_{ik} - \frac{\varkappa c^2}{4\pi}\left(E_i E_k + H_{*i}H_{*k}\right) \end{aligned}\right\}.$$

Taking into account the characteristics of the space metric we are considering (see above), after some algebra we obtain non-zero components of the left hand side terms

$$A_{ik}A^{ki} = -\frac{2\omega^2}{1+\frac{\omega^2 r^2\sin^2\theta}{c^2}},$$

$${}^{*}\nabla_k A^{3k} = \frac{\omega}{r^2\sin^2\theta\left(1+\frac{\omega^2 r^2\sin^2\theta}{c^2}\right)}\left\{1+\frac{2\omega^2 r^2\sin^2\theta}{c^2\left(1+\frac{\omega^2 r^2\sin^2\theta}{c^2}\right)}\right\},$$

$$2A_{1j}A^{\cdot j}_{1\cdot} - c^2 C_{11} = -\frac{\omega^2\sin^2\theta}{1+\frac{\omega^2 r^2\sin^2\theta}{c^2}} + \frac{\omega^4 r^2\sin^4\theta}{c^2\left(1+\frac{\omega^2 r^2\sin^2\theta}{c^2}\right)^2},$$

$$2A_{1j}A^{\cdot j}_{2\cdot} - c^2 C_{12} = -\frac{\omega^2 r\sin\theta\cos\theta}{1+\frac{\omega^2 r^2\sin^2\theta}{c^2}} + \frac{\omega^4 r^3\sin^3\theta\cos\theta}{c^2\left(1+\frac{\omega^2 r^2\sin^2\theta}{c^2}\right)^2},$$

$$2A_{2j}A^{\cdot j}_{1\cdot} - c^2 C_{21} = -\frac{\omega^2 r\sin\theta\cos\theta}{1+\frac{\omega^2 r^2\sin^2\theta}{c^2}} + \frac{\omega^4 r^3\sin^3\theta\cos\theta}{c^2\left(1+\frac{\omega^2 r^2\sin^2\theta}{c^2}\right)^2},$$

$$2A_{2j}A^{\cdot j}_{2\cdot} - c^2 C_{22} = -\frac{\omega^2 r^2\cos^2\theta}{1+\frac{\omega^2 r^2\sin^2\theta}{c^2}} + \frac{\omega^4 r^4\sin^2\theta\cos^2\theta}{c^2\left(1+\frac{\omega^2 r^2\sin^2\theta}{c^2}\right)^2},$$

$$2A_{3j}A^{\cdot j}_{3\cdot} - c^2 C_{33} = -\omega^2 r^2\sin^2\theta + \frac{\omega^4 r^4\sin^4\theta}{c^2\left(1+\frac{\omega^2 r^2\sin^2\theta}{c^2}\right)}.$$

We see that the left hand side of the chr.inv.-Einstein equations does not vanish. This means that a rotating space characterized by the considered metric is not Riemannian, if it is empty. To be Riemannian, such a space must be filled with a distributed matter so that the right hand side of the Einstein equations equalized the non-zero left hand side.

Using the obtained left hand side of the chr.inv.-Einstein equations, as well as the formulae for the electromagnetic field characteristics ϱ, J^i, U_{ik} (see page 34), we get the above chr.inv.-Einstein equations in the final form

$$\left.\begin{aligned} & \frac{\omega^2}{1+\frac{\omega^2 r^2\sin^2\theta}{c^2}} = \frac{\varkappa c^2}{16\pi}\left(E_i E^i + H_{*i}H^{*i}\right) \\ & \frac{\omega}{r^2\sin^2\theta\left(1+\frac{\omega^2 r^2\sin^2\theta}{c^2}\right)}\left\{1+\frac{2\omega^2 r^2\sin^2\theta}{c^2\left(1+\frac{\omega^2 r^2\sin^2\theta}{c^2}\right)}\right\} = \\ & \qquad = -\frac{\varkappa c}{4\pi}\,\varepsilon^{3km}E_k H_{*m} \\ & \frac{\omega^2(2+\sin^2\theta)}{1+\frac{\omega^2 r^2\sin^2\theta}{c^2}} - \frac{\omega^4 r^2\sin^4\theta}{c^2\left(1+\frac{\omega^2 r^2\sin^2\theta}{c^2}\right)^2} = \\ & \qquad = \frac{\varkappa c^2}{4\pi}\left(E_1 E_1 + H_{*1}H_{*1}\right) \\ & \frac{\omega^2 r\sin\theta\cos\theta}{1+\frac{\omega^2 r^2\sin^2\theta}{c^2}} - \frac{\omega^4 r^3\sin^3\theta\cos\theta}{c^2\left(1+\frac{\omega^2 r^2\sin^2\theta}{c^2}\right)^2} = \\ & \qquad = \frac{\varkappa c^2}{4\pi}\left(E_1 E_2 + H_{*1}H_{*2}\right) \\ & \frac{\omega^2 r\sin\theta\cos\theta}{1+\frac{\omega^2 r^2\sin^2\theta}{c^2}} - \frac{\omega^4 r^3\sin^3\theta\cos\theta}{c^2\left(1+\frac{\omega^2 r^2\sin^2\theta}{c^2}\right)^2} = \\ & \qquad = \frac{\varkappa c^2}{4\pi}\left(E_2 E_1 + H_{*2}H_{*1}\right) \\ & \frac{\omega^2 r^2(2+\cos^2\theta)}{1+\frac{\omega^2 r^2\sin^2\theta}{c^2}} - \frac{\omega^4 r^4\sin^2\theta\cos^2\theta}{c^2\left(1+\frac{\omega^2 r^2\sin^2\theta}{c^2}\right)^2} = \\ & \qquad = \frac{\varkappa c^2}{4\pi}\left(E_2 E_2 + H_{*2}H_{*2}\right) \\ & 3\omega^2 r^2\sin^2\theta - \frac{\omega^4 r^4\sin^4\theta}{c^2\left(1+\frac{\omega^2 r^2\sin^2\theta}{c^2}\right)} = \\ & \qquad = \frac{\varkappa c^2}{4\pi}\left(E_3 E_3 + H_{*3}H_{*3}\right) \end{aligned}\right\},$$

where the right hand side is expressed through the chr.inv.-electric strength vector E^i and the chr.inv.-magnetic strength pseudovector H^{*i} of the field (see page 34 for detail).

Note that the dimension of the electric and magnetic field strengths here is $[\mathrm{gram}^{1/2}\,\mathrm{cm}^{-3/2}]$ as well as everywhere in the

relativistic electrodynamics. To avoid confusion, we note that in our earlier works for these quantities we used the "electromagnetic" dimension $[\mathrm{gram}^{1/2}\,\mathrm{cm}^{-1/2}\,\mathrm{sec}^{-1}]$, as is customary in Classical Electrodynamics and technology. It is different from the above by a unit coefficient, the dimension of which is the same as that of the velocity of light.

Mathematically, the obtained chr.inv.-Einstein equations mean that a rotating space filled with an electromagnetic field of the specific configuration, as indicated in the equations, is Riemannian. Therefore, the above Einstein equations are the *Riemannian conditions* for this space metric. That is, we can consider a rotating space in the General Theory of Relativity only if it is filled with an electromagnetic field of the specific structure determined by the Einstein equations.

14 The structure of the electromagnetic field

To obtain some information about the structure of the particular electromagnetic field determined by the obtained Einstein equations, we analyze the equations in detail.

The scalar and tensorial equations give trivial relations between E and H.

Since just one component ${}^*\nabla_k A^{3k}$ of the vectorial Einstein equation is non-zero, ${}^*\nabla_k A^{1k}=0$ and ${}^*\nabla_k A^{2k}=0$ give

$$\varepsilon^{1km}E_k H_{*m}=\varepsilon^{123}E_2H_{*3}+\varepsilon^{132}E_3H_{*2}=0,$$
$$\varepsilon^{2km}E_k H_{*m}=\varepsilon^{213}E_1H_{*3}+\varepsilon^{231}E_3H_{*1}=0,$$

from which, since $\varepsilon^{123}=-\varepsilon^{132}=\varepsilon^{312}$ and so on, we obtain

$$E_2H_{*3}-E_3H_{*2}=0,$$
$$E_1H_{*3}-E_3H_{*1}=0.$$

The non-zero vectorial Einstein equation means

$$\varepsilon^{3km}E_k H_{*m}=\varepsilon^{312}E_1H_{*2}+\varepsilon^{321}E_2H_{*1}=$$
$$=-\frac{4\pi\omega}{\varkappa c\,r^2\sin^2\theta\left(1+\frac{\omega^2r^2\sin^2\theta}{c^2}\right)}\left\{1+\frac{2\omega^2r^2\sin^2\theta}{c^2\left(1+\frac{\omega^2r^2\sin^2\theta}{c^2}\right)}\right\},$$

which, taking into account that (see page 34)

$$\varepsilon^{ikm}=\frac{e^{ikm}}{\sqrt{h}},\quad e^{123}=+1,\quad e^{312}=-e^{132}=e^{123}=+1,$$

gives the following

$$E_1H_{*2}-E_2H_{*1}=$$
$$=-\frac{4\pi\omega}{\varkappa c\sin\theta\sqrt{1+\frac{\omega^2r^2\sin^2\theta}{c^2}}}\left\{1+\frac{2\omega^2r^2\sin^2\theta}{c^2\left(1+\frac{\omega^2r^2\sin^2\theta}{c^2}\right)}\right\}.$$

Taking the above into account, we conclude that the electromagnetic field determined by the obtained Einstein equations is characterized by the system of relations

$$\left.\begin{aligned}
&E^2+H^2=\frac{16\pi\omega^2}{\varkappa c^2\left(1+\frac{\omega^2r^2\sin^2\theta}{c^2}\right)}\\
&E_2H_{*3}-E_3H_{*2}=0\\
&E_1H_{*3}-E_3H_{*1}=0\\
&E_1H_{*2}-E_2H_{*1}=\\
&\quad=-\frac{4\pi\omega}{\varkappa c\sin\theta\sqrt{1+\frac{\omega^2r^2\sin^2\theta}{c^2}}}\left\{1+\frac{2\omega^2r^2\sin^2\theta}{c^2\left(1+\frac{\omega^2r^2\sin^2\theta}{c^2}\right)}\right\}\\
&E_1E_1+H_{*1}H_{*1}=\\
&\quad=\frac{4\pi}{\varkappa c^2}\left\{\frac{\omega^2(2+\sin^2\theta)}{1+\frac{\omega^2r^2\sin^2\theta}{c^2}}-\frac{\omega^4r^2\sin^4\theta}{c^2\left(1+\frac{\omega^2r^2\sin^2\theta}{c^2}\right)^2}\right\}\\
&E_1E_2+H_{*1}H_{*2}=\\
&\quad=\frac{4\pi}{\varkappa c^2}\left\{\frac{\omega^2r\sin\theta\cos\theta}{1+\frac{\omega^2r^2\sin^2\theta}{c^2}}-\frac{\omega^4r^3\sin^3\theta\cos\theta}{c^2\left(1+\frac{\omega^2r^2\sin^2\theta}{c^2}\right)^2}\right\}\\
&E_2E_2+H_{*2}H_{*2}=\\
&\quad=\frac{4\pi}{\varkappa c^2}\left\{\frac{\omega^2r^2(2+\cos^2\theta)}{1+\frac{\omega^2r^2\sin^2\theta}{c^2}}-\frac{\omega^4r^4\sin^2\theta\cos^2\theta}{c^2\left(1+\frac{\omega^2r^2\sin^2\theta}{c^2}\right)^2}\right\}\\
&E_3E_3+H_{*3}H_{*3}=\\
&\quad=\frac{4\pi}{\varkappa c^2}\left\{3\omega^2r^2\sin^2\theta-\frac{\omega^4r^4\sin^4\theta}{c^2\left(1+\frac{\omega^2r^2\sin^2\theta}{c^2}\right)}\right\}
\end{aligned}\right\},$$

which at small ω simplifies to

$$\left.\begin{aligned}
&E^2+H^2=\frac{16\pi\omega^2}{\varkappa c^2}\\
&E_2H_{*3}-E_3H_{*2}=0\\
&E_1H_{*3}-E_3H_{*1}=0\\
&E_1H_{*2}-E_2H_{*1}=-\frac{4\pi\omega}{\varkappa c\sin\theta}\\
&E_1E_1+H_{*1}H_{*1}=\frac{4\pi\omega^2(2+\sin^2\theta)}{\varkappa c^2}\\
&E_1E_2+H_{*1}H_{*2}=\frac{4\pi\omega^2r\sin\theta\cos\theta}{\varkappa c^2}\\
&E_2E_2+H_{*2}H_{*2}=\frac{4\pi\omega^2r^2(2+\cos^2\theta)}{\varkappa c^2}\\
&E_3E_3+H_{*3}H_{*3}=\frac{12\pi\omega^2r^2\sin^2\theta}{\varkappa c^2}
\end{aligned}\right\}.$$

Please note that $E^2 = E_i E^i = h_{ik} E^i E^k$ and $H^2 = H_{*i} H^{*i} = = h_{ik} H^{*i} H^{*k}$. The θ denotes the polar angle, i.e., $\sin\theta = 1$ and $\cos\theta = 0$ in the laboratory located at the equator.

What do the above relations between the electric and magnetic strength of the field mean and how to implement them in a real laboratory is rather better to ask engineers.

15 Non-quantum teleportation in the condition of a real laboratory using a strong electromagnetic field

Looking at the obtained Einstein equations (see page 46), you can see that the mechanical rotation of space, which appears due to the non-holonomity of the space-time, can be replaced by the magnetic or electric strength of the electromagnetic field that fills the space. Two natural questions arise in this regard: 1) Why is this even possible? 2) Is it possible to increase the space-time non-holonomity by an electromagnetic field in a real laboratory to such a level as to realize the non-quantum teleportation condition?

1. To understand why this is possible, you need to understand what is the three-dimensional rotation of space due to the non-holonomity of the space-time. An ordinary three-dimensional rotation is expressed in terms of $g_{ik} \neq 0$ in the space metric and, therefore, can be removed by a coordinate transformation (moving to another, non-rotating coordinate system on the observer's reference body). On the contrary, a rotation resulting from the non-orthogonality of the time lines to the three-dimensional spatial section originates from $g_{0i} \neq 0$ in the metric, and, therefore is not removable by a coordinate transformation; this is one of the fundamental properties of the observer's reference space.

For example, consider an observer in a laboratory located on the surface of the Earth. For him, the ordinary rotation expressed in terms of $g_{ik} \neq 0$, which can be removed by a coordinate transformation, is the rotation of an observed external body, say, the Moon. On the contrary, the non-removable rotation expressed in terms of $g_{0i} \neq 0$ is the rotation of his reference body, the Earth, around its own axis.

In terms of the basis vectors $\vec{e}_{(\alpha)}$ tangential to the curved coordinate lines of the Riemannian space (see page 35),

$$g_{0i} = e_{(0)} e_{(i)} \cos(x^0; x^i), \quad v_i = -c\, e_{(i)} \cos(x^0; x^i),$$

which means that the linear velocity v_i of such rotation is merely a manifestation of the inclination of the time coordinate lines to the three-dimensional spatial section. Cosine takes numeric values from $+1$ to -1. The length of the tangential basis vectors is equal to 1 in the absence of perturbing factors and decreases with increasing curvature of the coordinate lines. Therefore, such rotation of space cannot be mechanically increased to superluminal speed.

On the other hand, according to the obtained Einstein equations, the stronger the electromagnetic field, the faster the rotation of space: the limit for increasing the rotation of space is only the power of the electromagnetic field generator installed in your laboratory. This is because the angular velocity ω of rotation of space contained in them (and in the teleportation condition) has the same origin as the angular velocity ω in the definition of v_i.

As a result, we arrive at the conclusion that there are two types of rotation of space, which cannot be removed by a coordinate transformation. The source of the first type of rotation is a mechanical rotation of the observer's reference body, say, the planet Earth. Such rotation cannot exceed the speed of light. The second type is a "virtual rotation" that appears in a space filled with a distributed matter, due to the non-zero right hand side of the Einstein equations. Such "virtual rotation" is formally added to the first type of rotation of space, despite the fact that the observer's reference body still mechanically rotates at its own rotation speed, as before. This summation occurs because the angular velocity ω of both types of rotation has the same mathematical origin. For example, the Einstein equations showed that such "virtual rotation" can be as fast as the electromagnetic field strong.

This situation is similar to that with the equations of motion of particles. A free particle travels along a geodesic (i.e., shortest) trajectory. The equation of its motion is the equation of geodesic line: the right hand side of the equation is equal to zero. If an external factor perturbs the particle's motion, it deviates from the geodesic line. In this case, its motion is non-geodesic, and the equation of its motion contains the deviating force on the right hand side.

2. Now a second question arises: can we increase ω with an electromagnetic field to the level necessary to implement the teleportation condition in a real laboratory? To answer this question, let us consider the scalar chr.inv.-Einstein equation we have obtained (see page 46)

$$E^2 + H^2 = \frac{16\pi\omega^2}{\varkappa c^2 \left(1 + \frac{\omega^2 r^2 \sin^2\theta}{c^2}\right)}.$$

If the electric component of the electromagnetic field is much weaker than its magnetic component ($E \ll H$), then in the first order approximation we obtain the relation

$$\omega \approx \sqrt{\frac{\varkappa c^2}{16\pi}}\, H$$

connecting the angular velocity of the "virtual rotation" of space with the magnetic strength of the electromagnetic field (which is the source of this "virtual rotation").

On the other hand, the non-quantum teleportation condition is a rotating space filled with an electromagnetic field has the form (see page 45)

$$\omega r^2 \sin^2\theta \frac{d\varphi}{dt} = c^2,$$

where we assume that the space rotates with the linear velocity $v_3 = \omega r^2 \sin^2\theta$ along the φ-axis (geographical latitude),

$\omega = const$ is the angular velocity of this rotation, and the last multiplier is the coordinate velocity $\widetilde{\omega}$ of the teleporting particle along the φ-direction (we assume that the particle travels either in the same or in the opposite direction in which the space rotates).

Assume that the observer's laboratory is located on the Earth's equator. In this case, $\sin\theta = 1$. Then the ω necessary to launch a particle onto a teleportation trajectory in the observer's laboratory has the form

$$\omega = \frac{c^2}{\widetilde{\omega} r^2}.$$

Substituting here the formula for ω obtained above from the scalar chr.inv.-Einstein equation, we obtain the magnetic strength required for non-quantum teleportation in the condition of the earth-bound laboratory

$$H \approx \sqrt{\frac{16\pi}{\varkappa}}\,\frac{c}{\widetilde{\omega} r^2}.$$

That is, as soon as the magnetic strength inside the experimental setup reaches a numerical value according to this formula (and with the configuration of the electromagnetic field according to the obtained Einstein equations), a teleportation channel opens between this experimental setup and another remote experimental setup located anywhere else in the Universe. Synchronization of these two experimental setups is implemented using the same fine tuning of the magnetic field configuration and other characteristics, which allows physical bodies to be teleported only between these two setups, and not to some other place in the Universe.

Regarding the specific numerical value of H, necessary to implement the teleportation condition in the earth-bound laboratory, it depends on the understanding of the physical sense of the $\widetilde{\omega}$ and r in the above formula, as well as on the system of dimensions of electromagnetic quantities. Meanwhile, even on the basis of draft calculations and other information (that cannot be made public), we are sure that such an experimental setup is quite possible using a super-powerful pulsed magnetic field generator. These specific calculations, as well as the creation of such an experimental setup, are a task for engineers rather than for a theoretical physicist who is far from technology.

A century ago, Nikola Tesla claimed that the use of superstrong electromagnetic fields will allow us to travel instantly to any point in the Universe. We have no idea where he got this information from. Nevertheless, we are very glad that the words he uttered a century ago have now received a solid mathematical foundation in Einstein's theory.

Submitted on January 24, 2022

References

1. Zelmanov A. L. Chronometric Invariants. Translated from the 1944 PhD thesis, American Research Press, Rehoboth, New Mexico, 2006.
2. Zelmanov A. L. Chronometric invariants and accompanying frames of reference in the General Theory of Relativity. *Soviet Physics Doklady*, 1956, v. 1, 227–230 (translated from *Doklady Academii Nauk USSR*, 1956, v. 107, issue 6, 815–818).
3. Zelmanov A. L. On the relativistic theory of an anisotropic inhomogeneous universe. *The Abraham Zelmanov Journal*, 2008, vol. 1, 33–63 (translated from the thesis of the *6th Soviet Conference on the Problems of Cosmogony*, USSR Academy of Sciences Publishers, Moscow, 1957, 144–174).
4. Rabounski D and Borissova L. Particles Here and Beyond the Mirror. The 3rd expanded edition, American Research Press, Rehoboth, New Mexico, 2012 (the 1st edition was issued in 2001).
   Rabounski D. et Borissova L. Particules de l'Univers et au delà du Miroir. American Research Press, Rehoboth, New Mexico, 2012 (French translation).
5. Borissova L. and Rabounski D. Fields, Vacuum, and the Mirror Universe. The 2nd expanded edition, Svenska fysikarkivet, Stockholm, 2009 (the 1st edition was issued in 2001).
   Borissova L. et Rabounski D. Champs, Vide, et Univers miroir. American Research Press, Rehoboth, New Mexico, 2010 (French translation).
6. Rabounski D. and Borissova L. On the possibility of instant displacements in the space-time of General Relativity. *Progress in Physics*, 2005, v. 1, issue 1, 17–19.
7. Bennett C. H., Brassard G., Crepeau C., Jozsa R., Peres A., and Wootters W. K. Teleporting an unknown quantum state via dual classical and Einstein-Podolsky-Rosen channels. *Physical Review Letters*, 1993, v. 70, 1895–1899.
8. Boschi D., Branca S., De Martini F., Hardy L., and Popescu S. Experimental realization of teleporting an unknown pure quantum state via dual classical and Einstein-Podolsky-Rosen Channels. *Physical Review Letters*, 1998, v. 80, 1121–1125.
9. Riebe M., Häffner H., Roos C. F., Hänsel W., Benhelm J., Lancaster G. P. T., Korber T. W., Becher C., Schmidt-Kaler F., James D. F. V., and Blatt R. Deterministic quantum teleportation with atoms. *Nature*, 2004, v. 429, 734–736.
10. Barrett M. D., Chiaverini J., Schaetz T., Britton J., Itano W. M., Jost J. D., Knill E., Langer C., Leibfried D., Ozeri R., and Wineland D. J. Deterministic quantum teleportation of atomic qubits. *Nature*, 2004, v. 429, 737–739.

Deflection of Light Rays and Mass-Bearing Particles in the Field of a Rotating Body

Dmitri Rabounski and Larissa Borissova

Puschino, Moscow Region, Russia
E-mail: rabounski@yahoo.com, lborissova@yahoo.com

As proved earlier, the space of a rotating body is Riemannian only if it is filled with a distributed matter (Progr. Phys., 2022, v.18, 31–49). In this paper we consider motion of massless (light-like) and mass-bearing particles in the space of a rotating body filled with an electromagnetic field, where the influence of gravitation is negligible. Solving the equations of motion of a particle that does not have an electric charge, we find that its motion deflects from a straight line due to the space curvature caused by the rotation of space. That is, the trajectories of light rays and mass-bearing particles are deflected near a rotating body due to the curvature of space caused by its rotation. This is one more fundamental effect of the General Theory of Relativity, in addition to the deflection of light rays in the field of a gravitating body.

In this small paper, which is a continuation of the previous one [1], we consider the equations of motion of a massless (light-like) particle and a mass-bearing particle in the space of a rotating body, which is filled with an electromagnetic field, and the influence of gravitation is negligible.

As proved in the previous paper, a rotating space has a significant curvature due to its space-time non-holonomity (non-orthogonality of the time lines to the three-dimensional spatial section). For this reason, we expect to find that the space curvature caused by the rotation of space deflects light rays and mass-bearing particles near a rotating body.

Please note that, as proved earlier using Einstein's equations [1], the space of a rotating body is Riemannian only if it is filled with a distributed matter, say, an electromagnetic field. Therefore, the above problem statement will not be valid and mathematically correct in an empty space or in a space filled only with a gravitational field. In the case we are considering, as in the previous article, the "space filler" is an electromagnetic field.

In this work, as well as in our other works, we use the mathematical apparatus of chronometric invariants, which are physically observable quantities in the General Theory of Relativity. This mathematical apparatus was created in 1944 by our esteemed teacher A. L. Zelmanov (1913–1987). Its basics can be learned from Zelmanov's publications [2–4], of which his 1957 presentation [4] is the most useful and complete, and also from our previous article [1]. For a deeper study of this mathematical apparatus, read the respective chapters of our monographs [5, 6], especially — the chapter Tensor Algebra and the Analysis in [6].

The equations of motion of both mass-bearing and massless (light-like) particles were studied in detail in our two monographs [5, 6]. The first one [5] focused onto free motion of particles, and the second one [6] focused onto non-geodesic motion of particles: the right hand side of the equations of non-geodesic motion is non-zero, and contains the external force deflecting the particles from geodesic (shortest) trajectories.

The chronometrically invariant equations of motion are the physically observable projections of the general covariant four-dimensional equations of motion onto the time line and the three-dimensional spatial section of a particular observer. Such projections are invariant along the spatial section of the observer (his observed space) and are expressed through the properties of his local reference space. Those who are interested in how the equations of motion are derived can refer to the respective chapters of our monographs, where all these equations are explained in detail.

In this paper we consider mass-bearing particles that do not have an electric charge, and massless (light-like) particles are not electrically charged by definition. As a result, the right hand side of the equations of their motion, containing the force acting on electrically charged particles from the electromagnetic field, is equal to zero. Therefore, these are free particles, and the equations of their motion are the equations of motion along geodesic lines.

The chr.inv.-equations of motion of a free mass-bearing particle describe the motion along an ordinary geodesic line

$$\left.\begin{aligned} &\frac{dm}{d\tau} - \frac{m}{c^2}\,F_i\,\mathrm{v}^i + \frac{m}{c^2}\,D_{ik}\,\mathrm{v}^i\mathrm{v}^k = 0 \\ &\frac{d(m\,\mathrm{v}^i)}{d\tau} + 2m\left(D^i_k + A^{\cdot i}_{k\cdot}\right)\mathrm{v}^k - m\,F^i + m\,\Delta^i_{nk}\,\mathrm{v}^n\mathrm{v}^k = 0 \end{aligned}\right\},$$

and the chr.inv.-equations of motion of a free massless (light-like) particle describe the motion along an isotropic geodesic line (a.k.a. a null geodesic line)

$$\left.\begin{aligned} &\frac{d\omega}{d\tau} - \frac{\omega}{c^2}\,F_i\,c^i + \frac{\omega}{c^2}\,D_{ik}\,c^i c^k = 0 \\ &\frac{d(\omega\,c^i)}{d\tau} + 2\omega\left(D^i_k + A^{\cdot i}_{k\cdot}\right)c^k - \omega\,F^i + \omega\,\Delta^i_{nk}\,c^n c^k = 0 \end{aligned}\right\}.$$

Here in the equations of motion and so forth, m is the relativistic mass of the travelling particle, ω is the relativistic frequency of the massless (light-like) particle, $d\tau$ is the physically observable time interval expressed through the linear velocity v_i of the rotation of space

$$d\tau = \sqrt{g_{00}}\, dt - \frac{1}{c^2} v_i dx^i,$$

$$v_i = -\frac{c\, g_{0i}}{\sqrt{g_{00}}}, \qquad v^i = -c\, g^{0i}\sqrt{g_{00}}\,,$$

and, respectively the chr.inv.-vector of the physically observable velocity of the travelling particle has the form

$$\mathrm{v}^i = \frac{dx^i}{d\tau}, \qquad \mathrm{v}_i\mathrm{v}^i = h_{ik}\mathrm{v}^i\mathrm{v}^k = \mathrm{v}^2,$$

which in the ultimate case transforms into the chr.inv.-vector of the physically observable velocity of light, the square of which is $c_i\, c^i = h_{ik}\, c^i c^k = c^2$.

Please note that, according to the theory of chronometric invariants, the square of any chr.inv.-quantity, and also lifting and lowering indices in chr.inv.-quantities is determined through the chr.inv.-metric tensor

$$h_{ik} = -g_{ik} + \frac{1}{c^2} v_i v_k, \quad h^{ik} = -g^{ik}, \quad h^i_k = -g^i_k = \delta^i_k,$$

which is obtained as the spatial chr.inv.-projection of the fundamental metric tensor $g_{\alpha\beta}$ and has all its properties everywhere in the observer's three-dimensional spatial section.

Concerning the physically observable characteristics of space, which are terms in the equations of motion, these are the chr.inv.-vector of the gravitational inertial force F^i (where $\mathrm{w} = c^2(1-\sqrt{g_{00}})$ is the gravitational potential), the antisymmetric chr.inv.-tensor of the angular velocity of rotation of space, A_{ik}, the symmetric chr.inv.-tensor of deformation of space, D_{ik}, and the chr.inv.-Christoffel symbols Δ^i_{jk}, (coherence coefficients of space), i.e.

$$F_i = \frac{1}{1-\frac{\mathrm{w}}{c^2}}\left(\frac{\partial \mathrm{w}}{\partial x^i} - \frac{\partial v_i}{\partial t}\right),$$

$$A_{ik} = \frac{1}{2}\left(\frac{\partial v_k}{\partial x^i} - \frac{\partial v_i}{\partial x^k}\right) + \frac{1}{2c^2}(F_i v_k - F_k v_i),$$

$$D_{ik} = \frac{1}{2}\frac{{}^{*}\partial h_{ik}}{\partial t}, \qquad D^{ik} = -\frac{1}{2}\frac{{}^{*}\partial h^{ik}}{\partial t},$$

$$\Delta^i_{jk} = h^{im}\Delta_{jk,m} = \frac{1}{2}h^{im}\left(\frac{{}^{*}\partial h_{jm}}{\partial x^k} + \frac{{}^{*}\partial h_{km}}{\partial x^j} - \frac{{}^{*}\partial h_{jk}}{\partial x^m}\right),$$

where the chr.inv.-operators of derivation have the form

$$\frac{{}^{*}\partial}{\partial t} = \frac{1}{\sqrt{g_{00}}}\frac{\partial}{\partial t}, \qquad \frac{{}^{*}\partial}{\partial x^i} = \frac{\partial}{\partial x^i} - \frac{g_{0i}}{g_{00}}\frac{\partial}{\partial x^0}.$$

In our further calculation of the deflection of light rays and mass-bearing particles in the field of a rotating body we will use the same space metric that we introduced in the previous paper [1]. This is the metric of a space, where the three-dimensional space rotates due to the non-holonomity of the space-time, but there is no field of gravitation (or, to be more exact, the influence of gravitation is negligible).

Assume that the space rotates along the equatorial axis φ, i.e., along the geographical longitudes, with the velocity $v_3 = \omega r^2\sin^2\theta$, where $\omega = const$ is the angular velocity of this rotation. Then, according to the definition of v_i,

$$v_3 = \omega r^2\sin^2\theta = -\frac{c\, g_{03}}{\sqrt{g_{00}}},$$

we obtain the metric of such a space

$$ds^2 = c^2dt^2 - 2\omega r^2\sin^2\theta\, dt\, d\varphi - \\ - dr^2 - r^2\left(d\theta^2 + \sin^2\theta\, d\varphi^2\right).$$

As you can see, the non-zero components of the fundamental metric tensor $g_{\alpha\beta}$ of this metric are equal to

$$g_{00} = 1, \qquad g_{03} = -\frac{\omega r^2\sin^2\theta}{c},$$

$$g_{11} = -1, \quad g_{22} = -r^2, \quad g_{33} = -r^2\sin^2\theta,$$

and, according to the definition of the chr.inv.-metric tensor h_{ik}, its non-zero components in the metric are equal to

$$h_{11} = 1, \qquad h_{22} = r^2, \qquad h_{33} = r^2\sin^2\theta\left(1 + \frac{\omega^2 r^2\sin^2\theta}{c^2}\right),$$

$$h^{11} = 1, \qquad h^{22} = \frac{1}{r^2}, \qquad h^{33} = \frac{1}{r^2\sin^2\theta\left(1+\frac{\omega^2r^2\sin^2\theta}{c^2}\right)},$$

where, since the matrix h_{ik} is diagonal, the upper-index components of h_{ik} are obtained as $h^{ik} = (h_{ik})^{-1}$ just like the invertible matrix components to any diagonal matrix.

Using the definition of the antisymmetric chr.inv.-tensor of the angular velocity of rotation of space, A_{ik}, we obtain that its non-zero components in the rotating space we are considering are equal to

$$A_{13} = \omega r\sin^2\theta, \qquad A_{31} = -A_{13},$$

$$A_{23} = \omega r^2\sin\theta\cos\theta, \qquad A_{32} = -A_{23},$$

$$A^{13} = \frac{\omega}{r\left(1+\frac{\omega^2r^2\sin^2\theta}{c^2}\right)}, \qquad A^{31} = -A^{13},$$

$$A^{23} = \frac{\omega\cot\theta}{r^2\left(1+\frac{\omega^2r^2\sin^2\theta}{c^2}\right)}, \qquad A^{32} = -A^{23}.$$

Using the definition of the chr.inv.-Christoffel symbols Δ^i_{jk} (coherence coefficients of space), after some algebra, we obtain formulae for their non-zero components in the rotating

space we are considering. They have the form

$$\Delta^1_{22} = -r,$$
$$\Delta^1_{33} = -r\sin^2\theta\left(1+\frac{2\omega^2r^2\sin^2\theta}{c^2}\right),$$
$$\Delta^2_{12} = \Delta^2_{21} = \frac{1}{r},$$
$$\Delta^2_{33} = -\sin\theta\cos\theta\left(1+\frac{2\omega^2r^2\sin^2\theta}{c^2}\right),$$
$$\Delta^3_{13} = \Delta^3_{13} = \frac{1}{r\left(1+\frac{\omega^2r^2\sin^2\theta}{c^2}\right)}\left(1+\frac{2\omega^2r^2\sin^2\theta}{c^2}\right),$$
$$\Delta^3_{23} = \Delta^3_{32} = \frac{\cot\theta}{1+\frac{\omega^2r^2\sin^2\theta}{c^2}}\left(1+\frac{2\omega^2r^2\sin^2\theta}{c^2}\right).$$

Now, using the obtained physically observable characteristics of the rotating space we are considering, we will modify the general formulae of the chr.inv.-equations of free motion (see above) in accordance with the space metric. As a result, we will obtain the chr.inv.-equations of motion of a free mass-bearing particle and a free massless (light-like) particle in the rotating space. The solution of these equations will show the effect of deflection of light rays and mass-bearing particles in the field of a rotating body.

Since $g_{00} = 1$ in the metric, and the rotation of space is stationary ($v_3 = \omega r^2\sin^2\theta$ is not time-dependent), then the gravitational potential $w = c^2(1-\sqrt{g_{00}})$ is equal to zero and, hence, the gravitational inertial force vanish, $F_i = 0$.

In addition, you can see that neither the fundamental metric tensor $g_{\alpha\beta}$ nor the chr.inv.-metric tensor h_{ik} of the metric are not time-dependent, the rotating space we are considering does not deform and, hence, the tensor of deformation of space vanish, $D_{ik} = 0$.

As a result, since $F_i = 0$ and $D_{ik} = 0$, the chr.inv.-equations of motion of a free mass-bearing particle in the rotating space we are considering take the simplified form

$$\left.\begin{aligned}&\frac{dm}{d\tau} = 0\\ &\frac{d(m\mathrm{v}^i)}{d\tau} + 2mA^{\cdot i}_{k\cdot}\mathrm{v}^k + m\Delta^i_{nk}\mathrm{v}^n\mathrm{v}^k = 0\end{aligned}\right\},$$

and the chr.inv.-equations of motion of a free massless (light-like) particle are simplified to the form

$$\left.\begin{aligned}&\frac{d\omega}{d\tau} = 0\\ &\frac{d(\omega c^i)}{d\tau} + 2\omega A^{\cdot i}_{k\cdot}c^k + \omega\Delta^i_{nk}c^nc^k = 0\end{aligned}\right\}.$$

The above equations are identical. Therefore they are solved in the same way and have the same solution.

Consider the above equations of motion of a free mass-bearing particle as a sample (the solution for a free massless particle will be the same).

The scalar equation of motion solves as $m = const$. With this solution taken into account, we substitute here the obtained formulae for the tensor of the angular velocity of rotation of space, A_{ik}, and the Christoffel symbols Δ^i_{jk}. As a result, neglecting higher order terms (otherwise the equations are unsolvable), we obtain the vectorial equations of motion in the component form suitable for their further analysis

$$\left.\begin{aligned}&\frac{d\mathrm{v}^1}{d\tau} - 2\omega r\sin^2\theta\,\mathrm{v}^3 - r\,\mathrm{v}^2\mathrm{v}^2 - r\sin^2\theta\,\mathrm{v}^3\mathrm{v}^3 = 0\\ &\frac{d\mathrm{v}^2}{d\tau} - 2\omega\sin\theta\cos\theta\,\mathrm{v}^3 + \frac{2}{r}\mathrm{v}^1\mathrm{v}^2 - \sin\theta\cos\theta\,\mathrm{v}^3\mathrm{v}^3 = 0\\ &\frac{d\mathrm{v}^3}{d\tau} + \frac{2\omega}{r}\mathrm{v}^1 + 2\omega\cot\theta\,\mathrm{v}^2 + \frac{2}{r}\mathrm{v}^1\mathrm{v}^3 + 2\cot\theta\,\mathrm{v}^2\mathrm{v}^3 = 0\end{aligned}\right\}.$$

Even a brief look at the obtained equations of motion shows that the three possible effects are conceivable:

1. The deflection of a travelling free particle along the geographic longitudes (the third equation in the above system);
2. The deflection of a travelling free particle along the geographic latitudes (the second equation);
3. The acceleration or braking of a travelling free particle in the radial direction (the first equation).

The problem is that the above system of differential equations is unsolvable in the general form. Therefore, we will consider a simplified particular case of the equations, and calculate all three of the above effects just for this case.

Consider a particle travelling at a very high radial velocity v^1 in the equatorial plane exactly along the radial axis to the origin of the coordinates. Say, a particle from the near-Earth space travels freely in the equatorial plane directly to the Earth's surface. In this case, the velocities of its deflection along the geographical latitudes and longitudes, v^2 and v^3, are negligible compared to v^1, and the above equations take the simplified form

$$\left.\begin{aligned}&\frac{d\mathrm{v}^1}{d\tau} - 2\omega r\,\mathrm{v}^3 - r\,\mathrm{v}^2\mathrm{v}^2 - r\,\mathrm{v}^3\mathrm{v}^3 = 0\\ &\frac{d\mathrm{v}^2}{d\tau} + \frac{2}{r}\mathrm{v}^1\mathrm{v}^2 = 0\\ &\frac{d\mathrm{v}^3}{d\tau} + \frac{2\omega}{r}\mathrm{v}^1 + \frac{2}{r}\mathrm{v}^1\mathrm{v}^3 = 0\end{aligned}\right\}.$$

In addition, we assume that the particle's velocity in the radial direction gains only a very small increment or decrement α' compared to its numerical value v^1, which, according to our initial assumption, is very large. As a result, we set $\mathrm{v}^1 = const$ in the equations of motion along the equatorially

longitudinal axis φ (third equation) and the latitudinal axis θ (second equation), but solve the equation of motion along the radial axis r (first equation) with respect to $\mathrm{v}^1 + \alpha'$, i.e., with respect to the small parameter α. Otherwise, the above system of differential equations is unsolvable.

1. Consider the third equation of motion (along the equatorial axis φ). With the above assumptions, this equation takes the form, respectively,

$$y' + ay + b = 0, \qquad \varphi'' + a\varphi' + b = 0,$$

where we used the following notations

$$y = \mathrm{v}^3 = \frac{d\varphi}{d\tau}, \quad a = \frac{2}{r}\,\mathrm{v}^1 = const, \quad b = \frac{2\omega}{r}\,\mathrm{v}^1 = const.$$

The above differential equations for the velocity $y = \mathrm{v}^3$ and the coordinate φ with respect to the physically observable time $\tau = x$ are solved as

$$y = \frac{C}{\mathrm{e}^{ax}} - \frac{b}{a}, \qquad \varphi = \frac{C_1}{\mathrm{e}^{ax}} - \frac{bx}{a} + C_2,$$

where the constants of integration found using the initial conditions $x = x_0 = 0$ and $y = y_0 = 0$, are equal to

$$C = \frac{b}{a} = \omega, \quad C_1 = -\frac{b}{a^2} = -\frac{\omega r}{2\mathrm{v}^1}, \quad C_2 = -C_1 = \frac{\omega r}{2\mathrm{v}^1}.$$

As a result, we obtain solutions for the particle's velocity $y = \mathrm{v}^3$ along the equatorial axis (along the geographic longitudes), as well as for the equatorial coordinate φ (geographical longitude) of the arrival point of this particle.

The obtained solution for the particle's velocity along the equatorial axis φ has the form

$$\mathrm{v}^3 = -\omega + \omega\mathrm{e}^{-\frac{2}{r}\mathrm{v}^1\tau}.$$

Here the first term $-\omega$ is the particle's basics equatorial velocity, the origin of which is the banally shift of the equatorial coordinate φ to its negative numerical values due to the Earth's turn over the particle's travel to the Earth.

The second, additional term means that a particle freely travelling to the surface of a rotating body gains an additional velocity directed along the equator (geographical longitudes) opposite to the rotation of the body.

The obtained solution for the equatorial coordinate φ of the arrival point of this particle has the form

$$\varphi = \varphi_0 - \omega\tau + \frac{\omega r}{2\mathrm{v}^1}\left(1 - \mathrm{e}^{-\frac{2}{r}\mathrm{v}^1\tau}\right).$$

The third, additional term of this solution means that a particle freely travelling to the surface of a rotating body is deflected along the equator (geographical longitudes) opposite to the rotation of the body.

All this is because the rotation of any body gets space curved near it, thereby creating a "slope of the hill" slowing "down" along the equator towards the rotation of this body. In other words, space is curved by a rotating body in the direction of its rotation. As a result, a particle freely travelling to a rotating body "rolls down the curvature hill" of space along the equator in the direction in which the body rotates.

The same effect is expected for light rays, since the equations of motion for a massless (light-like) particle and a massless particle are identical, and, hence, their solutions coincide (see above). Only the mass-bearing particle's velocity is replaced with the physically observable velocity of light.

Please note that, as Zelmanov showed in 1944 using the mathematical apparatus of chronometric invariants, the vectorial components of the physically observable velocity of light depend on the geometric properties of space, as well as on the physical properties of distributed matter, despite the fact that the square of the velocity remains invariant.

As a result, the solution for the equatorial coordinate φ of the arrival point of a light ray falling down from space onto the Earth's surface in the equatorial plane has the form

$$\varphi = \varphi_0 - \omega\tau + \frac{\omega r}{2c^1}\left(1 - \mathrm{e}^{-\frac{2}{r}c^1\tau}\right),$$

where c^1 is the physically observable velocity of light in the radial direction.

Since the Earth, as well as any other planet or star, has its own gravitational field, a mass-bearing particle freely travelling to its surface gains a substantial acceleration. In this case, the particle's radial velocity cannot be assumed to be constant even in the first order approximation. For this reason, we will calculate the numerical value of the above effect, which we theoretically discovered, for a light ray.

Consider a light ray travelling, say, from the Moon to the Earth's surface along the radial axis r in the equatorial plane of the Earth. In this case, the physically observable velocity of light is equal to $c^1 = -3\times10^{10}$ cm/sec, since the vector of the velocity of light is directed opposite to the reading of the radial coordinates, the origin of which is the centre of the Earth. The Earth rotates around its axis with the angular velocity $\omega = 1$ rev/day $= 1.16\times10^{-5}$ rev/sec, and the Earth's radius is equal to $r = 6.4\times10^8$ cm. As a result, we obtain that the curvature of space caused by the Earth's rotation around its axis deflects a light ray coming to the Earth's surface from the Moon ($\tau = 1$ sec) in the longitudinal direction in which the Earth rotates by the angle equal to

$$\Delta\varphi = \frac{\omega r}{2c^1}\left(1 - \mathrm{e}^{-\frac{2}{r}c^1\tau}\right) = 1.2\times10^{-7}\ \text{rev} = 0.16'',$$

where the main goal into the effect is made due to the first term, and the second term is equal to 1.5×10^{-41} and, therefore, can be neglected.

The effect calculated for the Earth is small. Meanwhile, this effect increases with the radius and rotation velocity of the cosmic body. For example, the Sun has the radius equal to $r = 7.0\times10^{10}$ cm, and rotates around its axis with the angular

velocity $\omega = 4.5 \times 10^{-7}$ rev/sec. Therefore, the curvature of space caused by the Sun's rotation around its axis deflects a light ray coming to the Sun's surface in the longitudinal direction in which the Sun rotates by the angle equal to

$$\Delta\varphi = 5.3 \times 10^{-7} \text{ rev} = 0.68''.$$

Obviously, this effect has a much larger numerical value near a rapidly rotating star, such as Wolf-Rayet stars or neutron stars.

2. Now consider the second equation of motion (along the geographical latitudes, where the polar angle θ is read from the North pole). With the same assumptions as those we used in the third equation above, neglecting higher order terms and taking the obtained solution $v^3 = -\omega$ into account, this equation takes the form, respectively,

$$y' + ay = 0, \qquad \theta'' + a\theta' = 0,$$

where

$$y = v^2 = \frac{d\theta}{d\tau}, \qquad a = \frac{2}{r} v^1 = const.$$

The above differential equations are solved as

$$y = \frac{C}{e^{ax}}, \qquad \theta = \frac{C_1}{e^{ax}} + C_2,$$

where the constants of integration found using the initial conditions $x = x_0 = 0$ and $y = y_0 = 0$, are equal to $C = 0$, $C_1 = 0$ and $C_2 = \theta_0$. As a result, the solutions take the final form

$$v^2 = 0, \qquad \theta = \theta_0,$$

i.e., a particle freely travelling to the surface of a rotating body is not deflected up or down the geographical latitudes.

3. Finally, consider the first equation of motion (along the radial coordinates). As is explained in the beginning, we assume that the particle's velocity in the radial direction gains a very small increment or decrement α' compared to its numerical value v^1, which, according to our initial assumption, is very large. Thus, we assume $v^1 = const$ and solve the first equation of motion with respect to $v^1 + \alpha'$, i.e., with respect to the small parameter α. Neglecting higher order terms and taking the obtained solutions $v^3 = -\omega$ and $v^2 = 0$ into account, the first equation of motion takes the form, respectively,

$$y' + b = 0, \qquad \alpha'' + b = 0,$$

where $y = \alpha'$ and $b = \omega^2 r = const$ (here r is the radius of the rotating body). These simplest equations are solved as

$$y = C - bx, \qquad \alpha = -\frac{bx^2}{2} + C_2 x + C_1,$$

where, using the initial conditions $x = x_0 = 0$, $\alpha = \alpha_0 = 0$ and $y = y_0 = 0$, we find that the constants of integration are equal to zero. As a result, we obtain

$$\alpha' = -\omega^2 r\tau, \qquad \alpha = -\frac{\omega^2 r\tau^2}{2}.$$

This solution means that a particle freely travelling to a rotating body gains an additional speed, and the length of its path is physically "stretched" due to the curvature of space caused by the body's rotation. As a result, the particle reaches the body later (with a delay in time) compared if the body did not rotate.

Thus, according to the obtained solution, the increment of the path length of a light ray that travelled, say, from the Moon to the Earth, and also the delay in time of its arrival are equal to

$$\alpha = -8.8 \times 10^{-2} \text{ cm}, \quad \Delta\tau = \frac{\alpha}{c^1} = 2.7 \times 10^{-12} \text{ sec},$$

while such corrections for a light ray that travelled from the Earth to the Sun are equal to

$$\alpha = -1.8 \times 10^{3} \text{ cm}, \quad \Delta\tau = \frac{\alpha}{c^1} = 5.9 \times 10^{-8} \text{ sec}.$$

So, we theoretically found that a particle travelling freely to a rotating body is deflected slightly from its radial trajectory in the equatorial direction, in which the body rotates, i.e., along the geographical longitudes. In addition, during the travel, the particle gains a small increase of its velocity, and its path is physically "stretched" for a little, as a result of which the particle reaches the body with a delay in time compared to if the body did not rotate.

These two effects take place both for mass-bearing particles and for light rays (massless light-like particles).

The origin of these effects is the space curvature caused by the rotation of space. When any body rotates, the space around it curves towards the direction of its rotation and the centre of the body (the centre of rotation), thereby creating a "slope of the hill" descending "down" along the equator in the direction, in which the body rotates, and also to the centre of the body. When a particle travels freely to a rotating body, it "rolls down" the slope of the space curvature along the equator in the direction, in which the body rotates, as well as to the centre of the body.

These are two new fundamental effects of the General Theory of Relativity, we have discovered "au bout d'un stylo" in addition to the Einstein effect of the deflection of light rays in the field of a gravitating body.

Submitted on May 5, 2022

References

1. Rabounski D. and Borissova L. Non-quantum teleportation in a rotating space with a strong electromagnetic field. *Progress in Physics*, 2022, v. 18, issue 1, 31–49.
2. Zelmanov A. L. Chronometric Invariants. Translated from the 1944 PhD thesis, American Research Press, Rehoboth, New Mexico, 2006.
3. Zelmanov A. L. Chronometric invariants and accompanying frames of reference in the General Theory of Relativity. *Soviet Physics Doklady*, 1956, v. 1, 227–230 (translated from *Doklady Academii Nauk USSR*, 1956, v. 107, issue 6, 815–818).

4. Zelmanov A. L. On the relativistic theory of an anisotropic inhomogeneous universe. *The Abraham Zelmanov Journal*, 2008, vol. 1, 33–63 (translated from the thesis of the *6th Soviet Conference on the Problems of Cosmogony*, USSR Academy of Sciences Publishers, Moscow, 1957, 144–174).

5. Rabounski D and Borissova L. Particles Here and Beyond the Mirror. The 3rd expanded edition, American Research Press, Rehoboth, New Mexico, 2012 (the 1st edition was issued in 2001).
Rabounski D. et Borissova L. Particules de l'Univers et au delà du Miroir. American Research Press, Rehoboth, New Mexico, 2012 (French translation).

6. Borissova L. and Rabounski D. Fields, Vacuum, and the Mirror Universe. The 2nd expanded edition, Svenska fysikarkivet, Stockholm, 2009 (the 1st edition was issued in 2001).
Borissova L. et Rabounski D. Champs, Vide, et Univers miroir. American Research Press, Rehoboth, New Mexico, 2010 (French translation).

Physics of Transcendental Numbers as Forming Factor of the Solar System

Hartmut Müller

Rome, Italy.
E-mail: hm@interscalar.com

Transcendental ratios of physical quantities can inhibit the occurrence of destabilizing parametric resonance and in this way, provide stability in systems of coupled periodic processes. In this paper we apply this approach to the solar system and show that it can explain the current set of rotational and orbital periods and distances including observed tendencies of their evolution.

Introduction

One of the unsolved fundamental problems in physics [1] is the stability of systems of a large number of coupled periodic processes, for instance, the stability of planetary systems. If numerous bodies are gravitationally bound to one another, perturbation models predict long-term highly unstable states [2] that contradict the physical reality of the solar system and thousands of exoplanetary systems.

Another issue is that in theory, there are infinitely many pairs of orbital periods and distances that fulfill Kepler's laws. Regrettably, Einstein's field equations do not reduce the theoretical variety of possible orbits, but increases it even more. As a consequence, the current orbital system of the Sun seems to be accidental, and its stability a miracle.

Furthermore, there is no known law concerning the rotation of celestial bodies besides conservation of the angular momentum [3] that they retain from the protoplanetary disk, so that also the current distribution of the rotational periods appears as to be accidental.

However, many planets in extrasolar systems like Trappist 1 or Kepler 20 have almost the same orbital periods as the large moons of Jupiter, Saturn, Uranus and Neptune [4]. Trappist 1 is 40 light years away from our solar system [5] and Kepler 20 nearly 1000 light years [6].

The question is, why they prefer similar orbital periods if there are infinite possibilities? Obviously, there are orbital periods preferred anywhere in the galaxy. Why these orbital periods are preferred? What makes them attractive?

In this paper, we introduce an approach to the problem of stability based on the physical interpretation of certain statements of number theory. This approach leads us to the conclusion that in real systems, bound periodic processes approximate transcendental frequency ratios that allow them to avoid destabilizing parametric resonance. We illustrate this conclusion on some well-known features of the solar system which are still unexplained.

Theoretical Approach

The starting point of our approach is the measurement as it is the source of data that allow us developing and proofing theoretical models of the reality. The result of a measurement is the ratio of physical quantities where one of them is the reference quantity called unit of measurement. Whether measuring a wavelength or phase, a frequency, the speed or duration of some process, the mass of a body or its temperature, initially this ratio is a real number, regardless of its subsequent interpretation as component of a vector or tensor, for example. As real value, this ratio can approximate an integer, rational, irrational algebraic or transcendental number. In [7] we have shown that the difference between rational, irrational algebraic and transcendental numbers is not only a mathematical task, but it is also an essential aspect of stability in systems of bound periodic processes. For instance, integer frequency ratios, in particular fractions of small integers, make possible parametric resonance that can destabilize such a system [8, 9]. For instance, asteroids cannot maintain orbits that are unstable because of their resonance with Jupiter [10]. These orbits form the Kirkwood Gaps, which are areas in the asteroid belt where asteroids are absent.

According to this idea, irrational ratios should not cause destabilizing resonance interactions, because irrational numbers cannot be represented as a ratio of integers. However, algebraic irrational numbers, being real roots of algebraic equations, can be converted to rational numbers by multiplication. For example, the algebraic irrational number $\sqrt{2} = 1.41421\ldots$ cannot become a frequency scaling factor in real systems of coupled periodic processes, because $\sqrt{2} \cdot \sqrt{2} = 2$ creates the conditions for the occurrence of parametric resonance. Thus, only transcendental ratios can prevent parametric resonance, because they cannot be converted to rational or integer numbers by multiplication.

Actually, it is transcendental numbers, that define the preferred frequency ratios which allow to avoid destabilizing resonance [11]. In this way, transcendental frequency ratios sustain the lasting stability of coupled periodic processes. With reference to the evolution of a planetary system and its stability, we may therefore expect that the ratio of any two orbital periods should finally approximate a transcendental number.

Among all transcendental numbers, Euler's number $e = 2.71828\ldots$ is unique, because its real power function e^x coincides with its own derivatives. In the consequence, Euler's number allows inhibiting parametric resonance between any coupled periodic processes including their derivatives.

Because of this unique property of Euler's number, we expect that periodic processes in real systems prefer frequency ratios close to Euler's number and its roots. The natural logarithms of those frequency ratios are therefore close to integer $0, \pm1, \pm2, \ldots$ or rational $\pm1/2, \pm1/3, \pm1/4, \ldots$ values. For rational exponents, the natural exponential function is always transcendental [12]. As shown by A. Khinchine [13], any rational number has a biunique presentation as a finite continued fraction. Consequently, we can present the natural logarithms of the frequency ratios we are looking for as finite continued fractions:

$$\ln(\omega_A/\omega_B) = \mathcal{F} = \langle n_0; n_1, n_2, \ldots, n_k \rangle \qquad (1)$$

ω_A and ω_B are the angular frequencies of two bound periodic processes A and B avoiding parametric resonance. We use angle brackets for continued fractions. All denominators $n_1, n_2, \ldots, n_k$ of a continued fraction including the free link n_0 are integer numbers. All numerators equal 1. The length of a continued fraction is given by the number k of layers.

Finite continued fractions represent all rational numbers in the sense that there is no rational number that cannot be represented by a finite continued fraction. This universality of continued fractions evidences that the distribution of rational logarithms (1) in the number continuum is fractal.

The first layer of this fractal is given by the truncated after n_1 continued fractions:

$$\langle n_0; n_1 \rangle = n_0 + \frac{1}{n_1}$$

The denominators n_1 follow the sequence of integer numbers ±1, ±2, ±3 etc. The second layer is given by the truncated after n_2 continued fractions:

$$\langle n_0; n_1, n_2 \rangle = n_0 + \cfrac{1}{n_1 + \cfrac{1}{n_2}}$$

Figure 1 shows the first and the second layer in comparison. As we can see, reciprocal integers $\pm1/2, \pm1/3, \pm1/4, \ldots$ are the attractor points of the fractal. In these points, the distribution density of rational logarithms (1) reaches a local maximum. Integers $0, \pm1, \pm2, \ldots$ define the main attractors. Consequently, integer arguments of the natural exponential function define attractor points of transcendental numbers and ranges of stability that allow bound periodic processes to avoid parametric resonance.

Figure 1 shows that integer logarithms $0, \pm1, \pm2, \ldots$ form the widest ranges of stability. Half logarithms $\pm1/2$ form smaller ranges, third logarithms $\pm1/3$ form the next smaller ranges and fourth logarithms $\pm1/4$ form even smaller ranges of stability etc. Increasing the length of the continued fraction (1), the distribution density of the transcendental frequency ratios ω_A/ω_B is increasing as well. Nevertheless, their distribution is not homogeneous, but fractal. Applying continued fractions and truncating them, we can represent the logarithms $\ln(\omega_A/\omega_B)$ as rational numbers $\langle n_0; n_1, n_2, \ldots, n_k \rangle$ and make visible their fractal distribution.

Fig. 1: The distribution of rational logarithms for $k = 1$ (above) and for $k = 2$ (below) in the range $-1 \leqslant \mathcal{F} \leqslant 1$.

Here I would like to underline that the application of continued fractions doesn't limit the universality of our conclusions, because continued fractions deliver biunique representations of all real numbers including transcendental. Therefore, the fractal distribution of transcendental ratios (1) is an inherent feature of the number continuum that we call the *Fundamental Fractal* [11].

The natural exponential function $\exp(\mathcal{F})$ of the rational argument $\mathcal{F} = \langle n_0; n_1, n_2, \ldots, n_k \rangle$ generates a fractal set of transcendental frequency ratios $\omega_A/\omega_B = \exp(\mathcal{F})$ which allow to avoid destabilizing parametric resonance and in this way, provide the lasting stability of periodic processes bound in systems regardless of their complexity. This conclusion we have exemplified [14] in particle physics, astrophysics, geophysics, biophysics and engineering.

For bound harmonic quantum oscillators, the continued fractions $\mathcal{F}$ define not only ratios of frequencies ω, oscillation periods $\tau = 1/\omega$ and wavelengths $\lambda = c/\omega$, but also ratios of accelerations $a = c \cdot \omega$, energies $E = \hbar \cdot \omega$ and masses $m = \omega \cdot \hbar/c^2$, which allow to avoid parametric resonance.

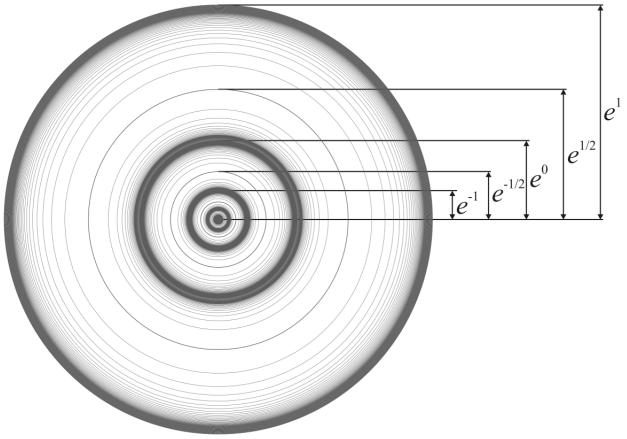

Fig. 2: The first layer ($k = 1$) of equipotential surfaces of the Fundamental Field in the 2D-projection in the range $-1 \leqslant \mathcal{F} \leqslant 1$.

The spatio-temporal projection of the Fundamental Fractal $\mathcal{F}$ is a fractal scalar field of transcendental attractors, the *Fundamental Field* [15]. The connection between the spatial and temporal projections is given by the speed of light $c = 299792458$ m/s. The constancy of c makes both projections isomorphic, so that there is no arithmetic or geometric

difference. Only the units of measurement are different. Figure 2 shows the 2D-projection $\exp(\mathcal{F})$ of its first layer. The Fundamental Field is topologically 3-dimensional, a fractal set of embedded spheric equipotential surfaces. The logarithmic potential difference defines a gradient directed to the center of the field that causes a central force of attraction creating the effect of a field source. Because of the fractal logarithmic hyperbolic metric of the field, also every equipotential surface is an attractor. The logarithmic scalar potential difference $\Delta\mathcal{F}$ of sequent equipotential surfaces equals the difference of sequent continued fractions (1) on a given layer:

$$\Delta\mathcal{F} = \langle n_0; n_1, \ldots, n_k\rangle - \langle n_0; n_1, \ldots, n_k + 1\rangle$$

Main equipotential surfaces at $k = 0$ correspond with integer logarithms (1); equipotential surfaces at deeper layers $k > 0$ correspond with rational logarithms.

The Fundamental Field is of pure arithmetic origin, and there is no particular physical mechanism required as field source. It is all about transcendental ratios of frequencies [11] that allow coupled periodic processes to avoid destabilizing parametric resonance. Hence, the Fundamental Field concerns all repetitive processes which share at least one characteristic – the frequency. Therefore, we postulate the universality of the Fundamental Field that affects any type of physical interaction, regardless of its complexity.

Property	Electron	Proton
$E = mc^2$	0.5109989461(31) MeV	938.2720813(58) MeV
$\omega = E/\hbar$	$7.76344 \cdot 10^{20}$ Hz	$1.42549 \cdot 10^{24}$ Hz
$\tau = 1/\omega$	$1.28809 \cdot 10^{-21}$ s	$7.01515 \cdot 10^{-25}$ s
$\lambda = c/\omega$	$3.86159 \cdot 10^{-13}$ m	$2.10309 \cdot 10^{-16}$ m

Table 1: The basic set of physical properties of the electron and proton. Data from Particle Data Group [21]. Frequencies, oscillation periods and wavelengths are calculated.

In fact, scale relations in particle physics [16, 17], nuclear physics [18, 19] and astrophysics [15, 20] obey the same Fundamental Fractal (1), without any additional or particular settings. The proton-to-electron rest energy ratio approximates the first layer of the Fundamental Fractal that could explain their exceptional stability [14]. Normal matter is formed by nucleons and electrons because they are exceptionally stable quantum oscillators. In the concept of isospin, proton and neutron are viewed as two states of the same quantum oscillator. Furthermore, they have similar rest masses. However, a free neutron decays into a proton and an electron within 15 minutes while the life-spans of the proton and electron top everything that is measurable, exceeding 10^{29} years [21]. The proton-to-electron ratio (tab. 1) approximates the seventh power of Euler's number and its square root:

$$\ln\left(\frac{E_p}{E_e}\right) = \ln\left(\frac{938.2720813\,\text{MeV}}{0.5109989\,\text{MeV}}\right) \simeq 7 + \frac{1}{2} = \langle 7; 2\rangle$$

In the consequence of this potential difference of the proton relative to the electron, the scaling factor $\sqrt{e}$ connects attractors of proton stability with similar attractors of electron stability in alternating sequence.

Applying Khinchine's [13] continued fraction method, we get the best approximation of the proton-to-electron ratio:

$$\ln\left(\frac{E_p}{E_e}\right) = 7 + \frac{1}{2} + \cfrac{1}{64 + \cfrac{9}{11}} = 7.515427769\ldots$$

Recent data [22] of the proton-to-electron ratio define the upper limit as 7.515427773 and the lower limit 7.515427702. The same method delivers for the neutron-to-proton ratio:

$$\ln\left(\frac{E_n}{E_p}\right) = \frac{1}{726}$$

By the way, $726 = 11 \cdot 11 \cdot 6$. The denominator 11 appears also in the W/Z-to-electron ratio [11], for example:

$$\ln\left(\frac{E_Z}{E_e}\right) = 12 + \frac{1}{11}$$

The unique properties of the electron and proton predestinate their physical characteristics as fundamental units. Table 1 shows the basic set of electron and proton units that can be considered as a *Fundamental Metrology* (c is the speed of light in a vacuum, $\hbar$ is the Planck constant). In [23] was shown that the fundamental metrology (tab. 1) is completely compatible with Planck units [24]. Originally proposed in 1899 by Max Planck, these units are also known as natural units, because the origin of their definition comes only from properties of nature and not from any human construct. Max Planck wrote [25] that these units, "regardless of any particular bodies or substances, retain their importance for all times and for all cultures, including alien and non-human, and can therefore be called natural units of measurement". Planck units reflect the characteristics of space-time.

We hypothesize that scale invariance according the Fundamental Fractal (1) calibrated on the physical properties of the proton and electron is a universal characteristic of organized matter and criterion of stability. This hypothesis we have called *Global Scaling* [14].

On this background, atoms and molecules emerge as stable eigenstates in fractal chain systems of harmonically oscillating protons and electrons. Andreas Ries [18] demonstrated that this model allows for the prediction of the most abundant isotope of a given chemical element.

In the following, we use the symbol $\mathcal{F}_e$ for the Fundamental Fractal (1) calibrated on the properties of the electron,

and the symbol $\mathcal{F}_p$ for the Fundamental Fractal calibrated on the properties of the proton. For example, $\mathcal{F}_e\langle 66\rangle$ means the main attractor 66 of electron stability. In the solar system, this attractor stabilizes the orbital period of Jupiter [7].

In [15] we applied the Fundamental Fractal (1) to planetary systems interpreting gravity as macroscopic attractor effect of transcendental frequency ratios in chain systems of harmonic quantum oscillators – protons and electrons. In [26] we demonstrated that the Fundamental Field (fig. 2) in the interval of the main attractors $\langle 49\rangle \leqslant \mathcal{F}_p \leqslant \langle 52\rangle$ of proton stability reproduces the 3D profile of the Earth's interior confirmed by seismic exploration. As well, the stratification layers in planetary atmospheres follow the Fundamental Field [27]. In [28] we have shown that the Fundamental Fractal determines the Earth axial precession cycle, the obliquity variation cycle as well as the apsidal precession cycle and the orbital eccentricity cycle. There we have also shown that recently discovered geological cycles, like the 27 million years' cycle [29], as well as the periodic variations in the movement of the Solar system through the Galaxy, substantiate their determination by the Fundamental Fractal.

The orbital and rotational periods of planets, planetoids and large moons of the solar system correspond with attractors of electron and proton stability [23]. This is valid also for exoplanets [4] of the systems Trappist 1 and Kepler 20. In [15] we have shown that the maxima in the frequency distribution of the orbital periods of 1430 exoplanets listed in [30] correspond with attractors of the Fundamental Fractal. As well, the maxima in the frequency distribution of the number of stars in the solar neighborhood as function of the distance between them correspond with attractors of the Fundamental Fractal [20].

Exemplary applications

Jupiter's orbital period $T_{\mathrm{O}}(Jupiter) = 4332.59$ days [31] approximates the main attractor $\mathcal{F}_e\langle 66\rangle$ of electron stability that equals the 66^{th} power of Euler's number multiplied by the oscillation period of the electron (see tab. 1):

$$\ln\left(\frac{T_{\mathrm{O}}(Jupiter)}{2\pi\cdot\tau_e}\right) = \ln\left(\frac{4332.59\cdot 86400\,\mathrm{s}}{2\pi\cdot 1.28809\cdot 10^{-21}\,\mathrm{s}}\right) = 66.00$$

Jupiter's distance from Sun approximates the main equipotential surface $\mathcal{F}_e\langle 56\rangle$ of electron stability that equals the 56^{th} power of Euler's number multiplied by the Compton wavelength of the electron. The aphelion 5.45492 AU = $8.160444\cdot 10^{11}$ m delivers the upper approximation:

$$\ln\left(\frac{A_{\mathrm{O}}(Jupiter)}{\lambda_e}\right) = \ln\left(\frac{8.160444\cdot 10^{11}\,\mathrm{m}}{3.86159\cdot 10^{-13}\,\mathrm{m}}\right) = 56.01$$

The perihelion 4.95029 AU = $7.405528\cdot 10^{11}$ m delivers the lower approximation:

$$\ln\left(\frac{P_{\mathrm{O}}(Jupiter)}{\lambda_e}\right) = \ln\left(\frac{7.405528\cdot 10^{11}\,\mathrm{m}}{3.86159\cdot 10^{-13}\,\mathrm{m}}\right) = 55.91$$

Now we can apply Kepler's 3^{rd} law of planetary motion and express the gravitational parameter μ_{Sun} of the Sun through Euler's number, the speed of light c in a vacuum and the oscillation period τ_e of the electron:

$$\mu_{Sun} = \tau_e\cdot c^3\cdot e^{36}$$

In logarithms, the cube of the mean orbit radius divided by the square of the orbital period $56\cdot 3 - 66\cdot 2 = 36$ results in the 36^{th} power of Euler's number. In this way, within our numeric physical approach, the gravitational parameter of the Sun does not appear to be accidental, but is stabilized by Euler's number and origins from the quantum physical properties of the electron.

In a similar way, we can derive the attractor that the gravitational parameter of Jupiter is approximating. Thanks to the negligible eccentricities of the orbits of Jupiter's large moons, we can use the mean orbit radius for calculations. Callisto's orbit radius $R_{\mathrm{O}}(Callisto) = 1.8827\cdot 10^9$ m approaches the equipotential surface $\mathcal{F}_e\langle 50\rangle$ of electron stability:

$$\ln\left(\frac{R_{\mathrm{O}}(Callisto)}{\lambda_e}\right) = \ln\left(\frac{1.8827\cdot 10^9\,\mathrm{m}}{3.86159\cdot 10^{-13}\,\mathrm{m}}\right) = 49.95$$

Callisto's orbital period $T_{\mathrm{O}}(Callisto) = 16.689$ days is approaching the attractor $\mathcal{F}_e\langle 60;2\rangle$ of electron stability:

$$\ln\left(\frac{T_{\mathrm{O}}(Callisto)}{2\pi\cdot\tau_e}\right) = \ln\left(\frac{16.689\cdot 86400\,\mathrm{s}}{2\pi\cdot 1.28809\cdot 10^{-21}\,\mathrm{s}}\right) = 60.45$$

For reaching both attractors, Callisto must still increase its orbital period by 10 hours and of course, its mean orbit radius as well. Now we can apply Kepler's 3^{rd} law of planetary motion and express the gravitational parameter $\mu_{Jupiter}$ of Jupiter through Euler's number:

$$\mu_{Jupiter} = \tau_e\cdot c^3\cdot e^{29}$$

In logarithms, the cube of the mean orbit radius divided by the square of the orbital period $50\cdot 3 - (60+1/2)\cdot 2 = 29$ results in the 29^{th} power of Euler's number. In this way, Jupiter's gravitational parameter approximates the attractor $\mathcal{F}_e\langle 29\rangle$ of electron stability.

Now we can derive the attractor that the gravitational parameter of the Earth is approximating. The orbital distance of the Moon from Earth approximates the equipotential surface $\mathcal{F}_e\langle 48;3\rangle$ of electron stability that equals the 48^{th} power of Euler's number and its cubic root multiplied by the electron wavelength. The apoapsis of the Moon $A_{\mathrm{O}} = 4.067\cdot 10^8$ m delivers the upper approximation:

$$\ln\left(\frac{A_{\mathrm{O}}(Moon)}{\lambda_e}\right) = \ln\left(\frac{4.067\cdot 10^8\,\mathrm{m}}{3.86159\cdot 10^{-13}\,\mathrm{m}}\right) = 48.41$$

Periapsis $3.626\cdot 10^8$ m delivers the lower approximation:

$$\ln\left(\frac{P_{\mathrm{O}}(Moon)}{\lambda_e}\right) = \ln\left(\frac{3.626\cdot 10^8\,\mathrm{m}}{3.86159\cdot 10^{-13}\,\mathrm{m}}\right) = 48.29$$

The orbital period $T_{\mathrm{O}}(Moon) = 27.32166$ days approaches the main attractor $\mathcal{F}_e\langle 61\rangle$ of electron stability:

$$\ln\left(\frac{T_{\mathrm{O}}(Moon)}{2\pi\cdot\tau_e}\right) = \ln\left(\frac{27.32166\cdot 86400\,\mathrm{s}}{2\pi\cdot 1.28809\cdot 10^{-21}\,\mathrm{s}}\right) = 60.95$$

For reaching this attractor, the Moon must increase its distance from Earth, and that's exactly what the Moon does [32]. However, our approach predicts an increase only until Moon's orbital period reaches the main attractor $\mathcal{F}_e\langle 61\rangle = 29.08$ days. Now we can apply Kepler's 3^{rd} law of planetary motion and express the gravitational parameter μ_{Earth} of the Earth through Euler's number:

$$\mu_{Earth} = \tau_e\cdot c^3\cdot e^{23}$$

In logarithms, the cube of the mean orbit radius divided by the square of the orbital period $(48 + 1/3)\cdot 3 - 61\cdot 2 = 23$ results in the 23^{th} power of Euler's number. Consequently, also the gravitational parameter of the Earth does not appear to be accidental, but origins from the quantum physical properties of the electron and is approaching a main attractor of the Fundamental Fractal.

In a similar way, we can derive the attractors that the gravitational parameters of other planets are approximating. Phobos' mean orbit radius approximates the equipotential surface $\mathcal{F}_e\langle 45;-3\rangle$ while its orbital period is stabilized by the attractor $\mathcal{F}_e\langle 56;2\rangle$. Consequently, the gravitational parameter of Mars approximates the attractor $\mathcal{F}_e\langle 21\rangle$, because $(45 - 1/3)\cdot 3 - (56 + 1/2)\cdot 2 = 21$:

$$\mu_{Mars} = \tau_e\cdot c^3\cdot e^{21}$$

The gravitational parameter of Uranus approximates the center of scale symmetry $(23 + 29)/2 = 26$ between the gravitational parameters of the Earth $\mathcal{F}_e\langle 23\rangle$ and Jupiter $\mathcal{F}_e\langle 29\rangle$:

$$\mu_{Uranus} = \tau_e\cdot c^3\cdot e^{26}$$

Neptune's gravitational parameter approaches the same attractor $\mathcal{F}_e\langle 26\rangle$, but for reaching it, Neptune's moon system must become larger. Saturn's gravitational parameter approximates the center of scale symmetry $(26 + 29)/2 = 27 + 1/2$ between the parameters of Uranus $\mathcal{F}_e\langle 26\rangle$ and Jupiter $\mathcal{F}_e\langle 29\rangle$:

$$\mu_{Saturn} = \tau_e\cdot c^3\cdot e^{27+1/2}$$

Because the scaling factor $\sqrt{e}$ links attractors of electron stability to corresponding attractors of proton stability, the mean orbit radius of Saturn's largest moon Titan approximates also the main equipotential surface $\mathcal{F}_p\langle 57\rangle$. Titan's apoapsis $A_{\mathrm{O}} = 1.25706\cdot 10^9$ m delivers the upper approximation:

$$\ln\left(\frac{A_{\mathrm{O}}(Titan)}{\lambda_p}\right) = \ln\left(\frac{1.25706\cdot 10^9\,\mathrm{m}}{2.10309\cdot 10^{-16}\,\mathrm{m}}\right) = 57.05$$

Periapsis $1.18668\cdot 10^9$ m delivers the lower approximation:

$$\ln\left(\frac{P_{\mathrm{O}}(Titan)}{\lambda_p}\right) = \ln\left(\frac{1.18668\cdot 10^9\,\mathrm{m}}{2.10309\cdot 10^{-16}\,\mathrm{m}}\right) = 56.99$$

And Titan's orbital period $T_{\mathrm{O}} = 15.945$ days is approaching the main attractor $\mathcal{F}_p\langle 68\rangle$ of proton stability:

$$\ln\left(\frac{T_{\mathrm{O}}(Titan)}{2\pi\cdot\tau_p}\right) = \ln\left(\frac{15.945\cdot 86400\,\mathrm{s}}{2\pi\cdot 7.01515\cdot 10^{-25}\,\mathrm{s}}\right) = 67.92$$

In this way, Saturn's gravitational parameter approximates also the attractor $\mathcal{F}_p\langle 35\rangle$, because $57\cdot 3 - 68\cdot 2 = 35$ results in the 35^{th} power of Euler's number, multiplied by the oscillation period of the proton:

$$\mu_{Saturn} = \tau_p\cdot c^3\cdot e^{35}$$

Besides conservation of angular momentum [33], there is no known law concerning the rotation of celestial bodies. The more remarkable is the correspondence of the rotation periods of planets, planetoids and large moons with attractors of the Fundamental Fractal (1) as shown in [15]. Here we give some of the most expressive examples.

In the solar system, the 66^{th} power of Euler's number stabilizes not only the orbital period 4332.59 days of Jupiter, but also the orbital period 686.971 days of Mars and the rotational period 9.074 hours of the planetoid Ceres, the largest body of the main asteroid belt that orbits the Sun between Mars and Jupiter. The difference lays in the reference units. While in the case of Jupiter's orbital period, the reference unit is the oscillation period of the electron $2\pi\tau_e$, in the case of Mars, it is the angular oscillation period of the electron τ_e:

$$\ln\left(\frac{T_{\mathrm{O}}(Mars)}{\tau_e}\right) = \ln\left(\frac{686.971\cdot 86400\,\mathrm{s}}{1.28809\cdot 10^{-21}\,\mathrm{s}}\right) = 66.00$$

And in the case of the rotational period of Ceres, the reference unit is the angular oscillation period of the proton τ_p:

$$\ln\left(\frac{T_{\mathrm{R}}(Ceres)}{\tau_p}\right) = \ln\left(\frac{9.07417\cdot 3600\,\mathrm{s}}{7.01515\cdot 10^{-25}\,\mathrm{s}}\right) = 66.01$$

The rotational periods of Mars and Earth approximate the next main attractor $\mathcal{F}_p\langle 67\rangle$ of proton stability:

$$\ln\left(\frac{T_{\mathrm{R}}(Mars)}{\tau_p}\right) = \ln\left(\frac{24.62278\cdot 3600\,\mathrm{s}}{7.01515\cdot 10^{-25}\,\mathrm{s}}\right) = 67.01$$

$$\ln\left(\frac{T_{\mathrm{R}}(Earth)}{\tau_p}\right) = \ln\left(\frac{23.93447\cdot 3600\,\mathrm{s}}{7.01515\cdot 10^{-25}\,\mathrm{s}}\right) = 66.98$$

Mercury's period 58.64615 days of rotation is approaching the main attractor $\mathcal{F}_p\langle 71\rangle$. Although Venus rotation is retrograde, its period 243.025 days approximates the attractor $\mathcal{F}_p\langle 72;2\rangle$ that coincides with $\mathcal{F}_e\langle 65\rangle$. The rotation of further planets, planetoids and moons of the solar system we have analyzed in [15].

Conclusion

The application of our numeric-physical approach to the analysis of the orbital and rotational periods of the planets, planetoids and moons of the solar system and thousands of exoplanets [15] leads us to the conclusion that the avoidance of orbital, rotational, proton and electron parametric resonances by approximation of transcendental ratios can be viewed as a basic forming factor of planetary systems.

Studies of circumstellar disks around young stars conclude [34] that the planet formation process is observationally required to be both fast and common. Solid planets in the solar system should have then formed within less than a few million years, which is a major challenge for terrestrial planet formation theories [35].

Perhaps, our approach can explain the fast consolidation of the solar system. In fact, the scale-invariant fractal distribution of transcendental Euler attractors of stability is an inherent feature of the number continuum and therefore given a priori and does not require a long history of random collisions to find them.

The circumstance that the gravitational parameters of the Sun and the planets approximate main numeric attractors of electron and proton stability could be an approach to achieve a deeper understanding of gravitation.

In modern theoretical physics, numerical ratios usually remain outside the realm of theoretical interest. In this work we have tried to elucidate the physical meaning of numerical ratios and to show their theoretical and practical importance.

Acknowledgements

The author is grateful to Leili Khosravi, Simona Muratori, Viktor Panchelyuga, Oleg Kalinin, Viktor Bart and Michael Kauderer for valuable discussions.

Submitted on April 27, 2022

References

1. Hansson J. The 10 Biggest Unsolved Problems in Physics. *International Journal of Modern Physics and Applications*,2015, v. 1, no. 1, 12–16.
2. Heggie D. C. The Classical Gravitational N-Body Problem. arXiv: astro-ph/0503600v2, 11 Aug 2005.
3. Colombo G. Rotational Period of the Planet Mercury. *Letters to Nature*, 1965, no. 5010, 575.
4. Müller H. Global Scaling of Planetary Systems. *Progress in Physics*, 2018, v. 14, 99–105.
5. Gillon M. et al. Seven temperate terrestrial planets around the nearby ultracool dwarf star TRAPPIST-1. *Nature*, 2017, v. 542, 456–460.
6. Hand E. Kepler discovers first Earth-sized exoplanets. *Nature*, 2011, https://doi.org/10.1038/nature.2011.9688
7. Müller H. On the Cosmological Significance of Euler's Number. *Progress in Physics*, 2019, v. 15, 17–21.
8. Dombrowski K. Rational Numbers Distribution and Resonance. *Progress in Physics*, 2005, v. 1, no. 1, 65–67.
9. Panchelyuga V.A., Panchelyuga M. S. Resonance and Fractals on the Real Numbers Set. *Progress in Physics*, 2012, v. 8, no. 4, 48–53.
10. Minton D. A., Malhotra R. A record of planet migration in the main asteroid belt. *Nature*, 2009, v. 457, 1109–1111.
11. Müller H. The Physics of Transcendental Numbers. *Progress in Physics*, 2019, vol. 15, 148–155.
12. Hilbert D. Über die Transcendenz der Zahlen e und π. *Mathematische Annalen*, 1893, v. 43, 216–219.
13. Khintchine A. Continued fractions. University of Chicago Press, Chicago, (1964).
14. Müller H. Global Scaling. The Fundamentals of Interscalar Cosmology. *New Heritage Publishers*, Brooklyn, New York, USA, ISBN 978-0-9981894-0-6, (2018).
15. Müller H. Physics of Transcendental Numbers meets Gravitation. *Progress in Physics*, 2021, v. 17, 83–92.
16. Müller H. Fractal Scaling Models of Natural Oscillations in Chain Systems and the Mass Distribution of Particles. *Progress in Physics*, 2010, v. 6, 61–66.
17. Müller H. Emergence of Particle Masses in Fractal Scaling Models of Matter. *Progress in Physics*, 2012, v. 8, 44–47.
18. Ries A. Qualitative Prediction of Isotope Abundances with the Bipolar Model of Oscillations in a Chain System. *Progress in Physics*, 2015, v. 11, 183–186.
19. Ries A., Fook M. Fractal Structure of Nature's Preferred Masses: Application of the Model of Oscillations in a Chain System. *Progress in Physics*, 2010, v. 4, 82–89.
20. Müller H. Physics of Transcendental Numbers Determines Star Distribution. *Progress in Physics*, 2021, v. 17, 164–167.
21. Zylaet P.A. al. (Particle Data Group), *Prog. Theor. Exp. Phys.*, 083C01, 2020 and 2021 update.
22. Physical constants. Particle Data Group, pdg.lbl.gov
23. Müller H. Scale-Invariant Models of Natural Oscillations in Chain Systems and their Cosmological Significance. *Progress in Physics*, 2017, v. 13, 187–197.
24. Astrophysical constants. Particle Data Group, pdg.lbl.gov
25. Planck M. Über Irreversible Strahlungsvorgänge. *Sitzungsbericht der Königlich Preußischen Akademie der Wissenschaften*, 1899, v. 1, 479–480.
26. Müller H. Quantum Gravity Aspects of Global Scaling and the Seismic Profile of the Earth. *Progress in Physics*, 2018, v. 14, 41–45.
27. Müller H. Global Scaling of Planetary Atmospheres. *Progress in Physics*, 2018, v. 14, 66–70.
28. Müller H. Physics of Transcendental Numbers on the Origin of Astrogeophysical Cycles. *Progress in Physics*, 2021, v. 17, 225–228.
29. Rampino M. R., Caldeira K., Zhu Y. A pulse of the Earth: A 27.5-Myr underlying cycle in coordinated geological events over the last 260 Myr. *Geoscience Frontiers*, 2021, v. 12, 101245.
30. Catalog of Exoplanets. Observatoire de Paris, http://exoplanet.eu/
31. NASA Planetary Fact Sheet – Metric (2019).
32. Bills B. G., Ray R. D. Lunar Orbital Evolution: A Synthesis of Recent Results. *Geophysical Research Letters*, 1999, v. 26, no. 19, 3045–3048.
33. Tiruneh G. Explaining Planetary-Rotation Periods Using an Inductive Method. arXiv:0906.3531, 2009.
34. Haisch K. E. et al. Disk frequencies and lifetimes in young clusters. *The Astrophysical Journal*, 2001, v. 553, L153–L156.
35. Montmerle T. et al. Solar System Formation and Early Evolution: the First 100 Million Years. *Earth, Moon, and Planets*, 2006, v. 98, 39–95.

Length Stretching and Time Dilation in the Field of a Rotating Body

Dmitri Rabounski and Larissa Borissova

Puschino, Moscow Region, Russia
E-mail: rabounski@yahoo.com, lborissova@yahoo.com

As was found in the first paper of this series of papers, the rotation of space produces a significant curvature (Progr. Phys., 2022, v.18, 31–49). In the second paper, we showed that light rays and mass-bearing particles are deflected near a rotating body due to the curvature of space caused by its rotation (ibid., 50–55). In this article we show that, since the rotation of the Earth around its axis curves the Earth's space making it "stretched" along the geographical longitudes, the measured length of a standard rod is greater when the rod is installed in the longitudinal direction. Due to the same reason, there is a time loss on board an airplane flying to the East (the direction in which the Earth's space rotates), and also a time gain when flying in the opposite direction, to the West. Both of the above effects are maximum at the equator (where the curvature of the Earth's space caused by its rotation is maximum and, therefore, space is maximally "stretched") and descrease towards the North and South Poles.

This paper is dedicated to the memory of Joseph C. Hafele, the outstanding American experimental physicist known due to his famous around-the-world-clocks experiment.

This is the third paper in the series of our papers on the effects of the space curvature caused by the rotation of space.

Recall that in the first paper [1], besides many other scientific results, it was found that the rotation of space produces a significant curvature due to its space-time non-holonomity (non-orthogonality of the time lines to the three-dimensional spatial section). In the second paper [2] that followed the first one, it was shown that light rays and mass-bearing particles are deflected near a rotating body due to the space curvature caused by the rotation of its space.

In particular, according to the formulae we have obtained, the curvature of the Earth's space, caused by its rotation, decreases from the equator, where it is maximum, to the geographical poles, and its effect depends on the direction of the measurement path with respect to the direction in which the Earth rotates.

This small paper is based of the previous two. We will calculate here the effects of length stretching and time loss/gain, which are due to the curvature of the Earth's space, caused by its rotation.

As always, we use the mathematical apparatus of chronometric invariants, which are physically observable quantities in the General Theory of Relativity. This mathematical apparatus was created in 1944 by our esteemed teacher A. L. Zelmanov (1913–1987) and published in his presentations [3–5], among which [5] is most complete. For a deeper study of this subject, read either our first article in this series [1] or the respective chapters in our monographs [6, 7].

Chronometrically invariant quantities are projections of four-dimensional (general covariant) quantities onto the line of time and the three-dimensional spatial section, which are linked to the physical space of a real observer, and are invariant everywhere along the spatial section (his observed space). They are calculated using operators of projection, which take the structure of space into account. Since a real space can be curved, inhomogeneous, anisotropic, deforming, rotating, be filled with distributed matter etc., the lines of real time can have different density of time coordinates, and the three-dimensional coordinate grids can have different density of real three-dimensional coordinates. Therefore, chronometrically invariant quantities are truly physically observables registered by the observer.

In particular, the physically observable chr.inv.-projection of the four-dimensional interval dx^α onto the time line of an observer is the interval of physically observable time

$$d\tau = \sqrt{g_{00}}\, dt - \frac{1}{c^2}\, v_i\, dx^i,$$

and the physically observable chr.inv.-projections of dx^α onto his spatial section are the regular three-dimensional coordinate intervals dx^i. Here v_i is the linear velocity of the three-dimensional rotation of space, which arises due to the non-holonomity of the space-time (non-orthogonality of the time lines to the three-dimensional spatial section). It is determined as

$$v_i = -\frac{c\, g_{0i}}{\sqrt{g_{00}}}, \qquad v^i = -c\, g^{0i} \sqrt{g_{00}}\,,$$

where g_{00} is expressed through the gravitational potential w as usually, i.e., $\mathrm{w} = c^2 (1 - \sqrt{g_{00}})$.

The fundamental metric tensor $g_{\alpha\beta}$, projected onto the three-dimensional spatial section of an observer, gives the chr.inv.-metric tensor h_{ik} of his space

$$h_{ik} = -g_{ik} + \frac{1}{c^2}\, v_i\, v_k, \quad h^{ik} = -g^{ik}, \quad h^i_k = -g^i_k = \delta^i_k,$$

which has all properties of $g_{\alpha\beta}$ in the three-dimensional spatial section. Using the chr.inv.-metric tensor, we can lift and

lower indices in chr.inv.-quantities, and also get their squares. Thus, the square of the three-dimensional physically observable interval on the spatial section is calculated as

$$d\sigma^2 = h_{ik}\,dx^i dx^k = \left(-g_{ik} + \frac{1}{c^2}\,v_i v_k\right) dx^i dx^k.$$

In our further calculations, we will use the same space metric that we used in two previous papers. This is the metric of a space, where the three-dimensional space rotates due to the non-holonomity of the space-time, but there is no field of gravitation. More precisely, we neglect the influence of the Earth's gravitation, since in our further examples we do not change the altitude above the Earth's surface, so the influence of the gravitational potential remains constant.

Assuming that the space rotates along the equatorial axis φ, i.e., along the geographical longitudes, with the linear velocity $v_3 = \omega r^2 \sin^2\theta$ (here $\omega = const$ is the angular velocity of this rotation), we obtain g_{03} from the definition of v_i,

$$v_3 = \omega r^2 \sin^2\theta = -\frac{c\,g_{03}}{\sqrt{g_{00}}},$$

and then we obtain the metric of such a space

$$ds^2 = c^2 dt^2 - 2\,\omega r^2 \sin^2\theta\, dt\, d\varphi - \\ - dr^2 - r^2\left(d\theta^2 + \sin^2\theta\, d\varphi^2\right).$$

The non-zero components of the fundamental metric tensor $g_{\alpha\beta}$ of this metric are obvious from the above

$$g_{00} = 1, \qquad g_{03} = -\frac{\omega r^2 \sin^2\theta}{c},$$
$$g_{11} = -1, \quad g_{22} = -r^2, \quad g_{33} = -r^2\sin^2\theta,$$

and the non-zero components of the chr.inv.-metric tensor h_{ik}, calculated from the above, are equal to

$$h_{11} = 1, \quad h_{22} = r^2, \quad h_{33} = r^2\sin^2\theta\left(1 + \frac{\omega^2 r^2 \sin^2\theta}{c^2}\right).$$

Now we have everything that is required for our further calculations.

So forth, we will calculate two effects due to the curvature of the Earth's space caused by its rotation.

First, we will calculate the effect of length stretching of a rod depending on its direction (in the equatorial, latitudinal and radial directions), as well as on the geographical latitude of the measurement site. According to the formulae for the Ricci curvature tensor and the scalar curvature, which we have obtained in the first paper [1, p. 45], the Earth's space is curved due to its rotation in the equatorial (longitudinal) direction, and its curvature decreases with the latitude from the equator, where the Earth's space is maximally "stretched", to the geographical poles of the Earth. Therefore, the measured length of a standard rod is expected to be greater when the rod is installed in the direction along the geographical longitudes, and this effect of length stretching is maximum at the equator and decreases with the geographical longitudes towards the North and South Poles.

Second, we will calculate the difference in time on board an aircraft flying Westward and Eastward. It is expected that the rotation of the Earth's space causes a time loss when flying Eastward, the direction in which the Earth's space rotates, and a time gain when flying in the opposite direction, to the West. We also expect that the mentioned effects of time loss and time gain are greater when the airplane travels along the equator (where the curvature of the Earth's space caused by its rotation is maximum and, therefore, space is maximally "stretched") and decrease from the equator towards the North and South Poles.

1. Consider a standard rigid rod of an elementary length dl_0, which is installed in a laboratory located somewhere on the surface of the Earth. Assume that the rod is installed in stages in three different positions: in the equatorial direction φ (along the geographical longitudes), in the polar direction θ (along the geographical latitudes), and in the radial direction r read from the centre of the Earth.

Using the formula for the square of the three-dimensional physically observable interval $d\sigma^2 = h_{ik}\,dx^i dx^k$ and the components of the physically observable chr.inv.-metric tensor h_{ik} we have obtained for an Earth-like rotating space (see above), we calculate the rod's length measured in each of the three indicated positions. It is respectively equal to

$$dl_r = \sqrt{h_{11}\,dr^2} = dr = dl_0,$$

$$dl_\theta = \sqrt{h_{22}\,d\theta^2} = r\,d\theta = dl_0,$$

$$dl_\varphi = \sqrt{h_{33}\,d\varphi^2} = \sqrt{1 + \frac{\omega^2 r^2 \sin^2\theta}{c^2}}\; r\sin\theta\, d\varphi = \\ = \sqrt{1 + \frac{\omega^2 r^2 \sin^2\theta}{c^2}}\; dl_0,$$

where $dr = dl_0$ is the length of an elementary segment along the radial r-axis, $r\,d\theta = dl_0$ is the length of an elementary arc along the latitudinal θ-axis (where θ is the polar angle read from the North Pole), and $r\sin\theta\,d\varphi = dl_0$ is the length of an elementary arc along the equatorial φ-axis.

As you can see from the above formulae, the rod retains its original physically observable length dl_0, when installed in the positions along the radial direction ($dl_r = dl_0$) and along the geographical latitudes ($dl_\theta = dl_0$).

However, when the rod is installed in the position along the geographical longitudes, i.e., along the equatorial direction in which the Earth's space rotates, its physically observable length dl_φ becomes greater by a small amount δl depending on the factor specific of the curvature of space caused by

its rotation [1, p. 45], i.e.,

$$dl_\varphi = \sqrt{1 + \frac{\omega^2 r^2 \sin^2\theta}{c^2}}\, dl_0 \simeq \left(1 + \frac{\omega^2 r^2 \sin^2\theta}{2c^2}\right) dl_0,$$

$$\delta l \simeq \frac{\omega^2 r^2 \sin^2\theta}{2c^2}\, dl_0.$$

Let us calculate the numerical value of this length stretching δl. The angular velocity of the Earth's rotation is equal to $\omega = 1$ rev/day $= 1.16 \times 10^{-5}$ rev/sec. The Earth's radius is equal to $r = 6.4 \times 10^8$ cm. Then the length stretching of a rod installed at the equator of the Earth in the direction along the longitudinal axis φ is equal to

$$\delta l \simeq 3.1 \times 10^{-14}\, dl_0$$

of the original length dl_0 of the rod. At the latitude of the Greenwich Observatory (51° North Lat., $\theta = 90° - 51° = 39°$) the length stretching of a rod installed along the longitudinal axis φ is less than at the equator and is equal to

$$\delta l \simeq 1.2 \times 10^{-14}\, dl_0,$$

and this effect of length stretching vanishes at the geographical poles of the Earth, since there $\sin\theta = 0$ and, hence,

$$\delta l = 0, \qquad dl_\varphi = dl_0.$$

So, we clearly see that the curvature of the Earth's space along the equatorial (longitudinal) axis, caused by the rotation of the Earth, and, as a result, the "stretching" of physical coordinates along the geographical longitudes, lead to the stretching of the physically observable length of a rod, installed in the position along the geographical longitudes.

The mentioned effect of length stretching is maximum at the equator, where the curvature of the Earth's space and the longitudinal stretching of physical coordinates caused by the Earth's rotation is maximum, and decreases towards the geographical poles, where the length stretching vanishes.

2. Consider an atomic clock installed on board an airplane flying, in stages, Westward and Eastward around the Earth. In this case, according to the definition of physically observable time, and taking the characteristics of an Earth-like rotating space into account (see above), the flight time τ registered on board the airplane is equal to

$$\tau = \left(1 - \frac{1}{c^2}\, v_3\, u^3\right) t = \left(1 - \frac{\omega r^2 \sin^2\theta}{c^2}\, u^3\right) t,$$

where t is the reference (coordinate) time counted using a reference clock installed at the point of departure (which is the same as at the point of arrival in an around-the-world flight), and u^3 is the linear coordinate velocity of the airplane, which is measured along the third, equatorial (longitudinal) axis φ as the difference in the geographical longitudes traveled by the airplane per second.

If the airplane stays at the airport, its coordinate velocity is equal to zero $u^3 = 0$ and, therefore, the second term in the above formula vanishes. In this case, the clock installed on board the airplane count the same time as the reference clock at the airport ($\tau = t$).

Since the Earth rotates from West to East, an airplane, when flying Eastward, travels in the same direction in which the Earth's space rotates (the airplane's velocity is co-directed with the rotation velocity of the Earth's space). As a result, the clock installed on board the airplane should register a time loss, the amount of which is calculated as

$$\delta\tau_{\text{East}} = -\frac{\omega r^2 \sin^2\theta}{c^2}\, u^3 t.$$

When an airplane flies Westward, its velocity is directed opposite the rotation velocity of the Earth's space. Accordingly, in this case, the clock on board the airplane should register a time gain, the amount of which is

$$\delta\tau_{\text{West}} = +\frac{\omega r^2 \sin^2\theta}{c^2}\, u^3 t.$$

Assume that the airplane flies along the equator around the Earth at a constant cruising speed of 800 km/hour, which means that $u^3 = +5.5 \times 10^{-6}$ rev/sec when flying Eastward and $u^3 = -5.5 \times 10^{-6}$ rev/sec when flying Westward. Thus, the airplane returns to its point of departure in a time interval $t = 1.8 \times 10^5$ sec. The angular velocity of the Earth's rotation is equal to $\omega = 1$ rev/day $= 1.16 \times 10^{-5}$ rev/sec and the Earth's radius is equal to $r = 6.4 \times 10^8$ cm. Thus, we obtain that the clock on board this airplane should register a time loss when flying Eastward and a time gain when flying Westward, which are respectively equal to

$$\delta\tau_{\text{East}} = -5.3 \text{ nanosec}, \quad \delta\tau_{\text{West}} = +5.3 \text{ nanosec}.$$

That is, the rotation of the Earth's space results in a 5.3 nanosecond loss in time on board an Eastward-flying airplane travelled around the world along the equator, i.e., in the direction in which the Earth's space rotates, and a 5.3 nanosecond gain of time when travelled around the world in the opposite direction, to the West.

The above effect of time loss and time gain caused by the rotation of the Earth's space decreases with the geographical latitude due to the sine of the polar angle, which is a multiplier in the above formulae. For example, when flying Eastward and Westward around the Earth along the Greenwich parallel (51° North Lat., $\theta = 39°$), the effect of time loss and time gain is respectively equal to

$$\delta\tau_{\text{East}} = -2.1 \text{ nanosec}, \quad \delta\tau_{\text{West}} = +2.1 \text{ nanosec}.$$

This effect obviously vanishes at the geographical poles of the Earth, since there $\sin\theta = 0$.

Yes, the expected loss/gain in the flight time is only 5.3 nanoseconds at the equator, and it decreases to the geographical poles. Compare, in the Hafele-Keating around-the-world-clocks experiment [8–10], the common effect of the relativistic addition of the Earth's rotation velocity to the airplane's velocity and also the decrease of the gravitational potential of the Earth with the flight altitude resulted a time loss of -59 ± 10 nanoseconds Eastward and a time gain of $+273 \pm 7$ nanoseconds Westward. The UK's National Measurement Laboratory commonly with the BBC repeated the Hafele-Keating experiment on its 25th anniversary in 2005, on board a London-Washington-London flight and with a better precision of ± 2 nanoseconds [11]. But even such a high measurement precision does not allow us to reliably register the expected 5.3 nanosecond loss/gain in the flight time (and this effect decreases to 2 nanoseconds at the middle latitudes).

Fortunately, the loss/gain in the flight time, caused by the rotation of the Earth's space, is a "cumulative effect": it depends linearly on the flight time (see the formula above). That is, when an airplane will "wind circles" around the Earth, the effect of time loss/gain on its board, caused by the rotation of the Earth's space, will increase with each revolution. And, after three-four-five revolutions around the Earth, the expected effect caused by the rotation of the Earth's space will be many times (or even dozens of times) higher than the measurement precision.

This is the real way to register the effect of time loss/gain, caused by the rotation of the Earth's space. "Winding circles" around the Earth is easier not using an airplane, but on board a spacecraft orbiting the Earth because it travels around the Earth two dozen times a day anyway and without the need of aviation kerosene. Thus, having an atomic clock installed on board an orbital spacecraft, the effect of time loss/gain, caused by the rotation of the Earth's space, can be accumulated to a surely measurable numerical value in just a few days, without doing anything for this.

The aforementioned effects of length stretching and time loss/gain, occurring due to the curvature of the Earth's space caused by its rotation, are new fundamental effects of the General Theory of Relativity. They are in addition to the effect of deflection of light rays and mass-bearing particles in the field of a rotating body, which we theoretically discovered earlier, and the well-known Einstein effect of deflection of light rays in the field of a gravitating body.

We dedicate this paper to the memory of Joseph C. Hafele (1933–2014), the outstanding American experimental physicist who initiated and later performed (together with Richard E. Keating) the famous around-the-world-clocks experiment, now known as the Hafele-Keating experiment [8–10].

We had an extensive correspondence with Joseph Hafele in the 2010s, in which we discussed various problems. Unfortunately, his sudden death had interrupted our acquaintance. He was a truly gentleman, good Catholic and a honest scientist who never compromised [12].

Surely he would be happy, if he read this article and saw it published.

Submitted on May 17, 2022

References

1. Rabounski D. and Borissova L. Non-quantum teleportation in a rotating space with a strong electromagnetic field. *Progress in Physics*, 2022, v. 18, issue 1, 31–49.
2. Rabounski D. and Borissova L. Deflection of light rays and mass-bearing particles in the field of a rotating body. *Progress in Physics*, 2022, v. 18, issue 1, 50–55.
3. Zelmanov A. L. Chronometric Invariants. Translated from the 1944 PhD thesis, American Research Press, Rehoboth, New Mexico, 2006.
4. Zelmanov A. L. Chronometric invariants and accompanying frames of reference in the General Theory of Relativity. *Soviet Physics Doklady*, 1956, v. 1, 227–230 (translated from *Doklady Academii Nauk USSR*, 1956, v. 107, issue 6, 815–818).
5. Zelmanov A. L. On the relativistic theory of an anisotropic inhomogeneous universe. *The Abraham Zelmanov Journal*, 2008, vol. 1, 33–63 (translated from the thesis of the *6th Soviet Conference on the Problems of Cosmogony*, USSR Academy of Sciences Publishers, Moscow, 1957, 144–174).
6. Rabounski D and Borissova L. Particles Here and Beyond the Mirror. The 3rd expanded edition, American Research Press, Rehoboth, New Mexico, 2012 (the 1st edition was issued in 2001).
   Rabounski D. et Borissova L. Particules de l'Univers et au delà du Miroir. American Research Press, Rehoboth, New Mexico, 2012 (French translation).
7. Borissova L. and Rabounski D. Fields, Vacuum, and the Mirror Universe. The 2nd expanded edition, Svenska fysikarkivet, Stockholm, 2009 (the 1st edition was issued in 2001).
   Borissova L. et Rabounski D. Champs, Vide, et Univers miroir. American Research Press, Rehoboth, New Mexico, 2010 (French translation).
8. Hafele J. Performance and results of portable clocks in aircraft. PTTI 3rd Annual Meeting, November 16–18, 1971, 261–288.
9. Hafele J. and Keating R. Around the world atomic clocks: predicted relativistic time gains. *Science*, July 14, 1972, v. 177, 166–168.
10. Hafele J. and Keating R. Around the world atomic clocks: observed relativistic time gains. *Science*, July 14, 1972, v. 177, 168–170.
11. Demonstrating relativity by flying atomic clocks. *Metromnia*, the UK's National Measurement Laboratory Newsletter, issue 18, Spring 2005.
12. Rabounski D. and Borissova L. In memoriam of Joseph C. Hafele (1933–2014). *Progress in Physics*, 2015, v. 11, issue 2, 136.

Space-Time Quantification

F. M. Sanchez[1], C. Bizouard[2], M. Grosmann[3], D. Weigel[4], R. Veysseyre[5], V. Kotov[6]

[1]Retired from Paris 11 University, France. E-mail: hol137@yahoo.fr
[2] Observatoire de Paris / SYRTE, PSL, France. E-mail: christian.bizouard@obspm.fr
[3] Retired Prof. of Physics, University of Strasbourg, France. Email: michelgrosmann@me.com
[4] Retired Prof. of Crystallography, University of Paris 6, France. Email: dominiqueweigel18@gmail.com
[5] Professeur Honoraire à l'Ecole Centrale de Paris, France. Email: renee.veysseyre@gmail.com
[6] Crimean Astrophysical Observatory, Russia. Email: vkotov43@mail.ru

The quantification of Length and Time in Kepler's laws implies an angular momentum quantum, identified with the reduced Planck's constant, showing a mass-symmetry with the Newtonian constant G. This leads to the Diophantine Coherence Theorem which generalizes the synthetic resolution of the Hydrogen spectrum by Arthur Haas, three years before Bohr. The Length quantum breaks the Planck wall by a factor 10^{61}, and the associated Holographic Cosmos is identified as the source of the Background Radiation in the Steady-State Cosmology. An Electricity-Gravitation symmetry, connected with the Combinatorial Hierarchy, defines the steady-state Universe with an invariant Hubble radius 13.812 milliard light-year, corresponding to 70.796 (km/s)/Mpc, a value deposed (1998) in a Closed Draft at the Paris Academy, confirmed by the WMAP value and the recent Carnegie-Chicago Hubble Program, and associated with the Eddington number and the Kotov-Lyuty non-local oscillation. This confirms definitely the Anthropic Principle and the Diophantine Holographic Topological Axis rehabilitating the tachyonic bosonic string theory. This specifies G, compatible with the BIPM measurements, but at 6 σ from the official value, defined by merging discordant measurements.

1 The Diophantine Coherence Theorem (DCT)

For connecting different physical measurements, Physics uses multiplication while addition is forbidden. But multiplication is a generalization of addition [1]. This paradox may be suppressed by considering only numerical ratios of the same physical quantity, as in the third Kepler law, *introducing Space and Time quanta* L_1 and T_1 [15]. Considered as a Diophantine Equation, which uses only natural numbers n, it resolves directly:

$$\begin{aligned}&(T_n/T_1)^2 = (L_n/L_1)^3 \equiv n^6\\ &\Rightarrow T_n = n^3 T_1 \;\;;\;\; L_n = n^2 L_1\,.\end{aligned} \tag{1}$$

This proceeds from the Holic Principle [27], a Diophantine form of the Holographic Principle, which states that Physics is described through the simplest degenerate Diophantine Equations, where the exponents identify with the dimensions 3 for Space, 2 for a 2D Time [39], 5 for Mass, and 7 for Field. The n-invariant L_n^3/T_n^2 is homogeneous to Gm_G, where G is Newton's gravitational constant, and m_G is a mass (here the usual central mass is divided by the factor $4\pi^2$). The other Kepler's law states that the orbital angular momentum per unit mass is an orbital invariant. Since the corresponding term L_n^2/T_n is proportional to n, this implies an orbital momentum quantum, identified to the reduced Planck constant, or *action quantum* $\hbar$, privileged by the particle physics in the spin concept. While the ratio of the kinematic parts of G and $\hbar$ are homogeneous to a speed, these two universal constants presents a symmetry by respect to the mass concept, implying the association of $\hbar$ with a mass $m_\hbar$:

$$L_n^3/T_n^2 = Gm_G \quad ; \quad L_n^2/T_n = n\hbar/m_\hbar\,. \tag{2}$$

Any mass pair $(m_G, m_\hbar)$ is associated to a series of Keplerian orbits $(L_n, T_n,)$:

$$L_n = \frac{(n\hbar)^2}{Gm_G m_\hbar^2} \quad ; \quad T_n = \frac{(n\hbar)^3}{G^2 m_G^2 m_\hbar^3}\quad . \tag{3}$$

For n = 1 and $m_G = m_\hbar = m$, the Special Non-Local Length and Time are:

$$L_{NL}(m) = \frac{\hbar^2}{Gm^3} \quad ; \quad T_{NL}(m) = \frac{\hbar^3}{G^2 m^5}\;. \tag{4}$$

Introducing the *formal* velocity $V_n = L_n/T_n$, this connects the reduced Planck energy $n\hbar/T_n$ with the gravitational potential energy pertaining to masses m_G and $m_\hbar$ and the energy $m_\hbar V_n^2$:

$$\begin{aligned}&V_n = L_n/T_n = Gm_G m_\hbar/n\hbar\\ &\Rightarrow n\hbar/T_n = Gm_G m_\hbar/L_n = m_\hbar V_n^2\,.\end{aligned} \tag{5}$$

With the Planck mass $m_P = \sqrt{\hbar c/G}$, where the light speed c is the third universal constant, this reads

$$\frac{n\hbar}{T_n} = \frac{Gm_G m_\hbar}{L_n} = m_\hbar V_n^2 \equiv m_\hbar\left(\frac{c}{nA}\right)^2 \quad ; \; A = \frac{m_P^2}{m_G m_\hbar}\;. \tag{6}$$

This is called the *Diophantine Coherence Theorem* (DCT).

2 The atom H and the Holographic Cosmos

Three years before Bohr, Arthur Haas [3] considered *the electron orbital period* in the Rutherford model, and the corresponding Planck energy $nh\nu = nh/T_n = n\,\hbar v_n/L_n$ where $v_n = 2\pi V_n$ is the orbital velocity. The correct Hydrogen spectrum is obtained by equalizing it with the electric potential energy $\hbar c/aL_n$, where $a \approx 137.0359991$ is the electric constant, and the double (virial) kinetic electron energy $m_e v_n^2$ (the useful physical constants are listed in Table 1):

$$n\hbar\frac{v_n}{L_n} = \frac{\hbar c}{aL_n} = m_e v_n^2 \equiv m_e\left(\frac{c}{na}\right)^2 . \tag{7}$$

Note that the so-called "properties of vacuum" ϵ_0 and μ_0 are unnecessary: they are only introduced for historical reasons, leading to the cumbersome, but official, choice of electrical units, hiding the true "electrical constant" a, whose inverse α, called "the fine structure constant" is of minor importance. For $n = 1$, this gives the bare Hass-Bohr radius: $r_{HB} = a\lambda\!\!\!^{-}_e$, where $\lambda\!\!\!^{-}_e \equiv \hbar/(m_e c)$ is the Reduced Electron wavelength (the effective electron mass effect defines the Bohr radius $r_B = r_{HB}/(1 + 1/p)$). This double equation shows up the same form that the above DCT (6), where additional 2π factors are integrated in the definitions of m_G and $m_{\hbar}$. The identification of potential energy terms implies $m_G m_{\hbar} = m_P^2/a$, thus in this case $A = a$. The simplest choice $m_{\hbar} = m_e$ implies the following m_G, where $m_N = am_e$ is *the Nambu mass, a quasi-quantum in Particle Physics* [17]:

$$m_{\hbar} = m_e \quad ; \quad m_G = \frac{m_P^2}{m_N} \quad ; \quad A = a\,. \tag{8}$$

This last mass is $m_G \approx 3.7939\times10^{12}$ kg, whose corresponding Special Length (4) is:

$$d_0 = L_{NL}(m_P^2/m_N) \approx 3.051\times10^{-96}\,\text{meter}\,. \tag{9}$$

This is the Cosmic Space Quantum d_0 breaking the "Planck Wall" by a factor 10^{61} which has been associated to the Cosmos holographic radius R_{hol} [14]:

$$\pi\left(\frac{R_{hol}}{l_P}\right)^2 = 2\pi\frac{R_{hol}}{d_0} \ . \tag{10}$$

This is the Bekenstein-Hawking Entropy formula of the Holographic Principle [6] where the *Planck Length*

$$l_P \equiv (G\hbar/c^3)^{1/2} \equiv L_{NL}(m_P)$$

is a basic holographic length. The Cosmos radius R_C has been defined by the natural *mono-chromatic* holographic extension:

$$\pi\left(\frac{R_{hol}}{l_P}\right)^2 = 2\pi\frac{R_{hol}}{d_0} = 2\pi\frac{R_C}{l_P} \ , \tag{11}$$

leading to:

$$\begin{aligned} R_{hol} &= 2L_{NL}(m_N) \approx 18.105\ \text{Giga light-year (Glyr)} \\ R_C &= 2L_{NL}(m_N^2/m_P) \approx 9.075\times10^{86}\ \text{meter}\,. \end{aligned} \tag{12}$$

Table 2 shows this symmetry between the Nambu mass m_N and the Planck mass m_P, whose large value is the source of the "Hierarchical Problem" [41]. From $P/\sqrt{a} \approx a_w n_t^3$, where $P = m_P/m_e$, these formula leads to a confirmation of the optimal G value in the ppb domain (Table 1), where $\beta = (H-p)^{-1}$

$$\left(\frac{P}{a_w}\right)^3 \approx \left(\frac{4\pi}{\sqrt{a}}\right)^8 \frac{(pH\beta^2)^5}{2} \approx \frac{aW}{137\,Z}\,(pH)^5\ (16\ \text{ppm}), \tag{13}$$

showing the role of the geometrical factor 4π.

Now $L_{NL}(\sqrt{m_P m_N}) \approx \lambda_{CMB}/2a_s^2$ ($2a_s^2 \sim a$), tying to 0.3% the strong coupling a_s and the nominal wavelength hc/kT_{CMB} of the Cosmic Microwave Background (CMB), whose source is lacking in the steady-state cosmology [7]. The simplest hypothesis is that the above Cosmos is this source. Indeed, the Wien CMB wavelength λ_{Wn} enters (0.1%):

$$4\pi\left(\frac{R_{hol}}{\lambda_{Wn}}\right)^2 \approx e^a. \tag{14}$$

This perfect holographic formula suggests that *the background would be coherent, meaning it brings information.* This could be the real significance of the CMB Anisotropy Statistics [29].

3 The gravitational hydrogen molecule

The Haas method was already applied to the *special three-body* dihydrogen molecule [13, p.391]:

$$n\hbar\frac{v_n}{L_n} = \frac{Gm_p m_H}{L_n} = m_e v_n^2\,, \tag{15}$$

The comparison with the above Haas equation implies the substitution: $a \to a_G = m_P^2/m_p m_H$, corresponding to the following m_G value:

$$m_{\hbar} = m_e \quad ; \quad m_G = m_{bc}\,; \quad A = a_G \tag{16}$$

where $m_{bc} = m_p m_H/m_e$ is close to the DNA bi-codon mass, which shows a central position in the Topological Axis [13], corresponding to the dimension 16. Indeed the topological term $f(16) = e^{16}$ is close to pH, and, more precisely, to $2n_t^4/a^3$ (0.04%).

For n = 1, this Haas-Sanchez radius R_{H_2} shows a direct Electricity-Gravitation symmetry, by respect to the Reduced Electron wavelength $\lambda\!\!\!^{-}_e = \hbar/m_e c$:

$$\begin{aligned} r_{HB} &= a\lambda\!\!\!^{-}_e = a\,\frac{\hbar}{m_e c} \\ R_{H_2} &= a_G\lambda\!\!\!^{-}_e = \frac{\hbar^2}{Gm_e m_p m_H} \equiv L_{NL}(m_0)\,, \end{aligned} \tag{17}$$

where $m_0 = (m_e m_p m_H)^{1/3}$. Note that a and a_G are very close to the last two terms of the Combinatorial Hierarchy 137 and $N_L + 137$, with $N_L = 2^{127} - 1$, the Lucas Number [12].

Table 1: Physical constants

Quantity	Value	Unit	10^{-9}
Electrical Constant a	137.035999084(21)	-	0.15
Electron Excess Magnetic moment d_e	1.00115965218096	-	0.26
Official Strong Coupling constant Optimal Strong Coupling Constant a_s [15]	8.45(5) 8.434502914	- -	
Proton/Electron mass ratio p	1836.152 673 43	-	0.06
Proton/Electron Wyler mass ratio p_W [33]	$6\pi^5$	-	exact
Neutron/Electron mass ratio n_t	1838.683 661 7	-	0.5
Hydrogen/Electron mass ratio H	1837.152 660 14	-	0.06
Hydrogen Relativist correction factor $\beta = 1/(H - p)$	1.0000266	-	
Optimal Muon/Electron mass ratio μ [14]	206.768 286 9	-	
Optimal Higgs Boson mass m_{Hg} [15]	$495^2 m_e$	-	
Action quantum $\hbar$	$1.054\,571\,81\,10^{-34}$	J s	exact
Official Gravitation Constant G_{off} Optimal Gravitation Constant G	$6.674\,30 \times 10^{-11}$ $6.67545272 \times 10^{-11}$ [14]	$kg^{-1}m^3s^{-2}$ $kg^{-1}m^3s^{-2}$	
Speed of light in vacuum c	299 792 458	m s^{-1}	exact
Optimal Fermi Constant $G_F = \hbar^3/cm_F^2$	$1.435\,851\,10^{-62}$	J m^3	
Optimal Fermi mass ratio $m_F/m_e = F = a_w^{1/2}$	573007.3652	-	
W boson mass ratio $W = m_W/m_e$	157298 ± 23	-	1.5×10^5
Z boson mass ratio $Z = m_Z/m_e$	178450 ± 4	-	2.3×10^4
Electron mass m_e	$9.109\,383\,701\,5\,10^{-31}$	kg	0.3
Boltzmann Constant k	$1.380649\,10^{-23}$	J K^{-1}	exact
Reduced Electron Wavelength $\lambda\!\!\!^{-}_e$	$3.861\,592\,675\,10^{-13}$	m	0.3
Measured CMB temperature T_{CMB} Optimal CMB Temperature T_{CMB}	2.725 5(6) 2.725 820 138 [14]	Kelvin K	
Optimal CMB Wien wavelength λ_{Wn}	$1.063\,082\,472\,10^{-3}$ [14]	m	
Optimal CMB reduced wavelength $\hbar\lambda_{CMB} = \hbar c/kT_{CMB}$	$8.400\,716\,617\,10^{-4}$ [14]	m	
Optimal CNB Temperature $T_{CNB} \equiv T_{CMB}(11/4)^{-1/3}$	1.945 597 [14]	Kelvin	
Optimal CNB reduced wavelength $\lambda\!\!\!^{-}_{CNB} = \hbar c/kT_{CNB}$	$1\,176\,956\,918\,10^{-3}$ [14]	m	
Optimal critical density $\rho_{cr} = 3c^2/8\pi GR^2$	$9.411\,979\,89\,10^{-27}$	kg $m^{-1/3}$	
Kotov P_0 period t_K	9600.606(12) [19]	s	1200

In R_{H_2} the speed c is eliminated: for this reason, a precise approximation was immediately guessed by the c-free "dimensional analysis", the so-called *Three Minutes Formula*, from the ternary symmetry Electron-Proton-Neutron (Closed Letter to the Paris Science Academy, March 1998) [22] (see Table 2). The associated Special time $T_{NL}(m_0)$ is very close (0.9%) to the time associated to the triplet: $\hbar$, the Fermi constant G_F and the associated critical steady-state density $\rho_{cr} = 3c^2/8\pi GR^2$ where $R = 2R_{H_2}$ and it is

$$\hbar^4/G_F^{5/2}\rho_{cr}^{3/2} \approx 3m_P^2 R_{hol}/cm_e m_Z$$

(0.01%), comforting the following steady-state Universe.

4 The Steady-State Universe revisited

A salient feature of the Universe is its critical character, relating its horizon radius R with its mass by $R = 2GM/c^2$. How-

Table 2: Values of the DCT Fundamental (n = 1) Radius $\hbar^2/Gm_G m_{\hbar}^2$ for specific values of m_G and $m_{\hbar}$. Planck mass: m_P. Nambu mass: $m_N = am_e$. Holographic ratio $u = R_{hol}/R$. Proton mass: m_p. Hydrogen mass: m_H. Mean Atomic mass: $m_0 = (m_e m_p m_H)^{1/3}$. Bicodon mass $m_{bc} = m_p m_H/m_e$. Photon mass $m_{ph} = \hbar/c^2 t_K \approx 1.2222 \times 10^{-55}$ kg. Graviton mass: $m_{gr} = m_{ph}/a_w \approx 3.7223 \times 10^{-67}$ kg [14]. Optimal Higgs boson mass: $m_{Hg} = 495^2 m_e$.

m_G	$m_{\hbar}$	Length	Symbol	Precision/offset
m_P^2/m_N	m_P^2/m_N	Space Quantum	d_0	exact
m_P^2/m_0	m_P^2/m_0	Topon	$\lambda\!\!\!^{-}_M$	exact
m_{bc}/a_w	$m_e\sqrt{a_w a_G}$	Reduced Electron Wavelength	$\lambda\!\!\!^{-}_e$	exact
m_P^2/m_N	m_e	Hass-Bohr radius $r_{HB} = a\lambda\!\!\!^{-}_e = r_B/(1+1/p)$	r_{HB}	exact
$a^3 m_P$	$\sqrt{m_p m_H}$	Background Wien Wavelength	λ_W	3.2×10^{-4}
m_{bc}	m_{bc}	Twice Kotov Length	$2l_K$	6.3×10^{-3}
m_{Hg}	m_{Hg}	$R\lambda\!\!\!^{-}_e/4\lambda\!\!\!^{-}_{CMB}$ $Ra_w^{1/2}/WZ^2$		- 0.23% + 0.25%
m_{bc}	m_e	Half Universe Radius	$R_{H_2} \equiv R/2$	exact
m_N	m_N	Half Holographic Cosmos radius	$R_{hol}/2$	exact
m_N^2/m_P	m_N^2/m_P	Half Cosmos Radius	$R_C/2$	exact
$u \times m_{bc}$	$\sqrt{m_{ph} m_{gr}}$	Cosmos radius	R_C	1.7×10^{-3}

ever, in the initial "flat universe" model [32], the total mass M is only matter, while in the present ΛCDM standard model, it is separated between a material part with relative density Ω_m and a so-called "dark energy" part with relative density $1 - \Omega_m$ [29]. We have noted that Ω_m is compatible with 3/10, which is both the density of the classical gravitational energy of a critical homogeneous ball and the density of the steady-state *non-relativist* recession kinetic energy [14]. While the standard cosmology uses an ad-hoc inflation to justify this observed critical condition, we consider rather the Universe as a particle (Topon) in the above Cosmos, with the Topon wavelength $\lambda\!\!\!^{-}_M \equiv \hbar/Mc = 2\hbar G/Rc^3 \equiv 2l_P^2/R$. Then, the critical condition results from the Bekeinstein-Hawking entropy holographic relation, as above (10), where the Topon appears as a secondary Length-Quantum, since the wavelength $\lambda\!\!\!^{-}_m$ associated for any particle of mass m is a whole multiple n_m of the Topon, in conformity with the Field Quantum Theory. The geometrical interpretation is clear: it is a sphere area described by a whole number of sweeping circles, illustrating the fact that multiplication is a series of additions:

$$\begin{aligned} 4\pi\left(\frac{R_{HB}}{l_P}\right)^2 &= \pi\left(\frac{R}{l_P}\right)^2 = 2\pi\,\frac{R}{\lambda\!\!\!^{-}_M} \equiv 2\pi n_m \frac{R}{\lambda\!\!\!^{-}_m} \\ \Rightarrow\quad M &= \frac{Rc^2}{2G} \equiv \frac{R_{H_2}c^2}{G}\ , \end{aligned} \tag{18}$$

identifying twice the above Haas-Sanchez's gravitational radius R_{H_2} with R, the steady-state Universe horizon radius, which is also the limit of a theoretical star radius when its number of atoms shrinks to one [21], a central length in astrophysics, leading to the Machian formula:

$$R = 2\frac{\hbar^2}{Gm_e m_p m_H} \quad \Rightarrow \quad M = \frac{m_P^4}{m_e m_p m_H}\ . \tag{19}$$

The effective electron mass $m'_e = m_e m_p/(m_p + m_e) \equiv M/n_e$, appears in the relation with Eddington number (Table 3) and introduces *n_e, the Universe Electron Quantum Number, canonical in Quantum Field Theory*. The Eddington Electron-Proton symmetry shows up in the following expression of the Large Number Correlation, where $\lambda\!\!\!^{-}_{pH}$ is the geometrical mean of the reduced wavelengths of the proton and Hydrogen:

$$\frac{m_P^2}{m_p m_e} = n_e^{1/2} = \frac{R}{2\lambda\!\!\!^{-}_{pH}}\ , \tag{20}$$

which is extended by very precise dramatic expressions involving the symmetry between the weak bosons of masses $m_W = Wm_e$ and $m_Z = Zm_e$:

$$n_e^{1/2} \approx \frac{(WZ)^4}{2} \approx \left(\frac{m_F^2}{m_p m_H}\right)^7 \left(\frac{aZ}{W}\right)^3\ , \tag{21}$$

where appears as well a Planck-Fermi symmetry. It relates $a_G = m_P^2/m_p m_H$ to W and Z, specifying the known relation $a_G \approx W^8$ [5].

In the Topological Axis, the above Topon corresponds to the orbital number $k = 7$, while the gauge bosons correspond to $k = 3$ (weak bosons W, Z) and $k = 5$ (strong GUT boson

X), letting a single place $k = 1$ for a *non-standard massive* Gluon [14].

The particular values of the topological function $f(k) = \exp(2^{k+1/2})$ for k = 7 and 6 show up in (0.06%):

$$\begin{aligned} n_e &\approx f(7) \times 153^2 \\ R/\lambda\!\!\!^{-}_e &\approx f(6)/6\,, \end{aligned} \tag{22}$$

where $(f(6))^2 \equiv f(7)$ implies that $m_p/m_e \approx 1836 \equiv 6 \times 2 \times 153$, the Diophantine approximation of the Wyler formula $p_W = 6\pi^5$ [33]. The spectroscopic number associated to k is $2(2k+1)$, where 2 is the spin degeneracy and $2k+1$ the number of magnetic states [15]. For $k = 6$, this is 26, the canonical dimension in the bosonic string theory [41].

This *invariable* Universe radius $R \approx 13.812$ Giga light-year (Glyr) of (19) is close to c times the variable standard Universe age. So the standard theoretical approach is correct, but not its Big Bang interpretation: it seems that a confusion is made somewhere between Time and Length, which readily occurs by putting $c = 1$. Moreover, the corresponding Hubble constant c/R is 70.793 (km/s)/Mpc, which is compatible with both the WMAP and the Carnegie-Chicago Hubble Program recent direct measurements (Table 3).

The above Universe gravitational potential energy $(3/10)\,Mc^2$ shows a Neutron Quantum Number (the number of neutron masses) very close (0.05%) to the large Eddington Number [14]. So it has nearly anticipated the correct Hubble Constant value (Table 3).

The Cosmos radius connects with the above radius R_{hol} and R by (27 ppm and 0.04%):

$$R_C(m_e/m_P)^2 \approx R_{hol}\left(\frac{WH}{3}\right)^2 \approx R\,(2F\,Z^2/3)\,, \tag{23}$$

confirming very precisely, since $1/(H-p) \approx 27$ ppm, the optimal weak W boson mass [14] (Table 1).

5 The Cosmic Microwave Background (CMB)

This Universe radius $R = 2R_{H_2}$ enters a 1D-2D holographic relation: $2\pi R/\lambda\!\!\!^{-}_e = 4\pi\lambda\!\!\!^{-}_p\lambda\!\!\!^{-}_H/l_P^2$. The extension to the 3D holographic relation using $\lambda\!\!\!^{-}_{H_2}$, the reduced wavelength of the dihydrogen molecule H_2, involves the reduced wavelength of the Cosmic Microwave Background (CMB) $\lambda\!\!\!^{-}_{CMB} = \hbar c/kT_{CMB}$:

$$2\pi\,\frac{R}{\lambda\!\!\!^{-}_e} = 4\pi\,\frac{\lambda\!\!\!^{-}_p\lambda\!\!\!^{-}_H}{l_P^2} \approx \frac{4\pi}{3}\left(\frac{\lambda\!\!\!^{-}_{CMB}}{\lambda\!\!\!^{-}_{H_2}}\right)^3, \tag{24}$$

leading to $T_{CMB} \approx (8G\hbar^4/3\lambda\!\!\!^{-5}_p)^{1/3}/k \approx 2.729$ Kelvin, which is once more, apart the holographic factor 8/3, a c-free three-fold (Mass, Length, Time) dimensional analysis, giving the energy kT_{CMB} from the constants G, $\hbar$, $\lambda\!\!\!^{-}_p$. Moreover, by substituting $a_G = R/2\lambda\!\!\!^{-}_e$ with the above Lucas Number N_L, this leads to a new holographic expression (analog to the area of a 4D sphere), which gives T_{CMB}, compatible with the measured value 2.7255(6) Kelvin [14]:

$$\begin{aligned} N_L &\approx 2\pi^2\,\frac{\lambda\!\!\!^{-3}_{CMB}}{\lambda\!\!\!^{-}_e\lambda\!\!\!^{-2}_H} \\ \Rightarrow T_{CMB} &= \frac{hc}{k\lambda_{CMB}} \approx 2.7258205\,\text{Kelvin}\,. \end{aligned} \tag{25}$$

The standard cosmology predicts a Neutrino background with temperature $T_{CNB} = T_{CMB} \times (4/11)^{1/3} \approx 1.946$ Kelvin. The total CMB photon number is $n_{ph} = (3\xi(3)/8\pi)(R/\lambda\!\!\!^{-}_{CMB})^3$, exceeding the total Hydrogen number $n_H = M/m_H = R\lambda_H/2l_P^2$. But in terms of energy, the matter dominates. So one must consider also the ratio between the critical energy density $u_{cr} = 3c^4/8\pi GR^2$ and the total background energy density $u_{cmb+cnb} = yu_{cmb}$, with $y = 1 + (21/8)(4/11)^{4/3} \approx 1.681322$ [24] and $u_{cmb} = (\pi^2/15)\,\hbar c/\lambda\!\!\!^{-4}_{CMB}$. We observed that these ratios are tied by an Eddingon type relation:

$$\left(2\frac{n_{ph}}{n_H}\right)^{1/2} \approx \frac{u_{cr}}{u_{cmb+cnb}} \;\Rightarrow\; T_{CMB} \approx 2.724\ \text{Kelvin}\,. \tag{26}$$

This confirms the existence of the Neutrino background. Now assuming that the total background Photon + Neutrino is the result of an ongoing Hydrogen-Helium transformation, producing $e_{He} = 6.40 \times 10^{14}$ Joule by kilogram of Helium, i.e. an efficiency $\epsilon_{He} = e_{He}/c^2 \approx 1/140$. The Helium mass density is $Y \times \rho_{bar}$; with the standard evaluation of baryonic density $\epsilon_{bar} = \rho_{bar}/\rho_{cr} \approx 0.045$ and $Y \approx 0.25$ [29], this leads to:

$$\begin{aligned} \left(\frac{\lambda\!\!\!^{-2}_{CMB}}{l_P R}\right)^2 &\approx \frac{8\pi^3 y}{45Y\epsilon_{bar}\epsilon_{He}} \approx 1.15\times 10^5 \\ \Rightarrow T_{CMB} &\approx 2.70\ \text{Kelvin}\,. \end{aligned} \tag{27}$$

In the standard model, the Universe age is far too small to explain a large Helium large density resulting from stellar activities [23]. Thus, it is not a real problem in the steady-state model.

6 The electron and the Kotov non-local period

This study confirms the central role of $\lambda\!\!\!^{-}_e$, the unit length in the Topological Axis [13]. So we look for a Diophantine series giving it for n = 1. This means:

$$\lambda\!\!\!^{-}_e \equiv \frac{\hbar}{m_e c} = \frac{\hbar^2}{Gm_G m_{\hbar}^2} \;\Rightarrow\; A \equiv \frac{m_P^2}{m_G m_{\hbar}} = \frac{m_{\hbar}}{m_e} \tag{28}$$

so that the fundamental (n = 1) energy is: $E \equiv m_{\hbar}c^2/A^2 = m_e c^2/A$. There is an *elimination of c* by considering the term A^2 as the product of the above gravitational constant $a_G = \hbar c/Gm_p m_H$ and the electro-weak one $a_w = \hbar^3/cG_F m_e^2$ [5], where G_F is the Fermi constant:

$$A^2 = a_G a_w \quad\Rightarrow\quad E = \frac{m_e c^2}{\sqrt{a_G a_w}} \tag{29}$$

Table 3: Prediction of Eddington Number ($N_E = 136 \times 2^{256}$) and Holo-physics formula for the *invariant* Hubble radius $R \approx 13.812$ Giga light-year (Gly) and the corresponding Hubble constant $H_0 = c/R$, which uses the length unit Megaparsec, compared to the main measurements. Lucas Number $N_L = 2^{127} - 1$. Topological Function $f(k) \equiv e^{2^{k+1/2}}$. Holographic ratio $u = R_{hol}/R$. For comparison, the so-called standard "Universe Age" is also presented, with unit in the c ratio.

Date	Source $R = 2GM/c^2$	Hubble radius Glyr	Hubble Cst. km s^{-1}/Mpc	Univ. "Age" Gyr
1945	Eddington Number [36] ; $N_E \approx (3/10)\, Mm_p/M_H m_n$	13.812	70.793	
1927	Lemaître [34]	1.6	620	
1929	Hubble [35]	1.8	540	
1956	Humason, Maydal and Sandage [37]	5.4	180	
1958	Sandage [38]	13	75	
1998	$2\hbar^2/Gm_e m_p m_n$ Twice (3 mn Form.= Clsd Draft)	13.800	70.852	
2006	$2\hbar^2/Gm_e m_p m_n$ [22]	13.800	70.852	
2006	$2\, N_L \lambda\!\!\!^{-}_e$ [22]	13.889	70.397	
2017	$(WZ)^4(\lambda\!\!\!^{-}_p \lambda\!\!\!^{-}_H)^{1/2}$ [5] [13]	13.796 ± 0.002	70.87 ± 0.01	
2017	$\lambda\!\!\!^{-}_e f(6)/6$ [13]	13.821	70.744	
2017	$\lambda\!\!\!^{-}_e (3^3)^{3^3}/u$ [13]	13.812	70.793	
2017	$2\hbar^2/Gm_e m_p m_H$ [13] Machian Formula	13.812	70.793	
2017	$2(ct_K)^2/a_w \lambda\!\!\!^{-}_e$ [13]	13.812	70.793	
2017	$(2/u)^{2\times3\times5\times7} \lambda\!\!\!^{-}_e$ [14] Complete Holic Principle	13.856	70.565	
2021	$(6/\pi)^{r_B/\lambda\!\!\!^{-}_e} \lambda\!\!\!^{-}_e$ [15]	13.776	70.975	
2022	$2N_L \lambda\!\!\!^{-}_e (1 - (137^2 + \pi^2 + e^2)/pH)$	13.812 (Machian prob)	70.793	
1998	PDG (Particle Data Group)	14 ± 2	70 ± 10	11.5 ± 1.5
2002	PDG	13.7 ± 0.3	71 ± 3	15 ± 3
2005	Hubble Space Telescope	13.6 ± 1.5	72 ± 8	13.7 ± 0.2
2012	WMAP [28]	14.1 ± 0.2	69.3 ± 0.8	13.77 ± 0.06
2019	Riess group [30]	13.2 ± 0.3	74.2 ± 1.4	
2020	Planck mission [29]	14.5 ± 0.1	67.4 ± 0.5	13.82 ± 0.04
2020	HOLICOW [31]	13.4 ± 0.3	73.3 ± 1.8	
2021	Carnegie-Chicago Hubble Program [18]	14.0 ± 0.3	69.8 ± 1.6	

with $t_e \equiv \hbar/m_e c^2$ the electron period, this corresponds to the time:

$$t_e \sqrt{a_G a_w} \approx 9600.60\, s\,. \tag{30}$$

The identification with the Kotov P_0 period $t_K \approx 9600.606\,(12)$ s [16, 19] corresponds to $G \approx 6.6754527$ SI, specified to 10^{-8} by the Single-Electron Radius $R_1 \approx (4\pi p/p_W)^2 a_w c t_K$ [14] and consistent with the BIPM measurements [25], but at 6 σ from the official value, a mean between *discordant* measurements. With the Fermi mass $m_F = m_e\sqrt{a_w}$, close to the mean nucleotide mass [13], the Lepton Mu mass m_μ, $u = R_{hol}/R$, the critical density $\rho_{cr} = 3c^2/8\pi G R^2$, $m_{GF} = (m_P m_F)^{1/2}$, this defines our optimal strong coupling a_s:

$$\begin{aligned}
m_G &= \frac{m_e m_p m_H}{m_F^2} \\
m_\hbar/m_P &= \frac{m_F}{(m_p m_H)^{1/2}} \equiv \frac{m_\mu^2}{m_e m_N} \equiv 2\pi \frac{a_s m_p m_H}{m_e m_F} \\
(GG_F)^{1/2} &\equiv \left(\frac{\hbar}{m_{GF}}\right)^2 = \frac{\hbar}{(m_p m_H)^{1/2}} \frac{\lambda\!\!\!^{-2}_e}{t_K} \\
\frac{G_F}{Gm_P^2 l_P^2} &\approx \frac{a^4 m_P m_\mu}{m_e^2}\,(0.2\%) \\
\frac{\hbar}{(G_F \rho_{cr})^{1/2}} &\approx \frac{\lambda\!\!\!^{-2}_e}{u^{1/16} l_P}\,(0.01\%)
\end{aligned} \tag{31}$$

exhibiting a symmetry between canonical area speeds. Note that $2\, ct_K \approx L_{NL}(m_{bc})$, confirming once more the bi-codon

mass, which enters also a relation involving the Cosmos, the Photon and Graviton masses [14] (Table 3). Moreover, with $P = m_P/m_e$, $F = m_P/m_e$, $H = m_H/m_e$, $p = m_p/m_H$, and the precise variant (0.14 ppm) of the Golden Number: $\Phi_0 = P/(a_w H)^3 \approx ((4\pi/3)(H/p)^2)^{1/3}$, one observes:

$$\begin{aligned} \frac{L_{NL}(m_{GF})}{r_{HB}} &\equiv \left(\frac{P}{F^3}\right)^{1/2} \frac{1}{a} \approx \Phi_0^2 \ (15\ ppm) \\ cT_{NL}(m_{GF}) &\equiv l_P \left(\frac{P}{F}\right)^{5/2} \\ &\approx \left(\frac{R_{hol}\,\lambda\!\!\!^{-}_e}{2}\right)^{1/2} \frac{1}{d_e^2} \ (74\ ppm) \end{aligned} \tag{32}$$

where d_e is the canonical Excess Electron Magnetic Moment (Table 1). This specifies the holographic relations $a^2 \approx (4\pi/3)p^{3/2}$ and $F^5/Pa^3 \approx \eta$, with $\eta = 1 + 2/(3 \times 139)$ (ppb precision) [15], where 139 is the complete Atiyah form [26], adding the dimensions of the four algebra (octonion, quaternion, complex, real): $139 = 137 + 2 = 2^7 + 2^3 + 2^1 + 2^0 \approx i^{-i\pi}$, and $3 \times 139 + 2 = 419$, the positive crystallographic number [40] in the superstring dimensions 10D and 11D [41], see Table 7 in [15]. Moreover, $T_{NL}(m_{GF}) \approx 19.14$ ms, typical of the Human nervous system, and the third octave down the flat La tone (Lab) for $La_3(A_4) = 442.9$ Hz, an anthropic argument far more pertinent and precise than the rough standard ones, principally based on a *cosmic Big Bang scenario* [5].

7 Conclusions

The quantification of Length and Time implies, through the Diophantine treatment of the Kepler laws, an angular momentum quantum identified with the reduced Planck constant $\hbar$. This leads to the Diophantine Coherence Theorem (DCT) which has the same structure than the Hass formulation in the Hydrogen atom spectrum. The DCT shows that the real invariant quantity is the Frequency, so that the Energy conservation would mean a Frequency Accordance, or "Coherence Principle", mandatory in Practical Holography; the DCT conforms with the Harmony Principle of Pythagoras, the father of Natural Philosophy, the very root of Science. This confirms the pertinence of the Quantum Field Theory, where any Particle Field is defined by a whole number, entering the Holographic principle in the revisited critical steady-state Universe. In particular, both the Electron Quantum Number and the Neutron Quantum Number play a central role. The Universe Length Quantum (Topon) is associated to a Universe Time quantum ("Chronon" $t_M = \lambda\!\!\!^{-}_M/c$), which may be looked as the period of the *Permanent Bang oscillation matter-antimatter* [42].

The DCT shows that the Haas-Bohr radius is a *pseudo* length quantum, while the Universe itself appears as a pseudo quantum in a Cosmos, defined by the Holographic Principle where the Planck length is an intermediate holographic length, instead of the standard quantum. The Cosmic Length Quantum breaks the "Planck wall" by the factor 10^{-61}. The main pseudo length quantum is the reduced Electron Wavelength which shows, through the DCT and the Kotov non-local period, a symmetry between gravitation and electroweak interaction. The Kotov-Lyuty Non-Doppler oscillation was overlooked: it is however a sign of the non-local character of Quantum Cosmology. It is mandatory to check the Lyuty Non-Doppler Quasar measurements [16].

The Planck mass enters naturally in the DCT, but plays no role in Particle Physics. However, the standard spin formulation rejoins our conclusion that the reduced Planck constant $\hbar$ plays a more fundamental role than h. This is confirmed by the spiraling trajectory interpretation of the Single-Electron cosmic model [14].

The standard speed limit c excludes any explanation of the wave packet reduction phenomena, which requires a non-local or tachyonic Physics. So, it is logical that the bosonic string theory, which introduces tachyon, is confirmed by the Diophantine Topological Axis. Indeed, the central bosonic dimension $d = 26$ corresponds to the non-local universe radius (Machian Formula). The Holographic Principle and the DNA bi-codon mass are both decisive. So the DNA could be an helix-hologram, opening the way towards bio-computing [20]. The c-free Elementary Non-Local Three Minutes Formula giving the Universe half-radius is now fully established: this means a tight harmony between the Universe and Human Consciousness, a special and decisive manifestation of the Anthropic Principle.

Acknowledgements

The authors are indebted to the philosophers Dominique Tassot and Nadia Guemidi, the computer scientists Laurent Gueroult, Denis Gayral and Joël Croissant, and the mathematicians Jacques Bailhache, Jacques de Wiele and Alain Molinier for useful discussions.

Received on April 20, 2022

References

1. Poincare H. La Science et l'Hypothèse, ch.1. Sur la nature du raisonnement mathématique. Flammarion, Paris,, 1968, p. 37.
2. Haas A. E. Über die elektrodynamische... *Sitzungsberichte der kaiserlichen Akademie der Wissenschaften in Wien*, 1910, v. 2a, 119–144.
3. Hermann A. The Genesis of Quantum Theory (1899-1913), Ch. 5. Transl. Claude W. Nash C. W., The MIT Press Cambridge, Massachusetts, and London, England, 1974.
4. Durham I. T. Sir Arthur Eddington and the Foundations of Modern Physics, arXiv: quant-ph/0603146v1.
5. Carr B. J. and Rees M. J. The anthropic principle and the structure of the physical world. *Nature*, 1979, v. 278, 605–612.
6. Bousso R. The Holographic Principle. *Reviews of Modern Physics*, 2002, v. 74 (3), 825–874.
7. Bondi H. and Gold T. The steady-state theory of the expanding universe. *Monthly Notices of the Roy. Astron. Soc.*, 1948, v. 108, 252.
8. Hoyle F. A new model for the expanding Universe. *Monthly Notices of the Roy. Astron. Soc.*, 1948, v. 108, 372–382.

9. Eddington A. S. The Fundamental Theory. Appendix: The Evaluation of the Cosmical Number. Cambridge University Press, 1949.
10. Lehmer D. Tests for primality by the converse of the Fermat's theorem. *Bulletin of the Am. Soc.*, 1927, v. 33 (3), 327.
11. Feynman R. Conférence Nobel (The Character of Physical Law). Seuil 1965/1980.
12. Bastin T. and Kilmister C. W. Combinatorial Physics. World Scientific, 1995.
13. Sanchez F. M. A Coherent Resonant Cosmology Approach and its Implications in Microphysics and Biophysics. *Quantum Systems in Physics, Chemistry and Biology, PTCP*, 2017, v. 23, 375–407. viXra: abs/1601.0011.
14. Sanchez F. M., Kotov V., Grosmann M., Weigel D., Veysseyre R., Bizouard C., Flawisky N., Gayral D. and Gueroult L. Back to Cosmos. *Progress in Physics*, 2019, v. 15 (2), 327.
15. Sanchez F. M., Kotov V., Grosmann M., Weigel D., Veysseyre R., Bizouard C., Flawisky N., Gayral D. and Gueroult L. Towards Science Unification through Number Theory. *A. P. Math*, 2021, v. 11 (1), 27–62.
16. Kotov V. A. and Lyuty V. M. The 160-min. Periodicity in the optical and X-ray observations of extragal. objects. *C.R.A.S.*, 1990, v. 310 (2), 743–748.
17. Nambu H. An Empirical Mass Spectrum of Elem. Particles. *Prog. Theor. Phys.*, 1952, v. 7 (5), 595–596.
18. Freedman W. L. Measurements of the Hubble Constant; Tensions in Perspective. *The Astrophysical Journal*, 2021, v. 919, (1), 16–38.
19. Kotov V. A. and Haneychuk V. I. Oscillations of solar photosphere: 45 years of observations. *Astronomische Nachrichten*, 2020, v. 341, 6–7.
20. Petoukhov. The genetic code, 8-dimensional hyper-complex numbers and dyadic shifts. 2015, 1–108. arXiv: 1102.3596.
21. Davies P. The Accidental Universe. Cambridge U. P., 1993, p. 50.
22. Sanchez F. M. Current Issues in Cosmology. Towards the grand unified Holic Theory. Pecker and Narlikar, C.U.P., 2006, pp. 257–260.
23. Burbidge G. Current Issues in Cosmology. The state of cosmology. Pecker and Narlikar, Cambridge U. P., 2006, pp. 257–260, 2006.
24. Zyla P. A. *et al.*/, Neutrinos in cosmology. *Prog. Theor. Exp. Phys. (Part. Data Gr.)*, 2020, v. 083C01.
25. Quinn T., Speake C., Parks H. and Davis R. The BIPM measurements of the Newtonian constant of gravitation. *G. Phil.Trans. R. Soc.*, 2014, v. A372.
26. Atiyah M. The Fine Structure Constant. *Heidelberg Laureate Forum*, 2018
27. Sanchez F. M. The Holic Principle. ANPA 16 Proc., Cambridge, 1995, 324–344.
28. Bennet C. L. *et al.* Nine Year Wilkinson Microwave Anisotropie Probe (WMAP), Final Maps and Results. *Astrophysical Journal Supplement*, 2013, v. 208 (2), 20.
29. Aghanim A. *et al.* Planck 2018 results. VI. Cosmological Parameters. *Astronomy and Astrophysics*, 2020, v. 641 (A6), 1–73.
30. Riess A. G. *et al.* Large Magellanic Cloud Cepheid Standards Provide a 1% Foudation for the Determination of the Hubble Constant and Stronger Evidence for Physics beyond Λ_{CDM}. *Astrophysical Journal*, 2019, v. 876, 85.
31. Wong K. C. *et al.* HOLICOW-XIII. A 2.4 per cent measurement of H_0 from lensed quasars: 5.3 σ between early and late Universe probes. *Monthly Notices of the Royal Ast.Soc.*, 2020, v. 498 (1).
32. Einstein A. and de Sitter W. On the relation between the expansion and the mean density of the universe. *Proc. Nat. Acad. USA*, 1932, v. 8 (2), 213–214.
33. Wyler A. Les groupes des potentiels de Coulomb et de Yukawa. *C. R.A. S.*, 1971, v. A271, 186–188.
34. Lemaître G. Un Univers homogène de masse constante et de rayon croissant rendant compte de la vitesse radiale des nébuleuses extra-galactiques. *Ann. Soc.Sc. Bruxelles*, 1927, 47–49.
35. Hubble E. P. A Relation between distance and radial velocity among extra-galactic nebulea. *Proc. Nat. Acad. USA*, 1929, v. 15, 163–173.
36. Eddington A. S. The Fundamental Theory. Cambridge, 1946.
37. Humason M. L. and Mayal N.U. and Sandage A.R. A Relation between distance and radial velocity among extra-galactic nebulea. *Astronomical Journal*, 1956, v. 61, 97–162.
38. Sandage A. R. Current Problems in the Extragalactic Distance Scale. *Astronomical Journal*, 1958, v.127, 513.
39. Bars I. Noncommutative Gauge Theory As the Foundation of 2T-Physics in Field Theory. *Phys. Rev. D*, 2001, v. 64.
40. Veysseyre R., Veysseyre H. and Weigel D. Counting, Types and Symbols of Crystallographic Point Symmetry Operations of Space En. *Applicable Algebra in Engineering, Communication and Computing*, 1992, v. 5, 53–70.
41. Salam A. Overview of particle physics. *The New Physics*, 1992, 481–491.
42. Sanchez F. M., Kotov A. V. and Bizouard C. Towards a synthesis of two cosmologies: the steady-state flickering Universe. *Journal of Cosmology*, 2011, v. 17, 7225–7237.

Iso-Representation of the Deuteron Spin and Magnetic Moment via Bohm's Hidden Variables

Ruggero Maria Santilli

The Institute for Basic Research, 35246 U. S. 19N, Suite 215, Palm Harbor, FL 34684, USA.
E-mail: research@i-b-r.org

In this paper, we review and upgrade the iso-representation of the spin 1/2 of nucleons according to the isotopic branch of hadronic mechanics, known as *hadronic spin,* which is characterized by an isotopy of Pauli's matrices with an explicit and concrete realization of Bohm's *hidden variable* λ and show, apparently for the first time, that it allows a consistent and time invariant representation of the spin $J_D = 1$ of the Deuteron in its true ground state, that with null angular contributions $L_D = 0$. We then show, also apparently for the first time, that the indicated hadronic spin allows a numerically exact and time invariant representation of the magnetic moment of the Deuteron with the numeric value $\lambda = 2.65557$.

1 The Einstein-Podolsky-Rosen argument

In the preceding paper [1], we have outlined the axiom-preserving completion of 20th century applied mathematics into *iso-mathematics,* (see [2] for an extended presentation and [5–7] for independent studies), and the related *iso-mechanical branch of hadronic mechanics* (see [3] for a detailed treatment, [8–10] for independent studies and [11–13] for recent reviews) which isotopic methods have been used for the verification in [14, 15] of the 1935 historical argument by A. Einstein, B. Podolsky and N. Rosen that *Quantum mechanics is not a complete theory* [16] (see [17] for the proceedings of the *2020 Teleconference in the EPR Argument*, and its overviews [18, 19]).

Via the use of said isotopic methods, [1] achieved, apparently for the first time, a non-relativistic and relativistic representation of *all* characteristics of the muons (including their recently measured anomalous magnetic moment) as an extended and naturally unstable hadronic bound state of electrons and positrons produced free in the spontaneous decay with the lowest mode.

In the subsequent paper [20], we showed that said isotopic methods confirm the 1983 experimentally unresolved deviations [21] from the conventional formulation of time dilation for composite particles such as the muons, in favor of its axiom-preserving isotopic completion. We indicated in [20] that said deviations are due to incompatibility of the conventional time dilation with the time-irreversible character of the muon decay voiced since 1967 by R. M. Santilli [22] (see the 1995 full treatment [3]) and independently voiced in 1968 by D. I. Blokhintsev [23] for the incompatibility of the conventional time dilation with internal non-local effects of composite particles.

In this paper, we review and upgrade the notion of *hadronic spin* first introduced in [3, Section 6.8, page 250] and then used for verification [14] of the EPR argument [16] as well as in other applications [4]. The new notion of hadronic spin is then used for the characterization of the spin 1/2 of the nucleons, and realized via an isotopy of Pauli's matrices with an explicit and concrete realization of Bohm's *hidden variable* λ [43]. We then show, apparently for the first time, that said hadronic spin allows the first known exact and time-invariant representation of the spin $S_D = 1$ of the deuteron in the true ground state, that with null contributions from angular momenta $L_D = 0$.

We then show, also apparently for the first time, that said hadronic spin allows a numerically exact and time-invariant representation of the magnetic moment of the Deuteron with $\lambda = 2.65557$.

A technical understanding of this paper requires a technical knowledge at least of [2, 3]. A preliminary understanding of this paper requires a knowledge of reviews [11–13].

2 Iso-representation of the Deuteron spin

As it is well known, the quantum mechanical spin 1/2 of nucleons is characterized by the fundamental irreducible representation of the special unitary Lie algebra SU(2) which is notoriously given by the celebrated *Pauli matrices*

$$\sigma_1 = \begin{pmatrix} 0 & 1 \\ 1 & 0 \end{pmatrix}, \quad \sigma_2 = \begin{pmatrix} 0 & -i \\ i & 0 \end{pmatrix}, \quad \sigma_3 = \begin{pmatrix} 1 & 0 \\ 0 & -1 \end{pmatrix}, \tag{1}$$

(where σ_3 is set hereon along the spin direction) with commutation rules

$$[\sigma_i, \sigma_j] = \sigma_i\sigma_j - \sigma_j\sigma_i = i2\epsilon_{ijk}\sigma_k \,. \tag{2}$$

The value $S = 1/2$ of the nucleon spin is characterized by the eigenvalue equations on a Hilbert space $\mathcal{H}$ over the field of complex numbers C with basis $|b\rangle$

$$\begin{aligned} &S_k = \tfrac{1}{2}\,\sigma_k \,, \\ &\sigma_3\,|b\rangle = \pm|b\rangle \,, \\ &\hat{\sigma^2}\,|b\rangle = (\sigma_1\sigma_1 + \sigma_2 v_2 + \sigma_3\sigma_3)\,|b\rangle = 3\,|b\rangle \,. \end{aligned} \tag{3}$$

A serious insufficiency of quantum mechanics in nuclear physics, which is fully supportive of the EPR argument [16], is that the representation of the spin $1/2$ of nucleons via Pauli matrices does not allow a representation of the Deuteron spin $S_D = 1$ under the conditions of its experimental detection, that is, in its ground state with null orbital contributions $L_D = 0$. In fact, the sole possible *stable* bound state between a proton and a neutron permitted by quantum mechanics (qm) is the singlet

$$D = (n_\uparrow, n_\downarrow)_{qm}\,, \tag{4}$$

for which the total spin is null, $J_D = 0$. In an attempt of resolving this insufficiency while preserving quantum mechanics, nuclear physicists have assumed for about one century that the Deuteron is a bound state of a proton and a neutron in *excited orbits* such that $L_D = 1$ (see e.g. [25]).

When at Harvard University with DOE support, R. M. Santilli noted that the most effective way of resolving the above and other insufficiencies of quantum mechanics (see next section) is to *exit from its class of unitary equivalence.* Therefore, Santilli proposed in two 1978 memoirs [26, 27] and in two Springer Verlag monographs [28, 29], the EPR generalization / completion of quantum mechanics into a new discipline which he called *hadronic mechanics* (see the Abstract and [27, pages 684,749,777] and [29, page 112]).

Hadronic mechanics was conceived to be an *axiom-preserving, thus isotopic non-unitary image of quantum mechanics for the representation of the dimension, shape and density of hadrons in interior conditions with ensuing potential as well as non-potential interactions due to mutual penetration.*

The proposal voiced in [26]–[29] suggested the construction of the *time irreversible completion of quantum mechanics into hadronic mechanics with the basic time evolution* (see [27, (4.15.24), page 742], [29, (19), page 153] and [3, (4.3.1), page 154])

$$\begin{aligned} & i\,\frac{dA}{dt} = (A, H) = ARH - HSA = \\ & \qquad = (ATH - HTA) + (AJH + HJA)\,, \\ & A(t) = e^{HSti}\,A(0)\,e^{-itRH}\,, \\ & R = T + J\,,\ \ s = -T + J\,, \end{aligned} \tag{5}$$

which is called Lie-admissible / Jordan-admissible since the bracket (A, H) clearly contains a Lie algebra $(ATH - HTA)$ and a Jordan algebra $(AJH + HJA)$ content.

By recalling that quantum mechanics can only represent systems whose time reversal images verify causality laws (because Heisenberg's equation is invariant under anti–Hermiticity), the aim of Santilli's proposal (stemming from his DOE support) was to achieve a consistent treatment of systems whose time reversal image violate causality, which is the case for all energy-releasing processes, with particular reference to nuclear fusions and fossil fuel combustion.

In this paper, we study *stable nuclei* that, as such, are time-reversal invariant. Consequently, our study requires the *Lie-isotopic branch of hadronic mechanics,* called for brevity *iso-mechanics,* which is based on the completion of the quantum mechanical enveloping associative algebra of Hermitean operators $A, B, ...$ on $\mathcal{H}$ over C with product $A \times B = AB$ and multiplicative unit I into the new product (first introduced in [26, (3.710), page 352] and [29, (5), page 71])

$$A \star B = A\hat{T}B, \quad \hat{T} > 0\,, \tag{6}$$

called *iso-product* because associativity-preserving, the positive-definite quantity $\hat{T}$ being called the *isotopic element* and new compatible multiplicative unit

$$\hat{I} = 1/\hat{T} > 0, \quad \hat{I} \star A = A \star \hat{I} \equiv A\ \forall\ A\ \in \mathcal{H}\,, \tag{7}$$

called *iso-unit* with ensuing basis time evolution first introduced in [27, (4.15.59), page 752] (see also [29, (18), page 163, Vol. II] and [3, (3.1.6), page 81])

$$i\,\frac{dA}{dt} = [A, H]^\dagger = A\hat{T}H - H\hat{T}A\,, \tag{8}$$

$$\begin{aligned} & A(t) = e^{H\hat{T}ti}\,A(0)\,e^{-it\hat{T}H} = W(t)\,A(0)\,W(t)^\dagger\,, \\ & WW^\dagger \neq I\,, \end{aligned} \tag{9}$$

which is called Lie-isotopic because of the clear verification of the Lie algebra axioms by the new brackets $[A, H]^\star$, although in a generalized form.

Following the identification of the basic structure (6) to (8), Santilli constructed in the 1983 monograph [29] the systematic isotopies in the 1983 volume [29] of the various branches of Lie's theory (universal enveloping associative algebra, Lie's theorems, Lie's transformation groups, etc.), resulting in a theory nowadays known as the *Lie-Santilli iso-theory* [5] (see also [30, 31]).

Santilli then constructed the isotopies of all known spacetime symmetries [32]–[42]. In particular, systematic studies were conducted on the construction, classification and verification isotopies of the SU(2)-spin symmetry which can be found in [3, Chapter 6, page 209 on], in papers [33]–[37] with a summary in Section 3 of [12].

The *hadronic spin* (first introduced in [3, Section 6.8]) is the characterization of the spin of hadrons under strong interactions via the iso-irreducible, iso-unitary, iso-representations of the Lie-Santilli iso-symmetry $\widehat{\mathrm{SU}}(2)$.

The simplest possible case of spin $1/2$ of the nucleons can be outlined as following: all mathematical and physical aspects of the (regular [31]) isotopic branch of hadronic mechanics can be uniquely and unambiguously constructed via a simple, positive-definite *non-unitary transformation* set equal to the iso-unit of the new theory

$$UU^\dagger = \hat{I} > 0\ \neq\ I,\ \ \hat{T} = 1/\hat{I} = (UU^\dagger)^{-1} > 0\,, \tag{10}$$

provided said non-unitary transformation is applied to the *totality* of the quantum mechanical, mathematical and physical quantities and their operations *with no exception known to the author*, to prevent insidious inconsistencies in mixing mathematics and iso-mathematics that generally remain undetected by non-experts in the field.

The indicated correct use of the above procedure permits the map of all quantum mechanical quantities, including unit, product, Lie algebras, etc., into their hadronic formulations that are generally denoted with a "hat"

$$\begin{aligned} & I \ \to \ UIU^\dagger = \hat{I}\,, \\ & AB \ \to \ U(AB)U^\dagger = \\ & \quad = (UAU^\dagger)(UU^\dagger)^{-1}(UBU^\dagger) = \hat{A} \star \hat{B}\,, \\ & AB - BA = [A, B] \to U(AB - BA)U^\dagger = \\ & \quad = \hat{A} \star \hat{B} - \hat{B} \star \hat{A} = [\hat{A}, \hat{B}]^\star, \ \text{etc}\,. \end{aligned} \tag{11}$$

The hadronic spin $1/2$ for nuclear constituents is given by the iso-fundamental, iso-unitary, iso-irreducible iso-representation of the Lie-Santilli iso-algebra $\widehat{\mathrm{SU}}(2)$ under the condition of *iso-unimodularity*

$$\mathrm{Det}\,\hat{I} = 1\,. \tag{12}$$

The above condition allowed Santilli to characterize the basic iso-unit of iso-mechanics in terms of Bohm's *hidden variable* λ [43] which was presented for the first time in [3, (6.8.19), page 248], according to the rules

$$\begin{aligned} & \mathrm{Det}\,\hat{I} = \mathrm{Det}\,[(UU^\dagger)] = \mathrm{Det}\,[\mathrm{Diag}\,(g_{11}, g_{22})] = 1\,, \\ & g_{11} = g_{22}^{-1} = \lambda \geq 0\,, \end{aligned} \tag{13}$$

yielding the *iso-Pauli matrices* first proposed in [3, (6.8.20), page 248]

$$\begin{aligned} & \hat{\sigma}_k = U\sigma_k U^\dagger, \\ & UU^\dagger = \hat{I} = \mathrm{Diag}\,(\lambda^{-1}, \lambda), \ \ \hat{T} = \mathrm{Diag}\,(\lambda, \lambda^{-1}), \\ & \hat{\sigma}_1 = \begin{pmatrix} 0 & \lambda \\ \lambda^{-1} & 0 \end{pmatrix}, \ \ \hat{\sigma}_2 = \begin{pmatrix} 0 & -i\lambda \\ i\lambda^{-1} & 0 \end{pmatrix}, \\ & \hat{\sigma}_3 = \begin{pmatrix} \lambda^{-1} & 0 \\ 0 & -\lambda \end{pmatrix}, \end{aligned} \tag{14}$$

and then used in [14] for the verification of the EPR argument thanks to the evident inapplicability of Bell's theorem [44] due to the non-unitary structure of the theory.

It is easy to see that the iso-Pauli matrices verify the Lie-Santilli iso-commutation rules

$$\begin{aligned} & [\hat{\sigma}_i, \hat{\sigma}_j]^* = \hat{\sigma}_i \star \hat{\sigma}_j - \hat{\sigma}_j \star \hat{\sigma}_i = \\ & \quad = \hat{\sigma}_i \hat{T} \hat{\sigma}_j - \hat{\sigma}_j \hat{T} \hat{\sigma}_i = i2\epsilon_{ijk}\hat{\sigma}_k\,, \end{aligned} \tag{15}$$

showing the clear iso-morphism $\widehat{\mathrm{SU}}(2) \approx \mathrm{SU}(2)$.

The representation of the spin $1/2$ of nucleons despite its generalized structure is given by the iso-eigenvalues on an iso-state $|\hat{b}\rangle$ of the *Hilbert-Myung-Santilli iso-space* $\hat{\mathcal{H}}$ [45] over the iso-field of iso-complex iso-numbers $\hat{C}$ [46]

$$\begin{aligned} & \hat{S}_k = \hat{\tfrac{1}{2}} \star \hat{\sigma}_k = \tfrac{1}{2}\hat{\sigma}_k\,, \\ & \hat{\sigma}_3 \star |\hat{b}\rangle = \hat{\sigma}_3 \hat{T}\, |\hat{b}\rangle = \pm|\hat{b}\rangle\,, \\ & \hat{\sigma}^{\hat{2}} \star |\hat{b}\rangle = (\hat{\sigma}_1 \hat{T} \hat{\sigma}_1 + \hat{\sigma}_2 \hat{T} \hat{\sigma}_2 + \hat{\sigma}_3 \hat{T} \hat{\sigma}_3)\hat{T}\, |\hat{b}\rangle = 3\, |\hat{b}\rangle\,. \end{aligned} \tag{16}$$

As it is well known, *non-unitary theories violate causality,* and that is the case for the hadronic spin when considered in its projection on a conventional Hilbert space $\mathcal{H}$ over a conventional field C. Additionally, non-unitary transforms generally change the numeric value of the isotopic element which represent physical, measurable quantities (see next section). These and other problems are resolved by the reformulation of non-unitary time evolution (9) into the *iso-unitary iso-transformations* [47]

$$\begin{aligned} & WW^\dagger = \hat{I}, \quad W = \hat{W}\hat{T}^{1/2}\,, \\ & WW^\dagger = \hat{W} \star \hat{W}^\dagger = \hat{W}^\dagger \star \hat{W} = \hat{I}\,, \end{aligned} \tag{17}$$

under which reformulation the iso-unit, iso-product, Lie-Santilli iso-algebras, etc., are invariant,

$$\hat{I} \to \hat{W} \star \hat{I} \star \hat{W}^\dagger = \hat{I}' \equiv \hat{I}\,, \tag{18}$$

$$\begin{aligned} & \hat{A} \star \hat{B} \to \hat{W} \star (\hat{A} \star \hat{B}) \star \hat{W}^\dagger = \\ & \quad = \hat{A}' \star \hat{B}' = \hat{A}'\hat{T}'\hat{B}', \ \ \hat{T}' \equiv \hat{T}\,, \\ & \hat{A}' = \hat{W} \star A \star \hat{W}^\dagger, \ \ \hat{B}' = \hat{W} \star \hat{B} \star \hat{W}^\dagger\,, \\ & \hat{T} = (W^\dagger \star \hat{W})^{-1}\,. \end{aligned} \tag{19}$$

It should be noted that, by no means, hadronic spin solely characterizes the spin $1/2$ because it was conceived [26, 27] for the characterization of the most general possible notion of spin for an extended particle such as a hadron in the core of a star with ensuing *non-local contributions from the star environment* (see [3, 14], [34]–[37]) according to the *de Broglie-Bohm non-local theory* [48]. The notion of hadronic spin was then specialized to the spin of nucleons because of clear experimental evidence, rather than popular views in nuclear physics, establishing its value $1/2$.

The iso-representation of the Deuteron spin $J_D = 1$ in its true bound state with $L_D = 0$ via the hadronic spin is elementary. To see it, let us call for clarity *iso-protons, iso-neutron, iso-nucleons, iso-Deuteron and iso-Helium* (with corresponding symbols $\hat{p}, \hat{n}, \hat{N}, \hat{D}, \widehat{He}$), the particles and nuclei characterized by the hadronic spin. With reference to [3, Section 2.11, page 265 on] on the addition of hadronic spins, the most stable hadronic bound state of the iso-Deuteron as a

hadronic bound state of an iso-proton and an iso-neutron is given by the *axial triplet state.* The axial triplet coupling first identified in the new chemical species of magnecules (see [49, Chapter 8, page 303 on] and [50, 51]) and then used for the new Intermediate Controlled Nuclear Fusion [52–54] with iso-representation (Fig. 1)

$$\hat{D} = \begin{pmatrix} \hat{p}_\uparrow \\ \star \\ \hat{n}_\uparrow \end{pmatrix}. \tag{20}$$

3 Iso-representation of the Deuteron magnetic moment

Another serious limitation of quantum mechanics in nuclear physics has been the inability, in about one century of studies, to achieve an exact representation of nuclear magnetic moments via the tabulated values for the magnetic moments of the proton and of the neutron in vacuum [55]

$$\mu_p = +2.79285\,\mu_N, \quad \mu_n = -1.91304\,\mu_N\,, \tag{21}$$

where μ_N represents the *nuclear magneton.*

As an example, the magnetic moment predicted by quantum mechanics (qm) from values (21) for the magnetic moment of the Deuteron is given by

$$\mu_D^{qm} = \mu_p + \mu_n = (2.79285 - 1.91304)\,\mu_N = 0.87981\mu_N\,, \tag{22}$$

and does not represent the experimental value of the Deuteron magnetic moment

$$\mu_D^{ex} = 0.85647\,\mu_N\,, \tag{23}$$

due to a deviation in *excess* of about 3%,

$$\mu_D^{qm} - \mu_D^{ex} = 0.02334\,\mu_N \approx 2.95\%\,\mu_D^{ex}\,, \tag{24}$$

with larger deviations for heavier nuclei.

E. Fermi [56], V. F. Weisskopf [25] and other founders of nuclear physics formulated the hypothesis, hereon referred to as the *Fermi-Weisskopf hypothesis*, that in the transition from isolated particles in vacuum to members of a nuclear structure, protons and neutrons experience a deformation of their extended charge distribution with consequential change of their magnetic moments (21) while conserving their spin 1/2 (see the statement at the top of [25, page 31]).

The first numerically exact and time-invariant representation of the Deuteron magnetic moment (23) was achieved in 1994 by Santilli [57] (see also its subsequent extended study in [58]) thanks to the prior construction of the isotopic branch of hadronic mechanics for the representation of extended, thus deformable hadrons and related iso-symmetries [32]–[42] with the isotopic element

$$\hat{T} = \text{Diag}\left(\frac{1}{n_1^2}, \frac{1}{n_2^2}, \frac{1}{n_3^2}, \frac{1}{n_4^2}\right), \tag{25}$$

in which $n_k^2,\ k = 1, 2, 3$, represent the semi-axes of the *deformable* proton and of the nucleon under strong nuclear forces and n_4^2 repesents their density. Under the assumption, for simplicity, that the proton and the neutron in the Deuteron structure have the same dimension, shape and density, [57] reached a numerically exact and time invariant representation of the magnetic moment of the Deuteron in [57, (3.6), page 124] with the following values of the characteristic n-quantities (that are denoted with the symbols $b_\mu = 1/n_\mu$ in [57])

$$\begin{aligned} b_1 &= \frac{1}{n_1} = b_2 = \frac{1}{n_2} = 1.0028\,, \\ b_3 &= \frac{1}{n_3} = 1.662\,, \quad b_4 = \frac{1}{n_4} \end{aligned} \tag{26}$$

(whose derivation is not reviewed here for brevity), by therefore confirming the 1981 preliminary experimental verification of the Fermi-Weisskopf hypothesis via neutron interferometry [59].

In this paper, we present, apparently for the first time, a second numerically exact and time invariant representation of the magnetic moment of the Deuteron (23), with spin $S_D = 1$ in its ground state via the representation of Santilli's iso-Pauli matrices (14) by using the Clifford's algebra representation of the conventional Pauli matrices [60]–[64], whose representation is here assumed to be known for brevity.

Note that, when formulated on their associative enveloping algebra, the iso-Pauli matrices satisfy all algebraic properties of the conventional Pauli matrices. Consequently, we can use the conventional representation in its entirety and introduce the *representation of iso-Pauli matrices (14) in terms of Clifford algebra* $\tilde{\mathbf{G}}_3 = \tilde{\mathbf{G}}_3(\mathbf{R^3})$ with the iso-basis

$$\tilde{\mathbf{G}}_3 : \{1, \hat{\sigma}_1, \hat{\sigma}_2, \hat{\sigma}_3, \hat{\sigma}_1\hat{\sigma}_2, \hat{\sigma}_1\hat{\sigma}_3, \hat{\sigma}_2\hat{\sigma}_3, i := \hat{\sigma}_1\hat{\sigma}_2\hat{\sigma}_3\}, \tag{27}$$

and main properties

$$\begin{aligned} &\hat{\sigma}_1^2 = \hat{\sigma}_2^2 = \hat{\sigma}_3^2 = 1\,, \\ &\hat{\sigma}_{12} = \hat{\sigma}_1\hat{\sigma}_2 = -\hat{\sigma}_{21},\ \hat{\sigma}_{13} = \hat{\sigma}_1\hat{\sigma}_3,\ \hat{\sigma}_{23} = \hat{\sigma}_2\hat{\sigma}_3\,, \\ &\hat{\sigma}_{12}^2 = \hat{\sigma}_1\hat{\sigma}_2\hat{\sigma}_1\hat{\sigma}_2 = -\hat{\sigma}_1\hat{\sigma}_2\hat{\sigma}_2\hat{\sigma}_1 = -\hat{\sigma}_1^2\hat{\sigma}_2^2 = -1\,. \end{aligned} \tag{28}$$

The *standard basis* of unit iso-vectors $\{\hat{\sigma}_1, \hat{\sigma}_2, \hat{\sigma}_3\}$ define the x, y, z iso-coordinate axes, respectively. The *iso-spectral basis* is

$$\begin{pmatrix} \hat{u}_+ & \hat{\sigma}_1\hat{u}_- \\ \hat{\sigma}_1\hat{u}_+ & \hat{u}_- \end{pmatrix}, \tag{29}$$

where $\hat{u}_\pm := \frac{1}{2}(1 \pm \hat{\sigma}_3)$ are *mutually annihilating iso-idempotents*. In the standard iso-basis of $\hat{\mathbf{G}}_\mathbf{3}$,

$$\begin{aligned} &\{\hat{\sigma}_1,\ \hat{\sigma}_2 = i\hat{\sigma}_1\hat{\sigma}_3,\ \hat{\sigma}_3\}\,, \\ &\hat{i} = \hat{\sigma}_1\hat{\sigma}_2\hat{\sigma}_3\,, \end{aligned} \tag{30}$$

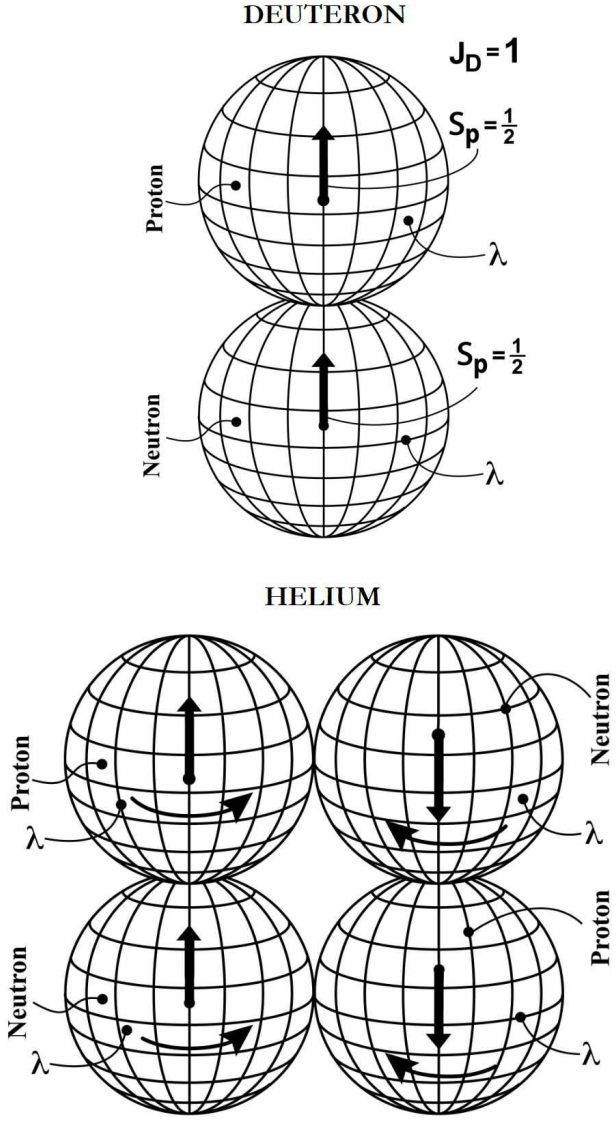

Fig. 1: In the top, we illustrate the structure of the iso-Deuteron as a hadronic bound state of an iso-proton and an iso-neutron in axial triplet coupling, thus representing for the first time the spin of the Deuteron $S_D = 1$ in its ground state, that with null angular contributions $L_D = 0$. The prefix "iso" represents the novel hadronic spin characterized by the iso-Pauli matrices, (14), with an explicit and concrete realization of Bohm's hidden variable λ. The axial triplet coupling was first identified in the new chemical species of magnecules (see [49, Chapter 8, page 303 on] and [50, 51]) and then used for the new Intermediate Controlled Nuclear Fusion [52–54]. In the bottom, we illustrate the structure model of the iso-Helium as a hadronc bound state under strong interactions of two iso-Deuterons in singlet coupling, which allows a representation of the null spin and magnetic moment of Helium in its ground state. It should be noted that the above model is not necessarily extendable to heavier stable nuclei due to the prior need of resolving the problem of nuclear stability caused by the natural instability of the neutron, which problem is planned for study in a subsequent paper (see [65] for a preliminary study).

is the *conventional unit* of the associative algebra $\tilde{\mathbf{G}}_\mathbf{3}$. It must be remembered that $\hat{\sigma}_k$ verify the property

$$\hat{\sigma}_k^2 = \hat{\sigma}_k \star \hat{\sigma}_k = 1\,, \tag{31}$$

for $k = 1, 2, 3$, where the $\star$ denotes the iso-product.

We now show that the hidden variable λ of the iso-Pauli matrices (14) can provide a second representation of the deformation of the magnetic moment of nucleons of [57, 58] with consequential exact representation of nuclear magnetic moments.

By introducing the realization of the hidden variable λ

$$\lambda = e^{\phi} \geq 0\,, \tag{32}$$

with respect to the basis of the *standard unit* of the iso-Pauli matrices $\hat{I}$, the *iso-reciprocal* $\hat{T}$ and the *iso-vector basis* $\{\hat{\sigma}_k\}$, are given by

$$\begin{aligned} \hat{I} &= \cosh\phi + \sigma_3 \sinh\phi = e^{\phi\sigma_3}\,, \\ \hat{T} &= \cosh\phi - \sigma_3 \sinh\phi = e^{-\phi\sigma_3}\,, \end{aligned} \tag{33}$$

Consequently

$$\begin{aligned} \hat{\sigma}_1 &= \sigma_1\hat{I} = \hat{T}\sigma_1\,, \\ \hat{\sigma}_2 &= \sigma_2\hat{I} = \hat{T}\sigma_2\,, \\ \hat{\sigma}_3 &= \sigma_3\hat{I} = \hat{I}\sigma_3\,. \end{aligned} \tag{34}$$

By recalling that σ_3 characterizes the nucleon spin $S = 1/2$, we reach the result that the replacement of the standard basis of the Clifford algebra $\mathbf{G_3}$ for Pauli matrices with the iso-Pauli matrices (14) implies the EPR completion of $\hat{\sigma}_3$ into the expression

$$\hat{\sigma}_3\,|\hat{b}\rangle = \sigma_3\,\hat{I}\,|\hat{b}\rangle = \sigma_3\,e^{\phi\sigma_3}\,|\hat{b}\rangle\,. \tag{35}$$

Recall that the quantum mechanical (qm) relationship between magnetic moments μ and spins S occurs via the gyromagnetic factor g,

$$\mu = gS\,, \tag{36}$$

and that the corresponding relation for the isotopic branch of hadronic mechanics (hm) is given by an expression of the type [57]

$$\mu_{hm}\,|\hat{b}\rangle = KgS\,|\hat{b}\rangle\,, \tag{37}$$

where K is an iso-renormalization constant of the gyromagnetic factor g created by the new notion of hadronic spin $1/2$. By using property (28), we reach the relation

$$\mu_{hm}\,|\hat{b}\rangle = e^{\phi\sigma_3}\mu_{qm}\,|\hat{b}\rangle = e^{\phi\sigma_3}gS\,|\hat{b}\rangle\,. \tag{38}$$

Recall also that: 1) Bohm's hidden variable λ is associated with the *spin* of a particle according to (14); 2) The proton and the neutron have the same spin $1/2$ and essentially the same mass, thus being characterized by the same λ; 3) The quantum mechanical representation of the magnetic moment

of the Deuteron is *in excess* of about 3% according to (24). By selecting the value for conformity with the selected spin orientation (Fig. 1)

$$\sigma_3 \, |\hat{b}\rangle = -|\hat{b}\rangle \, , \tag{39}$$

we can write the expression per each nucleon

$$\mu_{hm,k} \approx (1 + \phi\sigma_3) \, \mu_{qm,k} = (1 - \phi) \, \mu_{qm.k}, \;\; k = p, n \, , \tag{40}$$

from which we obtain the iso-renormalized value of the magnetic moment of the proton and of the neutron

$$\hat{\mu}_p = +(1-\phi) \, 2.79285 \, \mu_N, \;\; \hat{\mu}_n = -(1-\phi) \, 1.91304 \, \mu_N \, , \tag{41}$$

with corresponding value for the magnetic moment of the Deuteron

$$\begin{aligned} \mu_D^{hm} &= (1 - \phi) \, 2.79285 - (1 - \phi) \, 1.91304 \, \mu_N = \\ &= (1 - \phi) \, 0.87981 \, \mu_N = \mu_D^{ex} = 0.85647 \, \mu_N \, . \end{aligned} \tag{42}$$

From this, we obtain the numeric value

$$\phi = 1 - 0.87981/0.85647 = 1 - 0.02334 = 0.97666 \, , \tag{43}$$

with corresponding *numeric value of Bohm's hidden variable for the Deuteron*

$$\lambda = e^{\phi} = e^{0.97666} = 2.65557 \, , \tag{44}$$

by thereby achieving the desired exact representation of the magnetic moment of the Deuteron in terms of Bohm hidden variable λ. Its invariance over tine follows fom the derivation of iso-Pauli matrices (14) from the Lie-Santilli iso-symmetry $\hat{\mathcal{P}}(3.1)$ [39]–[41].

The iso-representation of the magnetic moment of $4 - He - 2$ as the *iso-Helium* $\widehat{He}(2)$ is a consequence (Fig. 1). The study of the iso-representation for heavier stable nuclei was initiated in [65], but its in-depth achievement requires the still missing consistent representation of nuclear stability against the natural instability of the neutron, which problem is planned for study in a subsequent paper.

We should finally note that in this section we have used the *standard Clifford algebra* and not the full isotopic Clifford algebra $\hat{\mathbf{G}}$ introduced by R. da Rocha and J. Vaz Jr. [66]. This is due to the fact that the full isotopy $\hat{\mathbf{G}}_3$ of $\mathbf{G_3}$ would have required the use of iso-product (6) with the isotopic element $\hat{T} = e^{-\phi\sigma_3} = 1/\hat{I}$, and the consequential lack of representation in (38) of the magnetic moment of the Deuteron for spin $S_D = 1$ in the ground state.

The understanding is however that the full iso-Clifford iso-algebra $\hat{\mathbf{G}}_{3N}$ is expected to be important for the numerically exact and time invariant representation of the spins and magnetic moments of nuclei with $A \geq 2$ nucleons.

In a nutshell, we can say that the Copenhagen interpretation of quantum mechanics deals with the simplest possible realization of quantum axioms, while the EPR completion of quantum into hadronic mechanics deals with progressively broader realizations of the same axioms for systems with progressively increasing complexity.

4 Acknowledgments

The author would like to thank Prof. G. Sobczyk for consultations in the representation of the isotopic Pauli matrices via the conventional Clifford's algebras. Thanks are also due for penetrating critical comments received from the participants of the *2020 International Teleconference on the EPR argument* and the *2021 International Conference on Applied Category Theory and Graph-Operad-Logic.* Additional thanks are due to various colleagues for technical controls and to Mrs. Sherri Stone for linguistic control of the manuscript. The author is solely responsible for the content of this paper.

Received on May 20, 2022

References

1. Santilli R. M. Representation of the anomalous magnetic moment of the muons via the Einstein-Podolsky-Rosen completion of quantum into hadronic mechanics. *Progress in Physics*, 2021, v. 17, 210–215. http://www.santilli-foundation.org/muon-anomaly-pp.pdf.
2. Santilli R. M. Elements of Hadronic Mechanics. Volumes I, Mathematical Foundations. Ukraine Academy of Sciences, Kiev, 1995. http://www.santilli-foundation.org/docs/Santilli-300.pdf.
3. Santilli R. M. Elements of Hadronic Mechanics. Volumes II, Theoretical Foundations. Ukraine Academy of Sciences, Kiev, 1994. http://www.santilli-foundation.org/docs/Santilli-301.pdf.
4. Santilli R. M. Elements of Hadronic Mechanics. Volumes III, Experimental Verifications. Ukraine Academy of Sciences, Kiev, 2016. http://www.santilli-foundation.org/docs/elements-hadronic-mechanics-iii.compressed.pdf.
5. Sourlas D. S. and Tsagas G. T. Mathematical Foundation of the Lie-Santilli Theory. Ukraine Academy of Sciences, Kiev, Ukraine, 1993. http://www.santilli-foundation.org/docs/santilli-70.pdf.
6. Ganfornina R. M. F. and Valdes J. N. Fundamentos de la Isotopia de Santilli. International Academic Press, Palm Harbor, FL, 2001. http://www.i-b-r.org/docs/spanish.pdf. English translation: Algebras, Groups and Geometries,2015, v. 32, 135–308 (2015) http://www.i-b-r.org/docs/Aversa-translation.pdf.
7. Georgiev S. Foundations of IsoDifferential Calculus. Vol 1. – Iso-Differential and Iso-Integral Calculus for Iso-Functions in One Variable. Vol 2. – Iso-Differential and Iso-Integral Calculus for Iso-Functions in Several Variables. Vol. 3 – Iso-Ordinary Iso-Differential Equations. Vol. 4 – Iso-Differential Equations. Vol.5 – Iso-Stochastic Iso-Differential Equations. Vol. 6 – Theory of Iso-Measurable Iso-Functions. Nova Publishers, New York, NY, 2014 (I), 2014 (II), 2014 (III), 2015 (IV), 2015 (V), 2016 (VI), 2022 (I new ed.).
8. Aringazin A. K., Jannussis A., Lopez F., Nishioka M. and Vel-janosky B. Santilli's Lie-Isotopic Generalization of Galilei and Einstein Relativities. Kostakaris Publishers, Athens, Greece, 1991. http://www.santilli-foundation.org/docs/Santilli-108.pdf.
9. Kadeisvili J. V. Santilli's Isotopies of Contemporary Algebras, Geometries and Relativities, Second edition. Ukraine Academy of Sciences, Kiev, 1997. http://www.santilli-foundation.org/docs/Santilli-60.pdf.
10. Gandzha I. and Kadeisvili J. V. New Sciences for a New Era: Mathematical, Physical and Chemical Discoveries of Ruggero Maria Santilli. Sankata Printing Press, Nepal, 2011. http://www.santilli-foundation.org/docs/RMS.pdf.
11. Santilli R. M. Studies on A. Einstein, B. Podolsky, and N. Rosen prediction that quantum mechanics is not a complete theory. I: Basic methods. *Ratio Mathematica*, 2020, v. 38, 5–69. http://www.eprdebates.org/docs/epr-review-i.pdf.

12. Santilli R. M. Studies on A. Einstein, B. Podolsky, and N. Rosen prediction that quantum mechanics is not a complete theory. II: Apparent proof of the EPR argument. *Ratio Mathematica*, 2020, v. 38, 71–138. http://www.eprdebates.org/docs/epr-review-ii.pdf.
13. Santilli R. M. Studies on A. Einstein, B. Podolsky, and N. Rosen prediction that quantum mechanics is not a complete theory. III: Illustrative examples and applications. *Ratio Mathematica*, 2020, v. 38, 139–222. http://www.eprdebates.org/docs/epr-review-iii.pdf.
14. Santilli R. M. Isorepresentation of the Lie-isotopic SU(2) Algebra with Application to Nuclear Physics and Local Realism. *Acta Applicandae Mathematicae*, 1998, v. 50, 177–190. http://www.santilli-foundation.org/docs/Santilli-27.pdf.
15. Santilli R. M. Studies on the classical determinism predicted by A. Einstein, B. Podolsky and N. Rosen. *Ratio Mathematica*, 2019, v. 37, 5–23. http://www.eprdebates.org/docs/epr-paper-ii.pdf.
16. Einstein A., Podolsky B., and Rosen N. Can quantum-mechanical description of physical reality be considered complete? *Phys. Rev.*, 1935, v. 47, 777–791. http://www.eprdebates.org/docs/epr-argument.pdf.
17. Beghella-Bartoli S. and Santilli R. M., eds, Proceedings of the 2020 Teleconference on the Einstein-Podolsky-Rosen argument that "Quantum mechanics is not a compete theory". Curran Associates, New York, NY, 2021. http://www.proceedings.com/59404.html (printed), 60007.html (electronic). http://www.santilli-foundation.org/epr-table-of-content.pdf (TOC).
18. Santilli R. M. Overview of historical and recent verifications of the EPR argument and their applications to physics, chemistry and biology. APAV - Accademia Piceno Aprutina dei Velati, Pescara, Italy, 2021. http://www.santilli-foundation.org/epr-overview-2021.pdf.
19. Dunning-Davies J. A Present Day Perspective on Einstein-Podolsky-Rosen and its Consequences. *Journal of Modern Physics*, 2021, v. 12, 887–936.
20. Santilli R. M. Apparent Unsettled Value of the Recently Measured Muon Magnetic Moment. *Progress in Physics*, 2022, v. 18, 15–18. http://www.santilli-foundation.org/docs/muon-meanlife-2022.pdf
21. Aronson S. H., Bock G. J., Cheng J. Y., and Fischbach E. Energy dependence of the fundamental parameters of the $K^0 - \bar{K}^0$ system. *Phys. Rev. D*, 1983, v. 28, 495–503.
22. Santilli R. M. Embedding of Lie-algebras into Lie-admissible algebras. *Nuovo Cimento*, 1967, v. 51, 570. http://www.santilli-foundation.org/docs/Santilli-54.pdf.
23. Blokhintsev D. I. The Philosophy of Quantum Mechanics. JINR (in Russian), 1965. Springer (in English), 1968.
24. Bohm D. A Suggested Interpretation of the Quantum Theory in Terms of "Hidden Variables". *Physical Review*, 1952, v. 85, 166–182. http://journals.aps.org/pr/abstract/10.1103/PhysRev.85.166.
25. Blatt J. M. and Weisskopf V. F. Theoretical Nuclear Physics. Wiley and Sons, 1952.
26. Santilli R. M. On a possible Lie-admissible covering of Galilei's relativity in Newtonian mechanics for nonconservative and Galilei form-non-invariant systems. *Hadronic J.*, 1978, v. 1, 223–423. http://www.santilli-foundation.org/docs/Santilli-58.pdf.
27. Santilli R. M. Need of subjecting to an experimental verification the validity within a hadron of Einstein special relativity and Pauli exclusion principle. *Hadronic J.*, 1978, v. 1, 574–901. http://www.santilli-foundation.org/docs/santilli-73.pdf.
28. Santilli R. M. Foundation of Theoretical Mechanics. Vol. I, The Inverse Problem in Newtonian Mechanics. Springer-Verlag, Heidelberg, Germany, 1978. http://www.santilli-foundation.org/docs/Santilli-209.pdf.
29. Santilli R. M. Foundation of Theoretical Mechanics. Vol. II, Birkhoffian Generalization of Hamiltonian Mechanics. Springer-Verlag, Heidelberg, Germany, 1983. http://www.santilli-foundation.org/docs/santilli-69.pdf.
30. Kadeisvili J. V. An introduction to the Lie-Santilli isotopic theory. *Mathematical Methods in Applied Sciences*, 1996, v. 19, 134–168. http://www.santilli-foundation.org/docs/Santilli-30.pdf.
31. Muktibodh A. S. and Santilli R. M. Studies of the Regular and Irregular Isorepresentations of the Lie-Santilli Isotheory. *Journal of Generalized Lie Theories*, 2007, v. 11, 1–32. http://www.santilli-foundation.org/docs/isorep-Lie-Santilli-2017.pdf.
32. Santilli R. M. Lie-isotopic Lifting of Special Relativity for Extended Deformable Particles. *Lettere Nuovo Cimento*, 1983, v. 37, 545–555. http://www.santilli-foundation.org/docs/Santilli-50.pdf.
33. Santilli R. M. Lie-isotopic Lifting of Unitary Symmetries and of Wigner's Theorem for Extended and Deformable Particles. *Lettere Nuovo Cimento*, 1983, v. 38, 509–516. http://www.santilli-foundation.org/docs/Santilli-51.pdf.
34. Santilli R. M. Isotopies of Lie Symmetries. I: Basic theory. *Hadronic J.*, 1985, v. 8, 8–33. http://www.santilli-foundation.org/docs/santilli-65.pdf.
35. Santilli R. M. Isotopies of Lie Symmetries. II: Isotopies of the rotational symmetry. *Hadronic J.*, 1985, v. 8, 36–59. http://www.santilli-foundation.org/docs/santilli-65.pdf.
36. Santilli R. M. Rotational isotopic symmetries. ICTP Communication No. IC/91/261, 1991. http://www.santilli-foundation.org/docs/Santilli-148.pdf.
37. Santilli R. M. Isotopic Lifting of the SU(2) Symmetry with Applications to Nuclear Physics. *JINR Rapid Comm.*, 1993, v. 6, 24–36. http://www.santilli-foundation.org/docs/Santilli-19.pdf.
38. Santilli R. M. Isotopic generalization of the Poincaré symmetry. ICTP Communication No. IC/91/45, 1991. http://www.santilli-foundation.org/docs/Santilli-140.pdf.
39. Santilli R. M. Nonlinear, Nonlocal and Noncanonical Isotopies of the Poincaré Symmetry. *Moscow Phys. Soc.*, 1993, v. 3, 255–289. http://www.santilli-foundation.org/docs/Santilli-40.pdf.
40. Santilli R. M. Isotopies of the spinorial covering of the Poincaré symmetry. Communication of the Joint Institute for Nuclear Research, Dubna, Russia, No. E4-93-252, 1993.
41. Santilli R. M. Relativistic synthesis of the neutron from the hydrogen atom via the isospinorial covering of the iso-Poincaré symmetry. *Chinese J. System Eng. and Electr.*, 1995, v. 6, 177–202. http://www.santilli-foundation.org/docs/Santilli-18.pdf.
42. Santilli R. M. Iso-Minkowskian Geometry for the Gravitational Treatment of Matter and its Isodual for Antimatter. *Intern. J. Modern Phys. D*, 1998, v. 7, 351–385. http://www.santilli-foundation.org/docs/Santilli-35.pdf.
43. Bohm D. A Suggested Interpretation of the Quantum Theory in Terms of "Hidden Variables". *Physical Review*, 1952, v. 85, 166–182. journals.aps.org/pr/abstract/10.1103/PhysRev.85.166.
44. Bell J. S. On the Einstein Podolsky Rosen paradox. *Physics*, 1964, v. 1, 195–221.
45. Myung H. C. and Santilli R. M. Modular-isotopic Hilbert space formulation of the exterior strong problem. *Hadronic Journal*, 1982, v. 5, 1277–1366. http://www.santilli-foundation.org/docs/myung-santilli-1982.pdf.
46. Santilli R. M. Isonumbers and Genonumbers of Dimensions 1, 2, 4, 8, their Isoduals and Pseudoduals, and "Hidden Numbers" of Dimension 3, 5, 6, 7. *Algebras, Groups and Geometries*, 1993, v. 10, 273–322. http://www.santilli-foundation.org/docs/Santilli-34.pdf.
47. Santilli R. M. Invariant Lie-isotopic and Lie-admissible formulation of quantum deformations. *Found. Phys.*, 1997, v. 27, 1159–1177. http://www.santilli-foundation.org/docs/Santilli-06.pdf.
48. Goldstein S. Bohmian (de Broglie-Bohm) Mechanics. Stanford Encyclopedia of Philosophy, 2021. http://plato.stanford.edu/entries/qm-bohm/

49. Santilli R. M. Foundations of Hadronic Chemistry, with Applications to New Clean Energies and Fuels. Kluwer Academic Publishers, 2001. http://www.santilli-foundation.org/docs/Santilli-113.pdf. Russian translation: Aringazin A. K. i-b-r.org/docs/Santilli-Hadronic-Chemistry.pdf.
50. Pandhurneka C. P. and Zodape S. P. Santilli's Magnecules and Their Applications. *American Journal of Modern Physics*, 2017, v. 6, 64–73. http://www.santilli-foundation.org/docs/magnecules-2017.pdf.
51. Yang Y., Kadeisvili J. V. and Marton S. Experimental Confirmations of the New Chemical Species of Santilli Magnecules. *The Open Physical Chemistry Journal*, 2013, v. 5, 1–15. http://www.santilli-foundation.org/docs/Magnecules-2012.pdf.
52. Santilli R. M. The novel Intermediate Controlled Nuclear fusions, a report for its industrial realization. *Hadronic Journal*, 2008, v. 31, 15–43. http://www.santilli-foundation.org/docs/CNF-HJ.pdf.
53. Brenna R., Kuliczkowski T. and YingL. Verification of Santilli intermediate Controlled Nuclear Fusions without harmful radiations and the production of magnecular clusters. *New Advances in Physics*, 2011, v. 5, 9–21. http://www.santilli-foundation.org/docs/ICNF-2.pdf.
54. Lynch C. and Yang Y. Confirmations of Santilli Intermediate Nuclear Fusions of Deuteron and Carbon into Nitrogen without Radiations. *The Open Physical Chemistry Journal*, 2013, v. 5, 17–39. http://www.santilli-foundation.org/docs/ICNF-Conf-2013.pdf.
55. Vonsovsk S. Magnetism of Elementary Particles. Mir Publishers, 1975.
56. Fermi E. Nuclear Physics. University of Chicago Press, 1949.
57. Santilli R. M. A quantitative isotopic representation of the deuteron magnetic moment. in Proceedings of the International Symposium "Dubna Deuteron-93". Joint Institute for Nuclear Research, Dubna, Russia, 1994. http://www.santilli-foundation.org/docs/Santilli-134.pdf.
58. Santilli R. M. The Physics of New Clean Energies and Fuels According to Hadronic Mechanics. *Journal of New Energy, Special Issue*, 1998, 318 pages. http://www.santilli-foundation.org/docs/Santilli-114.pdf.
59. Rauch H. and Zeilinger A. Demonstration of SU(2) symmetry by neutron interferometers. *Hadronic Journal*, 1981, v. 4, 1280–1285. http://www.santilli-foundation.org/docs/rauch-zeilinger-1981.pdf.
60. Hestenes D. and Sobczyk G. Clifford Algebra to Geometric Calculus: A Unified Language for Mathematics and Physics, 2nd ed. Kluwer, 1992.
61. Doran C. and Lasenby A. Geometric Algebra for Physicists. Cambridge University Press, 2003.
62. Sobczyk G. New Foundations in Mathematics: The Geometric Concept of numbers. Birkhauser, New York, 2013.
63. Sobczyk G. Spacetime Vector Analysis. *Physics Letters A*, 1981, v. 84, 45–49.
64. Sobczyk G. Conformal Mappings in Geometric Algebra. *Notices of the AMS*, 2012, v. 59, 264–273.
65. Bhalekar A. A. and Santilli R. M. Exact and Invariant representation of nuclear magnetic moments and spins according to hadronic mechanics. *American Journal of Modern Physics*, 2016, v. 5, 56–92. http://www.santilli-foundation.org/docs/nuclear-MM-spins.pdf.
66. da Rocha R. and Vaz J. Jr. Isotopic liftings of Clifford algebras and applications in elementary particle mass matrices. *Int. J. Theor. Phys.*, 2007, v. 46, 2464–2487. arXiv: math-ph/0710.0832.

Gödel Time Travel With Warp Drive Propulsion

Patrick Marquet
Calais, France. E-mail: patrick.marquet6@wanadoo.fr

In the first part of this work,we recall the basic principles of the Alcubierre warp drive space-time within the extrinsic curvature formalism. In the created singular region, we consider a hollow object that carries a charged current all around its external shape which interacts with an electromagnetic potential. As a result, this comoving object placed inside the region will follow a Finslerian geodesic. This allows to re-define a new lapse function that contains the potential-charge interacting term which can be chosen arbitrarily large, in order to lower the energy density required for sustaining the space-time distortion. Ultimately, this new lapse function is adjusted so as to keep the warp drive energy tensor positive thus always satisfying the famous energy conditions. In the second part, we apply this result to the Gödel curves following our previous publication whereby it was shown that Gödel's metric is a physical model not bound to any astrophysical representation. In this perspective, we suggest a possible mode of time travel.

Notations

Space-time Greek indices α, β run from 0, 1, 2, 3.
Spatial Latin indices a, b run from 1, 2, 3.
Space-time signature is: +2 (Part I) and −2 (Part II).

PART I

1 The warp drive metric

1.1 The (3 + 1) formalism or ADM technique

Arnowitt, Deser and Misner (ADM) suggested a technique which leads to decompose the space-time into a family of spacelike hypersurfaces and parametrized by the value of an arbitrarily chosen time coordinate x^0 [1]. This *foliation* displays a proper time element dt between two nearby hypersurfaces labeled $x^0 = const$, $x^0 + dx^0 = const$ and the proper time element $cd\tau$ must be proportional to dx^0, thus we write:

$$cd\tau = N\,(x^\alpha, x^0)\,dx^0, \tag{1.1}$$

where, according to the ADM terminology, N is called the *lapse function*.

Let us now evaluate the 3-vector whose spatial coordinates x^a are lying in the hypersurface $x^0 = const$ and which is normal to it, on the second hypersurface $x^0 + dx^0 = const$, where these coordinates now become $N^a dx^0$. The vector N^a is called the *shift vector*. The 4-metric tensor covariant components are

$$(g_{\alpha\beta})_{\text{ADM}} = \begin{pmatrix} -N^2 - N_a N_b\, g^{ab} & N_b \\ N_a & g_{ab} \end{pmatrix}. \tag{1.2}$$

The line element corresponding to the hypersurfaces separation is therefore written as

$$\begin{aligned}(ds^2)_{\text{ADM}} &= \\ &= -N^2\,(dx^0)^2 + g_{ab}\,(N^a dx^0 + dx^a)(N^b dx^0 + dx^b) = \\ &= (-N^2 + N_a N^a)(dx^0)^2 + 2N_b\,dx^0 dx^b + g_{ab}\,dx^a dx^b,\end{aligned} \tag{1.3}$$

where g_{ab} is the 3-metric of the hypersurfaces. The contravariant components of the ADM metric tensor are

$$(g^{\alpha\beta})_{\text{ADM}} = \begin{pmatrix} -\dfrac{1}{N^2} & \dfrac{N^b}{N^2} \\ \dfrac{N^a}{N^2} & g^{ab} - \dfrac{N^a N^b}{N^2} \end{pmatrix}. \tag{1.4}$$

As a result, the hypersurfaces have a unit time-like normal with contravariant components:

$$u^\alpha = N^{-1}\,(1, -N^a)\,. \tag{1.5}$$

If the universe is approximated to a Minkowski space within an orthonormal coordinates frame of reference and where the fundamental 3-tensor satisfies $g^{ab} = \delta^{ab}$, the metric (1.3) becomes

$$ds^2 = -(N^2 - N_a N^a)\,c^2 dt^2 + 2N^a dx\,cdt + dx^a dx^b \tag{1.6}$$

or, in another notation,

$$ds^2 = -N^2 dt^2 + (dx + N^a\,cdt)^2 + dy^2 + dz^2. \tag{1.6bis}$$

The Einstein action can be written in terms of the metric tensor $(g_{\alpha\beta})_{\text{ADM}}$ as [2]

$$S_{\text{ADM}} = \int cdt \int N\left({}^{(3)}R - K^a_b\,K^b_a + K^2\right)\sqrt{{}^{(3)}g}\,dx^3 + \\ + \text{boundary terms},$$

where $K^a_a K^b_b = K^2$, and ${}^{(3)}R$ is the 3-Ricci scalar and stands for the *intrinsic curvature* of the hypersurface

$$x^0 = const, \quad \sqrt{{}^{(3)}g} = \sqrt{\det\|g_{ab}\|} \;\leftrightarrow\; \sqrt{-{}^{(4)}g} = N\sqrt{{}^{(3)}g}$$

so that

$$K_{ab} = (2N)^{-1}(-N_{a;b} - N_{a;b} + \partial_0\, g_{ab}) \tag{1.7}$$

represents the *extrinsic curvature*, and as such describes the manner in which the hypersurface $x^0 = const$ is embedded in the surrounding space-time. The rate of change of the 3-metric tensor g_{ab} with respect to the time label can be decomposed into "normal" and "tangential" contributions:

— The normal change is proportional to the extrinsic curvature $2K_{ab}/N$ of the hypersurface;

— The tangential change is given by the Lie derivative of g_{ab} along the shift vector N^a, namely:

$$\mathrm{L}_N\, g_{ab} = 2N_{(a;b)}\,. \tag{1.8}$$

With the choice of $N^a = 0$, we have a particular coordinate frame called *normal coordinates* according to (1.5) which is called an *Eulerian gauge*. Inspection shows that

$$K_{ab} = -u_{a;b} \tag{1.9}$$

which is sometimes called the *second fundamental form* of the 3-space. Six of the ten Einstein equations imply for K^a_b to evolve according to

$$\begin{aligned}\frac{\partial K^a_b}{c\,\partial t} + \mathrm{L}_N\, K^a_b &= \nabla^a\nabla_b\, N + \\ &+ N\left[R^a_b + K^a_a\, K^a_b + 4\pi\,(T - C)\;\delta^a_b - 8\pi T^a_b\right],\end{aligned} \tag{1.10}$$

$$C = T_{\alpha\beta}\, u^\alpha u^\beta, \tag{1.11}$$

where C is the matter energy density in the rest frame of normal congruence (time-like vector field) with $T = T^a_a$. Using the Gauss-Codazzi relations [3] one can express the Einstein tensor as a function of both the intrinsic and extrinsic curvatures. It is convenient here to introduce the 3-momentum current density $I_a = -\,u_c\, T^c_a$. So the remaining four equations finally form the so-called *constraint equations*

$$H = \frac{1}{2}\left({}^{(3)}R - K^a_b K^b_a + K^2\right) - 8\pi C = 0\,, \tag{1.12}$$

$$H_b = \nabla_a\left(K^a_b - K\,\delta^a_b\right) - 8\pi I_b = 0\,. \tag{1.13}$$

Therefore, another way of writing (1.11) eventually leads to the formula

$$C = \frac{1}{16\pi}\left({}^{(3)}R - K_{ab}K^{ab} + K^2\right). \tag{1.14}$$

1.2 Salient features of Alcubierre's theory

1.2.1 The Alcubierre metric

In 1994, M. Alcubierre showed that an arbitrary large velocity (superluminal) can be achieved by building a so-called *space-time warped region* (*bubble-like region*) progressing along the x-direction which is a time-like trajectory, without violating the law of relativity [4]. Inside the bubble, the proper time element $d\tau$ is equal to the coordinate time dt which is also the proper time of a distant observer, so any object in the bubble does not suffer any time dilation as it moves. Outside and inside the bubble, space-time remains flat. In the classical interpretation, the warp drive requires *contraction* of the front space, and *expansion* behind the same bubble in the chosen direction, quite in analogy to the inflationary phase of the expanding universe.

In terms of the ADM formalism, the Alcubierre metric is defined from a flat space-time, while the lapse function and the shift functions are chosen as

$$\left.\begin{aligned} N &= 1 \\ N^1 &= -v_s(t)\, f(r_s, t) \\ N^2 &= N^3 = 0 \end{aligned}\right\}. \tag{1.15}$$

Next, we define

$$r_s(t) = \sqrt{(x - x_s(t))^2 + y^2 + z^2} \tag{1.16}$$

as the distance outward from the center of a spaceship placed in the bubble, variable until R_B, which is the *radius of the bubble*. With respect to a distant observer, the apparent velocity of the ship (thus the bubble), is given by:

$$v_s(t) = \frac{dx_s(t)}{dt}\,, \tag{1.17}$$

where $x_s(t)$ is the trajectory of the bubble along the x-direction. Such a region is transported forward with respect to distant observers, along the x-direction, and any spacecraft placed at rest inside, has no local velocity, but always moves along a time-like curve, regardless of $v_s(t)$. We then have the line element of the *Alcubierre metric*

$$(ds^2)_{\mathrm{AL}} = -c^2dt^2 + \left[dx - v_s\, f(r_s, t)\, cdt\right]^2 + dy^2 + dz^2, \tag{1.18}$$

$$d\tau = dt\,, \tag{1.19}$$

Inside the spacecraft, the occupants will never suffer acceleration and so it is not difficult to show that the 4-velocity of a distant observer called *Eulerian observer* [5], has the following components:

$$(u^\alpha)_{\mathrm{E}} = \{c,\, v_s\, cf(r_s, t),\, 0,\, 0\}\,, \tag{1.20}$$

$$(u_\alpha)_{\mathrm{E}} = \{-c,\, 0,\, 0,\, 0\}\,. \tag{1.21}$$

The Eulerian observer is a special type of observer which refers to the Eulerian gauge defined above but with $N^1 \neq 0$, and as such, it follows time-like geodesic orthogonal to euclidean hypersurfaces. This observer starts out just inside the bubble shell at its first equator with zero initial velocity. Once during his stay inside the bubble, this observer travels along a time-like curve: $x = x_s(t)$ with a constant velocity nearing the ship's velocity: $v_s = dx_s/dt$. The Eulerian observer's velocity will always be less than the bubble's velocity unless $r_s = 0$,

i.e., when this observer is at the center of the spaceship located inside. After reaching the second region's equator, this observer decelerates and is left at rest while going out at the rear edge of the bubble.

The Eulerian observer's velocity is needed to evaluate the energy density required to create the bubble.(see below) The function $f(r_s, t)$ is so defined as to cause space-time to contract on the forward edge and equally expanding on the trailing edge of the *bubble* as stated above. This is easily verified by using the expansion of the volume elements $\theta = (u^\alpha)_{\mathrm{E};\alpha}$ given by

$$\theta = \frac{v_s\, df}{(dx)_{\mathrm{AL}}}\,. \tag{1.22}$$

1.2.2 The Alcubierre function

The function $f(r_s, t)$ is often referred to as a *top hat function* and Alcubierre originally chose the following form

$$f(r_s, t) = \frac{\tanh\{\sigma(r_s + R_B)\} - \tanh\{\sigma(r_s - R_B)\}}{2\tanh\{\sigma R_B\}}\,, \tag{1.23}$$

where $R_B > 0$ is the *radius of the bubble*, and σ is a *bump parameter* which can be used to "tune" the wall thickness of the bubble. The larger this parameter, the greater the contained energy density, for its shell thickness decreases. Moreover the absolute increase of σ means a faster approach of the condition

$$\lim f(r_s, t) = 1, \ \text{ for } \ r_s \in (-R_B, R_B)\,, \ \text{ otherwise } \ \sigma \to \infty.$$

In the ADM formalism the expansion scalar is shown to be

$$\theta = \partial_1 N^1 = -\mathrm{Trace}\, K_{ab}\,, \tag{1.24}$$

which, with (1.13), becomes

$$\theta = v_s \frac{df}{dr_s}\frac{x_s}{r_s}\,. \tag{1.24bis}$$

Note that the Natàrio warp drive evades the problem of contraction/expansion, by imposing the divergence free constraint to the shift vector $\nabla[v_s^2\, f^2(r_s, t)] = 0$ [6].

Obviously, the shape of the function f induces both a volume contraction and expansion ahead and behind of the bubble. Let us now write down the Alcubierre metric in the equivalent form

$$\begin{aligned}(ds^2)_{\mathrm{Al}} = &-\left[1 - v_s^2 f^2(r_s, t)\right] c^2 dt^2 - \\ &- 2 v_s\, f\, c dt\, dx + dx^2 + dy^2 + dz^2,\end{aligned} \tag{1.25}$$

which puts in evidence the covariant components of the metric tensor

$$\left.\begin{aligned}(g_{00})_{\mathrm{Al}} &= -[1 - v_s^2 f^2(r_s, t)] \\ (g_{01})_{\mathrm{Al}} &= (g_{10})_{\mathrm{Al}} = -v_s f(r_s, t) \\ (g_{11})_{\mathrm{Al}} &= (g_{22})_{\mathrm{Al}} = (g_{33})_{\mathrm{Al}} = 1\end{aligned}\right\}. \tag{1.26}$$

1.2.3 Energy conditions

With the components (1.26), the Einstein-Alcubierre tensor is written

$$(G^{\alpha\beta})_{\mathrm{Al}} = (R^{\alpha\beta})_{\mathrm{Al}} - \frac{1}{2}\,(g^{\alpha\beta})_{\mathrm{Al}}\, R\,, \tag{1.27}$$

$$(T^{\alpha\beta})_{\mathrm{Al}} = \frac{c^4}{8\pi}\,(G^{\alpha\beta})_{\mathrm{Al}}\,. \tag{1.28}$$

The *weak energy condition* (WEC) stipulates [7] that we must always have

$$C_{\mathrm{Al}} = (T^{\alpha\beta})_{\mathrm{Al}}\,(u_\alpha)_{\mathrm{E}}\,(u_\beta)_{\mathrm{E}} \geqslant 0 \tag{1.29}$$

From (1.14) we see that there in the Alcubierre space-time ${}^{(3)}R = 0$. Thus we get

$$C_{\mathrm{Al}} = \frac{1}{16\pi}\left(K^2 - K_{ab}K^{ab}\right), \tag{1.30}$$

$$\begin{aligned}C_{\mathrm{Al}} = \frac{1}{16\pi}\Big[&(\partial_1 N^1)^2 - (\partial_1 N^1)^2 - \\ &- 2\,(\partial_2 N^1)^2 - 2\,(\partial_3 N^1)^2\Big],\end{aligned} \tag{1.31}$$

$$\begin{aligned}(T^{00})_{\mathrm{Al}}\,(u_0)_{\mathrm{E}}\,(u_0)_{\mathrm{E}} = (T^{00})_{\mathrm{Al}} \ = \\ -\frac{c^4}{32\pi}\, v_s^2\left[\left(\frac{\partial f}{\partial y}\right)^2 + \left(\frac{\partial f}{\partial z}\right)^2\right] < 0\,.\end{aligned} \tag{1.32}$$

By taking into account the form of (1.23) we find the energy density:

$$(T^{00})_{\mathrm{Al}} = -\frac{c^4}{32\pi}\,(v_s)^2\left(\frac{df}{dr_s}\right)^2 \frac{y^2 + z^2}{r_s^2}\,. \tag{1.33}$$

This expression is unfortunately negative as measured by the Eulerian observer, and therefore it violates the weak energy conditions.

2 Reducing the energy density

2.1 A new configuration

Inside this bubble a spacecraft is engineered with a surrounding "shell" of thickness, $R_e - R_i$, where R_e is the outer radius, and R_i the inner radius. Now, let us consider a fluid of density ρ carrying a charge μ which fills this shell. By applying an electromagnetic field with a 4-potential A_α inside the shell, the whole spacecraft surrounded by the charge density will follow a specific *Finslerian geodesic* [8] provided the ratio μ/ρ remains constant all along the trajectory

$$ds_{\mathrm{shell}} = ds + \frac{\mu}{\rho}\, A_\alpha\, dx^\alpha, \tag{2.1}$$

where $ds = \sqrt{\eta_{\alpha\beta}\, dx^\alpha dx^\beta}$.

Therefore we may write the metric (neglecting the non-quadratic term)

$$(ds^2)_{\mathrm{shell}} = ds^2 + \left(\frac{\mu}{\rho}\, A_\alpha\, dx^\alpha\right)^2. \tag{2.2}$$

Now, the shell containing the charge μ which is acted upon by the potential A_a, must be included in the formulation of the metric (1.25). This can be achieved in a manner not too dissimilar to the one chosen in [9, 10]. First we have for the time component of the interaction term

$$\frac{\mu}{\rho}\, iA_0\, dx^0 = \frac{\mu}{\rho}\, \Phi\, cdt\,, \tag{2.3}$$

where Φ is the scalar potential. The metric tensor time component in (2.2) becomes

$$g_{00} = -\left(1 + \frac{\mu}{\rho}\,\Phi\right)^2. \tag{2.4}$$

The remaining spatial components $(\mu/\rho)A_a dx^a$ can be neglected if the 3-velocity of the global charges carrier (spacecraft) is low, since in this case the 3-density current is equal to $j_a = \mu \mathrm{v}_a \approx 0$. Hence, the metric (2.2) would reduce to

$$ds^2 = -\left(1 + \frac{\mu}{\rho}\,\Phi\right)^2 + dz^2 + dx^2 + dy^2. \tag{2.5}$$

In the framework of the Alcubierre metric, the spaceship shell is part of the warp drive bubble and as such the interaction term should be a function of r_s, R_B, σ, and the thickness $(R_e - R_i)$ but not the speed v_s.

Therefore we are led to define the lapse function as

$$N = \sqrt{1 + iS^2}\,, \tag{2.6}$$

where

$$S = \frac{1}{2}\left\{1 + \tanh\left[\sigma(r_s + R_e)^2\right]\right\}^{-\frac{a\Phi\mu}{\rho}}. \tag{2.7}$$

The dimensionless factor a delimits the shell thickness

$$\mathrm{a} = (R_e - R_i)^{-1} \int_{R_i}^{R_e} dR\,, \tag{2.7bis}$$

and (2.7) is verified from the center of the spacecraft location to the ext. bubble wall R_e, where $f = 1$.

The Alcubierre metric (1.25) can then be re-written as

$$\begin{aligned} ds^2 = &-\left[N^2 - v_s^2 f^2(r_s)\right] c^2 dt^2 - \\ &- 2v_s f(r_s)\, cdt\, dx + dz^2 + dx^2 + dy^2. \end{aligned} \tag{2.8}$$

From the internal radius R_i throughout the spacecraft interior, there is no charge, and we see that the space is Minkowskian so that the spacecraft and its occupants will never suffer any tidal forces nor time dilation as per (1.10bis).

From the metric (2.8), it is now easy to infer the Eulerian observer's velocity components. We have

$$c^2 = -c^2\left(N^2 - v_s^2 f^2\right)\left(\frac{dt}{d\tau}\right)^2 - 2v_s f c\,\frac{dt}{d\tau}\,u_{\mathrm{E}} + u_{\mathrm{E}}^2\,. \tag{2.9}$$

The Eulerian observer travels along the geodesic where he "sees"

$$\frac{dt}{d\tau} = N^{-1}, \tag{2.10}$$

which yields

$$0 = u_{\mathrm{E}}^2 - 2v_s f c N^{-1} u_{\mathrm{E}} + v_s^2 f^2 c^2 N^{-2} \tag{2.11}$$

and finally we obtain

$$u_{\mathrm{E}} = v_s f c N^{-1}, \tag{2.12}$$

$$(u^\mu)_{\mathrm{E}} = \left\{cN^{-1},\, v_s f c N^{-1},\, 0,\, 0\right\}, \tag{2.13}$$

$$(u_\mu)_{\mathrm{E}} = \{-cN,\, 0,\, 0,\, 0\}\,. \tag{2.14}$$

2.2 The energy required for the propulsion

If we insert N into (1.30), the formula

$$C_{\mathrm{Al}} = (u_0)_{\mathrm{E}}\,(u_0)_{\mathrm{E}}\,T^{00} \tag{2.15}$$

yields the new energy density requirement

$$T^{00} = -\frac{c^4}{32\pi}\,\frac{v_s^2(y^2 + z^2)}{N^4 r_s^2}\left(\frac{df}{dr_s}\right)^2. \tag{2.16}$$

Now, recalling the form (2.6) for N, we have

$$N^4 = \left(1 + iS^2\right)^2 < 0\,. \tag{2.17}$$

Thus the energy conditions $T^{00} \geqslant 0$ are obviously always satisfied. Therefore we may choose the factor N (thereby S) arbitrarily large so as to substantially reduce the required energy density for the ship frame.

The higher the charge and the potential, the lower the energy requirement.

In the closed volume V of the spacecraft shell one can inject a flow of electrons according to the constant ratios

$$\frac{\mu}{\rho} = \frac{\sum_V e}{\sum_V m}\,. \tag{2.18}$$

We see that the leptonic lightweight would have the capacity to lower the negative energy even further. The splitting shell-inner part of the spacecraft frame, is really the hallmark of the theory here: it implies that the proper time τ of the inner part of the spacecraft is not affected by the term N.

PART II

In "The Time Machine" (1895), the novel by H. G. Wells, an English scientist constructs a machine which allows him to travel back and forth in time. The history of fascinating idea of time travel can be traced back to Kurt Gödel who found a solution of Einstein's field equations that contains closed time-like curves (CTCs) [11]. Those make it theoretically

feasible to go on journey into one's own past. In our previous publication [12], we formally demonstrated that Gödel's model was not just a mere (speculative) cosmological model as is was always accepted, but an ordinary metric with own physical properties.

Upon these results we develop here the bases for a possible time travel mode of displacement.

3 Reformulation of Gödel's metric (reminder)

The classical Gödel line element is generically given by the interval

$$ds^2 = a^2\left(dx_0^2 - dx_1^2 + dx_2^2\,\frac{e^{2x_1}}{2} - dx_3^2 + 2\,e^{x_1}dx_0\,dx_2\right) \quad (3.1)$$

or, equivalently,

$$ds^2 = a^2\left[-dx_1^2 - dx_3^2 - dx_2^2\,\frac{e^{2x_1}}{2} + (e^{x_1}dx_2 + dx_0)^2\right], \quad (3.2)$$

where $a > 0$ is a constant.

In our theory, we assumed that a is slightly space-time variable and we set

$$a^2 = e^{2U}. \quad (3.3)$$

As a result, the Gödel metric tensor components are conformal to the real Gödel metric tensor $g_{\mu\nu}$

$$(g_{\mu\nu})' = e^{2U}g_{\mu\nu}\,, \qquad (g^{\mu\nu})' = e^{-2U}g^{\mu\nu}. \quad (3.4)$$

The exact Gödel metric reads now

$$(ds^2)' = e^{2U}\left[dx_0^2 - dx_1^2 + dx_2^2\,\frac{e^{2x_1}}{2} - \right. \\ \left. - dx_3^2 + 2\,e^{x_1}(dx_0\,dx_2)\right]. \quad (3.5)$$

This implies that this metric is a solution of the field equations describing a peculiar perfect fluid [13–15]

$$G_{\mu\beta} = \varkappa\left[(\rho + P)\,u_\mu u_\beta - P g_{\mu\beta}\right]. \quad (3.6)$$

The model is likened to a fluid in rotation with mass density ρ and pressure P. The positive scalar U is shown to be:

$$U(x^\mu) = \int \frac{dP}{\rho + P}\,. \quad (3.7)$$

From (3.4) and (3.6) one formally infers that the flow lines of matter of the fluid follow conformal geodesics given by

$$s' = \int e^U ds\,. \quad (3.8)$$

The hallmark of the theory is the substitution (3.3): the Gödel space-time is no longer the representation of a cosmological model but it is relegated to the rank of an ordinary metric where its physical properties could allow for a possible replication.

4 Closed time-like curves

With Gödel one defines new coordinates (t, r, ϕ) which in the reformulated version lead to the line element

$$ds^2 = 4\,e^{2U}\Big[dt_{\rm G}^2 - dr^2 + (\sinh^4 r - \sinh^2 r)\,d\phi^2 + \\ + 2\,\sqrt{2}\,\sinh^2 r\,d\phi\,dt\Big]. \quad (4.1)$$

This metric exhibits the rotational symmetry of the solution about the chosen Gödel $t_{\rm G}$-time axis where $r = 0$ orthogonal to the hyperplane (x, y, z), since we clearly see that the spatial components of the metric tensor and its covariant derivative do not depend on f. For $r \geqslant 0$, we have $0 \leqslant \phi \leqslant 2\pi$. If a curve $r_{\rm G}$ is defined by $\sinh^4 r = 1$, that is

$$r_{\rm G} = \ln\left(1 + \sqrt{2}\right), \quad (4.2)$$

the circle $r > \ln(1 + \sqrt{2})$, i.e. $(\sinh^4 r - \sinh^2 r) > 0$ in the "hyperplane" $t_{\rm G} = 0$, is a *closed time-like curve* (which is not a *geodesic line*!). Here $r_{\rm G}$ is referred to as the *Gödel radius*.

The circle of radius $r_{\rm G}$ is a *light-like curve*, where the light cones are tangential to the hyperplane (x, y, z) of zero $t_{\rm G}$. Photons trajectories reaching this radius are closing up, therefore $r_{\rm G}$ constitutes a *chronal horizon* beyond which an observer located at the origin ($r = 0$) cannot detect them. The following quantity corresponds to $r_{\rm G}$, it is $(ds^2)' = e^{2U}ds^2 = 0$ with $e^{2U} \neq 0$.

For $r > r_{\rm G}$ the light cone opens up and tips over until its future part reaches the negative values of $t_{\rm G}$. In this an *achronal domain*, any closed curve is a time-like curve. The conformal line $s' = \int e^U ds$, the integral of which is performed over the curve length is always a time-like geodesic provided the following transformation is applied

$$t = t_{\rm G} + \tanh\left(\frac{r - r_{\rm G}}{r_{\rm G}}\right)\sqrt{x^2 + y^2}\,, \quad (4.3)$$

where $r - r_{\rm G}$ measures the distance from the Gödel radius onward. So long as $r < r_{\rm G}$, then t coincides with the Gödel time axis $t_{\rm G}$. When $r > r_{\rm G}$, then $t_{\rm G} = 0$ and the time coordinate t becomes space-like as viewed from within the Gödel space-time. The Gödel space coordinates should then be transformed as follows

$$x\,(\text{resp. } y, z) = x_{\rm G} - (x_{\rm G} + x_{\rm N})\tanh\left(\frac{r - r_{\rm G}}{r_{\rm G}}\right). \quad (4.4)$$

For $r < r_{\rm G}$, $x\,(\text{resp. } y, z)$ coincides with the Gödel space-time coordinates $x_{\rm G}\,(\text{resp. } y_{\rm G}, z_{\rm G})$ of the hyperplane (x, y, z). For $r > r_{\rm G}$, $x\,(\text{resp. } y, z)$ coincides with a new coordinate $x_{\rm N}\,(\text{resp. } y_{\rm N}, z_{\rm N})$ distinct from $x_{\rm G}\,(\text{resp. } y_{\rm G}, z_{\rm G})$.

5 Time displacement mode

5.1 Creating a "bubble" along a Gödel curve

As we demonstrated, the conformal factor e^{2U} is not related to the hypothetical cosmological constant Λ.

It is therefore possible to adjust the factor U in order to create a pressureless singularity within the new Gödel space-time. In the following such a singular region is likened to the warp drive "bubble" which is bound to move along a Gödel curve.

The bubble follows the trajectory $x_s(t)$ where the time coordinate t satisfies here (4.3). Therefore for $R \leqslant R_B$, the bubble is assumed to be ruled by the new Alcubierre metric (2.8) expressed with the signature -2

$$ds^2 = \left(N^2 - v_s^2 f^2\right) c^2 dt^2 - 2 v_s f(r_s)\, c dt\, dx - \\ - dz^2 - dx^2 - dy^2. \tag{5.1}$$

This space-time is thus regarded as *globally hyperbolic* and the bubble will never know whether it moves along a CTC. As a result,the bubble is seen by a specific observer (see below) as being transported forward along the x-direction *tangent* to a CTC beyond the Gödel radius r_{G}. In the absence of charge outside of the bubble ($R > R_B \to \infty$), there is $f = 0$ and we retrieve Gödel's metric (2.1).

5.2 Gödel chronal horizon

At the origin of the coordinate system, the axis of the light cone is orthogonal to the (x, y, z) hyperplane as described above by the metric (2.1). The circle of radius r_{G} is a *light-like curve*, where the light cones are tangential to the plane of constant (or zero) t and photons trajectories reaching this radius are closing up, therefore r_{G} constitutes a *chronal horizon*. Such an horizon is a special type of the *Cauchy horizon* beyond which an observer located at the origin ($r = 0$) cannot detect them. With increasing $r > r_{\mathrm{G}}$ the light cones continue to keel over and their opening angles widen until their future parts reach the negative values of t. In this an *achronal domain*, any closed curve is a time-like curve. As a result, the bubble follows a reversed chronological sequence with respect to the coordinate t.

The bubble moves backwards in time and travels into the past of a specific observer resting at $r = 0$ whose proper time satisfies $\tau = t$. After regressing, once $r < r_{\mathrm{G}}$, the bubble can return to the original causal domain at the departing coordinate time t, thus slightly aging with respect to the rest observer depending on its trip own time duration.

Concluding remarks

Without going into details of a sound engineering, we have just briefly sketched the basic principle of the existing theory using electromagnetism and charged current to suit the warp drive propulsion. Our approach heavily relies on a specific configuration describing a spacecraft located inside a warp drive bubble, which certainly deserves further scrutiny. In order to avoid an additional heavy treatment of the warp drive subject we have skipped some of the important aspects of the topic, as for example the causally separation of the bubble center to the outer edge of the bubble wall and beyond.

For further rigorous studies of classical warp drive physics, one can refer to [16–19]. Unlike our concept all of these theories rely on negative energy contributions also referred to as "exotic energy" or "exotic matter" [20]. Such form of energy has never been detected so far, although its theoretical production based on a L. de Broglie's publication [21] has been suggested in [22]. By introducing a "complex" potential, our warp drive concept does not require any form of exotic matter.

As a space-time short-cut Morris, Thorne et al. [23] derived a specific static wormhole comparable to the Einstein-Rosen-bridge. Combining two wormholes with a distorted one the authors could produce a time lag which would act as a time machine. Of particular interest is the recent paper published by Tippett and Tsang [24] where the Alcubierre warp is applied to a CTC. Like in our theory, a bubble of curvature travels along a closed trajectory and is ruled by a Rindler geometry. At any rate Exotic matter is still required.

Natàrio investigated an "optimal time travel" in the Gödel universe for a particle bound to accelerate along a CTC [25]. For this purpose, the well known Rocket Equation trajectories in general relativity are here applied to a CTC. Natàrio however keeps the factor $a = 1$ (and the cosmological constant $\Lambda = -\frac{1}{2}$), which necessarily restricts again this field of research to a finely tuned universe space-time. In contrast to all those attempts and related theories, the model we suggest here is derived from a reformulated Gödel metric that exhibits consistent physical properties which are known to exist. Because of this reformulation, new physical conditions render plausible a system which may accommodate a potential time machine.

The basic engineering we presented in here, pre-suppose a high level of technological accuracy, which is far from being reached by today's knowledge.

Billions of billions of distant galaxies must certainly harbour quite a great number of inhabitable worlds where advanced civilizations have certainly developed capabilities to allow for such interstellar propulsion modes. Indeed, our universe is 13.7 billion years old compared to the 4 billion years of our (marginal) Earth. Given this scale, an evolution difference of just one million years only between us and other extraterrestrial forms of thinking beings, is not unrealistic, and it implicitly means an incredible exponential degree of superior knowledge which is certainly beyond our common understanding.

Submitted on June 5, 2022

References

1. Arnowitt R., Deser S., Misner C. Dynamical structure and definition of energy in General Relativity. *Physical Review*, 1959, v. 116, no. 5, 1322–1330.
2. Kuchar K. Canonical methods of quantization. Quantum Gravity 2: A Second Oxford Symposium. Clarendon Press, Oxford Press, 1981, 329–374.

3. Wald R. General Relativity. University of Chicago Press, 1984.
4. Alcubierre M. The warp drive: hyper fast travel within General Relativity. *Classical and Quantum Gravity*, 1994, v. 11, L73–L77.
5. Marquet P. The generalized warp drive concept in the EGR theory. *The Abraham Zelmanov Journal*, 2009, v. 2, 261–287.
6. Natario J. Warp drive with zero expansion. arXiv: 0110086v3 [gr-qc] (2002).
7. Hawking S.W., Ellis G.F.R. The Large Scale Structure of Space-Time. Cambridge University Press, 1973.
8. Marquet P. Geodesics and Finslerian equations in the EGR theory. *The Abraham Zelmanov Journal*, 2010, v. 3, 90–100.
9. Loup F., Waite D., Halerewicz E.Jr. Reduced total energy requirements for a modified Alcubierre warp drive spacetime. arXiv: 01070975v1 [gr-qc] (2001).
10. Loup F., Waite D., Held R., Halerewicz E.Jr., Stabno M., Kuntzman M., Sims R. A causally connected superluminal warp drive spacetime. arXiv: 0202021v1 [gr-qc] (2002).
11. Gödel. K. An example of a new type of cosmological solutions of Einstein's field equations of gravitation. *Review of Modern Physics*, 1949, v. 21, no. 3.
12. Marquet P. The exact Gödel solution. *Progress in Physics*, 2021, v. 17, 133–138.
13. Eisenhart L.P. *Trans. Americ. Math. Soc.*, 1924, v. 26, 205–220.
14. Synge J.L. *Proc. London Math. Soc.*, 1937, v. 43, 37–416.
15. Lichnerowicz A. Les Théories Relativistes de la Gravitation et de l'Electromagnétisme. Masson et Cie, Paris, 1955.
16. Hiscock W.A. Quantum effects in the Alcubierre warp-drive spacetime. arXiv: 9707024 [gr-qc] (1997).
17. Ford L.H., Pfenning M.J. The unphysical nature of "warp drive". arXiv: 9707026 [gr-qc] (1997).
18. van den Broeck C. A warp drive with more reasonable total energy requirements. arXiv: 9905084 [gr-qc] (1999).
19. Santos-Pereira O.L., Abreu E.M.C., Ribeiro M.B. Charged dust solutions for the warp drive space-time arXiv: 210205119v1 [gr-qc] (2021).
20. Lobo F.S.N. Exotic solutions in General Relativity. Traversables wormholes and "warp drive" space-times. arXiv: 07104474v1 [gr-qc] (2007).
21. de Broglie L. Etude du mouvement des particules dans un milieu réfringent. *Annales de Institut Henri Poincaré*, 1973, v. XVIII, no. 2, 89–98.
22. Marquet P. Exotic matter: a new perspective. *Progress in Physics*, 2017, v. 13, 174–179.
23. Morris M.S., Thorne K.S., Yurtsever U. Wormholes, time machine and the weak energy condition. *Physical Rev. Lett.*, 1988, v. 61, no. 13, 1446–1449.
24. Tippett B.J., Tsang D. Traversable achronal retrograde domain in space-time. arXiv: 13107985v2 [gr-qc] (2013).
25. Natàrio J. Optimal time travel in the Gödel universe. arXiv: 1105619v2 [gr-qc] (2011).

Twin Universes Confirmed by General Relativity

Patrick Marquet
Calais, France. E-mail: patrick.marquet6@wanadoo.fr

The twin universes hypothesis was initially proposed by A. D. Sakharov followed by several astrophysicists in order to explain some unsolved questions mainly the current dark matter issue. However, no one could provide a physical justification as to the origin and existence of the second universe. We show here that general relativity formally yields two coupled field equations exhibiting an opposite sign, which lends support to Sakharov's conjecture. To this end, we use Cartan's calculus, in order to derive the differential form of Einstein's field equations. This procedure readily leads to a particular representation whereby the Einstein's field equation is classically inferred from the "Landau-Lifshitz superpotential". Since this superpotential is a fourth rank tensor (density-like), a second field equation naturally arises from the derivation, a result which has been so far totally obscured and overlooked in all classical treatments.

Notations

Space-time Greek indices α, β run from 0, 1, 2, 3 for local coordinates.
Space-time Latin indices a, b run from 0, 1, 2, 3 for a general basis.
Space-time signature is -2.
Einstein's constant is denoted by $\varkappa$.
We assume here that $c = 1$.

1 Differential calculus

1.1 The field equations in GR (short overview)

In General Relativity, the line element on the 4-dimensional pseudo-Riemannian manifold (M, g) is given by the interval $ds^2 = g_{ab}\, dx^a dx^b$. By varying the action $\mathcal{S} = \mathcal{L}_{\mathrm{E}}\, d^4x$ with respect to g_{ab} where the Lagrangian density is given by

$$\mathcal{L}_{\mathrm{E}} = g^{ab}\sqrt{-g}\left(\left\{{e \atop ab}\right\}\left\{{d \atop de}\right\} - \left\{{d \atop ae}\right\}\left\{{e \atop bd}\right\}\right), \tag{1}$$

one infers the symmetric Einstein tensor

$$G_{ab} = R_{ab} - \frac{1}{2}\, g_{ab}\, R\,, \tag{2}$$

where, as is well-known,

$$R_{bc} = \partial_a \left\{{a \atop bc}\right\} - \partial_c \left\{{a \atop ba}\right\} + \left\{{d \atop bc}\right\}\left\{{a \atop da}\right\} - \left\{{d \atop ba}\right\}\left\{{a \atop dc}\right\} \tag{3}$$

is the (symmetric) Ricci tensor whose contraction gives the curvature scalar R, and $\left\{{e \atop ab}\right\}$ denote the Christoffel symbols of the second kind.

The source free field equations are

$$G_{ab} = R_{ab} - \frac{1}{2}\, g_{ab}\, R + \Lambda\, g_{ab} = 0\,, \tag{4}$$

where Λ is usually called the cosmological constant. The second rank tensor G_{ab} is symmetric and is only function of the metric tensor components g_{ab} and their first and second order derivatives. Due to the Bianchi's identities the Einstein tensor is conceptually conserved

$$\nabla_a\, G^a_b = 0\,, \tag{5}$$

where ∇_a is the Riemann covariant derivative.

When a massive source is present, the field equations become

$$G_{ab} = R_{ab} - \frac{1}{2}\, g_{ab}\,(R - 2\Lambda) = \varkappa\, T_{ab}\,. \tag{6}$$

If ρ is the matter density, T_{ab} is here the tensor describing the pressure of a free fluid

$$T_{ab} = \rho\, u_a\, u_b\,. \tag{7}$$

1.2 The general structures on a manifold

Let us now consider a 4-manifold M referred to a vector basis e_α. A locally defined set of four linearly independent vector fields, determined by the dual basis θ^β of the local coordinates

$$\theta^\beta = \mathrm{a}^\beta_a\, dx^a \tag{8}$$

is called a *tetrad field* or *vierbein* [1].

On this manifold, it is well known that the connection coefficients $\Gamma^\gamma_{\alpha\beta}$ can be decomposed in the most general sense as

$$\Gamma^\gamma_{\alpha\beta} = \left\{{\gamma \atop \alpha\beta}\right\} + \mathrm{K}^\gamma_{\alpha\beta} + (\Gamma^\gamma_{\alpha\beta})\mathrm{s}\,, \tag{9}$$

where $\mathrm{K}^\gamma_{\alpha\beta}$ is the *contorsion tensor* which is built from the *torsion tensor* $T^\gamma_{\alpha\beta} = \frac{1}{2}\,(\Gamma^\gamma_{[\beta\alpha]} - \Gamma^\gamma_{\alpha\beta})$, and

$$(\Gamma^\gamma_{\alpha\beta})\mathrm{s} = \frac{1}{2}\, g^{\gamma\mu}\left(\mathrm{D}_\beta\, g_{\alpha\mu} + \mathrm{D}_\alpha\, g_{\beta\mu} - \mathrm{D}_\mu\, g_{\alpha\beta}\right) \tag{10}$$

is the *segment connection* formed with the general covariant derivatives of the metric tensor (denoted here by D instead of the Riemann symbol ∇)

$$\mathrm{D}_\gamma\, g_{\alpha\beta} = \partial_\gamma\, g_{\alpha\beta} - \Gamma_{\alpha\gamma\beta} - \Gamma_{\beta\gamma\alpha} \neq 0\,. \tag{11}$$

The connection $(\Gamma^{\gamma}_{\alpha\beta})_{\mathrm{S}}$ characterizes a particular property of the manifold related to a second type of structure, called the *segment curvature*. This additional curvature results from the variation of the parallel transported vector around a small closed path.

In a dual basis θ^{α}, the following 2-forms can be associated with any parallel transported vector along the closed path:

— a rotation curvature form

$$\Omega^{\alpha}_{\beta} = \frac{1}{2} R^{\alpha}_{\beta\gamma\delta}\, \theta^{\gamma} \wedge \theta^{\delta}, \tag{12}$$

— a torsion form

$$\Omega^{\alpha} = \frac{1}{2} T^{\alpha}_{\gamma\delta}\, \theta^{\gamma} \wedge \theta^{\delta}, \tag{13}$$

— a segment curvature form

$$\Omega = -\frac{1}{2} R^{\alpha}_{\alpha\gamma\delta}\, \theta^{\gamma} \wedge \theta^{\delta}. \tag{14}$$

These are the maximum admissible mathematical structures defining a general manifold.

1.3 The Cartan structure equations

We now introduce the *Cartan procedure*. This is a powerful coordinate calculus extensively used in the foregoing.

Let us first define the connection forms

$$\Gamma^{\alpha}_{\beta} = \left\{ {\alpha \atop \gamma\beta} \right\} \theta^{\gamma}. \tag{15}$$

The *first Cartan structure equation* is related to the torsion by [2, p. 40]

$$\Omega^{\alpha} = \frac{1}{2} T^{\alpha}_{\gamma\delta}\, \theta^{\gamma} \wedge \theta^{\delta} = d\theta^{\alpha} + \Gamma^{\alpha}_{\gamma} \wedge \theta^{\gamma}. \tag{16}$$

and the *second Cartan structure equation* is [2, p. 42]

$$\Omega^{\alpha}_{\beta} = \frac{1}{2} R^{\alpha}_{\beta\gamma\delta}\, \theta^{\gamma} \wedge \theta^{\delta} = d\Gamma^{\alpha}_{\beta} + \Gamma^{\alpha}_{\gamma} \wedge \Gamma^{\beta}_{\gamma}. \tag{17}$$

and $R^{\alpha}_{\beta\gamma\delta}$ are here the components of the curvature tensor in the most general sense.

Within the Riemannian framework alone (torsion free), $R^{\alpha}_{\beta\gamma\delta}$ reduces to the Riemann curvature tensor components and the first structure equation (16) becomes

$$d\theta^{\alpha} = -\Gamma^{\alpha}_{\gamma} \wedge \theta^{\gamma}. \tag{18}$$

We shall now define the absolute exterior differential D of a tensor valued p-form of type (r, s)

$$(\mathrm{D}\phi)^{i_1\ldots i_r}_{j_1\ldots j_s} = d\phi^{i_1\ldots i_r}_{j_1\ldots j_s} + \Gamma^{i_1}_{k} \wedge \phi^{k\, i_1\ldots i_r}_{j_1\ldots j_s} + \ldots - \Gamma^{k}_{j_1} \wedge \phi_{k\, j_2\ldots j_s}^{\,i_1\ldots i_r} - \ldots$$

As a simple example, the Bianchi identities can be simply written with the exterior differential as

$$\mathrm{D}\Omega^{\alpha} = \Omega^{\alpha}_{\beta} \wedge \theta^{\beta} \quad \text{(1st Bianchi identity)},$$

$$\mathrm{D}\Omega^{\alpha}_{\beta} = 0 \quad \text{(2nd Bianchi identity)}.$$

2 The differential Einstein equations

2.1 The Einstein action

We first recall the definition of the Hodge star operator for an oriented n-dimensional pseudo-Riemannian manifold (M, g), wherein the volume element is determined by g

$$\eta = \sqrt{-g}\, \theta^{0} \wedge \theta^{1} \wedge \theta^{2} \wedge \theta^{3}.$$

Let $\Lambda_k(\mathrm{E})$ be the subspace of completely antisymmetric multilinear forms on the real vector space E. The *Hodge star operator* $*$ is a linear isomorphism $\Lambda_k(\mathrm{M}) \to \Lambda_{n-k}(\mathrm{M})$, where $k \leqslant n$. If $\{\theta^0, \theta^1, \theta^2, \theta^3\}$ is an oriented basis of 1-forms, this operator is defined by

$$^{*}(\theta^{i_1} \wedge \theta^{i_2} \wedge \ldots\ \theta^{i_k}) =$$

$$= \frac{\sqrt{-g}}{(n-k)!}\, \varepsilon_{j_1\ldots j_n}\, g^{j_1 i_1} \ldots\ g^{j_k i_k}\, \theta^{j_{k+1}} \wedge \ldots \wedge \theta^{j_n}.$$

With this preparation, the Einstein action simply reads

$$^{*}R = R\,\eta\,. \tag{19}$$

To show this, we express this action in terms of tetrads. With $\eta^{\mu\nu} = {}^{*}(\theta^{\mu} \wedge \theta^{\nu})$ and taking into account (17) we have

$$\eta_{\beta\gamma} \wedge \Omega^{\beta\gamma} = \frac{1}{2}\, \eta_{\beta\gamma} R^{\beta\gamma}_{\mu\nu}\, \theta^{\mu} \wedge \theta^{\nu},$$

$$^{*}(\theta^{\mu} \wedge \theta^{\nu}) = \frac{1}{2}\, \eta_{\beta\gamma\sigma\rho}\, g^{\beta\gamma} \theta^{\sigma} \wedge \theta^{\rho},$$

i.e., we have

$$\eta_{\beta\gamma} = \frac{1}{2}\, \eta_{\beta\gamma\sigma\rho}\, \theta^{\sigma} \wedge \theta^{\rho}. \tag{20}$$

Thus, we have

$$\eta_{\beta\gamma} \wedge \theta^{\mu} \wedge \theta^{\nu} = \frac{1}{2}\, \eta_{\beta\gamma\sigma\rho}\, \theta^{\sigma} \wedge \theta^{\rho} \wedge \theta^{\mu} \wedge \theta^{\nu} = (\delta^{\mu}_{\beta}\, \delta^{\nu}_{\gamma} - \delta^{\mu}_{\gamma}\, \delta^{\nu}_{\beta})\, \eta\,,$$

$$\eta_{\beta\gamma} \wedge \Omega^{\beta\gamma} = \frac{1}{2}\, (\delta^{\mu}_{\beta}\, \delta^{\nu}_{\gamma} - \delta^{\mu}_{\gamma}\, \delta^{\nu}_{\beta})\, R^{\beta\gamma}_{\mu\nu}\, \eta = R\,\eta = {}^{*}R\,.$$

Taking also into account (20), we compute the absolute exterior differential $\mathrm{D}\eta_{\beta\gamma} = \frac{1}{2}\, \mathrm{D}(\eta_{\beta\gamma\sigma\rho}\, \theta^{\sigma} \wedge \theta^{\rho})$. In an orthonormal frame $\eta_{\beta\gamma\sigma\rho}$ is constant and $\mathrm{D}\,\eta_{\beta\gamma\sigma\rho} = 0$. This manifests the fact that in the *Riemannian framework* (metric connection), orthonormality is preserved under parallel transfer. Therefore, $\mathrm{D}\eta_{\beta\gamma} = \eta_{\beta\gamma\sigma\rho}\, \mathrm{D}\theta^{\sigma} \wedge \theta^{\rho}$.

Now, keeping in mind that the basis θ^{σ} is a tensor 1-form of the type (1,0), the first structure equation reads

$$\mathrm{D}\theta^{\sigma} = \Omega^{\sigma},$$

$$\mathrm{D}\eta_{\beta\gamma} = \eta_{\beta\gamma\sigma\rho}\, \Omega^{\sigma} \wedge \theta^{\rho} = \Omega^{\sigma} \wedge \eta_{\beta\gamma\sigma}\,.$$

The latter equation is zero for the Riemannian connection $\mathrm{D}\,\eta_{\beta\gamma} = 0$. In the same way, we can show that

$$\mathrm{D}\eta^{\beta\gamma}_{\alpha} = d\eta^{\beta\gamma}_{\alpha} + \Gamma^{\beta}_{\delta} \wedge \eta^{\delta\gamma}_{\alpha} + \Gamma^{\alpha}_{\delta} \wedge \eta^{\beta\delta}_{\alpha} - \Gamma^{\delta}_{\alpha} \wedge \eta^{\beta\gamma}_{\delta} = 0 \tag{21}$$

with $\eta^{\beta\gamma}_{\alpha} = {}^{*}(\theta^{\beta} \wedge \theta^{\gamma} \wedge \theta_{\alpha})$ (all indices are raised or lowered with $g_{\alpha\beta}$ from $g = g_{\alpha\beta}\, \theta^{\alpha} \otimes \theta^{\beta}$).

2.2 The Einstein field equations

From (20), we infer that

$$\eta_{\beta\gamma\delta} = \eta_{\beta\gamma\delta\lambda}\,\theta^{\lambda}. \tag{22}$$

Under the variation $\delta\theta^{\beta}$ of the orthonormal tetrad fields θ^{β}, we have

$$\delta\,(\eta_{\beta\gamma}\wedge\Omega^{\beta\gamma}) = \delta\eta_{\beta\gamma}\wedge\Omega^{\beta\gamma} + \eta_{\beta\gamma\delta}\wedge\delta\Omega^{\beta\gamma\delta}.$$

Now, using (20) and (22) yields

$$\delta\eta_{\beta\gamma} = \frac{1}{2}\,\delta\,(\eta_{\beta\gamma\delta\lambda}\,\theta^{\delta}\wedge\theta^{\lambda}) = \delta\theta^{\delta}\wedge\eta_{\beta\gamma\delta}\,.$$

Hence, applying the varied second structure equation

$$\delta\Omega^{\beta\gamma} = d\,\delta\Gamma^{\beta\gamma} + \delta\Gamma^{\beta}_{\eta}\wedge\Gamma^{\eta\gamma} + \Gamma^{\beta}_{\eta}\wedge\delta\Gamma^{\eta\gamma},$$

we obtain

$$\begin{aligned}\delta\,(\eta_{\beta\gamma}\wedge\Omega^{\beta\gamma}) &= \delta\theta^{\delta}\wedge(\eta_{\beta\gamma\delta}\wedge\Omega^{\beta\gamma}) + d\,(\eta_{\beta\gamma}\wedge\delta\Gamma^{\beta\gamma}) -\\ &- d\eta_{\beta\gamma}\wedge\delta\Gamma^{\beta\gamma} + \eta_{\beta\gamma}\wedge(\delta\Gamma^{\beta}_{\eta}\wedge\Gamma^{\eta\gamma} + \Gamma^{\beta}_{\eta}\wedge\delta\Gamma^{\eta\gamma})\,,\end{aligned} \tag{23}$$

and from the second line we extract $d\eta_{\beta\gamma} + \eta_{\beta\gamma}\wedge(\Gamma^{\eta}_{\gamma} + \Gamma_{\beta\eta})$, which is just $\mathrm{D}\eta_{\beta\gamma}$.

However, we know that $\mathrm{D}\eta_{\beta\gamma} = 0$, and finally, the varied Einstein action is

$$\begin{aligned}\delta\,(\eta_{\beta\gamma}\wedge\Omega^{\beta\gamma}) = \delta\theta^{\beta}\wedge(\eta_{\beta\gamma\delta}\wedge\Omega^{\gamma\delta}) + d\,(\eta_{\beta\gamma}\wedge\delta\Gamma^{\beta\gamma}) +\\ + (\text{exact differential}).\end{aligned} \tag{24}$$

The global Lagrangian density $\mathcal{L}$ in the presence of matter is written as

$$\mathcal{L} = -\frac{1}{2\varkappa}\,{}^{*}R + \mathcal{L}_{\text{matter}}\,.$$

Setting up ${}^{*}T_{\beta}$ as the energy-momentum 3-form for *bare matter* we have the Lagrangian density for the varied matter

$$\delta\mathcal{L}_{\text{matter}} = -\,\delta\theta^{\beta}\wedge{}^{*}T_{\beta}$$

and taking into account (24), the global variation is

$$\delta\mathcal{L} = -\,\delta\theta^{\beta}\wedge\left(\frac{1}{2\varkappa}\,\eta_{\beta\gamma\delta}\wedge\Omega^{\gamma\delta} + {}^{*}T_{\beta}\right) + (\text{exact differential}).$$

We eventually arrive at the field equations in the differential form

$$-\,\frac{1}{2}\,\eta_{\beta\gamma\delta}\wedge\Omega^{\gamma\delta} = \varkappa\,{}^{*}T_{\beta}\,, \tag{25}$$

where T_{α} is related to the energy-momentum tensor $T_{\alpha\beta}$ by $T_{\alpha} = T_{\alpha\beta}\,\theta^{\beta}$.

In the same manner, we can obtain $G_{\alpha} = G_{\alpha\beta}\,\theta^{\beta}$ for the Einstein tensor $G_{\alpha\beta}$ (see Appendix A).

2.3 The energy-momentum tensor

It is well known however, that $G_{\alpha\beta}$ is intrinsically conserved while the massive tensor $T_{\alpha\beta}$ is not. This is because the gravitational field is not included in $T_{\alpha\beta}$. To restore conservation for the energy-momentum tensor, we start by reformulating (25) in the form

$$-\,\frac{1}{2}\,\Omega_{\beta\gamma}\wedge\eta^{\beta\gamma}_{\ \ \alpha} = \varkappa\,{}^{*}T_{\alpha}\,. \tag{25bis}$$

Then, we use the second structure equation under the following form

$$\Omega_{\beta\gamma} = d\Gamma_{\beta\gamma} - \Gamma_{\mu\beta}\wedge\Gamma^{\mu}_{\gamma} \tag{26}$$

so that we obtain

$$d\Gamma_{\beta\gamma}\wedge\eta^{\beta\gamma}_{\ \ \alpha} = d(\Gamma_{\beta\gamma}\wedge\eta^{\beta\gamma}_{\ \ \alpha}) + \Gamma_{\beta\gamma}\wedge\eta^{\beta\gamma}_{\ \ \alpha}\,. \tag{27}$$

Then, using (21) in (26), we infer

$$\begin{aligned}d\Gamma_{\beta\gamma}\wedge\eta^{\beta\gamma}_{\ \ \alpha} &= d\,(\Gamma_{\beta\gamma}\wedge\eta^{\beta\gamma}_{\ \ \alpha}) +\\ &+\Gamma_{\beta\gamma}\wedge(-\Gamma^{\beta}_{\delta}\wedge\eta^{\delta\gamma}_{\ \ \alpha} - \Gamma^{\gamma}_{\delta}\wedge\eta^{\beta\delta}_{\ \ \alpha} + \Gamma^{\delta}_{\alpha}\wedge\eta^{\beta\gamma}_{\ \ \delta})\,.\end{aligned} \tag{28}$$

Adding the second contribution of (26) to (28), we obtain the Einstein field equations in a new form, which is

$$-\,\frac{1}{2}\,d(\Gamma_{\beta\gamma}\wedge\eta^{\beta\gamma}_{\ \ \alpha}) = \varkappa\,({}^{*}T_{\alpha} + {}^{*}t_{\alpha})\,, \tag{29}$$

where we denote

$${}^{*}t_{\alpha} = -\,\frac{1}{2\varkappa}\,\Gamma_{\beta\gamma}\wedge(\Gamma_{\delta\alpha}\wedge\eta^{\beta\gamma\delta} - \Gamma^{\gamma}_{\delta}\wedge\eta^{\beta\delta}_{\ \ \alpha})\,, \tag{30}$$

and the quantity ${}^{*}t_{\alpha}$ is interpreted as the energy-momentum (pseudo-tensor) of the gravitational field generated by this distributed matter.

Equation (29) readily implies the conservation law

$$d\,({}^{*}T_{\alpha} + {}^{*}t_{\alpha}) = 0\,. \tag{31}$$

Writing

$$t_{\alpha} = t_{\alpha\beta}\,\theta^{\beta}\,, \tag{32}$$

we see that $t_{\alpha\beta}$ describes the gravitational field, which can be expressed, for example, by the Einstein-Dirac pseudo-tensor [3, p. 61].

From (30) we verify that $t_{\alpha\beta}$ is not symmetric. To correct this problem, we shall not apply the Belinfante symmetrization procedure [4]. Instead, we will modify the field differential equations. We first revert to the field equations (25) in which we insert $\eta^{\alpha\beta\gamma} = \eta^{\alpha\beta\gamma\delta}\,\theta_{\delta}$. With (26) this yields

$$-\,\frac{1}{2}\,\eta^{\alpha\beta\gamma\delta}\,\theta_{\delta}\wedge(d\Gamma_{\beta\gamma} - \Gamma_{\mu\beta}\wedge\Gamma^{\mu}_{\gamma}) = \varkappa\,{}^{*}T^{\alpha} \tag{33}$$

leading to

$$-\,\frac{1}{2}\,\eta^{\alpha\beta\gamma\delta}\,d(\Gamma_{\beta\gamma}\wedge\theta_{\delta}) = \varkappa\,({}^{*}T^{\alpha} + {}^{*}t^{\alpha})\,, \tag{34}$$

where

$$ {}^{*}t^{\alpha} = -\frac{1}{2}\varkappa\,\eta^{\alpha\beta\gamma\delta}(\Gamma_{\mu\beta}\wedge\Gamma^{\mu}_{\gamma}\wedge\theta_{\delta}-\Gamma_{\beta\gamma}\wedge\Gamma_{\mu\delta}\wedge\theta^{\mu})\,. \quad (35) $$

We see that ${}^{*}t^{\alpha}$ is unaffected by the exterior product terms in the bracket, therefore $t_{\alpha\beta}$ is now symmetric. In that case, we idendify ${}^{*}t^{\alpha}$ with the Landau-Lifshitz 3-form ${}^{*}t^{\alpha}_{\mathrm{L-L}}$, which yields the corresponding pseudo-tensor $t^{\alpha\beta}_{\mathrm{L-L}}$.

3 The 4th rank tensor equation

3.1 The first set of Einstein's field equations

Multiply (34) by $\sqrt{-g}$. Then, taking $\eta_{\alpha\beta\gamma\delta}=-\frac{1}{2}\sqrt{-g}\,\varepsilon_{\alpha\beta\gamma\delta}$ into account, we find a new form for the field equations

$$ -d\,(\sqrt{-g}\,\eta^{\alpha\beta\gamma\delta}\,\Gamma_{\beta\gamma}\wedge\theta_{\delta}) = 2\varkappa\,\sqrt{-g}\,({}^{*}T^{\alpha}+{}^{*}t^{\alpha}_{\mathrm{L-L}}) \quad (36) $$

or

$$ d\,(\sqrt{-g}\,\Gamma^{\beta\gamma}\wedge\eta^{\alpha}_{\beta\gamma}) = 2\,\sqrt{-g}\,({}^{*}T^{\alpha}+{}^{*}t^{\alpha}_{\mathrm{L-L}})\,. \quad (37) $$

From these equations follows immediately the differential conservation law

$$ d\Big[\,\sqrt{-g}\,({}^{*}T^{\alpha}+{}^{*}t^{\alpha}_{\mathrm{L-L}})\Big] = 0\,. \quad (38) $$

A tedious calculation eventually shows that

$$ d\,(\sqrt{-g}\;\Gamma^{\beta\gamma}\wedge\eta^{\alpha}{}_{\beta\gamma}) = \frac{1}{\sqrt{-g}}\,H^{\alpha\beta\nu\gamma}{}_{,\beta\gamma}\,\eta_{\nu}\,, \quad (39) $$

where

$$ H^{\alpha\beta\nu\gamma} = -g\,(g^{\alpha\nu}g^{\beta\gamma}-g^{\beta\nu}g^{\gamma\alpha}) \quad (40) $$

is the "Landau-Lifshitz superpotential" [5, eq. 101.2]. Therefore the field equations read here

$$ H^{\alpha\beta\nu\gamma}{}_{,\beta\gamma} = 2\varkappa\,\Big[-g\,(T^{\alpha\nu}+t^{\alpha\nu}_{\mathrm{L-L}})\Big]. \quad (41) $$

Explicitly, we have

$$ H^{\alpha\beta\nu\gamma}{}_{,\beta\gamma} = \partial_{\beta}\Big\{\,\partial_{\gamma}\,[-g\,(g^{\alpha\nu}g^{\beta\gamma}-g^{\beta\nu}g^{\gamma\alpha})]\Big\}. \quad (42) $$

Remark: It is essential to note that the quantities $t^{\alpha\nu}_{\mathrm{L-L}}$ do not represent a true tensor. Indeed, the gravitational field can be transformed away at any point and its energy is not localizable. This is why the left hand side of (41) and (42) exhibits ordinary derivatives instead of covariant ones.

The 4th rank tensor $H^{\alpha\beta\nu\gamma}{}_{,\beta\gamma}$ can be regarded as a special choice of $R^{\alpha\nu}$ — the Ricci tensor, where all first derivatives of the metric tensor cancel out at this given point.

The Landau-Lifshitz pseudo-tensor has the form

$$ \begin{aligned}(-g)\,t^{\alpha\nu}_{\mathrm{L-L}} = \frac{1}{2\varkappa}\Big\{&{}^{\#}g^{\alpha\nu}{}_{,\lambda}\,{}^{\#}g^{\lambda\mu}{}_{,\mu}-{}^{\#}g^{\alpha\lambda}{}_{,\lambda}\,{}^{\#}g^{\nu\mu}{}_{,\mu}+\\ &+\frac{1}{2}\,g^{\alpha\nu}g_{\lambda\mu}\,{}^{\#}g^{\lambda\theta}{}_{,\rho}\,{}^{\#}g^{\rho\mu}{}_{,\theta}+g_{\mu\lambda}g^{\theta\rho}\,{}^{\#}g^{\alpha\lambda}{}_{,\theta}\,{}^{\#}g^{\nu\mu}{}_{,\rho}-\\ &-\Big(g^{\alpha\lambda}g_{\mu\theta}\,{}^{\#}g^{\nu\theta}{}_{,\rho}\,{}^{\#}g^{\mu\rho}{}_{,\lambda}+g^{\nu\lambda}g_{\mu\theta}\,{}^{\#}g^{\alpha\theta}{}_{,\rho}\,{}^{\#}g^{\mu\rho}{}_{,\lambda}\Big)+\\ &+\frac{1}{8}\,(2g^{\alpha\lambda}g^{\nu\mu}-g^{\alpha\nu}g^{\lambda\mu})(2g_{\theta\rho}g_{\delta\tau}-g_{\rho\delta}g_{\theta\tau})\,{}^{\#}g^{\theta\tau}{}_{,\lambda}\,{}^{\#}g^{\rho\delta}{}_{,\mu}\Big\},\end{aligned} \quad (43) $$

where ${}^{\#}g^{\alpha\nu}=\sqrt{-g}\,g^{\alpha\nu}$.

When velocities are low and the gravitational field is weak (42) reduces to

$$ H^{0\,i\,0\,j}{}_{,ij} = \partial_{i}\Big\{\,\partial_{j}\,[-g\,(g^{00}g^{ij}-g^{i0}g^{j0})]\Big\}, \quad (44) $$

where $i,j,\ldots=1,2,3$ are the spatial indices. We can write this equation in mixed indices by lowering one of the space indices

$$ H^{0\;0\,j}_{\;i\;\;,ij} = \partial_{i}\,\partial_{j}\,(-gg^{00}\delta^{j}_{i})\,. \quad (45) $$

When $i=j$, the Newton law is retrieved through the weak potential $g^{00}=1+2\psi$ as (45) reduces to the Laplacian

$$ \partial_{i}\,\partial_{i}\,g^{00} = \Delta\psi\,, \quad (46) $$

so that we obtain the well-known Poisson equation

$$ \Delta\psi = G\rho\,, $$

where G is Newton's constant.

Therefore, at the Newtonian approximation, we can write the *generalized Poisson equation*, which has the form

$$ H^{0\,i\,0\,j}{}_{,ij} = 2\varkappa\,\sqrt{-g}\,(T^{00}+t^{00}_{\mathrm{L-L}})\,, \quad (47) $$

where the Newtonian pseudo-tensor $t^{00}_{\mathrm{L-L}}$ reads

$$ \begin{aligned}(-g)\,t^{00}_{\mathrm{L-L}} = \frac{1}{2\varkappa}\Big\{&{}^{\#}g^{00}{}_{,k}\,{}^{\#}g^{kn}{}_{,n}-{}^{\#}g^{0k}{}_{,k}\,{}^{\#}g^{0n}{}_{,n}+\\ &+\frac{1}{2}\,g^{00}g_{kn}\,{}^{\#}g^{kr}{}_{,l}\,{}^{\#}g^{ln}{}_{,r}+g_{nk}\,g^{rl}\,{}^{\#}g^{0k}{}_{,r}\,{}^{\#}g^{0k}{}_{,l}-\\ &-\Big(g^{0k}g_{nr}\,{}^{\#}g^{0r}{}_{,l}\,{}^{\#}g^{nl}{}_{,k}+g^{0k}g_{nr}\,{}^{\#}g^{0r}{}_{,l}\,{}^{\#}g^{nl}{}_{,k}\Big)+\\ &+\frac{1}{8}\,(2g^{0k}g^{0n}-g^{00}g^{kn})(2g_{rl}g_{sm}-g_{ls}g_{rm})\,{}^{\#}g^{rm}{}_{,k}\,{}^{\#}g^{ls}{}_{,n}\Big\}.\end{aligned} \quad (48) $$

Unlike the classical Newtonian theory, the static bare mass density generally produces a gravitational field, which is described by $t^{00}_{\mathrm{L-L}}$ at the considered point.

Remark: A slightly variable cosmological term L term induces a stress energy tensor of vacuum which restores a conserved property of the r.h.s. of equation (6) thus avoiding the use of the ill-defined gravitational field pseudo-tensor as shown in [6, 7].

3.2 The second set of Einstein's field equations

The *second rank* tensor field equations have been inferred from a *fourth rank* tensor density like. It is then natural to consider a second set of field equations which is contained in the former.

A close inspection of the "Landau-Lifshitz superpotential" (40) leads to the obvious choice for this second field equation

$$ d\,(\sqrt{-g}\,\Gamma^{\gamma\alpha}\wedge\eta^{\beta}_{\gamma\alpha}) = \frac{1}{\sqrt{-g}}\,H^{\alpha\beta\nu\gamma}{}_{,\gamma\alpha}\,\eta_{\nu}\,, \quad (49) $$

$$ H^{\alpha\beta\nu\gamma}{}_{,\gamma\alpha} = 2\varkappa\,\sqrt{-g}\,(T^{\beta\nu}+t^{\beta\nu}_{\mathrm{L-L}}). \quad (50) $$

Note that (41) and (50) are linked using a common index. Furthermore, each set of field equations differ from a sign.

Proof: Let us label the "negative" equation as

$$ {}^{(-)}H^{\alpha\beta\nu\gamma}{}_{,\gamma\alpha} = \partial_\alpha \left\{ \partial_\gamma \left[-g \left(g^{\alpha\nu} g^{\beta\gamma} - g^{\beta\nu} g^{\gamma\alpha} \right) \right] \right\}. \qquad (51) $$

Now in the same manner as for (44), equation (51) reduces to

$$ {}^{(-)}H^{i00}{}_{,ij} = \partial_i \left\{ \partial_j \left[-g \left(g^{i0} g^{0j} - g^{00} g^{ij} \right) \right] \right\}. \qquad (52) $$

Lowering one of the space indices we obtain

$$ {}^{(-)}H^{i00}{}_{j\,,ij} = \partial_i \left(\partial_j \, g g^{00} \delta^j_i \right), \qquad (53) $$

which is just the opposite to $H^{0\,0j}_{i\,,ij} = \partial_i \partial_j \left(-g g^{00} \delta^j_i \right)$ (45).

Had we set $i = j$, we would have found

$$ {}^{(-)}\Delta\psi = -\Delta\psi \,. \qquad (54) $$

As a consequence, the right member of the Poisson equation (in our orthonormal frame) should also reverse sign

$$ {}^{(-)}(G\rho) = -\,G\rho \,. \qquad (55) $$

Since the Einstein constant is here a common factor, we infer that mass densities of each field equations differ from a sign as well as the gravitation potential ψ.

Therefore, in the framework of the Newtonian approximation we find two opposite field tensors which induce two opposite energy density tensors which we label as

$$ {}^{(+)}\left(T^{00} + t^{00}_{\text{L–L}} \right) \quad \text{and} \quad {}^{(-)}\left(T^{00} + t^{00}_{\text{L–L}} \right). \qquad (56) $$

3.3 Two antagonist manifolds

Conservation properties lead to the following evident corresponding equivalences

$$ H^{\alpha\beta\nu\gamma}{}_{,\beta\gamma} \to {}^{(+)}G^{\alpha\nu} = \varkappa \left[{}^{(+)}(T^{\alpha\nu} + t^{\alpha\nu}_{\text{L–L}}) \right]. \qquad (57) $$

$$ H^{\alpha\beta\nu\gamma}{}_{,\gamma\alpha} \to {}^{(-)}G^{\beta\nu} = \varkappa \left[{}^{(-)}(T^{\beta\nu} + t^{\beta\nu}_{\text{L–L}}) \right]. \qquad (58) $$

Hence, the field equation (57) can be regarded as being defined on a "positive" manifold with respect to the "negative" manifold on which is defined the field equation (58).

Remark: One should always bear in mind that both ${}^{(+)}G^{\alpha\nu}$ and ${}^{(-)}G^{\beta\nu}$ are coupled through the 4th rank tensor $H_{\beta\alpha\gamma\mu}$, which necessarily imposes that indices must keep their respective label. The "intertwined" metrics are then

$$ {}^{(+)}ds^2 = {}^{(+)}g_{\alpha\nu} dx^\alpha dx^\nu, \qquad {}^{(-)}ds^2 = {}^{(-)}g_{\beta\nu} dx^\beta dx^\nu, \qquad (59) $$

and, in the "vierbein" (tetrad) formalism, we have

$$ {}^{(+)}g_{\alpha\nu} = \mathrm{e}^a_\alpha \, \mathrm{e}^b_\nu \, \eta_{ab} \,, \qquad {}^{(-)}g_{\beta\nu} = \mathrm{e}^a_\beta \, \mathrm{e}^b_\nu \, \eta_{ab} \,, \qquad (60) $$

where η_{ab} is the Minkowski tensor.

One thus writes the *Pfaffian metrics* as

$$ {}^{(+)}ds^2 = \eta_{ab} {}^{(+)}\eta^a \eta^b, \qquad {}^{(-)}ds^2 = \eta_{ab} {}^{(-)}\theta^a \theta^b, \qquad (61) $$

$$ {}^{(+)}\theta^\alpha = \mathrm{e}^a_\alpha \, dx^\alpha, \qquad {}^{(-)}\theta^a = \mathrm{e}^a_\beta \, dx^\beta, \qquad (62) $$

The common basis 1-form $\theta^b = \mathrm{e}^b_\nu \, dx^\nu$ outlines the coupling between the metrics.

Obviously, in a flat space-time, ${}^{(+)}g_{\alpha\nu}$ and ${}^{(-)}g_{\beta\nu}$ coincide with η_{ab} meaning that the twin universes emerge from curvature.

Conclusions and outlook

The twin universe hypothesis recently saw a revived interest.

Several astrophysicists conjectured that it could provide an appropriate explanation to the puzzle of the dark energy and dark matter issues and other unsolved observational data questions [8–15]. However, all these theories do not justify the origin of the double universe which remains a pure arbitrary statement, not relying on any sound physical grounds. In here we showed that General Relativity formally confirms the existence of two coupled Einstein's field equations characterizing two co-existing antagonist manifolds.

General Relativity further shows that there exists at most two such field equations [16].

We hope that this formal demonstration will help to substantiate the current research in astrophysics.

Appendix. Classical Einstein tensor retrieved from the differential equations

Using (12), the field equations

$$ -\frac{1}{2} \, \eta_{\beta\gamma\delta} \wedge \Omega^{\gamma\delta} = \varkappa \, {}^*T_\beta \qquad (A1) $$

can be written in the form

$$ -\frac{1}{4} \, \eta_\alpha{}^\mu{}_\nu \, \theta^\sigma \wedge \theta^\delta R^\nu{}_{\mu\sigma\delta} = \varkappa \, T_{\alpha\beta} \, \eta^\beta. \qquad (A2) $$

We first use the following relations

$$ \eta^\alpha \wedge {}^*\theta^\alpha, \qquad (A3) $$

$$ \eta_\alpha = \frac{1}{3!} \left(\eta_{\alpha\beta\gamma\delta} \, \theta^\beta \wedge \theta^\gamma \wedge \theta^\delta \right) = \frac{1}{3!} \, \theta^\beta \wedge \eta_{\alpha\beta} \,. \qquad (A4) $$

Then, applying the following Riemannian identities

$$ \theta^\beta \wedge \eta_\alpha = \delta^\beta_\alpha \, \eta \,, $$

$$ \theta^\gamma \wedge \eta_{\alpha\beta} = \delta^\gamma_\beta \, \eta_\alpha - \delta^\gamma_\alpha \, \eta_\beta \,, $$

$$ \theta^\delta \wedge \eta_{\alpha\beta\gamma} = \delta^\delta_\gamma \, \eta_{\alpha\beta} + \delta^\delta_\beta \, \eta_{\gamma\alpha} + \delta^\delta_\alpha \, \eta_{\beta\gamma} \,, $$

$$ \theta^\varepsilon \wedge \eta_{\alpha\beta\gamma\delta} = \delta^\varepsilon_\delta \, \eta_{\alpha\beta\gamma} - \delta^\varepsilon_\gamma \, \eta_{\delta\alpha\beta} + \delta^\varepsilon_\beta \, \eta_{\gamma\delta\alpha} - \delta^\varepsilon_\alpha \, \eta_{\beta\gamma\delta} \,, $$

we obtain

$$
\begin{aligned}
&-\frac{1}{4}\,R^{\mu\nu}{}_{\sigma\tau}\Big[\,\delta^{\tau}_{\nu}\,(\delta^{\sigma}_{\mu}\,\eta_{\alpha}-\delta^{\sigma}_{\nu}\,\eta_{\mu})+\\
&\qquad+\delta^{\tau}_{\mu}\,(\delta^{\sigma}_{\alpha}\,\eta_{\nu}-\delta^{\sigma}_{\nu}\,\eta_{\alpha})+\delta^{\tau}_{\alpha}\,(\delta^{\sigma}_{\nu}\,\eta_{\mu}-\delta^{\sigma}_{\mu}\,\eta_{\nu})\,\Big]=\\
&=-\frac{1}{2}\,R^{\mu\nu}{}_{\mu\nu}\,\eta_{\alpha}+R^{\mu\nu}{}_{\alpha\nu}\,\eta_{\mu}= \qquad (A5)\\
&=-\frac{1}{2}\,R^{\beta\nu}{}_{\alpha\nu}\,\eta_{\beta}-\frac{1}{2}\,\eta^{\beta}_{\alpha}\,R^{\mu\nu}{}_{\mu\nu}\,\eta_{\beta}=\\
&=\left(R^{\beta}_{\alpha}-\frac{1}{2}\,\delta^{\beta}_{\alpha}\,R\right)\eta_{\beta}\,.
\end{aligned}
$$

Submitted on October 10, 2021

References

1. Marquet P. Lichnerowicz's theory of spinors in General Relativity: the Zelmanov approach. *The Abraham Zelmanov Journal*, 2012, v. 5, 117–133.
2. Kramer D., Stephani H., Hertl E., MacCallum M. Exact Solutions of Einstein's Field Equations. Cambridge University Press, 1979.
3. Dirac P.A.M. General Theory of Relativity. Princeton University Press, 2nd edition, 1975.
4. Rosenfeld L. Sur le tenseur d'impulsion-énergie. *Académie royale de Belgique*, *Mémories des Classes des Sciences*, t. 18, 1940.
5. Landau L., Lifshitz E. The Classical Theory of Fields. Addison-Wesley, Reading, 1962.
6. Marquet P. The gravitational field: a new approach. *Progress in Physics*, 2013, v. 3, 62–66.
7. Marquet P. Vacuum background field in General Relativity. *Progress in Physics*, 2016, v. 12, 314–316.
8. Sakharov A.D. Cosmological model of the Universe with a time vector inversion. *Journal of Experimental and Theoretical Physics*, 1980, v. 52, 349–351.
9. Farnes J. A unifying theory of dark energy and dark matter: negative mass and matter creation within a modified ΛCDM framework. *Astronomy and Astrophysics*, 2018, v. 620, A92.
10. Hossenfelder S. A bi-metric theory with exchange symmetry. *Physical Review D*, 2008, v. 78, 044015.
11. Hossenfelder S. Static scalar field solutions in symmetric gravity. arXiv: 160307075v2 [gr-qc] (2016).
12. Damour T., Kogan I.I. Effective Lagrangians and universality classes of nonlinear bigravity. *Physical Review D*, 2002, v. 66, 104024.
13. Damour T., Kogan I.I., Papazoglou A. (2002). Non-linear bigravity and cosmic acceleration. *Physical Review D*, 2002, v. 66, 104025.
14. Petit J.P., d'Agostini G. Cosmological bi-metric model with interacting positive and negative mass and two different speed of light, in agreement with the observed acceleration of the universe. *Modern Physics Letters A*, 2014, v. 29; no. 34.
15. Petit J.P., d'Agostini G. Negative mass hypothesis in cosmology and the nature of dark energy. *Astrophysics and Space Science*, 2014, no. 354, 611–615.
16. Marquet P. Twin universes: a new approach. *Progress in Physics*, 2019, v. 15, 64–67.

PROGRESS IN PHYSICS

A Scientific Journal on Advanced Studies in Theoretical and Experimental Physics, including Related Themes from Mathematics. This journal is registered with the Library of Congress (DC, USA).

Electronic version of this journal:
http://www.ptep-online.com

Postal Address

Department of Mathematics and Science,
University of New Mexico,
705 Gurley Ave., Gallup, NM 87301, USA

ISSN: 1555-5534 (print)
ISSN: 1555-5615 (online)

Standard Address Number: 297-5092
Printed in the United States of America

October 2022 **Vol. 18, Issue 2**

CONTENTS

Information for Authors

Progress in Physics has been created for rapid publications on advanced studies in theoretical and experimental physics, including related themes from mathematics and astronomy. All submitted papers should be professional, in good English, containing a brief review of a problem and obtained results.

All submissions should be designed in LaTeX format using *Progress in Physics* template. This template can be downloaded from *Progress in Physics* home page http://www.ptep-online.com

Preliminary, authors may submit papers in PDF format. If the paper is accepted, authors can manage LaTeXtyping. Do not send MS Word documents, please: we do not use this software, so unable to read this file format. Incorrectly formatted papers (i.e. not LaTeXwith the template) will not be accepted for publication. Those authors who are unable to prepare their submissions in LaTeXformat can apply to a third-party payable service for LaTeX typing. Our personnel work voluntarily. Authors must assist by conforming to this policy, to make the publication process as easy and fast as possible.

Abstract and the necessary information about author(s) should be included into the papers. To submit a paper, mail the file(s) to the Editor-in-Chief.

All submitted papers should be as brief as possible. Short articles are preferable. Large papers can also be considered. Letters related to the publications in the journal or to the events among the science community can be applied to the section *Letters to Progress in Physics*.

All that has been accepted for the online issue of *Progress in Physics* is printed in the paper version of the journal. To order printed issues, contact the Editors.

Authors retain their rights to use their papers published in *Progress in Physics* as a whole or any part of it in any other publications and in any way they see fit. This copyright agreement shall remain valid even if the authors transfer copyright of their published papers to another party.

Electronic copies of all papers published in *Progress in Physics* are available for free download, copying, and re-distribution, according to the copyright agreement printed on the titlepage of each issue of the journal. This copyright agreement follows the *Budapest Open Initiative* and the *Creative Commons Attribution-Noncommercial-No Derivative Works 2.5 License* declaring that electronic copies of such books and journals should always be accessed for reading, download, and copying for any person, and free of charge.

Consideration and review process does not require any payment from the side of the submitters. Nevertheless the authors of accepted papers are requested to pay the page charges. *Progress in Physics* is a non-profit/academic journal: money collected from the authors cover the cost of printing and distribution of the annual volumes of the journal along the major academic/university libraries of the world. (Look for the current author fee in the online version of *Progress in Physics*.)

How to Couple the Space-Time Curvature With the Yang-Mills Theory

Patrick Marquet
Calais, France. E-mail: patrick.marquet6@wanadoo.fr

We suggest here a new approach to couple space-time curvature with the three fundamental forces (interactions) of the standard model described by the Yang-Mills Theory. This is achieved through the extension of the Einstein tensor in the framework of the Weyl formalism (Weyl-Einstein tensor) which is known to exhibit a particular 4-vector referred to as the Weyl-Einstein vector. The Weyl-Einstein manifold so defined admits a tangent Minkowski space at a given point, where this particular vector asymptotically identifies with the Yang-Mills gauge field vectors. As a result, the Weyl-Einstein tensor implicitly interacts with the particles' masses and fields provided by the Yang-Mills equations. Assuming that the principle of equivalence always holds, a very simple grand unification with gravity could be achieved in this way.

Notations

Space-time Greek indices α, β run from 0, 1, 2, 3 for local coordinates.
Latin indices a, b are the group indices.
Space-time signature is -2.
We assume here that $c = 1$.

Introduction

Fields Φ are used to describe the fundamental particles known in modern physics. In Quantum Electrodynamics such fields associated with these particles must be chosen consistent with the symmetries in nature which include for example the space-time symmetries of Special Relativity. The fields Ψ are either scalars (neutral or charged) with spin-zero/spin-1 particles, or fermions with spin-$\frac{1}{2}$ particles. Initially, it was thought that these symmetries should be global symmetries, not depending on the position in space and time. However, it is well known that the laws of electromagnetism possess another *local symmetry*, in which charge is locally conserved, meaning that charged fields have a phase (in the exponent) that varies freely from point to point. This feat led Yang and Mills to suggest that local symmetries be extended from this U(1) group to non *Abelian symmetries* based on *local* gauge invariance which open the way to unify the electromagnetism, weak and strong interactions: U(1) × SU(2) × SU(3) is today known as the *standard model* elaborated by Glashow, Weinberg, Salam and Ward (1979 Nobel Prize). As we know, this theory implies the existence of *gauge fields* $A_\mu(x)$, which are necessarily part of a new covariant derivative $\mathrm{D}_\mu = \partial_\mu - i\mathrm{e}Am(x)$, where e is a coupling constant (see §2.1). In a curved space-time, the classical theory makes use of the Riemann derivative ∇_μ, and D_μ is thus generalized to $\nabla_\mu - i\mathrm{e}A_\mu(x)$ (see, for example, [1, p. 68]). However, the gauge fields $A_\mu(x)$, do not account for the space-time curvature except in the case of the electromagnetic field alone through the Einstein field equations.

Herein, we tackle this problem in a different way:

a) We start by defining a *Weyl connection* that exhibits a particular 4-vector (Weyl-Einstein vector) which induces extended curvature tensors;

b) From these curvatures is inferred the *Weyl-Einstein tensor* which is conceptually conserved like its standard counterpart which it generalizes;

c) A simple relation is established whereby the Weyl-Einstein 4-vector is asymptotically related to the Yang-Mills field vectors.

All three contributions (electromagnetic, weak and strong interactions) are then permitted to interact with the Weyl-Einstein 4-tensor through their respective gauge field vectors alone. A simple grand unification could be achieved through this particular coupling.

1 The Weyl-Einstein tensor

1.1 The curvatures

1.1.1 General issues

Following Lichnerowicz [2], we start by defining the *symmetric Weyl-Einstein connection* on a semi-metric 4-manifold denoted by $\mathfrak{M}$, i.e.

$$W^\alpha_{\mu\nu} = \Gamma^\alpha_{\mu\nu} - \frac{1}{2}\, g^{\alpha\beta}\left(g_{\mu\beta}J_\nu + g_{\nu\beta}J_\mu - g_{\mu\nu}J_\beta\right) \tag{1.1}$$

or, in another form,

$$W^\alpha_{\mu\nu} = \Gamma^\alpha_{\mu\nu} - \frac{1}{2}\left(\delta^\alpha_\mu J_\nu + \delta^\alpha_\nu J_\mu - g_{\mu\nu}J^\alpha\right). \tag{1.1bis}$$

From the point m in the neighbourhood of the Lorentz manifold denoted (M, g), where $\exists$ is a congruence of differentiable lines such that $\forall m' \in (\mathrm{M}, \mathrm{g})$, we may have the conformal metric

$$ds^2_{\mathrm{W}} = e^J ds^2, \tag{1.1ter}$$

where $J = \int_m^{m'} J_\mu dx^\mu$.

In general, the form $dJ = J_\mu dx^\mu$ is non-integrable. The 4-vector J_μ is referred to as the *Weyl-Einstein vector*.

1.1.2 The Weyl-Einstein 4th rank curvature tensor

With the Weyl connection $W^\alpha_{\mu\nu}$ we construct the *Weyl-Einstein curvature tensor* which is assumed to have the standard form of the Riemann-Christoffel tensor

$$(R^\alpha_{\ \beta\mu\nu})_{\rm W} = \partial_\nu W^\alpha_{\ \beta\mu} - \partial_\mu W^\alpha_{\ \beta\nu} + W^\lambda_{\ \beta\mu} W^\alpha_{\ \lambda\nu} - W^\lambda_{\ \beta\nu} W^\alpha_{\ \lambda\mu}\,. \quad (1.2)$$

Inspection shows that the following identity takes place

$$(R^\rho_{\ \alpha\beta\mu})_{\rm W} + (R^\rho_{\ \mu\alpha\beta})_{\rm W} + (R^\rho_{\ \beta\mu\alpha})_{\rm W} = 0\,. \quad (1.3)$$

Using the Riemann covariant derivative denoted using a semi-colon, the Bianchi identity also reads

$$(R^\rho_{\ \alpha\beta\mu})_{{\rm W}\,;\delta} + (R^\rho_{\ \alpha\delta\beta})_{{\rm W}\,;\mu} + (R^\rho_{\ \alpha\mu\delta})_{{\rm W}\,;\beta} = 0\,. \quad (1.3\text{bis})$$

Let us now express $(R_{\mu\nu\alpha\beta})_{\rm W}$ with the metric connection ∇_β. Setting $(\Gamma^\rho_{\nu\alpha})_{\rm J} = \frac{1}{2}\,(\delta^\rho_\nu J_\alpha + \delta^\rho_\alpha J_\nu - g_{\nu\alpha} J^\rho)$, we obtain

$$\begin{aligned}(R_{\mu\nu\alpha\beta})_{\rm W} = {} & R_{\mu\nu\alpha\beta} + g_{\mu\rho}\nabla_\beta(\Gamma^\rho_{\nu\alpha})_{\rm J} - \\ & - \frac{1}{2}\,g_{\mu\rho}\left[\nabla_\alpha(\Gamma^\rho_{\nu\beta})_{\rm J} + \nabla_\nu(\Gamma^\rho_{\alpha\beta})_{\rm J}\right] + \\ & + g_{\mu\rho}\left[(\Gamma^\rho_{\lambda\beta})_{\rm J}(\Gamma^\lambda_{\nu\alpha})_{\rm J} - (\Gamma^\rho_{\lambda\alpha})_{\rm J}(\Gamma^\lambda_{\nu\beta})_{\rm J}\right] + \\ & + g_{\mu\nu}\left[\partial_\alpha(\Gamma^\rho_{\beta\rho})_{\rm J} - \partial_\beta(\Gamma^\rho_{\alpha\rho})_{\rm J}\right].\end{aligned} \quad (1.4)$$

1.1.3 The Weyl-Einstein 2nd rank tensor

Relation (1.4) eventually leads to the contracted tensor

$$\begin{aligned}(R^\delta_{\ \alpha\beta\delta})_{\rm W} = (R_{\alpha\beta})_{\rm W} = {} & R_{\alpha\beta} + \nabla_\nu(\Gamma^\nu_{\alpha\beta})_{\rm J} - \nabla_\beta(\Gamma^\nu_{\alpha\nu})_{\rm J} + \\ & + (\Gamma^\lambda_{\alpha\beta})_{\rm J}(\Gamma^\nu_{\lambda\nu})_{\rm J} - (\Gamma^\lambda_{\alpha\rho})_{\rm J}(\Gamma^\rho_{\lambda\beta})_{\rm J}\end{aligned}$$

we then have the splitting

$$(R_{\alpha\beta})_{\rm W} = (R_{(\alpha\beta)})_{\rm W} + (R_{[\alpha\beta]})_{\rm W}\,, \quad (1.5)$$

where

$$\begin{aligned}(R_{(\alpha\beta)})_{\rm W} = {} & R_{\alpha\beta} + \nabla_\nu(\Gamma^\nu_{\alpha\beta})_{\rm J} - \frac{1}{2}\left[\nabla_\beta(\Gamma^\nu_{\alpha\nu})_{\rm J} + \nabla_\alpha(\Gamma^\nu_{\beta\nu})_{\rm J}\right] + \\ & + (\Gamma^\lambda_{\alpha\beta})_{\rm J}(\Gamma^\nu_{\lambda\nu})_{\rm J} - (\Gamma^\lambda_{\alpha\rho})_{\rm J}(\Gamma^\rho_{\lambda\beta})_{\rm J}\,,\end{aligned} \quad (1.6)$$

$$(R_{[\alpha\beta]})_{\rm W} = \partial_\alpha(\Gamma^\nu_{\beta\nu})_{\rm J} - \partial_\beta(\Gamma^\nu_{\alpha\nu})_{\rm J}\,. \quad (1.6\text{bis})$$

So forth, we check that $(\Gamma^\rho_{\nu\rho})_{\rm J} = \frac{1}{2}\,(\delta^\rho_\nu J_\rho + \delta^\rho_\rho J_\nu - g_{\nu\rho}J^\rho) = \frac{1}{2}\,(J_\nu + 4J_\nu - J_\nu) = 2J_\nu$. Thus we get

$$(R_{(\alpha\beta)})_{\rm W} = R_{\alpha\beta} - \frac{1}{2}\,(g_{\alpha\beta}\nabla_\nu J^\nu + J_\alpha J_\beta)\,, \quad (1.7)$$

$$(R_{[\alpha\beta]})_{\rm W} = 2\,(\partial_\alpha J_\beta - \partial_\beta J_\alpha) = 2J_{\alpha\beta}\,. \quad (1.8)$$

1.1.4 The Weyl-Einstein curvature scalar

Applying the contraction $R_{\rm W} = g^{\nu\alpha}(R_{\nu\alpha})_{\rm W}$, one obtains

$$\begin{aligned}R_{\rm W} = {} & R - \nabla_\rho\left[g^{\nu\alpha}(\Gamma^\rho_{\nu\alpha})_{\rm J}\right] - \nabla_\rho\left[g^{\nu\rho}(\Gamma^\rho_{\nu\rho})_{\rm J}\right] - \\ & - g^{\nu\alpha}\left[(\Gamma^\rho_{\nu\alpha})_{\rm J}(\Gamma^\nu_{\nu\rho})_{\rm J} - (\Gamma^\lambda_{\nu\rho})_{\rm J}(\Gamma^\rho_{\lambda\alpha})_{\rm J}\right],\end{aligned} \quad (1.9)$$

i.e.,

$$R_{\rm W} = R - \left(\nabla_\rho J^\rho + \frac{1}{2}\,J^2\right). \quad (1.10)$$

1.2 The Weyl-Einstein tensor

Here we omit the subscript $_{\rm W}$ for clarity. Unlike the Riemann-Christoffel curvature tensor, the Weyl curvature tensor is no longer antisymmetric on the pair of indices $\mu\nu$

$$R_{\mu\nu\alpha\beta} + R_{\nu\mu\alpha\beta} = g_{\mu\nu}J_{\alpha\beta}\,, \quad (1.11)$$

or, in another form,

$$R^{\mu\nu}_{\ \ \alpha\beta} + R^{\nu\mu}_{\ \ \alpha\beta} = g^{\mu\nu}J_{\alpha\beta}\,. \quad (1.11\text{bis})$$

Raising the index α in the equation (1.3bis) and contracting on α and μ as well as on μ and δ, we obtain

$$R^{\mu\delta}_{\ \ \beta\mu\,;\delta} + R^{\mu\delta}_{\ \ \mu\delta\,;\beta} = 0\,. \quad (1.12)$$

We next replace $R^{\mu\delta}_{\ \ \delta\beta}$ by its value taken from (1.11bis), and we eventually find

$$R^{\mu\delta}_{\ \ \mu\delta\,;\beta} + 2R^{\mu\delta}_{\ \ \beta\mu\,;\delta} + 2g^{\mu\delta}J_{\delta\beta\,;\mu} = 0\,, \quad (1.13)$$

$$\left(R^{(\delta)}_{\ (\beta)} - \frac{1}{2}\,\delta^\delta_\beta R\right)_{;\delta} = -\,J^\delta_{\ \beta\,;\delta}\,, \quad (1.14)$$

which is just the conservation law for the tensor (re-instating the subscript $_{\rm W}$ and changing the indices)

$$(G_{\alpha\beta})_{\rm W} = (R_{(\alpha\beta)})_{\rm W} - \frac{1}{2}\left(g_{\alpha\beta}R_{\rm W} - 2J_{\alpha\beta}\right). \quad (1.15)$$

We call $(G_{\alpha\beta})_{\rm W}$ the *Weyl-Einstein tensor* expressed with the Riemannian derivatives. Lets us note that $(G_{\alpha\beta})_{\rm W}$ is no longer symmetric. In the pure Riemannian regime, this tensor obviously reduces to the usual Einstein tensor

$$G_{\alpha\beta} = R_{\alpha\beta} - \frac{1}{2}\,g_{\alpha\beta}R\,. \quad (1.16)$$

2 The unification

2.1 A short overview of the Yang-Mills theory

2.1.1 The principle of gauge invariance

Let us recall that a general Lie group G is defined by the representation of a group element denoted U in terms of its generators T^a

$$\mathrm{U} = \exp\left(-i\mathrm{e}\sum_{a=1}^{n}\mathrm{T}^a\mathrm{k}_a\right), \quad (2.1)$$

where e is a coupling constant generalizing the fundamental electronic charge e in the electromagnetic case. The group element U is defined by the values of the N constants k_a, and T^a are hermitian generators satisfying the associated Lie algebra

$$[\mathrm{T}^a,\, \mathrm{T}^b] = i\,\mathrm{C}^{abc}\,\mathrm{T}_c\,, \tag{2.2}$$

where C^{abc} are the real antisymmetric structure constants defining the algebra.

The SU(2) group is defined in terms of the set of all *unitary unimodular matrices* with (2×2) complex elements. The related constraints are known to be

$$\det\|\mathrm{U}\| = 1\,, \tag{2.3}$$

$$\mathrm{U}^{+}\mathrm{U} = \mathrm{U}\mathrm{U}^{+} = \mathrm{I}\,, \tag{2.4}$$

where I is the unit matrix, and U^{+} is the Hermitian conjugate of the matrix U.

2.1.2 Electromagnetism and local gauge invariance U(1)

Consider non-hermitian complex charged scalar fields written in terms of the real fields $\Phi_1(x)$ and $\Phi_2(x)$

$$\Phi(x) = \frac{1}{\sqrt{2}}\,[\Phi_1(x) + i\,\Phi_2(x)]\,, \tag{2.5}$$

$$\Phi^{+}(x) = \frac{1}{\sqrt{2}}\,[\Phi_1(x) - i\,\Phi_2(x)]\,.$$

The classical Lagrangian for this charged scalar field is

$$\mathcal{L} = \partial^{\mu}\Phi^{+}\,\partial_{\mu}\Phi - m^2\Phi^{+}\Phi\,, \tag{2.6}$$

where the first term corresponds to the *kinetic energy* of the scalar field, and the second the *potential energy* of the massive field (mass of the charged particle).

Noether's theorem states that the symmetry of charge conservation is equivalent to the invariance of $\mathcal{L}$ under the group U(1) of continuous phase rotations, specified by a single parameter k.

We then check that this Lagrangian is invariant under the continuous group of phase rotations of Φ called the *global Abelian gauge group* U(1)

$$\Phi(x) \to \Phi(x)\exp i\,\mathrm{k}\,, \tag{2.7}$$

$$\Phi^{+}(x) \to \Phi(x)\exp(-i\,\mathrm{k})\,, \tag{2.7bis}$$

with the real parameter k.

Eqs. (2.7) and (2.7bis) should be true even when the parameter k depends on x^{μ}, thus the phase difference between distinct space-time points is *unobservable*: it is called the *local gauge invariance principle*. However inspection shows that the kinetic energy Lagrangian $\partial^{\mu}\Phi^{+}\partial_{\mu}\Phi$ is not invariant under the local gauge transformation

$$\Phi(x) \to \Phi(x)\exp(-i\,\mathrm{k})\,\mathrm{Q}(x)\,. \tag{2.8}$$

This is because the derivative may now operate on the variable parameter $\mathrm{k}(x)$. To remedy this problem one is forced to introduce a new covariant derivative

$$\mathrm{D}_{\mu} = \partial_{\mu} - i\,\mathrm{e}A_{\mu}(x)\,, \tag{2.9}$$

where Q is the quantity of the charges of the fields Φ which is proportional to the fundamental electronic unit e.

Here, the vector field $A_{\mu}(x)$ transforms as

$$A_{\mu}(x) \to A_{\mu}(x) + \partial_{\mu}\,\mathrm{k}(x)\,. \tag{2.10}$$

Hence, it is also necessary to include a kinetic energy term in $\mathcal{L}$ which takes into account the introduction of the new gauge field $A_{\mu}(x)$. This is achieved by adding the term

$$(\mathcal{L})^{\mathrm{kin}}_{A} = -\frac{1}{4}\,F^{\mu\nu}F_{\mu\nu}\,, \tag{2.11}$$

where we retrieve the electromagnetic field strength tensor

$$F_{\mu\nu} = \partial_{\mu}A_{\nu} - \partial_{\nu}A_{\mu}\,. \tag{2.12}$$

The new Lagrangian is now

$$\mathcal{L} = -\frac{1}{4}\,F^{\mu\nu}F_{\mu\nu} + \mathcal{L}'[\Phi,\, \Phi^{+}\,\mathrm{D}_{\mu}\Phi\,\mathrm{D}_{\mu}\Phi^{+}]\,. \tag{2.13}$$

The tensor $F_{\mu\nu}$ is obviously invariant under the gauge transformation of (2.8), so $(\mathcal{L})^{\mathrm{kin}}_{A}$ is also gauge invariant. This symmetry group is the Abelian group U(1) with a single commuting generator $\mathrm{T}^1 = \mathrm{Q}$ satisfying

$$[\mathrm{T}^1,\, \mathrm{T}^1] = 0\,. \tag{2.14}$$

Unlike the classical theory, the equations of motion are obtained by varying the action $\mathcal{L}$ with respect to A_{μ} for the fixed Φ, i.e.,

$$\partial_{\nu}\left[\frac{\mathcal{L}}{\partial\,(\partial_{\nu}A_{\mu}(x))}\right] - \frac{\partial\mathcal{L}}{\partial A_{\mu}(x)} = 0\,, \tag{2.15}$$

or, in another form,

$$\partial_{\nu}F^{\mu\nu}(x) = \frac{\partial\mathcal{L}}{\partial A_{\mu}(x)}\,. \tag{2.16}$$

From this equation, the current density is easily inferred

$$\mathrm{I}^{\mu}(x) = -\,\frac{1}{\mathrm{e}}\,\frac{\partial\mathcal{L}}{\partial A_{\mu}(x)}\,, \tag{2.17}$$

$$\mathrm{I}^{\mu}(x) = i\left[\Phi^{+}(x)\frac{\partial\mathcal{L}}{\partial\,(\mathrm{D}_{\mu}\Phi^{+})} - \Phi^{\sigma+}(x)\frac{\partial\mathcal{L}}{\mathrm{D}_{\mu}\Phi^{+}}\right], \tag{2.18}$$

which is conserved

$$\partial_{\mu}\mathrm{I}^{\mu} = 0\,. \tag{2.19}$$

The associated charge is given by

$$\mathrm{Q} = \int I^{0}(x)\,d^3x = \int i\left\{\Phi^{+}\,\mathrm{D}_{\mu}\Phi - \mathrm{D}^{\mu}\,\Phi^{+}\Phi\right\}d^3x\,, \tag{2.20}$$

which also remains unchanged with time

$$\frac{d\mathrm{Q}}{dt} = 0\,, \tag{2.21}$$

$$\int \partial x_0\, \mathrm{I}^0(x)\, d^3x = 0\,, \tag{2.22}$$

or, equivalently, $\int \partial_\mu \mathrm{I}^\mu(x)\, d^3x = 0$.

This result is formally equivalent to the classical theory, but it also shows that this new approach remains a particular case of a higher symmetry principle which rules modern physics.

2.2 The unification

2.2.1 The gauge invariance of the Weyl-Einstein connection

If we were to define a Weyl-Einstein covariant derivative just as in (2.9), the connection coefficients $\mathrm{W}^\tau_{\mu\sigma}$ should be invariant under the conformal relation

$$g_{\alpha\beta} \to \mathrm{U}\, g_{\alpha\beta}\,, \tag{2.23}$$

where $U(x) > 0$ is a real scalar. Conformal invariance is here simply achieved by implementing the additional gauge condition

$$J_\mu \to J_\mu - \partial_\mu \mathrm{U} \tag{2.24}$$

as oneself can be easily convinced.

2.2.2 The Weyl-Einstein-Yang-Mills relation

Let us consider the time-like geodesic ds_W spanned by the connexion coefficients $\mathrm{W}^\tau_{\mu\sigma}$ (1.1ter). To this geodesic is associated the 1-form $dJ = J_\mu dx^\mu$. Likewise, we write the Minkowskian line element as ds to which we associate the Yang-Mills 1-form $dA = A_\mu dx^\mu$ where A_μ is the generic term that stands for every gauge field of any of the first three Yang-Mills interactions. A specific unification between the Yang-Mills theory and space-time curvature can be thus achieved through the interaction between the Yang-Mills gauge field and vectors and the Weyl-Einstein vector J_μ. Such a relation can be set so as to maintain the euclidean character of the Yang-Mills theory within the Weyl-Einstein formalism. To this end, we write

$$\frac{dJ}{dA} = 1 + \ln\left(\frac{ds_\mathrm{W}}{ds}\right), \tag{2.25}$$

$$dJ = dA\left[1 + \ln\left(\frac{ds_\mathrm{W}}{ds}\right)\right]. \tag{2.26}$$

When $ds_\mathrm{W} \to ds$, the 4-vector J_μ identifies with the Yang-Mills gauge field vector.

The Yang-Mills physics always takes place in the Minkowski space that is asymptotic to the genuine Weyl-Einstein manifold $\mathfrak{M}$. In this way, the vector J_μ inherent to space-time curvature is regarded as "embedding" all the Yang-Mills gauge fields thereby providing a specific unification as described below.

2.3 Application to the Yang-Mills interactions

2.3.1 The weak interaction (SU(2) symmetry)

Writing classically the group element as

$$\mathrm{U} = \exp\left[\, -i\,\mathrm{h}\,\mathrm{T}^a\,\mathrm{k}_a\right], \qquad a = 1, 2, 3\,, \tag{2.27}$$

with the generators

$$\mathrm{T}^a = \frac{\sigma^a}{2}\,, \tag{2.28}$$

where σ^a are the three 2×2 Pauli spin matrices

$$\sigma^1 = \begin{pmatrix} 0 & 1 \\ 1 & 0 \end{pmatrix},\ \sigma^2 = \begin{pmatrix} 0 & -i \\ i & 0 \end{pmatrix},\ \sigma^3 = \begin{pmatrix} 1 & 0 \\ 0 & -1 \end{pmatrix}, \tag{2.29}$$

which satisfy [4, p. 2]

$$\mathrm{Tr}\left(\frac{\sigma^a}{2}\frac{\sigma^b}{2}\right) = \frac{1}{2}\,\delta^{ab}, \tag{2.30}$$

$$\mathrm{Tr}\,\frac{\sigma^a}{2} = 0\,. \tag{2.31}$$

Here we must introduce three vector gauge fields B^a_μ, which are conveniently represented by the vector field

$$B_\mu(x) = \mathrm{T}^a B_{a\mu}(x)\,. \tag{2.32}$$

The transformation properties of B_μ are obtained from :

$$B_\mu(x) \to B_\mu(x) - \mathrm{T}^a\partial_\mu \mathrm{k}^a(x) + i\,\mathrm{h}\,\mathrm{k}^a(x)\,[\mathrm{T}^a,\, B_\mu(x)]\,, \tag{2.33}$$

where h is the relevant coupling constant.

Here T^a satisfy the commutation relations with different structure constants

$$[\mathrm{T}^a,\, \mathrm{T}^b] = i\,\mathrm{f}^{abc}\,\mathrm{T}_c\,. \tag{2.34}$$

Using (2.30) in (2.33), then multiplying by T^b and taking the trace, we have the transformations laws of the individual gauge field $B^a_\mu(x)$

$$B^a_\mu(x) \to B^a_\mu(x) - \partial_\mu \mathrm{k}^a(x) + \mathrm{h}\,\mathrm{f}^a_{\ bc}\,\mathrm{k}^b(x)\,B^c_\mu(x)\,, \tag{2.35}$$

and the general form of the covariant derivative is

$$D_\mu = \partial_\mu - i\,\mathrm{h}\,B_\mu\,. \tag{2.36}$$

The SU(2) group relevant for matter representation is determined by the generators T^a, so that (2.36) is expressed by

$$\mathrm{D}_\mu = \partial_\mu - i\,\mathrm{h}\,B_{a\mu}\,\mathrm{T}^a, \tag{2.37}$$

where B_μ is here related to J_μ through equation (2.26).

2.3.2 The SU(3) symmetry

We finally illustrate the strong interaction (gluons) by defining the non-Abelian symmetry SU(3) whose elementary group element with 8 real parameters reads

$$\mathrm{U} = \exp\left[-i\,\mathrm{g}\,\frac{\lambda_a}{2}\,\mathrm{k}^a\right], \qquad a = 1,\ldots,8\,. \tag{2.38}$$

The λ^a are the eight Gell-Mann 3×3 Hermitian traceless matrices [5]

$$\lambda_1 = \begin{pmatrix} 0 & 1 & 0 \\ 1 & 0 & 0 \\ 0 & 0 & 0 \end{pmatrix}, \quad \lambda_2 = \begin{pmatrix} 0 & -i & 0 \\ i & 0 & 0 \\ 0 & 0 & 0 \end{pmatrix},$$

$$\lambda_3 = \begin{pmatrix} 1 & 0 & 0 \\ 0 & -1 & 0 \\ 0 & 0 & 0 \end{pmatrix}, \quad \lambda_4 = \begin{pmatrix} 0 & 0 & 1 \\ 0 & 0 & 0 \\ 1 & 0 & 0 \end{pmatrix},$$

$$\lambda_5 = \begin{pmatrix} 0 & 0 & -i \\ 0 & 0 & 0 \\ i & 0 & 0 \end{pmatrix}, \quad \lambda_6 = \begin{pmatrix} 0 & 0 & 0 \\ 0 & 0 & 1 \\ 0 & 1 & 0 \end{pmatrix},$$

$$\lambda_7 = \begin{pmatrix} 0 & 0 & 0 \\ 0 & 0 & -i \\ 0 & i & 0 \end{pmatrix}, \quad \lambda_8 = \begin{pmatrix} 1 & 0 & 0 \\ 0 & 1 & 0 \\ 0 & 0 & -2 \end{pmatrix},$$

and the representation of SU(3) acting on the matter field triplet

$$\psi(x) = \begin{matrix} \psi_1 \\ \psi_2 \\ \psi_3 \end{matrix} \tag{2.39}$$

is just the group element U. Accordingly, the Lagrangian for the SU(3) gauge bosons interacting with the above fermion triplet can be computed to give

$$\mathcal{L} = -\frac{1}{4}\,F^{\mu\nu}{}_k\,F_{\mu\nu}{}^k + i\,{}^\circ\psi_a\,\gamma^\mu_k\left[\partial_\mu - i\,\mathrm{g}\,S^k_\mu\left(\frac{\lambda}{2}\right)^a_{a'}\right]\psi^{a'}, \tag{2.40}$$

where ${}^\circ\psi_a$ is the complex conjugate spinor and where the field strength tensor is

$$F^{\mu\nu}_{\ \ k} = \partial^\mu S^\nu_k(x) + \mathrm{g}\,\mathrm{e}^{lm}_k\,\mathrm{k}_n(x)\,F^\mu_l\,F^\nu_n\,, \quad k,l,n = 1,\ldots,8\,. \tag{2.41}$$

Here, we have the correspondence $S^\mu \to J^\mu$.

2.3.3 Example of the gauge group U(1) × SU(2)

Using (2.29), we can construct explicit examples of the generators T^a needed to describe the transformation of matter multiplet under SU(2) which we will couple with the electromagnetic boson under U(1). We first introduce three vector gauge fields B^a_μ which may be written in the form [6, p. 53, eq. 2.91]

$$B_\mu = \left(\frac{\sigma_a}{2}\right)B^a_\mu = \frac{1}{2}\begin{vmatrix} B^3_\mu & B^1_\mu - i\,B^2_\mu \\ B^1_\mu + i\,B^2_\mu & -B^3_\mu \end{vmatrix}. \tag{2.42}$$

These are the gauge bosons transforming as the adjoint of SU(2) we couple with the gauge boson transforming as U(1).

The kinetic term of the resulting Lagrangian is given by

$$(\mathcal{L})^{\mathrm{kin}} = -\frac{1}{4}\,(B^a_{\mu\nu}\,B_a^{\mu\nu} + F^{\mu\nu}\,F_{\mu\nu})\,. \tag{2.43}$$

Here, the combination $C_\mu = B_\mu + A_\mu$ which takes place in the Euclidean tangent space is identified to the Weyl-Einstein 4-vector J_μ at this point.

All these examples illustrate how the Yang-Mills gauge field vectors actually interact with the Weyl-Einstein 4-vector through equation (2.26).

Conclusion

In this short paper, we have only sketched a possible representation of how space-time curvature can couple with the Yang-Mills Theory in a non-trivial way.

For each type of interaction, we show that the Yang-Mills gauge fields are asymptotically connected to the space-time curvature through the Weyl-Einstein 4-vector. This amounts to state that the first three interactions are defined in the euclidean space-time which is tangent to the Weyl-Einstein manifold at the point where this 4-gauge vector is chosen.

This particular interaction appears as a new coupling between the Weyl-Einstein space-time geometry and the various particles/fields satisfying the Yang-Mills theory. In a sense, such a coupling could be regarded as the realization of a new representation of Einstein's field equations with a source. In the classical General Relativity, the Riemannian field equations disregard the Weyl-Einstein vector and they just display an energy-momentum tensor on the right hand side as a source. The insertion of such a tensor was never entirely satisfactory to Einstein's opinion who always claimed that the right hand side of his equations was somewhat "clumsy". Einstein's argument should not be hastily dismissed: indeed, while his tensor exhibits a conceptually conserved property, the energy-momentum tensor as a source does not, which leaves the theory with a major inconsistency [7]. For a massive tensor, the problem has been cured by introducing the so-called pseudo-tensor that conveniently describes the gravitational field of the mass so that the 4-momentum vector of both matter and its gravity is conserved (for example, the Einstein-Dirac pseudo-density) [8, 9]. Unfortunately by essence, this pseudo-tensor can be transformed away at any point by a change of coordinates that naturally shows the non-localizability of the gravitational energy [10]. At any rate, a pseudo-tensor is not suitable to be represented on the right hand side of the field equations. This is of course a stumbling-block which has plagued General Relativity for more than a century. Moreover, unlike the Einstein tensor, the energy-momentum tensors are mainly antisymmetric and symmetrization is thus always required "afterwards" through the Belinfante procedure. To evade the initial problem one is led to introduce

a vacuum energy-momentum field energy that is "excited" in the vicinity of a mass to produce the gravitational field [11, 12]. Far from the mass, this (real) vacuum energy tensor never vanishes and guarantees the conservation of the source tensor on the right hand side of the field equations. However, several constraints are needed to be implemented which might be viewed as a loss of generality of the theory [13].

Let us note in passing that the most important Einstein solutions are derived from source-free equations as for example the famous Schwarzschild metric [14]. In the frame of our theory, the field equations in the post-Newtonian approximation should certainly deserve further scrutiny which is beyond the scope of this paper. In conclusion, we suggest here to correlate gauge fields so that unification of the three fundamental interactions with Einstein's General Theory of Relativity can be achieved in a very simple way. The principle of equivalence implies that gravity is thus indirectly related to each type of particles described in the Yang-Mills Theory.

Many topics such as the fermion and scalar quantum numbers in the electroweak model, or the spontaneous symmetry breakdown and the Higgs mechanism have not been discussed here.

We are however convinced that the introduction of the Weyl-Einstein formalism in the theory does not conflict with these results, and that it constitutes one of the permissible unifying theory between gauge theories.

Submitted on June 2, 2022

References

1. Hawking S. W., Ellis G. F. R. The Large Scale Structure of Space-Time. Cambridge University Press, 1987.
2. Lichnerowicz A. Les espaces variationnels généralisés. *Annales scientifiques de l'École Normale Supérieure*, série 3, t .62, 1945, 339–384.
3. Weyl H. On generalized Riemann matrices. *Annals of Mathematics*, 1934, v. 35, no. 4, 714–729.
4. Greiner W., Müller B. Gauge Theory of Weak Interaction. Springer-Verlag, 2009.
5. Gell-Mann M. The eightfold way: a theory of strong interaction symmetry. *Cal. Inst. of Technology*, TID 12608 CSTL-20, 1961.
6. Ross G. R. Grand Unified Theories. Benjamin/Cummings Publ. Co., Menlo Park (California), 1985.
7. Landau L., Lifshitz E. The Classical Theory of Fields. Addison-Wesley, Reading, 1962.
8. Tonnelat M. A. Les Théories unitaires de l'Électromagnétisme et de la Gravitation. Gauthier-Villars, Paris, 1965.
9. Dirac P.A.M. General Theory of Relativity. Princeton University Press, 2nd edition, 1975.
10. Straumann N. General Relativity and Relativistic Astrophysics. Springer-Verlag, 1984.
11. Marquet P. The gravitational field: a new approach. *Progress in Physics*, 2013, v. 3, 62–66.
12. Marquet P. Vacuum background field in General Relativity. *Progress in Physics*, 2016, v. 12, 314–316.
13. Marquet. P. Some insights on the nature of the vacuum background field in General Relativity. *Progress in Physics*, 2016, v. 12, 366–367.
14. Kramer D., Stephani H., Hertl E., MacCallum M. Exact Solutions of Einstein's Field Equations. Cambridge University Press, 1979.

Physics of Irrational Numbers

Hartmut Müller

Rome, Italy.
E-mail: hm@interscalar.com

In systems of coupled periodic processes, lasting frequency ratios can cause significant physical effects, which depend on the type of real numbers the ratios are approximating. Rational frequency ratios can cause parametric resonance and amplification, while approaching irrational frequency ratios can avoid them. In this paper we discuss physical effects that can be caused by frequency ratios approximating some irrational algebraic and transcendental numbers. We illustrate this approach on some features of the solar system which are still unexplained.

Introduction

In this paper, we introduce an approach that bases on the physical interpretation of certain statements of the number theory. In modern theoretical physics, numerical ratios usually remain outside the realm of theoretical interest. In this work we try to elucidate the physical meaning of numerical ratios and to show their theoretical and practical importance for resolving some fundamental problems of physics.

One of the unsolved fundamental problems in physics [1] is the stability of systems of a large number of coupled periodic processes, for instance, the stability of planetary systems. If numerous bodies are considered to be gravitationally bound to one another, perturbation models predict long-term highly unstable states [2] that contradict the physical reality of the solar system and thousands of exoplanetary systems.

In our previous publications we have applied our numeric-physical approach to the analysis of the orbital and rotational periods of the planets, planetoids and moons of the solar system and thousands of exoplanets [3] with the conclusion that the avoidance of orbital and rotational parametric resonances by approximation of transcendental ratios can be viewed as a basic forming factor of planetary systems [4].

Another unsolved fundamental problem is the imperishability of motion and interaction, and the inexhaustibility of energy. This question seems to be out of the realms of modern physics. Indeed, until now, all the sources of energy we are currently using – from electricity to radioactivity – were discovered by chance. This fact and the incapacity of inventing new energy sources evidences the lack of comprehention. For instance, the research of the predicted thermonuclear fusion has been going on for 60 years without success [5, 6].

Likewise, the nature of gravitational energy is still a mystery [7]. For instance, what is the propelling force of the orbital motion? Naturally, there is no propelling of orbital motion, the planets are in perpetual free fall. However, the orbital velocity of a planet is very high, 30 kilometers per second in the case of the Earth. The impulse of a planet is therefore enormous and sweeps away everything that gets in its trajectory. Where does this kinetic energy come from? Perhaps, this question seems naive to the physicist who is ready to answer immediately: Besides the primordial kinetic energy of the protoplanetary disk, the potential energy of the gravity field of the star is the source of the kinetic energy of planetary motion. However, this answer only readdresses the question. Then what is the source of gravitational energy? Is it the alleged ability of a mass to curve space-time? Then what causes this ability?

Obviously, the concept of mass is not complete since the numerical values of particle masses still remain a mystery. Where do the observed masses of elementary particles come from? This is the biggest, and oldest, unresolved enigma in fundamental particle physics. There is the widespread, but erroneous, belief that the Higgs boson resolves the origin of particle masses. This is not the case. It merely replaces one set of unknown parameters (particle rest energies) with an equally unknown set of parameters (coupling constants to the Higgs field), so nothing is gained in the fundamental understanding of masses [8].

Is there a hidden inexhaustible source of energy in the universe? Then why can energy not be generated or consumed, but only converted?

The earliest constants of motion discovered were momentum and kinetic energy, which were proposed in the 17^{th} century by René Descartes and Gottfried Leibniz on the basis of collision experiments, and later refined by Euler, Lagrange, d'Alembert and Hamilton. In theoretical physics, Noether's first theorem connects the conservation of energy with the homogeneity of time, supposing that the laws of physics do not change over time. Noether's theorem states that conservation laws apply in a physical system with conservative forces. A conservative force is a force with the property that the total work done in moving a particle between two points is independent of the path taken. Equivalently, if a particle travels in a closed loop, the total work done by a conservative force is zero. In short, a conservative force is a force that conserves energy. Hence, Noether's theorem leads to circular reasoning. It does not explain the cause of energy conservation [9]. Perhaps, no physical principle can explain the origin of energy, because every physical process presupposes the existence of

another physical process that serves as its energy source. This non ending chain of energy converters suggests that the imperishability of motion and interaction, and the inexhaustibility of energy must have a non-physical cause.

Our numeric-physical approach leads us to the conclusion that motion and interaction, including energy as well as other constants of motion are caused by attractors of numeric fields. We illustrate this conclusion on some features of the solar system which are still unexplained.

Theoretical Approach

The starting point of our approach is frequency as obligatory characteristic of a periodic process. As the result of a measurement is always a *ratio* of physical quantities, one can measure only *ratios* of frequencies. This ratio is always a real number. Being a real value, a frequency ratio can approximate an integer, rational, irrational algebraic or transcendental number. In [10] we have shown that the difference between rational, irrational algebraic and transcendental numbers is not only a mathematical task, but it is also an essential aspect of stability in systems of bound periodic processes. For instance, integer frequency ratios, in particular fractions of small integers, make possible parametric resonance that can destabilize such a system [11, 12]. This is why asteroids cannot maintain orbits that are unstable because of their resonance with Jupiter [13]. These orbits form the Kirkwood gaps that are areas in the asteroid belt where asteroids are absent.

According to this idea, irrational ratios should not cause destabilizing resonance interactions, because irrational numbers cannot be represented as a ratio of integers. However, algebraic irrational numbers, being real roots of algebraic equations, can be converted to rational numbers by multiplication. For example, the algebraic irrational number $\sqrt{2} = 1.41421\ldots$ cannot become a frequency scaling factor in real systems of coupled periodic processes, because $\sqrt{2} \cdot \sqrt{2} = 2$ creates the conditions for the occurrence of parametric resonance. Thus, only transcendental ratios can prevent parametric resonance, because they cannot be converted to rational or integer numbers by multiplication. Actually, it is transcendental numbers, that define the preferred frequency ratios which allow to avoid destabilizing resonance [14]. In this way, transcendental frequency ratios sustain the lasting stability of coupled periodic processes. With reference to the evolution of a planetary system and its stability, we may therefore expect that the ratio of any two orbital periods should finally approximate a transcendental number [15].

However, the issue is to clarify the type of number a measured ratio corresponds to. Because of the finite resolution of any measurement, there is no possibility to know it for sure. The obtained value is always an approximation and therefore, it is very important to know the amount of its uncertainty.

It is remarkable that approximation interconnects all types of real numbers – rational, irrational algebraic and transcendental. In 1950, Aleksandr Khinchin [16] made a very important discovery: He could demonstrate that simple continued fractions deliver biunique representations of all real numbers, rational and irrational. Whereas infinite continued fractions represent irrational numbers, finite continued fractions represent always rational numbers. In this way, any irrational number can be approximated by finite continued fractions, which are the convergents and deliver always its nearest and quickest rational approximation.

It is notable that the best rational approximation of an irrational number by a finite continued fraction is not a task of computation, but only an act of termination of the continued fraction recursion. For example, the golden ratio $\phi = (\sqrt{5}+1)/2 = 1.618\ldots$ has a biunique representation as simple continued fraction that contains only the number 1:

$$\phi = 1 + \cfrac{1}{1 + \cfrac{1}{1 + \cfrac{1}{1 + \ldots}}}$$

As the continued fraction of ϕ is periodic, it meets a quadratic equation evidencing that ϕ is algebraic:

$$\phi = 1 + \frac{1}{\phi} \qquad \phi^2 - \phi - 1 = 0$$

In order to save space, in the following we use angle brackets to write down continued fractions, for example the golden ratio $\phi = \langle 1; 1, 1, \ldots \rangle$. So long as the sequence of denominators is considered as infinite, this continued fraction represents the irrational number ϕ. If the continued fraction will be truncated, the sequence of denominators will be finite and we get a convergent that is always the nearest rational approximation of the irrational number ϕ.

In the case of ϕ, the approximation process is very slow because of the small denominators. Only the 10^{th} approximation gives the correct third decimal of ϕ. In fact, the denominators in the continued fraction of ϕ are the smallest possible and consequently, the approximation speed is the lowest possible. The golden ratio ϕ is therefore treated as the 'most irrational' number in the sense that a good approximation of ϕ by rational numbers cannot be given with small quotients. On the contrary, transcendental numbers can be approximated exceptionally well by rational numbers, because their continued fractions contain large denominators and can be truncated with minimum loss of precision. For instance, the simple continued fraction of Archimedes' number $\pi = 3.1415927\ldots = \langle 3; 7, 15, 1, 292, \ldots \rangle$ delivers the following sequence of rational approximations:

$\langle 3 \rangle = 3$
$\langle 3; 7 \rangle = 22/7 = 3.\overline{142857}$
$\langle 3; 7, 15 \rangle = 3.14150943396226$
$\langle 3; 7, 15, 1 \rangle = 3.1415929\ldots$

Already the 2nd approximation delivers the first two decimals correctly. Therefore, 22/7 is a widely used Diophantine approximation of π. The 4th approximation shows already six correct decimals. This special arithmetic property of continued fractions [17] of transcendental numbers has the consequence that transcendental numbers are distributed near by rational numbers of small quotients or close to integers, like $e^3 = 20.08\ldots$ or $\pi^3 = 31.006\ldots$. This can create the impression that complex systems like the solar system provide ratios of physical quantities that approximate rational numbers. More likely, they approximate transcendental numbers [4], which are located close to rational numbers.

Naturally, a continued fraction of π or any other real transcendental number cannot be periodic, otherwise it would meet an algebraic equation. For example, the continued fractions of the algebraic irrationals $\sqrt{2} = \langle 1; 2, 2, 2, \ldots \rangle$ and $\sqrt{3} = \langle 1; 1, 2, 1, 2, \ldots \rangle$ are periodic. In contrast to them, a generalized continued fraction of Euler's number contains all natural numbers in sequence as numerators and denominators and therefore, it cannot be periodic:

$$e = 2 + \cfrac{1}{1 + \cfrac{1}{2 + \cfrac{2}{3 + \cfrac{3}{4 + \ldots}}}}$$

The following generalized continued fraction [18] of π contains all natural numbers factorizing the numerators:

$$\pi = 2 + \cfrac{2}{1 + \cfrac{1 \cdot 2}{1 + \cfrac{2 \cdot 3}{1 + \cfrac{3 \cdot 4}{1 + \ldots}}}}$$

These continued fractions do not only evidence that π and e are not algebraic, but make comprehensible the increase of the approximation speed with every next convergent. In addition, it becomes clear that Archimedes' number π can be approximated faster than Euler's number e.

Among all transcendental numbers, Euler's number $e = 2.71828\ldots$ is unique, because its real power function e^x coincides with its own derivatives. In the consequence, Euler's number allows avoiding parametric resonance between any coupled periodic processes including their derivatives.

Because of this unique property of Euler's number, we expect that periodic processes in real systems prefer frequency ratios close to Euler's number and its roots. The natural logarithms of those frequency ratios are therefore close to integer $0, \pm 1, \pm 2, \ldots$ or rational $\pm 1/2, \pm 1/3, \pm 1/4, \ldots$ values. For rational exponents, the natural exponential function is always transcendental [19]. Since every rational number has a biunique representation as a simple finite continued fraction, we can represent the logarithms of the frequency ratios we are looking for as finite continued fractions:

$$\ln(\omega_A/\omega_B) = \mathcal{F} = \langle n_0; n_1, n_2, \ldots, n_k \rangle \qquad (1)$$

ω_A and ω_B are the angular frequencies of two bound periodic processes A and B avoiding parametric resonance. We use angle brackets for continued fractions. All denominators $n_1, n_2, \ldots, n_k$ of a continued fraction including the free link n_0 are integer numbers. All numerators equal 1. The length of a continued fraction is given by the number k of layers.

The canonical form (all numerators equal 1) does not limit our conclusions, because any continued fraction with partial numerators different from 1 can be transformed into a canonical continued fraction using the Euler equivalent transformation [20]. Therefore, finite canonical continued fractions represent all rational numbers in the sense that there is no rational number that cannot be represented as a finite canonical continued fraction. This universality of canonical continued fractions evidences that the distribution of rational logarithms (1) is fractal. As it is an inherent feature of the number continuum, we call it the *Fundamental Fractal* [14].

The first layer of this fractal is given by the truncated after n_1 continued fractions:

$$\langle n_0; n_1 \rangle = n_0 + \frac{1}{n_1}$$

The denominators n_1 follow the sequence of integer numbers ± 1, ± 2, ± 3 etc. The second layer is given by the truncated after n_2 continued fractions:

$$\langle n_0; n_1, n_2 \rangle = n_0 + \cfrac{1}{n_1 + \cfrac{1}{n_2}}$$

Figure 1 shows the first and the second layer in comparison. As we can see, reciprocal integers $\pm 1/2, \pm 1/3, \pm 1/4, \ldots$ are the attractor points of the fractal. In these points, the distribution density of rational logarithms (1) reaches a local maximum. Integers $0, \pm 1, \pm 2, \ldots$ define the main attractors having the widest ranges. Half logarithms $\pm 1/2$ form smaller attractor ranges, third logarithms $\pm 1/3$ form the next smaller ranges and so forth. Increasing the length of the continued fraction (1), the distribution density of the transcendental frequency ratios ω_A/ω_B is increasing as well. Nevertheless, their distribution is not homogeneous, but fractal. Applying continued fractions and truncating them, we can represent the logarithms $\ln(\omega_A/\omega_B)$ as rational numbers $\langle n_0; n_1, n_2, \ldots, n_k \rangle$ and make visible their fractal distribution.

The linear projection $\mathcal{E} = \exp(\mathcal{F})$ of the fundamental fractal (fig. 1) is a fractal scalar field of transcendental attractors that we call the *Euler field* [3]. Figure 2 (central part) shows the 2D-projection of its first layer. The Euler field is topologically 3-dimensional, a fractal set of embedded

Fig. 1: The distribution of rational logarithms for $k = 1$ (above) and for $k = 2$ (below) in the range $-1 \leqslant \mathcal{F} \leqslant 1$.

spheric equipotential surfaces. The potential difference defines a gradient directed to the center of the field that causes a central force of attraction creating the effect of a field source. Because of the fractal logarithmic hyperbolic metric of the field, also every equipotential surface is an attractor. The logarithmic scalar potential difference $\Delta\mathcal{F}$ of sequent equipotential surfaces equals the difference of sequent continued fractions (1) on a given layer:

$$\Delta\mathcal{F} = \langle n_0; n_1, \ldots, n_k \rangle - \langle n_0; n_1, \ldots, n_k + 1 \rangle$$

Main equipotential surfaces at $k = 0$ correspond with integer logarithms; equipotential surfaces at deeper layers $k > 0$ correspond with rational logarithms.

The Euler field is of pure arithmetic origin, and there is no particular physical mechanism required as field source. Hence, we postulate the universality of the Euler field that should affect any type of physical interaction, regardless of its complexity. Corresponding with (1), the Euler field generates a fractal set of transcendental frequency ratios $\omega_A/\omega_B = \mathcal{E}$ which allow to avoid destabilizing parametric resonance and in this way, provide the lasting stability of periodic processes bound in systems regardless of their complexity. This conclusion we have exemplified [21] in particle physics, astrophysics, geophysics, biophysics and engineering.

In several publications we have shown that the Euler field determines the orbital periods of thousands of exoplanets and large bodies in the solar system [3] as well as their gravitational parameters [4]. Astrophysical and geophysical cycles [22] as well as periodic biophysical processes [10] obey the Euler field. Finally, the Euler field determines the proton-to-electron ratio and the W/Z-to-electron ratio as well as the temperature 2.725 K of the cosmic microwave background radiation [14]. All these findings suggest that the cosmological significance of the Euler field is that of a universal stabilizer.

The radii of the equipotential surfaces of the Euler field $\mathcal{E} = e^{\mathcal{F}}$ are integer and rational powers of Euler's number. However, not only Euler's number $e = 2.71828\ldots$ defines a fractal scalar field of its integer and rational powers, but in general, every prime, irrational and transcendental number does it. While the fundamental fractal (fig. 1) is always the same distribution of rational logarithms, the structure of the corresponding fundamental field changes with the logarithmic base. Here it is important to notice that no fundamental field can be transformed in another by scaling (stretching), because $\log_a(x) - \log_b(x)$ is a nonlinear function of x. In this way, every prime, irrational or transcendental number generates a unique fundamental field of its own integer and rational powers that causes physical effects which are typical for that number. For instance, the golden ratio $\phi = \langle 1; 1, 1, \ldots \rangle$ makes difficult its rational approximation, since its continued fraction does not contain large denominators. Hence, the fundamental field of its integer and rational powers should be a perfect inhibitor of resonance amplification. We propose to name this field after Hippasus of Metapontum who was an ancient Greek philosopher and early follower of Pythagoras, and is widely credited with the discovery of the existence of irrational numbers, and the first proof of the irrationality of the golden ratio. Figure 2 (left part) shows the 2D-projection of the first layer of the Hippasus field $\mathcal{H} = \phi^{\mathcal{F}}$.

Although the golden ratio is irrational, it is a Pisot number, so its powers are getting closer and closer to whole numbers. This is why the Hippasus field can inhibit resonance within small frequency ranges only. Euler's number is not a Pisot number, so that the Euler field permits coupled periodic processes to avoid parametric resonance also over very large frequency ranges. Since the natural logarithm of the golden ratio is close to 1/2, small powers of the golden ratio can approximate main equipotential surfaces of the Euler field. For example, $\phi^2 = 2.618\ldots$ can serve as approximation of $e = 2.718\ldots$ Within small frequency ranges, this circumstance makes the Hippasus field a fast and simplified local approximation of the Euler field. In fact, as the continued fraction of the golden ratio contains only the number 1, approximations of the golden ratio can be achieved faster than approximations of Euler's number, since every extension of its continued fraction requires counting and additional computing. Therefore, systems of coupled periodic processes follow the Hippasus field within small frequency ranges only. For example, several authors [23, 24] have suggested that the Venus-to-Earth orbital period ratio 0.615 approximates the golden ratio $1/\phi = 0.618\ldots$ preventing Earth and Venus from parametric orbital resonance. However, the Hippasus field cannot prevent the whole solar system from orbital resonance. For instance, the Pluto-to-Venus orbital period ratio does not obey a power of the golden ratio, but approximates the 6^{th} power of Euler's number [10]. The 6^{th} power of Euler's number is in the range of the 12^{th} power of the golden ratio that approximates a whole number and hence cannot serve as a scaling factor that prevents parametric resonance.

Obviously, in systems with many coupled periodic processes, the Hippasus field can produce two opposing effects: over small frequency ranges, the Hippasus field can inhibit parametric resonance, but over large frequency ranges, it provides the long-period appearance of resonance amplification.

Furthermore in this paper, we introduce the Archimedes field $\mathcal{A} = \pi^{\mathcal{F}}$. Figure 2 (right part) shows the 2D-projection of its first layer. The radii of the equipotential surfaces of the Archimedes field are integer and rational powers of π.

According to our numeric physical approach, we interpret the fact that circumference / radius = π in the way that the transcendence of π makes possible circular motion. The transcendence of the circumference avoids interruptions and

makes impossible to define the start or endpoint of motion. Furthermore, Archimedes number π makes possible eternal oscillation. This is why it is impossible to *completely* stop oscillations, for example, the thermal oscillations of atoms. According to our approach, the origin of the zero point energy phenomenon lies in the transcendence of π.

Proven by Theodor Schneider [25] in 1937, the perimeter of an ellipse is transcendental. Elliptical or circular motion is the only way to move with acceleration without propulsion. The absence of propulsion makes this motion eternal. In this way, the transcendence of π makes possible eternal accelerated motion. Hence, Archimedes' number appears to be a universal source of kinetic energy and promoter of orbital and rotational motion.

In the framework of our approach, gravity is a physical effect caused by numeric attractors [3]. They cause mass accretion forming a celestial body and determine its movement in space and time. In this way, planets, stars, planetary systems and galaxies are materializations of numeric attractors. These attractors exist long before a star or planet is formed. In order to reach an attractor, the accelerated displacement of matter causes the force conventionally interpreted as gravity. Numeric attractors are primary; mass accretion is secondary. In this way, gravitation is not caused by the body mass, and it is not a physical property of a celestial body at all. We suppose that fundamental numeric attractors cause all types of physical interaction.

As well, the appearance of a field source is only a scaling effect. A field is not created by a charge, but the charge is a scaling effect of the field. The gradient of the field is the force of attraction that indicates the location of the energy source. The attractor is the energy source. Matter falls down to the attractor because in this way it gains energy. This is why the core of a planet is hot. On the contrary, in the assumption that mass is the source of gravity, and in accordance with Newton's shell theorem, the Preliminary Reference Earth Model [26] affirms the *decrease* of the gravity acceleration with the depth. However, this hypothesis is still under discussion. In 1981, Stacey and Holding [27, 28] reported anomalous measures (larger values than expected) of the gravity acceleration in deep mines and boreholes.

According to our approach, the acceleration of free fall should *increase* with the vicinity to the field singularity, but follow the logarithmically hyperbolic fractal metric of the fundamental numeric field. In [29] we have shown that the Euler field reproduces the 3D profile of the Earth's interior confirmed by seismic exploration. As well, the stratification layers in planetary atmospheres follow the Euler field [30].

Are there attractors of the Euler field that coincide with attractors of the Archimedes field? Since $e = 2.71828\ldots$ and $\pi = 3.14159\ldots$ are transcendental, there are no rational powers of these numbers that can produce identical results. Therefore, in general, Archimedes-attractors are different from Euler-attractors. However, some of them are so close to each other that they form common attractors. It is not difficult to compute the exponents of two transcendental numbers that define a common attractor. The ratio of their logarithms is a fractal dimension that equals $\mathrm{D} = \ln\pi = 1.144729\ldots$ Representing D as continued fraction $\langle 1; 7, -11, \ldots\rangle$, we immediately find 8/7 as the first approximation. Consequently, multiples of 8/7 define pairs of Euler-attractors of stability and Archimedes-attractors of motion that are very close to each other. For example, this is valid for $\mathcal{E}\langle 56\rangle$ and $\mathcal{A}\langle 49\rangle$. We will study this and other examples in the paragraph *Exemplary Applications*. Naturally, our description of possible physical effects caused by the fields $\mathcal{A}, \mathcal{E}, \mathcal{H}$ does not claim to be complete.

Exemplary Applications

Let us start with an application of the Euler field that demonstrates its ability of avoiding parametric resonance over extremely large scale-differences. For instance, Venus' distance from Sun approximates the main equipotential surface $\mathcal{E}_e\langle 54\rangle$ of the Euler field of the *electron* that equals the 54^{th} power of Euler's number multiplied by the Compton wavelength of the electron λ_e. The aphelion 0.728213 AU = $1.08939 \cdot 10^{11}$ m delivers the upper approximation:

$$\ln\left(\frac{A_{\mathrm{O}}(Venus)}{\lambda_e}\right) = \ln\left(\frac{1.08939 \cdot 10^{11}\,\mathrm{m}}{3.86159 \cdot 10^{-13}\,\mathrm{m}}\right) = 54.00$$

The perihelion 0.718440 AU = $1.07477 \cdot 10^{11}$ m delivers the lower approximation:

$$\ln\left(\frac{P_{\mathrm{O}}(Venus)}{\lambda_e}\right) = \ln\left(\frac{1.07477 \cdot 10^{11}\,\mathrm{m}}{3.86159 \cdot 10^{-13}\,\mathrm{m}}\right) = 53.98$$

This means that Venus' orbit derives from the Euler field of the electron. In other words, Venus' orbit is of subatomic origin. This is not a random coincidence. Jupiter's distance from Sun approximates the main equipotential surface $\mathcal{E}_e\langle 56\rangle$ of the same electron Euler field. The aphelion 5.45492 AU = $8.160444 \cdot 10^{11}$ m delivers the upper approximation:

$$\ln\left(\frac{A_{\mathrm{O}}(Jupiter)}{\lambda_e}\right) = 56.01$$

The perihelion 4.95029 AU = $7.405528 \cdot 10^{11}$ m delivers the lower approximation:

$$\ln\left(\frac{P_{\mathrm{O}}(Jupiter)}{\lambda_e}\right) = 55.91$$

As well, Jupiter's orbital period 4332.59 days derives from the Euler field of the electron. In fact, it equals the 66^{th} power of Euler's number multiplied by the oscillation period of the electron ($\tau_e = \lambda_e/c = 1.28809 \cdot 10^{-21}$ s is the angular oscillation period of the electron):

$$\ln\left(\frac{T_{\mathrm{O}}(Jupiter)}{2\pi \cdot \tau_e}\right) = \ln\left(\frac{4332.59 \cdot 86400\,\mathrm{s}}{2\pi \cdot 1.28809 \cdot 10^{-21}\,\mathrm{s}}\right) = 66.00$$

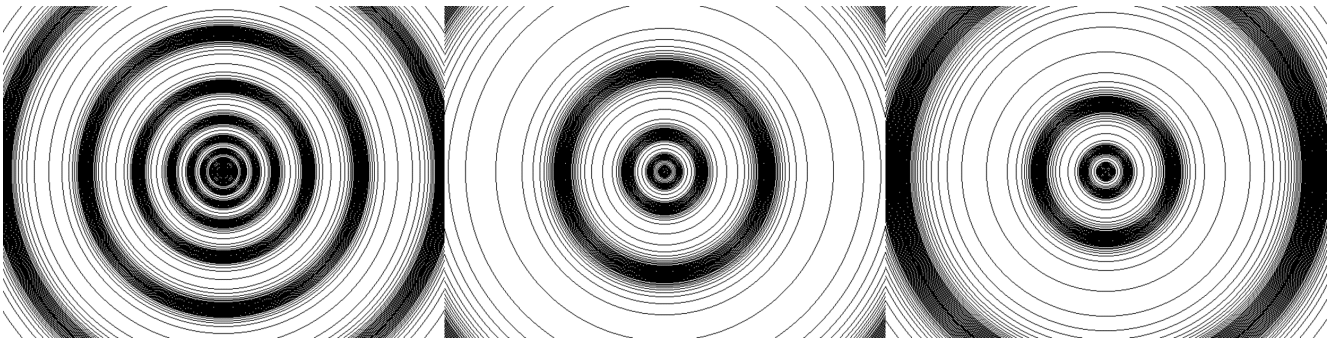

Fig. 2: The image shows the 2D-projection of the first layer ($k = 1$) of equipotential surfaces of the Hippasos Field $\mathcal{H} = \phi^{\mathcal{F}}$ (left), the Euler Field $\mathcal{E} = e^{\mathcal{F}}$ (center), and the Archimedes Field $\mathcal{A} = \pi^{\mathcal{F}}$ (right) of the Fundamental Fractal $\mathcal{F}$. The fields are shown to the same scale.

The same is valid for the orbital period 686.98 days (1.88 years) of the planet Mars that equals the 66^{th} power of Euler's number multiplied by the *angular* oscillation period of the electron:

$$\ln\left(\frac{T_{\mathrm{O}}(Mars)}{\tau_e}\right) = \ln\left(\frac{686.98 \cdot 86400\,\mathrm{s}}{1.28809 \cdot 10^{-21}\,\mathrm{s}}\right) = 66.00$$

Consequently, the ratio of the orbital periods of Jupiter and Mars equals 2π:

$$T_{\mathrm{O}}(Jupiter) = 2\pi \cdot T_{\mathrm{O}}(Mars)$$

This transcendental ratio allows Mars to avoid parametric orbital resonance with Jupiter and evidences that Jupiter and Mars are not planets of different systems, but bound together in the same conservative system (the solar system).

Also the orbital period 224.701 days of Venus derives from the Euler field of the electron, and it is stabilized by the main attractor $\mathcal{E}_e\langle 63\rangle$:

$$\ln\left(\frac{T_{\mathrm{O}}(Venus)}{2\pi \cdot \tau_e}\right) = 63.00$$

The complete (polar) rotational period $T_{\mathrm{R}}(Sun) = 34$ days of the Sun approximates the same attractor:

$$\ln\left(\frac{T_{\mathrm{R}}(Sun)}{\tau_e}\right) = 63.00$$

Consequently, the scaling factor 2π connects the orbital period of Venus with the rotational period of the Sun:

$$T_{\mathrm{O}}(Venus) = 2\pi \cdot T_{\mathrm{R}}(Sun)$$

Needless to say that these numeric relations cannot be derived from Kepler's laws or Newton's law of gravitation. Fig. 3 shows how Archimedes' number bonds together rotational and orbital periods. The scale symmetry of this connection not only reveals the Sun as the engine of planetary motion, but also the special role of Mercury. The connection of its rotation with the orbital motion of the Earth is surprising and encourages further investigation.

In general, orbital periods are stabilized by the Euler field of the electron, and rotational periods by the Euler field of the proton. For instance, the rotational periods of Earth and Mars derive from the angular oscillation period $\tau_p = \lambda_p/c$ of the proton ($\lambda_p = 2.10309 \cdot 10^{-16}$ m is the Compton wavelenght of the proton). They approximate the same attractor $\mathcal{E}_p\langle 67\rangle$. Mars' sidereal rotational period 24.62278 hours delivers the upper approximation:

$$\ln\left(\frac{T_{\mathrm{R}}(Mars)}{\tau_p}\right) = \ln\left(\frac{24.62278 \cdot 3600\,\mathrm{s}}{7.01515 \cdot 10^{-25}\,\mathrm{s}}\right) = 67.01$$

Earth' sidereal rotational period 23.93447 hours delivers the lower approximation:

$$\ln\left(\frac{T_{\mathrm{R}}(Earth)}{\tau_p}\right) = \ln\left(\frac{23.93447 \cdot 3600\,\mathrm{s}}{7.01515 \cdot 10^{-25}\,\mathrm{s}}\right) = 66.98$$

It is notable that the proton-to-electron ratio itself approximates the 7^{th} power of Euler's number and its square root:

$$\ln\left(\frac{\lambda_e}{\lambda_p}\right) = \ln\left(\frac{3.86159 \cdot 10^{-13}\,\mathrm{m}}{2.10309 \cdot 10^{-16}\,\mathrm{m}}\right) \simeq 7 + \frac{1}{2} = \mathcal{E}\langle 7; 2\rangle$$

In the consequence of this potential difference of the proton relative to the electron, the scaling factor $\sqrt{e} = 1.64872\ldots$ connects Euler field attractors of proton stability with similar attractors of electron stability in alternating sequence. In [4] we have applied Khinchine's [16] continued fraction method of approximation to the proton-to-electron ratio.

As we mentioned in the paragraph *Theoretical Approach*, multiples of 8/7 define pairs of Euler-attractors of stability and Archimedes-attractors of motion and energy that are very close to each other. For example, this is valid for $\mathcal{E}_e\langle 56\rangle$ and $\mathcal{A}_e\langle 49\rangle$, because 56/49 = 8/7. This coincidence underlines the significance of the attractor $\mathcal{E}_e\langle 56\rangle$ that determines the orbit of the largest planet in the Solar system. If we apply the exponent 49 to Euler's number, we discover that $\mathcal{E}_e\langle 49\rangle$ corresponds with the radius of the Sun. In this way, the coincidence of $\mathcal{E}_e\langle 56\rangle$ with $\mathcal{A}_e\langle 49\rangle$ identifies the Sun as energy source and Jupiter as main orbital body of the Solar system.

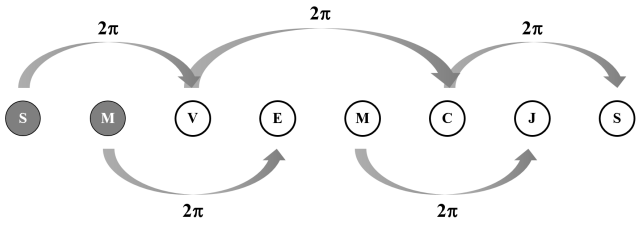

Fig. 3: From left to right: the *rotational* periods of the Sun (S) and Mercury (M), and the *orbital* periods of Venus (V), Earth (E), Mars (M), Ceres (C), Jupiter (J), and Saturn (S), coupled by the scaling factor 2π of the Archimedes field.

Interestingly, it is not the radius of the photosphere that coincides with the equipotential surface $\mathcal{E}_e\langle 49\rangle$, but the radius of the corona. It is noticeable that no complete theory yet exists to account for the extremely high temperature of the corona that reaches up to 20 million Kelvin. Despite great advances in observations and modelling, the problem of solar and stellar heating still remains one of the most challenging problems of space physics [31]. According to our approach, this heating could be a physical effect caused by numeric attractors of the Archimedes field.

Conclusion

According to our numeric-physical approach, numeric fields like $\mathcal{A}, \mathcal{E}$ are primary. Through their physical effects, they not only determine the frequency ratios of elementary particles, but also the setting of orbital and rotational periods in planetary systems. Modern theoretical physics is oriented towards equations, even if they cannot be solved. The language of equations is based on conservation rules, which, however, describe the behavior of model processes under certain ideal conditions of equilibrium. Nevertheless, the search for an equation describing the observed process is often considered a priority task of theoretical research. In this case, as a rule, numerical ratios are considered random. We consider this work to contribute to the idea that great unification in physics cannot be achieved as long as numerical ratios remain outside the realm of theoretical interest.

Acknowledgements

The author is grateful to Leili Khosravi, Veronika Müller, Viktor Panchelyuga, Oleg Kalinin, Viktor Bart and Michael Kauderer for valuable discussions.

Submitted on June 25, 2022

References

1. Hansson J. The 10 Biggest Unsolved Problems in Physics. *International Journal of Modern Physics and Applications*, 2015, v. 1, no. 1, 12–16.
2. Heggie D. C. The Classical Gravitational N-Body Problem. arXiv: astro-ph/0503600v2, 11 Aug 2005.
3. Müller H. Physics of Transcendental Numbers meets Gravitation. *Progress in Physics*, 2021, vol. 17, 83–92.
4. Müller H. Physics of Transcendental Numbers as Forming Factor of the Solar System. *Progress in Physics*, 2022, v. 18, 56–61.
5. Jacquinot J. Fifty years in fusion and the way forward. *Nucl. Fusion*, 2010, v. 50, 014001.
6. Lidsky L. M. The Trouble With Fusion. *MIT Technology Review*, October 1983.
7. Adler R. J. et al. Vacuum catastrophe: An elementary exposition of the cosmological constant problem. *American Journal of Physics*, 1995, v. 63 (7), 620–626.
8. Hansson J. Physical Origin of Elementary Particle Masses. arXiv: 1402.7033v1 [physics.gen-ph] 4 Feb 2014.
9. Brown H. R. Do symmetries "explain" conservation laws? The modern converse Noether theorem vs pragmatism. arXiv:2010.10909v2 [physics.hist-ph] 15 Jun 2021.
10. Müller H. On the Cosmological Significance of Euler's Number. *Progress in Physics*, 2019, v. 15, 17–21.
11. Dombrowski K. Rational Numbers Distribution and Resonance. *Progress in Physics*, 2005, v. 1, no. 1, 65–67.
12. Panchelyuga V.A., Panchelyuga M. S. Resonance and Fractals on the Real Numbers Set. *Progress in Physics*, 2012, v. 8, no. 4, 48–53.
13. Minton D. A., Malhotra R. A record of planet migration in the main asteroid belt. *Nature*, 2009, v. 457, 1109–1111.
14. Müller H. The Physics of Transcendental Numbers. *Progress in Physics*, 2019, vol. 15, 148–155.
15. Müller H. Global Scaling of Planetary Systems. *Progress in Physics*, 2018, v. 14, 99–105.
16. Khintchine A. Continued fractions. University of Chicago Press, Chicago, 1964.
17. Perron O. Die Lehre von den Kettenbrüchen. 1950.
18. Yiu P. The Elementary Mathematical Works of Leonhard Euler. Florida Atlantic University, 1999, pp. 77–78.
19. Hilbert D. Über die Transcendenz der Zahlen e und π. *Mathematische Annalen*, 1893, v. 43, 216–219.
20. Skorobogatko V. Ya. The Theory of Branched Continued Fractions and mathematical Applications. Moscow, Nauka, 1983.
21. Müller H. Global Scaling. The Fundamentals of Interscalar Cosmology. *New Heritage Publishers*, Brooklyn, New York, USA, ISBN 978-0-9981894-0-6, (2018).
22. Müller H. Physics of Transcendental Numbers on the Origin of Astrogeophysical Cycles. *Progress in Physics*, 2021, v. 17, 225–228.
23. Pletser V. Orbital Period Ratios and Fibonacci Numbers in Solar Planetary and Satellite Systems and in Exoplanetary Systems. arXiv: 1803.02828 (2018).
24. Butusov K. P. The Golden Ratio in the solar system. *Problems of Cosmological Research*, vol. 7, Moscow–Leningrad, 1978.
25. Schneider T. Arithmetische Untersuchungen elliptischer Integrale. *Mathematische Annalen*, 1937, v. 113, 1–13.
26. Dziewonski A. M., Anderson D. L. Preliminary reference Earth model. Physics of the Earth and Planetary Interiors, 1981, v. 25, 297–356.
27. Stacey F. D. et al. Constraint on the planetary scale value of the Newtonian gravitational constant from the gravity profile within a mine. *Phys. Rev. D*, 1981, v. 23, 1683.
28. Holding S. C., Stacey F. D., Tuck G. J. Gravity in mines. An investigation of Newton's law. *Phys. Rev. D*, 1986, v. 33, 3487.
29. Müller H. Quantum Gravity Aspects of Global Scaling and the Seismic Profile of the Earth. *Progress in Physics*, 2018, v. 14, 41–45.
30. Müller H. Global Scaling of Planetary Atmospheres. *Progress in Physics*, 2018, v. 14, 66–70.
31. Erdelyi R., Ballai I. Heating of the solar and stellar coronae: a review. *Astronomische Nachrichten*, 2007, v. 328, no. 8, 726–733.

Proposed Laboratory Measurement of the Gravitational Repulsion Predicted by Quantum Celestial Mechanics (QCM)

Franklin Potter

Sciencegems.com, 8642 Marvale Drive, Huntington Beach, CA 92646 USA. E-mail: frank11hb@yahoo.com

Quantum Celestial Mechanics (QCM) predicts the quantization of the orbital angular momentum per unit mass for bodies orbiting a central mass in response to attractive and repulsive gravitational accelerations. Applications to the Solar System, multi-planet exosystems, and to the Pluto system of 5 moons suggest its validity. A laboratory experiment to check this constraint is proposed.

1 Introduction

The gravitational constant G has now been measured by several new techniques, including a dynamic measurement by resonating beams [1] and a simple pendulum laser interferometer [2]. Both methods as well as Advanced LIGO and other gravitational sensors could also measure the repulsive gravitational acceleration predicted by the quantization of angular momentum per unit mass constraint [3] of Quantum Celestial Mechanics (QCM).

Although the Pluto system with its 5 satellites has already been a definitive test of this constraint [4], and its successful applications to the Solar System and numerous multi-planet exosystems have been achieved [5], an Earth-bound laboratory measurement confirmation is preferred.

According to QCM, which is derived from the general relativistic Hamilton-Jacobi equation, the quantization of orbital angular momentum L per unit mass μ constraint of the orbiting body, with quantization integer m, depends upon the total angular momentum L_T for the system of total mass M_T as

$$L/\mu = m\, L_T/M_T\,. \tag{1}$$

Recall that all orbits are equilibrium orbits for Newtonian gravitation for a central mass M and orbit distance r because the radial acceleration

$$\ddot{r} = -\frac{GM}{r^2} + \frac{L^2}{\mu^2\, r^3}\,. \tag{2}$$

But for QCM, the subset of allowed equilibrium orbits are the ones that obey

$$\ddot{r} = -\frac{GM}{r^2} + \frac{m\,(m+1)\,L_T^2}{M_T^2\, r^3} \tag{3}$$

for circular orbits. Therefore, a very small radial displacement from the equilibrium radius r_{eq} of orbit results in an acceleration in the opposite direction.

2 Lab experiment parameters

In order to mimic a Keplerian circular orbit, one would place an ideal rotating metal cylinder of mass M and radius R at a distance r from the gravitational detector. A simple estimation of the parameters for a laboratory scale measurement is made by assuming that the detector is essentially a point mass M_d responding instead of an extended geometrical object. Therefore,

$$r_{eq} = \frac{m\,(m+1)\,L_T^2}{GM\,M_T^2} \approx \frac{m\,(m+1)\,R^4\omega^2 M}{4G\,(M+M_d)^2}\,. \tag{4}$$

Inserting some reasonable values: $M = 5\,\text{kg}$, $R = 5\,\text{cm}$, $M_d = 2\,\text{kg}$, and $m = 1$, the first equilibrium radius will be at $r_{eq} \approx 4781\omega^2$ metre. For $r_{eq} = 1$ metre, i.e. fit in a lab room,

$$\omega \approx 0.0145\,\text{rad/s} \approx 8.3\,\text{rot/hr}\,. \tag{5}$$

By varying the rotation rate ω of the cylinder one can sweep back and forth through several equilibrium radii for $m = 1, 2, 3, ...$ to observe attractive and repulsive accelerations at $r_{eq} = 2r_0, 6r_0, 12r_0, ...$ sensed by the detector, with rapidly decreasing interaction accelerations with increasing r_{eq}.

Acknowledgements

The author thanks Sciencegems.com for support and H. G. Preston for insightful discussions on methods to test Quantum Celestial Mechanics.

Received on August 2, 2022

References

1. Brack T., Balabdaoui F., *et al*. Dynamic measurement of gravitational coupling between resonating beams in the hertz regime. *Nature Physics*, 2022. //doi.org/10.1038/s41567-022-01642-8.
2. Parks H. V. and Faller J. E. A simple pendulum laser interferometer for determining the gravitational constant. *Phil. Trans. A Math. Phys. Eng. Sci.*, 2014, v. 372 (2026).
3. Preston H. G. and Potter F. Exploring large-scale gravitational quantization without $\hbar$ in planetary systems, galaxies, and the Universe. arXiv: gr-qc/0303112.
4. Potter F. Update on Pluto and Its 5 Moons Obeying the Quantization of Angular Momentum per Unit Mass. *Prog. in Phys.*, 2016, v. 12 (1), 56–58.
5. Potter F. Multi-planet exosystems all obey orbital angular momentum quantization per unit mass predicted by Quantum Celestial Mechanics(QCM). *Prog. in Phys.*, 2013, v. 9 (3), 29–30.

An Observational Test of Doppler's Theory Using Solar-System Objects

John "Jack" D. Wilenchik
Phoenix, Arizona, USA. E-mail: wilenchik1@me.com

The scientific community widely accepted Christian Doppler's theory that light Doppler-shifts, even though it was proposed without empirical evidence and never tested on objects with well-known velocities like solar-system planets and moons. I conducted a test of Doppler's theory on a handful of planets and moons (Venus, Ganymede, Europa, and Ceres) using high-resolution data from the Keck Observatory's High Resolution Echelle Spectrometer (HIRES). In doing so, I was careful not to apply the automatic Doppler (heliocentric) corrections for movement of the earth that are normally applied when reducing such data. After comparing the observed shifts to actual velocities given by the NASA/JPL Horizons ephemeris system, I found both observations that agreed and disagreed with their Doppler-predicted values, which is an indication for more expansive tests. I also identified a significant problem with the Doppler explanation for "inclined" spectral lines, which can be found in the spectra of Jupiter and Saturn.

1 Introduction

This year is the 180th anniversary of Christian Doppler's hypothesis that colors of light shift due to movement by the source or observer [4]. Doppler's original paper describing his hypothesis was purely theoretical, and it reached conclusions that were quickly recognized as erroneous in their own time. For example, Doppler suggested that the actual color of every star was white or yellow, and that the stars' apparent colors (red, blue, etc.) were due solely to their radial velocities with respect to the earth [4, §5].* Nevertheless, the last sentence of his original paper proved to be prophetic: in "[t]he distant future," he wrote, his theory would "offer astronomers a welcome means of determining the motions and distances" of distant stars and other objects whose velocities are otherwise "immeasurable." [4, §11].

The instruments of the 19th Century lacked the resolution needed to test Doppler's theory on celestial objects with known velocities, like solar-system planets and moons [8]. As astronomer William Huggins wrote in 1868: "[t]he great relative velocity of light to the known planetary velocities, and to the probable motions of the few stars of which the parallax is known, showed that any alternations of position which might be expected from [Doppler shift] in the lines of the stellar spectra would not exceed a fraction of the interval between the double line D [sodium doublet line D], for that part of the spectrum." [8, p. 530]. "I have devoted much time," Huggins continued, "[and] I hope to accomplish the detection of so small an amount of change... [but] [t]he difficulties of this investigation I have found to be very great..." [*Id.*]. The first astronomer(s) to apply Doppler's theory therefore focused on targets whose velocities could not be rigorously and independently measured, like distant stars and nebulae or gases on the solar surface [7, 8].

But a modern spectrometer like the Keck Observatory's "High Resolution Echelle Spectrometer" (HIRES) is more than capable of performing the "William Huggins Test". I report the results of a test of Doppler's theory on solar-system planets and moons using the shift in their D lines, much like William Huggins intended.

2 Methodology

I searched the Keck Observatory Archive (KOA)† for solar-system data from the HIRES, particularly planets and moons with low axial rotation [11] ‡. The HIRES has a precision on the order of meters per second and has been heavily used in searches for exoplanets; accordingly, its archives contain comparatively few observations of solar-system objects [2,3]. A handful of observations were used: two observations of Venus in 2007 and 2009, one of Ganymede in 2009, one of Europa in 2009, and one of the dwarf planet Ceres in 2005. The data for various observations of Mercury were also considered, but the signal-to-noise ratio was deemed to be too

*In 1868, astronomer William Huggins described Doppler's error as "obvious": "Doppler endeavored...to account for the remarkable differences of colour which some of the binary stars present, and for some other phenomena of heavenly bodies. That Doppler was not correct in making this application of his theory is obvious from the consideration that even if a star could be conceived to be moving with a velocity sufficient to alter its colour sensibly to the eye, still no change of colour would be perceived, for the reason that beyond the visible spectrum, at both extremities, there exists a store of invisible waves which would be at the same time exalted or degraded into visibility, to take the place of the waves which had been raised or lowered in refrangibility by the star's motion. No change of colour, therefore, could take place until the whole of those invisible waves of force had been expended, which would only be the case when the relative motion of the source of light and the observer was several times greater than that of light." [8, p. 530-31].

†The Keck archive can be accessed from //koa.ipac.caltech.edu/cgi-bin/KOA/nph-KOAlogin . The particular datasets used herein are identified in Appendix "A."

‡Rates of rotation were calculated from [1]; or in the case of Venus, also from [6] (indicating that Venus' atmosphere rotates sixty times faster than its surface).

low (and airmass too high) to be included in this exploratory study.

The KOA offers data that has already been reduced and extracted by the Keck Observatory "MAKEE" pipeline ("MAuna Kea Echelle Ex-traction"). However, that pipeline normally applies a "heliocentric correction" of up to around ±30 km/s, which is designed to account for the putative Doppler effect of movement of the earth at the time of observation. MAKEE can be run manually with heliocentric corrections turned "off"; and so I downloaded the same raw science and calibration data that was used to generate the extracted data in the archives, then I re-extracted it using MAKEE without heliocentric corrections. Because I made no effort to account for the effect of the bodies' (or the earth's) axial rotations on Doppler shift, I treated it as a source of error in their calculated radial velocity (see E_{calc} in Table 1). The speed of axial rotation for each object in this study was between ±0.01 and 0.15 km/s, and earth's rotation was estimated at 0.5 km/s, so E_{calc} was never greater than ±0.52 km/s. Putative relativistic effects were calculated to be less than 0.01 km/s and therefore neglected. Finally, the measured Doppler shift in the D lines was compared to radial velocity as given by the NASA/JPL Horizons ephemeris system. More details on methodology are included in Appendix "A."

3 Results

Figure 1 shows plots of the measured and calculated Doppler shifts. While the Sodium absorption lines in Venus' and Ceres' atmospheres appeared at or near their Doppler-predicted positions, the lines in Ganymede and Europa did not. The mean absolute difference (weighted by error) in between measured (Doppler) and calculated (JPL Horizons) velocity for Ganymede and Europa was 9.24 ± 0.72 km/s. These results are also shown in Table 1.

Space-based (Hubble) spectroscopy confirms Na D absorption lines in the atmospheres of both Ganymede and Europa*, which tends to discount telluric interference as a cause for the discrepancy. Its magnitude (9.24 km/s) would also tend to discount atmospheric winds and other internal dynamics.

The discrepancy is less if the lines are compared to the Doppler-predicted shift in solar light reflecting from the body, which is given by:

$$R_{reflect} = R_{helio} + R_{calc} + \frac{R_{helio}R_{calc}}{c} \qquad (1)$$

(where R_{helio} is the object's heliocentric velocity, R_{calc} is its geocentric velocity, and c is the speed of light *in vacuo*)†. However, the bodies' spectra do not show separate lines for reflected light (albedo) and light originating from the object, as Doppler's theory would predict.

*See Observation ID "o51u02040" (Ganymede) and "od9l140m0" (Europa) in the ESA Hubble Science Archive, http://hst.esac.esa.int/ehst/.

†For a derivation of this equation, please see Appendix "B."

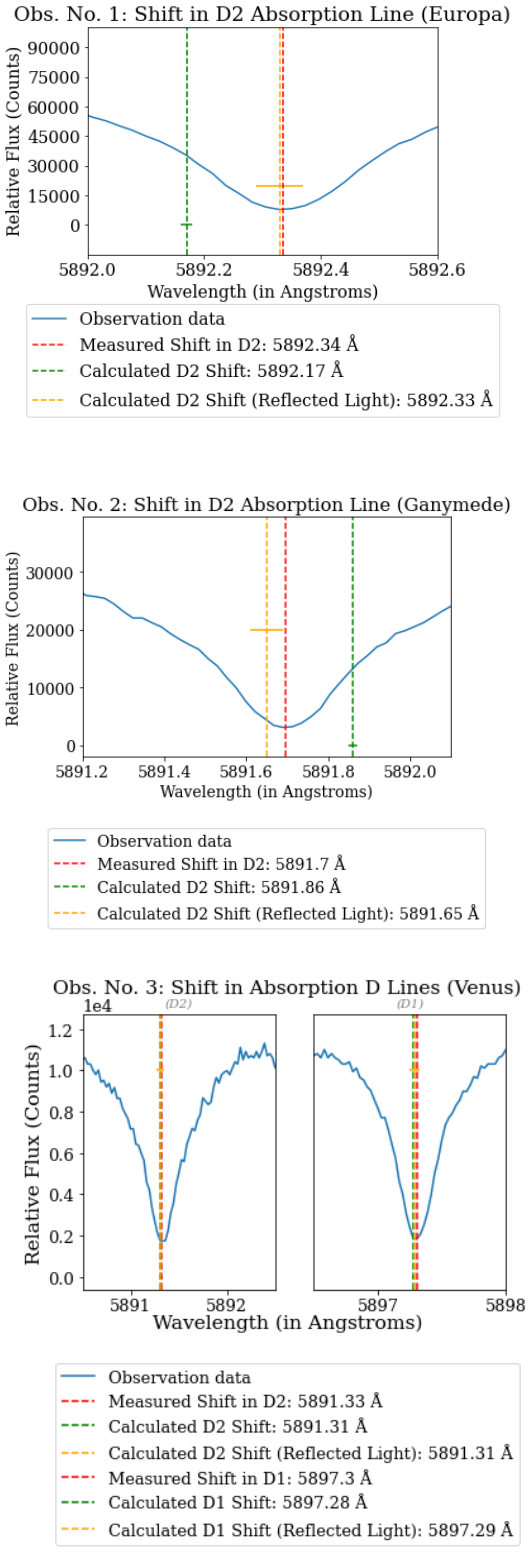

Fig. 1: Plots of the shifts in the D lines (actual and predicted) for the five observations. Error is thinner than the lines, except for the yellow lines (the predicted shifts in albedo), which had more significant error due to the calculated rotation of the sun. (*See also* Table 1.)

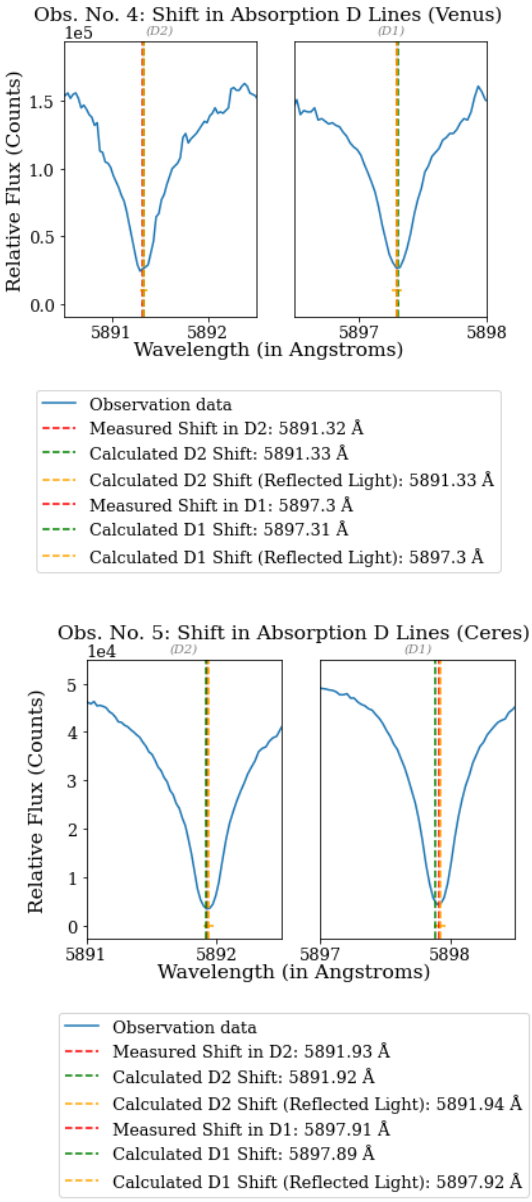

Fig. 1 (cont.)

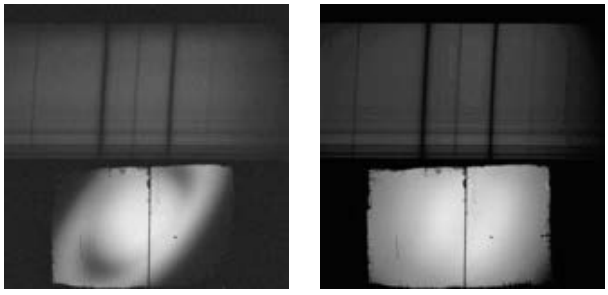

Fig. 2: At top left is an image of the spectrum of Saturn taken on June 25, 2018. Below it is the corresponding camera image of Saturn, which demonstrates the placement of the spectroscopic slit across the face of the planet. At top right is a spectrum of Jupiter taken on June 25, 2018, and below it is the corresponding camera image, which again demonstrates placement of the slit. The linear inclination in both planets' spectra is apparent. (Data source: [10], observations nos. 224 and 225.).

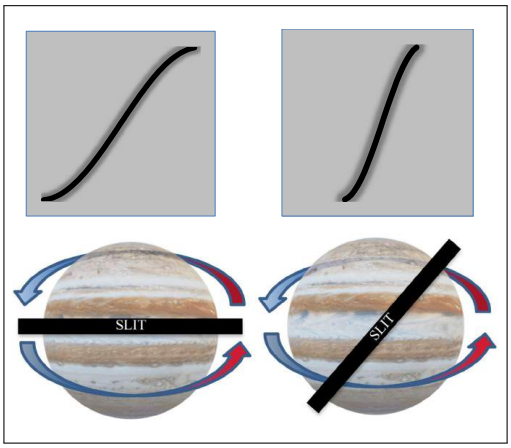

Fig. 3: At top (in gray) are illustrations of the expected sinusoidal pattern of spectral lines that are Doppler-shifted by the rotation of a spherical body. At bottom is shown the corresponding placement of a theoretical spectroscopic "slit" on the planet's surface.

3.1 Concerns with the Doppler modeling of planetary spectral line inclinations

The spectra of Jupiter and Saturn are known to be "tilted", or to exhibit a linear inclination (Figure 2). Historically, the cause of this inclination was deemed to be Doppler shift due to each planet's rotation about its own axis [5, 9]. However, the radial velocities of points across a spherical rotating body should exhibit a curved, sinusoidal pattern (Figure 3). The observed "tilt" is always linear, which suggests a cause other than Doppler shift.

4 Conclusion

Christian Doppler's theory that light Doppler-shifts was accepted and widely applied without an observational test on solar-system planets and moons, due to historical limitations on the resolution of available spectrometers. This "Huggins Test" used a small sample of modern high-resolution spectroscopic observations but nevertheless turned up observations that were inconsistent with their Doppler-predicted values. Further, there is substantial doubt concerning whether the inclined spectral lines of bodies like Jupiter and Saturn can be reasonably explained as a Doppler effect caused by their axial rotation. These results support conducting more expansive tests of the Doppler theory, using modern high-

resolution spectroscopy on solar-system objects with well-known velocities.

Disclosures

No outside funding was received to assist with the preparation of this article, and the author declares no conflicts of interest.

Supplemental Documents

A Python script that will reproduce my data reduction and analysis is available on Zenodo, (doi:10.5281/zenodo.6240436) as "Doppler_Test.py". [11].

Data Availability

The data underlying the results presented in this paper are fully contained on Zenodo [11]. They are also available from their original sources on the Keck Observatory Archive, https://www2.keck.hawaii.edu/koa/public/koa.php.

Acknowledgments

This research made use of the Keck Observatory Archive - (KOA), which is operated by the W. M. Keck Observatory and the NASA Exoplanet Science Institute (NExScI), under contract with the National Aeronautics and Space Administration. Profound thanks go to Dr. Zach Cano for his invaluable advice and assistance, as well as to Dr. Francisco Pina, Dr. Rafael Brahm and Dr. Christina Thöne.

Received on August 11, 2022

References

1. Cox A. Allen's Astrophysical Quantities, 4th Ed. Springer, 1999.
2. Vogt S., Allen S., Bigelow B., Bresee L., Brown B., Cantrall T., Conrad A., Couture M., Delaney C., Epps H., Hilyard D., Horn E., Jern N., Kanto D., Keane M., Kibrick R., Lewis J., Osborne J., Pardeilhan G., Pfister T., Ricketts T., Robinson L., Stover R., Tucker D., Ward J. & Wei M. HIRES: the high resolution echelle spectrometer on the Keck 10-m telescope. *Proc. SPIE* 2198, Instrumentation in Astronomy VIII, 1994. doi:10.1117/12.176725.
3. Butler R., Vogt S., Laughlin G., Burt J., Rivera E., Tuomi M., Teske J., Arriagada P., Diaz M., Holden B. & Keiser S. The LCES HIRES/Keck Precision Radial Velocity Exoplanet Survey. *AJ*, 2017, v. 153, 5. doi:10.3847/1538-3881/aa66ca.
4. Doppler C. Über das farbige Licht der Doppelsterne (Concerning the Coloured Light of Double Stars). *Royal Bohemian Society Of Sciences*, 1842. https://bit.ly/3qpUJpc.
5. Giver L. Line Inclinations in Equatorial Spectra of Jupiter and Saturn. *Astrophysical Journal*, 1964, v. 139, 727. doi:10.1086/147798.
6. Horinouchi T., Hayashi Y., Watanabe S., Yamada M., Yamazaki A., Kouyama T., Taguchi M., Fukuhara T., Takagi M., Ogohara K., Murakami S., Peralta J., Limaye S., Imamura T., Nakamura M., Sato T. & Satoh T. How waves and turbulence maintain the super-rotation of Venus' atmosphere. *Science*, 2020, v. 368, 405–409. doi:10.1126/science.aaz4439.
7. Huggins W. VII. Further observations on the spectra of the sun, and of some of the stars and nebulæ, with an attempt to determine therefrom whether these bodies are moving towards or from the earth. *Proc. R. Soc. London Ser. I*, 1868a, v. 16, 382–386. doi:10.1098/rspl.1867.0080.
8. Huggins W. XXI. Further observations on the spectra of some the stars and nebulæ, with an attempt to determine therefrom whether these bodies are moving towards or from the earth, also observations on the spectra of the sun and of comet II. *Phil. Trans. R. Soc. London, Ser. I*, 1868b, 158, p. 529–565. doi:10.1098/rstl.1868.0022.
9. Moore J. Spectroscopic Observations of the Rotation of Saturn. *Publications Of The Astronomical Society Of The Pacific*, 1939, v. 51, 274. doi:10.1086/125081.
10. Schmidt C. Rapid Imaging Planetary Spectrograph: 2018 Mercury Exosphere Data [Dataset, version 1]. *Zenodo*, 2019. doi:10.5281/zenodo.3588493.
11. Wilenchik J. An Observational Test of Doppler's Theory Using Solar System Objects [Dataset, version 2]. *Zenodo*, 2022. doi:10.5281/zenodo.6240436.

Appendix "A"

Version 6.4 of "MAKEE" was used to extract and reduce the Keck Archive data. The version of MAKEE that was used is dated May 2019 and available for download from: https://sites.astro.caltech.edu/~tb/makee/makee_6.4-2019.tar.gz.

MAKEE was run in a command terminal using Ubuntu 20.04.3 LTS. The MAKEE pipeline requires at least four "FITS" (Flexible Image Transport System) images to reduce and calibrate data: an image of the object; an image to find the "trace" of the echelle orders (which can simply be the image itself, although a star is often used); flat image(s); and an image of the arc lamp for wavelength calibration. Each image in the Keck Observatory Archive (KOA) is assigned a unique "KOAID." The KOAID for each of the raw science and calibration images used in this paper (as well as the CCD and orders extracted) are listed in Table 2.

To remove the heliocentric correction, MAKEE was run using the "-nohc" option. The "-koa" option was also used, which outputs the processed data into ".tbl" files. Finally, in order to run MAKEE, the user must specify a CCD number to be extracted (using the "ccd=*" argument). The final command for processing each observation was "makee [Object.fits] [Trace.fits] [Flat.fits] [Arc.fits] ccd = [CCD No.] -nohc -koa." An optional "log=*.txt" argument sends the command-line output into a "*.txt" file.

After running MAKEE, the region of the Sodium D lines (5890 – 5900 Å) was identified in the extracted orders. The wavelength, flux and error spectrum in the region of the D line(s) was then manually extracted into a ".csv" file (which is contained in the Zenodo depository and named "*_full.csv" for each observation). In Observations No. 1 and 2 (Europa and Ganymede), the D1 line fell beyond the extracted orders, and so only the D2 lines were used. The D lines in Observation No. 5 fell across two different orders; and so the data in Order #7 was used for the D1 line and part of the D2 line, with the remaining data for the D2 line coming from Order #6. Postscript images of the orders for all extractions can be found in the "logs" folder on Zenodo, along with the MAKEE command-line output logs.

Table 1: Summary of Observation Data and Results. (All velocities in km/s.)

Observation No.	**1**	**2**	**3**	**4**	**5**
Target Name	Europa	Ganymede	Venus	Venus	Ceres
Epoch (UT)	12/13/09 4:56	12/11/09 4:53	6/6/07 5:32	1/7/09 4:33	6/17/05 5:54
Exposure (sec)	30	20	500	500	300
Keck Image ID	HI.20091213.17797	HI.20091211.17597	HI.20070606.19972	HI.20090107.16390	HI.20050617.21254
R_{calc}	+30.05	+14.29	-14.04	-12.78	+16.89
E_{calc}	±0.51	±0.51	±0.52	±0.52	±0.51
$R_{Doppler}$	+40.34	+6.09	-13.62	-13.88	+18.25
$E_{Doppler}$	±0.03	±0.05	±0.17	±0.36	±0.48
$\Delta_{Doppler}$	+10.29	-9.20	+0.42	-1.10	+1.36
$E_{\Delta Doppler}$	±0.51	±0.51	±0.55	±0.63	±0.70
R_{helio}	+7.83	-10.91	+0.23	-0.23	+1.43
E_{helio}	±1.99	±1.99	±2.00	±2.00	±1.99
$R_{reflect}$	+37.82	+3.38	-13.81	-13.01	+18.32
$E_{reflect}$	±2.05	±2.05	±2.07	±2.07	±2.05
$\Delta_{reflect}$	+2.52	+2.71	+0.19	-0.87	-0.07
$E_{\Delta reflect}$	±2.05	±2.05	±2.07	±2.10	±2.11
A	1.52	1.47	1.72	1.76	1.25

Legend

R_{calc} = the target object's calculated geocentric velocity at the date and time of observation, from the NASA/JPL Horizons ephemeris system.

E_{calc} = uncertainty in the target's calculated geocentric velocity, due to axial rotation of the earth and target body.

$R_{Doppler}$ = Doppler-measured radial velocity.

$E_{Doppler}$ = uncertainty in the Doppler-measured radial velocity (see Appendix "A" for methodology).

$\Delta_{Doppler}$ = $(R_{Doppler} - R_{calc})$, i.e. the discrepancy in between Doppler-measured velocity ($R_{Doppler}$) and Horizons-calculated velocity (R_{calc}).

$E_{\Delta Doppler}$ = uncertainty in $\Delta_{Doppler}$, i.e. $\sqrt{(E_{calc})^2 + (E_{Doppler})^2}$.

R_{helio} = target object's calculated heliocentric velocity, based on the NASA/JPL Horizons ephemeris system.

E_{helio} = error in the object's heliocentric velocity due to rotation of the sun and target (which were combined in quadrature). Solar rotation was estimated at $]pm1.99$ km/s (based on values from [1]. I used a solar equatorial circumference of 2.720984 million miles, then divided by a rotation period of 26.24 days, to obtain a rotational velocity at the solar equator of 1992.86 m/s.)

$R_{reflect}$ = predicted Doppler shift of solar light reflecting from the target, given by $(R_{calc} + R_{helio})$.

$E_{reflect}$ = error in $R_{reflect}$, i.e. $\sqrt{(E_{calc})^2 + (E_{helio})^2}$.

$\Delta_{reflect}$ = $R_{Doppler} - R_{reflect}$, i.e. the difference in between Doppler-measured velocity ($R_{Doppler}$) and predicted Doppler shift in solar light reflecting form the target ($R_{reflect}$).

$E_{\Delta reflect}$ = uncertainty in $\Delta_{reflect}$, i.e. $\sqrt{(E_{helio})^2 + (E_{Doppler})^2 + (E_{calc})^2}$.

A = averaged airmass (as reported in the image's FITS header).

Table 2: Keck Observatory Archive Datasets

Observation No.	1 (Europa)	2 (Ganymede)	3 (Venus)	4 (Venus)	5 (Ceres)
Object KOIAD	HI.20091213.17797	HI.20091211.17597	HI.20070606.19972	HI.20090107.16390	HI.20050617.21254
Trace (star) ID	HI.20091213.08389	HI.20091211.10571	HI.20070607.01296	HI.20090107.16390	HI.20050616.06005
Flat KOAID	HI.20091213.13363	HI.20091211.13478	HI.20070606.17769	HI.20090107.15456	HI.20050617.19496
Arc KOAID	HI.20091213.10643	HI.20091211.12272	HI.20070606.16831	HI.20090107.01375	HI.20050617.11120
CCD	3	3	2	2	2
Order(s)	11	11	13	13	6,7

To calculate the parameters for a Gaussian fit to each of the Sodium D lines, the "curve_fit" function in Python's SciPy package was used ("SciPy: Scientific Library for Python" version 1.7.3). The error spectrum in the MAKEE-generated data tables (column #7, "Error") was input as "sigma" in the "curve_fit" routine. This produced parameters for the best-fit Gaussian function for each D line, as well as an estimated covariance. The standard deviation in the Gaussian centerline was calculated from the covariance; and this standard deviation was used for error in the measured Doppler shift of each D line. Finally, for those observations in which both D lines could be detected, an average of the two shifts was calculated (weighted by error) to reach a final Doppler shift; and the errors in the shift of each D line were combined in quadrature to reach final error values.

Final shifts were recorded as $R_{Doppler}$ in Table 1, and final errors were recorded as $E_{Doppler}$. The Python code used for these calculations is included in the "Zenodo" depository (as "Doppler_Test.py"), and when run it will reproduce the data analysis and figures used in this paper. Python version 3.9.7 was used.

Appendix "B"

The equation for finding the predicted Doppler shift in solar spectra that are being reflected from a target under observation from the earth ($R_{reflect}$), and expressed in terms of velocity (km/s), is:

$$R_{reflect} = R_{helio} + R_{calc} + \frac{R_{helio}R_{calc}}{c} \tag{2}$$

where R_{helio} is the target's heliocentric velocity, R_{calc} is its geocentric velocity, and c is the speed of light *in vacuo*. To derive this equation, we start with the general Doppler equation for wavelength as a function of radial velocity, which represents the initial Doppler-shifted wavelength of solar light reaching the target (λ_{helio}):

$$\lambda_{helio} = \frac{R_{helio}}{c}\,\lambda_0 + \lambda_0 \tag{3}$$

where λ_0 the target's wavelength at rest. To determine the final observed wavelength after light reflects from the target ($\lambda_{observed}$), we must apply a second Doppler shift to account for the target's geocentric velocity:

$$\lambda_{observed} = \frac{R_{calc}}{c}\,\lambda_{helio} + \lambda_{helio} \tag{4}$$

$$\lambda_{observed} = \lambda_{helio}\left(\frac{R_{calc}}{c} + 1\right). \tag{5}$$

Finally, in order to express the observed wavelength as a shift in velocity ($R_{reflect}$), and as a function of the target's heliocentric and geocentric velocities, we must again use the Doppler equation (this time solved for radial velocity) and make the proper substitutions for $\lambda_{observed}$ and λ_{helio}:

$$R_{reflect} = \left(\frac{\lambda_{observed} - \lambda_0}{\lambda_0}\right) c \tag{6}$$

$$R_{reflect} = \left(\frac{\lambda_{helio}\left(\frac{R_{calc}}{c} + 1\right) - \lambda_0}{\lambda_0}\right) c \tag{7}$$

$$R_{reflect} = \left(\frac{\left(\frac{R_{helio}\,\lambda_0}{c} + \lambda_0\right)\left(\frac{R_{calc}}{c} + 1\right) - \lambda_0}{\lambda_0}\right) c \tag{8}$$

$$R_{reflect} = \left(\frac{R_{helio}}{c} + 1\right)(R_{calc} + c) - c \tag{9}$$

$$R_{reflect} = R_{helio} + R_{calc} + \frac{R_{helio}R_{calc}}{c}\,. \tag{10}$$

On Action in the Spacetime Continuum

Pierre A. Millette

E-mail: pierre.millette@uottawa.ca, Ottawa, Canada

In this paper, we investigate the role of action $\mathcal{S}$ in the Spacetime Continuum (*STC*) as provided by the Elastodynamics of the Spacetime Continuum (*STCED*). We find that energy applies to three-dimensional space, while action applies to four-dimensional spacetime. Planck's reduced constant $\hbar$ corresponds to an elementary quantum of action S_0, with action units being the same as those of angular momentum. We thus find that action is the fundamental four-dimensional spacetime scalar quantity corresponding to energy for three-dimensional space. This helps explain why equations of motion in the Spacetime Continuum are determined by minimizing action, not energy, using the principle of least (or stationary) action. The contribution of a path, in the path integral formulation of quantum mechanics and quantum field theory, depends on the number of elementary quanta of action S_0 in the path.

1 Introduction

In this paper, we investigate the role of action $\mathcal{S}$ in the Spacetime Continuum (*STC*) as provided by the Elastodynamics of the Spacetime Continuum (*STCED*) [1–3]. *STCED* is a natural extension of Einstein's General Theory of Relativity which blends continuum mechanical and general relativistic descriptions of the Spacetime Continuum. The introduction of strains in the Spacetime Continuum as a result of the energy-momentum stress tensor allows us to use, by analogy, results from continuum mechanics, in particular the stress-strain relation, to provide a better understanding of the general relativistic spacetime.

2 Elastodynamics of the Spacetime Continuum

The stress-strain relation for an isotropic and homogeneous Spacetime Continuum is given by [1, 3]

$$2\bar{\mu}_0\,\varepsilon^{\mu\nu} + \bar{\lambda}_0\,g^{\mu\nu}\varepsilon = T^{\mu\nu} \tag{1}$$

where $\bar{\lambda}_0$ and $\bar{\mu}_0$ are the Lamé elastic constants of the Spacetime Continuum: $\bar{\mu}_0$ is the shear modulus (the resistance of the Spacetime Continuum to *distortions*) and $\bar{\lambda}_0$ is expressed in terms of $\bar{\kappa}_0$, the bulk modulus (the resistance of the Spacetime Continuum to *dilatations*), in a four-dimensional continuum as:

$$\bar{\lambda}_0 = \bar{\kappa}_0 - \tfrac{1}{2}\,\bar{\mu}_0\,. \tag{2}$$

$T^{\mu\nu}$ is the general relativistic energy-momentum stress tensor, $\varepsilon^{\mu\nu}$ the Spacetime Continuum strain tensor resulting from the stresses, and

$$\varepsilon = \varepsilon^{\alpha}{}_{\alpha}\,, \tag{3}$$

the trace of the strain tensor obtained by contraction, is the volume dilatation ε defined as the change in volume per original volume [4, see pp. 149–152] and is an invariant of the strain tensor. It should be noted that the structure of (1) is similar to that of the field equations of general relativity,

$$R^{\mu\nu} - \tfrac{1}{2}\,g^{\mu\nu}R = -\varkappa\,T^{\mu\nu} \tag{4}$$

where $R^{\mu\nu}$ is the Ricci curvature tensor, R is its trace, $\varkappa = 8\pi G/c^4$ and G is the gravitational constant (see [2, Ch. 2] for more details).

In *STCED*, as shown in [1, 3], energy propagates in the Spacetime Continuum as wave-like *deformations* which can be decomposed into *dilatations* and *distortions*. *Dilatations* involve an invariant change in volume of the Spacetime Continuum which is the source of the associated rest-mass energy density of the deformation. On the other hand, *distortions* correspond to a change of shape (shearing) of the Spacetime Continuum without a change in volume and are thus massless.

Thus deformations propagate in the Spacetime Continuum by longitudinal (*dilatation*) and transverse (*distortion*) wave displacements. This provides a natural explanation for wave-particle duality, with the massless transverse mode corresponding to the wave aspects of the deformations and the massive longitudinal mode corresponding to the particle aspects of the deformations.

The rest-mass energy density of the longitudinal mode is given by [1, see Eq. (32)]

$$\rho c^2 = 4\bar{\kappa}_0\varepsilon \tag{5}$$

where ρ is the rest-mass density, c is the speed of light, $\bar{\kappa}_0$ is the bulk modulus of the *STC* as seen previously, and ε is the volume dilatation given by (3).

3 Action in the Spacetime Continuum

In a previous paper [5], we considered dislocations in the Spacetime Continuum as a framework for quantum physics. In a subsequent paper [6], we expressed Planck's constant in terms of the Burgers spacetime dislocation constant b_0, given by

$$\hbar = \frac{\bar{\kappa}_0\,b_0^4}{c}\,, \tag{6}$$

where $\bar{\kappa}_0$ is the Spacetime Continuum bulk modulus, b_0 is the Burgers spacetime dislocation constant, c is the speed of light

in vacuo and $\hbar$ is Planck's reduced constant. This equation can be considered to be a definition of Planck's reduced constant $\hbar$. We consider this equation in greater detail.

On the right-hand side of the equation, we have the Spacetime Continuum bulk modulus constant $\bar{\kappa}_0$ in units of energy density [J m^{-3}], that is energy per 3-D volume. We can multiply $\bar{\kappa}_0$ by a 3-D volume to convert it to energy. However, $\bar{\kappa}_0$ is a Spacetime Continuum constant. We need a conversion in terms of the 4-D spacetime volume.

The right-hand side of (6) also includes the term b_0^4 which can be taken to be the 4-D volume of a four-dimensional elementary hypercube of side $b_0 = 1.616 \times 10^{-35}$ m. This 4-D hypervolume has units of [m^4] while the four-dimensional Spacetime Continuum hypervolume consists of three space dimensions and one time dimension with units [m^3 s]. This requires that one of the four-dimensional hypercube dimensions b_0 be divided by c to convert it to a time elementary dimension $t_0 = b_0/c = 5.39 \times 10^{-44}$ s as is observed in (6). Eq. (6) can thus be written as

$$\hbar = \bar{\kappa}_0 \, b_0^3 \, \frac{b_0}{c} = \bar{\kappa}_0 \, b_0^3 \, t_0 = \bar{\kappa}_0 \, V_0^{STC} \tag{7}$$

where V_0^{STC} is the four-dimensional elementary Spacetime Continuum hypervolume and $\hbar$ has units of [J s] which are units of action $\mathcal{S}$.

Hence multiplying $\bar{\kappa}_0$ by a 3-D space volume converts it to energy, while multiplying it by a 4-D spacetime volume converts it to action. Energy applies to three-dimensional space, while action applies to four-dimensional spacetime. From (7), we see that Planck's reduced constant corresponds to an elementary quantum of action S_0:

$$\hbar = \bar{\kappa}_0 \, V_0^{STC} = S_0 \tag{8}$$

which has units of [J s]. Action units are the same as those of angular momentum, but this equivalence is accidental. The basic nature of $\hbar$ is an action, not an angular momentum. Calling $\hbar$ a "spin" quantity is an unfortunate misnomer from the early days of quantum mechanics. It needs to be called more appropriately an action quantity, i.e. the fundamental quantum of action of the Spacetime Continuum.

We thus find that action is the fundamental four-dimensional spacetime scalar quantity corresponding to energy for three-dimensional space. This helps explain why equations of motion in the Spacetime Continuum are determined by minimizing action, not energy, using the principle of least (or stationary) action given by

$$\delta \mathcal{S} = 0 \tag{9}$$

where the action $\mathcal{S}$ is expressed in terms of the Lagrangian L of the system as

$$\mathcal{S} = \int_{t_1}^{t_2} L\left(q(t), \dot{q}(t), t\right) \, dt \tag{10}$$

where $q = (q_1, q_2, ..., q_N)$ are the N generalized coordinates defining the configuration of the system and $\dot{q}$ denotes the time derivative of q.

In Lagrangian field theory, the action is written in terms of the Lagrangian density $\mathcal{L}$ specified in terms of one or more fields $\phi(x)$ and their derivatives $\partial_\mu \phi$ as [7, see p. 15ff]

$$\mathcal{S} = \int_{x_1}^{x_2} \mathcal{L}\left(\phi(x), \partial_\mu \phi\right) \, d^4 x \, . \tag{11}$$

The path integral formulation of quantum mechanics and quantum field theory is a generalization of the action principle of classical mechanics [8]. Interestingly enough, Feynman who developed this formulation [9]

> ... belie[ved] that the path integral captures the fundamental physics, and that hamiltonians and Hilbert space are merely mathematical methods for evaluating path integrals. [10, see p. 143]

In *STCED*, the path integral between two points x_1 and x_2 can be understood to be equivalent to the different possible wave paths between the two points.

The propagation amplitude $G(x_2; x_1)$ between the points x_1 and x_2 is determined from the path integral using the appropriate action for the system under consideration. One can see that since the contribution of a path is proportional to $e^{i\mathcal{S}/\hbar}$ [10, see p. 146], then, from (8), it is equivalent to $e^{i\mathcal{S}/S_0}$. In other words, the contribution of a path depends on the number of elementary quanta of action S_0 in the path.

The quantization of action implied by the above, points to the approach required to achieve quantization of path integrals in quantum physics. Coupled with the understanding that equations of motion in the Spacetime Continuum are determined by minimizing action as per (9) provides an indication for its potential application to the development of a quantized theory of path integrals.

4 Discussion and conclusion

In this paper, we have investigated the role of action $\mathcal{S}$ in the Spacetime Continuum as provided by the Elastodynamics of the Spacetime Continuum (*STCED*). We have found that multiplying the Spacetime Continuum bulk modulus constant $\bar{\kappa}_0$ by a 3-D space volume converts it to energy, while multiplying it by a 4-D spacetime volume converts it to action. Hence energy applies to three-dimensional space, while action applies to four-dimensional spacetime. Planck's reduced constant $\hbar$ corresponds to an elementary quantum of action S_0, with action units being the same as those of angular momentum. We thus find that action is the fundamental four-dimensional spacetime scalar quantity corresponding to energy for three-dimensional space. This helps explain why equations of motion in the Spacetime Continuum are determined by minimizing action, not energy, using the principle of least (or stationary) action. In particular, the contribution of a path, in the path integral formulation of quantum mechanics and quantum

field theory, depends on the number of elementary quanta of action S_0 in the path.

Received on August 24, 2022

References

1. Millette P. A. Elastodynamics of the Spacetime Continuum. *The Abraham Zelmanov Journal*, 2012, vol. 5, 221–277.
2. Millette P. A. Elastodynamics of the Spacetime Continuum: A Spacetime Physics Theory of Gravitation, Electromagnetism and Quantum Physics. American Research Press, Rehoboth, NM, 2017.
3. Millette P. A. Elastodynamics of the Spacetime Continuum, Second Expanded Edition. American Research Press, Rehoboth, NM, 2019.
4. Segel L. A. Mathematics Applied to Continuum Mechanics. Dover Publications, New York, 1987.
5. Millette P. A. Dislocations in the Spacetime Continuum: Framework for Quantum Physics. *Progress in Physics*, 2015, vol. 11 (4), 287–307.
6. Millette P. A. The Burgers Spacetime Dislocation Constant b_0 and the Derivation of Planck's Constant. *Progress in Physics*, 2015, vol. 11 (4), 313–316.
7. Peskin M. E., Schroeder D. V. An Introduction to Quantum Field Theory. Westview Press, Boulder, CO, 1995.
8. Padmanabhan T. Quantum Field Theory: The Why, What and How. Springer, Cham, CH, 2016.
9. Feynman R. P. Space-Time Approach to Non-Relativistic Quantum Mechanics. *Rev. Mod. Phys.*, 1948, v. 20, 367–387. Reprinted in Schwinger, J., ed. Selected Papers on Quantum Electrodynamics. Dover Publications, New York, 1958, pp 321–341.
10. Stone M. The Physics of Quantum Fields. Springer-Verlag, New York, 2000.

Black Hole Universe – A Complete Structure of the Entire Spacetime

T. X. Zhang

Department of Physics, Alabama A&M University, Normal, Alabama 35762. E-mail: tianxi.zhang@aamu.edu

A complete hierarchically layered structure of the entire spacetime is established in accordance with the black hole universe model that the author comprehensively developed on the basis of the three fundamentals without any other hypothetical entities: (1) Newton's cosmological principle (CP) of spacetime homogeneity and isotropy in a large scale, (2) Einstein's general theory of relativity (GR) that describes the effect of matter on spacetime, and (3) Zhang's principle of spacetime black hole equivalence (SBHEP) that postulates spacetimes and black holes to be equivalent (i.e. a black hole wraps a spacetime and a spacetime encloses a black hole). This alternative cosmological model not only explains all the observations of the universe without relying on any other hypothetical entities, but also overcomes all the cosmic difficulties based on the well-developed physics. Our universe is a black hole or spacetime and the observed starlike, massive, and/or supermassive black holes are child universes or subspacetimes of our black hole universe. The author's previous studies have fully and self-consistently described and explained various aspects of black hole universe such as its origin, structure, expansion, evolution, acceleration, emission, entropy, cosmic microwave background radiation, and so on. This study, by constructing the inside of the child universes of our black hole universe, to further develop a complete structure of the entire spacetime and provide us a complete new view to the inside of a black hole and a unique solution of the spacetime singularity.

1 Introduction

A physical cosmology is a branch of study in physics and astrophysics for the physical origin and evolution of the universe. A successful cosmological model should be simple, significant, and complete. Simplicity of a cosmological model refers to that the model is straight-forward and can simply and fully describe the universe based on the currently well-developed laws and theories of physics and astrophysics without making hypotheses that not only are non-testable but also violate the laws of physics and astrophysics. Significance of a cosmological model refers to that the model is important and can significantly explain all the observations of the universe and overcome all the cosmic problems without having any difficulty or without relying on any hypothetical entities. Completeness of a cosmological model refers to that the model is in its totality/entirety and can completely interpret the origin and evolution of development of the entire spacetime rather than only a finite part of the infinite universe or spacetime.

The standard big bang model of the universe (BBU) was developed on the two solid bases: (1) Einstein's general relativity (GR) that describes the effect of matter on spacetime [1] and (2) Newton's cosmological principle (CP) of spacetime isotropy and homogeneity. The Einsteinian field equation given in GR along with the Friedmann-Lemaitre-Robertson-Walker (FLRW) metric of spacetime derived from CP leads to the Friedmann equation (FE) that governs the development and dynamics of the universe [2]. The big bang theory has made incredible successes in explaining the universe, but there exist innumerable problems and difficulties. Solutions of these problems and difficulties severely rely on an increasing number of hypothetical entities (HEs) such as dark matter, dark energy, inflation, big bang singularity, and so on [3]. Therefore, BBU consists of GR, CP, and innumerable HEs, i.e. BBU = {GR, CP, HE, HE, HE,....} (see the blue part of Figure 1). Although it has only two bases (GR and CP), the BBU is neither simple and significant because of severely relying on an increasing number of HEs, which have not yet been and may never be tested or falsified, nor complete because of being finite and thus having unknown (or unable to answer) outside and prehistory.

Recently, the author has developed a new physical cosmology called black hole universe (BHU) [4-5]. Instead of making many HEs as the BBU did, the BHU proposes a new principle to the cosmology - the Principle of Spacetime Black Hole Equivalence (SBHEP) [6] - in an attempt to explain all the existing observations of the universe and overcome all the existing problems and difficulties. Standing on the three bases (GR, CP, and SBHEP), this new cosmological theory - BHU = {GR, CP, SBHEP} (see the red part of Figure 1) - can fully explain the universe in various aspects as well as to conquer all the cosmic problems according to the well-developed physics neither making any other HEs nor including any other unsolved difficulties [7-12]. GR and CP are common to both BBU and BHU. The BBU stands on two legs unstably so that it needs many crutches (or HEs) for support, while the BHU stands on three legs stably without needing any other props. In the BHU, a single SBHEP simply removes all of those innumerable HEs made in the BBU.

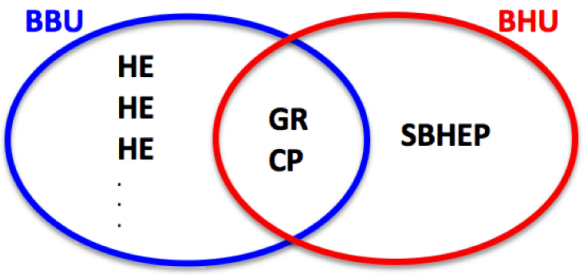

Fig. 1: The BBU versus the BHU [6, 12]. The BBU is developed on the basis of GR and CP with innumerable HEs to explain observations and overcome cosmic problems and difficulties. The BHU is developed on the basis of GR, CP and SBHEP. With one more base, SBHEP, the BHU can also perfectly explain all the existing observations of the universe and meantime overcome the cosmic problems and difficulties in terms of the well-developed physics without needing any other HEs.

The BHU is simple and significant because it does not rely on any HEs, but can fully explain the observations of the universe and overcome the cosmic problems and difficulties in terms of well-developed physics. It is also complete because the entire spacetime is infinite without unknown outside and prehistory. In the previous studies, the author has comprehensively explained various aspects of the universe, including its origin, structure, evolution, expansion, acceleration, cosmic microwave background (CMB) radiation, entropy, emissions of dynamic starlike, massive, and supermassive black holes such as gamma ray bursts, X-ray flares from galactic centers, and quasars, and so on [5-12]. However, the structure of the entire spacetime previously developed was only down to the level of the child universes of our black hole universe, i.e. the observed starlike, massive, and/or supermassive black holes. This study extends the structure of the entire spacetime into the deep insides of the child universes. This effort will provide us a complete structure of the entire spacetime and meantime shows us a brand new view to the insides of black holes, which may solve the black hole singularity issue.

2 Complete structure of the entire spacetime

According to the black hole model of the universe, our four-dimensional (4D) spacetime universe is a black hole, which is an extremely suppermassive and has been fully expanded with mass about a half hundred sextillions of solar masses, radius about forty-three hundred Mpc (or one Hubble length), and surface gravitational field about one third nanometer per second square [5-6]. All the inside, currently observed, starlike, massive, and/or supermassive black holes are subspacetimes (or child universes) of our black hole universe. Figure 2 shows the two-level or layer structure of any sized black hole or spacetime, including our black hole universe, and its child black holes. A black hole is a spacetime and its child black holes are its subspacetimes. For our black hole universe, the child universes or subspacetimes are the observed starlike, massive, and/or supermassive black holes. This hierarchically layered structure of spacetimes and subspacetimes genuinely overcomes the horizon problem, which was identified to exist in the big bang model of the universe primarily by Charles Misner in 1960s [13] and solved by Alan Guth in 1980s with the hypothesis of cosmic inflation [14] according to a field that does not correspond to any physical field. Therefore, in the black hole model of the universe, there does not exist the horizon problem at all. The scale of a black hole or spacetime should be much larger than that of its child black holes or subspacetimes.

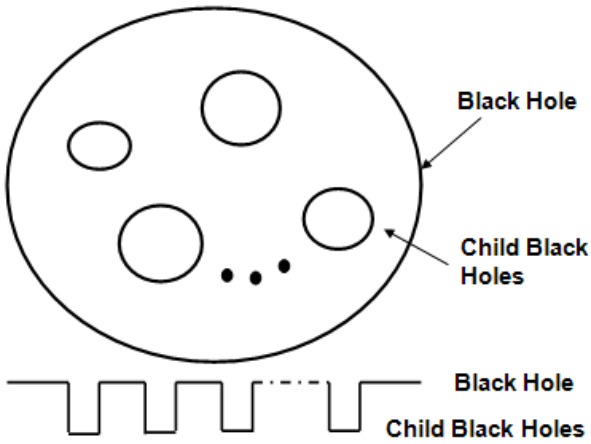

Fig. 2: The two-level or layer structure of a black hole or spacetime. Inside a black hole or spacetime, there are a number of child black holes or subspacetimes. For an example, inside our black hole universe, there are a number of child black hole universes or subspacetimes, which are the observed starlike, massive, and/or supermassive black holes.

Inside a black hole or spacetime, there are a number of child black holes or subspacetimes rather than singularity at the center as described conventionally. Outside a black hole or spacetime, there are a number of parallel sister black holes or spacetimes. Figure 3 shows a three-level or layer structure of a black hole or spacetime with both its inside and outside. The black hole or spacetime and all the parallel sister black holes or spacetimes are child black holes or subspacetimes of the mother black hole. Here, for the sketch to be simple, we have only drawn, inside each black hole or spacetime, three child black holes or subspacetimes. For our black hole universe, the observed starlike, massive, and/or supermassive black holes are its child universes or subspacetimes. The outside parallel universes are its sister universes. Our black hole universe and all the parallel sister universes are child universes or subspacetimes of the mother universe. Figure 4 sketches the four layers of the black hole universe from the child universe up to the grandmother universe which contains the aunt universes, mother universe, sister universes, cousin universes, our universe itself, child universes, and niece uni-

verses. Here again for the sketch to be simple, we only drew three universes for each layer. If the whole space is finite, then the matter in the whole space is finite and thus the number of layers is finite. Otherwise, it has infinite layers and the outermost layer corresponds to the limit of zero degree for the absolute temperature, zero for the density, and infinity for the radius and mass. A complete cosmological model suggests that the entire universe or spacetime must be infinite. For the black hole universe model to appropriately explain CMB, we favored and suggested that the entire spacetime to be infinite and eternal and include infinite universes, which are layered hierarchically [7].

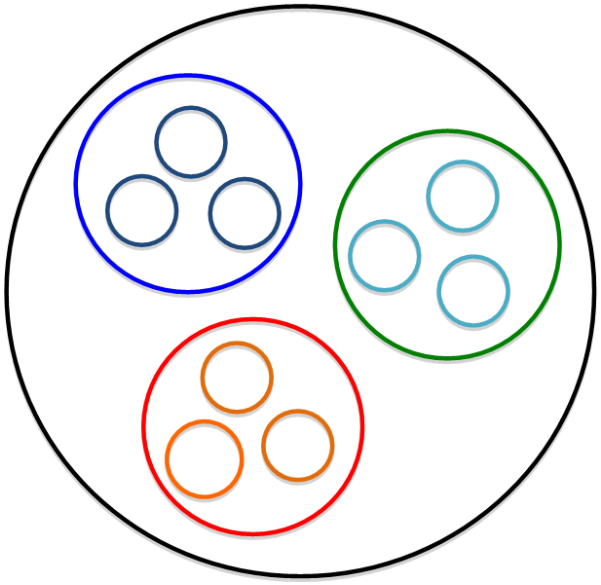

Fig. 3: The three-level or layer structure of a black hole or spacetime. Inside a black hole or spacetime (e.g. the one coded as green), there are a number of child black holes or subspacetimes. Outside the black hole or spacetime, there are a number of sister black holes (e.g., the ones coded as blue and red, respectively). Inside each of sister black holes, there are also a number of its child black holes. The black hole and all sister black holes are all the child black holes or subspacetimes of the mother black hole (coded as black). For our black hole universe, its inside has a number of the child black hole universes or subspacetimes, which are the observed starlike, massive, and/or supermassive black holes. Its outside has a number of sister black hole universes. Our black hole universe and all sister black hole universes are child black hole universes of the mother black hole universe.

For the infinite entire spacetime (called the grand universe), it has infinite layers [5-6, 12]. Figure 5 shows the infinite hierarchically layered structure of the infinite entire spacetime. The top layer is the entire spacetime, i.e. the grand universe, whose mass (M), radius (R), and entropy (S) are infinitely large; while the density (ρ) and temperature (T) (hence pressure) are infinitely small. The bottom layer is the layer of child universes, which are finite, referring to the

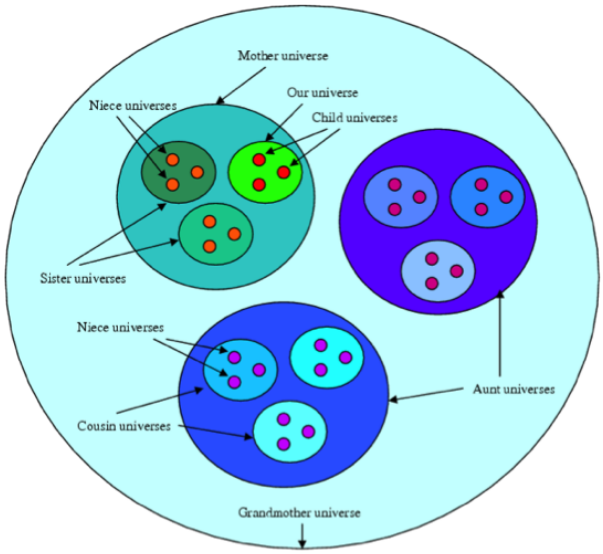

Fig. 4: The four-level or layer structure of our black hole universe up to the grandmother universe [5]. Inside our universe, there are a number of child universes, which are the observed starlike, massive, and/or supermassive black holes. Outside our universe, there are a number of sister universes who also have their own child universes named as niece universes. Our universe and all sister universes are child universes or subspacetimes of the mother universes. Parallel to the mother universe, there are a number of aunt universes who also have their child and grandchild universes or subspacetimes. The mother universe and all aunt universes are child universes or subspacetimes of the grandmother universe.

observed starlike, massive, and/or supermassive black holes. The second layer from the bottom is our universe. The child universe is a subspacetime of our universe; our universe is a subspacetime of the mother universe; the mother universe is a subspacetime of the grandmother universe, and so on. This infinitely layered structure of the entire spacetime can also be represented by using the mathematical set concepts as U = {...{F, F, F, ...{G, G, G, ...{A, A, A, ...{S, S, S, ...{C, C, C, ..., C}}}}...}. Here the child universes (also the niece universes) are null sets (i.e. C = { } and N = { }); the sister universes are sets of niece universes, S = {N, N, N, ...N}; our universe is a set of child universes, O = {C, C, C, ..., C}; the mother universe is the set of our universe and sister universes, M = {S, S, S, ..., O}; the aunt universes are sets of cousin universes, A = {Co, Co, Co, ..., Co}; the grandmother universe is the set of aunt universes and the mother universe, G = {A, A, A, ..., M}; and so on. The grand universe or the entire spacetime U is the grand set of all universes.

This previously developed infinitely layered structure of the infinite entire universe may not be complete, since it does not give what there are inside the child black hole universes. The structure of the entire universe shown in Figure 5 is only from the grand universe down to the child universes, which are currently observed starlike, massive, and/or supermassive

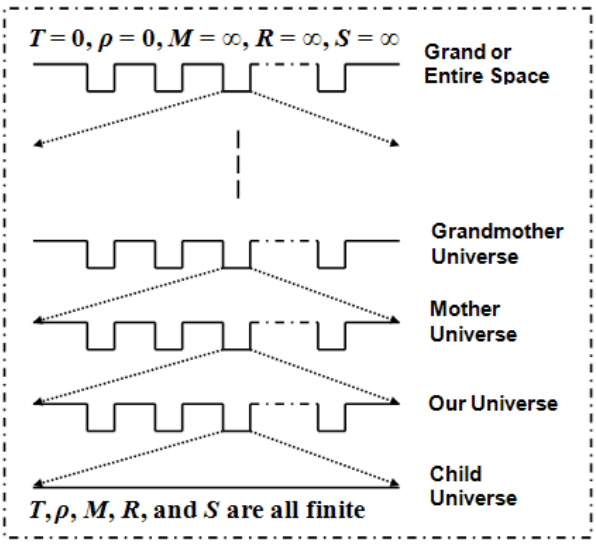

Fig. 5: The hierarchically layered structure of the entire universe, previously developed [6, 12]. It is incomplete because the bottom layer is only down to the child universes, suggested to be empty spacetimes or null sets. The child universes are subspacetimes of the universe in which we live in. Similarly, our universe is a subspacetime of the mother universe, and so on. The top or outmost layer is the entire space of all subspacetimes.

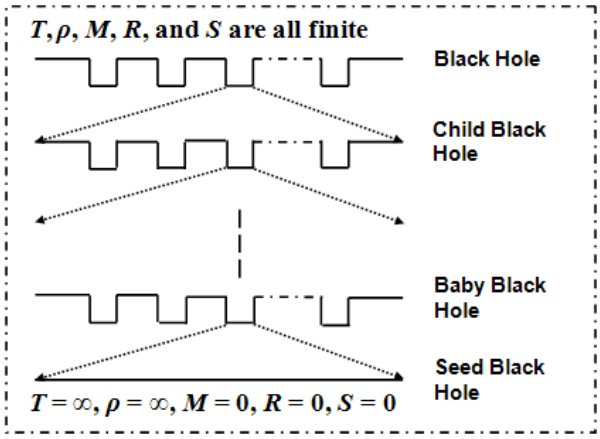

Fig. 6: The hierarchically layered structure of black holes or child black hole universes. Inside any sized black hole or spacetime, which is homogeneous and isotropic in the large or spacetime scale according to Newton's cosmological principle, there are a number of child black holes or subspacetimes. Inside a child black hole, there are a number of grandchild black holes, and so on in analogy. The bottommost is the seed black holes, which are infinitely small and are child black holes or subspacetime of a baby black holes.

blackholes. To have a complete structure of the entire spacetime, we need construct the inside of the child universes. According to Figure 2, any sized black hole or spacetime has a number of its child black holes or subspacetimes, like our black hole universe that has a great number of starlike, massive, and/or supermassive black holes as the child black hole universes. Therefore, inside a starlike, massive, or supermassive black hole, there may be in general a number of child black holes; inside a child black hole, there may be a number of grandchild black holes, and so on (see Figure 6). The innermost or bottommost layer is called seed black holes, which are infinitely small in size, mass, and entropy, but have infinitely large density, temperature, and pressure. The seed black holes are the child black holes of a baby black hole. This infinitely layered structure for the inside of a black hole or a spacetime can also be represented by using the mathematical set concepts. A black hole is a set of child black holes; a child black hole is a set of grandchild black holes, and so on in analogy. The baby black hole is a set of seed black holes, which are represented as null sets. A seed black hole has infinitely small mass, radius, and entropy, but infinitely large density, temperature, and pressure.

This hierarchically layered structure of a black hole provides us a completely new view to the inside of a black hole. At present, on what the inside of a black hole is, it is still an unsolved big open mysterious question in physics, since the Einsteinian general relativity is failed to be applicable to describe the inside of a black hole. Conventionally, most of scientists believe that matter once falling into a black hole will be gravitationally collapsed or drawn to the center point and form a dreaded singularity, where the known laws of physics break down and thus the picture of a black hole inside can be no longer trusted. As the matter inside a black hole is all drawn to the singular point at the center, there should be no matter and hence empty within the event horizon, except for the singular point at the center, which contains all matter of the black hole and thus has infinite density and temperature (see Figure 7). The matter density may be represented as the delta function of the radial distance. A recent notable study suggests that black hole are holograms [15]. This black hole holographic hypothesis considers a black hole as a holographic projection from a flat system of quantum particles that remains gravity-free. Though it may solve the clash between general relativity and quantum mechanics, the hologram model of black hole is still not fully understood. According to the black hole universe model, spacetime and black hole are equivalent. Our universe is a black hole and the observed starlike, massive, and/or supermassive black holes are subspacetimes of our 4D spacetime universe. The Einsteinian general relativity, a theory that describes the effect of matter on spacetime, is applicable to also describe the matter effect on a subspacetime, i.e. the inside of a black hole. The matter inside a black hole does not fall into the center point to form a singular point, but may form a number of child black holes or subspacetimes, which have scales much smaller than the black hole. The infinitely layered structure of a black hole as shown in Figure 6 shows the inside of a black hole to be infinite asymptotically singular spacetmes.

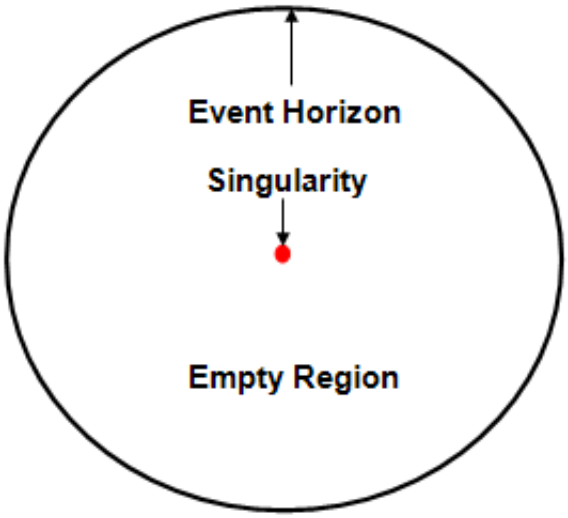

Fig. 7: The singularity of black hole. Conventionally, the matter falling into a black hole will be gravitationally collapsed or drawn to the center point and form a dreaded singularity, where the matter density goes to infinity. This will leads to the most interior region of a black hole does not have matter or is an empty space.

Considering the starlike, massive, and/or supermassive black holes to be child universes of our black hole universe, we can have the hierarchically layered structure of a child black hole universe from the hierarchically layered structure of a black hole given by Figure 6 through replacing the words "Black Hole" by "Child Universe", "Child Black Hole" by "Grandchild Universe", "Baby Black Hole" by "Baby Universe", and "Seed Black Hole" by "Seed Universe", and so on in analogy (see Figure 8). Then, combining Figure 5, which shows the infinite hierarchically layered structure of the entire spacetime that the author previously developed with the bottommost layer to be the child universes, with Figure 8, which shows the infinite hierarchically layered structure of the child universe, we can obtain the complete structure of the entire spacetime as shown in Figure 9. The top layer is the entire spacetime (or grand universe), whose mass, radius, and entropy are infinitely large; while the density, temperature, and pressure are infinitely small. The bottom layer is the layer of seed universes, whose mass, radius, and entropy are infinitely small; while the density, temperature, and pressure are infinitely large. The second layer from the bottom is the layer of baby universe. It is the mother universe of the seed universe. Infinitely going up in analogy, we have the layer of grandchild universes which are child universes or subspacetimes of the child universe of our universe. Our universe is a subspacetime of the mother universe; the mother universe is a subspacetime of the grandmother universe; and so on. This infinitely layered complete structure of the entire spacetime can also be represented by using the mathematical set concepts as U = {...{F, F, F, ...{G, G, G, ...{A, A, A, ...{S, S, S, ...{C, C, C, ..., {Gc, Gc, Gc, ...{....{Ba, Ba, Ba, ...{Se, Se, Se, ...} }...}}}}}}...}. The radii or masses of these universes, from the entire spacetime or grand universe to the seed universes, can be $\{\infty^{\infty}$, ..., ∞^{N}, ..., ∞^{2}, ∞^{1}, ..., M^{N}, ..., M^{2}, M, 1, M^{-1}, M^{-2}, ..., M^{-N}, ..., ∞^{-1}, ∞^{-2}, ..., ∞^{-N}, ..., $\infty^{-\infty}\}$ or simply say from infinitely large ∞^{∞} to infinitely small $\infty^{-\infty}$. This clear structure or picture of the entire spacetime exhibits the completeness of the black hole universe model. Any cosmological model without clearly describing its outside and inside cannot be a complete cosmology. Our next paper will establish the full origin and evolution of the entire spacetime and further give a full description not only to the present universe, but also its past and future or pre- and post-histories.

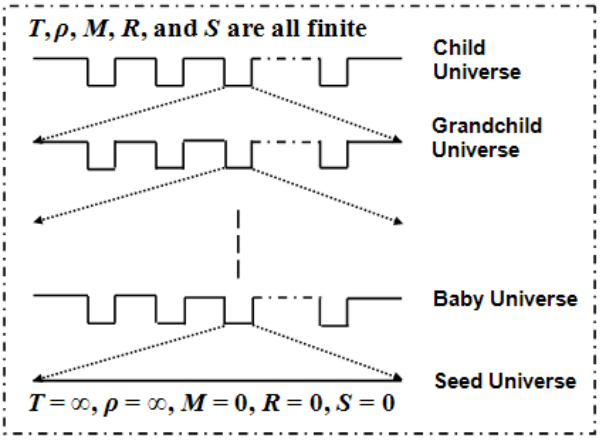

Fig. 8: The hierarchically layered structure of a child universe. Inside a child universe, there are a number of grandchild universes; inside a grandchild universe, there are a number of grand-grandchild universes; and so on in analogy. The bottommost layer is the level of seed universes, which are child universes or subspacetimes of a baby universe.

3 Summary

This study has established a complete structure for the infinite entire spacetime to be infinite hierarchically layered. First, we have constructed the internal structure of black holes or child universes as shown in Figure 6 or Figure 8. Then, we have combined the infinite hierarchically layered structure for the inside of child universes shown in Figure 8 with the previously developed infinite hierarchically layered structure of the entire spacetime that was only down to the child universes shown in Figure 5 to form the complete structure of the entire spacetime that is down to the infinitely small seed universes shown in Figure 9. The top layer is the entire spacetime, i.e. the grand universe, which has infinitely large mass, radius, and entropy and infinitely small density, temperature, and pressure. The bottom layer is the layer of seed universes, which has infinitely small mass, radius, and entropy and infinitely large density, temperature, and pressure. From the infinitely large top layer of the entire spacetime or the grand

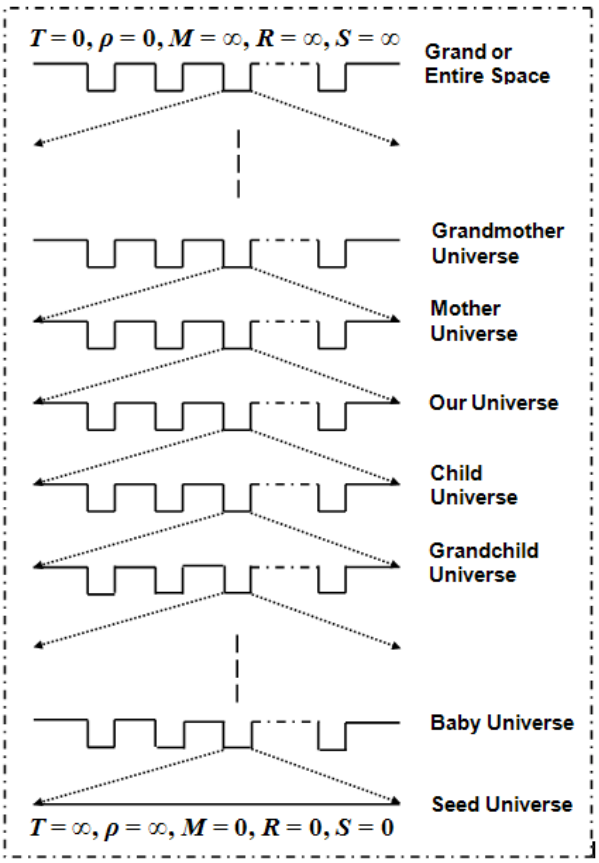

Fig. 9: The complete structure of the entire spacetime. The top or outermost layer is the entire spacetime, which is infinitely large. The bottom or innermost layer is the seed universe, which is infinitely small. The second layer from the bottom is the baby universe, which is the mother universe of the seed universe. Infinitely going up or out in analogy, they are grandchild, child, and our universes. Our universe is a subspacetime of the mother universe; the mother universe is a subspacetime of the grandmother universe; and so on.

universe to the infinitely small bottom layer of the seed universes, there are infinite layers. Our universe is about the middle finite large layer. Above or outside our universe, there are mother universes, grandmother universes, and so on. Below or inside our universe, there are child universes, grandchild universes, and so on. In addition to the complete structure of the entire spacetime, this study has also revealed the inside of black hole or child universes. This provides us a complete new view to the inside of black holes and a unique solution of the spacetime singularity as infinite asymptotically singular spacetimes.

Acknowledgements

The work was partially supported by the NSF/REU program (Grant #: PHY-1559870). The author is also thankful to the University's Title III Program for travel support of his attending conferences.

Received on August 10, 2022

References

1. Einstein A. Die Grundlage der Allgemeinen Relativitatstheorie. *Annalen der Physik*, 1916, v. 354, 769–822.
2. Friedmann A. Über die Möglichkeit einer Welt mit konstanter negativer Krümmung des Raumes. *Zeitschrift für Physik*, 1924, v. 21, 326–332.
3. Arp H. *et al*. An Open Letter to the Scientific Community – Signed by Scientists/Engineers/Researchers. *New Scientist*, 22 May 2004.
4. Zhang T. X. A New Cosmological Model: Black Hole Universe. *American Astronomical Society 211st Meeting*, 2007, Abstract #152.04.
5. Zhang T. X. A New Cosmological Model: Black Hole Universe. *Progress in Physics*, 2009, v. 2, 3–11.
6. Zhang T. X. Principle of Spacetime and Black Hole Equivalence. *Progress in Physics*, 2016, v. 12, 353–361.
7. Zhang T. X. Cosmic Microwave Background Radiation of Black Hole Universe. *Astrophysics and Space Science*, 2010, v. 330, 157–165.
8. Zhang T. X. Quasar Formation and Energy Emission in Black Hole Universe. *Progress in Physics*, 2012, v. 3, 48–53.
9. Zhang T.X. Frederick C. Acceleration of Black Hole Universe. *Astrophysics and Space Science*, 2014, v. 349, 567–573.
10. Zhang T. X.v Gamma Ray Bursts and Black Hole Universe. *Astrophysics and Space Science*, 2015, v. 358, article.id. #14, DOI 10.1007/s10509-015-2409-1, 8 pp.
11. Zhang T. X., Wilson C. & Schamschula M P. X-ray Flares from Sagittarius A* and Black Hole Universe. *Progress in Physics*, 2016, v. 12, 61–67.
12. Zhang T. X. The Principles and Laws of Black Hole Universe. *Journal of Modern Physics*, 2018, v. 9, 1838–1859.
13. Misner C. W., Coley A. A., Ellis G. F. R., Hancock M. The Isotropy of the Universe. *The Astrophysical Journal*, 1968, v. 151, 431–457.
14. Guth A. H. Inflationary Universe: A Possible Solution to the Horizon and Flatness Problems. *Physical Review D*, 1981, v. 23, 347–356.
15. Rinaldi E. *et al*. Matrix-Model Simulations Using Quantum Computing Deep Learning and Lattice Monte Carlo. *PRX Quantum*, 2022, v. 3, 0120324.

Lamb Shift in Discrete Time

Young Joo Noh

E-mail: yjnoh777@gmail.com, Seongnam, Korea

Lamb shift is the energy difference between the two energy levels of $2S_{1/2}$ and $2P_{1/2}$ of a hydrogen atom. This cannot be explained by the existing relativistic quantum mechanics, but was explained by the interaction of electrons and vacuum in quantum field theory. However, in this paper, I tried to explain the Lamb shift as a result of the previous paper [1] that causal delay in a discrete time perspective causes the charge change. As a result, the charge change caused an additional energy change in the existing fine structure of hydrogen, and the value was approximated.

1 Introduction

In my previous paper [1], I showed that the concept of causal delay in discrete time provides a correction for minimal coupling in electromagnetic interactions, and that this correction causes energy-scale-dependent changes in the charge and mass of elementary particles. An application example of such a result was attempted to explain the anomalous magnetic moment. In this paper, I will try to explain Lamb shift as another application example.

Like the anomalous magnetic moment, the Lamb shift is not explained by the existing relativistic quantum mechanics, but by the quantum field theory, a completely different paradigm. However, the changes in charge and mass due to the concept of causal delay open the possibility that these can be explained within the scope of modified relativistic quantum mechanics.

2 Nonrelativistic approximation of the modified Dirac equation

In the previous paper [1], it was shown that the Hamiltonian of electromagnetic interacting particles in terms of causal delay and the newly defined charge and mass dependent on energy scales are as follows

$$\mathrm{H} - q'\phi = \vec{\alpha}\cdot\left(\vec{p} - q'\vec{A}\right) + \beta m' \,, \tag{1}$$

where

$$\begin{aligned} m' &= f_{1r} m \\ q' &= (1 - f_{2r})\, q \end{aligned} \tag{2}$$

$$\begin{aligned} f_{1r} &= \mathrm{Re}\,(f_1) = \frac{1}{3}\,\mathrm{Re}\left(\frac{\mathrm{e}^{-i\Delta x\cdot p}}{\mathrm{e}^{-i\Delta x\cdot p} + 2\left(\mathrm{e}^{-i\Delta x\cdot\Delta p} - 1\right)}\right) \\ f_{2r} &= \mathrm{Re}\,(f_2) = \frac{1}{3}\,\mathrm{Re}\left(\frac{2\mathrm{e}^{-i\Delta x\cdot\Delta p}}{\mathrm{e}^{-i\Delta x\cdot p} + 2\left(\mathrm{e}^{-i\Delta x\cdot\Delta p} - 1\right)}\right). \end{aligned} \tag{3}$$

The Dirac equation satisfied by the electromagnetic interacting particle with mass m' and charge q' is as follows when expressed with two-component spinors ψ_A and ψ_B

$$(H - q'\phi)\begin{pmatrix}\psi_A\\ \psi_B\end{pmatrix} = \vec{\alpha}\cdot\left(\vec{p} - q'\vec{A}\right)\begin{pmatrix}\psi_A\\ \psi_B\end{pmatrix} + \beta m'\begin{pmatrix}\psi_A\\ \psi_B\end{pmatrix}. \tag{4}$$

Eq. (4) becomes the following system of equations

$$\begin{aligned} (H - q' - m')\,\psi_A &= \vec{\sigma}\cdot\left(\vec{p} - q'\vec{A}\right)\psi_B \\ (H - q' + m')\,\psi_B &= \vec{\sigma}\cdot\left(\vec{p} - q'\vec{A}\right)\psi_A \,. \end{aligned} \tag{5}$$

Since $\vec{A} = 0$ and ϕ is static in a hydrogen atom,

$$\psi(\vec{r}, t) = \mathrm{e}^{-iEt}\psi(\vec{r}), \quad E = m' + \varepsilon \,. \tag{6}$$

Then, in the second of (5), the following expression is obtained

$$\begin{aligned} (E - q'\phi + m')\,\psi_B(\vec{r}) &= \vec{\sigma}\cdot\vec{p}\,\psi_A(\vec{r}) \\ \psi_B(\vec{r}) &= (2m' + \varepsilon - q'\phi)^{-1}\,\vec{\sigma}\cdot\vec{p}\,\psi_A(\vec{r}) \\ &\cong \frac{1}{2m'}\left(1 - \frac{\varepsilon - q'\phi}{2m'}\right)\vec{\sigma}\cdot\vec{p}\,\psi_A(\vec{r}) \,. \end{aligned} \tag{7}$$

Since m' and q' are only parameters, the first of (5) is as follows

$$\begin{aligned} (\varepsilon - q'\phi)\,\psi_A &= \vec{\sigma}\cdot\vec{p}\,\frac{1}{2m'}\left(1 - \frac{\varepsilon - q'\phi}{2m'}\right)\vec{\sigma}\cdot\vec{p}\,\psi_A \\ &= \frac{q'}{4m'^2}\,(\vec{\sigma}\cdot\vec{p}\phi)\,(\vec{\sigma}\cdot\vec{p}\psi_A) + \\ &\quad + \frac{1}{2m'}\left(1 - \frac{\varepsilon - q'\phi}{2m'}\right)(\vec{\sigma}\cdot\vec{p})^2\,\psi_A \,. \end{aligned} \tag{8}$$

Therefore, the results of the relativistic correction of the modified Dirac equation can be obtained as follows

$$\begin{aligned} \varepsilon\psi_A &= \left\{\frac{\vec{p}^2}{2m'} + q'\phi - \frac{\vec{p}^4}{8m'^3} - \frac{q'}{4m'^2}\nabla\phi\cdot\nabla + \right. \\ &\quad \left. + \frac{q'}{4m'^2}\,\vec{\sigma}\cdot(\nabla\phi\times\vec{p})\right\}\psi_A \\ &= \left\{H'_0 + H'_{rel} + H'_D + H'_{SO}\right\}\psi_A \,. \end{aligned} \tag{9}$$

Eq. (9) is the same as just replacing m and q with m' and q' in the existing equation. In Section 3, I briefly review the fine structure of hydrogen, and in Section 4, how m' and q' of each term in (9) change the fine structure will be discussed. This discussion will be limited to only $2S_{1/2}$ and $2P_{1/2}$.

3 Fine structure of hydrogen

The Hamiltonian representing the fine structure of hydrogen is as follows

$$H = \frac{\vec{p}^2}{2m} - \frac{\alpha}{r} - \frac{\vec{p}^4}{8m^3} + \frac{1}{8m^2}\nabla^2 V_C + \frac{\alpha}{2m^2}\frac{\vec{S}\cdot\vec{L}}{r^3} = H_0 + H_{rel} + H_D + H_{SO}\,. \tag{10}$$

The changes in the energy of $2S_{1/2}$ and $2P_{1/2}$ by the last three terms of (10) are known as follows. Eq. (11) is the expectation value of each Hamiltonian, and the subscripts S and P denote $2S_{1/2}$ and $2P_{1/2}$

$$\begin{aligned}\Delta_{rel} &= \langle H_{rel}\rangle_S - \langle H_{rel}\rangle_P = -\frac{1}{12}\,m\alpha^4\\ \Delta_D &= \langle H_D\rangle_S - \langle H_D\rangle_P = \langle H_D\rangle_S = \frac{1}{16}\,m\alpha^4\\ \Delta_{SO} &= \langle H_{SO}\rangle_S - \langle H_{SO}\rangle_P = -\langle H_{SO}\rangle_P = \frac{1}{48}\,m\alpha^4\,.\end{aligned} \tag{11}$$

According to (11), the relativistic correction term lowers the energy of both $2S_{1/2}$ and $2P_{1/2}$, but the energy value of $2S_{1/2}$ has a lower energy value than $2P_{1/2}$ by $m\alpha^4/12$, and the Darwin term increases only the energy of $2S_{1/2}$ by $m\alpha^4/16$, and spin-orbit term lowers the energy of only $2P_{1/2}$ by $m\alpha^4/48$. The sum of all three effects is 0, so the energies of $2S_{1/2}$ and $2P_{1/2}$ are the same as a result. In other words, the Lamb shift cannot be explained by the existing relativistic quantum mechanics.

However, as we will see in the next chapter, the change in charge due to the causal delay effect causes a slight change in the expectation value of each Hamiltonian, which may explain the Lamb shift.

4 Corrections of fine structure

4.1 Modified Coulomb potential energy

First, let's try to find the charges q'_e and q'_p of the electron and the proton interacting in a hydrogen atom from (2)

$$\begin{aligned}q'_p &= \left(1 - f^p_{2r}\right)e\\ q'_e &= -\left(1 - f^e_{2r}\right)e\,.\end{aligned} \tag{12}$$

In a reference frame where the proton is at rest, first about the proton*,

$$\begin{aligned}&p_\mu = \left(E_p = m_p, 0, 0, 0\right)\ \ ,\ \ \Delta p_\mu = 0\\ &\Delta x\cdot p = E_p\,\Delta t_p = 1.\end{aligned} \tag{13}$$

$$q'_p = \left(1 - \frac{1}{3}\,\mathrm{Re}\left(\frac{2\mathrm{e}^{-i\Delta x\cdot\Delta p}}{\mathrm{e}^{-i\Delta x\cdot p} + 2\left(\mathrm{e}^{-i\Delta x\cdot\Delta p} - 1\right)}\right)\right)e = \left(1 - \frac{2}{3}\,\cos 1\right)e \equiv de\,. \tag{14}$$

About the electron,

$$\begin{aligned}\Delta x\cdot p &= \Delta t_e\left(E - \frac{\vec{p}^2}{\gamma m_e}\right) \cong \Delta t_e\; m_e = 1\\ \Delta x\cdot\Delta p &= \Delta t_e\left(\Delta E - \frac{\vec{p}\cdot\Delta\vec{p}}{\gamma m_e}\right) = \Delta t_e\;\Delta V\,.\end{aligned} \tag{15}$$

Using (15) and $\Delta p \ll p$, we get

$$\begin{aligned}q'_e &= -\left(1 - \frac{1}{3}\,\mathrm{Re}\left(\frac{2\mathrm{e}^{-i\Delta x\cdot\Delta p}}{\mathrm{e}^{-i\Delta x\cdot p} + 2\left(\mathrm{e}^{-i\Delta x\cdot\Delta p} - 1\right)}\right)\right)e\\ &= -\frac{2 - \frac{2}{3}\,\cos(\Delta x\cdot p)}{9 - 8\,\cos(\Delta x\cdot\Delta p)}\,e = \frac{-(d+1)\,e}{9 - 8\,\cos(\Delta t_e\;\Delta V)}\,.\end{aligned} \tag{16}$$

If the potential due to the proton is defined as (17), the $q'\phi$ related to the potential energy of the electron in (9) becomes (18)

$$\phi \equiv \frac{q'_p}{r}\,. \tag{17}$$

$$\begin{aligned}q'_e\phi &= -\frac{k\alpha}{r\,(9 - 8\,\cos(\Delta t_e\;\Delta V))}\,,\\ k &\equiv d\,(d+1) = 1.049\,.\end{aligned} \tag{18}$$

What we now need to do is to find the explicit expression for ΔV in (18). In (3), Δp represents the change in the momentum of an electron due to the interaction, which means that when the momentum of a free electron is p, the electromagnetic field is "turned on" and the momentum after the interaction is $p + \Delta p$. Therefore, in (18), ΔV means the value obtained by subtracting the potential energy of the free electron from the potential energy of the electron in a hydrogen atom, that is, Coulomb potential energy $-\alpha/r$. And, since $\Delta t_e = 1/m$,

$$q'_e\phi = -\frac{k\alpha}{r\,(9 - 8\,\cos(\alpha/mr))}\,. \tag{19}$$

At (19), $q'_e\phi$ is not exactly equal to the potential energy of the electron. Eq. (19) becomes $-k\alpha/r$ for large r, so it is somewhat different from the Coulomb potential energy $-\alpha/r$. So, to be equal to the Coulomb potential energy at a large r, the modified Coulomb potential energy must be defined as follows

$$V_m \equiv \frac{q'_e\phi}{k} = -\frac{\alpha}{r\,(9 - 8\,\cos(\alpha/mr))}\,. \tag{20}$$

Eq. (20) approximates the Coulomb potential energy well at large r. For example, at Bohr radius $a_0 = 1/m\alpha$, the ratio of modified Coulomb potential energy to Coulomb potential energy is as follows

$$\frac{V_m}{V_C} = \frac{1}{9 - 8\,\cos\alpha^2} = 0.99999999\,. \tag{21}$$

However, for small r, especially around $r = b \equiv \alpha/m = a_0\,\alpha^2 = 2.82\times10^{-15}$ m, that is, the closer to the proton (proton

*See the definition of causal delay time $\Delta t \equiv 1/m$ in the previous paper [1].

radius $r_p = 0.84 \times 10^{-15}$ m), the more it deviates from the Coulomb potential energy.

Considering the potential energy in the proton, assuming that the charges are uniformly distributed, the potential energy is a linear function with respect to r^2, so the overall potential energy function is as follows

$$\begin{aligned} r < r_p : V_{in} &= \frac{\alpha}{2r_p}\left[\left(\frac{r}{r_p}\right)^2 - 1.12\right] \\ r \geq r_p : V_m &= -\frac{\alpha}{r(9 - 8\,\cos(b/r))}\,. \end{aligned} \tag{22}$$

At $r < r_p$, the effect of fine structure by (10) is negligible, and the same is true for (9).

4.2 Mass change effect

As can be seen from (2), the mass also changes according to the energy scale. We discuss how the change in mass affects the energy of the electron in hydrogen. The energy of the electron is

$$E = \sqrt{m^2 + \vec{p}^2} + V \cong m + \frac{\vec{p}^2}{2m} - \frac{\vec{p}^4}{8m^3} + V\,. \tag{23}$$

In (23), $\vec{p}^2/2m$ and V are in order of $m\alpha^2$, and $-\vec{p}^4/8m^3$ is in order of $m\alpha^4$. Meanwhile, $\vec{p}^2/2m + V$ is invariant with respect to mass change. The reason is that, when the charge is constant, $mv^2/r = -e|\vec{E}|$, the change in mass cancels out the change in velocity. Thus, the energy change due to mass change appears in the term $-\vec{p}^4/8m^3$, which is α^2 times smaller than $\vec{p}^2/2m$ or V. That is, the energy change given by the mass change is α^2 times the energy change due to the charge change, so it can be ignored. Therefore, mass will be treated as a constant from now on.

Now, let's examine how each of the terms in (9) changes the fine structure.

4.3 Nonrelativistic term

$$H_0' = \frac{\vec{p}^2}{2m} + kV_m \Rightarrow \frac{\vec{p}^2}{2m} + V_m\,. \tag{24}$$

$P^2/2m + V_m$ in (24) is used to converge to the nonrelativistic Hamiltonian H_0 at large r. This is possible because the physics is invariant to the gauge transformation of electromagnetic potential energy. Also, convergence to the nonrelativistic Hamiltonian H_0 at large r means that each term of H' can be considered as a perturbation to H_0.

Now we need to find the expectation value $\langle H_0'\rangle_{S,P}$. In (10), the expectation value of H_0 is $\langle H_0\rangle = \langle V_C\rangle/2$ by the virial theorem, which does not strictly apply to H_0'. However, since the expectation value of H_0' mostly contributes to the large r part, and $V_m \cong V_C$ in the large r, the virial theorem can be approximately applied to the expectation value of H_0'. Thus

$$\left\langle H_0'\right\rangle_{S,P} \cong \frac{\langle V_m\rangle_{S,P}}{2}\,. \tag{25}$$

What we want to calculate is

$$\Delta_0' = \left\langle H_0'\right\rangle_S - \left\langle H_0'\right\rangle_P = \frac{1}{2}\left\{\langle V_m\rangle_S - \langle V_m\rangle_P\right\}\,. \tag{26}$$

And the function of the eigenstates $2S_{1/2}$ and $2P_{1/2}$ to be used in the calculation, that is, the solution of the Schrödinger equation is as follows.

$$\begin{aligned} \psi_{n=2,l=0,m=0} &= \frac{1}{\sqrt{8\pi a_0^3}}\left(1 - \frac{r}{2a_0}\right)\mathrm{e}^{-r/2a_0} \\ \psi_{n=2,l=1,m=0} &= \frac{1}{4\sqrt{2\pi a_0^3}}\,\frac{r}{a_0}\,\mathrm{e}^{-r/2a_0}\,\cos\theta\,. \end{aligned} \tag{27}$$

Eq. (26) is calculated as follows

$$\begin{aligned} \langle V_m\rangle_S &= \int_{r_p}^{\infty} 4\pi r^2\,\frac{-\alpha}{r\,(9 - 8\,\cos(b/r))}\,\frac{1}{8\pi a_0^3}\times \\ &\quad\times\left(1 - \frac{r}{a_0} + \frac{r^2}{4a_0^2}\right)\mathrm{e}^{-r/a_0}\,dr \\ &= -\frac{m\alpha^6}{2}\int_{0.3}^{\infty}\frac{1}{9 - 8\,\cos(1/r')}\times \\ &\quad\times\left(r' - \alpha^2 r'^2 + \frac{\alpha^4}{4}r'^3\right)\mathrm{e}^{-\alpha^2 r'}\,dr'\ \ (r = br') \\ \langle V_m\rangle_P &= \int_{r_p}^{\infty} 4\pi r^2\,\frac{2}{3}\,\frac{-\alpha}{r(9 - 8\,\cos(b/r))}\times \\ &\quad\times\frac{1}{32\pi a_0^3}\,\frac{r^2}{a_0^2}\,\mathrm{e}^{-r/a_0}\,dr \\ &= -\frac{m\alpha^{10}}{24}\int_{0.3}^{\infty}\frac{1}{9 - 8\,\cos((1/r')}r'^3\mathrm{e}^{-\alpha^2 r'}\,dr' \\ \Delta_0' &= -\frac{m\alpha^6}{4}\int_{0.3}^{\infty}\frac{1}{9 - 8\,\cos(1/r')}\times \\ &\quad\times\left(r' - \alpha^2 r'^2 + \frac{\alpha^4}{6}\,r'^3\right)\mathrm{e}^{-\alpha^2 r'}\,dr'\,. \end{aligned} \tag{28}$$

Unfortunately, the integral of (28) cannot be calculated analytically, but can be approximated. In the above integral, the factor $1/(9 - 8\,\cos(b/r))$ converges to 1 at large r. Its shape resembles a step function. This means that the integral is dominant at large r, so it can be calculated with the factor $1/(9 - 8\,\cos(b/r)) \cong 1$. So

$$\begin{aligned} &\langle V_m\rangle_S \cong \langle V_C\rangle_S\,,\ \langle V_m\rangle_P \cong \langle V_C\rangle_P \\ &\therefore \Delta_0' \cong \frac{1}{2}\left\{\langle V_C\rangle_S - \langle V_C\rangle_P\right\} = 0\,. \end{aligned} \tag{29}$$

Consequently, it can be said that the energy difference between $2S_{1/2}$ and $2P_{1/2}$ by V_m is very small.

4.4 Relativistic correction term

$$H'_{rel} = -\frac{\vec{p}^4}{8m^3} = -\frac{1}{2m}(E - V_m)^2 \,. \tag{30}$$

In (30), E is the expectation value of H'_0, so the desired value is

$$\begin{aligned}\Delta'_{rel} &= \left\langle H'_{rel}\right\rangle_S - \left\langle H'_{rel}\right\rangle_P \\ &= -\frac{1}{2m}\Big\{\left(E_S^2 - E_P^2\right) - 2\left(E_S\left\langle V_m\right\rangle_S - E_P\left\langle V_m\right\rangle_P\right) + \\ &\quad + \left(\left\langle V_m^2\right\rangle_S - \left\langle V_m^2\right\rangle_P\right)\Big\} \\ &\cong -\frac{1}{2m}\left\{\left\langle V_m^2\right\rangle_S - \left\langle V_m^2\right\rangle_P\right\} \,.\end{aligned} \tag{31}$$

The first and second terms in the second line of (31) can be ignored by the results in the previous chapter $\langle V_m\rangle_S \cong \langle V_m\rangle_P, E_S \cong E_P$

$$\begin{aligned}\left\langle V_m^2\right\rangle_S &= \int_{r_p}^{\infty} 4\pi r^2 \frac{\alpha^2}{r^2\left(9 - 8\,\cos(b/r)\right)^2}\left|\psi_{200}\right|^2 dr \\ \left\langle V_m^2\right\rangle_P &= \int_{r_p}^{\infty} 2\pi r^2 \frac{2}{3}\frac{\alpha^2}{r^2\left(9 - 8\,\cos(b/r)\right)^2}\left|\psi_{210}\right|^2 dr \,.\end{aligned} \tag{32}$$

In (32), it is a rough approximation, but if we put factor $1/(9 - \cos(b/r))^2 \simeq 1$

$$\begin{aligned}&\left\langle V_m^2\right\rangle_S \simeq \left\langle V_C^2\right\rangle_S \,,\ \left\langle V_m^2\right\rangle_P \simeq \left\langle V_C^2\right\rangle_P \\ &\therefore \Delta'_{rel} \simeq -\frac{1}{2m}\left\{\left\langle V_C^2\right\rangle_S - \left\langle V_C^2\right\rangle_P\right\} = \Delta_{rel} \,.\end{aligned} \tag{33}$$

According to (33), the correction by the relativistic correction term is also expected to be small.

4.5 Spin-orbit term

$$\begin{aligned}H'_{SO} &= \frac{q'_e}{4m^2}\,\vec{\sigma}\cdot(\nabla\phi\times\vec{p}) \\ &= \frac{k\alpha}{2m^2}\,\frac{1}{9 - 8\,\cos(b/r)}\,\frac{\vec{S}\cdot\vec{L}}{r^3} \\ &= \frac{1}{2m^2}\,\frac{kV_m}{r^2}\,\vec{S}\cdot\vec{L} \,.\end{aligned} \tag{34}$$

In (34), the spin-orbit term H'_{SO} is also expressed as modified Coulomb potential energy. This means that the gauge transformation can be performed so that H'_{SO} also converges to H_{SO} at large r. Thus

$$H'_{SO} = \frac{1}{2m^2}\,\frac{V_m}{r^2}\,\vec{S}\cdot\vec{L} \,. \tag{35}$$

On the other hand, using (36),

$$\begin{aligned}&\left\langle nljm_j\left|\vec{S}\cdot\vec{L}\right|nljm_j\right\rangle = \frac{1}{2}\left\{j(j+1) - l(l+1) - \frac{3}{4}\right\} \\ &\left\langle\vec{S}\cdot\vec{L}\right\rangle_S = 0 \,,\ \left\langle\vec{S}\cdot\vec{L}\right\rangle_P = -1 \,.\end{aligned} \tag{36}$$

Expectation values are:

$$\begin{aligned}\left\langle H'_{SO}\right\rangle_S &= 0 \\ \left\langle H'_{SO}\right\rangle_P &= -\frac{\alpha}{2m^2}\left\langle\frac{1}{9 - 8\,\cos(b/r)}\,\frac{1}{r^3}\right\rangle_P \\ &\cong -\frac{\alpha}{2m^2}\left\langle\frac{1}{r^3}\right\rangle_P = \left\langle H_{SO}\right\rangle_P \,.\end{aligned} \tag{37}$$

The difference between the spin-orbit term before and after charge correction is

$$\Delta'_{SO} - \Delta_{SO} = -\left\langle H'_{SO}\right\rangle_P + \left\langle H_{SO}\right\rangle_P \cong 0 \,. \tag{38}$$

Therefore, the charge change has little contribution to the spin-orbit term.

4.6 Darwin term

$$H'_D = -\frac{q'_e}{4m^2}\,\nabla\phi\cdot\nabla \,. \tag{39}$$

If we get the expectation value of (39), we get

$$\begin{aligned}\left\langle\psi\left|H'_D\right|\psi\right\rangle &= -\frac{1}{4m^2}\int\psi^\dagger\left(q'_e\nabla\phi\cdot\nabla\right)\psi\,d^3\vec{r} \\ &= -\frac{1}{8m^2}\int q'_e\nabla\phi\cdot\nabla\left(\psi^\dagger\psi\right)d^3\vec{r} \\ &= \frac{1}{8m^2}\int\psi^\dagger\psi\nabla\cdot\left(q'_e\nabla\phi\right)d^3\vec{r} \,.\end{aligned} \tag{40}$$

Consequently

$$H'_D = \frac{1}{8m^2}\,\nabla\cdot\left(q'_e\nabla\phi\right) \,. \tag{41}$$

where

$$q'_e = -\frac{(d+1)\,e}{9 - 8\,\cos(b/r)} \,, \quad \phi = \frac{de}{r} \,. \tag{42}$$

In (41), if $q'_e = -e$ and $q'_p = e$, it becomes H_D. H'_D is

$$\begin{aligned}H'_D &= \frac{1}{8m^2}\left(\nabla q'_e\cdot\nabla\phi + q'_e\nabla^2\phi\right) \\ &= \frac{k\alpha}{8m^2}\left\{\frac{\partial}{\partial r}\frac{1}{(9 - 8\,\cos(b/r))}\,\frac{1}{r^2} + \right. \\ &\quad \left. + \frac{4\pi\delta(\vec{r})}{9 - 8\,\cos(b/r)}\right\} \,.\end{aligned} \tag{43}$$

In (43), the Darwin term is expressed as a quantity related to the second order derivative of the modified Coulomb potential energy. This means that there is no gauge degree of freedom in the Darwin term, so the value of k in the equation must be maintained.

Expectation values are:

$$\begin{aligned}
\langle H'_D\rangle_S &= \frac{k\alpha}{8m^2}\int_{r_p}^{\infty} 4\pi r^2\,\frac{\partial}{\partial r}\frac{1}{(9-8\,\cos(b/r))}\times\\
&\times\frac{1}{r^2}\left|\psi_{200}\left(\vec{r}\right)\right|^2 dr\\
&+\frac{k\alpha}{8m^2}\int_{\vec{r}_p}^{\infty}\frac{4\pi\,\delta\left(\vec{r}\right)}{9-8\,\cos(b/r)}\left|\psi_{200}\left(\vec{r}\right)\right|^2 d^3\vec{r}\\
&=\frac{4\pi k\alpha}{8m^2}\left\{\left[\frac{1}{9-8\,\cos(b/r)}\left|\psi_{200}(\vec{r})\right|^2\right]_{r_p}^{\infty}-\right.\\
&\left.-\int_{r_p}^{\infty}\frac{1}{9-8\,\cos(b/r)}\,\frac{\partial}{\partial r}\left|\psi_{200}(\vec{r})\right|^2 dr\right\} \qquad (44)\\
&+\frac{4\pi k\alpha}{8m^2}\,\frac{\left|\psi_{200}\left(\vec{r}_p\right)\right|^2}{9-8\,\cos(b/r_p)}\\
&\cong-\frac{4\pi k\alpha}{8m^2}\int_{r_p}^{\infty}\frac{\partial}{\partial r}\left|\psi_{200}\left(\vec{r}\right)\right|^2 dr\\
&=\frac{4\pi k\alpha}{8m^2}\left|\psi_{200}\left(\vec{r}_p\right)\right|^2\cong\frac{km\alpha^4}{16}\,.\\
\langle H'_D\rangle_P &\cong\frac{4\pi k\alpha}{8m^2}\left|\psi_{210}\left(\vec{r}_p\right)\right|^2=O\left(m\alpha^8\right).
\end{aligned}$$

As can be seen from (44), the Darwin term by charge correction works mostly in the $2S_{1/2}$ state. Thus

$$\Delta'_D=\langle H'_D\rangle_S-\langle H'_D\rangle_P\cong\langle H'_D\rangle_S\cong\frac{km\alpha^4}{16}\,. \qquad (45)$$

Therefore, the difference between the Darwin term before and after charge correction is

$$\Delta'_D-\Delta_D\cong(k-1)\,\frac{m\alpha^4}{16}=57.67\,m\alpha^6\,. \qquad (46)$$

In (11), the existing Darwin term acts only on the $2S_{1/2}$ state to increase its energy by $m\alpha^4/16$, and in (46), the effect of charge correction by causal delay further increases the energy of the $2S_{1/2}$ state by $57.67\,m\alpha^6$.

5 Conclusions

From a discrete time point of view, causal delay gives energy scale-dependent changes to the mass and charge of elementary particles. In this paper, as a result of applying it to the Lamb shift, it was obtained that the change in the charge value increases the energy of $2S_{1/2}$ by about $57.67\,m\alpha^6$ =1076 MHz mostly by the Darwin term. This is slightly different from the experimental value of 1057.86 MHz, but it is a good result as an approximation. If numerical integration can be done accurately, I think it will be close to the actual value.

Received on September 2, 2022

References

1. Noh Y. J. Anomalous Magnetic Moment in Discrete Time. *Progress in Physics*, 2021, v. 17, 207–209.
2. Noh Y. J. Propagation of a Particle in Discrete Time. *Progress in Physics*, 2020, v. 16, 116–122.
3. Lamb W. E., Retherford R. C. Fine Structure of the Hydrogen Atom by a Microwave Method. *Physical Review*, 1947, v. 72 (3), 241–243.
4. Bethe H. A., Jackiw R. Intermediate Quantum Mechanics. The Benjamin Cummings Publishing Company, 1986.
5. Wachter A. Relativistic Quantum Mechanics. Springer, 2011.
6. Cohen-Tannoudji C., Diu B., Laloe F. Quantum Mechanics. Hermann, Paris, France, 1977.

A Quantitative Representation of Particle Entanglements via Bohm's Hidden Variable According to Hadronic Mechanics

Ruggero Maria Santilli

The Institute for Basic Research, 35246 U. S. 19N, Suite 215, Palm Harbor, FL 34684, USA.
E-mail: research@i-b-r.org

In this note, we first recall the 1935 historical view by A. Einstein, B. Podolsky and N. Rosen according to which *"Quantum mechanics is not a complete theory"* (EPR argument), because of the inability by quantum mechanics to provide a quantitative representation of the *interactions* occurring in particle entanglements. We then show, apparently for the first time, that the completion of quantum entanglements into the covering *EPR entanglements* formulated according to hadronic mechanics provides a *quantitative representation of the interactions occurring in particle entanglements* by assuming that their continuous and instantaneous communications at a distance are due to the overlapping of the wave packets of particles, and therefore avoiding superluminal communications. According to this view, entanglement interactions result to be non-linear, non-local and not derivable from a potential, and are represented via Bohm's variable λ hidden in the quantum mechanical *associative* product of Hermitean operators $AB = A \times B$ via explicit and concrete, axiom-preserving realizations $A\hat{\times}B = A\lambda B$, with ensuing *non-unitary* structure, multiplicative unit $U1U^\dagger = \hat{I} = 1/\lambda$, $\hat{I}\hat{\times}A = A\hat{\times}\hat{I} = A$, *inapplicability'* of Bell's inequalities and consequential validity of Bohm's hidden variables. We finally introduce, also apparently for the first time, the completion of quantum computers into the broader *EPR computers* characterizing a collection of extended electronic components under continuous entanglements, and show their apparent faster computation, better cybersecurity and improved energy efficiency.

According to clear experimental evidence dating back to the early part of the past century, particles that were initially bounded together and then separated, can continuously and instantaneously influence each other at a distance, not only at the particle level (see e.g. [1, 2] and papers quoted therein), but also at the classical level [3].

The above experimental evidence is generally *assumed* to be represented by quantum mechanics and, therefore, particle entanglements are widely called *quantum entanglement* (Figure 1). However, Albert Einstein strongly criticized such an assumption because it would imply superluminal communications that violate special relativity. This occurrence motivated the 1935 historical view by A. Einstein, B. Podolsky and N. Rosen according to which *"Quantum mechanics is not a complete theory"* (EPR argument) [4].

In fact, quantum mechanics can only represent interactions derivable from a potential while *no* quantum mechanical potential is conceivably possible to represent continuous and instantaneous interactions at a distance. More explicitly, the quantum mechanical equation for two interacting particles with coordinates $r_k,\ k = 1, 2$ on a Hilbert space $\mathcal{H}$ over the field C of complex numbers is given by the familiar Schrödinger equation (for $\hbar = 1$)

$$\left[\Sigma_{k=1,2}\ \frac{1}{2m_k}\ p_k p_k + V(r)\right]\psi(r) = E\,\psi(r)\,. \tag{1}$$

When the two particles are entangled, in view of the absence of any possible potential $V(r)$, the above equation becomes

$$\begin{aligned}
&\Sigma_{k=1,2}\ \frac{1}{2m_k}\ p_k p_k \psi(r_1)\psi(r_2) = \\
&= \left[\Sigma_{k=1,2}\ \frac{1}{2m_k}\left(-i\frac{\partial}{\partial_{r_k}}\right)\left(-i\frac{\partial}{\partial_{r_k}}\right)\right]\psi(r_1)\psi(r_2) = \\
&= E\,\psi(r_1)\psi(r_2)
\end{aligned} \tag{2}$$

and *can only represent two free particles* characterized by the individual wave functions $\psi(r_k)$ without any possible or otherwise known interaction.

At the *2020 International Teleconference on the EPR argument* [5–7], R. M. Santilli proposed the new notion of *Einstein-Podolsky-Rosen entanglement* (Sect. 7.2.3, p. 61 of [6]) which is based on the sole conceivable interaction responsible for particle entanglements, that due to the overlapping of the wave packets of particles (Figure 2), thus being non-linear as first suggested by W. Heisenberg [8], non-local as first suggested by L. de Broglie and D. Bohm [9] and non derivable from a potential as first suggested by R. M. Santilli at Harvard University under DOE support [13, 14], because of contact, thus continuous and instantaneous character, by therefore voiding the need for superluminal communications.

The non-linear, non-local and non-potential character of the assumed interactions render them ideally suited for their representation via the *isotopic (i.e. axiom-preserving branch of hadronic mechanics,* [15–17]), comprising *iso-mathematics and iso-mechanics* (see [18] for an outline, [19–21] for a

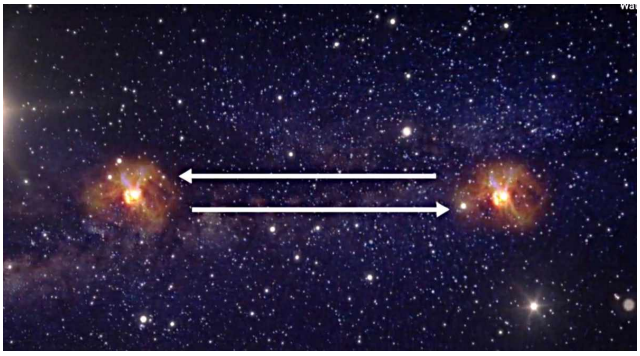

Fig. 1: In this figure, we illustrate the entanglement of particles with continuous and instantaneous interactions at a distance, and recall the argument by A. Einstein, B. Podolsky and N. Rosen on the lack of completeness of quantum mechanics due to its inability to represent said entanglement in a way compatible with special relativity [4].

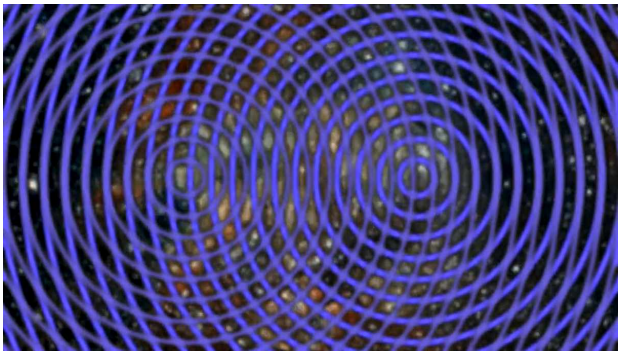

Fig. 2: In this figure, we illustrate the new Einstein-Podolsky-Rosen entanglement of particles introduced by R. M. Santilli in the 2020 overview [6] which is characterized by contact, therefore continuous and instantaneous interactions due to the overlapping of the wave packets of particles represented via Bohm's hidden variable (9), by therefore avoiding the need for superluminal interactions.

review and [22–30] for independent studies) which are characterized by the isotopy $\hat{\xi}:\{\hat{A},\hat{B},...,A\hat{\times}B\}$ of the universal enveloping associative algebra $\xi:\{A,B,...,AB=A\times B\}$ of quantum mechanical Hermitian operators $A,B,...$ with *iso-product* (first introduced in Eq. (5), p. 71 of [14])

$$\hat{A}\hat{\times}\hat{B}=\hat{A}\hat{T}\hat{B},\ \ \hat{T}>0\,, \tag{3}$$

where $\hat{T}$, called the *isotopic element,* is positive-definite but possesses otherwise an unrestricted functional dependence on coordinates, momenta, wave function and any other needed local variable, with related *iso-unit*

$$\begin{aligned}&\hat{I}=1/\hat{T}>0\,,\\ &\hat{I}\hat{\times}A=\hat{A}\hat{\times}\hat{I}=\hat{A},\ \forall\,\hat{A}\in\hat{\xi}\,,\end{aligned} \tag{4}$$

completion of Lie's theory into the *Lie-Santilli iso-theory* [14] (see [23, 28] for independent studies) with iso-brackets for an N-dimensional iso-algebra

$$[X_i\hat{,}X_j]=X_i\hat{\times}X_j-X_j\hat{\times}X_i=X_i\hat{T}X_j-X_j\hat{T}X_i=C_{ij}^kX_k\,, \tag{5}$$

iso-Heisenberg's equation (first proposed in Eq. (18), p. 163 of [14])

$$i\,\frac{dA}{dt}=[A\hat{,}H]=A\hat{\times}H-H\hat{\times}A\,, \tag{6}$$

and related *iso-Schrödinger's equation*

$$H\hat{\times}|\hat{\psi}\rangle=H\hat{T}|\hat{\psi}\rangle=E|\hat{\psi}\rangle\,. \tag{7}$$

Since the isotopic element $\hat{T}$ is *hidden* in the abstract axiom of associativity and becomes visible only in the isotopic realization (3)

$$A\hat{\times}(B\hat{\times}C)=(A\hat{\times}B)\hat{\times}C\,, \tag{8}$$

R. M. Santilli proposed in Sect. 6.8, p. 150 on, Eq. (5.8.19) in particular, of [16], as part of the isotopy of the SU(2) spin algebra and Pauli's matrices in particular, the *identification of the isotopic element $\hat{T}$ with Bohm's hidden variable λ* [31]

$$\lambda=\hat{T}(r,p,\psi,...)\,, \tag{9}$$

and consequential realization of the iso-unit $\hat{I}=1/\lambda$, with a variety of explicit and concrete realizations that, for the entanglement of two particles, are of the type [21]

$$\begin{aligned}&\lambda=\hat{T}=1/\hat{I}=\Pi_{\alpha=1,2}\,\text{Diag.}\left(\frac{1}{n_{1,\alpha}^2},\frac{1}{n_{2,\alpha}^2},\frac{1}{n_{3,\alpha}^2},\frac{1}{n_{4,\alpha}^2}\right)e^{-\Gamma},\\ &n_{\mu,\alpha}>0,\quad \Gamma>0,\ \ \mu=1,2,3,4,\ \ \alpha=1,2\,,\end{aligned} \tag{10}$$

providing:

1) A representation of the dimension and shape of particles via semi-axes $n_{k,\alpha}^2$, $k=1,2,3$ normalized to $n_{k,\alpha}=1$, $k=1,2,3$, $\alpha=1,2$ for the vacuum.

2) A representation of the density of particles via $n_{4,\alpha}^2$ normalized to the value $n_{\mu,\alpha}^2=1$ for the vacuum.

3) A representation of the non-potential character of the interactions due to the mutual penetration of particles via the exponential term e^{Γ}, where $\Gamma(\hat{r},\hat{p},\hat{\psi},...)$ is a positive-definite quantity with an unrestricted functional dependence on iso-coordinates $\hat{r}=r\hat{I}=r/\lambda$, iso-momenta $\hat{p}$, iso-wave-functions $\hat{\psi}(\hat{r})$, and other local variables.

By recalling the basic expression of the *iso-linear iso-momentum* characterized by the completion of the local Newton-Leibnitz differential calculus into the non-local *iso-differential calculus* [32] (see [29, 30] for independent studies)

$$\begin{aligned}\hat{p}\hat{\times}\hat{\psi}(\hat{r})&=\hat{p}\hat{T}(\hat{r},...)\psi(\hat{r})=-i\,\hat{\frac{\partial}{\partial_{\hat{r}}}}\hat{\psi}(\hat{r})=\\ &=-i\hat{I}(\hat{r},...)\,\frac{\partial}{\partial_{\hat{r}}}\hat{\psi}(\hat{r})=-i\,\frac{1}{\lambda}\,\frac{\partial}{\partial_{r/\lambda}}\hat{\psi}(r/\lambda)\,,\end{aligned} \tag{11}$$

the non-relativistic version of the EPR entanglement is characterized by the iso-Schrödinger equation (see [16] for the relativistic extension)

$$\begin{aligned}
&\Sigma_{k=1,2}\, \tfrac{1}{2m_k}\, \hat{p}_k \hat{\times} \hat{p}_k \hat{\times} \hat{\psi}(\hat{r}) = \\
&= \left[\Sigma_{k=1,2}\, \tfrac{1}{2m_k} \left(-i\hat{I}\tfrac{\partial}{\partial \hat{r}_k}\right)\left(-i\,\hat{I}\tfrac{\partial}{\partial \hat{r}_k}\right)\right] \hat{\psi}(\hat{r}) = \\
&= \left\{\Sigma_{k=1,2}\left[-\tfrac{\hat{I}^2}{2m_k}\left(\tfrac{\partial}{\partial \hat{r}_k}\right)\left(\tfrac{\partial}{\partial \hat{r}_k}\right) - \tfrac{\hat{I}}{2m_k}\left(\tfrac{\partial \hat{I}}{\partial \hat{r}_k}\right)\left(\tfrac{\partial}{\partial \hat{r}_k}\right)\right]\right\} \hat{\psi}(\hat{r}) = \qquad (12)\\
&= \left\{\Sigma_{k=1,2}\left[-\tfrac{\hat{I}^2}{2m_k}\left(\tfrac{\partial}{\partial \hat{r}_k}\right)\left(\tfrac{\partial}{\partial \hat{r}_k}\right) - \tfrac{\Gamma}{2m_k}\left(\tfrac{\partial \Gamma}{\partial \hat{r}_k}\right)\left(\tfrac{\partial}{\partial \hat{r}_k}\right)\right]\right\} \hat{\psi}(\hat{r}) = \\
&= \hat{E} \hat{\times} \hat{\psi}(\hat{r}) = E\hat{\psi}(\hat{r}) = E\hat{\psi}(\hat{r}_1) \hat{\times} \hat{\psi}(\hat{r}_2)\,,
\end{aligned}$$

with the following primary characteristics:

1. Iso-equation (9) characterizes a *new entanglement interaction* represented by Bohm's hidden variable $\lambda = \hat{T}$ which is absent in quantum mechanical equation (2);

2. The new entanglement interaction is manifestly *nonlinear* (in the wave-function), yet the theory is *iso-linear* [15, 16], namely, it is linear on the Hilbert-Myung-Santilli iso-space $\hat{\mathcal{H}}$ [33] with iso-states $|\psi\rangle$ and iso-normalization [12]

$$\langle \psi | \hat{\times} | \hat{\psi} \rangle = \langle \psi | \lambda | \hat{\psi} \rangle = \lambda\,, \qquad (12)$$

over Santtilli iso-field $\hat{C}$ of *iso-real, iso-complex or iso-quaternionic iso-numbers* [34]

$$\hat{n} = n\hat{I} = \frac{n}{\lambda} \qquad (13)$$

with iso-superposition principle $\psi(\hat{r}) = \hat{\psi}(\hat{r}_1 \hat{\times} \hat{\psi}(\hat{r}_2)$;

3. The new entanglement interaction is manifestly *nonlocal* in the sense of occurring in *volumes* represented by the iso-unit $\hat{I} = 1/\lambda$ and characterized by the overlapping of two volumes $V_k = (1/n^2_{1,k}, 1/n^2_{2,k}, 1/n^2_{3,k})$, $k = 1, 2$, each being on ontological grounds as big as experimental measurements can allow;

4. The new entanglement interaction is manifestly of contact, zero-range character, thus not being derivable from a potential, and therefore avoiding the need for superluminal interactions required by quantum entanglements [4];

5. The new entanglement interaction verifies, by conception and construction, the abstract axioms of relativistic quantum mechanics although realized via the indicated universal iso-associative envelope [35–37].

It should be indicated that (12) can be equally derived via a *non-unitary transformation* of quantum mechanical equation (2)

$$\begin{aligned}
&U \times 1 \times U^\dagger = \frac{1}{\lambda} = \hat{I}\,,\\
&U \times (A \times B) \times U^\dagger = A' \lambda B',\ \ \lambda = (U \times U^\dagger)^{-1}\,, \qquad (14)\\
&A' = U \times A \times U^\dagger,\ \ B' = U \times B \times U^\dagger\,.
\end{aligned}$$

The *invariance* of the numeric value of Bohm's hidden variable is then assured by the *Lorentz-Poincaré-Santilli iso-symmetry* [20] with structure [38]

$$\begin{aligned}
&U = \hat{U} \times \hat{T}^{1/2}\\
&\hat{U} \hat{\times} \hat{U}^\dagger = \hat{U}^\dagger \hat{\times} \hat{U} = \frac{1}{\lambda}\,.
\end{aligned} \qquad (15)$$

It may be of some interest to indicate the expected EPR completion of other branches of physics, such as the completion of quantum computers into new computers, here suggested under the name of *EPR computers,* for the description of extended electronic constituents in global, continuous and instantaneous communications, by therefore approaching the new notion of living organisms attempted in [39], with the following expected advances:

1) Faster computations, since all values of Bohm hidden variable λ are very small according to all available fits of experimental data [6], with ensuing rapid convergence of iso-perturbative series (see also Corollary 3.7.1, p. 128 of [20]). As a confirmation of this expectation, we recall the achievement via iso-mathematics and iso-chemistry of the first known *attractive* force between the *identical* electrons of valence coupling (see Chapter 4 of [40]), resulting in a *strong valence bond* that allowed the first known numerically exact representation of the experimental data for the hydrogen [41] and water [42] molecules with iso-perturbative calculations at least one thousand times faster than their conventional chemical counterparts.

2) Better cybersecurity, due to the formulation via iso-mathematics, with the consequential availability of iso-cryptograms equipped with an algorithm changing the numeric value of the iso-unit with such a frequency to prevent a solution within a finite period of time (Appendix 2C, p. 84 of [15] and [43]).

3) Increased energy efficiency, due to the fact that EPR entanglements are caused by *interactions without potential energy,* thus being more energy efficient than quantum computers.

The following comments are now in order:

I. Verifications of the EPR argument. In 1964, J. S. Bell [44] released a theorem according to which, under the assumption of quantum mechanics, the representation of the spin 1/2 of particles via Pauli's matrices, statistical independence and other assumptions, *a system of point-like particles with spin* 1/2 *does not admit a classical counterpart,* by therefore preventing any possibility of recovering Einstein determinism [4] under the indicated assumptions. The theorem was proved by showing that a certain expression D^{Bell} (whose explicit value depends on the relative conditions of the particles) is always *smaller* than the corresponding classical value D^{Clas},

$$D^{Bell} < D^{Clas}\,, \qquad (16)$$

for all possible values of D^{Bell}.

By assuming that nuclear forces have a non-linear, nonlocal and non-potential component represented via the isotopic element $\hat{T}$, R. M. Santilli initiated in 1981 [10] the studies on the inevitable *completion of Heisenberg's uncertainties and Bell's inequalities for strong interactions.*

Following the achievement of maturity for iso-mathematics and iso-mechanics, by representing the *extended* character of nuclear constituents via the *isotopic completion of Pauli's matrices with Bell's hidden variables* [16], today called the *Pauli-Santilli iso-matrices* formulated on a Hilbert-Myung-Sanilli iso-space [33] over Santilli iso-fields C [34] (see Eqs. (6.8.20), p. 254 of [16])

$$\hat{\sigma}_k = U\sigma_k U^\dagger, \quad UU^\dagger = \hat{I} = 1/\hat{T} = \text{Diag.}(\lambda^{-1}, \lambda),$$
$$\hat{\sigma}_1 = \begin{pmatrix} 0 & \lambda \\ \lambda^{-1} & 0 \end{pmatrix}, \quad \hat{\sigma}_2 = \begin{pmatrix} 0 & -i\lambda \\ i\lambda^{-1} & 0 \end{pmatrix}, \tag{17}$$
$$\hat{\sigma}_3 = \begin{pmatrix} \lambda^{-1} & 0 \\ 0 & -\lambda \end{pmatrix},$$

with *iso-commutation rules*

$$[\hat{\sigma}_i, \hat{\sigma}_j] = \hat{\sigma}_i \hat{\times} \hat{\sigma}_j - \hat{\sigma}_j \hat{\times} \hat{\sigma}_i = i2\epsilon_{ijk}\hat{\sigma}_k\,, \tag{18}$$

and *conventional spin* $1/2$ *iso-eigenvalues*

$$\hat{\sigma}_3 \hat{\times} |\hat{b}\rangle = \hat{\sigma}_3 \hat{T} |\hat{b}\rangle = \pm |\hat{b}\rangle\,,$$
$$\hat{\sigma}^{\hat{2}} \hat{\times} |\hat{b}\rangle = (\hat{\sigma}_1 \hat{T} \hat{\sigma}_1 + \hat{\sigma}_2 \hat{T} \hat{\sigma}_2 + \hat{\sigma}_3 \hat{T} \hat{\sigma}_3)\hat{T} |\hat{b}\rangle = 3|\hat{b}\rangle\,. \tag{19}$$

R. M. Santilli proved in 1998 the following *completion of Bell's inequalities for strong interactions* (Eq. (5.8), p. 189 of [11])

$$D^{HM} = \frac{1}{2}(\lambda_1 \lambda_2^{-1} + \lambda_1^{-1}\lambda_2)\, D^{Bell}\,, \tag{20}$$

where λ_1 and λ_2 are the hidden variables of the two particles. Additionally, Santilli proved that D^{HM} can indeed be equal to the corresponding D^{Clas} with specific examples, by therefore confirming Einstein's view on the possible recovering of classical determinism.

Finally, by combining the results of [10] and [11], in 2019 R. M. Santilli [12] (see the review in [20]) proved the following *completion of Heisenberg's uncertainties for strong interactions* (Eq. (35), p. 14 of [12])

$$\Delta r\, \Delta p \approx \frac{1}{2} \left| \langle \hat{\psi}(\hat{r}) | \hat{\times} [\hat{r}, \hat{p}] \hat{\times} | \hat{\psi}(\hat{r}) \rangle \right| \ll \frac{1}{2} \hat{T} = \frac{\lambda}{2} \tag{21}$$

establishing that *the standard deviations Δr and Δp, individually as well as their product, progressively approach Einstein's classical determinism with the increase of the density in the interior of hadrons, nuclei, and stars, and achieve a full classical determinism at the limit of Schwarzschild's horizon for which $\lambda = \hat{T} = 0$.*

In essence, verifications [10–12] of the EPR argument establish that Bell's inequalities are *valid* for the electromagnetic interactions of point-like particles, including electrons and photons, with ensuing lack of hidden variables.

By contrast, following half a century of mathematical, theoretical and experimental studies in the field, this author believes that Bell's inequalities are *inapplicable,* in favor of their completions via hadronic mechanics [10–12], for composite systems of particles at short mutual distances, including hadrons [20] and leptons [47], because the exact representation of their experimental data requires non-unitary transforms of quantum models, under which none of Bell's assumptions can be formulated, with ensuing validity of Bohm's hidden variables.

It then follows that any experiment proving the *violation* of Bell's inequalities, as defined by the above equations, is a direct experimental verification of hadronic mechanics.

II. Conditions of validity of hadronic mechanics. Recall that the wave packet of one electron is identically null only at infinity and, consequently, the universe is a single integrated structure much similar to the total EPR entanglement of living organisms [39]. Recall also that the universe will never admit one single final theory for the representation of all its complexities. Under these recollections, this author believes that the isotopic branch of hadronic mechanics can indeed provide a first axiomatically consistent representation of *stable,* thus time reversible systems, while the genotopic branch of hadronic mechanics can provide a first axiomatically consistent representation of energy-releasing processes, including nuclear fusions and fossil fuel combustion [20], and the hyperstructural branch of hadronic mechanics can at least initiate the search for an axiomatically consistent representation of life [39], here referred to a quantitative representation of the difference between organic and inorganic molecules.

III. Conditions of validity of quantum mechanics. By recalling that "point-like wave packets" do not exist in nature, and that quantum mechanics is identically and uniquely recovered by iso-mathematics and iso-mechanics for $\lambda = \hat{T} = 1$, this author believes that the Copenhagen interpretation of quantum mechanics provides an excellent representation of *stable systems of particles at mutual distances allowing their effective approximation as being point-like,* by therefore solely admitting action-at-a-distance potential interactions, with ensuing validity for atomic structures, particles in accelerators, crystals and numerous other systems. Despite these justly historical achievements, following half a century of studies in the field, this author believes that *quantum mechanics cannot be exactly valid for particle entanglements, as shown in this note, as well as for all composite systems of particles at short mutual distances, thus including leptons, hadrons, nuclei and stars* [17].

It is appropriate in the latter respect to note that the widespread assumption that a single theory, quantum mechanics, can represent all possible complexities of the universe, has

been kept for about one century in oblivion of:

A) Clear experimental evidence in various fields of *deviations* of physical reality from quantum predictions in favor of *exact* representations via hadronic mechanics, including deviations in: nuclear physics [45]; electrodynamics [46–48]; nuclear physics [45]; condensed matter physics [49]; heavy ion physics [50]; time dilation for composite particles [51]; Bose-Einstein correlation [52, 53]; cosmology [54, 55]; and other fields.

B) The insufficiencies of quantum mechanics in nuclear physics due to its inability over one century under large public funds to achieve [19–21]: a quantitative representation of the synthesis of the neutron from the hydrogen in the core of stars; an exact representation of nuclear magnetic moments; an exact representation of the spin of nuclei in their true ground state (that without the usual orbital excitations); a representation of the stability of nuclei despite the huge Coulomb repulsion between nuclear protons; a representation of the stability of neutrons when members of a nuclear structure; and other insufficiencies.

C) The inability by quantum mechanics to allow a consistent treatment of energy-releasing processes, including nuclear fusions, due to their time irreversibility compared to the known time-reversibility of quantum mechanics (e.g. because of the invariance of Heisenberg's equation under anti-Hermiticity and for other reasons). Under these conditions, the same Schrödinger equation has to be applied for both, the forward and backward time evolutions, with ensuing violation of causality due to unavoidable solutions in which the effect precedes the cause. This violation of causality may explain the lack of achievement to date of controlled nuclear fusion [56].

Consequently, the continuation of the century-old use and support of quantum mechanics for all possible conditions existing in the universe in oblivion of the teaching by Einstein, Podolsky and Rosen, in oblivion of vast opposing experimental evidence, and in oblivion of fundamental unresolved nuclear problems, may continue to have widely negative implications for our rapidly deteriorating environment.

Acknowledgements

The author would like to thank for critical comments the participants of the *2020 International Teleconference on the EPR argument*. Additional thanks are due to Mrs. Sherri Stone for linguistic control of the manuscript.

This note has been written from 9-20 to 9-30, 2022, at the Pietra Blue Resort, Polignano a Mare, Bari, Italy.

Received on October 9, 2022

References

1. Aspect A. *et al*. Experimental Realization of Einstein-Podolsky-Rosen-Bohm Gedankenexperiment: A New Violation of Bell's Inequalities. *Phys. Rev. Lett.*, 1982, v. 49, 91–94. http://ui.adsabs.harvard.edu/abs/1982PhRvL..49...91A
2. Eigen G. Measurements of the Polarization Correlation of the Two-Photon System Produced in Positron-Electron Annihilation. *Proceedings of the 2020 Teleconference on the EPR argument*, Curran Associates, New York, 823–843, 2021.
3. Berkowitz R. Macroscopic systems can be controllably entangled and limitlessly measured. *Physics Today*, July 2021, 16–18.
4. Einstein A., Podolsky B., and Rosen N. Can quantum-mechanical description of physical reality be considered complete? *Phys. Rev.*, 1935, v. 47, 777–791. http://www.eprdebates.org/docs/epr-argument.pdf
5. Beghella-Bartoli S. and Santilli R. M., eds, Proceedings of the 2020 Teleconference on the Einstein-Podolsky-Rosen argument that "Quantum mechanics is not a compete theory". Curran Associates, New York, NY, 2021. http://www.proceedings.com/59404.html (printed), 60007.html (electronic). http://www.world-lecture-series.org/level-xii-epr-teleconference-2020 (recorded lectures).
6. Santilli R. M. Overview of historical and recent verifications of the Einstein-Podolsky-Rosen argument and their applications to physics, chemistry and biology. APAV - Accademia Piceno Aprutina dei Velati, Pescara, Italy, 2021. http://www.santilli-foundation.org/epr-overview-2021.pdf
7. Dunning-Davies J. A Present Day Perspective on Einstein-Podolsky-Rosen and its Consequences. *Journal of Modern Physics*, 2021, v. 12, 887–936. http://www.scirp.org/journal/paperinformation.aspx?paperid=109219
8. Heisenberg W. *Nachr. Akad. Wiss. Gottingen*, 1953, v. IIa, 111. http://link.springer.com/chapter/10.1007/978-3-642-70079-8_23
9. Goldstein S. Bohmian (de Broglie-Bohm) Mechanics. Stanford Encyclopedia of Philosophy, 2021. http://plato.stanford.edu/entries/qm-bohm/
10. Santilli R. M. Generalization of Heisenberg's uncertainty principle for strong interactions. *Hadronic Journal*, 1981, v. 4, 642–657. http://www.santilli-foundation.org/docs/generalized-uncertainties-1981.pdf
11. Santilli R. M. Isorepresentation of the Lie-isotopic SU(2) Algebra with Application to Nuclear Physics and Local Realism. *Acta Applicandae Mathematicae*, 1998, v. 50, 177–190. http://www.santilli-foundation.org/docs/Santilli-27.pdf
12. Santilli R. M. Studies on the classical determinism predicted by A. Einstein, B. Podolsky and N. Rosen. *Ratio Mathematica*, 2019, v. 37, 5–23. http://www.eprdebates.org/docs/epr-paper-ii.pdf
13. Santilli R. M. Foundation of Theoretical Mechanics. Vol. I, The Inverse Problem in Newtonian Mechanics. Springer-Verlag, Heidelberg, Germany, 1978. http://www.santilli-foundation.org/docs/Santilli-209.pdf
14. Santilli R. M. Foundation of Theoretical Mechanics. Vol. II, Birkhoffian Generalization of Hamiltonian Mechanics. Springer-Verlag, Heidelberg, Germany, 1983. http://www.santilli-foundation.org/docs/santilli-69.pdf
15. Santilli R. M. Elements of Hadronic Mechanics. Vol. I, Mathematical Foundations. Ukraine Academy of Sciences, Kiev, 1995. http://www.santilli-foundation.org/docs/Santilli-300.pdf
16. Santilli R. M. Elements of Hadronic Mechanics. Vol. II, Theoretical Foundations. Ukraine Academy of Sciences, Kiev, 1995. http://www.santilli-foundation.org/docs/Santilli-301.pdf
17. Santilli R. M. Elements of Hadronic Mechanics. Vol. III, Experimental Verifications. Ukraine Academy of Sciences, Kiev, 2016. http://www.santilli-foundation.org/docs/elements-hadronic-mechanics-iii.compressed.pdf
18. Anderson R. Outline of Hadronic Mathematics, Mechanics and Chemistry as Conceived by R. M. Santilli. *American Journal of Modern Physics*, 2016, v. 6, 1–16. http://www.santilli-foundation.org/docs/HMMC-2017.pdf

19. Santilli R. M. Studies on A. Einstein, B. Podolsky, and N. Rosen prediction that quantum mechanics is not a complete theory. I: Basic methods. *Ratio Mathematica*, 2020, v. 38, 5–69. //eprdebates.org/docs/epr-review-i.pdf
20. Santilli R. M. Studies on A. Einstein, B. Podolsky, and N. Rosen prediction that quantum mechanics is not a complete theory. II: Apparent proof of the EPR argument. *Ratio Mathematica*, 2020, v. 38, 71–138. //eprdebates.org/docs/epr-review-ii.pdf
21. Santilli R. M. Studies on A. Einstein, B. Podolsky, and N. Rosen prediction that quantum mechanics is not a complete theory. III: Illustrative examples and applications. *Ratio Mathematica*, 2020, v. 38, 139–222. //eprdebates.org/docs/epr-review-iii.pdf
22. Aringazin A. K., Jannussis A., Lopez F., Nishioka M. and Veljanosky B. Santilli's Lie-Isotopic Generalization of Galilei and Einstein Relativities. Kostakaris Publishers, Athens, Greece, 1991. http://www.santilli-foundation.org/docs/Santilli-108.pdf
23. Sourlas D. S. and Tsagas Gr. T. Mathematical Foundation of the Lie-Santilli Theory. Ukraine Academy of Sciences, 1993. http://www.santilli-foundation.org/docs/santilli-70.pdf
24. Lohmus J., Paal E. and Sorgsepp L. Non-associative Algebras in Physics. Hadronic Press, 1994. http://www.santilli- foundation.org/docs/Lohmus.pdf
25. Kadeisvili J. V. Santilli's Isotopies of Contemporary Algebras, Geometries and Relativities, Second edition. Ukraine Academy of Sciences, Kiev, 1997. http://www.santilli-foundation.org/docs/Santilli-60.pdf
26. Jiang C.-X. Foundations of Santilli Isonumber Theory. International Academic Press, 2001. http://www.i-b-r.org/docs/jiang.pdf
27. Ganfornina R. M. F. and Valdes J. N. Fundamentos de la Isotopia de Santilli. International Academic Press, Palm Harbor, FL, 2001. www.i-b-r.org/docs/spanish.pdf. English translation: Algebras, Groups and Geometries,2015, v. 32, 135–308 (2015) http://www.i-b-r.org/docs/Aversa-translation.pdf
28. Gandzha I. and Kadeisvili J. V. New Sciences for a New Era: Mathematical, Physical and Chemical Discoveries of Ruggero Maria Santilli. Sankata Printing Press, Nepal, 2011. http://www.santilli-foundation.org/docs/RMS.pdf
29. Georgiev S. Foundations of IsoDifferential Calculus. Vol 1. – Iso-Differential and Iso-Integral Calculus for Iso-Functions in One Variable. Vol 2. – Iso-Differential and Iso-Integral Calculus for Iso-Functions in Several Variables. Vol. 3 – Iso-Ordinary Iso-Differential Equations. Vol. 4 – Iso-Difference Equations. Vol.5 – Iso-Stochastic Iso-Differential Equations. Vol. 6 – Theory of Iso-Measurable Iso-Functions. Nova Publishers, New York, NY, 2014 (I), 2014 (II), 2014 (III), 2015 (IV), 2015 (V), 2016 (VI), 2022 (I new ed.).
30. Georgiev S. Iso-Mathematics. Lambert Academic Publishing, 2022.
31. Bohm D. A Suggested Interpretation of the Quantum Theory in Terms of "Hidden Variables". *Physical Review*, 1952, v. 85, 166–182. http://journals.aps.org/pr/abstract/10.1103/PhysRev.85.166
32. Santilli R. M. Nonlocal-Integral Isotopies of Differential Calculus, Mechanics and Geometries. *Rendiconti Circolo Matematico Palermo, Suppl.*, 1996, v. 42, 7–82. http://www.santilli-foundation.org/docs/Santilli-37.pdf
33. Myung H. C. and Santilli R. M. Modular-isotopic Hilbert space formulation of the exterior strong problem. *Hadronic Journal*, 1982, v. 5, 1277–1366. http://www.santilli-foundation.org/docs/myung-santilli-1982.pdf
34. Santilli R. M. Isonumbers and Genonumbers of Dimensions 1, 2, 4, 8, their Isoduals and Pseudoduals, and "Hidden Numbers" of Dimension 3, 5, 6, 7. *Algebras, Groups and Geometries*, 1993, v. 10, 273–322. http://www.santilli-foundation.org/docs/Santilli-34.pdf
35. Santilli R. M. Lie-isotopic Lifting of Special Relativity for Extended Deformable Particles. *Lettere Nuovo Cimento*, 1983, v. 37, 545–555. http://www.santilli-foundation.org/docs/Santilli-50.pdf
36. Santilli R. M. Isotopic Generalizations of Galilei and Einstein Relativities. Intern. Academic Press, 1991. Vol. I: http://www.santilli-foundation.org/docs/Santilli-01.pdf Vol. II: http://www.santilli-foundation. org/docs/Santilli-61.pdf
37. Aringazin A. K., Jannussis A., Lopez F., Nishioka M. and Veljanosky B. Santilli's Lie-Isotopic Generalization of Galilei and Einstein Relativities. Notes from R. M. Santilli's 1990 Lectures at the ICTP, Trieste, Italy. Kostakaris Publishers, Athens, Greece, 1991. http://www.santilli-foundation.org/docs/Santilli-108.pdf
38. Santilli R. M. Invariant Lie-isotopic and Lie-admissible formulation of quantum deformations. *Found. Phys.*, 1997, v. 27, 1159–1177. http://www.santilli-foundation.org/docs/Santilli-06.pdf
39. Santilli R. M. and Vougiouklis T. New Conception of Living Organisms and its Representation via Lie-Admissible H_v-Hyperstructures. *Algebras, Groups and Geometries*, 2020, v. 37, 741–764. http://www.santilli-foundation.org/docs/Santilli-Vougiouklis-2020-epr.pdf
40. Santilli R. M. Foundations of Hadronic Chemistry, with Applications to New Clean Energies and Fuels. Kluwer Academic Publishers, 2001. http://www.santilli-foundation.org/docs/Santilli-113.pdf. Russian translation: Aringazin A. K. http://i-b-r.org/docs/Santilli-Hadronic-Chemistry.pdf
41. Santilli R. M. and Shillady D. D. A new isochemical model of the hydrogen molecule. *Intern. J. Hydrogen Energy*, 1999, v. 24, 943. http://www.santilli-foundation.org/docs/Santilli-135.pdf
42. Santilli R. M. and Shillady D. D. A new isochemical model of the water molecule. *Intern. J. Hydrogen Energy*, 2000, v. 25, 173. http://www.santilli-foundation.org/docs/Santilli-39.pdf
43. Wade M. I. and Gill T. L. Isonumbers and RGB Image Encryption. *Algebras, Groups and Geometries*, 2021, v. 37, 103–119. http://www.santilli-foundation.org/docs/wade-gill-2021.pdf
44. Bell J. S. On the Einstein Podolsky Rosen paradox. *Physics*, 1964, v. 1, 195–200. http://cds.cern.ch/record/111654/files/vol1p195-200_001.pdf
45. Santilli R. M. Iso-Representation of the Deuteron Spin and Magnetic Moment via Bohm's Hidden Variables. *Progress in Physics*, 2022, v. 18, 74–81. http://www.santilli-foundation.org/docs/PiP-paper-3-22.pdf
46. Miller J. P., de Rafael E. and Roberts B. Lee. Muon (g-2): experiment and theory. *Rep. Prog. Phys.*, 2007, v. 70, 795–881. http://news.fnal.gov/2021/04/first-results-from-fermilabs-muon-g-2-experiment-strengthen-evidence-of-new-physics/
47. Santilli R. M. Representation of the anomalous magnetic moment of the muons via the Einstein-Podolsky-Rosen completion of quantum into hadronic mechanics. *Progress in Physics*, 2021, v. 17, 210–215. http://www.santilli-foundation.org/muon-anomaly-pp.pdf
48. Santilli R. M. Representation of the anomalous magnetic moment of the muons via the novel Einstein-Podolsky-Rosen entanglement. In: Guzman J. C., ed. Scientific Legacy of Professor Zbigniew Oziewicz: Selected Papers from the International Conference "Applied Category Theory Graph-Operad-Logic". Word Scientific, in press. http://www.santilli-foundation.org/ws-rv961x669.pdf
49. Fadel M., Zibold T., Decamps B. and Treutlein Ph. Spatial entanglement patterns and Einstein-Podolsky-Rosen steering in Bose-Einstein condensates. *Science*, 2018, v. 360, 409–415. http://www.santilli-foundation.org/Basel-paper.pdf
50. Schukraft J. Heavy-ion physics with the ALICE experiment at the CERN Large Hadron Collider. *Trans. R. Soc.*, 2012, v. A370, 917–932. http://royalsocietypublishing.org/doi/10.1098/rsta.2011.0469
51. Santilli R. M. Apparent Unsettled Value of the Recently Measured Muon Magnetic Moment. *Progress in Physics*, 2022, v. 18, 15–18. http://www.santilli-foundation.org/docs/muon-meanlife-2022.pdf

52. Santilli R. M. Nonlocal formulation of the Bose-Einstein correlation within the context of hadronic mechanics. *Hadronic J.*, 1992, v. 15, 1–50 and v. 15, 81–133. http://www.santilli-foundation.org/docs/Santilli-116.pdf

53. Cardone F. and Mignani R. Nonlocal approach to the Bose-Einstein correlation. *Europ. Phys. J.*, 1998, v. C4, 705–728.

54. Ahmar H., Amato G., Kadeisvili J. V., Manuel J., West G. and Zogorodnia O. Additional experimental confirmations of Santilli's IsoRedShift and the consequential lack of expansion of the universe. *Journal of Computational Methods in Sciences and Engineering*, 2013 v. 13, 321–375. http://www.santilli-foundation.org/docs/IRS-confirmations-212.pdf

55. Santilli R. M. Experimental Verifications of IsoRedShift with Possible Absence of Universe Expansion, Big Bang, Dark Matter, and Dark Energy. *The Open Astronomy Journal* 2010, v. 3, 124. http://www.santilli-foundation.org/docs/Isoredshift-Letter.pdf

56. Santilli R. M. Apparent resolution of the Coulomb barrier for nuclear fusions via the irreversible Lie-admissible branch of hadronic mechanics. *Progress in Physcs*, 2022, in press. http://www.santilli-foundation.org/docs/hyperfusion-2022.pdf

Apparent Resolution of the Coulomb Barrier for Nuclear Fusions Via the Irreversible Lie-admissible Branch of Hadronic Mechanics

Ruggero Maria Santilli

The Institute for Basic Research, 35246 U. S. 19N, Suite 215, Palm Harbor, FL 34684, USA.
E-mail: research@i-b-r.org

In this paper, we report decades of mathematical, theoretical, experimental and industrial studies aiming at the resolution of the Coulomb barrier for nuclear fusions, here referred to the extremely big *repulsive* Coulomb force between natural nuclei that has prevented the achievement of controlled nuclear fusion to date. The studies have been done via the Lie-isotopic completion (for reversible processes) and Lie-admissible completion (for irreversible processes) of quantum mechanics into the various branches of hadronic mechanics. We first outline the prior representations via hadronic mechanics of: the synthesis of the neutron from the Hydrogen in the core of stars; the experimental data of the Deuteron in its true ground state (that with null orbital contributions); the stability of the neutron under strong nuclear forces; and the nuclear stability despite strongly repulsive protonic forces. Thanks to these preceding studies, we present apparently for the first time: 1) The prediction by hadronic mechanics of the existence of new, negatively charged, unstable nuclei, called *pseudo-nuclei* and denoted with the symbol $\tilde{N}$ (patent pending), which are characterized by a strongly attractive hadronic bond of electrons and natural nuclei, by therefore resolving the Coulomb barrier since pseudo-nuclei would be *attracted* (rather than repelled) by natural nuclei, with ensuing new conception of nuclear fusions here called *hyperfusions;* 2) The identification of engineering means for the synthesis of pseudo-nuclei which is given by the hadronic reactors for the synthesis of the neutron from the proton and the electron; 3) Laboratory evidence according to which the synthesis of pseudo-nuclei and related hyperfusions appear to be the origin of the limited, yet sustained and controlled excess energy achieved by the *Intermediate Controlled Nuclear Fusions.*

1 Introduction

As it is well known, nuclear fusions have indeed been achieved at various energies, but none of them has achieved to date the *sustainability and controllability* necessary for industrial usages, such as the production of electricity, due to a number of yet unresolved theoretical and engineering problems, such as:

Problem 1: Means to resolve the *repulsion* between natural, positively charged nuclei, called the *Coulomb barrier,* which reaches very big repulsive values of the macroscopic order of Newtons at the mutual distances of about 1 fm necessary to activate attractive strong nuclear forces,

$$F = Z\,\frac{e^2}{r^2} = \\ = Z\,(8.99\times 10^9)\,\frac{(1.60\times x10^{-19})^2}{(10^{-15})^2} = Z\times 230\,\mathrm{N}\,, \tag{1}$$

where Z represents the number of proton-proton pairs.

Problem 2: Means to control the anti-parallel coupling of nuclear spins, in which absence there would be a violation of the angular momentum conservation law with nuclear fusions solely possible at random.

Problem 3: Means to achieve "clean" nuclear fusions, ideally referring to those without the emission of harmful radiations and without the release of radioactive waste.

In this paper, we study, apparently for the first time, the possibility of synthesizing new, negatively charged, unstable nuclei, hereon called *pseudo-nuclei,* which are characterized by a strongly attractive bond between negatively charged electrons and positively charged natural nuclei.

In the event the synthesized nuclei have a sufficient mean life, pseudo-nuclei would bypass the Coulomb barrier (Problem 1) because they would be *attracted* (rather than repelled) by natural, positively charged nuclei all the way to mutual distances 10^{-13} cm = 1 fm needed to activate strong nuclear interactions.

Pseudo-nuclei also offer realistic possibilities for a resolution of Problem 2, because, in view of their opposite charges and magnetic moments, pseudo-nuclei would couple automatically with natural nuclei in anti-parallel spin alignment.

Engineering tests are expected to initiate with the synthesis of *light* pseudo-nuclei, whose fusion with natural nuclei would be the best arena for the possible resolution of Problem 3.

We shall hereon identify generic nuclei N with the familiar expression $N(Z, A, J, u)$ where Z represents the total number of protons, A represents the total number of protons and neutrons, J represents the nuclear spin, and u represents the mass in Atomic Mass Units, also denoted amu. We shall also

use tabulated symbols for individual nuclei, such as: H for Hydrogen, D for Deuteron, C for Carbon, *etc*. Measurements of nuclear data used in this paper are available from [1–4].

Our feasibility study shall initiate with the synthesis of the smallest possible pseudo-nucleus, here called the *pseudo-Deuteron-2e* and denoted with the symbol $\tilde{D}_{2e}$ (Figs. 1, 2, 3), according to the reaction

$$(\beta_{\uparrow}^{-},\beta_{\downarrow}^{-}) + D(1,2,1) \to \tilde{D}_{2e}(1,2,1)\,, \tag{2}$$

where: the subindex $2e$ represents the total number of bonded electrons; the total charge of the pseudo-nucleus is *negative,* $Z^{tot} = -1$ (since it is the result of one positive + and two negative − elementary charges); and the electron pair with antiparallel coupling is an expected image at short distances of Pauli's exclusion principle in molecular structures.

The existence of synthesis (2) would evidently imply the existence of the *pseudo-Deuteron-3e* with structure

$$(\beta_{\uparrow}^{-},\beta_{\downarrow}^{-}) + \beta_{\downarrow}^{-} + D(1,2,1_{\uparrow}) \to \tilde{D}_{3e}(1,2,1/2_{\uparrow})\,, \tag{3}$$

with intriguing characteristics due to the very big magnetic moment of the third electron for nuclear standards, and ensuing possibility of resolving Problem 2.

Following a quantitative representation of pseudo-Deuterons, in this paper we shall study the possible fusion of pseudo-nuclei and natural nuclei, called *hyperfusion* and here referred to nuclear fusions without the Coulomb barrier and with natural antiparallel spin alignments, including the following possible hyperfusion

$$\begin{aligned} &\tilde{D}_{2e}(1,2,1) + C(6,12,0) \to \to N(7,14,1) + \beta_{\uparrow}^{-} + \beta_{\downarrow}^{-} \\ &\Delta_N = 10.272\,\text{MeV}\,, \end{aligned} \tag{4}$$

and others that apparently occurred in recently measured excess heat in nuclear fusions to be reviewed in Sect. 4.

In order to conduct the indicated feasibility study, in this paper we shall adopt:

1) The 1935 historical argument by A. Einstein, B. Podolsky and N. Rosen that *Quantum mechanics is not a complete theory* [5];

2) The historical verifications of the EPR argument by W. Heisenberg [6], L. de Broglie [7] and D. Bohm [8], as well as the recent verifications by R. M. Santilli [9–11];

3) The experiments establishing deviations of quantum mechanical predictions from physical reality in various fields, including: nuclear physics [12]; electrodynamics [13–15]; condensed matter physics [16]; heavy ion physics [17]; time dilation for composite particles [18, 19]; Bose-Einstein correlation [20, 21]; cosmology [22, 23]; and various epistemological arguments [24–26].

4) The *approximate validity* of quantum mechanics in nuclear physics due to its inability over one century of achieving [27–29]: a quantitative representation of the fundamental synthesis of the neutron from a proton and an electron in the core of stars; an exact representation of nuclear magnetic moments; an exact representation of the spin of nuclei in their true ground state (that without the usual orbital excitations); a quantitative representation of the stability of neutrons when members of a nuclear structure; a quantitative representation of the stability of nuclei despite the huge Coulomb repulsion between nuclear protons; and other insufficiencies.

5) The completion of quantum mechanics into hadronic mechanics [30–32] (see [33] for an outline and [27–29] for a review); and the studies conducted during the *2020 International Teleconference on the EPR Argument* [34] (see its overviews [36,37] and monographs [38]–[47] for independent studies).

By using a language specifically intended for nuclear physicists, in Sect. 2 we review the branches of hadronic mechanics used in our study [48]–[76]; in Sect. 3, we show that hadronic mechanics allows a quantitative representation of the synthesis of the pseudo-nuclides; in Sect. 4, we show that the synthesis of pseudo-Deuterons appears to be verified by the sustainable and controllable excess energy produced by the *Intermediate Controlled Nuclear Fusions* (ICNF) [77]–[146]; and in Sect. 5 we summarize the results.

For the self-sufficiency of this presentation, in the appendices we outline preceding studies playing a crucial role for the consistent derivation and application of pseudo-nuclei. In Appendix A, we study the possible resolution of Problem 3 (nuclear fusions without harmful radiations); in Appendix B, we outline the representation via hadronic mechanics of the synthesis of the neutron from a proton and an electron (which is fundamental for the synthesis of pseudo-nuclei); and in Appendix C we present, apparently for the first time, the representation of nuclear stability permitted by hadronic mechanics despite the natural instability of the neutron and despite the strongly repulsive protonic forces in which absence no resolution of the Coulomb barrier for nuclear fusions appears to be plausible.

2 Selection of the basic methods

2.1 Basic notions of hadronic mechanics

Recall that, according to Einstein, Podolsky and Rosen [5], the primary limitation of quantum mechanics in nuclear physics is its *locality,* namely, the representation of protons and neutrons as *massive points*. Therefore, the foundations of hadronic mechanics were built in the late 1970's by R. M. Santilli at Harvard University under DOE support [48, 49] for the primary purpose of representing the actual dimension, shape and density of protons and neutrons in a form invariant over time.

Recall also that quantum mechanical point-particles can solely admit linear, local and potential interactions, hereon called *Hamiltonian interactions* (and technically identified as *variationally self-adjoint (SA) interactions* [48]).

By contrast, clear nuclear data establish that nuclear vol-

umes are generally *smaller* than the sum of the volumes of the constituent protons and neutrons. Consequently, when they are members of a nuclear structure, protons and neutrons are generally in conditions of partial mutual penetration of their dense charge distributions, resulting in additional interactions that are: *non-linear* in the wave function, as first studied by W. Heisenberg [6]; *non-local* in the sense of occurring over volumes, as first studied by L. de Broglie [7]; and of contact, thus zero-range type, *not derivable from a potential,* as first studied by R. M. Santilli [49]. The latter interactions are hereon called *non-Hamiltonian interactions* (and are technically identified as *variationally non-self-adjoint (NSA) interactions* [48]).

2.2 Lie-isotopic branch of hadronic mechanics

In Sect. 3, we shall study the representation of *stable,* thus time reversible nuclei. Their possible bonds with electrons are also reversible over time since the decay of pseudo-nuclei reproduce the original, permanently stable constituents.

In this section, we outline the branch of hadronic mechanics suggested for the consistent representation of time reversible systems, which is known as the *isotopic branch* and comprises the novel *iso-mathematics* [30] (see also [43, 47]) and *iso-mechanics* [31] (see also [38] and [45]), where the prefix "iso" is intended in the Greek meaning of denoting *preservation of the original axioms.*

By recalling that quantum mechanics is based on Lie algebras, the above methods are also known as *Lie-isotopic formulations* to indicate that they are based on the isotopies of Lie algebras not treated here for brevity [49] (see also [39]).

Recall that quantum mechanics is characterized by a universal enveloping algebra of Hermitean operators A, B, with conventional associative product $A \times B = AB$ on a Hilbert space $\mathcal{H}$ with states $|\psi\rangle$ and normalization $\langle\psi|\psi\rangle = 1$ over the field of complex numbers C, Schrödinger equation $H(r,p)|\psi\rangle = E|\psi\rangle$, canonical commutation rules and the familiar quantum mechanical methods used in nuclear physics over the past century.

Santilli achieved the first known representation of non-Hamiltonian/NSA interactions in a time-reversible way via a *new operator* called the *isotopic element* and indicated with the symbol $\hat{T}$, which is sandwiched in between all possible quantum products AB, resulting in the new, associativity-preserving product called *iso-product* (Eq. (5), p. 71 of [49])

$$A \star B = A\hat{T}B, \quad \hat{T} = \hat{T}(\hat{\psi}, ...) > 0\,, \tag{5}$$

with ensuing generalized multiplicative unit, called *iso-unit* and related identity axion

$$\begin{aligned} &\hat{I}(\hat{\psi}, ...) = 1/\hat{T}(\hat{\psi}, ...) > 0\,, \\ &I \star A = A \star I = A\,, \end{aligned} \tag{6}$$

where the dependence on $\hat{\psi}$ represents non-linearity in the appropriate iso-space of iso-mechanics.

For the case of the Deuteron as a two-body bound state according to hadronic mechanics, the isotopic element has a realization of the type [29, 36]

$$\begin{aligned} &\hat{T}(\hat{\psi}, ...) = 1/\hat{I}(\hat{\psi}, ...) = \\ &= \prod_{\alpha=1,2} \text{Diag}\left(\tfrac{1}{n_{1,\alpha}^2}, \tfrac{1}{n_{2,\alpha}^2}, \tfrac{1}{n_{3,\alpha}^2}, \tfrac{1}{n_{4,\alpha}^2}\right) e^{-\Gamma(\hat{\psi},...)}\,, \\ &n_{\mu,\alpha} > 0, \quad \Gamma > 0, \quad \mu = 1,2,3,4, \quad \alpha = 1,2\,, \end{aligned} \tag{7}$$

by therefore characterizing:

1) The dimension and shape of the proton and neutron via semi-axes $n_{k,\alpha}^2$, $k = 1, 2, 3$ (with n_3 parallel to the spin);

2) The density $n_{4,\alpha}^2$ of the proton and of the neutron with normalizations for the vacuum to the value $n_{\mu,\alpha}^2 = 1$.

3) Non-Hamiltonian/NSA interactions between the proton and the neutron caused by the mutual penetration of their dense charge distribution, which interactions are represented via the exponential term $e^{\Gamma(\hat{\psi},...)} > 0$, where Γ is positive-definite but possesses otherwise an unrestricted functional dependence on all needed local variables.

Despite their simplicity, isotopies (5)-(6) requested the step-by-step, completion of all aspects of quantum mechanics into iso-mechanics, as illustrated by the basic *Schrödinger-Santilli iso-equation* (Ch. 5, p. 182 on, [31])

$$H \star |\hat{\psi}\rangle = H(r,p)\,\hat{T}(\hat{\psi}, ...)\,|\hat{\psi}\rangle = E\,|\hat{\psi}\rangle\,, \tag{8}$$

as well as the *Heisenberg-Santilli iso-equation* for an observable A

$$\begin{aligned} i\,\frac{dA}{dt} &= [A, H]^\star = \\ &= A \star H - H \star S = A\hat{T}H - H\hat{T}A\,, \end{aligned} \tag{9}$$

whose time-reversibility is assured by the conservation of the total energy,

$$i\,\frac{dH}{dt} = [H, H]^\star \equiv 0\,, \tag{10}$$

as well as the invariance of (9) under anti-Hermiticity,

$$[A, H]^\star \equiv -[A, H]^{\star\dagger}\,. \tag{11}$$

As clearly illustrated by iso-equation (8)-(9), the representation of stable nuclei via iso-mechanics requires *two operators,* the conventional Hamiltonian H for the representation of Hamiltonian/SA interactions and the isotopic element $\hat{T}$ for the representation of the dimension, shape, density and non-Hamiltonian/NSA interactions of protons and neutrons in a nuclear structure.

To reach a preliminary understanding of the subsequent sections, interested readers should be aware that, despite their simplicity, Eqs. (5)-(6) require a step-by-step completion of *all* aspects of 20th century applied mathematics into the novel iso-mathematics, with no exception known to the author, including the new: *iso-numbers* [50] (see also [42])

$$\hat{n} = n\hat{I}\,; \tag{12}$$

iso-functions [49] (see also [38]) $\hat{f}(\hat{r}) = [f(r\hat{I})]\,\hat{I}$; and iso-differential calculus [51] (see also [46])

$$\begin{aligned} &\hat{d}\hat{r} = \hat{T}d(r\hat{I}) = dr + r\hat{T}d\hat{I}, \\ &\frac{\hat{\partial}\hat{f}(\hat{r})}{\hat{\partial}\hat{r}} = \hat{I}\,\frac{\partial\hat{f}(\hat{r})}{\partial\hat{r}}\,, \end{aligned} \tag{13}$$

that allowed the completion of the iso-Schrödinger and iso-Heisenberg representations

$$\begin{aligned} &\hat{p}\star|\,\hat{\psi}(\hat{r})\,\rangle = -\hat{i}\star\hat{\partial}_{\hat{r}}|\,\hat{\psi}(\hat{r})\,\rangle = -i\,\hat{I}\partial_{\hat{r}}|\,\hat{\psi}(\hat{r})\,\rangle\,, \\ &\left[\hat{r}_i,\hat{p}_j\right]^{\star}\star|\,\hat{\psi}(\hat{r})\,\rangle = -i\,\hat{\delta}_{ij}|\,\hat{\psi}(\hat{r})\,\rangle = -i\,\hat{I}\delta_{ij}|\,\hat{\psi}(\hat{r})\,\rangle\,, \\ &\left[\hat{r}_i,\hat{r}_j\right]^{\star}\star|\,\hat{\psi}(\hat{r})\,\rangle = [\hat{p}_i,\hat{p}_j]^{\star}\star|\,\hat{\psi}(\hat{r})\,\rangle = 0\,, \end{aligned} \tag{14}$$

as well as the completion of the Heisenberg uncertainties for point particles under electromagnetic interactions into the *Heisenberg-Santilli iso-uncertainties* for extended hadrons under strong interactions [9–12]

$$\Delta r\,\Delta p = \frac{1}{2}\,|\,\langle\,\hat{\psi}\,|\star[\hat{r},\hat{p}]^{*}\star|\,\hat{\psi}\,\rangle\,| \approx \frac{1}{2}\hat{T} \;\ll\; 1\,. \tag{15}$$

It should be finally noted that all aspects of iso-mathematics and iso-mechanics can be constructed very simply via a systematic non-unitary transformation of *all* the corresponding 20th century formulations [52], e.g.,

$$\begin{aligned} &UU^{\dagger} = \hat{I}(\hat{\psi},...) = 1/\hat{T} > 0\,, \\ &\hbar = 1 \;\to\; U\hbar U^{\dagger} = \hat{I}\,, \\ &r \;\to\; UrU^{\dagger} = \hat{r}\,, \\ &p \;\to\; UpU^{\dagger} = \hat{p}\,, \\ &U(AB)U^{\dagger} = \hat{A}\hat{T}\hat{B}\,, \\ &U(H|\,\psi\,\rangle U^{\dagger} = \hat{H}\star|\,\hat{\psi}\,\rangle = \\ &\quad = \left[\frac{1}{\hat{2}\star\hat{m}}\sum_{k=1,2,3}\hat{p}_k\star\hat{p}_k + \hat{V}(\hat{r})\right]\star|\,\hat{\psi}\,\rangle = \\ &\quad = \hat{E}\star|\,\hat{\psi}\,\rangle = E|\,\hat{\psi}\,\rangle\,. \end{aligned} \tag{16}$$

The invariance over time of the numeric values of the isotopic element and of the iso-unit is finally assured by the reformulation of conventional non-unitary transformations (15) into the *iso-unitary iso-transformations* of hadronic mechanics [52]

$$\begin{aligned} &WW^{\dagger} = \hat{I}, \quad W = \hat{W}\hat{T}^{1/2}\,, \\ &WW^{\dagger} = \hat{W}\star\hat{W}^{\dagger} = \hat{W}^{\dagger}\star\hat{W} = \hat{I}\,, \end{aligned} \tag{17}$$

under which

$$\begin{aligned} &\hat{I}\to\hat{I}' = \hat{W}\star\hat{I}\star\hat{W}^{\dagger}\equiv\hat{I}\,, \\ &\hat{A}\star\hat{B}\to\hat{W}\star(\hat{A}\star\hat{B})\star\hat{W}^{\dagger} = \\ &\quad = \hat{A}'\star\hat{B}' = \hat{A}'\hat{T}\hat{B}'\,, \\ &\hat{A}' = \hat{W}\star A\star\hat{W}^{\dagger}),\;\hat{B}' = \hat{W}\star\hat{B}\star\hat{W}^{\dagger}\,, \\ &\hat{T} = (W^{\dagger}\star\hat{W})^{-1}\,. \end{aligned} \tag{18}$$

The invariance of isotopic formulation then follows (see [29] for a technical review via *iso-symmetries,* namely, the isotopic completion of 20th century space-time symmetries).

2.3 Lie-admissible branch of hadronic mechanics

In Sect. 4, we shall study apparent nuclear fusions that are permitted by pseudo-Deuterons without Coulomb barrier and with a natural antiparallel alignment of nuclear spins. The primary difference between stable nuclei and nuclear fusions is that the former constitute time reversible systems, thus allowing their treatment via time reversible isotopic methods, while the latter are *irreversible over time* by therefore requiring for their consistent treatment the *irreversible branch of hadronic mechanics* known as *Lie-admissible or genotopic formulations* [53]–[70] (see [30–32] for a general treatment), where the prefix "geno" is intended this time in the Greek sense of *inducing new axioms.*

In the author's view, an important problem of nuclear fusions, that has remained essentially unaddressed for about one century, is that *the representation of nuclear fusions via quantum mechanics generally violates causality,* because the same Schrödinger equation applies for both, the fusion process as well as its time reversal image which requires the spontaneous disintegration of the synthesized nucleus, resulting in solutions that generally admit effects preceding their cause.

The primary objective of Santilli's research in the late 1970's at Harvard University under DOE support was the construction of the EPR completion of time reversible quantum mechanics into an irreversible form representing nuclear fusions without causality problems. The study was essentially along the Ph. D. thesis at the University of Torino, Italy, on the time irreversible, Lie-admissible generalization of quantum mechanics [53, 54, 56].

The need for new clean nuclear energies to contain the deterioration of our environment (that was already visible in the late 1970's), joint with the lack of controlled nuclear fusions, stimulated a considerable volume of research in the period 1977–1985 under DOE support, including papers [57]–[61] five *Workshops on Lie-admissible formulations* [61], the *First International Conference on Nonpotential Interactions and their Lie-Admissible Treatment* [62], the first *Workshops on Hadronic Mechanics* [63, 64], and various reprint volumes, such as [65]. The post-1985 references on Lie-admissible

mathematics and mechanics are too numerous for comprehensive quotations. We here merely quote *The third international conference on the Lie-admissible treatment of non-potential interactions* [66] and special contributions [67]–[70].

As a main aspect in the representation of nuclear fusions via irreversible genotopic methods let us recall that quantum mechanics is a time reversible theory beginning with its axiomatic structure. In particular, the right modular action of the Hermitean Hamiltonian on a Hilbert state, $H|\psi\rangle = E|\psi\rangle$, is equivalent to the corresponding left modular action, $\langle\psi|H = -\langle\psi|E'$, $E' \equiv E$, and the same holds for isotopic methods in view of the Hermiticity of the isotopic element $\hat{T} = \hat{T}^\dagger$.

Following extensive studies, the foundations of irreversible formulations were achieved in the 1979 Harvard University paper [57] via the following inequivalent right and left modular actions of a Hamiltonian on a Hilbert state. The right modular action (indicated with the symbol >) is assumed to represent *motion forward in time,* while the left modular action (indicated with the symbol <) is assumed to represent *motion backward in time,* with forward ("for") and backward ("bac") geno-Schödinger equations

$$\begin{aligned} &\hat{H} \equiv \hat{H}^\dagger, \\ &\hat{H} > |\psi\rangle = \hat{H}\hat{R}|\psi\rangle = E^{for}|\psi\rangle, \\ &\langle\psi| < \hat{H} = \langle\psi|\hat{S}\hat{H} = \langle\psi|E^{bac}, \end{aligned} \tag{19}$$

which assure irreversibility whenever the *genotopic operators* $\hat{R}, \hat{S}$ are different

$$\hat{R} \neq \hat{S}, \quad E^{for} \neq E^{bac}, \tag{20}$$

isotopic formulations being a particular case for $\hat{R} = \hat{S} = \hat{T}$.

Note that *genotopic formulations maintain the observability of the total energy* [31], by therefore avoiding the use of complex-valued Hamiltonians to represent irreversibility with the consequential loss of observability.

According to the above assumptions, geno-mathematics (geno-mechanics) essentially consists of *two* inequivalent iso-mathematics (iso-mechanics), one with *all* products ordered to the right and the other ordered to the left.

By using (19), the *genotopic time evolution* (for the simple case $\hat{t} = t$) is given by (Eqs. (19), p. 153 of [49])

$$\begin{aligned} \hat{A}(t) = e^{Hti}_{>} > \hat{A}(0) < e_{<}e^{-itH} = \\ = e^{H\hat{S}ti}\hat{A}(0)\, e^{-it\hat{S}H}, \end{aligned} \tag{21}$$

with infinitesimal form

$$\begin{aligned} i\frac{\hat{d}\hat{A}}{\hat{d}t} = (\hat{A}, \hat{H}) = \\ = \hat{A} < \hat{H} - \hat{H} > \hat{A} = \hat{A}\hat{S}\hat{H} - \hat{H}\hat{R}\hat{A} = \\ = (\hat{A}\hat{T}\hat{H} - \hat{H}\hat{T}\hat{A}) + (\hat{A}\hat{J}\hat{H} - \hat{H}\hat{J}\hat{A}), \\ \hat{S} = \hat{T} + \hat{J}, \quad \hat{R} = -\hat{T} + \hat{J}. \end{aligned} \tag{22}$$

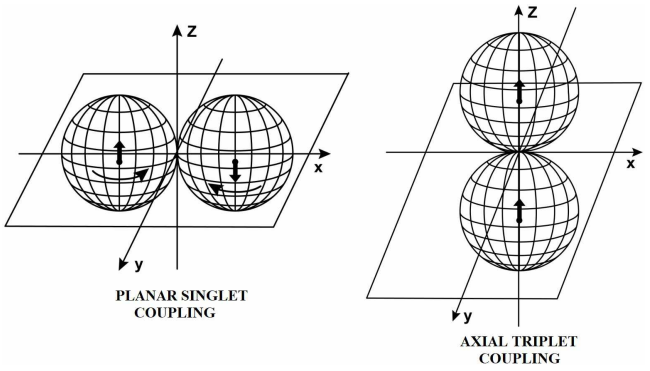

Fig. 1: In this figure, we illustrate the two stable bound states of particles with spin predicted by hadronic mechanics, which are given by the "planar singlet coupling" on the left and the "axiom triplet coupling" on the right.

The important methodological, as well as historical feature of genotopic formulations is that their brackets (A, H) are *jointly Lie-admissible and Jordan-admissible* according to the American mathematician A. A. Albert [71], in the sense that the antisymmetric brackets $[A, B]^\star$ verify the Lie algebra axioms, while the symmetric brackets $\{A, B\}^\star$ verify the Jordan axioms.

Intriguingly, the symmetric term of brackets (21) provides a representation of the *external terms* $\hat{F}^{NSA}$ of Lagrange's and Hamilton's equations as one can see for the particular case

$$\begin{aligned} &\hat{S} = 1, \quad \hat{R} = -1 + \frac{\hat{F}}{\hat{H}}, \\ &i\frac{\hat{d}\hat{A}}{\hat{d}t} = (\hat{A}, \hat{H}) = \hat{A}\hat{H} - \hat{H}\hat{A} + \hat{A}\hat{F}, \end{aligned} \tag{23}$$

by therefore realizing Jordan's wish that his symmetric algebra may, one day, see physical applications (for details, see Sect. 2 of [27]).

Recall that iso-mathematics and iso-mechanics can be constructed with the sole use of *one*, single, non-unitary transformation of the conventional applied mathematics and quantum mechanics, Eqs. (16). Similarly, geno-mathematics and geno-mechanics can be constructed, this time, via *two* different non-unitary transformations of conventional applied mathematics and quantum mechanics, and this includes the lifting of quantum mechanical nuclear models with sole potential interactions into their covering hadronic models with potential, as well as contact, non-potential interactions (see [52] for brevity).

3 Negatively charged pseudo-Deuterons

3.1 Basic assumptions

As indicated in Sect. 1, no study of pseudo-nuclei, with ensuing resolution of the Coulomb barrier for nuclear fusions, appears to be plausible without the prior resolution of a number of basic problems in nuclear physics, beginning with the

resolution of the *locality* of quantum mechanics via the invariant representation of the dimension, shape and density of protons and neutrons outlined in Sect. 2.

In this section, we outline the second necessary requirement for the indicated task, the numerically exact and time invariant representation of the experimental data of the Deuteron in its true ground state (that with null orbital contributions) under the assumption that the neutron is an extended structureless neutral particle with spin 1/2.

The indicated task additionally requires the representation according to hadronic mechanics (outlined in Appendix B) of the synthesis of the neutron from a proton and an electron in the core of stars. In fact, the neutron synthesis is prohibited by quantum mechanics for numerous technical reasons, despite the huge proton-electron Coulomb *attraction,* with ensuing expectation that pseudo-nuclei are not possible because not allowed by quantum mechanics.

The latter view is quickly dispelled by the century old evidence that the neutron is indeed synthesized in the core of stars from a proton and an electron, by therefore confirming the Einstein-Podolsky-Rosen argument that *Quantum mechanics is not a complete theory* [5].

In turn, the representations of *all* characteristics of the neutron during its synthesis from the proton and the electron have allowed the resolution of the last nuclear problems needed for the study of pseudo-nuclei, which are given by the understanding of nuclear stability despite the neutron natural instability and despite the huge repulsive protonic forces. The latter resolutions are presented apparently for the first time in Appendix C.

3.2 Representation of the Deuteron experimental data

As it is well known, the only stable bound state between a proton and a neutron predicted by quantum mechanics (qm) is the singlet coupling

$$D = (p_\uparrow, n_\downarrow)_{qm}\,, \tag{24}$$

for which the total spin would be zero, $J_D = 0$, contrary to clear experimental evidence for which the spin of the Deuteron is $J_D = 1$.

For the intent of maintaining quantum mechanics as an exact discipline in nuclear physics, the spin of the Deuteron is generally associated to a collection of *orbital states* $L_D = 1$ (see e.g. [75]), which association is however contrary to the experimental evidence for which *the spin of the Deuteron has the value* $J_D = 1$ *in the true ground state,* namely, a state for which all excited orbital contributions are null.

Following the non-relativistic and relativistic representations of all characteristics of the neutron in its synthesis from the proton and the electron [84]–[103], the numerically exact and time invariant representation of all the experimental data of the Deuteron in its true ground state has been achieved by R. M. Santilli [29, 77, 78, 83] (see also [79–81]).

Under the assumption that the neutron is an extended structureless particle, the representation of the spin $J_D = 1$ was achieved via the notion of *hadronic spin* (first introduced in Sect. 6.8, p. 250 of [31] and [10]) which is given by iso-unitary, iso-irreducible iso-representations of the Lie-Santilli iso-algebra $\widehat{\mathrm{SU}}(2)$ whose iso-fundamental iso-representation can be constructed quite easily via the following *non-unitary* transformation of Pauli's matrices

$$UU^\dagger = \hat{I} = \mathrm{Diag}\,(\lambda^{-1}, \lambda)\,,\ \ \hat{T} = \mathrm{Diag}\,(\lambda, \lambda^{-1})\,, \tag{25}$$

including an explicit and concrete realization of Bohm's *hidden variables* λ [8], first introduced in Eqs. (6.8.20), p. 254 of [31], and resulting in the *iso-Pauli matrices* generally called *Pauli-Santilli iso-matrices*

$$\begin{aligned}
&\hat{\Sigma}_k = U\Sigma_k U^\dagger,\ \ \Sigma_k = \sigma_k \hat{I}\,,\\
&\hat{\sigma}_1 = \begin{pmatrix} 0 & \lambda \\ \lambda^{-1} & 0 \end{pmatrix},\ \ \hat{\sigma}_2 = \begin{pmatrix} 0 & -i\lambda \\ i\lambda^{-1} & 0 \end{pmatrix},\\
&\hat{\sigma}_3 = \begin{pmatrix} \lambda^{-1} & 0 \\ 0 & -\lambda \end{pmatrix},
\end{aligned} \tag{26}$$

and then used in various works (see e.g. [10]).

As one can see, the iso-Pauli matrices verify the iso-commutation rules

$$\begin{aligned}
[\hat{\sigma}_i, \hat{\sigma}_j]^* &= \hat{\sigma}_i \star \hat{\sigma}_j - \hat{\sigma}_j \star \hat{\sigma}_i = \\
&= \hat{\sigma}_i \hat{T} \hat{\sigma}_j - \hat{\sigma}_j \hat{T} \hat{\sigma}_i = i2\epsilon_{ijk}\hat{\sigma}_k\,,
\end{aligned} \tag{27}$$

showing the clear iso-morphism $\widehat{\mathrm{SU}}(2) \approx \mathrm{SU}(2)$, as well as the iso-eigenvalue equations on an iso-state $|\hat{b}\rangle$ of the *Hilbert-Myung-Santilli iso-space* $\hat{\mathcal{H}}$ [76] over the iso-field of iso-complex iso-numbers $\hat{C}$ [50]

$$\begin{aligned}
&\hat{S}_k = \frac{\hat{1}}{2} \star \hat{\sigma}_k = \frac{1}{2}\hat{\sigma}_k\,,\\
&\hat{\sigma}_3 \star |\,\hat{b}\,\rangle = \hat{\sigma}_3 \hat{T}\,|\,\hat{b}\,\rangle = \pm\,|\,\hat{b}\,\rangle\,,\\
&\hat{\sigma^2} \star |\,\hat{b}\,\rangle = (\hat{\sigma}_1 \hat{T} \hat{\sigma}_1 + \hat{\sigma}_2 \hat{T} \hat{\sigma}_2 + \hat{\sigma}_3 \hat{T} \hat{\sigma}_3)\hat{T}\,|\,\hat{b}\,\rangle = 3\,|\,\hat{b}\,\rangle.
\end{aligned} \tag{28}$$

The addition of hadronic spins (Sect. 6.11, p. 265 of [31]) allowed the identification of two stable couplings of spin 1/2 *extended* particles called *planar singlet coupling* and *axial triplet coupling* which are illustrated in Fig. 1.

The configuration of the Deuteron allowing the representation of the spin $J_D = 1$ in its true ground state is evidently the axial triplet coupling, first identified in Fig. 13, p 91 of [36] (Fig. 2)

$$\tilde{D} = \begin{pmatrix} \hat{p}_\uparrow \\ \star \\ \hat{n}_\uparrow \end{pmatrix}. \tag{29}$$

Two complementary, numerically exact and time invariant representations of the Deuteron magnetic moment

$$\mu_D^{ex} = 0.85647\,\mu_{\mathrm{N}}\,, \tag{30}$$

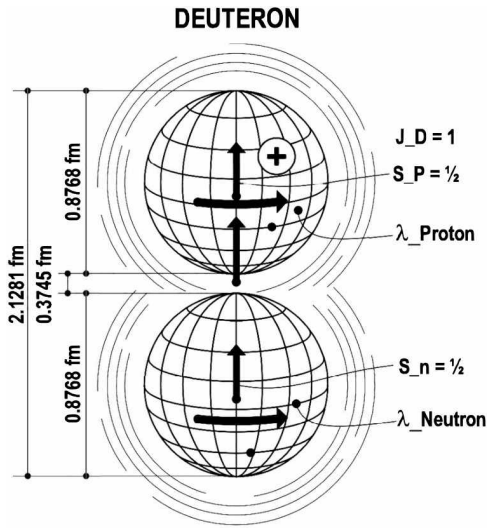

Fig. 2: In this figure, we reproduce known experimental data on the dimensions of the Deuteron [2] and its constituent proton and neutron [4], as well as their interpretation as a hadronic bound state in axial triplet coupling (Fig. 1), thus representing for the first time the spin of the Deuteron $S_D = 1$ in its ground state, that with null angular contributions $L_D = 0$ [83].

were achieved via hadronic mechanics. The first representation was reached in Eq. (3.6), p. 124 of the 1994 paper [77] (see also the 1998 monograph [78]) via the following numeric values of the characteristic quantities of isotopic element (26)

$$\begin{aligned} b_1 &= \frac{1}{n_1} = b_2 = \frac{1}{n_2} = 1.0028\,, \\ b_3 &= \frac{1}{n_3} = 1.662, \;\; b_4 = \frac{1}{n_4} = 1.653\,. \end{aligned} \tag{31}$$

The second representation of the magnetic moment of the Deuteron (35) was reached in the recent paper [83] via the realization of Bohm's hidden variable λ

$$\lambda = e^{\phi} \geq 0\,, \tag{32}$$

and the factorization (from Eq. (6.8.18), p. 254 of [31]),

$$\hat{\sigma}_3|\,\hat{b}\,\rangle = \sigma_3\hat{|}\,\hat{b}\,\rangle = \sigma_3 e^{\phi\sigma_3}|\,\hat{b}\,\rangle\,, \tag{33}$$

resulting in the relation

$$\mu_{hm}|\,\hat{b}\,\rangle = e^{\phi\sigma_3}\mu_{qm}|\,\hat{b}\,\rangle = e^{\phi\sigma_3} gS\,|\,\hat{b}\,\rangle\,, \tag{34}$$

from which the magnetic moment (35) is exactly represented via the following numeric value of Bohm's hidden variable λ [83]

$$\lambda = e^{\phi} = e^{0.97666} = 2.65557\,. \tag{35}$$

The invariance over time of the representations follows from the derivation of iso-Pauli matrices (31) from the isotopies of the Poincaré symmetry (see the general review [29] for brevity).

The representation of the rest energy and charge radius of the Deuteron (Fig. 2) were first achieved via the iso-Schrödinger equation of hadronic mechanics for a two-body, proton-neutron system (Fig. 12) [78] and then extended to a *restricted three-body system* comprising two protons and an electron (Fig. 13 and reviews [79–81]). The stability of the Deuteron despite the natural instability of the neutron is studied in Appendix C.

3.3 Predicted characteristics of the pseudo-Deuteron-2e

In this section, we study the possible bound state (2) of an electron pair and the Deuteron into a negatively charged unstable nucleus called *pseudo-Deuteron-2e* and denoted with the symbol $\tilde{D}_{2e}(1,2,1)$ (Sect. 1), conceptually proposed in Sect. 8.2.8, p. 96 of [36], and here studied at the non-relativistic level with the structure according to hadronic mechanics (hm)

$$[(\beta^-_{\uparrow},\beta^-_{\downarrow})_{hm} + D(1,2,1)]_{hm} = \tilde{D}_{2e}(1,2,1)\,, \tag{36}$$

where:

3.1.1) The bond between the electron pair and the Deuteron is primarily due to their very big *attractive* Coulomb force of 460 N at the mutual distance of 10^{-13} cm, Eq. (1), as well as non-Hamiltonian/NSA interactions caused by the motion of the electron pair within the wave packet of the Deuteron here presented as an example of the *Einstein-Podolsky-Rosen (EPR) entanglement* [12].

3.1.2) The electron pair in synthesis (36) is the valence electron bond represented via hadronic chemistry under the name of *isoelectronium* (see Chapter 4 on, [72] and applications [73, 74]) which is the sole valence electron pair with an *attractive force* known to this author despite their equal charges.

3.1.3) The electron pair and the Deuteron are assumed, for simplicity, to constitute single bodies in structure equations.

3.1.4) Synthesis (36) is assumed in first approximation to be reversible over time with spontaneous decay

$$\tilde{D}_{2e}(1,2,1) \;\to\; D(1,2,1) + \beta^-_{\uparrow} + \beta^-_{\downarrow}\,. \tag{37}$$

3.1.5) Synthesis (36) is studied via the iso-mathematics and iso-mechanics of hadronic mechanics outlined in Sect. 2.2 under the sole assumption of the following non-relativistic form of isotopic element (7) [29, 36]

$$\begin{aligned} &\hat{T}(\hat{\psi},...) = 1/\hat{I}(\hat{\psi},...) = \\ &= \prod_{\alpha=1,2} \text{Diag}\left(\frac{1}{n^2_{1,\alpha}}, \frac{1}{n^2_{2,\alpha}}, \frac{1}{n^2_{3,\alpha}}\right) e^{-\Gamma(\hat{\psi},...)}, \\ &n_{\mu,\alpha} > 0, \quad \Gamma > 0, \;\; \mu = 1,2,3 \;\; \alpha = 1,2\,. \end{aligned} \tag{38}$$

3.1.6) We assume that both the electron pair and the Deuteron are spherical with characteristic quantities $n_\mu = 1$, $\mu = 1,2,3$, by therefore reducing isotopic element (36) to its exponential term

$$\hat{T}(\hat{\psi},...) = 1/\hat{I}(\hat{\psi},...) = e^{-\Gamma(\hat{\psi},...)}. \tag{39}$$

3.1.7) To avoid insidious instabilities, the orbit of the electron pair around the Deuteron is assumed to be in a plane and a perfect circle on iso-spaces over iso- fields.

Following the study of synthesis (36) with two electrons, we shall study the synthesis with a bigger number of electrons, such as the *pseudo-Deuteron-3e* (Fig. 4).

A generic hyperfusion between a pseudo-nucleus $\tilde{N}_{ke}(Z_1, A_1, J_1)$ with k bonded electrons and a natural nucleus $N(Z_2, A_2, J_2)$ will be denoted

$$\begin{aligned} &\tilde{N}_{ke}(Z_1, A_1, J_1) + N(Z_2, A_2, J_2) \to \\ &\to N(Z_1 + Z_2, A_1 + A_2, J_1 + J_2) + k\beta^- \,. \end{aligned} \tag{40}$$

With reference to Fig. 3, we consider now the quantum mechanical Schrödinger equation for the bond of an electron pair with rest energy $M_{2e} = 1.022$ MeV to the Deuteron with rest energy $M_D = 1875.6129$ MeV

$$\left[-\frac{1}{2m} \sum_{k=1,2,3} p_k p_k + V_c(r) \right] | \psi(r) \rangle = E \, | \psi(r) \rangle \,, \tag{41}$$

where m is the reduced mass

$$m = \frac{M_D \times 2m_e}{M_d + 2M_e} \approx M_{2e} = 1.022 \text{ MeV} \,, \tag{42}$$

and the attraction is that of the Coulomb force between the electron pair and the proton

$$V_c = \frac{(+e) \times (-2e)}{r} = -2 \, \frac{e^2}{r} \,. \tag{43}$$

We now assume that the considered bond is characterized by a second interaction due to the overlapping of the wave packets of the electrons with that of the Deuteron (illustrated with the dashed area of Fig. 2), resulting in a deep EPR entanglement (Sect. 3 of [15]) with ensuing contact, non-Hamiltonian/NSA interactions represented by isotopic element (27).

In order to achieve an interaction in the iso-Schrödinger equation which is *additive* to the Coulomb interaction, we select the following simplified form of the isotopic element that has produced various numerically exact representations of experimental data [29]

$$\hat{T} = 1/\hat{I} = e^{+V_h(\hat{r})/V_c(\hat{r})} \,, \tag{44}$$

where $V_h(\hat{r})$ is the *Hulten potential* in the hadronic system of iso-coordinates $\mathrm{v}\hat{r} = r\hat{I}$

$$V_h(\hat{r}) = -K_h \, \frac{e^{b\hat{r}}}{1 - e^{b\hat{r}}} \,, \tag{45}$$

b represents the charge radius of the pseudo-Deuteron here assumed to be of the order of 2 fm,

$$R_{\tilde{D}} = b \approx 2 \, \text{fm} = 2 \times 10^{-13} \, \text{cm}, \tag{46}$$

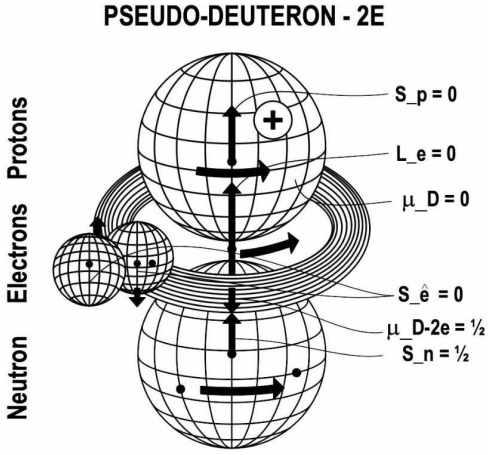

Fig. 3: In this figure, we illustrate the structure of the pseudo-Deuteron-2e predicted by hadronic mechanics as a bound state of an electron pair and a Deuteron (Sect. 3).

and K_h is the Hulten constant.

Under the above assumptions, the iso-Schrödinger equation in the structure of the pseudo-Deuteron is uniquely characterized by the following *non-unitary* transformation of the quantum mechanical description

$$\begin{aligned} &UU^\dagger = \hat{I} = 1/\hat{T} = e^{[-V_h(\hat{r})]/[-V_c(\hat{r})]} \approx 1 + \tfrac{\hat{V}_h(\hat{r})}{V_c(\hat{r})} + ... \\ &(UU^\dagger)^{-1} = \hat{T} = e^{V_h(\hat{r})/V_c(\hat{r})} \approx 1 - \tfrac{V_h(\hat{r})}{V_c(\hat{r})} + ... \end{aligned} \tag{47}$$

when applied to (41) (first studied in Sect. 5.1, p. 827 on, of the 1978 Harvard University memoir [82] and upgraded in Sect. 2.7.2 of [29]) with final result

$$\left[-\frac{1}{2m} \hat{\Delta}_{\hat{r}} - V_c(\hat{r}) - V_h(\hat{r}) \right] | \hat{\psi}(\hat{r}) \rangle = E_h \, | \hat{\psi}(\hat{r}) \rangle \,. \tag{48}$$

Recall that the Hulten potential behaves like the Coulomb potential at short distances (see Eq. (5.1.15), p. 885 of [82]),

$$V_h(\hat{r}) \approx \frac{k_h}{b\hat{r}} \,. \tag{49}$$

Consequently, the strongly attractive Hulten potential *absorbs* the attractive Coulomb potential with a mere redefinition K_h', of the constant K_h, resulting in the iso-Schrödinger equation

$$\left[-\frac{1}{2m_e} \hat{\Delta}_{\hat{r}} - K_h' \, \frac{e^{b\hat{r}}}{1 - e^{b\hat{r}}} \right] | \hat{\psi}(\hat{r}) \rangle = E_{be} \, | \hat{\psi}(\hat{r}) \rangle, \tag{50}$$

where E_{be} is the binding energy of the Hulten potential and $\bar{m}_e$ is the iso-renormalized mass of the electron, that is, the renormalization of the mass caused by non-Hamiltonian interactions.

For our initial feasibility study, we assume that the pseudo-Deuteron has the mass $m_{\tilde{D}} \approx 2m_e + m_D = 1.876 \, \text{MeV} - E_{be}$,

the mean life of $\tau_{\tilde{D}} \approx 1\,\text{s}$ and the charge radius $R_{\tilde{D}} = b^{-1} = 2 \times 10^{-13}\,\text{cm}$.

By following the structure model of pions as hadronic bound states of electrons and positrons of Eqs. (5.1.14), p. 836, [82], we reach the following *non-relativistic structure equations of the pseudo-Deuteron-2e*

$$\begin{aligned} &\left[\frac{1}{r^2}\left(\frac{d}{dr}r^2\frac{d}{dr}\right) + \tilde{2}\bar{m}_e\left(E_{be} + K'_h\frac{e^{-br}}{1-e^{-br}}\right)\right] = 0\,,\\ &m_{\tilde{D}} = 2m_e + m_D - E_{be}\,,\\ &\tau_{\tilde{D}}^{-1} = 2\pi\lambda^2\,|\hat{\psi}(0)|^2\,\frac{\alpha^2 E_1}{\hbar} = 1\,\text{s}\,,\\ &R_{\tilde{D}} = b^{-1} = 2\times 10^{-13}\,\text{cm}\,. \end{aligned} \tag{51}$$

The solution of the above equations was reduced (see Eqs. (5.1.32a) and (5.1.32b), p. 840 of [82]) to the numeric values of two parameters denoted k_1 and k_2 that, in our case, become

$$k_1[1-(k_2-1)2] = \frac{1}{2\hbar c}\left(m_{\tilde{D}}b^{-1}\right) = 2.5\times 10^{-2} m_{\tilde{D}}\,, \tag{52}$$

$$\frac{(k_2-1)^3}{k_1} = 2.9\times 10^{-6}\left(\tau_{\tilde{D}}^{-1}b^{-1}\right) = 1.45\times 10^{-19}\,, \tag{53}$$

whose numeric solutions are given by

$$k_2 \approx 1\,,\quad k_1 \approx 1.45\,. \tag{54}$$

As it is well known, the binding energy is represented by the familiar *finite* spectrum of the Hulten potential (Eq. (5.1.20), p. 837, [82]) that in our case has the null value

$$\begin{aligned} &E_{be} = -\frac{1}{4K_h k_2}\left(\frac{k_2}{N} - N\right)^2 = 0\,,\\ &k_2 = K_h\,\frac{m_{\tilde{D}}}{\hbar^2 b^2} = 1\,, \end{aligned} \tag{55}$$

suggesting the existence of *one and only one energy value* that with $N = 1$ and $E_{be} = 0$ as expected because contact interactions have no potential.

In conclusion, the use of non-Hamiltonian/NSA interactions yields structure model (54) of the pseudo-Deuteron-2e predicting the following rest energy

$$m_{\tilde{D}} \approx 2m_e + m_D = 1.876\,\text{MeV}, \tag{56}$$

with the evident understanding that the above value needs a correction via hadronic mechanics of the Coulomb binding energy which is currently under study.

3.4 Spin of the pseudo-Deuteron-2e

Evidently, the total spin of the electron pair in structure (36) is identically null, while the Deuteron-2e is represented in its ground state, thus implying that the orbital angular momentum of the electron pair has the value $L_{2e} = 0$. Consequently, the total angular momentum of the electron pair is null and *the spin of the pseudo-Deuteron-2e coincides with that of the conventional Deuteron.*

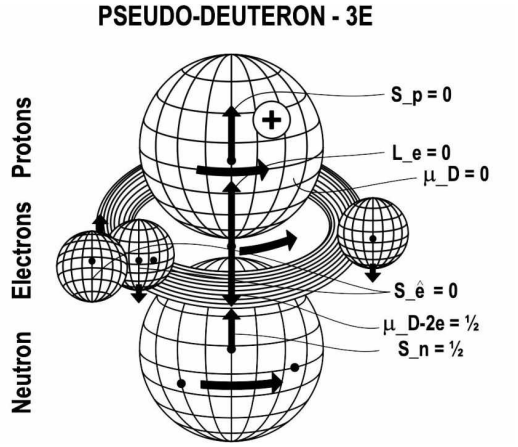

Fig. 4: In this figure, we illustrate the structure of the pseudo-Deuteron-3e predicted by hadronic mechanics as a bound state of an electron and a pseudo-Deuteron-2e (Sect. 3).

3.5 Magnetic moment of the pseudo-Deuteron-2e

Evidently, the magnetic moment of the electron pair in structure (36) is identically null. However, the *rotation* of the two elementary charges in the ground state creates a rather big magnetic moment (per nuclear standards) in the direction opposite that of the Deuteron magnetic moment.

In fact, the magnetic moment of the electron is given by

$$\begin{aligned} \mu_e^{spin} &= -9.284764\times 10^{-24}\,\text{J/T} =\\ &= 1838.2851\,\mu_{\text{N}}, \end{aligned} \tag{57}$$

(where J/T stands for Joules per Tesla and μ_{N} is the nuclear magnetron) thus being 2,162-times *bigger* than the magnetic moment of the Deuteron.

Direct calculations of the magnetic moment of elementary charges rotating within a dense hadronic medium are unknown at this writing. To have an order of magnitude of the magnetic moment of the pseudo-Deuteron-2e, we use the orbital magnetic moment of the electron in the synthesis of the neutrons from the Hydrogen in the core of star done in [84]–[97] (see also reviews [98]–[103]) which, in order to counter magnetic moment (57) to reach the neutron magnetic moment of $-1.9130\,\mu_{\text{N}}$, is given from (84) by $\mu_e = 1833.5801\,\mu_{\text{N}}$, resulting in the tentative prediction of the *magnetic moment of the pseudo-Deuteron-2e*

$$\mu_{\tilde{D}-2e} = -3.666\,\mu_{\text{N}}. \tag{58}$$

Evidently, a much bigger magnetic moment is predicted for the pseudo-Deuteron-3e.

4 Hyperfusion

4.1 Basic assumptions

In this section, we show that, according to our best understanding and documentation, the *Intermediate Controlled Nu-*

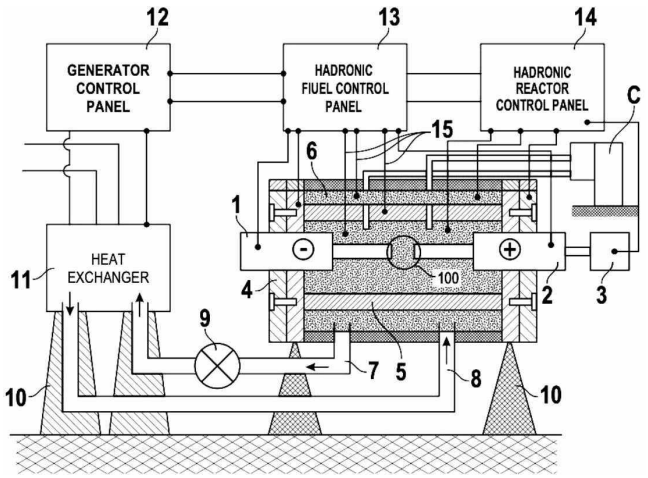

Fig. 5: In this figure, we provide a conceptual rendering of the main features of the hadronic reactor for the engineering realization of Intermediate Controlled Nuclear Fusions described in Sect. 4.3 according to Laws I-V of hadronic mechanics, including: 1. Stationary cathode; 2. Controllable anode; 3. Servomotor for the remote control of the electrode gap; 4. High pressure metal vessel; 5. External flanges; 6. Gaseous hadronic fuel, pump and tank; 7. Liquid coolant; 8. Outlet and inlet ports for the liquid coolant; 9. Liquid coolant pump; 10. Heat exchanger; 11. Electric power released to the grid; 12-13. Separate stands for the hadronic reactor and for the heat exchanger; 14. Electric power in; 15. DC power cables; 16. DC generator; 17. Variety of detectors for temperature, pressure, radiation, *etc*.; 18-20. Integrated remote and automatic control panels for the electric generator (19), hadronic fuel (20) and hadronic reactor (21), with automatic disconnect for any pre-set values for: outlet power; hadronic fuel temperature, pressure and flow; liquid coolant temperature, pressure and flow; *etc*; 21. Area in which the nuclear fusion occurs (for technical details see U. S. patents [129–131]).

clear Fusions (ICNF) tested from 2005 to 2016 [78] [104]–[128]: 1) Produce fully controlled energy without harmful radiations in excess of the used energy; 2) The production of excess energy via ICNF hadronic reactors has been limited to a few minutes for safety reasons, but it is expected to be continuous under sufficient funding and engineering; 3) The primary origin of the sustainable and controlled production of clean excess energy, here studied for the first time, appears to be primarily due to the capability by the ICNF technology of turning the nuclei of at least one of the two hadronic fuels into pseudo-nuclei (Sect. 3).

As done in the ICNF tests here considered, we assume that the hadronic fuels are *light, natural and stable elements* in their solid, liquid or gaseous form. The selection of their form is made following the engineering realization of the hadronic laws for nuclear fusions reviewed below.

Since ICNF are irreversible over time, in order to avoid the causality problems in the use of quantum mechanics or iso-mechanics identified earlier, all elaborations of ICNF are tacitly assumed to be done via the Lie-admissible geno-mathematics and geno-mechanics of Sect. 2.3.

4.2 Physical laws of controlled nuclear fusions according to hadronic mechanics

Following the quantitative representation of the neutron synthesis and its use for the exact representation of deuteron data, the physical laws of new clean nuclear energies predicted by hadronic mechanics have been presented for the first time in the 1998 monograph [78], specialized in the 2007 paper [104] and then developed at the scientific and industrial levels in subsequent years [105]–[128] according to the following classification:

Class I: Clean nuclear energies predicted via stimulated nuclear transmutations (Sect. III-4, p. 127 of [78]);

Class II: Clean nuclear energies predicted via controlled nuclear fusions (Sect. IV-3, p. 183 of [78]);

Class III: Clean energies predicted at the atomic-molecular level via contributions from energies of Class I and II (Sect. V-4, p. 287 of [78]).

In this section, we adopt the physical laws of Class II presented in Sect. 8, p. 149 of [104] and here specialized for the engineering realization of ICNF:

HADRONIC LAW I: Hadronic fusion reactors should have means for the systematic and controlled exposure of nuclei out of their electronic clouds. In the absence of such engineering means, it is assumed that nuclear fusions may indeed occur, but only at random.

HADRONIC LAW II: Whenever the nuclei of hadronic fuels have non-null spins, hadronic fusion reactors should have means for the systematic and controlled coupling of nuclear spins either in planar singlet or in axial triplet coupling (Fig. 1). In the absence of said engineering means, it is assumed that nuclear fusions may occur, but again, only at random.

HADRONIC LAW III: Hadronic fusion reactors should have means for the systematic and controlled transmutation of the nuclei of at least one of the two hadronic fuels into pseudo-nuclei (Sect. 3). In the absence of said engineering means, nuclear fusions remain possible but at a smaller efficiency rate.

HADRONIC LAW IV: The search for ICNF without the emission of harmful radiation or the release of radioactive waste should use light, natural and stable elements as hadronic fuels. Hadronic mechanics predicts that the use of heavy natural elements as hadronic fuels creates such instantaneous energy surges to trigger processes that may inevitably emit neutrons (see Appendix A for details).

HADRONIC LAW V: The energy used by hadronic reactors to achieve a desired energy output should be the minimal possible for the operation of all engineering components of the reactors. The Lie-admissible branch of hadronic mechanics predicts that any energy in excess of the indicated minimum creates instabilities with ensuing decrease of efficiency.

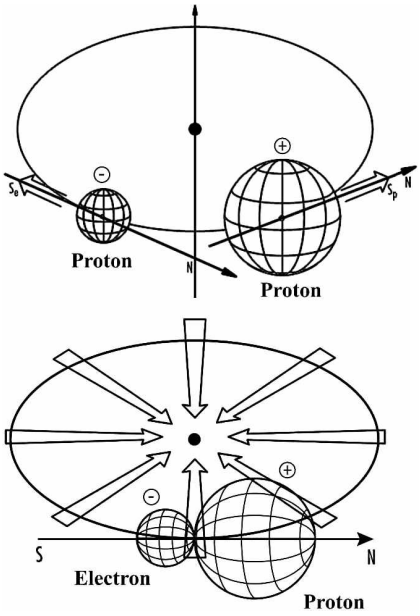

Fig. 6: In this figure, we illustrate the action of an electric DC arc between carbon electrodes submerged within a Hydrogen gas. The top view illustrates the ionization of the gas and the orientation of the proton and electron along a magnetic line, which occurs during the activation of the arc. The bottom view illustrates the compression of the plasma surrounding the arc in all radial directions toward its symmetry axis, which occurs during the disconnection of the arc [104].

4.3 Engineering realization and test of hadronic reactors for ICNF

The main principle for the engineering realization of ICNF according to Laws I-V suggested by decades of tests is the use of *DC arcs between carbon electrodes submerged within a gas.* This assumption implies that the first recommendable hadronic fuel is given by *Carbon C*$(6, 12, 0)$, while the second hadronic fuel is a properly selected, commercially available *gaseous fuel* flown through the arc to control its temperature and maximize efficiency (see U. S. patents [129–131]). Note that *Carbon nuclei have spin zero,* by therefore avoiding the need for the engineering realization of Hadronic Law II.

The action of submerged DC arcs on the gaseous hadronic fuel is the following:

1) Following their activation, DC arcs consume the point of the carbon electrode where they occur, with consequential disconnection and reconnection between points with the shortest distance. Hence, when activated, DC arcs consist of a continuous sequence of connection and disconnections generally occurring in [ms].

2) During their activation and under sufficient DC power (generally of a minimum of 40 kW), DC arcs ionize the gas, by creating a plasma in their surroundings comprising electrons, nuclei and atoms (left view of Fig. 6).

3) During their reconnection, DC arcs have been proved by the technology for the neutron synthesis (Fig. 11, 12 and Appendix B) to *compress* the surrounding plasma in all radial directions toward its symmetry axis (right view of Fig. 6).

Fig. 7: In the top figure, we show the main components of the Nitrogen hadronic reactor [105]; in the bottom left picture, we show the team of experimentalists from Princeton Gamma Spectroscopy Corporation [118]–[121] headed by L. Ying, President, who confirmed all results of [105]; in the bottom right picture, we show the confirmation of the lack of neutron or other harmful radiations by R. Brenna [110].

Consequently, to the author's best knowledge, submerged DC arcs provide the best known means for the verification of Hadronic Laws I-V, with particular reference to the synthesis of pseudo-nuclei (Hadronic Law III).

Hadronic reactors for the engineering realization of ICNF consist of: a metal vessel containing a gaseous hadronic fuel at pressure traversed by internal electrodes with remote means for the monitoring and control of the arc power, arc gap, gas pressure, gas temperature, vessel temperatures, gas flow through the arc, heat exchanger; a variety of neutrons and other detectors; interconnected, remote, monitoring and control panels of the various functions with automatic disconnect of all systems in the event of any deviation of the data from pre-set values (for details, see Fig. 5 and U. S. patents [129–131]).

In regards to manufacturing data, tests [104]–[109] were done via hadronic reactors comprising: cylindrical metal vessels with outside diameters ranging from 1 foot to 2 feet and length ranging from 2 feet to 6 feet, said vessels being certified to withstand internal pressures at least up to three times the expected operating pressure; electrodes fabricated form cylindrical graphite rods ranging from 1 to 2 inches diame-

ter with the non-consuming anode generally being 4 inches long and the consuming cathode generally being a minimum 6 inches long; a metal jacket surrounding said vessel containing a coolant (such as water) which is recirculated through a heat exchanger; specially designed control panels for the various functions; and other engineering means (Fig. 5).

All tests [104]–[109] were done via a 50 kW Miller Electric Dimension 1000, AC-DC converter operating at 40 kW by therefore supplying 0.866 kWh per minute. The reader should be aware that the use (in lieu of a commercially available AC-DC converter) of the special DC power unit for the neutron synthesis (Appendix B) provides a significant increase of the energy output due to special features of the DC arc not outlined here for brevity. All ICNF tests conducted from 2005 to 2019 by the U. S. publicly traded company *Thunder Energies Corporation,* now the private company *Hadronic Technologies Corporation* which owns all intellectual rights on ICNF. All ICNF tests were done from 2005 to 2016 with *private funds.*

Samples of the solid and gaseous hadronic fuels where taken for all ICNF tests outlined in Sects. 4.4, 4.5, 4.6, under the Trail of Custody by the technician Jim Alban before and after the tests and sent out for analysis by independent companies.

More specifically, laboratory bottles were filled up with the gaseous hadronic fuel at ambient temperature of about $80^{o}\,\mathrm{F} = 26^{o}\,\mathrm{C}$ before and after the activation of the reactor. Said samples were individually marked and shipped to *Oneida Research Services* (ORS) of Whitebnodo, New York, for the *two* different analyses of reports [118]–[124], the first for *molecular* counts and the second for *nuclear* counts with Atomic Mass Units from 2 u to 400 u, which were done via an Internal Vapor Analyzer, model 110-s operated with SOP MEL-1070. The generally low pressure of the various laboratory bottles were also marked and are reported in the individual ORS reports.

The following information is important for the proper interpretation of ORS reports: 1) The molecular and nuclear counts are inequivalent due to molecular anomalies caused by the DC arc discussed in Sect. 4.7; 2) The total number of nuclear counts before and after the tests are not the same because the Avogadro number is not conserved under nuclear fusions; 3) Reported nuclear counts generally refer to primary counts out of possible counts from 2 u to 400 u, thus implying that the sum of all counts per given sample does not necessarily add to 100; 4) The type of gas was not generally disclosed to ORS, thus implying that the used gaseous hadronic fuel is generally identified in a given report by the biggest number of reported counts; 5) The approximate character of the analyses is unquestionable, yet sufficient to establish the *existence* of an excess clean energy produced by ICNF, with the understanding that readers interested in the utmost possible accuracy should wait for proper funding.

Also under the Trail of Custody by Jim Alban, samples of the graphite used for the electrodes were taken before and after each test, marked and shipped to *Constellation Technology* of Largo, Florida, for analyses available in reports [125]–[128]. It should be noted that the latter analyses are for *solid* traces of new elements in the electrodes following tests, that confirm *some* of the nuclear fusions detected by the ORS analyses, but not all, since the primary nuclear fusions occur at the gaseous level.

Fig. 8: In this figure, we show the Oxygen hadronic reactor for the ICNF of Helium and Carbon into Oxygen (Sect. 4.5) with the structure outlined in Fig. 5, including: in the top view, the engineer Chris Lynch, the reactor, its control panel and the power unit; in the bottom left view, the scorching of the cathode despite its continuous cooling by the flow of the Helium; in the bottom right view, the production of steam operated by the author.

4.4 ICNF with the Nitrogen hadronic reactor [105]

The *Nitrogen hadronic reactor* ([105]–[107] and Fig. 7) was built according to the specifications described in Sect. 4.3 and in Fig. 5. In particular, the metal vessel was built out of Schedule 40 steel tube 1 foot $\times$ 2 feet with 1/2 inch thickness weighting 325 lbs plus side flanges weighting 125 lbs each for a total of 575 lbs certified to withstand 300 psi. All tests were done with gaseous hadronic fuels at 100 psi and for a maximum of *two minutes* due to the rapidity of the temperature surge.

Among the variety of tests with the Nitrogen hadronic reactor from 2005 to 2016, we outline below the following tests with the understanding that, to avoid an excessive length, all technical details are referred to [105]–[107]:

4.4.1 ICNF with Deuterium and Carbon

The Nitrogen hadronic reactor was filled up with a commercial grade Deuterium gas at 100 psi pressure under 40 kW DC power. Following two minutes of operation, the external temperature of the reactor went from 26° C to 150° C. Two laboratory bottles before and after the activation of the reactor were filled up with the gas at the pressure indicated in the reports, market HCN1 and HCN2, respectively and shipped to ORS. The results are available in [118] and will be analyzed for nuclear fusions in Sect. 4.7.

4.4.2 ICNF with Hydrogen and Carbon

The preceding results were confirmed by tests in the Nitrogen hadronic reactor with a commercial grade Hydrogen at 100 psi pressure and 40 kW DC power, as reported in Sect. 6 of [105] and in ORS report [120] for bottles market HC1 and HC2 (see Sect. 4.7 for their study). An important result of this test is that, under the same conditions of pressure, power, electrodes, *etc*. of the preceding test with Deuterium and Carbon, the operation with a hydrogen gas produced an energy excess bigger than that with Deuterium gas, since in two minutes of operation the temperature of the exterior wall of the reactor went from 26° C to 254° C with about 1.72% *increase* of the temperature compared to the test with Deuterium.

4.4.3 ICNF with Magnegas and Carbon

The most successful tests with the Nitrogen hadronic reactor occurred with the use as hadronic fuel of *magnegas,* the gaseous fuel with the new magnecular structure [72, 131] (Fig. 10). The results of the ORS analyses are reported in [120] for bottles marked MG1 and MG2. A main result of various tests is that the Nitrogen hadronic reactor operating with magnegas at 100 psi pressure under 40 kW power went from 26° C to 254° C in *one minute,* rather than the two minutes as for then Hydrogen-Carbon tests, thus implying a 3.44 increase of efficiency of the Deuteron-Carbon tests.

We should indicate the conduction of additional tests with the Nitrogen hadronic reactor by using various gaseous fuels whose analyses are available from [119].

4.5 ICNF with the Oxygen hadronic reactor

The Oxygen hadronic reactor (see [106]–[107], independent studies in [113], ORS reports [121, 122] and Fig. 8 in the present paper) was built in 2010 for testing the ICNF of Helium and Carbon into Oxygen, by therefore using Helium as the gaseous hadronic fuel.

The hadronic reactor comprised: a vertical 1 foot × 4 feet Schedule 40 steel cylinder certified to withstand 500 psi; a chamber surrounding said vessel for flowing water as coolant; the flow of the gaseous hadronic fuel through the electrodes for its cooling; and the remaining engineering component illustrated in Fig. 5.

The reactor was additionally built to test the feasibility of the new principle of combustion subsequently released in 2018 under the name of *HyperCombustion* [145] which is intended to achieve the full combustion of fossil fuels via a combination of a conventional combustion plus ICNF in Parts Per Million by Volume, ppmv.

For the test done in April 2010, the laboratory bottles prior and after the test were filled up with the internal gas at the pressure indicated in the reports, market HT1 and HT2 and shipped to ORS for analysis whose results are available from [121]. The tests were repeated in February 2011, market HE1 and HE2 and sent to ORS for analyses whose results are available from [122] (see Sect. 4.7 for their analysis).

The primary result of the tests was the proof under various eyewitnesses that, when filled up with Helium at 100 psi and operated with a 40 kW AC-DC converter, the Oxygen hadronic reactor did indeed produce a steam sustainable for two minutes after which the cooling system was insufficient to maintain the reactor at a constant temperature.

During additional tests done on May 15, 2011, with the Helium hadronic fuel at 150 psi, in two minutes of operation the mixture of Helium and synthesized Oxygen sent the internal temperature gauge off the 10 000° C limit and melted the top Helium recirculation port, with an impressive release of the incandescent interior gas after which all tests with the Oxygen hadronic reactor were terminated for safety. The technicians (who eyewitnessed the discharge at a distance) nicknamed *Dragons* the hadronic reactors (Dragons I, II and III for the Nitrogen, Oxygen and Silicon reactors, respectively).

4.6 ICNF with the Silicon hadronic reactor

The Silicon hadronic reactor ([106]–[108], video [109] and Fig. 9) was built to test the ICNF of Oxygen and Carbon into Silicon via the use of *air* as hadronic fuel, instead of pure Oxygen, because the natural mixture of 78% Nitrogen and 21% Oxygen is known to quench the Oxygen reactance experienced in Section 4.5.

The hadronic reactor consisted of a Schedule 40 steel tube with 1 foot diameter and 6 feet long certified to withstand a 5 000 psi pressure. Air was continuously pumped through the reactor at 1 000 psi. The arc was powered by a 50 kW AC-DC converter. The reactor was surrounded by a jacket as in Fig. 5 in which water was continuously pumped at ambient pressure. The superheated air and cooling water from the reactor were mixed to power an electricity producing turbine whose data are analyzed in Sect. 4.7. To avoid an excessive length, we suggest interested readers to view video [109] for a detailed description of this third hadronic reactor including the identification of the various members of the experimental team.

The analyses for the gaseous part of the test are available from ORS [123, 124], and the analyses for the solid part are

Fig. 9: In this figure, we illustrate the hadronic reactor for the ICNF of Oxygen and Carbon into Silicon (Sect. 4.6), with a structure outlined in Fig. 5 and described in detail in the video [109], including: in the top row, a front and rear view; in the middle view, the reactor and the touch screen for remote control; in the bottom view, one of control panels and some of the technicians (from the left) Chrys Lynch, Jim Alban and Michael Rodriguez eye-witnessing the sustainable and controllable production of steam from the turbine for the duration of 15 min.

available from Constellation Technology [125]–[128]. Independent studies are available from [110]–[117].

The main result of the tests with the Silicon hadronic reactor is that, under various eyewitness (see Fig. 9 and [109]), *the Silicon hadronic reactor did prove the capability by ICNF to produce clean excess energy for* 15 min *(fifteen minutes),* after which the remote monitoring and control panels automatically disconnected the operation for the inability of the cooling system to maintain the reactor temperature within a pre-set safety value. No additional tests were done with the Silicon hadronic reactor due to lack of funds for the construction of a properly engineered *prototype hadronic power plant.*

4.7 Representation of ICNF excess energy via hyperfusions

The ICNF tests conducted from 2015 to 2016 via the Nitrogen, Oxygen and Silicon hadronic reactors [104]–[109] were conceived, conducted and reported under the assumption that the Hadronic Laws for nuclear fusions available at that time [78] were verified by the processing, via a submerged DC arc, of the gaseous hadronic fuel into the new chemical species

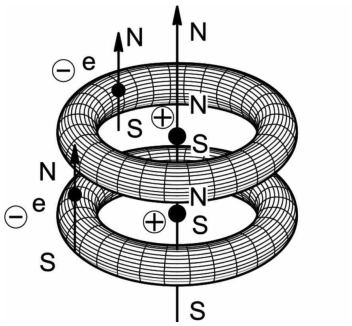

Fig. 10: In this figure, we illustrate the simplest possible case of the new chemical species of magnecules [72–74, 131], which is characterized by two atoms with a toroid polarization of their orbits caused by a DC arc which atoms are bonded together according to an axial triplet coupling thanks to their newly acquired magnetic field which does not exist in natural atomic configurations.

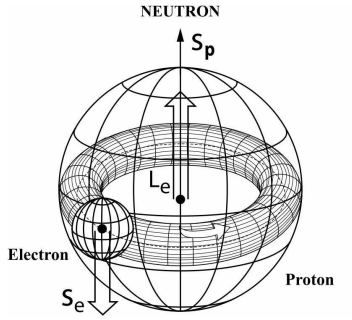

Fig. 11: In this figure, we illustrate the synthesis of the neutron from a proton and an electron in the core of stars according to hadronic mechanics reviewed in Appendix B [84]–[103].

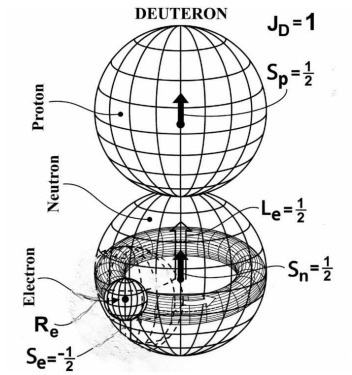

Fig. 12: A view of the structure of the Deuteron according to the synthesis of the neutron from a proton and an electron in the core of Stars ([83] and Appendix B).

of *magnecules* [72, 131] (see the MG1 counts in [120] for a sample of its anomalous chemical structure), due to the verification by magnecules such as $C \times D$ (Fig. 10) of Hadronic Laws I and II. The fusion $C \times D \to N$ was then supposed to be permitted by the compression of the magnecules during the disconnection of the DC arc (Fig. 6).

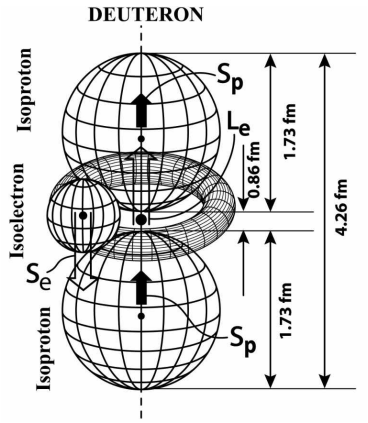

Fig. 13: In this figures, we illustrate the representation by hadronic mechanics of the stability of natural nuclei despite the natural instability of their neutrons. Said representation is intrinsic in the hadronic synthesis of the neutron from a proton and an electron (Appendix B), and it is given by the decoupling of the electron to assure a symmetric position between the two attracting protons (Appendix C). Note that the model implies the reduction of all matter in the universe to protons and electrons.

Subsequent studies have revealed that the sole creation of a magnecular structure for gaseous hadronic fuels is insufficient for a consistent representation of the nuclear fusions reported in the ORS nuclear counts for various reasons, including:

1) As shown below, the representation of ORS data on the fusion of Oxygen, Silicon and higher nuclei requires the prior fusion of two Deuterons into the Helium, which has not been achieved to date in a sustainable form via conventional engineering means;

2) Deuterium atoms are ionized by the DC current of the ICNF tests, by therefore resulting in Deuterons and electrons;

3) Explicit calculations done via the Ampere law have shown that the compression caused by the disconnection of the DC arc is unable to overcome the *extremely big Coulomb repulsion* between two Deuterons at 1 fm mutual distance, Eq. (1), by therefore rendering impossible their fusions into the Helium.

To the author's knowledge, the best possibility for two Deuterons to fuse into the Helium is that one of them acquires the form of pseudo-Deuteron (Sect. 3) since in that case all Hadronic Laws I-V are verified due to opposite charges and magnetic moments, including the planar spin coupling, under an extremely big Coulomb *attraction,* and the consequential inevitable activation of strong nuclear forces under which the fusion is inevitable. In this section, we study the excess clean energy produced by the ICNF [104]–[109] to illustrate the plausibility of their being in reality hyperfusions.

The excess energy produced by the Nitrogen hadronic reactor (Sect. 4.4.1) over the used energy in two minutes of 1.333 kWh was tentatively appraised in Sect. 4. Eq. (4.3) of [105] resulting in the value

$$\Delta E = E^{out} - E^{in} = \\ = 2.203 - 1.333\,\text{kWh} = 0.87\,\text{kWh}\,. \tag{59}$$

These preliminary appraisals were confirmed by the independent analysis [113]. By using a different method, Sect. 3.3 of the independent study [110] reached the value

$$\Delta E = 2.88\,\text{MJ} = 0.138\,\text{kWh}\,. \tag{60}$$

The tests of Sect. 4.4.2 then imply a clean excess energy of 1.73% bigger then that of (59), i.e.,

$$\Delta E = E^{out} - E^{in} = \\ = 2.823 - 1.333\,\text{kWh} = 1.49\,\text{kWh}\,. \tag{61}$$

For the case of magnegas as hadronic fuel (Sect. 4.4.3) we would then have an excess clean energy 3.44 times bigger that that of (59) in only one minute,

$$\Delta E = E^{out} - E^{in} = \\ = 23.656 - 0.666\,\text{kWh} = 2.99\,\text{kWh}\,. \tag{62}$$

It should be noted that the above preliminary appraisals are significantly *below* the excess energy actually produced by the hadronic reactors because said appraisals used the *external temperature* of the hadronic reactors, rather than the actual *internal temperature*. As an example, calculations done for the tests indicated in Section 4.1.2 with the Helium as hadronic fuel at 150 psi and the temperature of the internal gas in excess of 10 000° C in two minutes of operation we would have a multiple of value (62). The same large thermal values can be obtained from the tests of Section 4.6 with the Silicon hadronic reactor operating at 1 000 psi.

In view of the indicated insufficiencies of thermal calculations of excess clean energy produced by the hadronic reactors, in this section we present, apparently for the first time, an alternative approximate calculation of excess energy output based on the energy produced by the primary nuclear fusions reported in the ORS counts. Along these lines, [118] reports the following primary increased counts Δu among numerous other counts that are omitted in this first study for brevity,

$$\begin{aligned}
&(a)\ \ \Delta 2u : 18,550,801 - 16,075,402 = \\
&\qquad = 2,475,399\,\text{ppmv}\,, \\
&(b)\ \ \Delta 3u : 41,165 - 30,269 = 10,896\,\text{ppmv}\,, \\
&(c)\ \ \Delta 4u : 76 - 0 = 76\,\text{ppmv}\,, \\
&(d)\ \ \Delta 14u : 3,555 - 2,841 = 714\,\text{ppmv}\,, \\
&(e)\ \ \Delta 16u : 3,010 - 1,205 = 1,805\,\text{ppmv}\,, \\
&(f)\ \ \Delta 18u : 2,949 - 2,718 = 231\,\text{ppmv}\,, \\
&(g)\ \ \Delta 28u : 30,171 - 24,684 = 3,687\,\text{ppmv}\,.
\end{aligned} \tag{63}$$

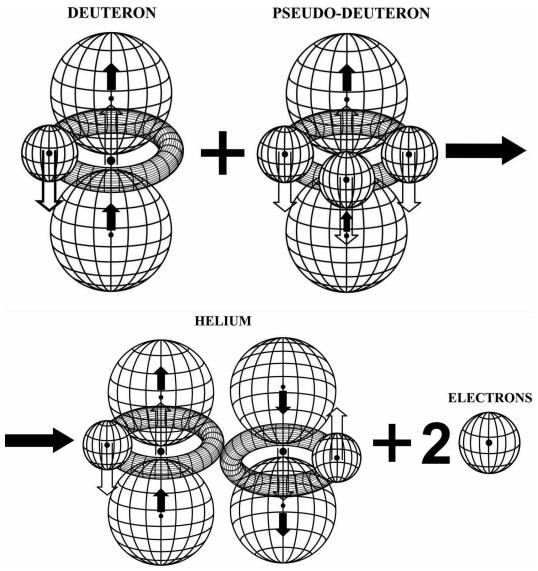

Fig. 14: In this figure, we illustrate the hyperfusion of a natural Deuteron and a pseudo-Deuteron-2e into the Helium plus the emission of an electron pair (Sects. 3 and 4).

Recall the following tabulated values (see e.g. [1])

$$\begin{aligned} &E_e = 0.511\,\text{MeV}\,,\\ &E_p = 938.272\,\text{MeV}\,,\quad E_n = 939.565\,\text{MeV}\,,\\ &E_D = 2.014102\,\text{u}\,,\quad E_{He} = 4.002603\,\text{u}\,,\\ &E_C = 12.00000\,\text{u}\,,\quad E_N = 14.003074\,\text{u}\,,\\ &E_O = 15.994915\,\text{u}\,,\quad E_{Si} = 27.976927\,\text{u}\,,\\ &1\,u = 931.5\,\text{MeV}\,. \end{aligned} \tag{64}$$

Recall also that the commercial grade Deuterium gas used for the tests contained a considerable percentage of Hydrogen. From our studies on the neutron synthesis (Appendix B), we expect that the reactor first synthesized the neutron according to the *endothermic* reaction (82)

$$\hat{e}^- + \hat{a} + p^+ \to n\,,\quad \Delta E_n = -0.782\,\text{MeV}\,. \tag{65}$$

Immediately following their synthesis, neutrons are compressed by the arc against the protons, by therefore synthesizing the Deuterium. This would explain the considerable increase of counts (a) in (63)

$$n + p \to D(1,2,1)\,,\quad \Delta E_D = 1.7045\,\text{MeV}\,. \tag{66}$$

Count (b) of (63) is interpreted as the synthesis of the Tritium with an energy balance here assumed, for simplicity, to be similar to that for the Deuterium. Count (c) of (63) is evidently the synthesis of the Helium from two Deuterons which, according to our view, can be best interpreted as the hyperfusion between a pseudo-Deuteron-2e and a natural Deuteron according to the general rule of (28) (Fig. 14),

$$\begin{aligned} &\tilde{D}_{2e}(1,2,1_\uparrow) + D(1,2,1_\downarrow) \to He(2,4,0) + \beta^-_\uparrow + \beta^-_\downarrow\,,\\ &\Delta E_{4\,u} = 23.8473315\,\text{MeV}\,. \end{aligned} \tag{67}$$

Count (d) of Eq. (63) is interpreted via the synthesis of the Nitrogen,

$$\begin{aligned} &\tilde{D}_{2e}(1,2,1) + C(6,12,0) \to N(7,14,1) + 2\beta^-\,,\\ &\Delta E_{14\,u} = 10.272582\,\text{MeV}\,. \end{aligned} \tag{68}$$

Count (e) is interpreted as due to the synthesis of the Oxygen

$$\begin{aligned} &\tilde{He}_{ke}(2,4,0) + C(6,12,0) \to O(8,16,0) + k\beta^-\,,\\ &\Delta E_{16\,u} = 7.161372\,\text{MeV}\,. \end{aligned} \tag{69}$$

Count (f) of (63) is evidently due to the synthesis of the Silicon

$$\begin{aligned} &\tilde{O}_{ke}(8,16,0) + C(6,12,0) \to Si(14,28,0) + k\beta^-\,,\\ &DeltaE_{15\,u} = 16.755822\,\text{MeV}\,. \end{aligned} \tag{70}$$

Even though incomplete, the above ICNF are sufficient to illustrate the sustainable and controllable production of clean energy by ICNF.

By using the data from (63) to (70), we have the following energy output for the counts of (63):
Deuterium synthesis: 2, 283, 555 MeV in ppmv which is given by the energy released by the Deuterium synthesis 2,475,399 ppmv $\times$ 1.7045 MeV = 4, 219, 317 MeV in ppmv *less* the energy needed for the neutron synthesis $2,475,399 \times 0.782 = 1,935,762$ MeV;
Helium synthesis: 76 ppmv $\times$ 23.8 MeV = 1, 808.8 MeV in ppmv;
Nitrogen synthesis: 714 ppmv $\times$ 10.3 MeV = 7, 354.2 MeV in ppmv;
Oxygen synthesis: $1,805 \times 7.2$ MeV = 12, 996 MeV in ppmv;
Silicon synthesis: 3, 687 ppmv $\times$ 16.7 MeV = 61, 573 MeV;
resulting in the total energy output of 54, 546, 518 MeV in ppmv corresponding to the total energy output of

$$54,546,518\,\text{MeV} = 2.43 \times 10^{-12}\,\text{kWh}\,. \tag{71}$$

By assuming that the gas in the reactor is a perfect gas, by assuming the related law

$$PV = nRT\,, \tag{72}$$

and by recalling that one mole contains 6.02×10^{23} particles, that is, 6.02×10^{17} *millions* of particles, the total energy output for data (63) is given by

$$\begin{aligned} &\Delta E = E^{out} - E^{in} =\\ &= 2.43 \times 10{-}12 \times n \times 6.02 \times 10^{17} - 1.333\,\text{kwh} \approx\\ &\approx n \times 14.628 \times 10^5\,\text{kwh}\,. \end{aligned} \tag{73}$$

For a first approximation of the number of moles n, we assume the conversions for: pressure 100 psi = 6.8 atm; length 1 foot = 2.54 cm; radius of the cylinder r = 1 foot = 13.97 cm; height of the cylinder h = 2 ft = 60.85 cm; and volume of the gas $V = \pi \times r^2 h = 3.14 \times 196 \times 60.85 = 37,455\,\text{cm}^3 = 37.45\,\text{L}$. Consequently, $PV = 6.8 \times 37.45 = 254.66$. Since the gas constant is given (in our units) by $R = 0.0821$, we have $PV/R = 254.66/0.0821 = 3,101.827$. Consequently, an approximate value of the total number of moles under the indicated assumptions is given by

$$n = 3 \times 10^3 \times \frac{1}{T}. \tag{74}$$

We now assume that the internal gas is Hydrogen and that its temperature varies from the expected 1 000 000° C in the small area of the nuclear fusions all the way to temperatures of the order of 1 000° C in the back of the reactor wall, resulting in an average temperature of the order of 10^5 C. A similar temperature value is reached via calculations based on the transmission of from 26° C to 150° C through a 1/2 inch steel wall within a period of time of the order of sixty seconds via a gas, such as Hydrogen, with the smallest possible density.

By using the equivalency 0° C ≡ 273.15 K, we have 150° C ≡ 423.15 K, our approximate value of the number of moles is given by

$$\begin{aligned} n = 3 \times 10^3 \times \frac{1}{T} = 3 \times 10^3 \times \frac{1}{423} \times 10^{-5} = \\ = 0.00704 \times 10^{-2} = 7.04 \times 10^{-4}\,. \end{aligned} \tag{75}$$

Corrections of the above value for the total number of moles of a Deuterium gas reduce the above value to

$$n \approx 7 \times 10^{-5}\,. \tag{76}$$

The approximate total output of controlled clean energy of the considered ICNF is then given by

$$\begin{aligned} \Delta E = E^{out} - E^{in} = \\ = 7 \times 10^{-5} \times 15 \times 10^5 - 1.333\,\text{kWh} \approx 100\,\text{kWh}\,. \end{aligned} \tag{77}$$

It is easy to see that, for the case of the tests of the Silicon hadronic reactor (Section 4.6) done at 1,000 psi of the gaseous hadronic fuel, the repetition of the above analysis yields a total sustainable and controllable, clean energy output of the order of 1,000 kWh, out of which the surplus electric energy released by a turbine operated electric generator is expected to be of the order of 100 kWh.

The author has no words to indicate again the approximate character of the above appraisal. More accurate calculations are planned for the forthcoming paper [146].

5 Concluding remarks

In this paper, we have recalled the generally forgotten insufficiencies of quantum mechanics in nuclear physics in view of its inability in about one century of achieving: A) A quantitative representation of the fundamental synthesis of the neutron from a proton and an electron in the core of stars; B) An exact representation of nuclear magnetic moments; C) An exact representation of the spin of nuclei in their true ground state (that without the usual orbital excitations); D) A quantitative representation of the stability of neutrons when members of a nuclear structure; E) A quantitative representation of the stability of nuclei despite the huge Coulomb repulsion between positive nuclear charges; and other insufficiencies.

We then recalled the largely forgotten experiments establishing deviations of quantum mechanical predictions from physical reality in various fields, including: electrodynamics; condensed matter physics; heavy ion physics; time dilation for composite particles; Bose-Einstein correlation; propagation of light within physical media; and in other fields.

We additionally recalled that *quantum mechanics is reversible over time* due to the invariance of Heisenberg's equation under anti-Hermiticity and for other reasons. Consequently, quantum mechanics cannot provide a consistent representation of energy-releasing processes such as nuclear fusion due to their *irreversibility over time.* In particular, we have shown that the treatment of nuclear fusions via quantum mechanics may violate causality laws (e.g., because of solutions in which effects precede the cause), because the same Schrödinger equation applies for nuclear fusions forward as well as backward in time.

We then recalled that the axiomatic origin of the above insufficiencies of quantum mechanics has been first identified in 1935 by A. Einstein, B. Podolsky and N. Rosen and rests in the *locality* of the theory (EPR argument) [5], beginning at the level of the Newton-Leibnitz calculus, due to the sole possibility of characterizing particles and nuclei as massive points, thus creating conceptual and technical difficulties in fusing two points into a third point.

We then briefly reviewed the EPR completion of quantum mechanics into hadronic mechanics for the characterization of particles and nuclei as *extended, thus deformable and hyperdense* under conventional, Hamiltonian interactions plus contact, thus zero-range, non-Hamiltonian interactions caused by mutual penetrations, with an elementary review of:

i) The Lie-isotopic (i.e. axiom-preserving) branch of hadronic mechanics including *iso-mathematics and iso-mechanics* (Sect. 2.2) for the representation of extended particles and their non-Hamiltonian interactions via the isotopic element $\hat{T} = \hat{T}^\dagger > 0$ of the universal enveloping iso-associative algebra of Hermitean operators with product $A \star B = A\hat{T}B$ and ensuing iso-Schrödinger equation $H \star |\psi\rangle = H\hat{T}|\psi\rangle = E|\psi\rangle$ with apparent resolution of quantum mechanical insufficiencies for *stable* nuclei.

ii) The Lie-admissible branch of hadronic mechanics, also called genotopic branch, including *geno-mathematics and geno-mechanics* (Sect. 2.3) based on forward enveloping algebra with ordered products to the right $A > b = ARB$, R-

> 0 representing motion forward in time, and backward enveloping algebra with ordered products to the left $A < B = ASB, S > 0$ representing motion backward in time, with the corresponding forward and backward geno-Schrödinger equations $H > |\psi^{for}\rangle = HR|\psi^{for}\rangle = E^{for}|\psi^{for}\rangle$, $\langle\psi^{bac}| < H = \langle\psi^{bac}|S\,H = E^{bac}\langle\psi^{bac}|$, and axiomatically consistent resolution of the quantum mechanical causality problems for irreversible processes whenever $R \neq S$.

Thanks to half a century preparatory studies on the above issues, in this paper we have presented apparently for the first time:

1) The prediction by hadronic mechanics of the existence of new, negatively charged, unstable nuclei, called *pseudo-nuclei,* which are characterized by a hadronic bond of negatively charged electrons and positively charged natural nuclei, by therefore resolving the Coulomb barrier since pseudo-nuclei would be *attracted* (rather than repelled) by natural nuclei, with ensuing new conception of nuclear fusions between pseudo-nuclei and natural nuclei, here called *hyperfusions* (Section 3);

2) The identification of engineering means for the synthesis of pseudo-nuclei which is given by the hadronic reactors for the synthesis of the neutron from the proton and the electron (Sects. 4.1-4.6 and Appendix B);

3) Laboratory evidence according to which the synthesis of pseudo-nuclei and related hyperfusions appear to be the origin of the limited, yet sustained and controlled excess energies achieved by the *Intermediate Controlled Nuclear Fusions* (Section 4.7).

In view of the inability by quantum mechanics in about one century under large public funds to achieve industrially applicable nuclear fusions, and the consequential, rapidly increasing deterioration of our environment, the author hopes that appropriate academic and governmental entities initiate the implementation of a true scientific democracy for qualified inquiries, which requires the continuation of the search for clean nuclear energies along quantum mechanical lines, *jointly* with the search based on new vistas, such as the forgotten EPR argument.

Appendices

A Is neutron radiation truly necessary for nuclear fusions?

As it is well known, it has been generally assumed for about one century that the emission of harmful neutrons is necessary for nuclear fusions (see e.g. [132]), as it is the case for the *Tokamak nuclear fusion* of Deuterium and Tritium into Helium plus neutron [133, 134]

$$\begin{aligned} &D(1,2,1) + D(1,3,1/2) \to He(2,4,0) + n\,,\\ &\Delta E = +17.6\,\text{MeV}\,. \end{aligned} \tag{78}$$

The author respectfully suggests the conduction of *experimental verifications* of the need for the emission of neutrons in Deuteron-type fusions prior to its systematic use under public support, in view of the following opposing evidence:

A.1. The need for the emission of neutrons in nuclear fusions was historically established for the fusions of *heavy nuclei* but, to the author's best knowledge, no quantitative study is currently available on a similar need for the fusion of *light nuclei,* such as the Deuterium and the Tritium.

A.2. It is known that, in the core of stars, Deuterons fuse into the Helium without neutron emission,

$$\begin{aligned} &D(1,2,1_\uparrow) + D(1,2,1_\downarrow) \to He(2,4,0)\,,\\ &\Delta E = +29.523\,\text{MeV}\,, \end{aligned} \tag{79}$$

since the Coulomb barrier is overcome by the extreme local pressures, while collective fusions leading to the explosion of the star are prohibited by the random spin alignment of fusion (79).

A.3. There exists valid evidence of excess heat creation in condensed matter due to nuclear fusions of light nuclei without the emission of neutrons [135–137].

A.4. The assumption of the necessary emission of neutrons in the fusion of light nuclei is based on a theory, quantum mechanics, which is only *approximately valid* in nuclear physics due to its inability in one century of achieving exact representations of basic nuclear data (Sect. 1).

A.5. Clear experimental evidence achieved in major physics laboratories has established the existence of deviations of quantum mechanical predictions from physical reality in various fields [12]–[26].

A.6. The unverified assumption of the necessary emission of neutrons in nuclear fusion is made in oblivion of the Einstein-Podolsky-Rosen argument that *Quantum mechanics is not a complete theory* [5].

A.7. The totality of the *intermediate Controlled Nuclear Fusions* occurred with the independently certified absence of any neutron emission [104]–[128].

Since sustainability has not been achieved in about one century for nuclear fusions with neutron emission, nuclear fusions without neutron emission should deserve the same scientific process.

B The synthesis of the neutron in a star

In 1920, E. Rutherford [138] suggested that the hydrogen atom in the core of stars is "compressed" into a new particle that he called the *neutron*

$$e^- + p^+ \to n\,. \tag{80}$$

In 1932, J. Chadwick [139] provided an experimental confirmation of the existence of the neutron.

In 1933, W. Pauli [140] pointed out that synthesis (80) violates the conservation of angular momentum.

In 1935, E. Fermi [141] submitted the hypothesis that the synthesis of the neutron occurs with the joint *emission* of a

neutral and massless particle ν with spin 1/2 that he called the *neutrino* (meaning "little neutron" in Italian)

$$e^- + p^+ \ \rightarrow \ n + \nu \, . \tag{81}$$

In 1978, R. M. Santilli [82] (see also the 2021 update [29]) identified various arguments according to which quantum mechanics is *inapplicable* to (rather than violated by) the neutron synthesis, beginning with the fact that the rest energy of the neutron is *bigger* than the sum of the rest energies of the proton and the electron,

$$\begin{aligned} &E_p = 938.272 \, \text{MeV} \, , \ \ E_e = 0.511 \, \text{MeV} \, , \\ &E_n = 939.565 \, \text{MeV} \, , \\ &\Delta E = E_n - (E_p + E_e) = 0.782 \, \text{MeV} > 0 \, , \end{aligned} \tag{82}$$

by therefore requiring a *positive binding energy* and resulting in a *mass excess* for which the Schrödinger and Dirac equations admit no physically meaningful solutions.

Consequently, when he was at Harvard University under support of the U.S. Department of Energy, R. M. Santilli proposed [49] the construction of the non-unitary Einstein-Podolski-Rosen completion of quantum mechanics into a new mechanics called *hadronic mechanics* (Sect. 2).

Following the achievement of mathematical and physical maturity [51] (see [30, 31] for detailed treatment), the Lie-isotopic branch of hadronic mechanics allowed the representation of *all* characteristics of the neutron at the non-relativistic and relativistic levels via a structure model of the neutron consisting of an electron e^- totally compressed inside the extended and dense proton p^+ in singlet coupling [84]–[89] (Figs. 11, 12 and 13).

At the non-relativistic level, the exact representation of the **mass, mean life and charge radius of the neutron** were achieved via structure equations of type (51) [84].

The exact representation of the **spin of the neutron** was achieved thanks to the appearance of the *internal orbital motion* of the electron within the extended and dense proton with angular momentum $L_e = 1/2$ (which is necessary to avoid major resistive forces), resulting in the following realization of Rutherford's original conception of the neutron, Eq. (80),

$$\begin{aligned} &\hat{e}^- + \hat{p}^+ \rightarrow \hat{e}^-_{spin} + \hat{e}^-_{orb} + \hat{p}^+ \rightarrow n \, , \\ &S^{spin}_{\hat{e}} + S^{orb}_{\hat{e}} + S^{spin}_{\hat{p}} = -\frac{1}{2} + \frac{1}{2} + \frac{1}{2} = \frac{1}{2} \, , \end{aligned} \tag{83}$$

(where the "hat" denotes treatment via hadronic mechanics) according to which *the spin of the neutron coincides with that of the proton,* as expected since the proton is assumed to be at rest in synthesis (80) and its mass is about 1 800 times that of the electron. Note that the internal orbital motion of the electron is impossible for quantum mechanics due to the representation of the proton as a point.

Recall that, in Rutherford's synthesis (80), we have the following tabulated magnetic moments of the electron, the proton and the neutron all considered in nuclear magnetrons

$$\begin{aligned} &\mu^{spin}_{\hat{e}} = +1838.285 \, \mu_{\text{N}}, \ \ \mu^{spin}_{\hat{p}} = +2.7/92 \, \mu_{\text{N}} \, , \\ &\mu^{spin}_{n} = -1.913 \, \mu_{\text{N}} \, , \end{aligned} \tag{84}$$

where one should note that the direction of the magnetic moment of the electron is the same as that of the proton because of the double inversion of the spin and of the charge. One should also note the very big value of the intrinsic magnetic moment of the electron for nuclear standards which is intrinsic in the synthesis of the neutron from the Hydrogen.

The exact representation of the **anomalous magnetic moment of the neutron** was achieved thanks to the indicated internal orbital motion of the electron with the value

$$\mu^{orb}_{\hat{e}} = -1842.990 \, \mu_{\text{N}} \, , \tag{85}$$

by keeping in mind that the orbital magnetic moment of the electron is opposite that of the proton due to opposite charges. The exact representation of the anomalous magnetic moment of the neutron was then reached via the sum [84]

$$\begin{aligned} &\mu^{spin}_{e} + \mu^{orb}_{e} + \mu^{spin}_{p} = \\ &= +1838.285 - 1842.990 + +2.792 \, \mu_{\text{N}} = \\ &= -1.913 \, \mu_{\text{N}} \, . \end{aligned} \tag{86}$$

The above representation is considered to be a confirmation of the internal orbital motion of the electron in synthesis (80) because of the representation of the *negative* value of the neutron magnetic moment.

The **relativistic representation** of all characteristics of the neutron in synthesis (80) was reached in the 1995 paper [89] (see review [28]) via the isotopies $\hat{\mathcal{P}}(3.1)$ of the spinorial covering of the Lorentz-Poincaré symmetry and cannot be reviewed here for brevity.

Following the mathematical and physical understanding of the neutron synthesis in the core of stars, Santilli and his associates conducted systematic experimental and industrial tests on the laboratory synthesis of the neutron from a commercial grade Hydrogen gas [90]–[97] (see also independent studies [98]–[103]). These tests eventually lead to the production and sale by the U.S. publicly traded company *Thunder Energies Corporation* (now the private company *Hadronic Technologies Corporation* http://www.hadronictechnologies.com) of the *Directional Neutron Source* (DNS) producing on demand a flux of low energy neutrons in the desired direction (Fig. 15).

In regard to the mass excess of synthesis (80), we should recall that the missing energy of 0.782 MeV cannot be provided by the relative kinetic energy between the electron and the proton because, at that energy, the electron-proton cross section is essentially null, thus prohibiting any synthesis.

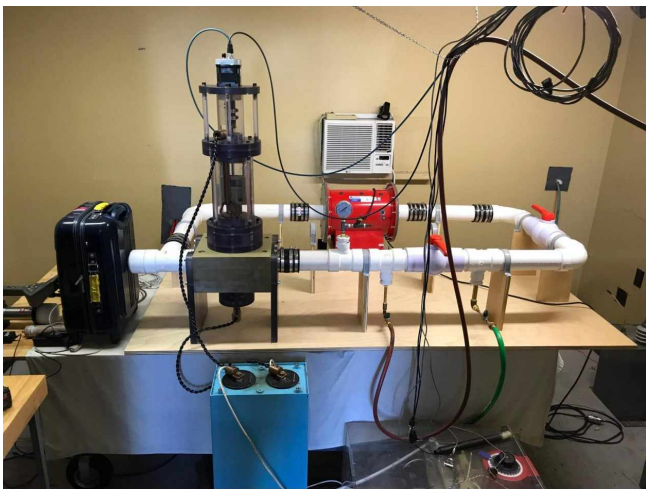

Fig. 15: In this figure, we illustrate the Directional Neutron Source (DNS) produced and sold by the U. S. publicly traded company Thunder Energies Corporation* which produces on demand a flux of low energy, directional neutrons synthesized from a commercial-grade Hydrogen gas contained in the loop of the hadronic reactor.
*Now www.hadronictechnologies.com

Similarly, said missing energy cannot be provided by a star such as our Sun, because the Sun synthesizes about 10^{38}–10^{39} neutrons *per second,* that would require such a big amount of energy (about 10^{38} MeV/s) to prevent a star from producing light due to insufficient internal temperature.

For these and other reasons, Santilli [142] proposed in 2007 the hypothesis that *the missing energy in the neutron synthesis is provided by space as a universal substratum with an extremely big energy density* needed for the characterization and propagation of electromagnetic waves and elementary particles. The missing energy is transferred from space to the neutron by a massless, chargeless and spinless longitudinal impulse called *etherino* and denoted with the letter $\hat{a}$ (from the Latin *aether*), according to the synthesis

$$\hat{e}^- + \hat{a} + \hat{p}^+ \to n\,, \tag{87}$$

where one should note that, contrary to the case of the neutrino in synthesis (81), the etherino is on the *left* of the synthesis as a condition to supply the missing energy.

Independently from the above studies, the Sun releases into light 2.3×10^{38} MeV/s [143], corresponding to about 4.3×10^6 t/s. Since in a Gregorian year there are 10^7 seconds, the loss of mass by the Sun ΔM_S per year due to light emission is given by

$$\Delta M_S = 10^{23} \text{ metric tons per year}\,. \tag{88}$$

This loss of mass is of such a size to cause a decrease of planetary orbits detectable in astrophysical laboratories, contrary to centuries of measurements on the stability of planetary orbits.

Therefore, Santilli proposed the etherino hypothesis [142] for the intent of representing the gravitational stability of the Sun via a return to the historical cosmological model based on the continuous creation of matter in the universe. In fact, the energy needed for the star to synthesize neutrons 10^{38} MeV/s is essentially equal to the energy needed for the neutron synthesis, by therefore representing the stability of the star with intriguing cosmological implications [22, 23], e.g. for supernova explosions and neutron stars.

Note that the *permanently stable* protons and electrons cannot possibly disappear from the universe during the neutron synthesis to be replaced by the hypothetical quarks. Note also that the neutron is naturally unstable (when isolated) and decays into the original stable constituents. The above features imply new recycling nuclear waste via their stimulated decay caused by photon irradiation with a suitable resonating frequency $\gamma^{res} = 1.293$ MeV and transmutations of the type [78, 95]

$$M\gamma^{res} + N(Z, A, J) \;\to\; N'(Z + M, A, J + K) + M\beta^-\,, \tag{89}$$

(where K is the spin corrections due to the emission of electrons) under which transmutations the long mean lives of nuclear waste can be reduced in a way proportional to the intensity of the gamma irradiation.

Additionally, we should mention that, following the compression of the electron within the proton, hadronic mechanics predicts the subsequent compression (evidently with a smaller probability) of an electron, this time, within a neutron, resulting in a *new negatively charged particle* called *pseudo-proton* $\tilde{p}^-$ [144] with an additional possibility of recycling nuclear waste via pseudo-proton irradiation and ensuing transmutations

$$M\tilde{p}^- + N(Z, A, J) \;\to\; N'(Z - M, A, J + K)\,, \tag{90}$$

under which long mean lives (calculated via hadronic mechanics) can be reduced to seconds.

C Representation of nuclear stability

We close this paper with an outline of the representation of nuclear stability according to hadronic mechanics.

C.1 Representation of nuclear stability despite the instability of the neutron

According to quantum mechanics, no stable nuclei should exist in nature because nuclei are assumed to be quantum mechanical bound states of protons, which are permanently stable, and neutrons which are naturally unstable, with a mean life of 879.6 ± 0.8 s and spontaneous decay [1]

$$n \;\to p^+ + e^- + \bar{\nu}\,. \tag{91}$$

Following decades of study of the problem, this author was unable to *formulate,* let alone solve, the above problem due to

the lack of any possible quantum mechanical representation of the synthesis of the neutron in a star.

Following a conceptual suggestion in [36], we here indicate, apparently for the first time, that the quantitative representation of nuclear stability despite the natural instability of the neutron is an intrinsic feature of the hadronic synthesis of the neutron from the proton and the electron because, starting from the hadronic structure of the neutron (Fig. 11 and Appendix B) with ensuing hadronic structure of the Deuteron as a two-body bound state of a proton and a neutron in axial triplet coupling (Fig. 12 and Sect. 3), the electron naturally decouples from the proton to acquire a position intermediate between the two protons (Fig. 13). Consequently, the decoupled electron assumes an intermediate position between the two attracting protons by occupying the distance between their charge distributions of 0.3745 fm, which would otherwise be empty according to available experimental data (Fig. 2, [2]). Intriguingly, the suggested decoupling allows a novel representation of the known *exchange forces* in nuclear physics because the transition of the decoupled electron from one proton to the other evidently implies a proton-neutron exchange.

Note that the indicated decoupling of the neutron is impossible for 20^{th} century physics. Note also that, in the preceding Deuteron model based on planar singlet couplings of Sect. IV-2.5, p. 171 of [78], the decoupling here considered is impossible while, for the axial triplet coupling the decoupled electron remains with null total angular momentum due to its motion within the nuclear medium, by therefore confirming the uniqueness and importance of the axial triplet coupling (Fig. 1). Note finally that the decoupling of nuclear neutrons into protons and electrons implies the reduction of all matter in the universe to protons and electrons.

C.2 Representation of nuclear stability despite repulsive protonic forces

Additionally, stable nuclei should not exist in nature according to quantum mechanics because equal charge nuclear protons *repel* each other with an extremely big Coulomb force of the order of hundreds of Newtons Eq. (1).

We here indicate, also apparently for the first time, that hadronic mechanics can indeed represent this second problem of nuclear stability via a mechanism similar to the achievement by quantum chemistry of a strongly *attractive* force between the *identical* electrons of valence couplings [72–74].

Let us consider the nucleus with the minimal number of proton pairs, which is evidently given by the Helium $He(2,4,0)$ [1]. Various measurements [3] have established that the Helium has a charge radius of 1.678 fm, against the radius of two protons and two neutrons each having the value of 0.841 fm [4] with the total radius of 1.678 fm .

The above measurements confirm the primary assumption of hadronic mechanics, according to which nuclei are composed by extended protons and neutrons in conditions of partial mutual penetration of their dense charge distributions with ensuing non-Hamiltonian interactions (Sect. 2).

Let us assume in first approximation that the Helium is a quantum mechanical (qm) bound state of two Deuterons with anti-parallel spins

$$He(2,4,0) = [\, D(1,2,1_\uparrow), D(1,2,1_\downarrow)\,]_{qm}\,. \tag{92}$$

We assume the representation of the non-Hamiltonian interactions via non-unitary transform (47) of the quantum model (92) thus yielding the expression

$$\begin{aligned} & U\left[\frac{1}{2m}\,\delta^{ij}p_ip_j + V_c(r)\right]|\,\psi(r)\,\rangle\,U^\dagger = \\ & = \left\{-\frac{1}{m}\,\hat\partial_{\hat r}\hat\partial_{\hat r} + V_c(\hat r)\left[1 - \frac{V_h(\hat r)}{V_c(\hat r)}\right]\right\}|\,\hat\psi(\hat r)\,\rangle = \\ & = \left[-\frac{1}{m}\,\hat\Delta_{\hat r} - K_h'\,\frac{e^{b\hat r}}{1-e^{b\hat r}}\right]|\,\hat\psi(\hat r)\,\rangle = E_h\,|\,\hat\psi(\hat r)\,\rangle\,, \end{aligned} \tag{93}$$

where the last expression has been reached by "absorbing" the Coulomb potential into the Hulten potential as in (50).

Consequently, the above analysis confirms that non-linear, non-local and non-potential nuclear interactions due to the mutual penetration of nucleons can be so strongly attractive to overcome repulsive Coulomb force between protons.

It is easy to see that the hadronic conversion of the repulsive Coulomb into a strongly attractive Hulten-type or other potentials also applies for other nuclear potentials, such as the *Yukawa potential* [147], the *Woods-Saxon potential* [148] and other potentials or their combination [149].

C.3 Representation of the Helium data

We now show that, following the overcoming of the repulsive ptotonic forces, non-Hamiltonian interactions remain so strong to represent the characteristics of Helium.

Note that the representation of the spin and magnetic moment of Helium follows from the antiparallel Deuteron spins of model (92). The representation of the rest energy, mean life and charge radius of Helium can be done via the hadronic structure model of the pion (Sect. 5.1, p. 827 on, [82]) and of the Deuteron (Sect. IV-2.5, p. 171 on, [78])

$$\begin{aligned} & \left[\frac{1}{r^2}\left(\frac{d}{dr}r^2\frac{d}{dr}\right) + \tilde m_d\left(E + K_h'\frac{e^{-br}}{1-e^{-br}}\right)\right] = 0\,, \\ & E_{he} = 2E_d - E_{be} = 3.7284\times 10^3\,\text{MeV}\,, \\ & \tau^{-1} = 2\pi\lambda^2\,|\hat\psi(0)|^2\,\frac{\alpha^2 E_1}{\hbar} = \infty\,, \\ & R = b^{-1} = 1\,\text{fm}, \end{aligned} \tag{94}$$

where $\hat m = m/\rho$ is the *iso-renormalized mass* of the Deuteron, that is, the mass renormalized from non-Hamiltonian interac-

tions (Eq. (5.1.7b), p. 833, of [82]) here adjusted for Helium

$$\tilde{m} = \tilde{E}_d = \frac{E_d}{\rho} = \frac{E_{he}}{2} = 1.8542 \times 10^3 \,\mathrm{MeV}\,, \qquad \rho = 1.0188 > 1\,, \tag{95}$$

The solution of Eqs. (94) was studied in all details in Sect. 5.1, p. 836 on, [82] (see also the recent review in [29]) and reduced to the numeric values of two parameters denoted k_1 and k_2, Eqs. (5.1.32a) and (5.1.32b), p. 840 [82], that become in our case

$$\tau = \frac{48 \times (137)^2}{4\pi bc} \frac{k_1}{(k_2 - 1)^3} = \infty\,, \tag{96}$$

$$E_{he} = k_1[1 - (k_2 - 1)2] \frac{2\bar{h}c}{b} = 3.7284 \times 10^3 \,\mathrm{MeV}\,, \tag{97}$$

with numeric solutions

$$k_2 = 1\,, \quad k_1 = 4.9\,, \tag{98}$$

that should be compared with the numeric solutions for the meson octet of [29, 82].

Intriguingly, the known finite spectrum of the Hulten potential (see Eq. (5.1.20), p. 837, [82])

$$BE_h = -\frac{1}{4K_h k_2} \left(\frac{k_2}{n} - n\right)^2\,, \quad k_2 = K_h \frac{\tilde{E}_d}{\hbar^2 b^2} = 1\,, \tag{99}$$

admits *only one value, Helium*, for $n = 1$, with null value of the binding energy, $BE_h = 0$, as expected for the sole *non-potential* interactions of model (94), since the representation of the Helium binding energy requires the addition of a *potential* force here left to interested readers.

In conclusion, the above model confirms that nuclear forces are some of the most complex forces in nature, since they include a linear, local and potential component represented by the Hamiltonian which is responsible for nuclear binding energies, plus a non-linear, non-local and non-potential component represented by the isotopic element which is responsible for the nuclear stability.

Acknowledgements

The author would like to thank for penetrating critical comments the participants of the *2020 International Teleconference on the EPR argument* and the *2021 International Conference on Applied Category Theory and Graph-Operad-Logic*. Additional thanks are due to the technicians Micahel Rodriguez, Jim Alban, Ray Jones and Chris Lynch for the recollection of 2005-2019 ICNF tests. Special thanks are due to Eng. S. Beghella-Bartoli for a critical reading of the manuscript, and to Mrs. Sherri Stone for linguistic control of the manuscript. The author is solely responsible for the content of this paper due to inevitable final controls of the manuscript.

Received September 29, 2022

References

1. KAERI Table of Nuclide, website. http://pripyat.mit.edu/KAERI/
2. Rau S., *et al*. Penning Ttrap measurements of the deuteron and the HD^+ molecular ion. *Nature*, 2020, v. 585, 43–47. http://doi.org/10.1038/s41586-020-2628-7
3. Krauth J. J., Schuhmann K. and Kottmann F, Measuring the α-particle charge radius with muonic helium-4 ions. *Nature*, 2021, v. 589, 527–531. http://www.nature.com/articles/s41586-021-03183-1
4. Pohl R. Antognini A. and Kottmann F. The size of the proton. *Nature*, 2010, v. 466, 213–216. http://www.nature.com/articles/nature09250
5. Einstein A., Podolsky B. and Rosen N. Can quantum-mechanical description of physical reality be considered complete? *Phys. Rev.*, 1935, v. 47, 777–780. http://www.eprdebates.org/docs/epr-argument.pdf
6. Heisenberg W. *Nachr. Akad. Wiss.* Gottingen, Germany, 1953, v. IIa, 111. http://link.springer.com/chapter/10.1007/978-3-642-70079-8-23
7. Geoldtesin S. Stanford Encyclopedia of Philosophy, Bohmian (de Broglie-Bohm) Mechanics, 2021. http://plato.stanford.edu/entries/qm-bohm/
8. Bohm D. A Suggested Interpretation of the Quantum Theory in Terms of "Hidden Variables". *Physical Review*, 1952, v. 85, 166–182. http://journals.aps.org/pr/abstract/10.1103/PhysRev.85.166
9. Santilli, R. M. Generalization of Heisenberg's uncertainty principle for strong interactions. *Hadronic Journal*, 1981, v. 4, 642–657. http://www.santilli-foundation.org/docs/generalized-uncertainties-1981.pdf
10. Santilli R. M. Isorepresentation of the Lie-isotopic SU(2) Algebra with Application to Nuclear Physics and Local Realism. *Acta Applicandae Mathematicae*, 1998, v. 50, 177–190. http://www.santilli-foundation.org/docs/Santilli-27.pdf
11. Santilli R. M. Studies on the classical determinism predicted by A. Einstein, B. Podolsky and N. Rosen. *Ratio Mathematica*, 2019, v. 37, 5–23. http://www.eprdebates.org/docs/epr-paper-ii.pdf
12. Santilli R. M. A quantitative representation of particle entanglements via Bohm's hidden variables according to hadronic mechanics. *Progress in Physics*, 2022, v. 18, 131–137. http://www.santilli-foundation.org/docs/pip-entanglement-2022.pdf
13. Miller J P., de Rafael E. and Roberts B. Lee. Muon (g2): experiment and theory. *Rep. Prog. Phys.*, 2007, v. 70, 795–881. http://news.fnal.gov/2021/04/first-results-from-fermilabs-muon-g-2-experiment-strengthen-evidence-of-new-physics/
14. Santilli R. M. Representation of the anomalous magnetic moment of the muons via the Einstein-Podolsky-Rosen completion of quantum into hadronic mechanics. *Progress in Physics*, 2021, v. 17, 210–215. http://www.santilli-foundation.org/muon-anomaly-pp.pdf
15. Santilli R. M. Representation of the anomalous magnetic moment of the muons via the novel Einstein-Podolsky-Rosen entanglement. In: Guzman J. C., ed. Scientific Legacy of Professor Zbigniew Oziewicz: Selected Papers from the International Conference "Applied Category Theory Graph-Operad-Logic". World Scientific, in press. http://www.santilli-foundation.org/ws-rv961x669.pdf
16. Fadel M., Zibold T., Decamps B. and Treutlein Ph. Spatial entanglement patterns and Einstein-Podolsky-Rosen steering in BoseEinstein condensates. *Science*, 2018, v. 360, 409–415. http://www.santilli-foundation.org/Basel-paper.pdf
17. Schukraft J. Heavy-ion physics with the ALICE experiment at the CERN Large Hadron Collider. *Trans. R. Soc.*, 2012, v. A370, 917–932. royalsocietypublishing.org/doi/10.1098/rsta.2011.0469
18. Cardone F., Mignani R. and Santilli, R. M. On a possible energy-dependence of the K^0 lifetime. Paper I *J. Phys. G: Part. Phys.*, 1992, v. 18, L61–L65. Paper II *J. Phys. G: Part. Phys.*, 1992, v. 18, L141–L144. http://www.santilli-foundation.org/docs/Santilli-32.pdf

19. Santilli R. M. Apparent Unsettled Value of the Recently Measured Muon Magnetic Moment. *Progress in Physics*, 2022, v. 18, 15–18. http://www.santilli-foundation.org/docs/muon-meanlife-2022.pdf
20. Santilli R. M. Nonlocal formulation of the Bose-Einstein correlation within the context of hadronic mechanics. *Hadronic J.*, 1992, v. 15, 1–50 and v. 15, 81–133. www.santilli-foundation.org/docs/Santilli-116.pdf
21. Cardone F. and Mignani R. Nonlocal approach to the Bose-Einstein correlation. . *Phys. J.*, 1998, v. C4, 705–728.
22. Ahmar H., Amato G., Kadeisvili J. V., Manuel J., West G. and Zogorodnia O. Additional experimental confirmations of Santilli's IsoRedShift and the consequential lack of expansion of the universe. *Journal of Computational Methods in Sciences and Engineering*, 2013, v. 13, 321–375. http://www.santilli-foundation.org/docs/IRS-confirmations-212.pdf
23. Santilli R. M. Experimental Verifications of IsoRedShift with Possible Absence of Universe Expansion, Big Bang, Dark Matter, and Dark Energy. *The Open Astronomy Journal*, 2010, v. 3, 124. http://www.santilli-foundation.org/docs/Isoredshift-Letter.pdf
24. Saldanha P. L. Inconsistency of a Realistic Interpretation of Quantum Measurements: a Simple Example. *Braz. J. Phys.*, 2020, v. 50, 438–441. http://doi.org/10.1007/s13538-020-00757-8
25. Svensson E. Y. Logical inconsistencies in quantum mechanics. arXiv: 1803.06162, 2018. http://arxiv.org/abs/1803.06162
26. Myrvold W. Philosophical Issues in Quantum Theory. *The Stanford Encyclopedia of Philosophy*, 2022. http://plato.stanford.edu/entries/qt-issues
27. Santilli R. M. Studies on A. Einstein, B. Podolsky, and N. Rosen prediction that quantum mechanics is not a complete theory. I: Basic methods. *Ratio Mathematica*, 2020, v. 38, 5–69. http://eprdebates.org/docs/epr-review-i.pdf
28. Santilli R. M. Studies on A. Einstein, B. Podolsky, and N. Rosen prediction that quantum mechanics is not a complete theory. II: Apparent proof of the EPR argument. *Ratio Mathematica*, 2020, v. 38, 71–138. http://eprdebates.org/docs/epr-review-ii.pdf
29. Santilli R. M. Studies on A. Einstein, B. Podolsky, and N. Rosen prediction that quantum mechanics is not a complete theory. III: Illustrative examples and applications. *Ratio Mathematica*, 2020, v. 38, 139–222. http://eprdebates.org/docs/epr-review-iii.pdf
30. Santilli, R. M. Elements of Hadronic Mechanics, Vol. I. *Mathematical Foundations. Ukraine Academy of Sciences, Kiev*, 1995. http://www.santilli-foundation.org/docs/Santilli-300.pdf
31. Santilli R. M. Elements of Hadronic Mechanics, Vol. II, *Theoretical Foundations. Ukraine Academy of Sciences, Kiev*, 1995. http://www.santilli-foundation.org/docs/Santilli-301.pdf
32. Santilli R. M. Elements of Hadronic Mechanics, Vol. III, *Experimental Verifications. Ukraine Academy of Sciences, Kiev*, 2016. http://www.santilli-foundation.org/docs/elements-hadronic-mechanics-iii.compressed.pdf
33. Anderson R. Outline of Hadronic Mathematics, Mechanics and Chemistry as Conceived by R. M. Santilli. *American Journal of Modern Physics*, 2016, v. 6, 1–16. http://www.santilli-foundation.org/docs/HMMC-2017.pdf
34. Beghella-Bartoli S. and Santilli R. M., eds. Proceedings of the 2020 Teleconference on the Einstein-Podolsky-Rosen argument that "Quantum mechanics is not a complete theory". Curran Associates, New York, 2021. http://www.proceedings.com/59404.html (printed). http://www.proceedings.com/60007.html (electronic). http://www.world-lecture-series.org/level-xii-eprteleconference-2020 (recorded lectures).
35. Santilli R. M. Overview of historical and recent verifications of the Einstein-Podolsky-Rosen argument and their applications to physics, chemistry and biology. APAV - Accademia Piceno Aprutina dei Velati, Pescara, Italy, 2021. http://www.santilli-foundation.org/epr-overview-2021.pdf
36. Santilli R. M. Overview of historical and recent verifications of the Einstein-Podolsky-Rosen argument and their applications to physics, chemistry and biology. APAV - Accademia Piceno Aprutina dei Velati, Pescara, Italy, 2021.
37. Dunning-Davies J. A Present Day Perspective on Einstein-Podolsky-Rosen and its Consequences. *Journal of Modern Physics*, 2021, v. 12, 887–936. www.scirp.org/journal/paperinformation.aspx?paperid=-109219
38. Aringazin A. K., Jannussis A., Lopez F., Nishioka M. and Vel-janosky B. Santilli's Lie-Isotopic Generalization of Galilei and Einstein Relativities. Notes from R. M. Santilli's 1990 Lectures at the ICTP, Trieste, Italy. Kostakaris Publishers, Athens, Greece, 1991. http://www.santilli-foundation.org/docs/Santilli-108.pdf
39. Sourlas D. S. and Tsagas Gr. T. Mathematical Foundation of the Lie-Santilli Theory. *Ukraine Academy of Sciences*, 1993. http://www.santilli-foundation.org/docs/santilli-70.pdf
40. Lohmus J., Paal E. and Sorgsepp L. Non-associative Algebras in Physics. Hadronic Press, 1994. http://www.santilli- foundation.org/docs/Lohmus.pdf
41. Kadeisvili J. V. Santilli's Isotopies of Contemporary Algebras, Geometries and Relativities, Second edition. *Ukraine Academy of Sciences*, Kiev, 1997. http://www.santilli-foundation.org/docs/Santilli-60.pdf
42. Jiang C.-X. Foundations of Santilli Isonumber Theory. *International Academic Press*, 2001. http://www.i-b-r.org/docs/jiang.pdf
43. Ganfornina R. M. F. and Valdes J. N. Fundamentos de la Isotopia de Santilli. International Academic Press, Palm Harbor, FL, 2001. http://www.i-b-r.org/docs/spanish.pdf
English translation: *Algebras, Groups and Geometries*, 2015, v. 32, 135–308, 2015. http://www.i-b-r.org/docs/Aversa-translation.pdf
44. Davvaz B. and Vougiouklis Th. A Walk Through Weak Hyperstructures and H_v-Structures. World Scientific, 2018.
45. Gandzha I. and Kadeisvili J. V. New Sciences for a New Era: Mathematical, Physical and Chemical Discoveries of Ruggero Maria Santilli. Printing Press, Nepal, 2011. http://www.santilli-foundation.org/docs/RMS.pdf
46. Georgiev S. Foundations of IsoDifferential Calculus. Vol 1. IsoDifferential and Iso-Integral Calculus for Iso-Functions in One Variable. Vol 2. Iso-Differential and Iso-Integral Calculus for IsoFunctions in Several Variables. Vol. 3 Iso-Ordinary Iso-Differential Equations. Vol. 4 Iso-Difference Equations. Vol. 5 Iso-Stochastic Iso-Differential Equations. Vol. 6 Theory of Iso-Measurable IsoFunctions. Nova Publishers, New York, NY, 2014 (I), 2014 (II), 2014 (III), 2015 (IV), 2015 (V), 2016 (VI), 2022 (I new ed.)
47. Georgiev S. Iso-Mathematics. Lambert Academic Publishing, 2022.
48. Santilli R. M. Foundation of Theoretical Mechanics. Vol. I The Inverse Problem in Newtonian Mechanics. Springer-Verlag, Heidelberg, Germany, 1978. http://www.santilli-foundation.org/docs/Santilli-209.pdf
49. Santilli R. M. Foundation of Theoretical Mechanics. Vol. II Birkhoffian Generalization of Hamiltonian Mechanics. Springer-Verlag, Heidelberg, Germany, 1983. http://www.santilli-foundation.org/docs/santilli-69.pdf
50. Santilli R. M. Isonumbers and Genonumbers of Dimensions 1, 2, 4, 8, their Isoduals and Pseudoduals, and "Hidden Numbers" of Dimension 3, 5, 6, 7. *Algebras, Groups and Geometries*, 1993, v. 10, 273–322. http://www.santilli-foundation.org/docs/Santilli-34.pdf
51. Santilli R. M. Nonlocal-Integral Isotopies of Differential Calculus, Mechanics and Geometries. *Circolo Matematico Palermo, Suppl.*, 1996, v. 42, 7–82. http://www.santilli-foundation.org/docs/Santilli-37.pdf
52. Santilli R. M. Invariant Lie-isotopic and Lie-admissible formulation of quantum deformations. *Found. Phys.*, 1997, v. 27, 1159–1177. http://www.santilli-foundation.org/docs/Santilli-06.pdf

53. Santilli R. M. Embedding of Lie-algebras into Lie-admissible algebras. *Nuovo Cimento*, 1967, v. 51, 570-585. http://www.santilli-foundation.org/docs/Santilli-54.pdf
54. Santilli R. M. Dissipativity and Lie-admissible algebras. *Meccanica*, 1969, v. 1, 3–12.
55. Santilli R. M. An introduction to Lie-admissible algebras. *Suppl. Nuovo Cimento*, 1968, v. 6, 1225.
56. Santilli R. M. On a possible Lie-admissible covering of Galilei's relativity in Newtonian mechanics for nonconservative and Galilei form-non-invariant systems. *Hadronic J.*, 1978, v. 1, 223–423. http://www.santilli-foundation.org/docs/Santilli-58.pdf
57. Santilli R. M. Initiation of the representation theory of Lie-admissible algebras of operators on bimodular Hilbert spaces. *Hadronic J.*, 1978, v. 3, 440–467. http://www.santilli-foundation.org/docs/santilli-1978-paper.pdf
58. Santilli R. M. Lie-Admissible Approach to the Hadronic Structure. International Academic Press, Vol. I, 1978. http://www.santilli-foundation.org/docs/Santilli-71.pdf Vol. II, 1982. http://www.santilli-foundation.org/docs/Santilli-72.pdf
59. Fronteau J., Tellez-Arenas A. and Santilli R. M. Lie-admissible structure of statistical mechanics. *Hadronic Journal*, 1979, v. 3, 130–176. http://www.santilli-foundation.org/docs/arenas-fronteau-santilli-1981.pdf
60. Myung H. C. and Santilli R. M., Eds. Proceedings of the Second Workshop on Lie-Admissible formulations.
Part A: Review Papers. *Hadronic Journal*, 1979, v. 2 (6). http://www.santilli-foundation.org/docs/hj-2-6-1979.pdf
Part B: Research Papers. *Hadronic Journal*, 1979, v. 3 (1). http://www.santilli-foundation.org/docs/hj-3-1-1979.pdf
61. Myung H. C. and Santilli R. M., Eds. Proceedings of the Third Workshop on Lie-Admissible Formulations. Part A: Mathematics. *Hadronic Journal*, 1981, v. 4 (2). http://www.santilli-foundation.org/docs/hj-4-2-1981.pdf Part B: Theoretical Physics. *Hadronic Journal*, 1981, v. 4 (3). http://www.santilli-foundation.org/docs/hj-4-3-1981.pdf Part C: Experimental Physics, and Bibliography. *Hadronic Journal*, 1981, v. 4 (4). http://www.santilli-foundation.org/docs/hj-4-4-1981.pdf
62. Arenas T., Fronteau J. and Santilli R. M., Eds. Proceedings of the First International Conference on Nonpotential Interactions and their Lie-Admissible Treatment.
Part A: Invited Papers. *Hadronic Journal*, 1982, v. 5 (2). http://www.santilli-foundation.org/docs/hj-5-2-1982.pdf
Part B: Invited Papers. *Hadronic Journal*, 1982, v. 5 (3). http://www.santilli-foundation.org/docs/hj-5-3-1982.pdf
Part C: Contributed Papers. *Hadronic Journal*, 1982, v. 5 (4). http://www.santilli-foundation.org/docs/hj-8-4-1982.pdf
Part D: Contributed Papers. *Hadronic Journal*, 1982, v. 5 (5). http: http://www.santilli-foundation.org/docs/hj-5-5-1982.pdf
63. Myung H. C. and Santilli R.M., Eds. Proceedings of the First Workshop on Hadronic Mechanics. *Hadronic Journal*, 1983, v. 6 (6). http://www.santilli-foundation.org/docs/hj-6-6-1983.pdf
64. Myung H. C. and Santilli R. M., Eds. Proceedings of the Second Workshop on Hadronic Mechanics. Vol. I. *Hadronic Journal*, 1984, v. 7 (5). http://www.santilli-foundation.org/docs/hj-7-5-1984.pdf Vol. II. *Hadronic Journal*, 1984, v. 7 (6). http://www.santilli-foundation.org/docs/hj-7-6-1984.pdf
65. Schoeber A., Ed. Irreversibility and Non-potentiality in Statistical Mechanics. Hadronic Press, 1984.
http://www.santilli-foundation.org/docs/Santilli-110.pdf
66. Tuladhar Bhadra Man, Ed. , Proceedings of the third international conference on the Lie-admissible treatment of non-potential interactions. Kathmandu University, Nepal, 2011.
Vol. I: http://www.santilli-foundation.org/docs/2011-nepal-conference-vol-1.pdf Vol. II: http://www.santilli-foundation.org/docs/2011-nepal-conference-vol-2.pdf
67. Dunning-Davies J. The Thermodynamics Associated with Santilli's Hadronic Mechanics. *Progress in Physics*, 2006, v. 4, 24–26. http://www.santilli-foundation.org/docs/Dunning-Davies-Thermod.PDF
68. Bhalekar A. A. Santilli's Lie-Admissible Mechanics. The Only Option Commensurate with Irreversibility and Nonequilibrium Thermodynamics. *AIP Conf. Proc.*, 2013, v. 1558, 702–722. http://www.santilli-foundation.org/docs/bhalekar-lie-admissible.pdf
69. Vougiouklis T. The Santilli theory 'invasion' in hyperstructures. *Algebras, Groups and Geometries*, 2011, v. 28, 83–104. http://www.santilli-foundation.org/docs/santilli-invasion.pdf
70. Santilli R. M. Lie-admissible invariant representation of irreversibility for matter and antimatter at the classical and operator levels. *Nuovo Cimento B*, 2006, v. 121, 443–485. http://www.santilli-foundation.org/docs http://Lie-admiss-NCB-I.pdf
71. Albert A. A. *Trans. Amer. Math. Soc.*, 1948, v. 64, 552–585.
72. Santilli R. M. Foundations of Hadronic Chemistry, with Applications to New Clean Energies and Fuels. Kluwer Academic Publishers, 2001. http: http://www.santilli-foundation.org/docs/Santilli-113.pdf Russian translation: Aringazin A. K. http: http://i-b-r.org/docs/Santilli-Hadronic-Chemistry.pdf
73. Santilli R. M. and Shillady D. D. A new isochemical model of the hydrogen molecule. *Intern. J. Hydrogen Energy*, 1999, v. 24, 943. http://www.santilli- foundation.org/docs/Santilli-135.pdf
74. Santilli R. M. and Shillady D. D. A new isochemical model of the water molecule. *Intern. J. Hydrogen Energy*, 2000, v. 25, 173. http://www.santilli-foundation.org/docs/Santilli-39.pdf
75. Blatt J. M. and Weisskopf V. F. Theoretical Nuclear Physics. Wiley and Sons, 1952.
76. Myung H. C. and Santilli R. M. Modular-isotopic Hilbert space formulation of the exterior strong problem. *Hadronic Journal*, 1982, v. 5, 1277–1366.
http://www.santilli-foundation.org/docs/myung-santilli-1982.pdf
77. Santilli R. M. A quantitative isotopic representation of the Deuteron magnetic moment. In: Proceedings of the International Symposium "Dubna Deuteron-3e". Joint Institute for Nuclear Research, Dubna, Russia, 1994. http://www.santilli-foundation.org/docs/Santilli-134.pdf
78. Santilli R. M. The Physics of New Clean Energies and Fuels According to Hadronic Mechanics. Special issue of the Journal of New Energy, 1998. http://www.santilli-foundation.org/docs/Santilli-114.pdf
79. Dhondge S. S. Santilli's Hadronic Mechanics Formation for the Deuteron. AIP Conference Proceedings 1648, 510009, 2015. doi: 10.1063/1.4912714.
http://www.santilli-foundation.org/docs/1.4912714(SS-Dhondge).pdf
80. Dhondge S. S. Studies on Santilli Three-Body Model of the Deuteron According to Hadronic Mechanics. *American Journal of Modern Physics*, 2016, V. 5 (2-1), 46–55.
http://www.santilli-foundation.org/docs/deuteron-2018.pdf
81. Muktibodh Arun S. Studies on Santilli Three-Body Model of the Deuteron According to Hadronic Mechanics. *American Journal of Modern Physics*, 2016, v. 5 (2-1), 17–36. http://www.santilli-foundation.org/docs/pdf4.pdf
82. Santilli R. M. Need of subjecting to an experimental verification the validity within a hadron of Einstein special relativity and Pauli exclusion principle. *Hadronic J.*, 1978, v. 1, 574–901. http://www.santilli-foundation.org/docs/santilli-73.pdf
83. Santilli R. M. Iso-Representation of the Deuteron Spin and Magnetic Moment via Bohm's Hidden Variables. *Progress in Physics*, 2022, v. 18, 74–81. http://www.santilli-foundation.org/docs/PiP-paper-3-22.pdf
84. Santilli R. M. Apparent consistency of Rutherford's hypothesis on the neutron as a compressed hydrogen atom. *Hadronic J.*, 1990, v. 13, 513–533. http://www.santilli-foundation.org/docs/Santilli-21.pdf

85. Santilli R. M. The notion of non-relativistic isoparticle. ICTP release IC/91/265, 1991. www.santilli-foundation.org/docs/Santilli-145.pdf

86. Santilli R. M. Apparent consistency of Rutherford's hypothesis on the neutron structure via the hadronic generalization of quantum mechanics, nonrelativistic treatment. ICTP communication IC/91/47, 1992. http://www.santilli-foundation.org/docs/Santilli-150.pdf

87. Santilli R. M. The synthesis of the neutron according to hadronic mechanics and chemistry. *Journal Applied Sciences*, 2006, v. 5, 32–47.

88. Santilli R. M. Recent theoretical and experimental evidence on the synthesis of the neutron. Communication of the Joint Institute for Nuclear Research, Dubna, Russia, No. E4-93-252, 1993.

89. Santilli R. M. Recent theoretical and experimental evidence on the synthesis of the neutron. *Chinese J. System Eng. and Electr.*, 1995, v. 6, 177–195. http://www.santilli-foundation.org/docs/Santilli-18.pdf

90. Santilli R. M. Apparent confirmation of Don Borghi's experiment on the laboratory synthesis of neutrons from protons and electrons. *Hadronic J.*, 2007, v. 30, 29–41. http://www.i-b-r.org/NeutronSynthesis.pdf

91. Santilli R. M. Confirmation of Don Borghi's experiment on the synthesis of neutrons. arXiv: physics/0608229v1. http://arxiv.org/pdf/physics/0608229v1.pdf

92. Santilli R. M. Documentation of scans from the Polimaster and SAM 935 detectors. http://www.neutronstructure.org/neutron-synthesis-3.htm http://www.neutronstructure.org/neutron-synthesis-2.htm

93. Burande C. S. On the experimental verification of Rutherford-Santilli neutron model. *AIP Conf. Proc.*, 2013, v. 158, 693–721. http://www.santilli-foundation.org/docs/Burande-2.pdf

94. Santilli R. M. and Nas A. Confirmation of the Laboratory Synthesis of Neutrons from a Hydrogen Gas. *Journal of Computational Methods in Sciences and Eng.*, 2014, v. 14, 405–414. http://www.hadronictechnologies.com/docs/neutron-synthesis-2014.pdf

95. Santilli R. M. Apparent Nuclear Transmutations without Neutron Emission Triggered by Pseudoprotons. *American Journal of Modern Physics*, 2015, v. 4, 15–18. http://www.sciencepublishinggroup.net/journal/paperinfo?journalid=122&doi=10.11648/j.ajmp.20150401.13

96. de Haan V. Possibilities for the Detection of Santilli Neutroids and Pseudo-protons. *American Journal of Modern Physics*, 2015, v. 5, 131–136. http://sciencepublishinggroup.com/journal/paperinfo?journalid=122

97. Norman R., Bartoli S. B., Buckley B., Dunning-Davies J., Rak J. and Santilli R. M. Experimental Confirmation of the Synthesis of Neutrons and Neutroids from a Hydrogen Gas. *American Journal of Modern Physics*, 2017, v. 6, 85–104. http://www.santilli-foundation.org/docs/confirmation-neutron-synthesis-2017.pdf

98. Driscoll R. B. Bohrs Atom Completed: the Rutherford-Santilli Neutron. APS Conf. Proc., April 5-8, 2003. http://ui.adsabs.harvard.edu/abs/2003APS..APR.D1009D/abstract

99. Chandrakant S. B. On the Rutherford-Santilli Neutron Model. AIP Conf. Proc., 2015, 1648, 510006, 10.1063/1.4912711. http://www.santilli-foundation.org/docs/1.4912711(CS-Burande(1)).pdf

100. Kadeisvili J. V. The Rutherford-Santilli Neutron. *Hadronic J.*, 2008, v. 31, 1–125. http://www.i-b-r.org/Rutherford-Santilli-II.pdf

101. Burande C. S. Santilli Synthesis of the Neutron According to Hadronic Mechanics. *American Journal of Modern Physics*, 2016, v. 5, 17–36. http://www.santilli-foundation.org/docs/pdf3.pdf

102. Burande C. S. Santilli Synthesis of the Neutron According to Hadronic Mechanics. *American Journal of Modern Physics*, in press, 2015. http://www.santilli-foundation.org/docs/

103. Bartoli S. B. Significance for the EPR Argument of the Neutron Synthesis from Hydrogen and of a New Controlled Nuclear Fusion without Coulomb Barrier. Proceedings of the 2020 Teleconference on the EPR argument, Curran Associates Conference Proceedings, New York, USA, 2021, 459–466.

104. Santilli R. M. The novel Intermediate Controlled Nuclear fusions, a report for its industrial realization. *Hadronic Journal*, 2008, v. 31, 15–42. http://www.santilli-foundation.org/docs/CNF-HJ.pdf

105. Santilli R. M. Experimental Confirmation of Nitrogen Synthesis from Deuterium and Carbon without harmful radiations. *New Advances in Physics*, 2010, v. 4, 17–41. http://www.santilli-foundation.org/docs/Nitrogen-synthesis-2010.pdf

106. Santilli R. M. Additional Confirmation of the Intermediate Controlled Nuclear Fusions without harmful radiation or waste. Proceedings of the Third International Conference on the Lie-Admissible Treatment of Irreversible Processes, Kathmandu University, 2011, 163–177. http://www.santilli-foundation.org/docs/ICNF-3.pdf

107. Santilli R. M. Intermediate Controlled Nuclear Fusions without the emission of radiations and without the release of radioactive waste, Lecture. http://www.world-lecture-series.org/level-v

108. Santilli R. M. Third Hadronic Reactor for Intermediate Controlled Nuclear Fusions without Radiations. Lecture. http://www.world-lecture-series.org/lecture-vc

109. Santilli R. M. Video presentation of the third hadronic reactor for the Nitrogen and Silicon syntheses. 2011. http://www.world-lecture-series.org/dragon-iii

110. Brenna R., Kuliczkowski T. and Ying L. Verification of Santilli intermediate Controlled Nuclear Fusions without harmful radiations and the production of magnecular clusters. *New Advances in Physics*, 2011, v. 5, 9–18. http://www.santilli-foundation.org/docs/ICNF-2.pdf

111. Brenna R., Kuliczkowski T. and Ying L. Report on Test for Silicon on the Nitrogen synthesis. Princeton Gamma Technologies report dated April 6, 2011. http://www.santilli-foundation.org/docs/PGTI-Anal-test1.pdf

112. Ying L., Cai W., J., Lynch C., Marton, Elliot S. and Yang Y. Experimental verification for Intermediate Controlled Nuclear Fusion. City College of New York, Preprint 2012, unpublished. http://www.santilli-foundation.org/docs/ICNF-Cai-paper-Ying.pdf

113. Kadeisvili J. V., Lynch C. and Yang Y. Confirmation of Santilli's intermediate controlled nuclear fusion of Deuterium and Carbon into Nitrogen without harmful radiation. *The Open Physical Chemistry Journal*, 2013, v. 5, 17–27. http://www.santilli-foundation.org/docs/ICNF-Conf-2013.pdf

114. Abundo U. Interpretation and enhancement of the excess energy of Rossi's reactor via Santilli neutroids and nucleoids. *Hadronic J.*, 2014, v. 37, 697–737. http://www.santilli-foundation.org/docs/abundo-paper-2014.pdf

115. Lanjewar R. B. A Brief Review of Intermediate Controlled Nuclear Syntheses (ICNS) without Harmful Radiations. *AIP Conference Proceedings*, 2015, v. 1648, 510–515. 10.1063/1.4912717. http://www.santilli-foundation.org/docs/1.4912717(RB-Lanjewar).pdf

116. Das Sarma I. B. Hadronic Nuclear Energy: An Approach Towards Green Energy. *American Journal of Modern Physics*, 2016, v. 5, 119–130. http://www.santilli-foundation.org/docs/pdf6.pdf

117. Ying L. Verification of Santilli's Intermediate Nuclear Harmful Radiation and the Production of Magnecular Clusters. Lecture, 2012 http://www.world-lecture-series.org/lecture-vd

118. Rossiter D., Director. IVA Report 184727-001 on comparative Nitrogen counts on samples of the Nitrogen synthesis. http://www.santilli-foundation.org/docs/nitrogen-tests-2010.pdf

119. Rossiter D., Director. IVA Report 200010 on comparative Nitrogen counts. http://www.santilli-foundation.org/docs/Oneida-analyses-2013.zip

120. Rossiter D., Director. IVA Report 184033-001 on comparative hydrogen and magnegas tests. http://www.santilli-foundation.org/docs/hydrogen-magnegas-2010.pdf

121. Rossiter D., Director. IVA Report 189920 on comparative Oxygen counts. http://www.santilli-foundation.org/docs/helium-carbon-fusion-I.pdf

122. Rossiter D., Director. IVA Report 189920 on comparative Oxygen counts. http://www.santilli-foundation.org/docs/helium-carbon-fusion-II.pdf

123. Rossiter D., Director. IVA Report 189920 on comparative Silicon counts. http://www.santilli-foundation.org/docs/IVAReport.189920.pdf

124. Rossiter D., Director. IVA Report 189920 on comparative Silicon count. http://www.santilli-foundation.org/docs/IVAReport.189920.pdf

125. Swartz D. Constellation Technologies first report on comparative Silicon counts. http://www.santilli-foundation.org/docs/Constellation-Si-10-13.zip

126. Swartz D. Constellation Technologies second report on comparative Silicon counts. http://www.santilli-foundation.org/docs/Constellation-Rep-Si-2.zip

127. Swartz D. Constellation Technologies third report on comparative Silicon counts. http://www.santilli-foundation.org/docs/Constell-Si-3.pdf

128. Swartz D. Constellation technologies Third report on comparative Silicon counts. http://www.santilli-foundation.org/docs/Constell-Silicon-10-14.pdf

129. Santilli R. M. Apparatus and method for recycling contaminated liquids. U. S. patent No. 6,540,966. http://pdfpiw.uspto.gov/.piw?docid=06540966

130. Santilli R. M. Durable and efficient equipment for the production of a combustible and non-pollutant gas from underwater arcs and method therefore. U. S. patent No. 6,183,604. http://patentimages.storage.googleapis.com/4c/ad/2b/8-74b5ffe4a2f12/US6183604.pdf

131. Santilli R. M. Method and Apparatus for the industrial production of new hydrogen-rich fuels. U. S. patent No. 9,700,870,B2. http://www.santilli-foundation.org/docs/Magnecule-patent.pdf

132. Eriksson J. Neutron Emission Spectrometry for Fusion Reactor Diagnosis Method Development and Data Analysis. *Acta Universitatis Upsalensis, Uppsala*, 2015. http://uu.diva-portal.org/smash/get/diva2:798599/FULLTEXT01.pdf

133. Wesson J. Tokamak, Oxford Science Publ., 2011.

134. Saxena Y. C. Tokamak: Q device for nuclear fusion. *Indian Journal fr Cryogenics*, 2016, v. 41, 2–18. http://www.researchgate.net/publication/306373246

135. Ke H. B., Wen P. and Wang W. H. The Excess Heat Capacity in Glass-forming Liquid Systems Containing Molecules. arXiv 1111.4826. http://arxiv.org/abs/1111.4826

136. Mizuno T. and Rothwell J. Increased Excess Heat from Palladium Deposited on Nickel in the 22nd International Conference for Condensed Matter Nuclear Science ICCF-22 Assisi, Italy, 2019. http://fdocuments.net/document/mizuno-increased-excess-mizuno-t-and-j-rothwell-increased-excess-heat-from-palladium.html?page=1

137. Iwamura Y., Itoh T. and Kasagi Ji. Research Article Excess Energy Generation using a Nano-sized Multilayer Metal Composite and Hydrogen Gas. *J. Condensed Matter Nucl. Sci.*, 2020, v. 33, 1–13. http://www.cleanplanet.co.jp/wp-content/uploads/J-Condensed-Matter-Nucl-Sci-33-2020-1.pdf

138. Rutherford E. Bakerian Lecture: Nuclear Constitution of Atoms. *Proc. Roy. Soc. A*, 1920, v. 97, 374–382. http://royalsocietypublishing.org/doi/10.1098/rspa.1920.0040

139. Chadwick J. *Proc. Roy. Soc. A*, 1932, v. 136, 692–723.

140. Rapports du Septième Conseil de Physique Solvay, Gauthier-Villars, Paris, 1933, 324.

141. Fermi E. Nuclear Physics. University of Chicago Press, 1949.

142. Santilli R. M. The etherino and/or the neutrino Hypothesis? *Found. Phys.*, 2007, v. 37, 670–695. http://www.santilli-foundation.org/docs/EtherinoFoundPhys.pdf

143. American Chemical Society. Energy from the Sun. http://www.acs.org/content/acs/en/climatescience/energybalance/energyfromsun.html

144. Santilli R. M. Apparent Experimental Confirmation of Pseudoprotons and their Application to New Clean Nuclear Energies. *International Journal of Applied Physics and Mathematics*, 2019, v. 9, 72–100. http://www.santilli-foundation.org/docs/pseudoproton-verification-2018.pdf

145. Santilli R. M. The Novel Hyper Combustion for the Complete Combustion of Fossil Fuels. *Intern. Journal of Chemical Engineering and Applications*, 2019, v. 10, 16. http://www.santilli-foundation.org/docs/hypercombustion-2019.pdf

146. Bartoli S. B. and Santilli R. M. Studies on the engineering realization of Intermediate Controlled Nuclear Fusions. to appear.

147. Yukawa, H. On the interaction of elementary particles. *Proc. Phys. Math. Soc. Jpn*, 1935, v. 17, 48–57.

148. Woods R. D. and Saxon D. S. Diffuse Surface Optical Model for Nucleon-Nuclei Scattering. *Physical Review*, 1954, v. 95, 577–578.

149. Reid R. V. Local phenomenological nucleon–nucleon potentials. *Annals of Physics*, 1962, v. 50, 411–448.

On the Nature of Some Cosmic Radiations

Anatoly V. Belyakov

Tver, Russia. E-mail: belyakov.lih@gmail.com

Frequency distributions of the spectrum of hydrogen and hydrogen-like elements help to determine the most probable excited elements spectral radio lines in outer space. Based on the geometrodynamic concept of J. Wheeler, the reason for the appearance of recombination radio lines is explained, and the background cosmic radiation maximum nature is established. The hydrogen atom limiting quantum number is calculated. It has been established that the wavelength during proton-electron recombination at the limiting quantum level coincides with the known 21 cm cold atomic hydrogen wavelength.

1 Introduction

Space is filled with various types of radiation, and some of them, such as the background cosmic (relic) radiation, recombination radio lines (RRL) and atomic hydrogen radiation at a wavelength of 21.1 centimeters, are of particular interest to researchers. The study of radio lines of excited atoms is the most effective method of astrophysical research to obtain the important information about various galactic and extragalactic objects. The spectrum of the relic radiation filling the Universe corresponds to the completely black body radiation spectrum with a temperature of 2.73 K. Its maximum falls at a wavelength of 1.9 mm.

The conditions for the occurrence of this kind of radiation exist in a cold rarefied interstellar medium. Under such conditions, in the process of electrons and ions recombination, some highly excited stable hydrogen atoms and other light elements can be formed with a quantum number theoretically possible up to $n = 1000$, where the electronic levels are still distinguishable; the atom limiting size is limited by the background nonthermal radio emission of the Galaxy and $n_{lim} = 1600$ [1].

High electronic levels are inhabited mainly due to recombinations, and radio lines most often manifest themselves during electron transitions between neighboring electronic levels. The spectral RRLs emitted during the transitions fall in the radio range. To date, the recombination radio lines of hydrogen have been registered in the scale from the infrared to the metre scale at $n = 10 \ldots 300$. At higher excitation levels, radio lines were observed in the process of absorption only [2–4].

Atomic hydrogen in the interstellar medium is observed due to emission and absorption in the 21 cm line. The hydrogen radio line is an effective means of studying the Universe, because there is about half the mass of galactic interstellar matter in the atomic hydrogen ground state form. It is assumed this spectral line to be the result of transitions between sublevels of the hyperfine structure of the hydrogen atom ground energy level. The reason for hyperfine splitting is the interaction of the nucleus spin and the electron spin, since these spins can be parallel or antiparallel. When the electron spin orientation is reversed, emission (or absorption) of quanta with the frequency of 1420 MHz occurs [5, 6].

2 On the shape of the spectra of frequency distributions

The presence and spectral lines intensity of specific sources depend on various factors, and usually a small part of the spectrum is realized. However, the averaging with respect to many sources in large space and time scales (infinite scales as an ultimate case) of all possible hydrogen atom electron transitions and the spectral lines corresponding to these transitions gives characteristic *frequency distributions* in accordance with the Balmer-Rydberg formula

$$W = \frac{m^2 n^2}{m^2 - n^2}\,, \tag{1}$$

where $m, n = 1, 2, 3 \ldots$ Moreover, in the range of $n, m = 10 \ldots 300$ (in radiation), the characteristic frequency distribution will correspond to the completely black body radiation spectrum with a temperature of about 3 K, and the characteristic frequency distribution over all remaining levels at $n, m = 300 \ldots 500$ will take a similar shape with a maximum of about 21 cm, see Fig. 1. Such a result to some extent explains the nature of these radiations. For example, the shape of the background radiation curve could be explained

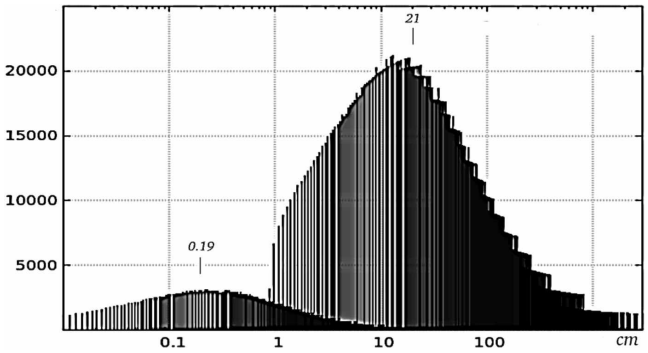

Fig. 1: Frequency distribution of the Balmer-Rydberg formula for $n, m = 10 \ldots 300$ (left) and for $n, m = 300 \ldots 1500$ (right).

by natural factors currently taking place. Details about frequency distributions and methods for their construction are given in [7, 8].

The radio lines of excited atoms provide information about the electron temperature, density, composition of the interstellar medium, and about other important parameters. However, finding useful RRL is a laborious task, because building even one spectrum for a single observed point at decameter waves requires many days of observations. Frequency distributions help solve this problem.

Fig. 2 shows the characteristic frequency distribution of the Balmer-Rydberg formula in the decameter range. The currently recorded radio links according to the data of [1] and [3] are also shown there. Although these lines belong to carbon, its atoms under these conditions are hydrogen-like. Designations, for example, $427\,\alpha$ means transition $428 \rightarrow 427$. At $n = 1530$ (this value, as will be shown below, is equal to the limiting value of n), good agreement with the experimental data is achieved.

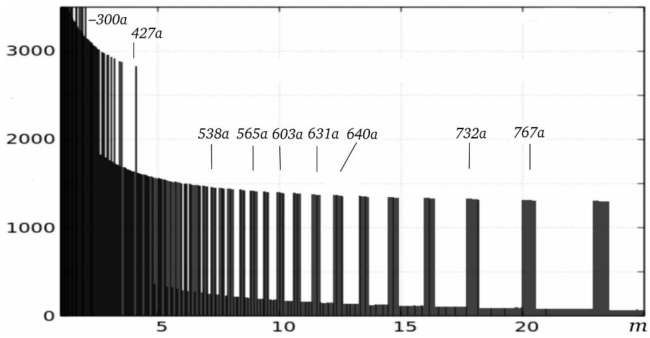

Fig. 2: Frequency distribution for hydrogen-like atoms at $n, m = 300 \ldots 1530$. The designated a-lines belong to carbon.

Not all lines are observable in practice, and not only and not so much for external reasons. As follows from the analysis of the characteristic frequency distributions, the most active radio lines are in fact a superposition (combination) of closely spaced spectral lines, when the electrons make a variety of transitions. Of course, the spectrograms constructed under the condition of the equiprobability of all possible electron transitions cannot completely coincide with the real radiation spectrum, but where the combinatorial factor is significant, the important spectral lines should be sought in the areas of concentration of spectral lines of the frequency distribution. The strong *widening* of radio links at large n [3] can also be explained by the summation, superposition, and combination of close frequencies.

3 Proton-electron contour and the nature of RRL

Recombination radio lines were recorded starting from $n \approx 10$, moreover, at $n \approx 100$ and more, only RRLs are observed. These features, as well as the recombination phenomenon itself, can be explained by considering the atom from the point of view of *J. Wheeler's geometrodynamic concept* [9].

According to Wheeler's concept, charged microparticles are singular points on a topologically non-unitary coherent and fractalized two-dimensional surface of our world, connected by a "wormhole", a vortex tube or a force current line of the drain-source type in an additional dimension, forming a closed *contour*. According to the adopted model [10], the vortex tube (contour) has mass M, radius r_e, and it is helically filled with some medium in the triple vortex thread form with radius r, circulating along the contour at a velocity v.

The parameters of an arbitrary proton-electron contour are defined in dimensionless units of the electron mass m_e, its classical radius r_e, and the speed of light c:

$$M = (an)^2 , \tag{2}$$

$$v = \frac{c_0^{1/3}}{(an)^2} , \tag{3}$$

$$r = \frac{c_0^{2/3}}{(an)^4} , \tag{4}$$

where a and c_0 are the reciprocal fine structure constant and the dimensionless speed of light c divided by [m/sec].

It is assumed the contour to be structured into ordered units (let's call them photons for short), and their number z is determined by the contour total length to the wavelength ratio. As a result, the formula is obtained:

$$z = \frac{n^6}{k\,W} , \tag{5}$$

where $k = 1.7 \ldots 1$ depending on the parameter n, and for large n can be accepted $k \approx 1$. The contour unit mass corresponding to one photon is equal to

$$m = \frac{M}{z} . \tag{6}$$

It is clear, a unit mass kinetic energy's changing during an electron transition from n_i to n_k orbit is:

$$E_k = \left(m_i v_i^2 - m_k v_k^2\right) \tag{7}$$

or, bearing in mind (2), (3), (5), and (6) and setting $n = n_i$ and $m = n_k$ in the Balmer formula, we obtain in units of $m_e c^2$:

$$E_k = k\,W\,c_0^{2/3}\left(\frac{1}{n_i^8} - \frac{1}{n_k^8}\right)\frac{1}{a^2} . \tag{8}$$

At the same time, the energy of the corresponding photon is:

$$E_h = \frac{hc}{\lambda} , \tag{9}$$

where Planck's constant is:

$$h = 2\pi\alpha m_e c r_e , \tag{10}$$

wavelength is:

$$\lambda = \frac{W}{R_\infty}\,, \tag{11}$$

and the Rydberg constant is:

$$R_\infty = \frac{1}{4\pi\alpha^3 r_e}\,. \tag{12}$$

Then the photon energy, taking into account (10), (11) and (12), in units of $m_e c^2$ is:

$$E_h = \frac{1}{2Wa^2}\,. \tag{13}$$

The ratio of a unit mass energy and a photon energy, bearing in mind (8) and (13), in units of $m_e c^2$ takes the form:

$$\frac{E_k}{E_h} = 2kW^2 c_0^{2/3}\left(\frac{1}{n_i^8} - \frac{1}{n_k^8}\right), \tag{14}$$

and for large n and for neighboring levels, when $W \approx n^3/2$

$$\frac{E_k}{E_h} = \frac{1}{2}\,kn^6 c_0^{2/3}\left(\frac{1}{n_i^8} - \frac{1}{n_k^8}\right), \tag{15}$$

where $n \approx \frac{1}{2}(n_i + n_k)$.

As the quantum number n grows, i.e. as the contour increases when an electron passes from the n_k level to the n_i level, there comes a moment when the increment of kinetic energy of a unit mass per photon is not enough to form the corresponding photon, and additional energy is required through external influence. In these cases the emission is preceded by an act of *recombination* – the capture of a free electron by an ion to one of the high levels, for example, photorecombination. Free electrons recombine with a proton or ions. An excess of energy equal to the difference between the electron energy and its binding energy in the atom is carried away with the quantum. During subsequent downward cascade transitions, RRL radiation occurs with frequencies $\nu \sim \Delta n/n^3$. Thus, from (15) it follows that for $n > 110$ the ratio E_k/E_h is always less than 1, and *all radio lines will already be recombination*. Moreover, the electron-proton recombination according to the type $\infty \to n$ at n close to 110 just forms quanta, with a frequency equal to the frequency of the relic radiation maximum.

At $n < 110$, in the millimeter range, there are possible transition where electrons can spontaneously move to lower levels, forming the corresponding spectral lines. These lines in the hydrogen spectrum are observed experimentally [1], and they are well revealed when the restriction $E_k/E_h > 1$ is introduced into the program for calculating the characteristic frequency distributions, Fig. 3. Without this condition, it is difficult to isolate them in the full spectrum. If one builds a frequency distribution with an inverse constraint $E_k/E_h < 1$, then one can make sure that RRLs can occur starting from $\lambda = 0.1$ mm, i.e. at $n \approx 10$.

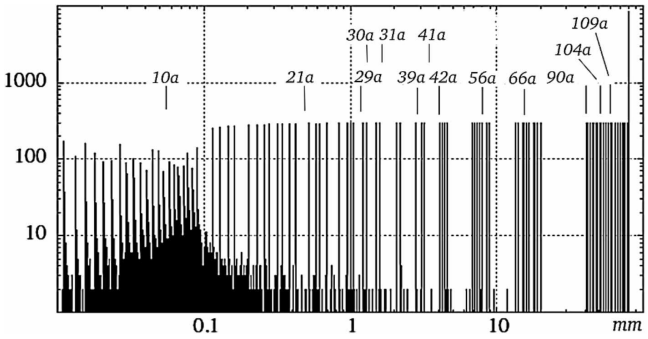

Fig. 3: Frequency distribution for hydrogen in the millimeter range at $n, m = 1 \ldots 130$ under the condition $E_k/E_h > 1$.

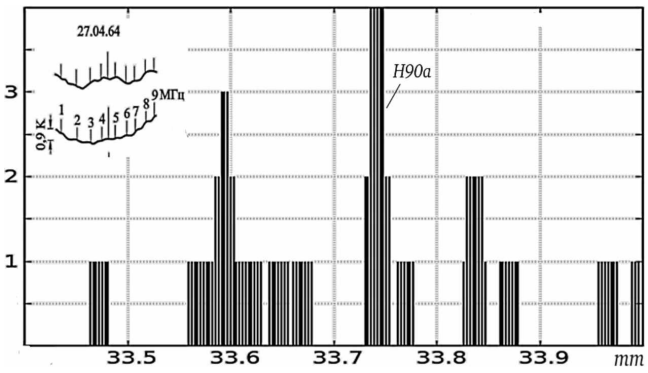

Fig. 4: Frequency distribution of the H90a line at $n, m = 50 \ldots 250$; 207 intervals per range. Top left – the line of hydrogen according to observations in Pushchino in the direction of the Omega Nebula compared with the control spectrogram with the antenna retracted from the source.

It is obvious that the detected radio lines in the range $n = 10 \ldots 110$ can be the result of the superposition of close spectral lines, both recombination and non-recombination ones, for example, the 33.76 mm radio line [11]. This line was one of the first to be discovered in space, perhaps because it is the combination of several very close lines, Fig. 4, and the central peak in the figure is not RRL. That is, the peak does not disappear when the restriction $E_k/E_h > 1$ is imposed. If there are other known restrictions or conditions, they can also be entered into the program for calculating the characteristic frequency distributions.

These distributions explain the features of some spectra noted by some authors. Thus, in [1], the profiles of the H29a, H30a, and H31a lines are given, which turned out to be two-humped, which the authors have given an exotic explanation to. However, the analysis of the spectrum in Fig. 5 narrow part shows that the two-humped profile of the mentioned lines is due to the presence of two closely spaced spectral lines.

In another case, the reason for the unusually low intensity of the H41a line, namely, more than 50 times lower than the intensity of the above lines, is clear from Fig. 3. Indeed, the H41a line height is 60 times lower than the neighboring lines height (in arbitrary units).

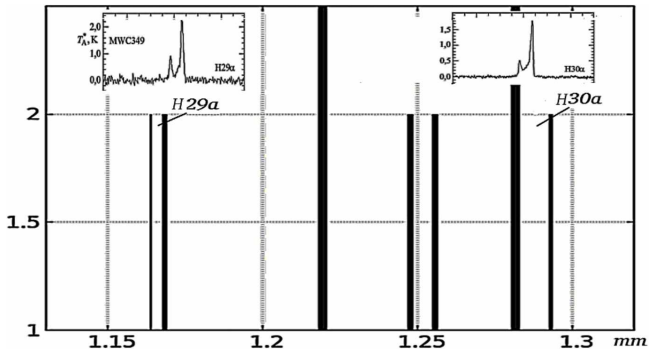

Fig. 5: Frequency distribution in the millimeter range of the H29a and H30a lines at $n, m = 30 \dots 70$, provided $E_k/E_h > 1$; 341 intervals per range. Above: RRL spectra obtained from the MWC349 source.

4 The hydrogen atom limiting size and the 21 centimeters line

It is believed the atom limiting size to be limited by the background non-thermal Galaxy radio emission and n cannot be more than 1500–1600. But the background radiation is not a constant, and more fundamental parameters are needed to accurately determine the limiting level.

In the adopted model based on Wheeler's geometrodynamics, the vortex thread radius r, which fills the proton-electron contour like a spiral, decreases as the contour increases according to (4). On the whole, the thread consists of three unit threads, and each of them can in the limit have the Planck size r_h [12]. Then, under the condition of their dense packing and based on geometric considerations, the vortex thread size (circumferential diameter) will be:

$$r_0 = \left(1 + 2/\sqrt{3}\right) r_h = 2.1547\, r_h\,, \tag{16}$$

where the Planck size is:

$$r_h = \left(\frac{\hbar\gamma}{c^3}\right)^{1/2} = 1.616 \times 10^{-35}\,\text{m} \;\text{ or }\; 5.735 \times 10^{-21}\, r_e\,, \tag{17}$$

where $\hbar = h/2\pi$, and γ is the gravitational constant.

Let us assume that in the limit the thread fills the contour in the spiral form, having turns being twisted into the last (tertiary) spiral structure, then the thread (by the Bohr atom general analogy) has the size:

$$r = a^2 r_0\,. \tag{18}$$

Then, when taking into account (4), (16), (17), and (18), one obtains the limiting quantum number value:

$$n_{lim} = \frac{c_0^{1/6}}{\left(1 + 2/\sqrt{3}\right)^{1/4} r_h^{1/4} a^{3/2}}\,. \tag{19}$$

Further, substituting the dimensionless value r_h in units of r_e, one obtains the limiting quantum number $n_{lim} = 1530$ and the proton-electron recombination wavelength for the transition $\infty \to n_{lim}$:

$$\lambda = \frac{n_{lim}^2}{R_\infty} = 21.3\,\text{cm}\,. \tag{20}$$

Thus, the recombination wavelength for the $\infty \to n_{lim}$ transition turned out to be actually equal to the hydrogen radio line 21.1 cm.

It is assumed some mechanism for the atomic hydrogen radiation appearance to exist in which when the atoms are impacting, there is their electron with different directions of spins exchanging [5, 6]. The very same transitions between the hyperfine structure sublevels of the hydrogen atom main energy level, as quantum calculations show, occur with a negligible probability of $2.85 \times 10^{-15}\,\text{sec}^{-1}$. Moreover, although there are analogs of the 21 cm line for atoms of hydrogen isotopes as well as for some other atoms whose nuclei have a nonzero spin moment, such lines are not found in astrophysical sources [5]. Therefore, the low probability and the absence of analogues of this radiation in other atoms make it possible to doubt the main reason for the radiation at 21 cm. It is logical to assume the recombination radiation to be the main reason. Its energy coincides with the spin reorientation energy, that in general creates radiation in a relatively narrow range of about 21 cm.

Thus, the situation with recombination at $n = 10$, where the photon energy is compared with the energy of a unit mass, which forms the background radiation maximum, is reproduced symmetrically at a higher level at $n = 1530$, where the photon energy is compared with the spin reorientation energy, which forms the recombination radiation maximum. This situation seems to be harmonious and logical.

5 Conclusion

It is shown that the frequency distributions make it possible to use the combinatorics factor to identify spectral regions with the most intense spectral lines of excited elements in outer space. In general, the range of cosmic radiation can be divided into two subranges: at $n = 1 \dots 300$ (mainly in radiation), which has a total maximum coinciding with the background (relic) radiation maximum and at $n = 300 \dots 1530$ (in mainly in absorption), which has a total maximum coinciding with the atomic hydrogen wavelength.

It has been established that the transition to recombination radiation is due to the equality of the recombination photon energy and the energy of a unit mass of the contour per one photon at $n \approx 110$, which corresponds to the background radiation maximum during the transition $\infty \to n$.

The limiting quantum level for hydrogen has been determined and it has been found that the photon recombination energy is at this level equal to the electron spin reorientation energy with respect to the atomic hydrogen nuclear spin.

Received on November 30, 2022

References

1. Sorochenko R. L., Gordon M. A. Recombination of Radio Lines. Physics and Astronomy. Fizmatlit, Moscow, 2003.
2. Pedlar A. *et al*. *Mon. Not. R. Astron. Soc.*, 1978, v. 182, 473.
3. Konovalenko A. A. Decametric astrospectroscopy. *Earth and Universe*, 1986, v. 5, 26–34.
4. Gordon M. A. and Sorochenko R. L., eds. Radio Recombination Lines: 25 Years of Investigation. 1990, *Proceeding of the IAU Colloquium 125*, Kluwer Academic Publishers.
5. http://ns1.andynet.org/~gmr/course/5.htm.
6. http://12apr.su/books/item/f00/s00/z0000038/st025.shtml.
7. Belyakov A. V. Finding the fine structure of the solutions of complicate logical probabilistic problems by the frequent distributions. *Progress in Physics*, 2010, v. 6 (4), 36–39.
8. Belyakov A. V. Combinatorics and frequency distributions as the determining factors of electron and nuclear spectra. *Progress in Physics*, 2022, v. 18 (1), 15–20.
9. Dewitt B. S. Quantum gravity. *Scientific American*, December 1983, v. 249, 112–129.
10. Belyakov A. V. Macro-analogies and gravitation in the microworld: further elaboration of Wheeler's model of geometrodynamics. *Progress in Physics*, 2012, v. 8 (2), 47–57.
11. http://www.prao.ru/History/history_6.html
12. Belyakov A. V. Determination of the neutrino mass. *Progress in Physics*, 2016, v. 12 (1), 34–38.

On the Nature of the Spacetime Continuum

Pierre A. Millette

E-mail: pierre.millette@uottawa.ca, Ottawa, Canada

In this paper, we summarize the nature of the Spacetime Continuum (STC) as provided by the Elastodynamics of the Spacetime Continuum (*STCED*). We note that, in addition to providing a physical explanation for inertial mass and for wave-particle duality, *STCED* covers the Physics of the Spacetime Continuum. We show that the dimensionality of the Spacetime Continuum could be deduced mathematically if the value of the Lamé elastic constants $\bar{\kappa}_0$, $\bar{\mu}_0$ and $\bar{\lambda}_0$ of the Spacetime Continuum could be determined experimentally. From Einstein's field equation for an isotropic and homogeneous STC, we derive the value of the Spacetime Continuum bulk modulus $\bar{\kappa}_0$ in terms of elementary constants. Understanding the nature of the Spacetime Continuum as provided by *STCED* provides a better understanding of the general relativistic spacetime.

1 Introduction

In this paper, we summarize the nature of the Spacetime Continuum (*STC*) as provided by the Elastodynamics of the Spacetime Continuum (*STCED*) [1–3]. *STCED* is a natural extension of Einstein's General Theory of Relativity which blends continuum mechanical and general relativistic descriptions of the Spacetime Continuum. The introduction of strains in the Spacetime Continuum as a result of the energy-momentum stress tensor allows us to use, by analogy, results from continuum mechanics, in particular the stress-strain relation, to provide a better understanding of the general relativistic spacetime.

2 Elastodynamics of the Spacetime Continuum

The stress-strain relation for an isotropic and homogeneous Spacetime Continuum is given by [1, 3]

$$2\bar{\mu}_0\,\varepsilon^{\mu\nu} + \bar{\lambda}_0\,g^{\mu\nu}\varepsilon = T^{\mu\nu} \tag{1}$$

where $\bar{\lambda}_0$ and $\bar{\mu}_0$ are the Lamé elastic constants of the Spacetime Continuum: $\bar{\mu}_0$ is the shear modulus (the resistance of the Spacetime Continuum to *distortions*) and $\bar{\lambda}_0$ is expressed in terms of $\bar{\kappa}_0$, the bulk modulus (the resistance of the Spacetime Continuum to *dilatations*):

$$\bar{\lambda}_0 = \bar{\kappa}_0 - \tfrac{1}{2}\,\bar{\mu}_0 \tag{2}$$

in a four-dimensional continuum. $T^{\mu\nu}$ is the general relativistic energy-momentum stress tensor, $\varepsilon^{\mu\nu}$ the Spacetime Continuum strain tensor resulting from the stresses, and

$$\varepsilon = \varepsilon^{\alpha}{}_{\alpha}\,, \tag{3}$$

the trace of the strain tensor obtained by contraction, is the volume dilatation ε defined as the change in volume per original volume [4, see pp. 149–152] and is an invariant of the strain tensor. It should be noted that the structure of (1) is similar to that of the field equations of General Relativity,

$$R^{\mu\nu} - \tfrac{1}{2}\,g^{\mu\nu}R = -\varkappa\,T^{\mu\nu} \tag{4}$$

where $R^{\mu\nu}$ is the Ricci curvature tensor, R is its trace, $\varkappa = 8\pi G/c^4$ and G is the gravitational constant (see [2, Ch. 2] for more details).

In *STCED*, as shown in [1, 3], energy propagates in the spacetime continuum (*STC*) as wave-like *deformations* which can be decomposed into *dilatations* and *distortions*. *Dilatations* involve an invariant change in volume of the Spacetime Continuum which is the source of the associated rest-mass energy density of the deformation. On the other hand, *distortions* correspond to a change of shape (shearing) of the Spacetime Continuum without a change in volume and are thus massless.

Thus deformations propagate in the Spacetime Continuum by longitudinal (*dilatation*) and transverse (*distortion*) wave displacements. This provides a natural explanation for wave-particle duality, with the massless transverse mode corresponding to the wave aspects of the deformations and the massive longitudinal mode corresponding to the particle aspects of the deformations.

The rest-mass energy density of the longitudinal mode is given by [1, see Eq. (32)]

$$\rho c^2 = 4\bar{\kappa}_0\varepsilon \tag{5}$$

where ρ is the rest-mass density, c is the speed of light, $\bar{\kappa}_0$ is the bulk modulus of the *STC* as seen previously, and ε is the volume dilatation given by (3).

3 The physicality of four-dimensional spacetime

Minkowski [5,7] first introduced the concept of a four-dimensional spacetime and the description of particles in this spacetime as worldlines in 1908. This has given rise to the question whether four-dimensional spacetime is real or a mathematical abstraction. Eddington [7] considered this question in 1921:

> It was shown by Minkowski that all these fictitious spaces and times can be united in a single continuum of four dimensions. The question is often raised whether this four-dimensional space-time is real, or merely a mathematical construction; perhaps it is sufficient to

> reply that it can at any rate not be less real than the fictitious space and time which it supplants.

Petkov [6, 7] provides a cogent summary of Minkowski's paper. Worldlines of particles at rest are vertical straight lines in a *space−ct* diagram, while particles moving at a constant velocity v are oblique lines and accelerated particles are curved lines. This provides a physical explanation for length contraction as a manifestation of the reality of a particle's extended worldline, where the cross-section measured by an observer moving relative to it (i.e. at an oblique line in the *space−ct* diagram), creates the difference in perceived length between a body at rest and one in movement. This is explored in greater detail in [8, 9]. Minkowski's work demonstrates the physicality of four-dimensional spacetime, and that indeed, four-dimensional physics is spacetime geometry.

The relation (2) between κ, and μ and λ can be generalized to N dimensions, and is given by [10, p. 769]

$$\kappa = \frac{2\mu + N\lambda}{N} \,. \tag{6}$$

The dimensionality of the Spacetime Continuum could thus be deduced mathematically if the value of the Lamé elastic constants $\bar{\kappa}_0$, $\bar{\mu}_0$ and $\bar{\lambda}_0$ of the Spacetime Continuum could be determined experimentally.

4 Physics of the Spacetime Continuum

From General Relativity and *STCED*, one can deduce the properties of the Spacetime Continuum, as *STCED* includes the physics of the Spacetime Continuum as an underlay of the theory.

The Spacetime Continuum is modelled as a four-dimensional differentiable manifold [11] endowed with a metric $g_{\mu\nu}$. It is a continuum that can undergo deformations and support the propagation of such deformations. A continuum that is deformed is strained.

An infinitesimal element of the unstrained continuum is characterized by a four-vector x^μ, where $\mu = 0, 1, 2, 3$. The time coordinate is $x^0 \equiv ct$.

A *deformation* of the Spacetime Continuum corresponds to a state of the *STC* in which its infinitesimal elements are displaced from their unstrained positions. Under deformation, the infinitesimal element x^μ is displaced to a new position $x^\mu + u^\mu$, where u^μ is the displacement of the infinitesimal element from its unstrained position x^μ.

The Spacetime Continuum is approximated by a deformable linear elastic medium that obeys Hooke's law. Under those conditions, for a general anisotropic continuum in four dimensions [12, see pp. 50–53],

$$E^{\mu\nu\alpha\beta}\varepsilon_{\alpha\beta} = T^{\mu\nu} \tag{7}$$

where $\varepsilon_{\alpha\beta}$ is the strain tensor, $T^{\mu\nu}$ is the energy-momentum stress tensor, and $E^{\mu\nu\alpha\beta}$ is the elastic moduli tensor.

The Spacetime Continuum is further assumed to be isotropic and homogeneous. This assumption is in agreement with the conservation laws of energy-momentum and angular momentum as expressed by Noether's theorem [13, see pp. 23–30]. For an isotropic medium, the elastic moduli tensor simplifies to [12]:

$$E^{\mu\nu\alpha\beta} = \bar{\lambda}_0(g^{\mu\nu}g^{\alpha\beta}) + \bar{\mu}_0(g^{\mu\alpha}g^{\nu\beta} + g^{\mu\beta}g^{\nu\alpha}) \tag{8}$$

where $\bar{\lambda}_0$ and $\bar{\mu}_0$ are the Lamé elastic constants of the Spacetime Continuum as seen previously in Section 2. Substituting (8) into (7), we obtain the stress-strain relation (1) seen previously in Section 2, for an isotropic and homogeneous Spacetime Continuum. The Spacetime Continuum is thus modelled as an elastic medium (see [3, pp. 16–18,24]).

Blair [14, p. 3–4] writes Einstein's field equation as

$$\mathbf{T} = \frac{c^4}{8\pi G}\,\mathbf{G}\,, \tag{9}$$

where $\mathbf{T}$ is the stress energy tensor, $\mathbf{G}$ is the Einstein curvature tensor and G is the universal gravitational constant. He notes the very large value of the proportionality constant. This leads him to point out that spacetime is an elastic medium that can support waves, but its extremely high stiffness means that extremely small amplitude waves have a very high energy density. He notes that the coupling constant $c^4/8\pi G$ can be considered as a modulus of elasticity (K) for spacetime. In similarity to the acoustic case, where the specific impedance $z = K/v$, he identifies the quantity c^3/G with the characteristic impedance of spacetime [14, p. 45].

Substituting for the Einstein curvature tensor in (9), the equation becomes

$$T^{\mu\nu} = \frac{c^4}{8\pi G}\,G^{\mu\nu} = \frac{c^4}{8\pi G}\left[R^{\mu\nu} - \tfrac{1}{2}\,g^{\mu\nu}R\right]. \tag{10}$$

For *STCED*, as seen in (7), the single modulus of elasticity of (10) is replaced by the elastic moduli tensor $E^{\mu\nu\alpha\beta}$ of rank 4, consisting of 256 components. For an isotropic and homogeneous Spacetime Continuum, the elastic moduli tensor is given by (8) and simplifies to two moduli, the shear modulus $\bar{\mu}_0$ for transverse waves and the bulk modulus $\bar{\kappa}_0$ for longitudinal waves, as seen previously in (1):

$$T^{\mu\nu} = 2\bar{\mu}_0\,\varepsilon^{\mu\nu} + \bar{\lambda}_0\,g^{\mu\nu}\varepsilon\,. \tag{11}$$

As shown in [2, §2.5], (10) and (11) can be combined and separated into a longitudinal relation

$$\frac{c^4}{8\pi G}\,R = 2(\bar{\mu}_0 + 2\bar{\lambda}_0)\,\varepsilon = 4\,\bar{\kappa}_0\,\varepsilon = \rho c^2 \tag{12}$$

where ρ is the rest-mass energy density present in the Spacetime Continuum, and a transverse relation

$$\frac{c^4}{8\pi G}\,R^{\mu\nu} = 2\bar{\mu}_0\,\varepsilon^{\mu\nu} - (\bar{\lambda}_0 + \bar{\mu}_0)\,g^{\mu\nu}\varepsilon \tag{13}$$

which becomes

$$\frac{c^4}{8\pi G}\, R^{\mu\nu} = 2\bar{\mu}_0 \left(\varepsilon^{\mu\nu} - \frac{1}{2}\, \frac{\bar{\lambda}_0 + \bar{\mu}_0}{\bar{\mu}_0}\, g^{\mu\nu}\varepsilon \right) \tag{14}$$

where $(\bar{\lambda}_0 + \bar{\mu}_0)/\bar{\mu}_0$ is a numerical factor.

We can derive the relationship between the Spacetime Continuum bulk modulus $\bar{\kappa}_0$ and known constants from relation (12) as follows:

$$\frac{c^4}{8\pi G}\, R = 4\,\bar{\kappa}_0\, \varepsilon\,, \tag{15}$$

where the constant $c^4/8\pi G$ has dimensions of [N], R has dimensions of $[\mathrm{m}^{-2}]$, $\bar{\kappa}_0$ has dimensions of $[\mathrm{N\,m}^{-2}]$ or $[\mathrm{J\,m}^{-3}]$, and ε is dimensionless. We need to express R as a dimensionless quantity and combine its constant factor with constant $c^4/8\pi G$. Curvature R is expressed in $[\mathrm{m}^{-2}]$. As shown in [15], the smallest Spacetime Continuum Burgers vector b_0 is equal to Planck's length

$$\ell_P = \sqrt{\frac{\hbar G}{c^3}}\,. \tag{16}$$

The curvature of this smallest surface element will be constant, such that we can write the curvature R as

$$R = \frac{\bar{R}}{\ell_P^2} \tag{17}$$

where $\bar{R}$ is the dimensionless curvature number in terms of the smallest surface element ℓ_P^2.

Substituting (17) and (16) into (15), we obtain

$$\frac{c^7}{8\pi\hbar G^2}\, \bar{R} = 4\,\bar{\kappa}_0\, \varepsilon\,, \tag{18}$$

where the units are $[\mathrm{N\,m}^{-2}]$. The dimensionless curvature $\bar{R}$ and, as seen in Section 2, the dimensionless volume dilatation ε corresponding to the change in volume per original volume $(\Delta V/V)$ [4, see pp. 149–152], result from the applied stresses leading to the deformation of the Spacetime Continuum.

The latter corresponds to the definition of the bulk modulus. The numerical factors can be included in the definition of the dimensionless curvature $\bar{R}$ and the dimensionless volume dilatation ε to obtain

$$\frac{c^7}{\hbar G^2}\, \frac{\bar{R}}{8\pi} = \bar{\kappa}_0\, (4\varepsilon)\,. \tag{19}$$

One option is to equate the terms having dimensions of $[\mathrm{N\,m}^{-2}]$ to obtain the Spacetime Continuum bulk modulus, with the understanding that there may be a numerical factor on the R.H.S. of (20):

$$\bar{\kappa}_0 = \frac{c^7}{\hbar G^2}\,. \tag{20}$$

From one of my previous articles [1, Eq. (150)], we then have

$$\bar{\mu}_0 = 32\bar{\kappa}_0 = 32\, \frac{c^7}{\hbar G^2}\,. \tag{21}$$

Numerically, $\bar{\kappa}_0 = 4.6\times10^{113}\,\mathrm{J/m^3}$ and $\bar{\mu}_0 = 1.5\times10^{115}\,\mathrm{J/m^3}$.

With these constants, we are now in a position to calculate the density of the Spacetime Continuum $\bar{\rho}_0$. Using the relation [1]

$$c = \sqrt{\frac{\bar{\mu}_0}{\bar{\rho}_0}}, \tag{22}$$

the density of the spacetime continuum is

$$\bar{\rho}_0 = 1.7 \times 10^{98}\,\mathrm{kg/m^3}. \tag{23}$$

This value is in the same ballpark as the vacuum energy density calculated by Carroll [16, see p. 173] ($\sim 10^{112}\,\mathrm{ergs/cm^3}$) from quantum mechanical considerations.

5 Mass in the Spacetime Continuum

We have considered the origin of inertial mass in the Spacetime Continuum in [17], where we showed that integrating (5) over the 3-D space volume,

$$\int_{V_3} \rho c^2\, \mathrm{d}V_3 = 4\bar{\kappa}_0 \int_{V_3} \varepsilon\, \mathrm{d}V_3\,, \tag{24}$$

and using

$$m = \int_{V_3} \rho\, \mathrm{d}V_3 \tag{25}$$

in (24), where m is the rest mass of the deformation, we obtain

$$mc^2 = 4\bar{\kappa}_0 \int_{V_3} \varepsilon\, \mathrm{d}V_3\,. \tag{26}$$

This demonstrates that mass is not independent of the Spacetime Continuum, but rather mass is part of the Spacetime Continuum fabric itself. Hence mass results from the dilatation of the Spacetime Continuum in the longitudinal propagation of energy-momentum in the Spacetime Continuum. Matter does not warp spacetime, but rather, matter *is* warped spacetime (i.e. dilated spacetime). The missing link in General Relativity is the understanding that the trace of the energy-momentum stress tensor is related to the trace of the Spacetime Continuum strain tensor and is proportional to the mass of matter as given by (5) and (26).

6 Discussion and conclusion

In this paper, we have summarized the nature of the Spacetime Continuum (*STC*) as provided by the Elastodynamics of the Spacetime Continuum (*STCED*), which provides a better understanding of general relativistic spacetime. We have shown that the dimensionality of the Spacetime Continuum could be deduced mathematically if the value of the Lamé elastic constants $\bar{\kappa}_0$, $\bar{\mu}_0$ and $\bar{\lambda}_0$ of the Spacetime Continuum

could be determined experimentally. From Einstein's field equation for an isotropic and homogeneous STC, we derive the value of the Spacetime Continuum bulk modulus $\bar{\kappa}_0$ in terms of elementary constants.

STCED provides a physical model of the nature of inertial mass, which also includes an explanation for wave-particle duality. Mass is shown to be the invariant change in volume of spacetime in the longitudinal propagation of energy-momentum in the spacetime continuum. Hence mass is not independent of the spacetime continuum, but rather mass is part of the spacetime continuum fabric itself.

Received on December 23, 2022

References

1. Millette P. A. Elastodynamics of the Spacetime Continuum. *The Abraham Zelmanov Journal*, 2012, vol. 5, 221–277.
2. Millette P. A. Elastodynamics of the Spacetime Continuum: A Spacetime Physics Theory of Gravitation, Electromagnetism and Quantum Physics. American Research Press, Rehoboth, NM, 2017.
3. Millette P. A. Elastodynamics of the Spacetime Continuum, Second Expanded Edition. American Research Press, Rehoboth, NM, 2019.
4. Segel L. A. Mathematics Applied to Continuum Mechanics. Dover Publications, New York, 1987.
5. Minkowski H. Space and Time. 80^{th} *Assembly of German Natural Scientists and Physicians*. Cologne, 21 September 1908. English translation reprinted in Lorentz H. A., Einstein A., Minkowski H, and Weyl H. The Principle of Relativity: A Collection of Original Memoirs on the Special and General Theory of Relativity. Dover Publications, New York, 1952, pp. 73–91.
6. Petkov V. Relativity and the Nature of Spacetime, 2^{nd} ed. Springer, New York, 2009, pp. 111–114.
7. Petkov V. Inertia and Gravitation: From Aristotle's Natural Motion to Geodesic Worldlines in Curved Spacetime. Minkowski Institute Press, Montreal, 2012, pp. 78–82.
8. Millette P. A. On Time Dilation, Space Contraction, and the Question of Relativistic Mass. *Progress in Physics*, 2017, vol. 13 (4), 202–255.
9. Millette P. A. On the Question of Acceleration in Special Relativity. *Progress in Physics*, 2017, vol. 13 (4), 215–219.
10. Kleinert H. Gauge Fields in Condensed Matter, Vol. II Stresses and Defects. World Scientific Publishing, Singapore, 1989.
11. Millette P. A. The Elastodynamics of the Spacetime Continuum as a Framework for Strained Spacetime. *Progress in Physics*, 2013, vol. 9 (1), 55–59.
12. Flügge W. Tensor Analysis and Continuum Mechanics. Springer-Verlag, New York, 1972.
13. Kaku M. Quantum Field Theory: A Modern Introduction. Oxford University Press, Oxford, 1993.
14. Blair D. G., ed. The Detection of Gravitational Waves. Cambridge University Press, Cambridge, 1991.
15. Millette P. A. The Burgers Spacetime Dislocation Constant b_0 and the Derivation of Planck's Constant. *Progress in Physics*, 2015, vol. 11 (4), 313–316.
16. Carroll S. M. Spacetime and Geometry: An Introduction to General Relativity. Addison Wesley, San Francisco, 2004.
17. Millette P. A. The Origin of Inertial Mass in the Spacetime Continuum. *Progress in Physics*, 2019, vol. 15 (2), 86–91.

Progress in Physics is an American scientifc journal on advanced studies in physics, registered with the Library of Congress (DC, USA): ISSN 1555-5534 (print version) and ISSN 1555-5615 (online version). The journal is peer reviewed.

Electronic version of this journal: http://www.ptep-online.com

Postal address:
Department of Mathematics and Science, University of New Mexico,
705 Gurley Avenue, Gallup, NM 87301, USA